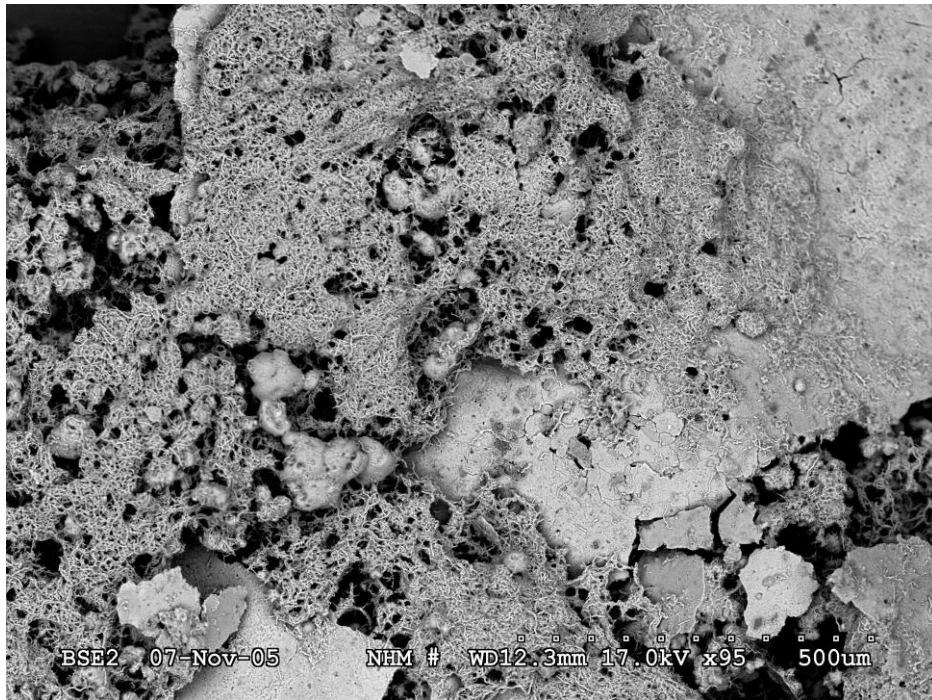


Deterioration Mechanisms and Durability of Sprayed Concrete for Rock Support in Tunnels



Per Hagelia

*“Comprehension is a prerequisite
for predictability”*

Ivan Th. Rosenqvist

Dit proefschrift is goedgekeurd door de promotor
Prof. dr. ir. K. van Breugel

Copromotor, Dr. **O. Çopuroğlu**

Samenstelling promotiecommissie:

Rector Magnificus, voorzitter

Prof. dr. ir. K. van Breugel,	Technische Universiteit Delft, promotor
Dr. O. Çopuroğlu,	Technische Universiteit Delft, copromotor
Prof. dr. ir. N. De Belie,	Universiteit Ghent, België
Prof. dr. H. Justnes,	Norges teknisk-naturvitenskaplige universitet, Noorwegen
Prof. dr. D. Damidot,	Ecole des Mines de Douai, Frankrijk
Prof. dr. ir. R. B. Polder,	Technische Universiteit, Delft
Dr. T.G. Nijland,	TNO Bouw en Ondergrond, Delft
Prof. dr. ir. E.M. Haas,	Technische Universiteit Delft, reservelid

Cover design by Per Hagelia

Cover picture: BSE image of layered Mn-Fe biofilm

Copyright © 2011 by P. Hagelia

ISBN-

Deterioration Mechanisms and Durability of Sprayed Concrete for Rock Support in Tunnels

Deterioration Mechanisms and Durability of Sprayed Concrete for Rock Support in Tunnels

Proefschrift

ter verkrijging van de graad van doctor
aan de Technische Universiteit Delft,
op gezag van de Rector Magnificus prof. ir. K.C.A.M. Luyben,
voorzitter van het College voor Promoties,
in het openbaar te verdedigen
op maandag 21 november 2011 om 15:00 uur

door

Per HAGELIA

Candidatus Scientiarum in geologie en mineralogie
van de Universiteit Oslo, Noorwegen

geboren te Gjerstad, Noorwegen

Acknowledgements

This work was carried out mainly within the framework of the project “Tunnel development” at the Technology Department, Norwegian Public Roads Administration (NPRA). The study was undertaken as a part time activity from late 2002 to early 2010. Firstly I wish to thank Alf T. Kveen for making way for a research project of this kind and Håvard Østlid for his advice and encouragements during early planning. I am especially indebted to my promotor Professor dr. ir. Klaas van Breugel and co-promotor Assistant Professor Oğuzhan Çopuroğlu for accepting me as PhD candidate in 2010 at the Faculty of Civil Engineering and Geosciences - Technical University of Delft. Your insightful assistance, generosity and genuine interest in my work are very much appreciated.

The project has in reality been performed as a free doctorate, which did not enjoy the opportunity of having a supervisor and a regular educational scheme. I therefore had to pick up almost everything by myself. This was possible due to my good colleagues in the Norwegian and international community. I owe special thanks to Reidar Kompen, Finn Fluge and Claus K. Larsen (NPRA) for discussions and the tickets you gave me to the world of concrete. Much of my literature survey was accomplished by the aid of the World Wide Web. My sincere thanks go to all of you around the globe who always responded so quickly to my reprint requests. Grethe Winge at the NPRA library is thanked for all help with getting hold of publications and reports: You also quickly learned who is sitting with the missing volumes!

Collaboration with Inger Kjersti Iden (IFE) and technical assistance by Hans-Jørgen Berg and Muriel Erambert (UiO) is gratefully acknowledged: it is always necessary to have experienced geologists within reach when it comes to analysis. Collaboration on thaumasite and popcorn calcite deposition with Ted Sibbick, Norah Crammond and Ian Longworth; formerly with BRE, Garston, Watford, is gratefully acknowledged. Discussions on concrete deterioration mechanisms with you and Sidney Diamond, Purdue University were of great importance. In addition several other people have made important contributions either as analysts or otherwise, as mentioned in the acknowledgements in each individual chapter. However, a few colleagues must be mentioned specially: Jacques Touret, Ecole des Mines, Paris; Arne Grønhaug & Kaare Flaate formerly at the Norwegian Road Research Laboratory (NRRL); Elisabeth Gundersen (NPRA) and Isabel Fernandes, Faculdade de Ciências, Universidade do Porto. Your sincere encouragements from time to time convinced me that my scientific work is important.

I wish to thank all good colleagues in my “home” Technology Department for always making a friendly and lively atmosphere in my surroundings. Also your assistance and invaluable moral support throughout 2003 while I was on a cancer treatment is most gratefully acknowledged. This incident indeed made me understand what sort of durable material you were made from. I am also indebted to Marc Ottelé at TU-Delft for translating texts into Dutch, to Jørn T. Abelsnes (NPRA) for printing the thesis and Kjersti Kvalheim Dunham, head of the Tunnel and Concrete Division at NPRA for encouragements.

Finally I express my most sincere gratitude to my family. At first I thank my parents Tonnie and Gunnar Hagelia for supporting me in my interest in geology and natural sciences ever since my childhood. Last but not least I thank Ayse and my boys Arman and Emre for being patient with me during the preparation of the manuscript and for being stuck with your X’box while I was busy.

Curriculum Vitae

Per Hagelia was born on November 18, 1955, in Gjerstad, Norway. After *Examen Artium* at Hornnes gymnas in 1975 he worked as a forest worker and metal worker in Gjerstad until 1977. In 1977 he commenced his studies at the University of Oslo and was otherwise much involved in organisation work, cultural activities, job employment at Bankenes Betalingsentral Oslo, geological field mapping for the Norwegian Geological Survey and laboratory work at University of Oslo and Institute for Energy Technology at Kjeller. In June 1989 he graduated as *Cand. Scient.* in structural geology, metamorphism and geochronology at the Geological Museum – University of Oslo.

From September 1989, he was employed as a geologist at the previous Norwegian Road Research Laboratory – Norwegian Public Roads Administration (NPRA) and was later on affiliated to the Materials Testing Division, the Geology and Tunnel Division and since 2008 the Tunnel and Concrete Division, at NPRA.

Hagelia is a co-founder and member of the national Forum for Alkali Reactions in Norway (FARIN). He has been involved in the arrangement of international conferences such as 11th Euroseminar on Microscopy of Building Materials 2007 and 13th International Conference on Alkali-Aggregate Reactions in Concrete 2008 as member of international board of reviewers and scientific committees. Hagelia has since 2006 been Vice-Chairman of the Abel Centre for Natural Sciences and Mathematics and is a co-founder of the annual AbelSeminar, both in Gjerstad. Since 2009 he has been a guest lecturer at the annual Concrete Microscopy Course - TU-Delft, the Netherlands and member of the Applied Petrography Group - Geological Society of London.

Summary

This thesis deals with deterioration mechanisms affecting steel fibre reinforced sprayed concrete used for rock support in tunnels. Physical and chemical degradation of sprayed concrete linings may contribute to destabilisation of the rock mass, involving increased maintenance costs, reduced service life, and a potential safety risk. The principal aims of this work were to a) provide an updated and modern diagnosis of chemical degradation phenomena occurring in steel fibre reinforced concrete used for rock support, b) investigate the reaction mechanisms involved including the possible interaction of different reaction schemes, c) characterise the environmental loads, mainly with respect to water chemistry, microbial activity and hydrogeology, and d) attempt to establish links between scientific findings and practical engineering issues, such as durability and life time aspects, maintenance/repair and consequences for rules and recommendations.

Black Shale environment. The first part of the thesis investigated the effects and causes of non-deleterious Thaumasite Formation (TF) and deleterious Thaumasite Sulfate Attack (TSA) leading to breakdown of the cement paste matrix within the Alum Shale environment. TF and TSA were closely associated with leaching, decalcification and Popcorn calcite deposition (PCD) and other forms of detrimental carbonation. The TF-TSA-carbonation reactions take place in response to cool ground waters carrying aqueous sulfate and bicarbonate. Two novel reaction mechanisms were found: a) the development of high crystallisation pressures resulting from high degree of supersaturation of thaumasite during deposition (“TF” is not always non-deleterious) and b) full scale TSA was most efficient after partial or complete decalcification of the cement paste matrix: Thaumasite had formed at the expense of remaining amorphous silica and secondary calcite (PCD). At low pH sulfuric acid caused outer leaching of concrete, making way for deep effects of aggressive ions. The process was developed to a moderate extent in modern sulfate resistant sprayed concretes within the Oslo Alum Shale environment but had caused localised spalling after <13 years. Previous workers have interpreted historically severe and rapid cement paste degradation in Alum Shale as related to secondary ettringite formation and sulfuric acid attack. However, petrographic analysis of historical test samples within this study proved this was due to a severe case of TSA and detrimental internal carbonation involving PCD and variable effects of acids.

The sources and release mechanisms of Alum Shale aggressives are complex and at least in the investigated cases different from the hitherto established mechanism, e.g. sulfide oxidation facilitated by catalytic oxidation of pyrite due to minor contents of a highly reactive monoclinic pyrrhotite. Anhydrite was found in Norwegian Alum Shale, as first reported herein. This mineral was responsible for most aqueous sulfate in the studied cases. Pyrite and pyrrhotite also contributed but were more persistent than expected. Influence of both sulfate reducing bacteria (SRB) and sulfide oxidising bacteria (*Acidithiobacillus sp.*) seems to be important for the development of sulfuric acids in the Alum Shale environment. Such bacteria are fertilised by ammonium which is leached from the shale. Bicarbonate in ground water originated both from calcite in Alum Shale, whilst the thaumasite carbonate in degrading concrete also contained a substantial amount derived from atmospheric carbon dioxide. Alum

Shale swelling seems partly governed by anhydrite-gypsum conversion and is also due to gypsum supersaturation and possibly clay minerals.

Subsea environment. A novel composite degradation mechanism was found in subsea tunnels, leading to partial to complete breakdown of the cement paste matrix and destructive steel fibre corrosion. This involved: a) acidification related to layered Mn-Fe biofilms (*Leptothrix sp.* and *Gallionella sp.*) and b) infiltration of saline ground waters and abiotic transformation of the cement paste matrix, due mainly to Mg-attack and TF-TSA-carbonation reactions. The cement pastes were transformed into magnesium-calcium silicate hydrate (M-C-S-H) with shrinkage cracks, reaching several mm to cm into concrete. Acid soluble secondary minerals formed. At advanced stages, gypsum had formed extensive deposits on the outer concrete surface, originating from Ca in leached concrete and sulfate from saline ground water. This represents a relatively mild acidification of mobile saline water, which occasionally reached the concrete/rock interface. Acidification was caused by redox reactions related to Mn and Fe biominerals, sulfuric acid derived from oxidation of sulfides (initially formed through temporary sulfate reduction within biofilms) and organic acids from dying biota. Steel fibres delivered reactants to the acid producing reactions. Steel corrosion was due to chlorides, acids from bacterial action, carbonation and OH⁻ consumption due to brucite deposition. The attack was rapid when processes a) and b) coincided at the same location, involving thinning of sprayed concrete at rates varying from < 0.5 mm/year to 10 mm/year.

Summary of degradations and engineering aspects. The present study has demonstrated cases of aggressive ground conditions leading to degradation of initially high quality sprayed concretes used for rock support. The most important deterioration mechanism was the composite bacterial and saline water attack in subsea tunnels. But also reactions involving thaumasite - internal carbonation associated with Alum Shale still represent a concern. Degradations within the freshwater environment are uncommon, and Alkali-Silica Reaction was unimportant. The NS- EN 206-1 Exposure Classes did not predict the extent and rate of the most severe attacks. Tunnel sprayed concrete used for rock support was also found to be influenced by the hydraulic gradient, bacterial activity and evaporation of water within the tunnels: Hypersaline waters developed from brackish waters due to drought caused by tunnel fans. These mechanisms facilitate a deeper penetration of aggressive solutions into sprayed concrete than what is the case for cast concrete subjected to similar water chemistries in mainly static water environments. Mobile waters, being typical of the tunnel environment, are sometimes very aggressive. Therefore the life time of concretes in the tunnel environment is sometimes deemed to be much shorter than their designed life time, which is 50 years. Issues related to maintenance, repair and future work were discussed.

Oslo, March 2011
Per Hagelia

Samenvatting

Dit proefschrift behandelt schademechanismen voor gewapend staalvezel spuitbeton dat gebruikt kan worden voor het ondersteunen van gesteente in tunnels. Fysische- en chemische degradatie van spuitbeton lagen kunnen destabilisatie veroorzaken van de rotsmassa, met verhoogde onderhoudskosten, vermindering van de levensduur, en een potentieel veiligheidsrisico. De belangrijkste doelstellingen van dit werk waren om a) een bijgewerkte en moderne diagnose van chemische degradatie fenomenen die voorkomen in gewapend staalvezel beton gebruikt voor gesteenteondersteuning te beschrijven b) te onderzoeken wat de reactiemechanismen zijn die betrokken zijn bij de mogelijke interactie tussen de verschillende reactie's c) te karakteriseren van de milieu-belastingen in relatie tot hoofdzakelijk water chemie, microbioactiviteit en hydrogeologie en d) een poging om de relatie tussen wetenschappelijke bevindingen en praktische issues, zoals duurzaamheid, levensduur aspecten, en onderhoud/repairatie en de bijbehorende gevolgen voor de regels en aanbevelingen vast te stellen.

Zwarte Shalie omgeving. In het eerste deel van het proefschrift is onderzoek gedaan naar de oorzaken en de gevolgen van niet-schadelijke Thaumasiet Formatie (TF) en schadelijke Thaumasiet Sulfaat Aantasting (TSA) wat leidt tot degradatie van de cementpasta binnen de Alum Shale omgeving. TF en TSA zijn nauw verbonden met uitloging, ontkalking en Popcorn Calciet neerslag (PCD) en andere vormen van schadelijke carbonatatie. De TF-TSA-koolzuur reacties vinden plaats doordat het koele grondwater sulfaat en bicarbonaat bevat. Twee nieuwe reactiemechanismen werden gevonden: a) de ontwikkeling van hoge kristallisatiedruk als gevolg van een hoge mate van thaumasite oververzadiging tijdens de neerslag ("TF" is niet altijd ongevaarlijk) en b) grootschalige TSA was het meest efficiënt na gedeeltelijke of volledige ontkalking van de cementpasta matrix: Thaumasiet werd gevormd ten koste van de resterende amorfe silica en secundaire calciet (PCD). Bij een lage pH graad veroorzaakt zwavelzuur uitloging van beton en maakt het op deze manier toegankelijk voor de schadelijke effecten van agressieve ionen. Dit proces ontwikkeld zich met name in veel gebruikt sulfaat bestendig gespoten beton in de Oslo-Alum Schalie omgeving, en veroorzaakte gelokaliseerde afspatting na <13 jaar. Eerdere onderzoekers hebben historisch ernstig en snelle cementpasta degradatie in Alum Schalie geïnterpreteerd in relatie tot secundaire ettringite vorming en zwavelzuur vorming. Echter, petrografische analyse van historische proefmonsters binnen dit onderzoek bleek dat dit voornamelijk te wijten was aan TSA en schadelijk interne carbonatatie met PCD en variabele effecten van zuren.

De oorzaak en de afgeefmechanismen van Alum Schalie agressieve bestanddelen zijn complex en ten minste in de onderzochte gevallen afwijkend van het tot dan toe bekende mechanisme, zoals sulfideoxidatie die door een katalytische oxidatie van pyriet welke veroorzaakt wordt door een kleine hoeveelheid van het zeer reactieve monoclinic pyrrhotiet. Anhydriet werd in het Noors Alum Schalie gevonden, zoals als eerst in dit proefschrift gemeld. Dit mineraal was verantwoordelijk voor het waterige sulfaat in de bestudeerde gevallen. Pyriet en pyrrhotiet dragen ook bij, maar waren meer bestand dan naar verwacht. Invloed van zowel sulfaat reducerende bacteriën (SRB) als sulfide oxiderende bacteriën (*Acidithiobacillus sp.*) lijken belangrijk te zijn voor de ontwikkeling van zwavelzuur in het

Alum Schalie omgeving. Dergelijke bacteriën worden gevoed door ammonium welke is uitgelooft uit de schalie. Bicarbonaat in het grondwater afkomstig van zowel calciet als Alum Schalie, terwijl de thaumasiet in verweerd beton is gecarbonateerd en bevatte daarbij ook een aanzienlijke hoeveelheid atmosferische kooldioxide. Alum Schalie uitzetting lijkt deels veroorzaakt door anhydriet-gips conversie en is ook wegens gips oververzadiging en uit eventuele kleimineralen.

Onderzeese omgeving. Een nieuw samengestelde degradatiemechanisme is gevonden in onderzeese tunnels, welke leidt tot een gedeeltelijke of volledige degradatie van de cementpasta matrix en staalvezels. Dit betrof: a) de verzuring gerelateerd aan gelaagde Mn-Fe biofilms (*Leptothrix* sp en *Gallionella* sp) en b) infiltratie van zout grondwater en biologische omzetting van de cementpasta matrix, voornamelijk als gevolg van Mg-aanval en TF-TSA-carbonatatie reacties. De cementpasta's zijn omgezet tot magnesium-calcium-silicaat hydraat (MCSH) met krimp-scheuren, tot enkele mm á cm in het beton. In zuur oplosbare secundaire mineralen zijn gevormd. In een gevorderd stadium, had gips uitgebreide afzettingen gevormd aan de buitenzijde van het betonoppervlak, afkomstig uit Ca in uitgelooft beton en sulfaat van zout grondwater. Dit vertegenwoordigt een relatief milde verzuring van het bewegend zout water, welke af en toe het beton/gesteente-overgangszone bereikte. Verzuring wordt veroorzaakt door redox reacties met betrekking tot Mn en Fe biomineralen, zwavelzuur afgeleid van oxidatie van sulfides (in eerste instantie gevormd door tijdelijke sulfaatreductie in biofilms) en organische zuren uit uitgestorven biota. Staalvezels leveren reactanten aan de zuur producerende reacties. Bewapenings corrosie is veroorzaakt door chloriden, zuren vrijkomend van bacteriële reacties, carbonatatie en OH-consumptie als gevolg van depositie bruciet. De aanval was snel wanneer processen a) en b) samen vielen op dezelfde locatie, waarbij het dunner worden van spuitbeton op percentages die varieerde van <0,5 mm / jaar tot 10 mm / jaar.

Samenvatting van de degradaties en technische aspecten. In de huidige studie is aangetoond dat agressieve terrein omstandigheden leiden tot degradatie van in eerste instantie een hoge kwaliteit gespoten beton welke gebruikt wordt voor gesteente ondersteuning. De belangrijkste degradatie mechanisme was een samengestelde bacteriële en zoutwater activiteit in de onderzeese tunnels. Maar ook reacties waarbij thaumasiet-interne carbonatatie geassocieerd met Alum Schalie vormen nog steeds een punt van zorg. Degradaties in een zoetwater-omgeving zijn zeldzaam, en alkali-silica reactie was onbelangrijk. De NS-EN 206-1 Blootgesteldeklassen kunnen niet voorspellen de mate en snelheid van de meest ernstige reactie's. Tunnel gespoten beton gebruikt voor gesteente-ondersteuning bleek ook te worden beïnvloed door de hydraulische gradiënt, bacteriële activiteit en de verdamping van water in de tunnels: extreem zoute water ontwikkeld op basis van brak water, als gevolg van droogte, veroorzaakt door tunnel fans. Deze mechanismen bevorderen een diepere penetratie van agressieve oplossingen in spuitbeton dan het geval is voor gegoten beton onderworpen aan soortgelijke chemicaliën in het vooral stilstaandwater. Bewegende wateren, die typisch zijn voor de tunnel omgeving, zijn soms erg agressief. Daarom is de levensduur van beton geacht in de tunnel omgeving veel korter te zijn dan hun ontworpen levensduur, welke 50 jaar is. Issue's in verband met onderhoud, reparatie en toekomstige werkzaamheden zijn uitvoerig besproken.

Oslo, maart 2011
Per Hagelia

Lists of minerals, chemical formulae, definitions and abbreviations:

Summary of minerals and chemical compositions.

Mineral	Chemical formula*
Albite	$\text{NaAlSi}_3\text{O}_8$
Almandine	$\text{Al}_2\text{Fe}_3(\text{SiO}_4)_3$
Anhydrite	CaSO_4
Annite	$\text{KFe}_3\text{AlSi}_3\text{O}_{10}(\text{OH},\text{F})_2$
Anorthite	$\text{CaAl}_2\text{Si}_2\text{O}_8$
Anorthoclase	$(\text{Na}_{0.85}\text{K}_{0.15})\text{AlSi}_3\text{O}_8$
Aragonite	CaCO_3
Birnessite	$\text{Ca}_{0.8}(\text{Mn}_4\text{O}_8) \cdot 2\text{H}_2\text{O}$
Bixbyite	Mn_2O_3
Brucite	$\text{Mg}(\text{OH})_2$
Brushite	$\text{CaPO}_3(\text{OH}) \cdot 2\text{H}_2\text{O}$
Buetschliite	$\text{K}_2\text{Ca}(\text{CO}_3)_2$
Buserite(-Na)	$\text{Na}_4\text{Mn}_{14}\text{O}_{27} \cdot 21\text{H}_2\text{O}$
Calcite	CaCO_3
Copiapite	$\text{Fe}^{2+}\text{Fe}^{3+} 4 (\text{SO}_4)_6(\text{OH})_2 \cdot 20\text{H}_2\text{O}$
Cristoballite	SiO_2
Dickite (a variety of kaolinite)	$\text{Al}_2\text{Si}_2\text{O}_5(\text{OH})_4(\text{HCONH}_2)$
Dolomite	$\text{CaMg}(\text{CO}_3)_2$
Ettringite	$3\text{CaO} \cdot \text{Al}_2\text{O}_3 \cdot 3\text{CaSO}_4 \cdot .32\text{H}_2\text{O}$
Ferrihydrite	$\text{Fe}(\text{OH})_3$
Gibbsite	$\text{Al}(\text{OH})_3$
Goethite	$\text{FeO}(\text{OH})$
Giniite	$\text{Fe}_4(\text{PO}_4)_4(\text{OH})_2 \cdot 2\text{H}_2\text{O}$
Gismondine	$\text{Ca}_2\text{Al}_4\text{Si}_4\text{O}_{16} \cdot 9(\text{H}_2\text{O})$
Gypsum	$\text{CaSO}_4 \cdot 2\text{H}_2\text{O}$
Hematite	Fe_2O_3
Kaolinite	$\text{Al}_4(\text{Si}_4\text{O}_{10})(\text{OH})_4$
Laumontite	$\text{CaAl}_2\text{Si}_4\text{O}_{12} \cdot 4(\text{H}_2\text{O})$
Magnesite	MgCO_3
Magnetite	Fe_3O_4
Manganosite	MnO
Marcasite	FeS_2
Margarite	$\text{CaAl}_2(\text{Al}_2\text{Si}_2)\text{O}_{10}(\text{OH})_2$
Mellite (an organic mineral)	$\text{Al}_2\text{C}_6(\text{COO})_6 \cdot 16\text{H}_2\text{O}$
Mg-calcite	$\text{Mg}_{0.064}\text{Ca}_{0.936}\text{CO}_3$
Microcline	KAlSi_3O_8
Montmorillonite	$\text{Na}_{0.3} (\text{Al}, \text{Mg})_2 \text{Si}_4\text{O}_{10} \cdot \text{OH}_2 \cdot 6\text{H}_2\text{O}$
Muscovite	$\text{KAl}_2(\text{Si}_3\text{Al})\text{O}_{10}(\text{OH},\text{F})_2$
Nordstrandite	$\text{Al}(\text{OH})_3$
Portlandite	$\text{Ca}(\text{OH})_2$
Pyrrhotite (hexagonal)	$\text{Fe}_{0.95}\text{S}_{1.05}$
Pyrrhotite (monoclinic)	$\text{FeS}_{1.14}$

Mineral	Chemical formula*
Quartz	SiO ₂
Rhodochrosite	MnCO ₃
Rutile	TiO ₂
Thaumasite	CaSiO ₃ •CaCO ₃ •CaSO ₄ •15H ₂ O
Thenardite	Na ₂ SO ₄
Todorokite	Mn ₆ O ₁₂
- Ca-todorokite	Ca _{0.8} (Mn ₄ O ₈) •2H ₂ O
- Na-todorokite	NaMn ₆ O ₁₂ •3H ₂ O
Titanomagnetite	Fe _{2.5} TiO _{0.5} O ₄

* The table does not include the more subtle chemical variations and substitutions which may occur in many of these minerals.

Abbreviations and definitions related to degradation of concrete.

Abbreviations	Process	Explanation
AAR	Alkali aggregate reaction	A general term covering ASR and ACR, leading to internal swelling and surface cracking of concrete. Most forms are relatively slow and long lasting.
ACR	Alkali carbonate reaction	A form of AAR which is related to dolomitic aggregates. Involves formation of brucite and Mg bearing gels. The mechanism is still debated.
ASR	Alkali silica reaction	The most common form of AAR due to formation of visco-elastic gel with high swelling pressure within the concrete, leading to distress. Caused by presence of micro crystalline or amorphous silica in the concrete aggregate which contributes Si to the pore water reacts with alkalis and calcium.
OR	Ordinary surface carbonation	Carbonation of the cement paste matrix by reaction with atmospheric CO ₂ . May lead to corrosion if steel reinforcement when reaching deep.
PCD	Popcorn calcite deposition	A form of internal carbonation with deposition of relatively coarse calcite related to influx of bicarbonate and associated decalcification of the cement paste matrix. Ultimately leading to very friable concrete, in contrast to most common effects of OR.

TF	Thaumasite Formation	Non-deleterious early stage deposition of thaumasite within voids and pre-existing microcracks. In Chapter 4 it was however demonstrated that thaumasite deposits resembling TF sometimes develop a high crystallisation pressure.
TSA	Thaumasite Sulfate Attack	Deleterious thaumasite growth forming at the expense of the cement paste matrix, ultimately degrading to a soft mush.

Descriptive terminology related to Thaumasite Sulfate Attack.

Terms	Explanation
Thaumasite types:	Criteria based on optical properties
<i>Thaumasite Type I</i>	A highly porous needle-like crystalline material. Colourless to very pale yellow in plane light. Birefringence; near isotropic to 1 st order white (0.000-0.005).
<i>Thaumasite Type II</i>	Closely spaced needle-like crystals forming quite massive flow like structures. Light straw yellow to bright yellow in plane light. Birefringence; 1 st order creamy white to pale yellow (0.005-0.007).
<i>Thaumasite Type III</i>	Dense well ordered needle-like crystals. Yellow tinted in plane light. Birefringence typically 2 nd order blue-green (0.007-0.027).
Zones 1-4:*	Used in the United Kingdom (UK) to describe the degree of TSA as based on microscale observations. This terminology was used in Chapter 3 in order to compare with UK experience.
<i>Zone 1</i>	Corresponds to non-degraded concrete with associated first signs of TF.
<i>Zone 2</i>	TSA can be seen in its earliest or most minor form, associated with microcracks and air voids frequently filled with thaumasite in the form of TF.
<i>Zone 3</i>	Aggregate particles are surrounded by halo-like deposits of thaumasite; scattered domains of TSA and a relatively large amount of microcracks filled with thaumasite in the form of TF.
<i>Zone 4</i>	TSA degradation is fully developed and the transformation of the cement paste into thaumasite is completed. This stage represents “full scale TSA”, frequently characterised by a soft thaumasite mush.

* A given “Zone” may occupy a few millimetres in a thin section or even reach structural scale dimensions.

Summary of abbreviations related to cement and concrete constituents.

Abbreviations	Formula*	Chemical name (mineral name)
C-S-H	CaO.SiO ₂ .H ₂ O	Calcium silicate hydrate
M-S-H	MgO.SiO ₂ .H ₂ O	Magnesium silicate hydrate
C-M-S-H	CaO.MgO.SiO ₂ .H ₂ O	Calcium magnesium silicate hydrate
C ₃ A	3CaO.Al ₂ O ₃	Tricalcium Aluminate
CH	Ca(OH) ₂	Calcium hydroxide (portlandite)
MH	Mg(OH) ₂	Magnesium hydroxide (brucite)
PC	Portland Cement	Cements with ordinary high C ₃ A contents (> 5 wt. %)
SF	SiO ₂ . xH ₂ O	Silica fume, also called microsilica
SRPC	Sulfate Resisting Portland Cement	Cements with low C ₃ A contents

* The table does not include the more subtle chemical variations and substitutions which may occur in many of these compounds.

Strength Classes used in Norway (NS-EN 206-1. Annex NA.4.3.2) and the equivalent CEN nomenclature.

NS-EN 206-1	B20	B25	B30	B35	B40*	B45	B55
EN 206-1	C20/25	C25/30	C30/37	C35/45	none	C45/55	C55/67

* B40 applied to sprayed concrete for rock support (e.g. Norwegian Concrete Association, Publication 7) until 2011: Strength Classes B30, B35 and B45 are now recommended

Rock mass classification based on the Q-system.

The Q-system is a combined rock mass classification method and geotechnical design system developed at the Norwegian Geotechnical Institute, which has been in use worldwide for about three decades. The Q-value, representing a measure of rock mass stability, is defined on the basis of six different engineering geological parameters:

$$Q = \frac{RQD}{J_n} \cdot \frac{J_r}{J_a} \cdot \frac{J_w}{SRF}$$

RQD = Rock Quality Designation

RQD is the total length of core pieces over 100 mm (between natural joints) expressed as a percentage of the core run length. During field mapping the RQD-value can easily be calculated by using the number of joints per cubic metre.

J_n = Join Set Number

These numbers vary from 0.5 for un-jointed rocks to 20 for completely earth-like material. RQD/J_n gives a description of the joint pattern and block size in the rock mass.

J_r = Joint Roughness Number

These numbers vary from 4 for discontinuous joints to 0.5 for slickensided joints. For joints with soft infilling a nominal value of $J_r = 1$ is used.

J_a = Joint Alteration Number

These numbers vary from 0.75 for healed joints to 20 for discontinuities with thick fillings of swelling clay. The J_a numbers depend generally on the thickness and mineralogy (friction properties) of the fillings. Occurrences of thin to very thin clay fillings (< 5 mm) are rated with $J_a = 8-12$. J_r/J_a gives an approximate indication of the friction angle along the joints or filled discontinuities.

J_w = Joint Water Reduction Factor

This parameter varies from 1.0 for dry rock masses to 0.05 for rock masses with very high inflow.

SRF = Stress Reduction Factor

The factor may vary from 1 for hard rocks with moderate stress to ≥ 20 for rocks with extremely high stress, or for cases of extreme squeezing or swelling. J_w/SRF gives a description of the active stress situation in the rock mass at the tunnelling depth.

The Q-system makes use of six detailed tables for appropriate choice of the parameter values. The requirement for rock reinforcement increases while the Q-value decreases. The Q-system also accounts for the span width of underground space. Commonly fibre reinforced sprayed concrete is used in conjunction with rock bolts ($Q > 0.1$). However, in extremely poor rock masses ($Q < 0.1$) reinforced ribs are also required. In exceptionally poor rock masses ($Q < 0.01$) reinforced ribs or cast concrete arches are employed. The relationship of the Q-value and rock reinforcement is embedded in the so-called Q-chart (Barton et al. 1974, Barton and Grimstad 2004, referenced in Chapters 1 and Chapter 2).

Table of contents

Summary	<i>i</i>
Samenvatting	<i>iii</i>
List of minerals, chemical formulae, definitions and abbreviations	<i>v</i>

Chapter 1 - Introduction 1

1.1 Background of the problem.....	1
1.1.1 Outline of previous investigations into sprayed concrete durability in Norway	2
1.1.2 Need for diagnosis and research into degradation mechanisms in sprayed concrete and its context	3
1.2 Aims and specific research objectives	4
1.2.1 Specific objectives of this study	4
1.3 Research strategy and methodology	5
1.3.1 Selection criteria.....	5
1.3.2 Field work and sampling strategy	5
1.3.3 Laboratory methods.....	6
1.4 The thesis constraints	6
1.5 Arrangement of the thesis	7
1.6 Original papers included in this thesis	8
1.7 References	9

Chapter 2 - Extended background..... 11

2.1 Uncertainties regarding tunnel concrete degradation phenomena in aggressive ground.....	11
2.1.1 Status regarding life time expectancy, durability results and standard documents	11
2.1.2 Recommendations of ITA Working Group 12; “Shotcrete Use”	12
2.1.3 Environmental loads acting upon sprayed concrete in tunnels	13
2.1.3.1 Significance of deformational loads.....	13
2.1.3.2 Significance of hydraulic gradient, volumetric flow rate and mobility of water	13
2.1.3.3 Significance of water chemistry, evaporation and origin of aggressive waters.....	14
2.1.3.4 Significance of microbial activity	14

2.2 Deterioration mechanisms encountered in Norwegian cast concrete and status as regards sprayed concrete in tunnels	14
2.2.1 Chloride ingress and reinforcement corrosion	14
2.2.2 Alkali Aggregate Reaction	15
2.2.3 Ordinary Carbonation.....	16
2.2.4 Leaching	16
2.2.5 Popcorn calcite deposition and internal deleterious carbonation	16
2.2.6 Acid attack.....	17
2.2.7 Sulfate attack	18
2.2.8 Magnesium attack	19
2.2.9 Frost action.....	19
2.2.10 Deformations within unstable rock mass	19
2.2.11 Biodegradation and other microbial effects?.....	20
2.3 References	20

Chapter 3 - Thaumasite and secondary calcite in some Norwegian concretes23

3.1 Introduction	23
3.2 Recent research in Norway and objectives of this work	24
3.3 Case studies	25
3.3.1 Sprayed concrete on Alum Shale in Oslo.....	25
3.3.2 Sprayed concrete in sulfate bearing ground in East Central Southern Norway	29
3.3.3 Sprayed concrete in contact with seawater.....	29
3.3.4 Steel fibre corrosion and role of silica fume in the TF-TSA-carbonation process.....	31
3.4 Discussion	31
3.4.1 TF – TSA – carbonation and formation conditions.....	31
3.4.2 Deterioration and service life of sprayed concrete	33
3.5 Conclusions	35
3.6 Acknowledgements	36
3.7 References	36

Chapter 4 - Thaumasite sulfate attack, popcorn calcite deposition and acid attack in concrete stored at the “Blindtarmen” test site Oslo, from 1952 to 1982.....37

4.1 Introduction	37
4.2 Outline of results from the Alum Shale Committee.....	39
4.2.1 Characterisation of Alum Shale and its properties.....	39
4.2.2 The Blindtarmen Test Site, 1952 to 1972 and beyond.....	40
4.3 Samples from Blindtarmen investigated in this study.....	42
4.3.1 Methods, sample handling and identification of unknowns.....	42
4.4 Microscopy of degradation products.....	45
4.4.1 Reference samples kept in tap water	45
4.4.2 Exposed samples displayed six reaction stages within their outer reaction zones.....	46
4.4.2.1 Stage 1: TF and local TSA.	46
4.4.2.2 Stage 2: Extensive decalcification of C-S-H and with PCD	47

4.4.2.3 Stage 3: Partial to extensive TSA at the expense of decalcified C-S-H and PCD	48
4.4.2.4 Stage 4: Replacement of thaumasite by PCD.....	48
4.4.2.5 Stage 5: Ordinary carbonation.....	48
4.4.2.6 Stage 6: Leached outermost concrete.....	48
4.5 Discussion	50
4.5.1 Chemical reaction mechanisms	50
4.5.2 Physical response related to thaumasite growth and decalcification with PCD.....	53
4.5.3 Physical response related to outer carbonation, acid leaching and iron staining	55
4.6 Comparison with modern sprayed concrete used for rock support: the durability – life time perspective	55
4.7 Conclusions	56
4.8 Glossary of definitions and abbreviations	57
4.9 Acknowledgements	58
4.10 References	58

Chapter 5 - C, O and S isotopic signatures in concrete which have suffered thaumasite formation and limited thaumasite form of sulfate attack61

5.1 Introduction	61
5.2 Background and objectives	62
5.3 Methods and samples	63
5.4 Results	64
5.4.1 Petrography of analysed micro domains	64
5.4.1.1 Åkebergveien road cut	64
5.4.1.2 Svartdal tunnel.....	64
5.4.1.3 Alum Shale.....	65
5.4.2 Stable isotopes.....	67
5.4.2.1 Åkebergveien	67
5.4.2.2 Svartdal tunnel.....	68
5.5 Discussion	69
5.5.1 Carbon isotopes	70
5.5.2 Sulfur isotopes.....	71
5.6 Conclusions	71
5.7 Acknowledgements	72
5.8 References	72

Chapter 6 - Sources of aqueous sulfate, bicarbonate and acid in Oslo Alum Shale, with implications for concrete durability, geotechnical properties and metal leaching75

6.1 Introduction	75
6.1.1 Objectives and strategy	76
6.2 Norwegian experience and recent research relevant to Black shale	76
6.2.1 Research results from Alum Shale within the Oslo Graben.....	76

6.2.2	Recent research into concrete degradation associated with Oslo Alum Shale.....	78
6.2.3	Outline of contemporary research progress	78
6.2.3.1	Sulfide oxidation and release mechanisms of sulfur compounds and acids.....	78
6.2.3.2	Carbonates, organic carbon and bicarbonate.....	82
6.3	Materials and methods	83
6.3.1	Field location and samples	83
6.3.2	Sample preparation and analytical methods.....	83
6.4	Results	86
6.4.1	Bacteria and bio-minerals in Tunnel water 320-06.....	86
6.4.2	Effects of leaching on bulk mineral composition.....	87
6.4.3	Alum Shale characterisation by SEM before and after leaching.....	88
6.4.4	Water chemistry	90
6.4.4.1	pH and Eh evolution during the 65 days leaching experiment	90
6.4.4.2	Waters 1 and 2 before and after leaching compared with tunnel water	91
6.4.4.3	Saturation indices	93
6.4.5	Stable isotopes.....	95
6.5	Discussion	97
6.5.1	Chemistry of water - Alum Shale interaction.....	97
6.5.1.1	Abiotic leaching experiment	97
6.5.1.2	Ca-sulfates contributed most of the aqueous sulfate	100
6.5.1.3	Tunnel water and ground water involving biotic and abiotic reactions	101
6.5.2.1	Source materials in Alum Shale powder deduced from abiotic leaching.....	101
6.5.2.2	Additional processes deduced from sprayed concrete and tunnel environment.....	103
6.6	Regional aspects: H ₂ S-gas and anhydrite in Alum Shale.....	106
6.6.1	H ₂ S gas release versus very rapid loss of pyrrhotite sulfur.....	106
6.6.2	Additional evidence of anhydrite in Alum Shale	106
6.7	Implications	107
6.7.1	Concrete degradation.....	107
6.7.2	Shale swelling mechanism	108
6.7.3	Metal leaching.....	108
6.7.4	Further work.....	109
6.8	Summary of findings and conclusions	109
6.9	Acknowledgements	111
6.10	References	111

Chapter 7 - Sprayed concrete deterioration due to layered Mn-Fe biofilms and saline ground waters in subsea tunnels117

7.1	Introduction	117
7.2	Materials and methods	118
7.2.1	Investigation and sampling of sprayed concrete in four subsea tunnels	118
7.2.2	Sample preparation and laboratory methods.....	120
7.3	Results	123
7.3.1	Tunnel observations and outline of forensic examination.....	123
7.3.1.1	Oslofjord subsea tunnel.....	123
7.3.1.2	Byfjord subsea tunnel.....	126
7.3.1.3	Freifjord subsea tunnel	127
7.3.1.4	Flekkerøy subsea tunnel.....	128

7.3.2 Micro characteristics of the abiotic saline ground water attack	129
7.3.2.1 Effects of Mg ingress on cement paste colour	129
7.3.2.2 Synopsis of micro structural features in thin section	131
7.3.3 Micro characteristics of Mn and Fe bacteria, biominerals and crust materials	133
7.3.3.1 Young Mn and Fe slimes and in situ formed Mn-platelets	133
7.3.3.2 Aged Mn-crust material and aged heavily encrusted Gallionella	135
7.3.3.3 Gypsum mush and crust deposits	136
7.3.3.4 Occurrence of a mellite-like carboxylate and phosphates related to saline water attack	137
7.3.3.5 Mn L-edge spectra of Mn-crust material	138
7.3.4 Stable isotopes	139
7. 4 Discussion	140
7. 4.1 Introductory remarks	140
7. 4. 2 Abiotic saline water attack	140
7. 4. 3 The bacterial attack and the acidification processes	141
7.4.3.1 Role of the metal oxidising bacteria	142
7.4.3.2 Mechanisms of acid production, reduction and reoxidation	142
7.4.3.3 Evolution of the attack and the significance of gypsum deposits	144
7.4.4 Some remarks to future work	144
7.4.5 Overall engineering judgement	145
7.5 Conclusions	145
7.6 Acknowledgements	146
7. 7 References	147

Chapter 8 - Deterioration mechanisms and durability of sprayed concrete in Norwegian tunnels.....149

8.1 Introduction	149
8.1.1 Norwegian experience, guidance and environmental classification	150
8.1.2 Objectives	151
8.2 Selection of sites, work strategy and summary of methods	152
8.2.1 Selection criteria	152
8.2.2 Hypotheses and work strategy	152
8.2.3 Water categories and concrete sampling with comments to rock mass rating data	153
8.2.4 Materials and methods	153
8.3 Results and discussion	153
8.3.1 Anatomy of chemical attack and consequences for sprayed concrete thickness	153
8.3.2 Concrete degradation phenomena studied within three water categories	154
8.3.3 Sprayed concrete in freshwater environments	158
8.3.3.1 Exposure conditions	158
8.3.3.2 Deterioration mechanisms and examples	158
8.3.4 Sprayed concrete in the Alum Shale environment	158
8.3.4.1 Exposure conditions	158
8.3.4.2 Deterioration mechanisms and examples	159
8.3.5 Sprayed concrete in saline ground water	159
8.3.5.1 Exposure conditions involving occurrences of hypersaline waters	159
8.3.5.2 Deterioration mechanisms and examples	160

8.3.6 Steel fibre corrosion due to chlorides, carbonation and bacterial attack.....	162
8.3.7 Insignificant traces of Alkali Silica Reaction (ASR)	162
8.3.8 Compressive strength of samples from subsea tunnels	163
8.4 The geological context	163
8.4.1 Significance of rock mass rating as regards sprayed concrete durability	163
8.4.2 The hydrogeological environment and effect of hydraulic gradient	164
8.5 Practical implications	165
8.5.1 Characterisation and classification of exposure conditions	165
8.5.2 Mitigation and remediation for new constrictions, maintenance and repair	166
8.5.3 Optimal timing of repair? A general socio-economic approach	166
8.6 Conclusions	167
8.7 Acknowledgements	167
8.8 References	168

Chapter 9 - Does the EN 206-1 Exposure Classification Apply to Tunnel Concrete?171

9.1 Introduction	171
9.1.1 Background, motivation and objectives	172
9.2 Norwegian sprayed concrete in tunnels	173
9.2.1 Norwegian specifications for sprayed concrete versus investigated concrete	173
9.2.2 Context of sprayed concrete in tunnels	174
9.2.3 An outline of the structural deterioration phenomena in sprayed concrete.....	175
9.3 Water environments	178
9.3.1 Freshwater environment.....	178
9.3.2 Alum Shale environment.....	178
9.3.3 Saline ground water environment with localised development of hypersalinity	180
9.3.3.1 A novel mechanism involving bacterial degradation.....	180
9.3.3.2 Significance of salinity, hypersalinity and evaporation	182
9.3.4 Characterisation of waters by hydrogen and oxygen stable isotopes.....	183
9.4 Exposure classification according to NS EN 206-1	184
9.4.1 Introduction	184
9.4.2 Classification and comparison with real life tunnel concrete	184
9.4.2.1 Freshwater environment.....	187
9.4.2.2 Alum Shale environment.....	187
9.4.2.3 Saline environment.....	187
9.5 Discussion of NS-EN 206-1	188
9.5.1 Evaporation and classification.....	188
9.5.2 Significance of dynamic water environments	190
9.5.2.1 Natural background.....	190
9.5.2.2 Dynamics in tunnels	190
9.5.3 What the standard does not tell: some recommendations	191
9.6 Conclusions	192
9.7 Acknowledgements	192
9.8 References	192

Chapter 10 - Conclusions, implications and further work.....195

10.1 General	195
10.2 Main conclusion of the thesis.....	195
10.2.1 Part 1 - The Black Shale environment	195
10.2.1.1 Reaction mechanisms in concrete	195
10.2.1.2 Sources and release mechanisms of aggressives.....	197
10.2.2 Part 2 – The subsea environment	198
10.2.2.1 Reaction mechanisms in concrete	198
10.2.2.2 Sources and release mechanisms of aggressives.....	198
10.2.3 Part 3 – Summary of deteriorations and engineering aspects	199
10.3 Implications and consequences based on present knowledge.....	200
10.3.1 Concrete in the Black shale environment.....	200
10.3.2 Concrete in subsea tunnels	201
10.3.3 Durability and engineering aspects	202
10.4 Recommendations for further work	202
10.4.1 A comment to the claimed beneficial effect of increased sprayed concrete thickness.....	202
10.4.2 Black shale environment	203
10.4.3 Subsea environment	204
10.4.4 Engineering aspects and durability prediction	204
10.5 References	205

Acknowledgements
Curriculum Vitae

Appendices on CD

Part 1 – Black shale environment

Appendix 1: Additional documentation to Chapter 3

A1-1	Summary of samples with systematic petrography
A1-2	X-ray diffraction data
A1-3	Micro analyses of thaumasite
A1-4	Images of thaumasite, decalcified cement paste matrix & secondary calcite

Appendix 2: Additional documentation to Chapter 4

A2-1	Forensic examination and identification of unknown samples from the Blindtarmen test site
A2-2	Outer reaction zones in exposed samples
A2-3	Microscopical images

Appendix 3: Additional documentation to Chapter 5

- A3-1 C, O and S stable isotope data of thaumasite and secondary calcite in sprayed concrete in contact with Alum Shale
- A3-2 Outline of stable isotope systematics

Appendix 4: Additional documentation to Chapter 6

- A4-1 Scanning Electron Microscopy (SEM)
- A4-2 X-ray diffraction (XRD)
- A4-3 Water chemical calculation using the computer code PHREEQC-2
- A4-4 Contribution of Ca-sulfates and Fe-sulfides to aqueous sulfate
- A4-5 Images of tunnel water with bacterial slime and Alum Shale sample
- A4-6 Microbes found in the Alum Shale environment

Part 2 – Subsea environment

Appendix 5: Additional documentation to Chapter 7

- A5-1 Results from Scanning Electron Microscopy (SEM)
- A5-2 Results from X-ray diffraction (XRD)
- A5-3 Results from Electron Microprobe Analysis (EMPA)
- A5-4 Images of tunnel concrete and biota
- A5-5 Summary of concrete samples with systematic petrography
- A5-6 Microbes found in the subsea environment
- A5-7 Mn L-edge spectra and STXM

Part 3 – Summary of deteriorations & engineering aspects

Appendix 6: Additional documentation to Chapter 8

- A6-1 Introduction
- A6-2 Freshwater environment
- A6-3 Lier railway tunnel
- A6-4 Alum Shale environment
- A6-5 Saline environment
- A6-6 Alkali-Silica Reaction (ASR)
- A6-7 Rating of water loads, Ca- and Fe-Mn deposits on subsea tunnel concrete

Appendix 7: Additional documentation to Chapter 9

- A7-1 Relationships of Durability Class and Exposure Class according to NS-EN 206-1
- A7-2 Characteristics of sprayed concrete versus cast concrete

Chapter 1

Introduction

“Forståelse er det eneste som gir forutsigbarhet”
Ivan Th. Rosenqvist

1.1 Background of the problem

This thesis deals with deterioration mechanisms affecting steel fibre reinforced sprayed concrete used for rock support. Norway has a very long experience with planning, construction and maintenance of tunnels. The Norwegian road authorities have been responsible for the construction of more than one thousand tunnels. Among these are thirty-one eight subsea tunnels, by far the largest number for any country. The tunnelling method is conventional drill and blast. The development towards modern sprayed concrete technology in Norway started already about fifty years ago. By about 1980 the country had taken a leading role in the development of robotized equipment, ultimately leading to a huge production capacity (Kompen 2008, Woldmo 2008). Over the latest decades sprayed concrete has become an integral part of all modern tunnel excavations and the annual sprayed volume is steadily increasing. Sprayed concrete differs from cast concrete in many respects (see Appendix 7). This material is special in that the main quality parameters are relatively more sensitive to the execution process than cast concrete. Hence a continuing focus on quality routines and good workmanship is very important for development of the technology. Fibre reinforced concrete absorbs energy due to deformational loads exerted by the rock mass. If cracks develop the material will to a certain extent behave ductilely (Morgan and Parker 2006). The durability is dependent on spray thickness as well as fibre dosage and material properties, e.g. when exposed to environmental loads. Presently sprayed concrete is used successfully both for construction and repair due to its flexibility and overall uniform quality.

In Norway steel fibre reinforced sprayed concrete and rock bolts are used as a final rock support method within a wide range of rock mass conditions. The spray thickness and requirement for rock bolts is designed after an assessment of rock mass stability on site (Barton and Grimstad 2004). Hence, loss of bearing capacity due to secondary physical or chemical degradation of the sprayed concrete lining is a very relevant problem to investigate, because such effects may contribute to destabilisation of the rock mass. This may involve reduced service life, potential safety risks and increased maintenance costs.

The present investigations were initiated by the Norwegian Public Roads Administration and were mostly, but not exclusively, focusing on sprayed concretes exposed to variably aggressive environments in road tunnels. This chapter presents a brief outline of the motivation of this thesis, aims, overall contents and a summary of the research strategies and methods. Chapter 2 gives an extended background for the various research topics.

1.1.1 Outline of previous investigations into sprayed concrete durability in Norway

A previous Norwegian durability project; “Proper use of sprayed concrete” at the Norwegian Public Roads Administration (1995-1997), dealt mainly with documentation of initial sprayed concrete quality and the resulting mechanical properties after some years in service. The previous Norwegian project was unique for its time, because only few international cases have hitherto been reported on the longer term durability of sprayed concrete. A vast number of tunnels were investigated. Despite evidence of some chemical deterioration no alarming features were reported. However, concrete in many of the investigated tunnels were still quite young. It was, therefore, concluded that several problems should be followed up at a later stage. Important remaining durability issues were related to potential effects of aggressive water leakages in subsea tunnels and the impact of Alkali Aggregate Reaction. Yet dry tunnel sections and freshwater leakages rarely showed signs of deterioration (Davik 1997 and references therein, Davik 1998).



Figure 1. Spalling in steel fibre reinforced sprayed concrete due to thaumasite sulfate attack and associated carbonation (Hagelia and Grønhaug 2000).

Back shale environment. The most significant concrete degradation phenomenon ever reported from Norway is represented by an extensive sulfate attack related to Alum Shale. However, the project “Proper use of sprayed concrete” did not investigate sprayed concrete within the Alum Shale environment. Alum Shale consists of anthracitic-graphitic carbon, quartz, feldspar, clay minerals, chlorite and pyrite with smaller amounts of pyrrhotite. Historically the attack was characterised by fast and sometimes complete cement paste degradation in buried cast concrete, interpreted to be due to ettringite attack under partial influence of sulfuric acids. The origin of sulfate and acids was regarded as due to oxidation of the iron sulfides residing in this Black shale. A semi-official Alum Shale Committee worked on the problem from 1947 to 1973. After extensive systematic testing the main problem was solved through improved concrete mix design, using sulfate resisting concretes and membranes in order to avoid direct contact between concrete and Alum Shale. Control on redox conditions within the shale was also recommended. Pertinent details may be found in Bastiansen et al. (1957), Moum and Rosenqvist (1959) and Fiskaa (1973).

In current practice sprayed concrete for rock support is sprayed directly on the harmful shale. Consequently NPRA investigated a 13 years old modern steel fibre reinforced sprayed

concrete made with Sulfate Resisting Portland Cement (SRPC) and silica fume. The concrete was sprayed on Alum Shale in a road cut (Figure 1). It was found that spalling here was caused by Thaumassite Sulfate Attack (TSA) with associated carbonation and destructive steel fibre corrosion (Grønhaug and Hagelia 2000, Hagelia and Grønhaug 2000). This finding triggered a further interest in sulfate attack, and notably the intriguing possibility that the old and more extensive attack perhaps represented a severe case of TSA.

Subsea environment. No systematic attempt was made in order to diagnose chemical deterioration phenomena (weathering). As a matter of fact only five thin sections of sprayed concrete used for rock support were investigated within the project “Proper use of sprayed concrete”, all of which represented quite sound concrete from four subsea tunnels. Steel fibre corrosion was reported, but this was mainly restricted to thin outer layers of carbonated sprayed concrete. However, there were also some reports on loose sprayed concrete in some young subsea tunnels (Røhrsveen and Lygre 1996). There were even some indications that microbial activity might have been involved and caused localised debris formation (Hansen 1995). It was inferred that such features most likely represented rebound from the spraying operation (Davik 1997). However, mineral identification by microscopy of thin sections, X-ray diffraction (XRD) and Scanning electron microscopy (SEM) was not undertaken on such materials. Thus, as yet the origin of loose or weathered concrete in subsea tunnels should be regarded as unknown.

1.1.2 Need for diagnosis and research into degradation mechanisms in sprayed concrete and its context

Clearly, there is a need for diagnosis and investigations into deterioration mechanisms in fibre reinforced sprayed concrete used for rock support. In previous work it seems generally assumed that experience from cement paste degradation in cast concrete can be directly applied to sprayed concrete (cf. Bernard 2008). However, in view of the special characteristics and context of sprayed concrete used for rock support in tunnels it seems rather unclear whether this assumption is entirely valid. Specific studies of cement paste degradation of sprayed concrete are in fact rare, although incidents of a combined effect due to freeze-thaw action and de-icing salts have been investigated (Beaupré et al. 1994). Research efforts have focused on corrosion of steel fibres in sprayed concrete (cf. Bernard 2008) but according to the present author’s knowledge the potentially corrosive effects of biota have not been investigated. Moreover, the International Tunnelling Association (ITA) has requested durability data from long term exposure of sprayed concrete (Franzén et al. 2001). Presently a state of the art report is missing.

A fundamental understanding of concrete deterioration mechanisms is significant for concrete technologists as well as for the owners of structures. Steady improvement of our codes and recommendations for the design of durable concrete structures requires a continuous flow of research results based on scientific characterisation and interpretation of phenomena observed in real life: The main research efforts should in the author’s opinion focus on the mechanisms which cause cracking, spalling and loss of cementitious properties in field concretes. Performance testing in the laboratory has proven possible for some concrete durability problems. However, assessment of the relevance and reliability of performance tests requires a basic knowledge related to how well they replicate experience from real life conditions. The interaction of sprayed concrete with rock mass and water loads in tunnels is complex, and not well documented. Obviously investigations into real life concrete must be done before any performance testing can be invented. Performance testing was beyond the scope of this thesis.

1.2 Aims and specific research objectives

The previous investigations (Chapter 1.1 and Chapter 2) suggest that the status and nature of chemical degradation mechanisms in sprayed tunnel concrete is virtually unknown, and perhaps also involve effects of biota. Evidently impact of the aggressive Black shale and subsea environments were most relevant for a study, whilst the fresh water environment was less harmful. Sprayed concrete without an external water load were regarded as less relevant in this study, with the notable exception of the uncertain status of Alkali-Silica Reaction. In general, the relative impact of mechanical loads/local stress conditions on overall deterioration state was not possible to assess (see Chapter 1.4 and Chapter 2.2.10).

Thus, the principal aims of this thesis were to a) provide an updated and modern diagnosis of degradation phenomena occurring in steel fibre reinforced concrete used for rock support, b) investigate the reaction mechanisms involved, including the possible interaction of different reaction schemes, c) characterise the environmental loads, mainly with respect to water chemistry and hydrogeology, d) identify sources of aggressives and e) invoke the consequences of the findings in relation to practical engineering issues, such as durability and life time aspects, maintenance/repair and consequences for design rules and recommendations. The research strategy (Chapter 1.3) was based on forensic principals.

1.2.1 Specific objectives of this study

The present investigations were based on concrete samples which had been exposed to environmental loads over periods of several years. The main focus was on the most important chemical mechanisms, i.e. the ones responsible for observed concrete distress under influence of aggressive ground waters. The specific objectives of the present study were:

- Investigate Thaumassite Sulfate Attack (TSA) and its relationship to leaching and internal detrimental carbonation in modern sprayed concrete exposed to Alum Shale environment.
- Provide the first petrographic study of historical concrete prisms previously exposed to Alum Shale ground water at the Blindtarmen test site and test the hypothesis that this classic sulfate attack in the Oslo region was caused by TSA rather than ettringite. Moreover, investigate the degradation mechanisms and long term durability of mixes used at the test site, and compare with the results from modern sprayed concrete.
- Investigate the sources and release mechanisms of aggressives in Alum Shale as highlighted by previous interpretation and recent research results, and establish the implications for Alum Shale characterisation, concrete durability and other engineering properties.
- Investigate deterioration mechanisms in steel fibre reinforced sprayed concrete in the subsea tunnel environment with emphasis on weathered and loose concrete, and establish the role of magnesium attack, sulfate attack and possible influence of bio-degradation.
- Summarise the status of sprayed concrete degradations encountered in sprayed concrete used for rock support in Norway, investigate the impact of the hydrogeological context and establish the current status of Alkali-Aggregate Reactions in Norwegian sprayed concrete, with a look to their effects on service life.
- Discuss the findings in relation to the concrete standard (NS EN 206-1) and if necessary suggest improvements for future revisions.

The details of the approaches and methods used are referred to in each individual chapter.

1.3 Research strategy and methodology

This section provides an outline of the strategy and methods relied on within this thesis. Further details are presented in Parts 1, 2 and 3 as well as in the Appendices.

1.3.1 Selection criteria

The tunnel sprayed concrete investigated within this work was selected on the basis of the following main criteria, most of which comply with recommendations of the ITA Working Group 12 (see details in Chapter 2.1.2):

- They should include typical ground conditions, involving hydro-geological variation and ground water compositions
- Deterioration characteristics should be representative and relevant for structural performance
- Investigations should mainly focus on the most common and modern concrete mixes
- The age of concretes should be variable, and
- Sufficient basic documentation should be available

Timing was optimal because many tunnels were now old enough to establish more clearly the effects of deterioration mechanisms, including slowly working Alkali-Aggregate Reaction.

1.3.2 Field work and sampling strategy

Sites for detailed investigations were selected after reconnaissance work and a study of available documentation. The sampling strategy aimed at a forensic examination of the sprayed concretes and the exposure conditions. It was hoped that the approach could bring about a pertinent characterisation of the state of deterioration as seen in a relevant broad context. Samples were selected such that deteriorated and seemingly intact concrete portions were represented. Most of the concrete cores displayed a complete cross section of the sprayed concrete slab and some few centimetres of the rock mass behind. Additional small samples of deteriorated concrete, surface deposits and suspect microbial matter were collected separately. Water samples were collected from tunnel water leakages with a variable interaction with sprayed concrete and ditch waters. Some pH measurements were done in the field. Further details may be found in Chapters 3 through 7.

Also historical test samples, which had been investigated by the previous Alum Shale Committee, were included. None of these samples had been investigated petrographically, whilst their history and exposure conditions were well established by previous workers. Hence, these concrete prism samples were investigated further in the light of evidence from modern sprayed concrete used for rock support in the Alum Shale environment.

Moreover, samples of Alum Shale were collected for characterisation of the shale constituents in a search for a deeper understanding of the origin of aggressives. The main idea in this case was to undertake a very detailed study of a local “system” of Alum Shale – sprayed concrete – water interaction in order to unveil as detailed as possible the influence of various components and release mechanisms.

1.3.3 Laboratory methods

Concrete petrography, by polarising microscopy of standard polished thin sections, was a main investigative method. Most thin section series covered the entire cross section of sprayed concrete and the rock behind, including features of the interfacial zone. X-ray diffraction (XRD) and Scanning electron microscopy (SEM) with microanalysis and imaging was undertaken on outer weak deposits, bacterial slime, interfacial deposits and other loose material, which could not safely be preserved in thin sections. SEM and Electron microprobe analysis (EMPA) was also utilised for analysis of a few thin sections.

Water chemical analyses were undertaken at an accredited laboratory. Particles were filtrated according to standard procedures prior to analysis. Important ions and elements were analysed along with pH, alkalinity and TOC. A leaching experiment was set up with crushed Alum Shale in water. Saturation indices were calculated for some waters using the computer code PHREEQC-2.

Stable isotopes of carbon, sulfur, oxygen and deuterium were analysed in selected solids and waters in order to put further constraints on sources of aggressives and chemical processes involved. Moreover, Scanning Transmission Soft X-ray Microscopy (STXM) was applied in an attempt to shed light on charge state distribution in a subsea tunnel deposit. The analytical methods are explained in appropriate detail in the relevant chapters below.

1.4 The thesis constraints

The effects of freeze-thaw action, microcracking due to mechanical loads of rock mass, fire damage and exhaust fumes were not investigated. Relationships of chemical deterioration and concrete compressive strength are briefly referred to in Part 3, but were not part of this work. The structural effects of ion poor ground waters were generally minor and only a few cases were investigated. Sprayed concretes in the Alum Shale environment were affected by mildly acidic to neutral pH conditions. Unfortunately, no modern case of very acidic Alum Shale attack on sprayed concrete was approached. In the subsea environment, however, the range of exposure conditions related to the investigated sprayed concretes was apparently representative. Microbes involved in the Alum Shale and subsea environments were only partly identified with certainty, as based on light microscopy. Future more rigorous work should take advantage of microbiological methodology involving DNA-fingerprinting, which is beyond the present author's expertise.

Chemical reaction schemes deduced solely from petrography are not considered to be rigorously balanced, which would have required a more detailed quantitative micro-analytical approach. Reactants and/or reaction products were in some instances presented with the prescript “±”, meaning they sometimes participate and sometimes not. This expression of reaction schemes, involving entire mineral assemblages, is frequently used in petrology.

As regards the durability aspect, sprayed concretes of different ages were mainly investigated in terms of alterations and material loss. Although there were clear examples of reduced service life of concretes located within chemically aggressive environments, it was comparably more difficult to make an assessment of concrete residual life time. Residual life time needs to be understood in a wider context, which was beyond the scope of this work. No further quantitative approach was attempted at this stage, as for example by using durability indices proposed in some literature.

Sprayed concretes made according to modern technology were investigated in this thesis. A few sprayed concretes made according to old technology (1965-1970) were also examined, but were not regarded as relevant for the present day durability status.

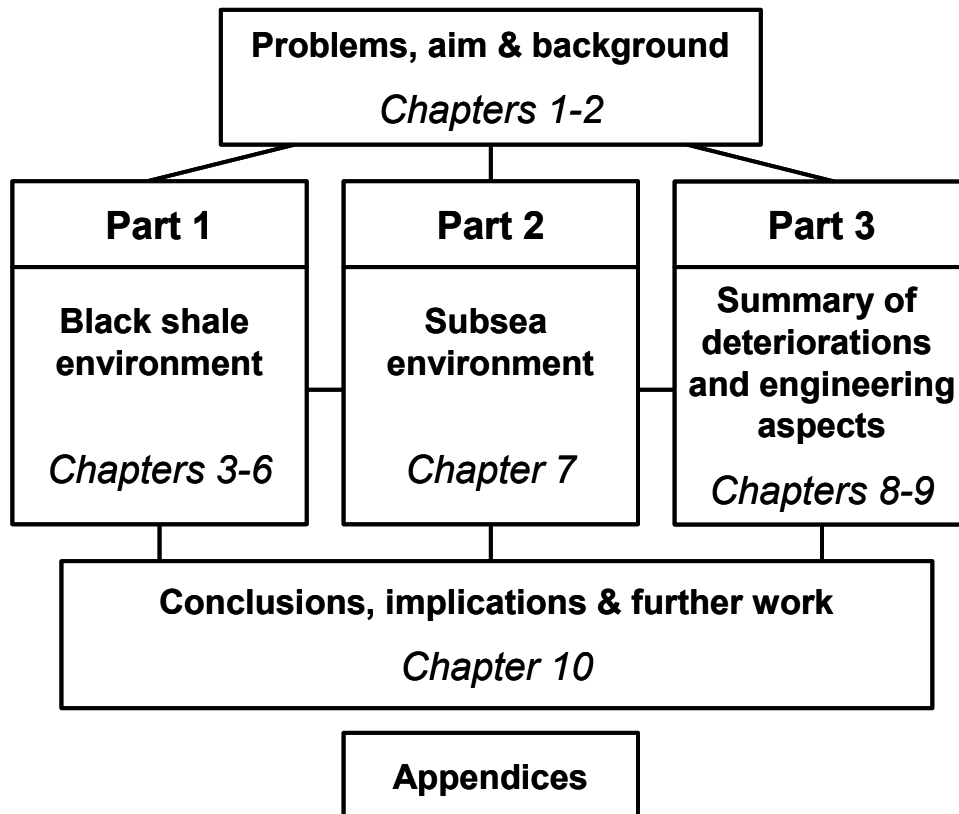


Figure 2 Arrangement of the thesis.

1.5 Arrangement of the thesis

Chapter 2 gives an extended background for the investigated problems. The main body of research is based on seven papers presented in Chapters 3 through 9 (included “as is”), as divided into three different thematic parts (Figure 2). The majority of the papers have been published, as listed in Chapter 1.6. Necessarily, some degree of duplication was unavoidable.

Part 1 is devoted to concretes exposed to the Black shale environment, mainly represented by Norwegian Alum Shale. Chapter 3 and Chapter 4 deal with deterioration mechanisms related to Alum Shale attack in modern sprayed concrete and historical test prisms, respectively. Chapter 4 provides the most complete insight into the overall processes. In Chapter 3 also one case of sulfate attack in subsea tunnel concrete was reported. Chapters 5 and 6 investigate the sources and release mechanisms of aggressive waters. Chapter 5 represents a pilot study of the possibility that stable isotopes may be used for the purpose of discriminating between sources, as based on detailed characterisation. Chapter 6 discusses the issue further in view of a multidisciplinary approach, and makes the final conclusions on sources, release mechanisms and effects related to Alum Shale waters.

Part 2, consisting of Chapter 7, is devoted to sprayed concrete exposed to the subsea environment. The chapter focuses on the specific characteristics of sprayed concrete degradation found in subsea tunnels, including reaction mechanisms, sources and release mechanisms of aggressives.

Part 3. Chapters 8 and 9 discuss the status of sprayed concrete deterioration within a wider context relevant to engineering. Each chapter gives a summary of the structurally important deterioration mechanisms as based on experience from a) fresh water environment,

b) Alum Shale environment and c) subsea environment. Chapter 8 also reports on the status of Alkali Aggregate Reaction in sprayed concrete, but mainly focuses on the impact of the geological context and practical implications. The impact of hydrogeology and rock mass classification is discussed in relation to durability of sprayed concrete. The chapter also briefly discusses implications as regards mitigation, maintenance and the prospects of “optimal timing of repair” within a socio-economic perspective. Chapter 9 is devoted to the consequences for the NS-EN 206-1 concrete standard. The relevance of present Exposure Classes is discussed. Also the potential effect of evaporation on the development of aggressiveness within tunnel space was assessed. Furthermore, hydro-geological processes and their potential impact on ground water aggressiveness are briefly discussed.

Chapter 10, summarises the conclusions drawn in Parts 1, 2 and 3, discusses the implications and the requirements for further work. This chapter also provides a critical comment to the inferred positive effect of an increased sprayed concrete thickness, being relevant to claims in Chapters 3, 4, 7, 8 & 9. Background documentation to each separate chapter is given in Appendices 1 through 7.

1.6 Original papers included in this thesis

Hagelia P, Sibbick RG, Crammond NJ and Larsen CK (2003): Thaumasite and secondary calcite in some Norwegian concretes. *Cement & Concrete Composites*, 25, 1131-1140 (Chapter 3)

Hagelia P and Sibbick RG (2009): Thaumasite Sulfate Attack, Popcorn Calcite Deposition and acid attack in concrete stored at the “Blindtarmen” test site Oslo, from 1952 to 1982. *Materials Characterisation*, 60, 686-699 (Chapter 4)

Iden KI and Hagelia P (2003): C, O and S isotopic signatures in concrete which have suffered thaumasite formation and limited thaumasite form of sulfate attack. *Cement & Concrete Composites*, 25, 839-846 (Chapter 5)

Hagelia P (2009): Sources of aqueous sulfate, bicarbonate and acid in Oslo Alum Shale with implications for concrete durability, geotechnical properties and metal leaching. (Chapter 6: Manuscript submitted to GFF)

Hagelia P (2009): Sprayed concrete deterioration due to layered Mn-Fe biofilms and saline ground waters in subsea tunnels (Chapter 7: In revision with *Cement & Concrete Research*)

Hagelia P (2008): Deterioration mechanisms and durability of sprayed concrete in Norwegian tunnels. *Proceedings of the 5th International Symposium on Sprayed Concrete – Modern Use of Wet Mix Sprayed Concrete for Underground Support*. Lillehammer 2008, p 180-197 (Chapter 8 as republished in slightly modified version in: *Underground Openings – Operations, Maintenance and Repair*, Norwegian Tunnelling Society, Publication 17, p 45-58)

Hagelia P (2008): Does the EN 206-1 Exposure Classification Apply to Tunnel Concrete? Nordic Exposure Sites – Input to revision of EN 206-1, *Workshop Proceedings from a Nordic Miniseminar*, Hirtshals 2008, p 241-263 (Chapter 9)

1.7 References

- Barton N and Grimstad E (2004): The Q-system following thirty years of development and application in tunnelling projects. Rock Engineering – Theory and Practice, Proceedings of ISRM Regional Symposium EUROCK 2004, Salzburg, Austria, pp 15-18.
- Bastiansen R, Moum J and Rosenqvist I Th (1957): Contribution to high-light certain construction problems associated with Alum Shale in Oslo. Norwegian Geotechnical Institute, Publication No. 22, Oslo, 69 pp. (in Norwegian with English summary).
- Beaupré d, Talbot C, Gendreau M, Pigeon M and Morgan DR (1994): Deicer salt scaling resistance of dry and wet-process shotcrete. ACI Materials, Vol. 91, No. 5, 487-494.
- Bernard ES (2008): Current deficiencies in the design of fibre reinforced shotcrete linings in hard rock. In: K Berg, C Hauck, R Kompen (Eds.), 5th International Symposium on Sprayed Concrete – Modern Use of Wet Mix Sprayed Concrete for Underground Support. Lillehammer, pp. 36-47.
- Davik KI (1997): Proper use of sprayed concrete in tunnels, Parts A, B, C, D, E and Final report (in Norwegian). Norwegian Public Roads Administration 1997.
- Davik KI (1998): Proper use of sprayed concrete in tunnels. Nordic Road and Transport Research 1998-1, 16-17.
- Fiskaa O (1973): Concrete in Alum Shale. Norwegian Geotechnical Institute, Publication No. 86, Oslo, 32 pp. (in Norwegian with English summary).
- Franzén T, Garshol KF and Tomisawa N (2001): ITA/AITES Accredited Material. Sprayed concrete for final linings: ITA working group report. Tunnelling and Underground Space Technology 16, p 295-309.
- Grønhaug A and Hagelia P (2000): Alum shale can damage sulfate resistant concrete. Betongindustrien Nr 3, 8-9 (in Norwegian).
- Hagelia P and Grønhaug A (2000): Thaumassite – infection causing concrete deterioration. Våre Veier Nr. 9, 54-55 (in Norwegian).
- Hansen BO (1996): Durability considerations related to sprayed concrete in subsea tunnels. Sprayed Concrete in Subsea Tunnels. NPRA Unpublished report October 1996 (In Norwegian).
- Kompen R (2008): How the use of fibres has developed in Norway. In: K Berg, C Hauck, R Kompen (Eds.), 5th International Symposium on Sprayed Concrete – Modern Use of Wet Mix Sprayed Concrete for Underground Support. Lillehammer, pp. 245-249.
- Morgan DR and Parker HW (2006): Shotcrete for underground support X. 10th International Conference on Shotcrete for Underground Support. Whistler, BC, Canada. American Society of Civil Engineers, 382p.
- Moum J and Rosenqvist I Th (1959): Sulphate Attack on Concrete in the Oslo Region. Journal of the American Concrete Institute, Proceedings, Volume 56, Title 56-18, 8 pp.
- Røhrsveen NG and Lygre JK (1996): Proper use of sprayed concrete in tunnels. MSc thesis, Norwegian Technical University, Trondheim (in Norwegian).
- Woldmo O (2008): The history of wet mixed sprayed concrete from a Norwegian perspective. In: K Berg, C Hauck, R Kompen (Eds.), 5th International Symposium on Sprayed Concrete – Modern Use of Wet Mix Sprayed Concrete for Underground Support. Lillehammer, pp.343-346.

Chapter 2

Extended background

“Durability is the ability of a material or structure to withstand its design service conditions for its design life without significant deterioration.”

Yunus Ballim

2.1 Uncertainties regarding tunnel concrete degradation phenomena in aggressive ground

2.1.1 Status regarding life time expectancy, durability results and standard documents

Standard planning routines and cost analysis for tunnel construction in Norway involve geological mapping, engineering geological characterisation of rock mass including geotechnical and geophysical measurements. However, the *environmental loads which act- or later will act upon sprayed concrete* tunnel linings are not well understood. The current state of knowledge as detailed in this chapter provides basis for the central research topics of this thesis.

Presently the designed life time, e.g. the life time expectancy, for Norwegian road tunnels is regarded as 50 years. For this reason the bearing capacity of the designed rock reinforcement should not be significantly disturbed during this time span. Sprayed concrete thickness and requirement for rock bolts should preferably be based on rock mass properties on site, according to the Q-system (Barton et al. 1974, Barton and Grimstad 2004). The Q-system has established a relationship between rock joint parameters and rock load (kg/cm^2). In contrast, the sprayed concrete thicknesses in Norwegian tunnels have until recently been designed mainly on qualitative criteria and “engineering judgement” as based on presence/absence of weakness zones, swelling clays and rock joint orientation. Sprayed concrete thicknesses are usually about 5-25 cm: increasing with decreasing rock mass quality.

The experience from the previous durability project (1995-1997): “Proper use of sprayed concrete in tunnels” (Davik 1997) was embedded in the document NB Publication No 7 “Sprayed concrete for rock support” (Norwegian Concrete Association 2003, 2011). This publication represents the standard specification for sprayed concrete in Norway, dealing with product specifications, guidance and testing of sprayed concrete. NB Publication 7 has recently been updated with the most recent European Standard for sprayed concrete (EN 14487, EN 14488 & EN 14489). This publication mainly refers directly to NS-EN 206-1 (with National Annexes) for Exposure Classes, Durability Classes and Strength Classes. Norwegian sprayed concrete used for rock support should be made according to the wet method. Durability class M40 is currently specified for subsea sections and Alum Shale

ground, otherwise M45 is utilised. Sprayed concretes are mainly specified as CEM 1 with added 4-15 % silica fume (SF) by cement weight. However, other pozzolanic mineral admixtures with a proven effect similar to SF are permitted. Water/binder ratios are mostly 0.40 to 0.50 and binder contents vary from about 400 to 550 kg/m³. Otherwise NB Publication 7 specifies that a maximum of 10 % of aggregate particles is allowed to exceed 8 mm in size. The setting accelerator has changed from water glass to mostly alkali-free Al-sulfate in more recent years. Until very recently steel fibre reinforcement has been employed, whilst synthetic fibres are now also used.

Davik (1997) summarised that *carbonation*, *leaching* and some *steel fibre corrosion* have been identified with certainty. The visual impression of deterioration is considered to be worse than the state indicated by laboratory analysis. However experience is as yet too scarce to establish how deteriorations will influence the service life and life cycle costs of sprayed concrete. Also the impact of alkali aggregate reaction and the long term impact of subsea water leakages remain to be investigated.

Available water chemical analysis from Norwegian underground environments (Bastiansen et al. 1957; Davik 1997) shows that tunnel concretes are subjected to variably aggressive ground conditions. The *interaction of ground water and sprayed concrete* used for rock support, therefore, represents a very important research field.

2.1.2 Recommendations of ITA Working Group 12; “Shotcrete Use”

A recent accredited publication from the International Tunnelling Association (Franzén et al. 2001) summarised 10 years of work on the durability problem. Their work was based on national reports incorporating a vast number of cases, applications, materials and ground conditions. The report stated that the evaluation of durability of sprayed concrete linings in underground work “turned out to be an extremely complex subject when trying to produce an overview and status description”. In most cases the standard quality and property parameters are available for time frames from 28 days to 120 days. *Tests carried out showing the effects of time spans of years were relatively seldom*. When damage had occurred, usually, this was “quite evidently caused by water and frost, chemical attack and situations causing extensive cracking and bond failure”. However, a state of the art report was considered to be “a bit premature”.

Working Group 12 recommended several ways to work on this issue, and considered that as much as possible should be known about the following four main durability aspects:

- Complete information about the exposure situation
- All necessary sprayed concrete material information, to be able to quantify exposure resistance parameters
- Duration of exposures, if necessary, split on the local set of processes; and
- Design basis and lifetime expectancy compared to specifications and work execution

The ITA working group stated that *durability of sprayed concrete is a relative term*, which depends on issues such as the present age of the structure compared to the specified service life expectancy and the actual exposure processes involved. ITA recommended that the “durability subject” should “be broken down into its individual components”. Moreover: “When trying to draw conclusions on durability, this can only be made based on documented experience from a wide range of applications and regions – in other words, by systematic data collection and comparison”. The present investigation took advantage of the recommendations from the ITA.

2.1.3 Environmental loads acting upon sprayed concrete in tunnels

The environmental loads acting on sprayed concrete are illustrated in Figure 1. In contrast to cast concrete structures such as bridges, buildings and retaining walls, sprayed concrete used for rock support is characterised by a relatively thin layer in direct contact with the adjacent rock mass. Such concrete is potentially influenced by instabilities present within the ambient rock mass as well as ground water loads. Tunnels are frequently located below the water table. Therefore, in principle, the sprayed concrete is subjected both to the chemical composition of the water as well as the ambient hydraulic gradient. Aggressive waters of various sources may attack from behind the sprayed concrete layer; from the outer concrete surface or along internal cracks.

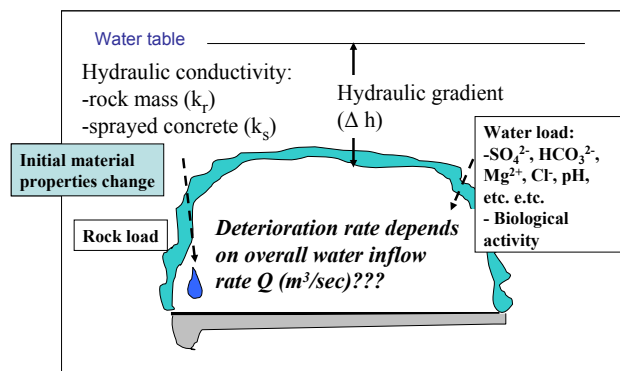


Figure 1 Principal aspect of environmental loads acting on sprayed concrete used for rock reinforcement in tunnels.

2.1.3.1 Significance of deformational loads

Mechanical loads may induce strains and creep in concrete structures, leading to micro-cracking (Taylor 1997, Hoseini et al. 2009). Such effects may induce a secondary permeability along with a direct strength reduction. Presumably relatively thin sprayed concrete layers are most vulnerable, as was also reported by Davik (1997).

2.1.3.2 Significance of hydraulic gradient, volumetric flow rate and mobility of water

Up to now the importance of the *hydraulic gradient* (“driving force) versus chemical attack by water loads has not been investigated. Moreover, although availability of water is a prerequisite for chemical concrete degradation (Taylor 1997), it is not yet known if there is a correlation between the extent of deterioration and *volumetric flow rate*. In view of the context illustrated in Figure 1 it is not obvious that deterioration mechanisms acting on tunnel concrete are exactly the same as the ones observed in cast concrete structures elsewhere. This is due to the fact that ground waters may be different from rain water, surface-near fresh waters or standard seawater. In the general case the aggressiveness of water towards concrete should not be regarded as constant over time. It is well established that ground water chemistry may change within a single site due to the complex temporal interaction of ground water and rock mass. Moreover the flow rate may also vary quite much over time (cf. Appelo and Postma 2005). The volumetric flow rates into Norwegian tunnels tend to diminish after a while, the effect of which seems to vary from place to place (Davik 1997). It is also very important that *static water* loads typical of cast concrete pillars in water are regarded as less aggressive than *mobile water* loads (Building Research Establishment 2003).

2.1.3.3 Significance of water chemistry, evaporation and origin of aggressive waters

According to the NS-EN 206-1 Exposure Classes the main aggressive ions to be accounted for are chloride, sulfate, magnesium and ammonium as well as pH. The standard also classifies verbally contact relationships with seawater and state of surface carbonation. The Norwegian version also includes a special class relevant to Alum Shale environment, but is otherwise mainly the same as EN 206-1. The standard does not describe or refer to water sampling routines and the likelihood of changing water chemistry over time, for example related to ground water – rock mass interaction or possible effects from drought within the tunnel environment, which should potentially lead to *evaporation* and an increased ionic strength and aggressiveness of water leakages.

This leads us to yet another important research problem, namely the origin of aggressive waters in general. Although the origin of aggressive water loads is usually regarded as known, the more specific sources and water chemical processes involved are not investigated in relation to tunnel engineering. However, successful planning, mitigation or repair may depend on a more explicit knowledge of sources and processes which govern the aggressiveness of waters. Such experience is generally not gathered in relation to tunnel projects but should be investigated further in light of basic achievements in water science.

2.1.3.4 Significance of microbial activity

There is currently a growing international awareness regarding biodegradation: Gaylarde et al. (2003) summarised the work of RILEM TC 183-MIB “Microbial impacts on building materials – Weathering and conservation”, showing that concrete, steel and several other building materials may degrade under influence from microbes. Hypothetically, subterranean concrete such as rough and tortuous sprayed concrete in tunnels should be more prone to biodegradation than cast concrete in open air.

2.2 Deterioration mechanisms encountered in Norwegian cast concrete and status as regards sprayed concrete in tunnels

During past decades several projects in Norway have been aiming at a better understanding of concrete deterioration. These investigations were essentially focusing on cast concrete structures, which represent a valuable basis for further durability studies. Most of the reported mechanisms are well known from elsewhere in the world. The present account gives a brief outline of the deterioration mechanisms previously encountered and summarises their status with respect to sprayed concrete used for rock support in tunnels. Details of individual projects, construction codes, guidelines and special mechanisms caused by industrial processes are omitted.

2.2.1 Chloride ingress and reinforcement corrosion

The main focus in Norway has been on chloride ingress and reinforcement corrosion, especially related to effects in coastal bridges. This has been investigated extensively in laboratory studies as well as at large scale in the field. Corrosion of steel may be initiated by carbonation of the cement paste or by chloride penetration. Both mechanisms are active within concretes exposed to coastal environments. Steel is protected by the very high alkaline pore water in the cement paste forming a passive layer of $\text{Fe}(\text{OH})_2$ which is thick enough to prevent further corrosion. Carbonation leads to a significant drop in cement pore water pH causing steel depassivation and formation of trivalent iron compounds (rust). However,

chloride penetration is different in that chlorine reacts directly with bivalent iron in the passive layer forming various trivalent iron corrosion products. Cl^- increases the solubility of $\text{Fe}(\text{OH})_2$ at very high pH, which is characteristic of pristine concrete pore waters (Taylor 1997). Rebar corrosion may be associated with expansive pressures exerted by the precipitation of iron oxides and -hydroxides which may cause cracking and spalling. In effect the rebar corrosion still represents an important challenge, notably due to previous practice with less good routines as regards rebar cover. Also early age cracking of high strength concretes (i.e. with low water/cement ratios) has represented a significant part of this problem. Chloride penetration is regarded as the main durability problem in Norwegian concrete bridges. However, improved routines for new constructions as regards concrete mix design and rebar cover have proven to be very efficient (cf. Norwegian Public Roads Administration 2007).

As regards steel fibre reinforced sprayed concrete, the effect of fibre corrosion due to chloride penetration in subsea tunnel sprayed concrete has for long been regarded as rather insignificant (Davik 1997; Norwegian Concrete Association 2003). However accumulated experience has shown that steel fibre corrosion is usually fast along cracks and fissures in sprayed concrete, leading to loss of ductility (cf. Kompen 2008). The specific role of chloride has been investigated briefly within this thesis.

2.2.2 Alkali Aggregate Reaction

Alkali Aggregate Reactions (AAR) also represents an important concern. The most common form of AAR: Alkali Silica Reaction (ASR) is a chemical reaction between the high alkaline concrete pore fluid ($\text{pH} \geq 12.5$) and reactive microcrystalline quartz or other forms of silica in the concrete aggregate. This leads to formation of swelling gels and a mechanical response in the form of cracking and distress of the concrete. The rate of ASR expansion increases with increasing temperature and humidity (cf. Taylor 1997). The most comprehensive and updated research may be found in the most recent proceedings of “the International Conference on Alkali Aggregate Reactions in Concrete” (Bérubé et al. 2000, Tang and Deng 2004, Broekmans and Wigum 2008).

Although reported several decades ago (e.g. Musæus 1962) it was not until the early nineteen nineties that the significance of ASR was acknowledged as an important problem in Norway (e.g. Jensen 1993): ASR had caused map cracking and expansion within bridges and hydroelectric power stations. The most common reactive aggregates in Norway are mylonite, meta-rhyolite, sandstone, meta-greywacke, clay and siltstone and other fine grained rocks with an appreciable amount of quartz (cf. Norwegian Concrete Association 2004). The reactive aggregates in Norway are regarded as slowly reacting, and significant damage caused by ASR is usually not apparent until about 15-25 years after construction. However, recently it has been reported that deleterious AAR (e.g. surface map cracking) may also develop after less than 8-10 years even in the rather cool Scandinavian climate (Hagelia and Lie Hansen 2008). Since 1993 detailed petrographic assessment as well as accelerated testing of aggregate reactivity has been embedded in our routines (cf. Norwegian Concrete Association 2008).

In Iceland scattered effects of ASR have been observed in relatively young sprayed concrete in road tunnels from ca 1990 and 1998. Icelandic sprayed concretes contain more than 7.5 kg/m^3 of $\text{Na}_2\text{O}_{\text{eq}}$, due to cement contents and water glass as setting accelerator. ASR gel was related to reactive components such as basaltic glass and undispersed silica fume. The latter was reportedly non-deleterious (Guðmundsson et al. 2008).

As yet the significance of AAR in Norwegian sprayed concrete is not established (Davik 1997 and references therein; Norwegian Concrete Association 2004). One of the

reasons for this is that the investigated tunnels are rather young and perhaps too early to expect any significant influence of this reaction. Also petrographic techniques, being crucial for the identification of AAR, have only been applied to a very limited extent to tunnel concrete. The potential of AAR in sprayed concrete has been assessed in view of a literature survey but no explicit conclusion could be drawn (Wigum and Hagelia 1998). However, it was considered that the presence of undispersed silica fume, the typically high cement contents of sprayed concretes and high sodium concentrations in subsea water leakages might enhance the potential for ASR.

The impact of ASR in tunnel sprayed concrete was studied further in the present dissertation.

2.2.3 Ordinary Carbonation

Ordinary surface carbonation is always present in bridge concrete as well as in sprayed concrete. According to Davik (1997) carbonation in sprayed concrete was restricted to the outermost 2-3 mm without signs of steel fibre corrosion inside the carbonation front. This form of carbonation also takes place along cracks and may then sometimes reach much deeper. Surface carbonation takes place when calcium hydroxide (portlandite) in the cement paste reacts with atmospheric CO₂ to form calcium carbonate (calcite) and water. Such carbonate is very fine grained and forms an outer protective coating with low permeability, thus preventing the interior portlandite and calcium silicate hydrate (C-S-H) from further reaction. Carbonation results in pore fluid pH dropping to 8-9 (Taylor 1997). The influence of surface carbonation was reported as part of the forensic examination during this work.

2.2.4 Leaching

Leaching of calcium from the cement paste matrix appears to be more common in sprayed concrete used for rock support than in bridge concrete. Formation of calcium carbonate stalactites has been encountered in several quite young tunnels, being most prominent in rather thin layers (< 5-6 cm) of sprayed concrete. This process leads to a drop in concrete pore water pH and loss of strength. There are indications that relatively early stage stalactite formation may lead to spalling of sprayed concrete later on (Davik 1997, 1998 and references therein). Notably in relatively thin concrete layers, such as sprayed concrete used for rock support, this may lead to undesirable effects in the long run. Development of stalactites does not only reflect leaching of calcium hydroxide (CH) but in a number of cases also involves decalcification of the cement calcium silicate hydrates (C-S-H) (Taylor 1997). In this thesis decalcification has been investigated in relation to several different deterioration mechanisms.

2.2.5 Popcorn calcite deposition and internal deleterious carbonation

Recently a new form of potentially deleterious internal carbonation has been described (Bromley and Pettifer 1997; Thaulow et al. 2000; Sibbick and Crammond 2001; Sibbick et al. 2003; Hagelia et al. 2001). Popcorn calcite deposition (PCD) in concrete refers to a relatively “coarse” form of popcorn shaped calcite deposition associated with Ca depleted cement paste. However, other calcite shapes form in the same process (Hagelia et al. 2001). This form of carbonation is completely different from the typical surface carbonation in that it usually

results in a quite porous, permeable and eventually a more or less friable cement paste matrix involving extensive steel corrosion. In contrast to ordinary carbonation, PCD forms in a through solution process which takes place when bicarbonate bearing ground waters enter the concrete interior. Accordingly, PCD does not sustain formation of a distinct protective carbonated surface layer. The term popcorn calcite has been used for some time to describe features of mm to cm sized popcorn like calcite cave deposits (speleothems) and similar formations associated with the Franklin Marble, USA and similar rock types (www.mindat.org).

Some Norwegian sprayed concretes were among the first reported with PCD (Hagelia et al. 2001, using the synonymous but now abandoned term “cornflake calcite”). PCD and its relationship to other deterioration processes were investigated further within this study.

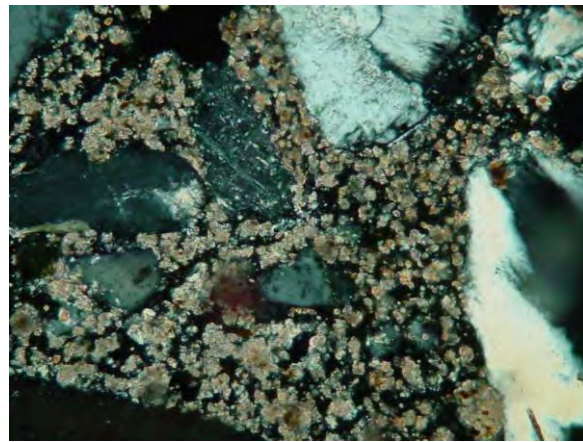


Figure 2: Popcorn calcite deposition (PCD) caused by extensive Ca depletion of the cement paste under influence of bicarbonate bearing ground water. Image width = 0.9 mm.

2.2.6 Acid attack

Acids of all kinds are more or less detrimental to concrete. This is mainly due to the fact that portlandite ($\text{Ca}(\text{OH})_2$) and C-S-H start to dissolve at $\text{pH} < 12.5$ (cf. Taylor 1997; Harris et al. 2002). Portlandite represents a somewhat subordinate phase within the cement paste matrix: yet portlandite guarantees for the very high pore fluid pH, thus stabilising the C-S-H and thereby sustaining the strength of the cement paste. Acid attack first consumes the portlandite and then subsequently the C-S-H. Also carbonated concrete is vulnerable due to the elevated solubility of calcite in acids, yet less than non-carbonated concrete where the highly soluble portlandite prevails. It is well established that the effect of even weak acids (pH about 5.5) can be very detrimental in highly mobile water, whilst being unimportant when the water load is static (cf. Building Research Establishment 2003). The most common reaction product in concrete after acid attack is gypsum (cf. Taylor). The most common sources of acidity are probably related to sulfide oxidation involving iron sulfide in bedrock as well as H_2S in sewers. Acid attack related to sulfide bearing Oslo Alum Shale is well known. However other environments in Norway are also characterised by Acid Rock Drainage (ARD). Examples of weaker acids are carboxylic and carbonic acids, the latter with pH near 5.7 in CO_2 -saturated freshwaters.

As yet, there are indications that sulfuric acids and likely carbonic acids were responsible for some attack on steel fibre reinforced sprayed concrete used for rock support on Oslo Alum Shale (Hagelia et al 2001). Acid attack has been investigated further within this thesis, with an emphasis on processes related to the Black shale and subsea environments.

2.2.7 Sulfate attack

Sulfate attack occurs among others in sewers and manure cellars. However the most prominent concrete sulfate attack in Norway is associated with the sulfide bearing Alum Shale. This represented a severe construction problem before and after World War II, also involving severe steel corrosion and internal swelling in the shale itself (cf. Bastiansen et al. 1957; Moum and Rosenqvist 1959). Cast concrete in contact with this Black Shale had caused quick and frequently complete degradation of the cement paste matrix. Investigations by the Alum Shale Committee (1947-1973) suggested this was due to secondary ettringite and sulfuric acid attack (Bastiansen et al. 1957, Fiskaa et al. 1971). Concrete made with Sulfate Resisting Portland Cement (SRPC) or Portland cement with added pozzolana resisted the attack to a great extent. The committee was apparently the first to report on the beneficial effect of silica fume. The Alum Shale Committee argued that a minor amount of very reactive monoclinic pyrrhotite was able to catalyse oxidation of abundant pyrite, being the reason for reactivity and swelling of Alum Shale. The swelling mechanism was investigated by Sopp (1966) but was not completely resolved. Swelling due to gypsum formation has however been observed (cf. Bastiansen et al. 1957). The Alum Shale Committee proposed that airing (oxidation) of ground waters prior to construction or alternatively permanent protection of the shale from oxidation should assist in solving the construction problems. Use of membranes to avoid direct contact with concrete and the harmful Alum Shale was also introduced.

However the Norwegian Public Roads Administration observed that a sprayed concrete made with SRPC and silica fume, exposed to Alum Shale, showed signs of deterioration (Grønhaug and Hagelia 2000). Forensic examination documented the influence of Thaumasite Sulfate Attack (TSA) in 2-13 years old steel fibre reinforced sprayed concretes in direct contact with Oslo Alum Shale (Hagelia and Grønhaug 2000). Locally TSA and internal carbonation in the form of Popcorn calcite had caused breakdown of the cement paste matrix, leading to localized spalling and through-corrosion of the steel fibres. It was therefore hypothesised that the classic sulfate attack in Oslo was perhaps a severe case of TSA rather than being caused by secondary ettringite (Hagelia et al. 2001). Other recent Norwegian cases involving thaumasite formation have been reported from a manure cellar, a bridge concrete influenced by seagull droppings and an industrial cooling pipe (Justnes and Rodum 2006).

TSA was first reported by Erlin and Stark (1965). This form of sulfate attack has been investigated mainly during the last ten to fifteen years. The most famous cases have been reported from the United Kingdom (Department of the Environment, Transport and the Regions 1999; Crammond 2003). TSA is usually found in a moist and cool environment (< 10 °C) although exceptions have been reported at higher temperatures: A summary on TSA in different structures and environments may be found in MacPhee and Diamond (2003), comprising 55 papers dealing with different aspects of thaumasite from many countries. Thaumasite is composed of Ca, Si, water, carbonate and sulfate; hence it attacks the C-S-H itself if also carbonate and sulfate are present. The initial non-destructive stage called Thaumasite Formation (TF) is characterised by deposition of thaumasite in voids and pre-existing cracks. Eventually, if the reaction is sustained, thaumasite forms as a non-cementitious replacement (TSA) at expense of the cement paste matrix. Ultimately the paste may be transformed into a mush. Several topics related to thaumasite formation conditions have been debated. The following themes are very relevant to the practitioner: a) It has been argued that thaumasite may require early stage formation of secondary ettringite (Bensted 2003, Crammond 2003) and b) that thaumasite cannot form in fully carbonated cement paste (Bellmann 2004).

Later work on Norwegian TSA related to the Alum Shale and subsea environments is reported by the present author within this thesis; including problems regarding the role of early ettringite and the significance of carbonation related to TSA.

2.2.8 Magnesium attack

Concrete in contact with seawater and saline ground waters is subjected to an appreciable amount of magnesium ingress which might gradually transform the cement paste matrix into a weaker material (cf. Taylor 1997). The process mainly involves breakdown of portlandite with precipitation of brucite ($\text{Mg}(\text{OH})_2$), substitution of Ca in C-S-H with Mg, leading to formation of Magnesium Silicate Hydrate (M-S-H) which is a non-cementitious material. In contrast to portlandite, brucite is insoluble and captures much of OH^- , thus lowering the pH in the pore solution. Yet cast concrete is usually only affected within the outermost surface, forming a protective layer. This effect has been observed after long term exposure of cast concrete in the North Sea (Maage 2008) and in tunnel concrete paving exposed to MgCl_2 (Justnes and Østvik 2008), reaching only about 1 mm depth.

In contrast, reports from the oldest Norwegian subsea tunnels, completed in 1982-1987, indicated high levels of total Mg across the bulk cement pastes, being associated with leaching and spalling (cf. Davik 1997 and references therein). Most likely this reflects formation of brucite and M-S-H and possibly also magnesium hydroxychloride.

The significance of magnesium attack was investigated further in this thesis.

2.2.9 Frost action

In Norway influence of frost damaged concrete is not uncommon in bridges and other structures. The effects depend on the initial concrete quality and the number of freeze/thaw cycles over time. It is also expected that sprayed concrete around tunnel entrances may suffer frost damage, notably because this material is not always frost resistant in terms of air content. However the general experience up to now is that frost damage in sprayed concrete is not a very important problem. Apparently sprayed concrete with quite low air contents were not damaged. Instead, frost action in Norwegian tunnels tends to act along joints in the rock mass rather than making damage to the sprayed concrete (Davik 1997, 1998). Recent work related to establishment of the Arctic Seed Vault in arctic Svalbard has demonstrated that spraying on permafrost rocks is also successful (Beck and Hansen 2008). Frost action was not investigated in this thesis.

2.2.10 Deformations within unstable rock mass

Sprayed concrete for rock support is by concept and definition subjected to an unstable rock mass. The possible effects on the overall strength and permeability depend strongly on the local scale interplay between rock mass properties and the rock reinforcement employed (i.e. thickness and strength of sprayed concrete, rock bolting etc.). One might hypothetically consider *early stage effects* if a structure has been under-dimensioned, and *later stage effects* where chemical deterioration mechanisms have been working over a period of time within cracked sprayed concrete. Bond strength between rock mass and sprayed concrete is also very important (Norwegian Concrete Association 2003, 2011) and might be weakened due to secondary concrete weathering reactions. Recent cases of rock fall in some Norwegian tunnels

probably reflect interplay of these mechanisms (Norwegian Public Roads Administration 2000-2008).

However, access to rigorously quantified rock mass parameters was in fact scarce and mostly absent, and no detailed documentation on real sprayed concrete thickness and strength variation was available. Thus, impact of unstable rock mass on the overall degree of chemical deteriorations as investigated herein remains uncertain.

2.2.11 Biodegradation and other microbial effects?

Rusty and black slimes are apparently quite common on sprayed concrete surfaces and ditches in Norwegian subsea tunnels. Some of these are iron bacteria which tend to clog drains systems (cf. Davik 1997, and references therein). However, Hansen (1996) investigating the Flekkerøy subsea tunnel, reported on loose concrete associated with rusty iron rich slimes and black deposits. According to him the “black deposits” were apparently most harsh to sprayed concrete. This phenomenon has as yet not been investigated but may indicate that micro-organisms also play a direct role in some concrete deterioration processes. Moreover, it is now well established that sulfide oxidising bacteria play a key role in iron sulfide oxidation and sulfate reduction processes. Accordingly such bacteria may enhance the formation rate of aqueous sulfate and sulfuric acid, for example within the Black Shale environment (Konhauser 2007). By contrast previous workers on Alum Shale only considered abiotic sulfate release mechanisms (cf. Bastiansen et al 1957).

Consequently the potential role of microbes related to rock – water – concrete interaction was investigated further within the Black Shale and subsea environments.

2.3 References

- Appelo CAJ and Postma D (2005): *Geochemistry, ground water and pollution* (2nd Ed.). A.A. Balkema Publishers, Leiden, 649 pp.
- Barton N, Lien R and Lunde J (1974): Engineering classification of rock masses for the design of tunnel support. *Rock Mechanics* 6, 189-236.
- Bastiansen R, Moum J and ITh Rosenqvist (1957): Contribution to high light certain construction problems associated with Alum Shale in Oslo. Norwegian Geotechnical Institute, Publication No. 22, Oslo, 69 pp. (In Norwegian with English summary).
- Beck T and Hansen R (2008): Sprayed concrete performance in arctic area – spraying on permafrost rock. In: K. Berg, C Hauck, R Kompen (Eds.). 5th International Symposium on Sprayed Concrete – Modern Use of Wet Mix Sprayed Concrete for Underground Support, Lillehammer, pp.17-25.
- Bensted J (2003): Thaumasite – direct, Woodfordite and other possible formation routes. *Cement and Concrete Composites*, 25, 873-877.
- Bellmann F (2004): On the formation of thaumasite $\text{CaSiO}_3 \cdot \text{CaSO}_4 \cdot \text{CaCO}_3 \cdot 15\text{H}_2\text{O}$: Part II. *Adv. Cem Res*, 16(3), 89-94.
- Bérubé MA, Fournier B and Durand B (eds.) (2000): *Alkali-Aggregate Reactions in Concrete*. Proceedings of 11th ICAAR, Quebec, Canada.
- Broekmans MATM and Wigum BJ (Eds.) (2008): *Proceedings of the 13th ICAAR*, Trondheim, Norway 1336 pp.
- Bromley AV, Pettifer K. (1997): Sulfide-related degradation of concrete in Southwest England. Building Research Laboratory Report, BR325. Published by CRC Ltd, Watford, Herts, pp 13-29

- Building Research Establishment (2003): BRE Special Digest 1 Concrete in aggressive ground. Parts 1-4.
- Crammond NJ (2003): The thaumasite form of sulfate attack in the UK. *Cement and Concrete Composites*, 25, 809-818.
- Davik KI (1997): Proper use of sprayed concrete in tunnels, Parts A, B, C, D, E and Final report (in Norwegian). Norwegian Public Roads Administration 1997.
- Department of the Environment, Transport and the Regions (1999): The thaumasite form of sulfate attack: risks, diagnosis, remedial works and guidance on new constructions. Report of the Thaumasite Expert Group, 180 pp.
- Erlin B and Stark DC (1965): Identification and occurrences of thaumasite in concrete. *Highway Research Record* 113, 108-113.
- European Standard EN 14487 Sprayed concrete, Parts 1 & 2
- European Standard EN 14488 Testing sprayed concrete, Parts 1 to 7
- European Standard EN 14487 Fibres for concrete, Parts 1 & 2
- Fiskaa O, Hansen H and Moum J (1971): Concrete in Alum Shale, Norwegian Geotechnical Institute, Oslo, Publication No. 86. 32pp (in Norwegian with English summary).
- Franzén T, Garshol KF and Tomisawa N (2001): ITA/AITES Accredited Material. Sprayed concrete for final linings: ITA working group report. *Tunnelling and Underground Space Technology* 16, p 295-309.
- Gaylarde C, Ribas Silva M and Warscheid (2003): Microbial impact on building materials: an overview. *RILEM TC 183-MIB. Materials and Structures*, 36, 342-352.
- Grønhaug A and Hagelia P (2000): Alum shale can damage sulfate resistant concrete. *Betongindustrien* Nr 3, 8-9 (in Norwegian).
- Guðmundsson G, Loftsson M, Sveinbjörnsson S, Wigum BJ and Harðarson BA (2008): Condition survey of sprayed concrete in Iceland. In: K Berg, C Hauck, R Kompen (Eds.), 5th International Symposium on Sprayed Concrete – Modern Use of Wet Mix Sprayed Concrete for Underground Support. Lillehammer, pp 157-168.
- Hagelia P and Grønhaug A (2000): Thaumasite – infection causing concrete deterioration. *Våre Veier*, Nr. 9 (in Norwegian).
- Hagelia P, Sibbick, RG, Crammond NJ, Grønhaug A and Larsen CK (2001): Thaumasite and subsequent secondary calcite deposition in sprayed concrete in contact with sulfide bearing Alum Shale, Oslo, Norway. 8th Euroseminar on Microscopy Applied to Building materials, p 131-138, Athens, Greece. September 2001.
- Hagelia P (2007): There is always more than one concrete degradation mechanism involved at each site. Presentation given at the Workshop “Forensic examination of concrete”, M.D.A. Thomas, I. Fernandes (Org.), 5th June, 11th EMABM Porto, Portugal, 2007.
- Hagelia P and Lie Hansen, K (2008): Lillehammer Olympic Park. In: P. Hagelia (Ed.), Pre-Conference Tour Guide of the 13th ICAAR, Norway, p 9-13.
- Hansen, BO (1996): Durability considerations related to sprayed concrete in subsea tunnels. *Sprayed Concrete in Subsea Tunnels*, NPRA Unpublished report (in Norwegian).
- Harris AW, Manning MC, Tearle WM and Tweed CJ (2002): Testing models of the dissolution of cement-leaching of synthetic CSH gels. *Cement and Concrete Research*, 32, 731-746.
- Hoseini M, Bindiganavile V and Banthia N (2009): The effects of mechanical stress on permeability of concrete: A review, *Cement and Concrete Composites*, 31, 213-220.
- Jensen V (1993): Alkali Aggregate Reaction in Southern Norway. Dr. Technicae thesis. The Norwegian Institute of Technology. University of Trondheim.
- Justnes H and Rodum E (2006): Case studies of thaumasite formation. In: V. M. Malhotra (Ed.), Seventh CANMET/ACI International Conference on Durability of Concrete, American Concrete Institute, SP-234 – 33, p 521-537.

- Justnes H and Østvik J-M (2008): Effect of magnesium chloride as dust binders on tunnel concrete paving. Proceedings of the 7th International Congress, Concrete: Construction's Sustainable Option, Dundee, July 2008.
- Kompen R (2008): Specifications for sprayed concrete, EN 14487 for sprayed concrete generally, Norwegian Concrete Association Publication No. 7 for rock support and NPRA Specifications for road tunnels. In: K. Berg, C Hauck, R Kompen (Eds.). 5th International Symposium on Sprayed Concrete – Modern Use of Wet Mix Sprayed Concrete for Underground Support, Lillehammer, 256-261
- Konhauser K. (2007): Introduction to Geomicrobiology. Blackwell Publishing, 425 pp.
- Maage M and Helland S (2008): Shore approach – 26 years of experience with high quality concrete in XS3 exposure. Nordic Exposure Sites – Input to Revision of EN 2006-1, Hirtshals Denmark, p 137-152.
- MacPhee D and Diamond S (Eds.) (2003): Thaumassite in Cementitious Materials. Special Issue, Cement and Concrete Composites, Vol. 25, No. 8.
- Moum J and Rosenqvist I Th (1959): Sulphate attack on concrete in the Oslo region. Journal of the American Concrete Institute, Proceedings, Paper 56 -18, 8 pp.
- Musæus H B (1962): Alkali-kiselsyre reaksjoner i betong. Thesis, the Norwegian Institute of Technology, Trondheim.
- Norwegian Concrete Association (2003): Sprayed Concrete for Rock Support, Publication No 7 (in Norwegian).
- Norwegian Concrete Association (2011). Sprayed Concrete for Rock Support, Publication No 7 (in English).
- Norwegian Concrete Association (2004): Alkali Aggregate Reactions in Concrete. Test Methods and Requirements to Test Laboratories, Publication No 32 (in Norwegian).
- Norwegian Concrete Association (2008): Durable Concrete with Alkali Reactive Aggregates, Publication No 21.
- Norwegian Public Roads Administration (2007): Process Code No. 2, 026. Standard specifications for highway construction (in Norwegian).
- Norwegian Public Roads Administration (2000-2008): Internal documents
- Norwegian Standard NS-EN 206-1, Concrete Part 1: Specification, performance, production and conformity (in Norwegian).
- Sibbick RG and Crammond NJ (2001): Microscopical investigation into recent field examples of the thaumasite form of sulfate attack (TSA). 8th Euroseminar Applied to Building Materials, p 261-269 Athens, Greece, September 2001.
- Sibbick RG, Crammond NJ and Metcalf D (2003): The microscopical characterisation of thaumasite. Cement and Concrete Composites 25, 831-837
- Sopp OI (1966): Contribution to understanding the Alum Shale swelling mechanism. Thesis, University of Oslo (in Norwegian).
- Tang M and Deng M (eds.) (2004): Proceedings of the 12th International Conference on Alkali-Aggregate Reactions in Concrete, Beijing, China.
- Taylor HFW (1997): Cement Chemistry (2nd Ed.). Thomas Telford Publishing, 459pp
- Thaulow N, Lee RJ, Wagner K and Sahu (2000): The form, extent and significance of Carbonation. In: Calcium hydroxide in concrete. Materials Science of Concrete, 191-202.
- Wigum BJ and Hagelia P (1998): Evaluation of the potential for Alkali Aggregate Reactions in Norwegian sprayed concrete based on literature survey an international experience (in Norwegian). P-533 Bestandige betongkonstruksjoner, Alkalireaktivitet. Internal report no. 2009, Norwegian Road Research Laboratory.

Chapter 3

Thaumasite and secondary calcite in some Norwegian concretes

*“In stark contrast to the limited damage potential
for conventional sulfate attack, TSA damage
is in principle unlimited”*

Donald MacPhee & Sidney Diamond

Thaumasite formation (TF) and limited Thaumasite form of sulfate attack (TSA) has recently been detected in several Norwegian sprayed concretes. TF and TSA is frequently associated with contemporaneous and late stage internal calcite formation by: a) decalcification of calcium silicate hydrate (C-S-H): b) decomposition of thaumasite associated with secondary liberation of SO_4^{2-} and occasional formation of subordinate gypsum; c) supersaturation of fluids in voids. Popcorn calcite and other textural forms were characteristic for these reactions. Also co-precipitation of Popcorn calcite + thaumasite, as well as later stage dissolution of both minerals occurred. The entire process was represented by a drop in pore fluid pH from about 13 towards 5-7. In this paper we study the *TF-TSA –carbonation* process in several environments: 1) Three examples of 2-13 years old steel fibre reinforced sprayed concrete made with Sulfate Resisting Portland Cement (SRPC) and silica fume in contact with carbon-, calcite- and sulfide bearing Alum Shale: 2) Two examples of ca. 30 years old, and severely damaged, SRPC based sprayed concrete within the Alum Shale: 3) One 16 years old sprayed concrete made with Portland Cement (PC) and possibly fly ash in presence of sulfate bearing ground water and 4) One 10 years old steel fibre reinforced sprayed concrete in a sub-sea tunnel with inflow of somewhat modified seawater. This PC based concrete with silica fume had suffered localised crumbling and mush formation after less than 5 years. The critical factors for thaumasite formation are discussed together with consequences for further deterioration and timing of repair.

Keywords: Sprayed concrete, thaumasite, calcite, durability, Norway

3.1 Introduction

During the last decade it has become increasingly apparent that formation of thaumasite represents an important degradation mechanism in concrete. The early non-deleterious stage called Thaumasite formation (TF) is characterised by thaumasite growth restricted to pre-existing voids and micro cracks. In deleterious Thaumasite sulfate attack (TSA) thaumasite forms at the expense of calcium silicate hydrate (C-S-H), ultimately

involving total disintegration of the cement paste matrix. Until very recently, neither TF nor TSA had been detected in Norway. Yet, during past decades a severe form of cement paste deterioration occurred in concretes associated with sulfide bearing Alum Shale in the Oslo region. This was previously attributed to ettringite and was compared to similar extensive forms of sulfate attack in the London district (cf. Moum and Rosenqvist [1]). However, in 2000 the Geology and Tunnel Division at the Norwegian Public Roads Administration (NPRA) detected TF and local spalling caused by TSA mush formation in a deteriorated 13 years old steel fibre reinforced sprayed concrete in contact with Alum Shale (Hagelia and Grønhaug [2]). This particular concrete was made with Sulfate Resisting Portland Cement (SRPC) and 5-10 % silica fume, which is typical for mixes used in contact with the Alum Shale. We now believe that the old and more extensive sulfate attack observed within the Oslo area was in fact severe cases of TSA (Hagelia et al. [3]).

During the last 15 years the use of steel fibre reinforced sprayed concrete in Norway has increased dramatically. The largest volume is used as tunnel support in conjunction with rock bolts. In order to maintain stability of the rock mass around the tunnel space, it is important that the spray thickness (usually about 5-25 centimetres, depending on local conditions) does not become significantly reduced with time. Thus, extensive deterioration should certainly not be allowed to take place. Yet, sprayed concretes made with SRPC are employed in direct contact with the harmful Alum Shale, and Ordinary Portland Cement (OPC) may also be used in contact with other sulfide bearing rock types. TSA has now been encountered in a wide range of structures made with such cements around the world. The environmental loads, which favour TSA, are of various kinds, including structures affected by seawater. In most cases studied TSA had occurred in a wet and cool environment (DETR [4], Crammond [5]). It is therefore not unlikely that this form of sulfate attack may occur in sprayed concrete in sub-sea tunnels as well as in bridge pillars. Although TSA has not yet been detected in Norwegian bridges, this may well be due to current characterisation strategy, which seldom involves petrography, SEM and X-ray diffraction analysis.

3.2 Recent research in Norway and objectives of this work

A collaborative investigation programme was set up by the Building Research Establishment (BRE), UK and the Norwegian Public Roads Administration (NPRA), Norway in 2000. Our work involves field investigations, sampling, core extraction, petrography, X-ray diffraction, Scanning electron microscopy, Electron Microprobe analysis and water chemistry analysis by Ion Chromatography. We have found TF and TSA within high quality sprayed concretes in Oslo, even in concretes of less than 2 years age. TF and TSA were frequently associated with contemporaneous and late stage *decalcification* of both C-S-H and thaumasite, which in both cases leads to the formation of unusual forms of internal secondary calcite (e.g. Popcorn calcite and several other textural forms). This suggests the existence of a *TF-TSA – carbonation process*. The thaumasite breakdown seldom involved gypsum formation, leading to secondary liberation of sulfate ions with a potential for further attack. Secondary calcite deposits were also abundant in air- and entrapment voids and notably at the concrete – Alum Shale interface where initial permeability frequently was elevated (cf. Hagelia et al. [3]). The aim of the present contribution is to:

- 1) Summarise results from the BRE-NPRA collaboration, including structures subjected to a variety of environmental loads
- 2) Discuss the conditions which have led to the TF-TSA-internal carbonation process
- 3) Put constraints on the possibility for further reactions and durability

3.3 Case studies

Table 1 gives a summary of the investigated concrete structures and their environment. All samples were collected in 2000. Sprayed concretes were made by the wet method unless otherwise stated. In general the concrete aggregates did not contain chemical components, which could have contributed significantly to TF and TSA. Hence the TF-TSA-carbonation process here seems to have been triggered mainly by the action of aggressive ground water. Although all four zones of TSA development (e.g. [4]) were encountered, it should be noted that the most advanced stage (i.e. “Zone 4”) in most cases was limited to a few rather small domains/zones less than 1-2 mm across. All samples have been carbonated by ordinary surface carbonation to normal depths of about 1-3 mm. The internal TSA- related carbonation was frequently much more extensively developed than surface carbonation, and resulted in a quite friable, permeable and brittle concrete. This internal carbonation was characterised by relatively coarse-grained largely non-interlocking calcite, comprising a great variety of textural forms. Popcorn calcite is preferred herein instead of “cornflake calcite”, previously used by authors because the calcite crystals formed have three-dimensional shapes similar to popcorn.

Table1: Summary of investigated sprayed concretes. See text for further details.

Locality	Type of structure	Age of concrete	Ground conditions	TSA development (see ref. [4])
-Åkeberg, Oslo	Road cut	13 and 30 years	Alum Shale	Zones 1-4 -mush
-Ekeberg, Oslo	Highway tunnel	8 years	Alum Shale/Clay stone	Zones 1-4
-Svartdal, Oslo	Highway tunnel	2 years	Alum Shale	Zones 1-4
-Oslo	Civil Defence Shelter	Ca. 25-35 years	Alum Shale (swelling)	Zones 1-3
-East Norway	Access tunnel to hydropower plant	16 years	Metasediments with black gneiss	Locally Zones 1-3
-Freifjord	Sub -sea road tunnel	10 years	Modified sea water	Zones 3-4 -mush

3.3.1 Sprayed concrete on Alum Shale in Oslo

The Upper Cambrian – Lower Ordovician Alum Shale in Oslo is a black shale, which consists of nearly anthracitic carbon, quartz, feldspar, clay minerals and chlorite. Calcite as well as sulfides, e.g. pyrite and subordinate amounts of very reactive monoclinic pyrrhotite, occurs as abundant laminae and veins. Pyrrhotite is held responsible for the sulfate attack, since it oxidises very easily and causes catalytic oxidation of adjacent pyrite with release of sulfate ions and associated production of sulfuric acid. Alum Shale is known for its swelling properties in contact with air, and gypsum growth may be part of the swelling mechanism [1]. Natural weathering products involve significant jarosite and some gypsum, whereas other sulfates such as hexahydrate were probably subordinate (cf. Neumann [6]). The first three cases from Oslo have been reported in a previous paper [3], and a brief summary with additional comments is given herein.

Åkebergveien road cut. This first documented occurrence of thaumasite in Norwegian concrete [2] consists of 2-3 layers of steel fibre reinforced sprayed concrete made in 1987. The concrete was made with SRPC and 5-10 % silica fume (not well dispersed with some lumps exceeding 100 microns in size), and water glass as setting accelerator. The w/c –ratio was about 0.45-0.5. TF and limited TSA occurs a) quite near the open outer surface immediately beneath ordinary surface carbonation, b) in vicinity of the concrete – Alum Shale

interface, as well as c) internally in entrapment voids between layers and in their surroundings. Thaumaside of Type 1 and 2 (as classified under the Optical Microscope in [4]) and all four stages of TSA development (i.e. Zones 1-4) were encountered [3]. At present this concrete has become deteriorated with extensive rusty surface deposits (from oxidation of sulfides) as well as calcite efflorescence being apparent. The aggregate did not contain any sulfate and carbonate source materials, except from minor amounts of calcite fines. The concrete was consistently moist with scattered tiny leakages throughout the spray. Spalling had started to develop in association with a 10-20 mm wide layer of thaumaside + calcite (mush zone). Other deformations in the sprayed concrete suggest that its initial shear strength had been significantly reduced since 1987. Destructive steel fibre corrosion was restricted to within the carbonated TSA mush zone, whilst fibres were intact or of limited degradation in the more sound, yet still friable zones with TF-TSA -carbonation.

Secondary internal calcite formation frequently involved the decalcification of C-S-H. This was closely associated with calcite ± subordinate gypsum formation at the expense of thaumaside. This breakdown reaction occurred both within the intact sprayed concrete as well as at an internal surface against the thaumaside + calcite mush zone, which was in contact with air. Presence of gypsum tends to be more common near the zone of ordinary surface carbonation. Calcite deposits with no obvious relationship to thaumaside or C-S-H were also frequently encountered in air- and entrapment voids. In general the calcite varied in form from blocky, branched/dendritic, popcorn- and cornflake like forms to acicular crystals.

Table2: Summary of water analyses

Locality	pH	Cl ⁻ mg/l	NO ₃ ⁻ mg/l	SO ₄ ²⁻ mg/l	CO ₃ ²⁻ mg/l	Na ⁺ mg/l	K ⁺ mg/l	Mg ²⁺ mg/l	Ca ²⁺ mg/l	Sulfate Class (ref. [4])
Åkeberg 1	7.6	29	25	1841	274	26	22	110	615	3
Ekeberg 1	7.0	10	18	592	100	25	16	20	106	2
Ekeberg 2	7.0	10	14	2031	56	43	22	74	574	3
East-N 4	5.70	16.9	nd	111	na	3.2	7.8	2.3	59.9	1
East-N 5	5.67	13.2	nd	106	na	3.5	4.4	2.8	38.5	1
East-N 6-1	5.66	15.8	nd	102	na	11.0	5.0	1.5	58.5	1
East N 6-2	6.06	12.8	nd	105	na	3.4	nd	3.9	38.9	1
Freifjord 1	7.0	5600	na	460	na	na	na	158	1425	2
Freifjord 2	7.3	18200	na	2400	na	na	na	1100	2200	3
Freifjord 3	7.3	17400	na	2200	na	na	na	1095	2290	3
Sea water	7.8	18980	0.7	2652	140	10561	380	1272	400	3

One water sample taken as it leaked from a crack through the sprayed concrete had a pH of 7.6 (cf. Table 2 for water chemistry and Sulfate Class). This water composition is probably not very different from unaffected ground water behind. However, non-oxidised ground waters in Alum Shale may be slightly acidic due to predomination of ferrous iron. As regards oxidised water in the vadose zone, pH may be 3-4 or slightly less, due to oxidation of ferrous iron and hydrolysis of ferric iron (cf. [1]).

TF-TSA and carbonation had also attacked remnants of a previous sprayed concrete layer from 1970. This concrete was made with SRPC, but without silica fume. Further details from this severely degraded spray were reported in [3].

Ekeberg highway tunnel. The steel fibre reinforced sprayed concrete in this tunnel was placed in 1992, and the concrete mix was essentially the same as at Åkebergveien. w/c -ratio was about 0.45. Due to previous experience sprayed concrete was not applied on wet Alum Shale, but instead the rock surface was dried (as much as possible) using compressed air just before the spraying operation in order to achieve bonding [7]. Silica fume (ca. 8% by cement weight) was in this case well dispersed throughout the matrix. Yet TF, and limited TSA were found. Calcite stalactites and rust deposits were commonly observed in presence of water

leakages throughout the concrete. This was usually also associated with steel fibre corrosion in several places, although apparently not usually very severe. The overall TF-TSA internal carbonation process was somewhat less well developed than at Åkebergveien, but all features were broadly similar. Type 1-2 thaumasite and Zones 1-4 were all encountered. The pH range within the ground water was about 4-5 within this Alum Shale sequence just after blasting [7]. Water samples collected in 2000 from leaks associated with calcite stalactites as well as rusty brown deposits along a crack through the concrete had a pH of about 7. The water compositions may have been slightly modified by the concrete (cf. Table 2 for water chemistry and Sulfate Class).

Svartdal highway tunnel. The spraying method and concrete mix were essentially similar to the Ekeberg tunnel, although it also contains a small amount of limestone aggregate. The reported w/c ratio was slightly above 0.4 [7], and we have found that silica fume was very well dispersed. In fact all cores were extracted the day before the tunnel was officially opened for traffic in August 2000, when the sprayed concrete was already about 2 years old. Surprisingly the TF –limited TSA –carbonation process was also found in this younger concrete (Zones 1-4, predominated by thaumasite Type 1-2). The steel fibres were occasionally slightly corroded, when in contact with the secondary calcite. TSA within most samples was restricted to rather thin zones (< 1.5 mm) in the vicinity of the concrete Alum Shale interface and elsewhere [3]. Although secondary calcite frequently had formed at the expense of C-S-H and thaumasite, additional euhedral calcite coexists with thaumasite in some large entrapment voids. Some of them were multiple crystals resembling Popcorn calcite (Figure 1). This paragenesis represents simultaneous deposition of thaumasite and calcite, rather than partial thaumasite decomposition. We have also found occasional evidence of a *later stage partial dissolution* of this assemblage (Fig. 3 in [3]), most likely due to the action of somewhat acidic water.

An Al-sulfate suspension (5-8 % by cement weight [7]) was used as a rapid setting accelerator where the tunnel cuts through Alum Shale, but locally water glass also had been used. Comparison of samples of both types indicated a quite similar development of the TF-TSA-carbonation process. However, the long term effect of the Al-sulfate accelerator, as a contributor to TSA is as yet not clear: 1) In contrast to water glass, this accelerator allows for a rapid build-up of a much thicker spray in a single spraying round. Hence, the amount of entrapment voids and other discontinuities may be rather small, thereby reducing the number of nucleation sites for TF and TSA [cf. 4]; 2) The chemical stability of this added sulfate is to our knowledge not documented for the ambient environmental loads, thus representing a potential internal sulfate- and aluminium source.

Water samples were not analysed chemically during construction. The investigated concrete was locally moist or wet in 2000; however, no uncontaminated water sample could be collected. During construction the reactivity of Alum Shale was, however, determined by chemical analysis of milled samples according to a standard method [7]. The Alum Shale immediately behind one of our samples suggested virtual absence of reactive sulfur (= 0.00 %). Total- and soluble sulfur were estimated to 7.87 % and 0.03 %, respectively. However, in view of the high reactivity of the Alum Shale sulfides this was of no surprise. The reactive component was very probably oxidised and lost before analysis. The ground water here most likely belongs to Sulfate Classes 2-3 and $\text{pH} \leq 7$ similar to the Ekeberg Alum Shale (Table 2). In fact the Svartdal- and Ekeberg tunnels have been excavated in exactly the same Alum Shale sequence in close vicinity of each other.

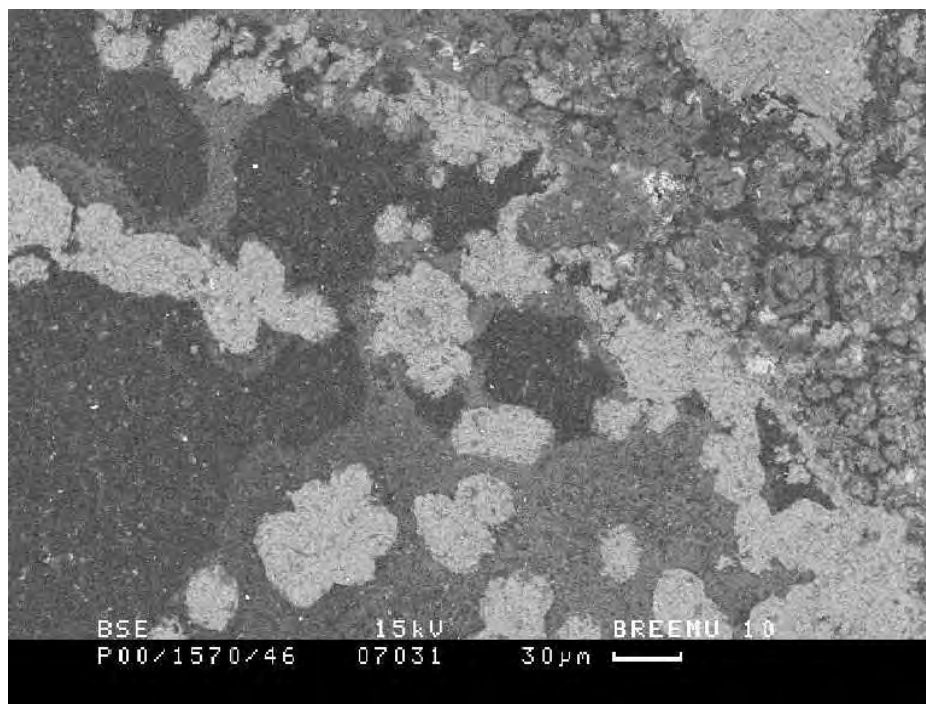


Figure 1: Co-precipitation of Popcorn calcite (bright) and surrounding Type 1-2 thaumasite (grey) in a partly filled entrapment void within 2 years old sprayed concrete in the Svartdal tunnel (BS-image). This TF-PCD process requires elevated concentrations of calcium and carbonate ions relative to sulfate ions. Notice the presence of very porous cement hydrates (granular/grey) next to aggregate (upper right), which may represent loss of calcium and silicon. See text for details. Scale bar = 30 μm .

Abandoned Civil Defence Shelter in Oslo. Sprayed concrete (dry method, fibre free) was applied directly on Alum Shale in the late sixties or early seventies. Due to the earlier focus on sulfate attack in the Oslo region it was expected that all concrete constructions here were made with SRPC. This was however not easy to confirm due to severe deterioration. In 2000 about 1-5 m^2 areas of very friable sprayed concrete had spalled and fallen down in several places. Jarosite and gypsum were frequently observed at the now exposed Alum Shale, and internal swelling within the outer surface of the shale had obviously contributed a lot to this extreme spalling. Rust deposits occurred on the surface. In the sprayed concrete TF and TSA (Zones 1-3, thaumasite Type 1-2) were clearly present as a major cause of the observed degradation, at least within a 5 mm thick layer in contact with the Alum Shale. The concrete adjacent to the shale was usually represented by microcracks, now heavily filled with secondary carbonate, some of which had apparently been derived from thaumasite. Also abundant gypsum crystals as void filling, plus ettringite were observed to be contributing to degradation. The main degradation was still in the form of abundant surface parallel microcracks variously filled with thaumasite, gypsum, ettringite and calcite, which were co-habiting within relatively small domains. These sulfate deposits were often closely associated with abundant calcite deposits probably secondary, which were filling pre-existing surface parallel micro cracks within the cement paste and aggregates particles. These aggregate particles and the surrounding cement paste matrix have clearly been degraded by a 'sulfate type' degradation at an earlier time. The sulfate minerals causing this degradation have since been either washed out and the micro crack subsequently filled with secondary calcite precipitate, or the thaumasite / gypsum and ettringite have become unstable and converted to calcite. Mottled and Popcorn-like carbonation was also observed within the cement paste in several places, and must have contributed to the overall loss of strength.

3.3.2 Sprayed concrete in sulfate bearing ground in East Central Southern Norway

An access tunnel leading down to an underground hydro power station was also investigated. The ground conditions here were characterised by somewhat elevated sulfate and calcium contents in ground water, as evidenced with historically known surface precipitation of bitter salt (gypsum with some epsomite), due to the rather dry climate in this part of Norway (Neumann [6]). The bedrock was characterised by various quartz-feldspar-mica gneisses and black gneiss (“shale”), which is equivalent to Alum Shale having additionally suffered higher temperature deformation during the Caledonian Orogeny. Locally within the tunnel jarosite and some gypsum had formed by weathering of the black gneiss. The present 1984 fibre free sprayed concrete was made with Portland Cement with about 8 % C₃A and most likely with Fly ash (i.e. Norcem MP30 with 20 %, Class F). Water glass was used as setting accelerator [7].

Locals tell that the tunnel was initially characterised by abundant water leakages, this being the main motivation for a sprayed concrete lining. In fact extensive white surface efflorescence was present, thus confirming the presence of significant water action at an earlier time. Several rusty brown deposits also occur, both on the concrete surface and as heavy rust-coloured sludge at the base. Sampling and petrography by the NPRA in 1997 indicated presence of a few Fly ash like fragments. White efflorescence consisted of abundant calcite (including stalactites) as well as “powder” and “cotton wool” deposits of thenardite. Thenardite might have formed from sulfate ions present in the ground water and sodium from water glass. It was not obvious that this sodium sulfate had caused any significant degradation of the concrete. Non-deleterious secondary ettringite and occasional minor non-deleterious ASR-gel was identified in air voids in the thin sections, but no thaumasite was found in the 1997 material. This may not necessarily imply absence of TF or TSA at that time, since sampling was restricted to a rather small section of the tunnel.

In 2000 BRE and NPRA extracted more cores as well as water samples. One core contained a 5-10 mm friable TSA + calcite layer (Zones 1-3, thaumasite Type 1-2) at the concrete – black gneiss interface. Some thaumasite was locally observed in association with deleterious ettringite deposits within surface parallel micro cracks. Popcorn calcite deposition (PCD) within thaumasite deposits was also noted. Apparently the formation of thaumasite and thenardite was associated with black gneiss. The patterns of surface efflorescence with calcite and thenardite had not changed since 1997 and the sprayed concrete tunnel lining presently appeared to be quite dry and sound. Thin sections generally indicated an overall quite dense and sound cement paste matrix. It seems possible at the present time that the secondary reactions have reached a stage where sprayed concrete permeability is at a minimum, or perhaps more likely the ground water level has been significantly lowered. The water samples from cracks through concrete have different composition than the ones in Oslo Alum Shale; pH ranges from about 5.7-6.1. Calcium and sulfate contents were low (e.g. Sulfate Class 1 see Table 2), which probably explains the limited development of the TF-TSA-carbonation process here.

3.3.3 Sprayed concrete in contact with seawater

The 5000 m long *Freiffjord sub-sea tunnel*, located near Kristiansund, was opened for traffic in 1992, and steel fibre reinforced sprayed concrete was made with about 6-8 % silica fume and Norcem RP 38: a rapidly setting Portland Cement that contains about 8 % C₃A. Water glass was used as a setting accelerator and the reported w/c ratio was in the order of 0.37-0.47 [7-8]. Systematic investigations including tunnel mapping and laboratory analysis

were undertaken in 1996 as part of a major project on durability of sprayed concrete. It was concluded (Davik [8]) that there was no evidence of “chemical attack” on the local concrete lining. However, by 1996 calcite stalactites were abundant and in several restricted areas the concrete had been partially to completely transformed into a mush. These deteriorated concretes were located within a sequence of banded gneiss with layers of marble, and were typically associated with water leakages. The mush occurred as loose layers on the surface of more sound sprayed concrete and had usually also been accumulated as a sludge at the base. This phenomenon was thought by some authorities to have been caused by rebound during the spraying operation, while others claim this was not so.

Investigations based on about 20-100 mm size samples of less deteriorated white and friable remnants of sprayed concrete, within the now washed away mush, clearly shows that deterioration was caused by TSA. Even in fairly solid remnants of an initially 50-100 mm thick spray [8], full scale TSA (Zones 3-4) was observed (Figure 2). TF had occasionally formed along micro cracks that post dated the paste matrix, which had already been transformed into a friable TSA – depleted C-S-H assemblage (i.e. some TF was locally secondary to TSA). Thaumasisites of Types 1-3 were found. In contrast to the Oslo concretes, thaumasite Types 2-3 here appear to be a lot more dense and massive. Secondary carbonation was very extensive in all forms described above, and some gypsum and ettringite were also detected. The steel fibre reinforcement was frequently completely transformed into a rusty Fe-hydroxide most notably in presence of abundant Popcorn calcite and other forms of calcite. From sound concrete samples elsewhere in the Freifjord sub-sea tunnel it was apparent that the silica fume was not well dispersed (i.e. globules <50-100 μm). However, there was no sign of silica fume globules within the TF-TSA affected areas, suggesting that this amorphous phase might have been incorporated into the thaumasite by chemical reaction.

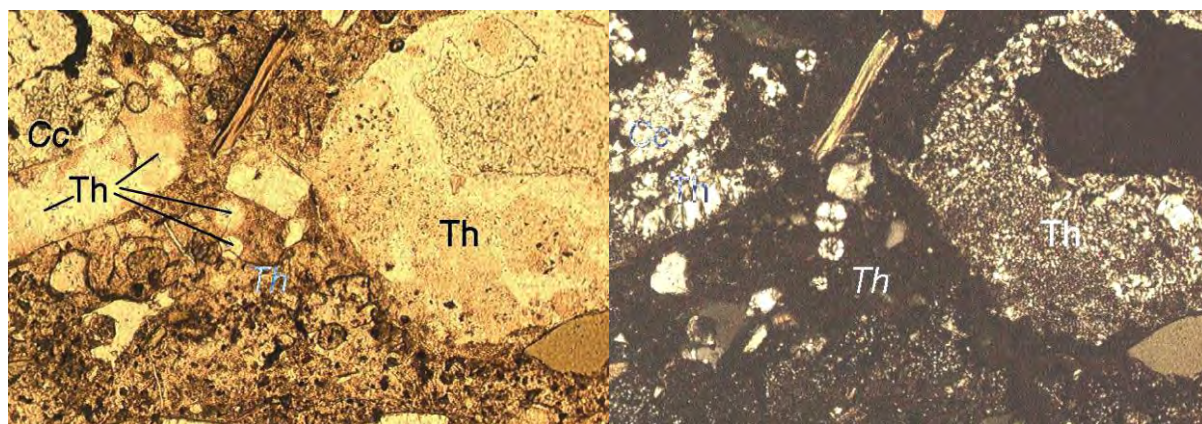


Figure 2: TF and TSA (Zone 3) in a small remnant of sprayed concrete from within a TSA-mush in the Freifjord sub sea tunnel. Thaumasisite of Type 2 (Th) occurs: a) in two large entrapment voids with subsequent calcite deposition (Cc in left void): b) in smaller air voids and c) as thaumasite of Type 1 and 2 scattered about in depleted cement paste (area around and below Th). Plane polarised light and crossed polars, respectively. Horizontal fields of view 1 mm.

Published water analyses [8] from the TSA affected tunnel sections, probably collected from cracks in vicinity of degraded concrete, had pH from 7.0-7.3, high contents of SO_4^{2-} , Mg^{2+} , Cl^- and very high Ca^{2+} , suggesting modified seawater (Table 2). Carbonate ion concentrations are as yet not available. Calcite in the marble layers may represent a potential carbonate source for thaumasite and secondary internal calcite. However, calcite is very slightly soluble at pH about 7 and calls upon another carbonate source. Hence a contribution

from atmospheric CO₂ should not be excluded. The high Mg²⁺ and Cl⁻ contents in water suggest influence by other processes as well.

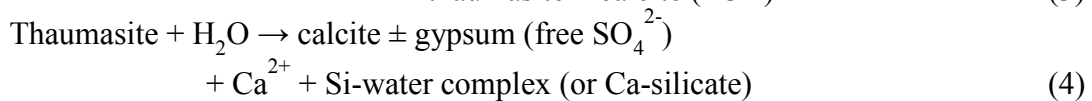
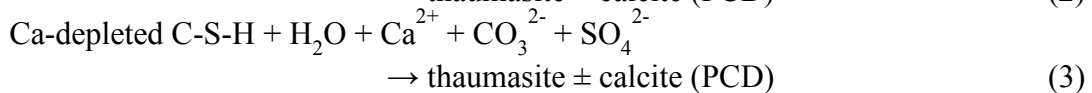
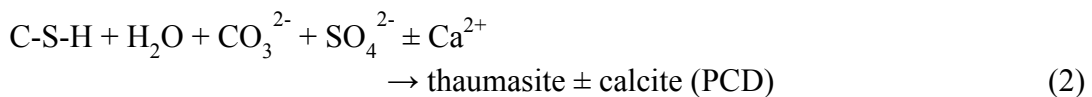
3.3.4 Steel fibre corrosion and role of silica fume in the TF-TSA-carbonation process

All observations indicate that it was the presence of internal carbonation that was most crucial to fibre corrosion. Steel fibres in presence of single thaumasite deposits in air voids were occasionally marginally corroded [3]. In contrast, corrosion was completely destructive in thaumasite-calcite mush. Within domains of well-developed Zones 3-4 with extensive carbonation, marginal steel fibre corrosion was usually observed. It is significant that the most severely corroded fibres were always in direct contact with calcite, and frequently in the form of Popcorn calcite deposition (PCD). It should be noted that this form of internal carbonation invariably results in a quite porous, permeable and more or less friable cement paste matrix, which hence stands in marked contrast to the effects caused by ordinary surface carbonation. Silica fume appears to delay the development of TSA in concretes on Oslo Alum Shale (cf. [3]), but yet this does not appear to inhibit deleterious reactions, even when well dispersed.

3.4 Discussion

3.4.1 TF – TSA – carbonation and formation conditions

The TF- TSA – carbonation process requires a steady drop in pore fluid pH from about 13 towards neutral, and which takes place in presence of sulfate- and carbonate sources in a wet and cool environment (cf. [3]). These conditions were prevailing in all cases studied herein. The sprayed concrete layers sitting on rock surfaces were subjected to *hydraulic gradients*, and the TF-TSA- carbonation process was typically more advanced in presence of water leakages. There was substantial evidence to suggest that ground water seepage through concrete was not only restricted to minor cracks, but in fact frequently affected the bulk cement paste matrix. Our data show that ground waters with neutral to somewhat acidic pH have mixed with pristine alkaline pore fluids in these concretes. The petrographic observations suggest the following schematic chemical reactions, implicitly also involving breakdown of portlandite:



The breakdown of C-S-H according to reaction (1) takes place when pore fluid pH drops below about 12.5. Carbonation in the form of PCD involved breakdown of portlandite as well as C-S-H [3]. Recent work by Sahu et al. ([10] and references therein) suggests that carbonation of C-S-H is governed by bi-carbonation, a process which takes place below pH = 11. Thaumasite appears to be stable at pH ranging from about 11 – 6 (Gaze and Crammond [9]). The various calcite assemblages are probably stable within the pH interval 10 to 7. Ground water in contact with sulfide oxidation processes should in general have pH less than 7. Yet, calcite veins in Alum Shale most likely acted as a buffer, and probably sustained a pH near 7. Reaction (6) involving acidic water appeared to be uncommon.

Calcium carbonate efflorescence and stalactites were surface expressions of the decalcification of C-S-H-gel (e.g. Ca depletion of C-S-H). The internal calcite deposits associated with depleted cement paste represent the “root zone” of this process. If sulfate and carbonate ions are present, thaumasite forms by replacement (e.g. TSA) after some degree of cement paste decalcification (reaction 3), rather than by direct decomposition of un-depleted C-S-H (reaction 2). Early stage TF, with or without PCD (Figure 1) in voids and cracks, seemingly precipitated from a fluid (similar to reaction 3, except silicon from Si-water complexes instead of depleted solid state C-S-H). Thaumasite later breaks down to form calcite and minor gypsum as pH drops further towards neutral. The essential scarcity of gypsum and thus apparent liberation of SO_4^{2-} (reaction 4) needs to be explained, since the stoichiometric proportions of the components CaCO_3 and CaSO_4 in thaumasite are 1 : 1. This most likely reflects the solubility product of gypsum, which is two orders of magnitude higher than calcite. It seems significant that the assemblage gypsum + calcite usually occurred near the surface in contact with ordinary carbonation. Gypsum most probably precipitated here due to surface drying of the concrete. Thus, internally in a concrete where thaumasite breaks down to calcite, *sulfate ions are available for further attack*. The secondary availability of this aggressive anion is a function of the TF-TSA-Cc reaction progress. Gaze and Crammond [9] have demonstrated experimentally that “carbonation of thaumasite” is very efficient at 5 °C in specimens in contact with atmospheric CO_2 . Stable isotopic signatures (C and O) in Oslo sprayed concretes indeed suggest partial influence from atmospheric CO_2 in the overall TF-TSA -carbonation process (Iden and Hagelia [11]).

A significant result [3] was that secondary ettringite was not very common in the Oslo sprayed concretes and did not appear to have predated formation of thaumasite. Preliminary analysis suggests that the compositions of Oslo thaumasite vary from almost pure Si end-member to 1-2 wt. % Al_2O_3 [3,7]. As a system component Al was apparently not important here; 1) Norwegian SRPC's have had quite uniform and low C_3A contents around 1 % for perhaps three decades (cf. [3]); 2) The ground water associated with Alum Shale in Oslo typically contains trace amounts of Al [1]. This offers a plausible explanation to the apparent scarcity of ettringite. But further analysis and more detailed SEM work is required to elucidate the ettringite problem in the TF-TSA-carbonation process, notably in view of associated pore fluid pH, which when dropping below 10.7 does not sustain ettringite stability.

Recent experimental synthesis of very Al-poor thaumasite made from an CaO -sucrose slurry mixed with sodium silicate, sodium sulfate, sodium carbonate, and with little or no sodium aluminate, shows very interesting results (Barnett et al. [12]). Precipitation of end-member- and Al-poor thaumasite under a nitrogen blanket was accompanied with significant amounts of calcite and an as yet unidentified amorphous phase (Th<Cc< amorphous). The co-precipitation of quite poorly formed thaumasite and Popcorn calcite depicted in Figure 1 may, therefore, well represent a similar process. The possibility that an amorphous phase is present interstitially between thaumasite needles cannot be excluded, and the identification and quantification of this may in case have a direct bearing on the TF-TSA-carbonation reaction

progress. One might speculate that the unidentified amorphous phase has a composition similar to thaumasite, and that this may be part of the explanation for the nearly isotropic Type 1 thaumasite. These experimental results also highlight a warning, in that the petrographer should take great care when attempting to discriminate between thaumasite – calcite deposits and calcite formed from thaumasite decomposition.

Comparison of Tables 1 and 2 suggests a good agreement between degree of TSA development and established Sulfate Classes as defined in reference [4]. It is noteworthy that the TF-TSA-carbonation reaction mechanism does not seem to be very sensitive to the C_3A contents in the cements, since the investigated cases represent a variation from ca. 1-8 % of this clinker phase. The role of Ca^{2+} , CO_3^{2-} and other ionic species should be investigated further, together with the influence from atmospheric carbon dioxide. These important constituents in thaumasite were not investigated to any great extent within the present study.

3.4.2 Deterioration and service life of sprayed concrete

Although the currently used SRPC based mixes with silica fume appear to have eliminated the most severe forms of TSA in the Oslo region [1], a systematic durability study is still required. Based on preliminary data, Hagelia et al. [3] suggested that the “lifetime” of such sprayed concrete on Alum Shale probably is 15-20 years. Service life is a matter of definition that varies from one site to the next. In our context service life of sprayed concrete is a function of;

- 1) The chemical reaction rates involved in deterioration (depending on material properties and environmental loads).
- 2) The relationship between chemical reaction stages and bearing capacity of sprayed concrete (i.e. when it becomes weaker and thinner than specifications for the local rock mass conditions).
- 3) The local traffic and safety conditions (traffic prognosis, alternative routes when a tunnel tube must be closed, public safety, etc).

Thus, a more precise and site-specific knowledge of these relations should provide a good basis for forecasting the optimal (i.e. most cost-effective) timing of repair.

We have investigated the available cores from modern sprayed concrete in Oslo and estimated the fraction of the initial sprayed thickness (assuming no loss of material), which was influenced by the TF-TSA-carbonation process. These rather uniform sprayed concretes were typically attacked from both sides of the sprayed slab, yet with variably developed internal degradation [3]. The TF-TSA-carbonated thickness/Initial thickness -ratio has increased roughly, from 0 to 13 years (Figure 3). The most reacted concrete in the Åkebergveien road cut had started to develop localised TSA-calcite mush with associated extensive steel fibre corrosion, spalling and other evidence of strength loss. This suggests that, for these SRPC based mixes sitting on Alum Shale; the *initiation time* is somewhat less than 13 years. In fact structural deterioration by TF-TSA-carbonation had already started to propagate. It is expected that the trend hereafter will establish TSA at an even faster rate. A quite “critical stage” has been reached, and timing of repair depends mostly on traffic- and safety considerations.

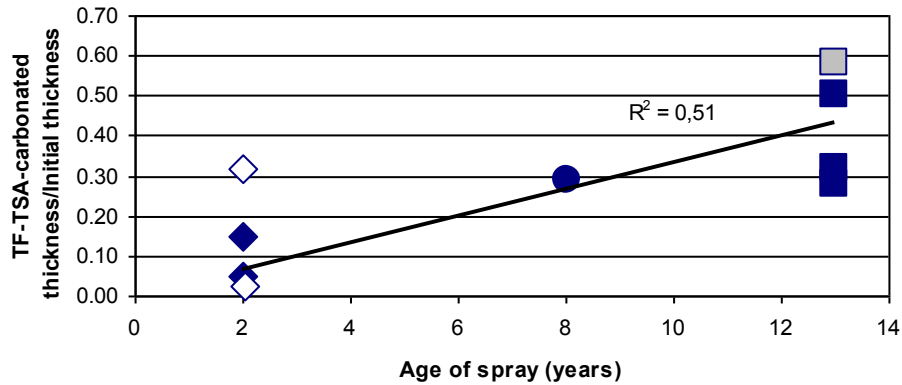


Figure 3 – Development of the TF – TSA – carbonation with time in modern steel fibre reinforced sprayed concretes made with SRPC and silica fume in contact with Oslo Alum Shale. w/c about 0.4-0.5. Squares = Åkebergveien cut (grey filled symbol contains some 1970 spray); Filled circle = Ekeberg tunnel; Diamonds = Svartdal tunnel: Open diamonds made with Al-sulfate accelerator: Filled symbols, with water glass accelerator. The TF-TSA-carbonated thickness in each core represents the sum of bleached- surface parallel zones within which this reaction was developed.

The sprayed concretes in tunnel linings (i.e. Svartdal and Ekeberg) should perhaps have a shorter initiation time than sprayed concrete in the Åkebergveien road cut, due to the higher hydraulic gradients involved in tunnels. Indeed, the flow rate of aggressive waters through concrete should have a bearing on the TF-TSA-Cc reaction progress. This should be investigated further.

In the Freifjord sub sea tunnel Portland Cement based sprayed concrete with silica fume was attacked by modified seawater. Evidently the initiation time for the TF-TSA-carbonation process was in this case < 5 years in presence of several focused water leakages. Elsewhere in this tunnel, where influence from seawater is small, the sprayed concrete was a lot more durable [7,8].

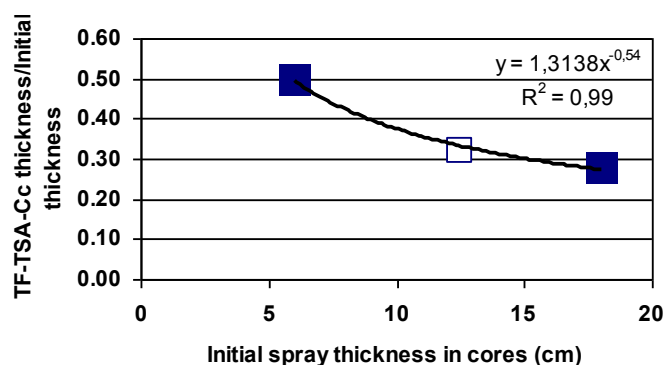


Figure 4: TF-TSA-carbonation development in 13 years old sprayed concrete cores at Åkebergveien as function of initial spray thickness. The open square symbol represents a core with some internal reaction plus a soft TSA- calcite mush layer (2 cm) and a reaction zone (1 cm) within a spall just outside the mush. The remaining cores (filled squares) contained TSA mostly at micro scale. The equation is empirical. A core with a remnant of 30 years old spray was excluded. All cores were extracted from consistently moist concrete.

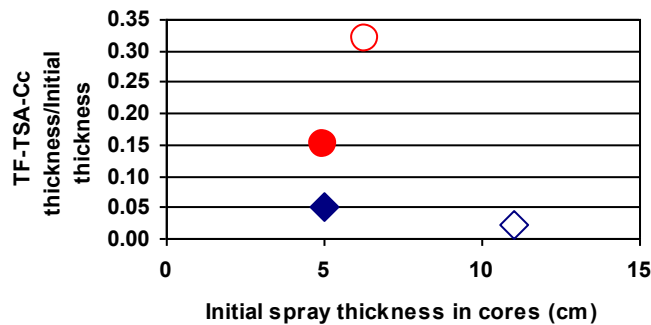


Figure 5: TF-TSA-carbonation development in 2 years old sprayed concrete in the Svartdal highway tunnel as function of initial spray thickness. Open symbols = with Al-sulfate; Filled symbols = with water glass. Notice that the most reacted cores were extracted from surface wet concrete (circular symbols), whilst the least reacted were from surface dry concrete (diamonds).

There was also a significant influence on deterioration rate from the initial thickness of the spray, as well as presence- or absence of water *: Figure 4 shows the development of the TF-TSA-carbonation process as a function of initial spray thickness at Åkebergveien. All cores here were extracted from consistently moist concrete and there is a good negative correlation between initial thickness and state of reaction. An equivalent diagram for the Svartdal cores is shown in Figure 5, representing concrete with more variable initial characteristics. Also in this younger sprayed concrete the degree of reaction was perhaps essentially influenced by water. The most reacted cores were extracted from moist concrete, in contrast to the least reacted cores being surface dry. Yet, different influences from the two different setting accelerators here cannot be excluded; an Al-sulfate admixture bearing surface wet core was much more influenced by the TF-TSA-carbonation process than an approximately equivalent surface wet core made with water glass. A comparison of the pore structure and microchemistry in these cores is required in order to test this hypothesis.

3.5 Conclusions

- 1) The TF-TSA –carbonation process in sprayed concrete was triggered by admixture of sulfate- and carbonate-bearing ground waters with mildly acidic to neutral pH.
- 2) The process requires fluid flow through the bulk cement paste matrix, and was found in concretes associated with sulfide oxidation as well as in seawater environment.
- 3) The reaction progress is sensitive to spray thickness.
- 4) TF-TSA-carbonation does not seem to be very sensitive *either* to the C_3A contents within the 1-8 % interval, *or* to the degree of dispersion of silica fume.
- 5) Steel fibre corrosion begins in presence of Popcorn calcite depositions (PCD) and other relative coarse and porous calcites. Destructive fibre corrosion was commonly associated with soft thaumasite + calcite mush formation.
- 6) The lifetime of TSA affected SRPC- and PC based steel fibre reinforced sprayed concretes, made with 5-10 % silica fume, is much shorter than the designed lifetime (= 50 years) for Norwegian tunnel concrete.

* The effect of spray thickness is, however, complex as discussed further in Chapter 10.

3.6 Acknowledgements

The authors are indebted to Simon Lane, Neil Gape, Derek Metcalf, Margaret Gavin (BRE); Muriel Erambert, Hans Jørgen Berg (Geological Museum, Oslo); Per Geir Sigursen and Ian Willoughby (NPRA) for technical assistance. Arne Grønhaug (NPRA) is thanked for discussions. Ove Lars Strømme and Ole Fromreide are thanked for information/samples from the Freifjord tunnel, and information from the Ekeberg tunnel, respectively. PH acknowledges an invitation to come and visit BRE and the receipt of a travel grant from the Norwegian Public Roads Administration in 2001. The authors would also like to thank the UK government's Construction Directorate for funding the BRE works on TSA, and an anonymous reviewer for relevant comments.

3.7 References

- 1 Moum J, Rosenqvist IT, "Sulphate Attack on Concrete in the Oslo Region". Journal of the American Concrete Institute, Proceedings Vol 56, Title 56-18, 1959, 8 pp.
- 2 Hagelia P, Grønhaug A, "Thaumasite – infection causing concrete deterioration", *Våre Veger* nr. 9, 2000, pp 54-55 (in Norwegian).
- 3 Hagelia P, Sibbick RG, Crammond NJ, Grønhaug A, Larsen CK, "Thaumasite and subsequent secondary calcite deposition in sprayed concretes in contact with sulfide bearing Alum Shale, Oslo, Norway". 8th Euroseminar on Microscopy Applied to Building Materials, Athens, Greece, September 2001. pp 131-138.
- 4 Department of Environment, Transport and the Regions, "The thaumasite form of sulfate attack: Risks, diagnosis, remedial works and guidance on new construction", Report of the Expert Group, DETR London, 1999, 180 pp.
- 5 Crammond NJ, "The occurrence of thaumasite in modern construction – A review", *Cement & Concrete Composites* 24. Special edition (ed. P. Brown), 2002, pp 393-402.
- 6 Neumann H, "The Minerals of Norway", *Norges geologiske undersøkelse*, 1985, *Skrifter* 68, 278 pp (in Norwegian).
- 7 Norwegian Public Roads Administration (internal documents).
- 8 Davik KI, "Proper use of sprayed concrete in tunnels", Part B Sub-sea tunnels (in Norwegian). Norwegian Public Roads Administration 1997, 66 pp.
- 9 Gaze ME, Crammond NJ, "The formation of thaumasite in a cement: lime: sand mortar exposed to cold magnesium and potassium sulfate solutions", *Cement and Concrete Composites* 22, 2000, pp 209-222.
- 10 Sahu S, Badger S, Thaulow N, "Mechanism of thaumasite formation in concrete". *Cement and Concrete Composites* (this volume).
- 11 Iden IK, Hagelia P, "C, O and S isotopic signatures in concretes which have suffered thaumasite formation and limited thaumasite form of sulfate attack". *Cement and Concrete Composites* (this volume).
- 12 Barnett SJ, Macphee DE, Lachowski EE, Crammond NJ, "XRD, EDX and IR analysis of solid solution between thaumasite and ettringite". *Cement and Concrete Research* 32, 2002, pp 1-12.

Chapter 4

Thaumasite sulfate attack, popcorn calcite deposition and acid attack in concrete stored at the “Blindtarmen” test site Oslo, from 1952 to 1982

*“There are two systems in the universe;
geology and theology –
petrography is the connecting link”
Vladimir E. Wolkodoff*

In past decades concrete in contact with Oslo Alum Shale suffered severe deterioration, frequently involving quick and complete degradation of the cement paste matrix. The Norwegian Alum Shale Committee (1947-1972) concluded that this was due to secondary ettringite deposition and acid attack. The most resistant concrete mixes were based on Sulfate Resisting Portland Cements or those containing a pozzolanic supplementary cementitious mineral. However, the present work concludes that this “classic” sulfate attack was triggered by deleterious Thaumasite Sulfate Attack and Popcorn Calcite Deposition in close association with effects of externally derived acid attack. This paper provides an outline of the previous work and the first petrographic documentation of concrete prisms previously exposed at the “Blindtarmen” test site. Two important novel reaction mechanisms were also found: 1) the development of high crystallisation pressure associated with Thaumasite Formation, and 2) full scale Thaumasite Sulfate Attack was most efficient after partial or complete decalcification of calcium silicate hydrate: thaumasite had formed at the expense of remaining amorphous silica and associated secondary popcorn calcite. Comparison with modern sprayed concrete on Alum Shale shows that influence of Thaumasite Sulfate Attack and internal carbonation was faster under a hydraulic gradient than under static conditions.

Keywords: Thaumasite Sulfate Attack; Popcorn calcite; Acid attack; Concrete mix design; Sprayed concrete lifetime

4.1 Introduction

The Upper Cambrian – Lower Ordovician Alum Shale in Norway has historically caused a lot of problems related to construction activities. This black shale may cause swelling and heave of foundations, corrosion of steel pipes and reinforcements and notably the development of an unusual severe form of sulfate attack on concrete. During past decades

the concrete sulfate attack, which is the subject of this paper, involved partial to complete degradation of the cement paste matrix, sometimes within less than one year. This was caused by presence of Alum Shale particles in the concrete aggregate and direct contact between concrete and Alum Shale or ground water derived from the shale.

Alum Shale varies in regard to composition, geological setting and metamorphic grade. Occurrences of harmful Alum Shale are essentially restricted to within the Permo-Carboniferous Oslo Graben. However, several varieties of Alum Shale are not harmful and they occur both within the Oslo region and elsewhere. Although Alum shales are easily detected from their high carbon contents, it may be comparably much more difficult to unveil their reactivity. It was, therefore, of utmost importance to understand the mechanisms that were responsible for the behaviour of the Alum Shale.

A semi-official “Alum Shale Committee” was established in 1947 in order to unravel the nature of the shale and the mechanisms behind swelling, steel corrosion and concrete deterioration. Further development of the infrastructure after the Second World War, notably in the capital city of Oslo, was much dependant on results from the committee. The Alum Shale Committee investigated the Alum Shale problem through site inspection and laboratory investigations of shales and concrete. This involved a long term test program for the performance of several concrete mixes set up in a specially designed underground test site at Blindtarmen within an Alum Shale environment in the city centre of Oslo (Figure 1). As a result of the pioneering work by the Alum Shale Committee, Sulfate Resisting Portland Cement (SRPC) with silica fume (SF) now represent the prime ingredients used for concrete construction within the reactive Alum Shale environment.

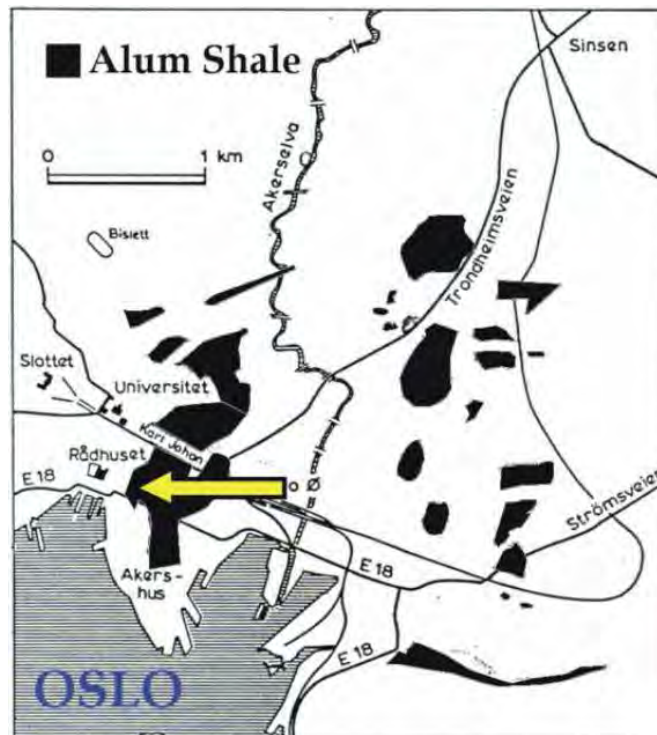


Figure 1: Alum Shale outcrops in Oslo with arrow showing the location of the previous Blindtarmen test site.

It was concluded from these investigations that the concrete attack was caused by extensive ettringite formation caused by sulfide oxidation and sometimes associated with acid attack. The attack was compared to certain severe sulfate attacks caused by some London clays (cf. [1]). However, recently it has been established that sulfate attack observed in modern sprayed concretes in tunnels within the Alum Shale instead were caused by non-deleterious Thaumate Formation (TF) and limited deleterious Thaumate Sulfate Attack (TSA) at the expense of the calcium silicate hydrate (C-S-H) (e.g. Hagelia and Grønhaug [2]). Associated contemporaneous and later stage internal carbonation in the form of Popcorn Calcite Deposition (PCD) was typical, and evidence for late stage acid dissolution of thaumate and calcite was also detected. This occurred in SRPC concrete with SF [3, 4]. Due to the description of the old attack we have argued in previous papers that this must have represented a severe case of TSA with associated deleterious carbonation and acid attack. In order to verify this hypothesis (e.g. [3]) it was decided to retrieve the remaining samples at Blindtarmen, which according to the latest reports still were located at Blindtarmen in 2000 ([5]; Ulf Fredriksen, personal communication 2000). The old samples from Blindtarmen were expected to represent very valuable information about the long term (48 years in 2000) performance of SRPC and pozzolanic PC in this aggressive environment. Moreover, concrete petrography based on thin section studies was not conducted by the Alum Shale Committee. The objectives of this paper were to:

- Give an outline of the main results of the Alum Shale Committee, with focus on the story of the Blindtarmen test site.
- Present the first petrographic examination of concrete prisms stored at the previous Blindtarmen test site: provide an updated diagnosis of the deterioration mechanism and investigate the long term durability of mixes relevant to lifetime of sprayed concrete used for rock support in tunnels.

4.2 Outline of results from the Alum Shale Committee

4.2.1 Characterisation of Alum Shale and its properties

The work of the Alum Shale Committee was very detailed, systematic and well thought out. The important findings will be given in the following a brief account. Swelling of the Alum Shale was described from several field cases and involved slow, fast and delayed heaves amounting to several decimetres. The Alum Shale Committee considered that several processes within the shale were responsible for swelling: the mechanism is still not well understood (cf. [7]) although gypsum is probably involved. The modal composition of Oslo Alum Shale exhibits considerable variation, mainly consisting of carbon (anthracitic or “pre-graphite” stage), quartz, feldspars, clay minerals, chlorite, pyrite, minor amounts of pyrrhotite and calcite as veins and lamina [6, 8]. The sulfate source was considered to be minor contents of very reactive disordered monoclinic pyrrhotite ($\text{FeS}_{1.14}$) and associated more abundant pyrite (usually 6-7 %). According to the Alum Shale Committee, oxidation of pyrrhotite had a catalytic effect on pyrite-oxidation due to an electrochemical process. Unweathered Alum Shales with pyrrhotite sulfur contents of 0.01-0.71 wt. % had caused building damage, whilst undamaged constructions were found in areas with 0.00-0.026 wt. % pyrrhotite derived sulfur. No threshold value could, however, be established, although < 0.001 % pyrrhotite sulfur was considered safe. Acid attack on steel and concrete was interpreted to relate to iron

sulfide oxidation followed by formation and precipitation of ferric iron hydroxides, because oxidation of ferrous to ferric iron was related to a drop in pH from ca 6 to < 3 [1]). The surface weathering products of Alum Shale frequently involved gypsum, epsomite and jarosite.

Chemical and XRD analysis of concrete deterioration products suggested compositions quite similar to ettringite, yet without a full match. Significant amounts of calcite were also detected. Material from white halos (Figure 2) around alum shale aggregate in both construction concrete as well as Blindtarmen test concrete were characterised by a refractive index of 1.496. The Alum Shale Committee concluded that this most probably was representing a water bearing sulfate mineral, possibly aluminate sulfate (ettringite). A DTA curve of this sort of material [6] showed a very pronounced endothermic peak at 150-160 °C. Recently it has, however, been pointed out that both the refractive index and DTA data may as well be indications of thaumasite rather than ettringite [3].

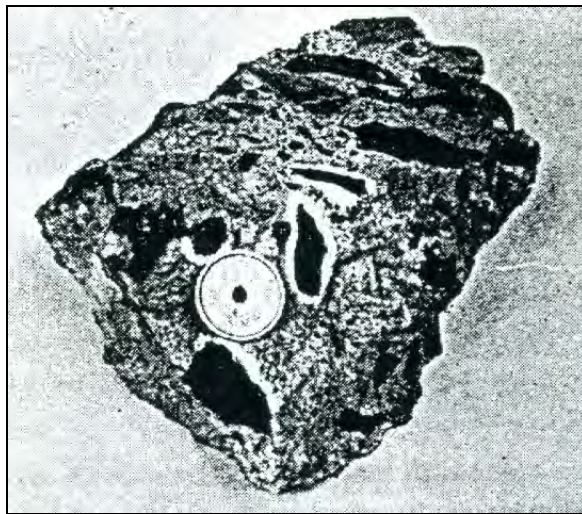


Figure 2: Old construction concrete with white “halos” of reaction products around Alum Shale aggregate particles [1].

4.2.2 The Blindtarmen Test Site, 1952 to 1972 and beyond

The Blindtarmen Test Site was established within an abandoned small tunnel branch of the Oslo sewer system, which had in fact never been in use. The field experiments started in January 1952. The ground conditions here were characterised by sulfate bearing ground water with a well documented previous record of severe concrete deterioration. The exposure conditions were divided into two groups. One set of samples was kept at a high level exposed to fluctuating ground water level (depending on seasonal variation) whilst another set was kept at the base of the tunnel, being more or less constantly submerged in ground water. In general, the submerged samples had suffered more severe attack than the prisms stored at the higher level. The water chemistry at the Blindtarmen test site was analysed several times and typical results are given in Table 1. The most acidic waters had the highest sulfate contents, being typical of Acid Rock Drainage. Sulfate concentrations even exceeding 4 g/l have been reported [9]. Chemical analysis of deteriorated concrete prisms showed they had absorbed significant amounts of sulfate, iron and carbonate [9]. The deteriorations observed in the Blindtarmen test specimens, therefore, reflect accumulated effects of variations in acidity, bicarbonate and sulfate loads over time.

Table 1: Typical water chemistry of Blindtarmen ground waters [1, 9]. All concentrations in grams/litre.

Sample	pH	Fe ³⁺	Fe ²⁺	SO ₃	Cl	Ca ²⁺	Al
I	5.38	Trace	0.358	2.3136	0.421	n.a.	Trace
II	6.14	Trace	0.412	0.544	0.491	n.a.	Trace
III	5.00	Trace	0.244	2.109	0.343	n.a.	Trace
IV	4.89	Trace	0.229	2.104	0.347	n.a.	Trace
Sept 55 B	6.22	Trace	0.36	2.31	0.42	n.a.	Trace
22/5/53 B	3.91	0.03	0.70	3.43	0.21	0.76	0.26
22/5/53 H1	2.95	0.08	0.93	3.57	0.19	0.74	0.22

Altogether 212 individual concrete prisms (10 x 10 x 40 cm) representing sixteen different concrete mixes were placed at the test site in 1952 (Series 1-9); in 1957 (Series 10-14) and in 1960 (Series 15 and 16). Reference samples from each series were kept in tap water [9]. The concrete aggregate consisted of a coarse fraction (5-20 mm) of crushed limestone (weakly metamorphosed, containing 81 % calcite) and a fine fraction of natural quartz – feldspar rich fluvio-glacial sand (0.1 – 10 mm). The binders used were Norwegian Standard Portland Cement (Nor PC), Danish seawater cement (with 10 % pozzolana in the form of diatomaceous clay called molére), Finnish Ferrari cement, American sulfate resistant Type 5, English Sulfacrete, Danish Type 5 and Danish Marine Cement (with 10 % molére). The sample series were placed at Blindtarmen just 6-14 days after hardening, in order to mimic real life conditions [9]. Further details about concrete mixes, additives and performance are summarised in Table 2.

The performance of individual concrete prisms varied much, and the results in Table 2 represent averages of several samples in each series. According to [5] volume loss and visual observations were regarded as the most important criteria in evaluating the degree of chemical attack in the different sample series. After a comparison of all 16 samples series at age 11 years it was concluded that:

- The reference Series 1 consisting of Norwegian Portland cement (Nor PC) without additives was heavily attacked by the Alum Shale ground water with volume loss of 6 %.
- The volume loss increased to 20 % when about 8 % of the natural fine quartz sand was replaced by crushed calcite (Series 9) and to 30 % by a similar level of replacement by very finely crushed limestone (Series 8).
- By using cements with C₃A contents lower than 5 % (i.e. SRPC) or by replacing 15 % of Nor PC by highly reactive pozzolana (silica fume, trass and diatomaceous clay), the volume loss was not more than 0.2-1.7 %.
- Use of air entrainment agents into Nor PC based Series 5 and 10 seemed to have had an overall negative effect, with volume loss corresponding to about 35 % and 5 %, respectively.

These conclusions are also corroborated by the loss of strength and the measured differences in permeability (Table 2). Length measurements undertaken until 5 ¾ years of exposure (Series 1 through 9) revealed that length increases were only very small and erratic. However, to the present authors this seems to be compatible with a predominating thaumasite sulfate attack, which in contrast to ettringite does not involve much total expansion [10, 11].

According to [5] the most intact samples, 55 prisms in total, belonging to Series 1, 4, 6, 11, 12, 15 and 16, were returned to the Blindtarmen test site in late 1972 for future workers to report. Twelve reference samples belonging to the same sample series' were stored in tap

water at NBI, Oslo. However, it turned out that all samples were removed from the test site in 1982 without any further reporting. Yet in 2001 we obtained some sample slices, both exposed and reference samples, which had been stored at NBI since then. These samples represent the basis of the present work.

4.3 Samples from Blindtarmen investigated in this study

4.3.1 Methods, sample handling and identification of unknowns

The exposed samples had lost parts of the outer surfaces and were otherwise characterised by notable bleached and very friable outer reaction zones. Table 3 gives a summary of the investigated samples with reference to main characteristics as received. The sample slices (1-2 cm thick) had been cut at right angle to the major prism axes, and were at first photographed and visually documented. The slices were dried at 40°C for 24 hours and then vacuum impregnated with a low viscosity epoxy containing a blue dye. One thin section was prepared from each concrete slice, covering a cross section from the outer rusty surface deposit to the sounder interior. After lapping the thin sections were covered by a removable glass cover slip, thus allowing for SEM. For the main petrographic work on degradation mechanisms we used standard polarising microscopes. SEM analysis, using 15kV beam energy and 5×10^{-10} amp beam current and micro analytical Energy Dispersive X-ray Spectroscopy (EDX) capability was used for the chemical analysis of relatively sound cement matrixes in unknown samples and reference samples.

Most of the exposed samples had lost their numbers, although a few individual specimens belonging to Series 1 with Nor PC could readily be identified along with the reference samples. By comparing petrographic and chemical characteristics of unknown samples with available reference samples and mix details given by the Alum Shale Committee [9] we have been able to identify which of the concrete mixes were at hand. The overall results strongly suggested that eight of the exposed samples belonged to the original Series 1 (Nor PC without additives); one sample belonged to Series 8 (Nor PC with 8 % limestone fines) and one specimen of Series 12 (Nor PC with added 15 % German trass) was also present. Only the latter sample (our number 1647/7), had performed very well with just minor loss of outer concrete material. Series 8 (1647/12) was severely affected as were the specimens belonging to Series 1. It was, however, not possible to identify individual prism numbers. Further details of the procedures and analytical results may be found in [12]. The results are summarised in Table 4.

Part 1 – Black Shale environment

Table 2: Synthesis of Blindtarmen test data from [5] and [9]; * SF = silica fume from Fiskaa Verk; ** Slag from Christiania Spigerverk. *** = Franzefoss limestone. Strength data recalculated from kp/cm² in original work.

Series/ cement type	Additives (% of cement weight) or air entrainment (% additional air volume)	w/c	Permeability (cm/s) of ref. samples (1967)	Volume loss (dm ³)/ exposure time (start to 1972)	- Compressive strength in ref. samples (year measured) - % strength loss on exposure	Overall performance
1/ Nor PC (11.9 % C ₃ A)	None	0.50	1.1 x 10 ⁻¹⁰	0.50/ 20 yrs	- 48 MPa (1957) - 28 %	Severe attack
2/ Danish SRPC (5% C ₃ A & 10 % molère)	None	0.50	7.5 x 10 ⁻¹¹	0.10/ 20 yrs	- 55 MPa (1972) - 35 %	Good
3/ Finnish Ferrari Cement	None	0.51		0.13/ 20 yrs	Not established	Good
4/ American Type 5 SRPC (3.3 % C ₃ A)	None	0.50	1.7 x 10 ⁻¹²	0.09/ 20 yrs	- 50 MPa (1957) - 1-9 %	Very good
5/ Nor PC	Air entrained (4 %)	0.52	2.5 x 10 ⁻¹⁰	2.10/ 20 yrs	- 41 MPa (1957) - 34-53 %	Very severely attacked
6/ 85 % Nor PC	15 % SF*	0.62	1.04 x 10 ⁻¹¹	0.10/ 20 yrs	- 46 MPa (1972) - 31 %	Good
7/ 85 % Nor PC	15 % slag**	0.50	1.01 x 10 ⁻¹¹	1.40/ 20 yrs	- 37 MPa (1957) - 16-44 %	Severe attack
8/ Nor PC	8 % crushed limestone fines (D ₅₀ = 0.01 mm)***	0.52	7.1 x 10 ⁻¹¹	2.66/ 20 yrs	- 46 MPa (1957) - 30-31 %	Very severely attacked
9/ Nor PC	8 % crushed calcite fines (D ₅₀ = 0.03 mm)	0.51	1.6 x 10 ⁻¹⁰	1.56/ 18.9 yrs	- 54 MPa (1957) - 29-50 %	Severe attack
10/ Nor PC	Air entrained (4.3 %)	0.50	n.a	0.26/ 14.2 yrs	Not established -	Severe attack
11/ English sulfacrete (2.6 % C ₃ A)	None	0.50	n.a	0.06/ 14.2 yrs	- 72 MPa (1972) - 7 %	Very good
12/ 85 % Nor PC	15 % Trass	0.50	n.a	0.02/ 14.2 yrs	- 50 MPa (1972) - 6 %	Very good
13/ 85 Nor PC	15 % Trass & crushed calcite sand replacing sand fraction	0.50	n.a	0.11/ 14.2 yrs	Not established	Good
14/ 45 % Nor PC	45 % Trass 10 % Portlandite	0.50	n.a	0.06/ 14.2 yrs	- 44 MPa (1972) - 22 %	Very Good
15/ Danish Type 5 SRPC (0.9 % C ₃ A)	None	0.50	n.a	0.01/ 11.2 yrs	- 70 MPa (1972) - 16 %	Very good
16/ Danish Marine cement (0.9 % C ₃ A with 10 % molère)	None	0.50	n.a	0.01/ 11.2 yrs	- 66 MPa (1972) - 3 %	Very good

Note: 8 % of the sand fraction in Series no 8 and 9 was replaced by calcium carbonate fines.

Table 3: Blindtarmen sample data as received. Mix details from Fiskaa et al. [9].

Sample No.	Original No.	Old	Mix details where known	Condition as received
P01/1647/3	Series 1-18 <i>Exposed</i>		1952: Norwegian PC: 390 kg/m ³ w/c = 0.50	Up to 25mm of material loss from corners of the sample. Underlying area of ~10mm is rather soft and crumbly.
P01/1647/6	Unknown <i>Exposed</i>		Unknown	Up to 35mm of material loss from corners of the sample. Underlying area of ~10mm is rather soft and crumbly.
P01/1647/7	Unknown <i>Exposed</i>		Unknown	Outer heavily carbonated and carbonate encrusted surface. Slight material loss <2mm, corners up to max. 5 mm.
P01/1647/8	Unknown <i>Exposed</i>		Unknown	Up to 20mm of material loss from top corners of the sample.
P01/1647/9	Unknown <i>Exposed</i>		Unknown	Up to 20mm of material loss from top corners of the sample.
P01/1647/10	Unknown <i>Exposed</i>		Unknown	Up to 27mm of material loss from top corners of the sample.
P01/1647/11	Unknown <i>Exposed</i>		Unknown	Up to 15mm of material loss from top corners of the sample. Some outer surface softening.
P01/1647/12	Series 8 <i>Exposed</i>		1952: Nor PC with 8 % crushed limestone fines: 390 kg/m ³ w/c = 0.52	Up to 25mm of material loss from top corners of the sample.
P01/1647/13	Unknown <i>Exposed</i>		Unknown	Up to 30mm of material loss from top corners of the sample.
P01/1647/14	Unknown <i>Exposed</i>		Unknown	Up to 25mm of material loss from top corners of the sample.
P01/1647/17	Series 6-20 <i>Reference kept in tap water</i>		1952: Norwegian PC 85% silica fume 15%: 390 kg/m ³ w/c = 0.62	Sound.
P01/1647/18	Series 8-20 <i>Reference kept in tap water</i>		1952: Norwegian PC 390 kg/m ³ : limestone filler w/c = 0.52	Sound.
P01/1647/19	Series 11-10 <i>Reference kept in tap water</i>		1952: English sulfacrete w/c = 0.50	Sound.
P01/1647/20	Series 12-10 <i>Reference kept in tap water</i>		1952: Norwegian PC 85% natural pozzolana 15%: 390 kg/m ³ w/c = 0.50	Sound.

Table 4: Summary of identified samples (interpretation from [12]).

Sample numbers	Alum Shale Committee: Series numbers
P01/1647/3	Series 1-18 Nor PC
P01/1647/6	Series 1 Nor PC
P01/1647/7	Series 12 85% Nor PC & 15% natural pozzolana (German Trass)
P01/1647/8	Series 1 Nor PC
P01/1647/9	Series 1 Nor PC
P01/1647/10	Series 1 Nor PC
P01/1647/11	Series 1 Nor PC
P01/1647/12	Series 8 Nor PC & 8 % crushed limestone in sand fraction
P01/1647/13	Series 1 Nor PC
P01/1647/14	Series 1 Nor PC

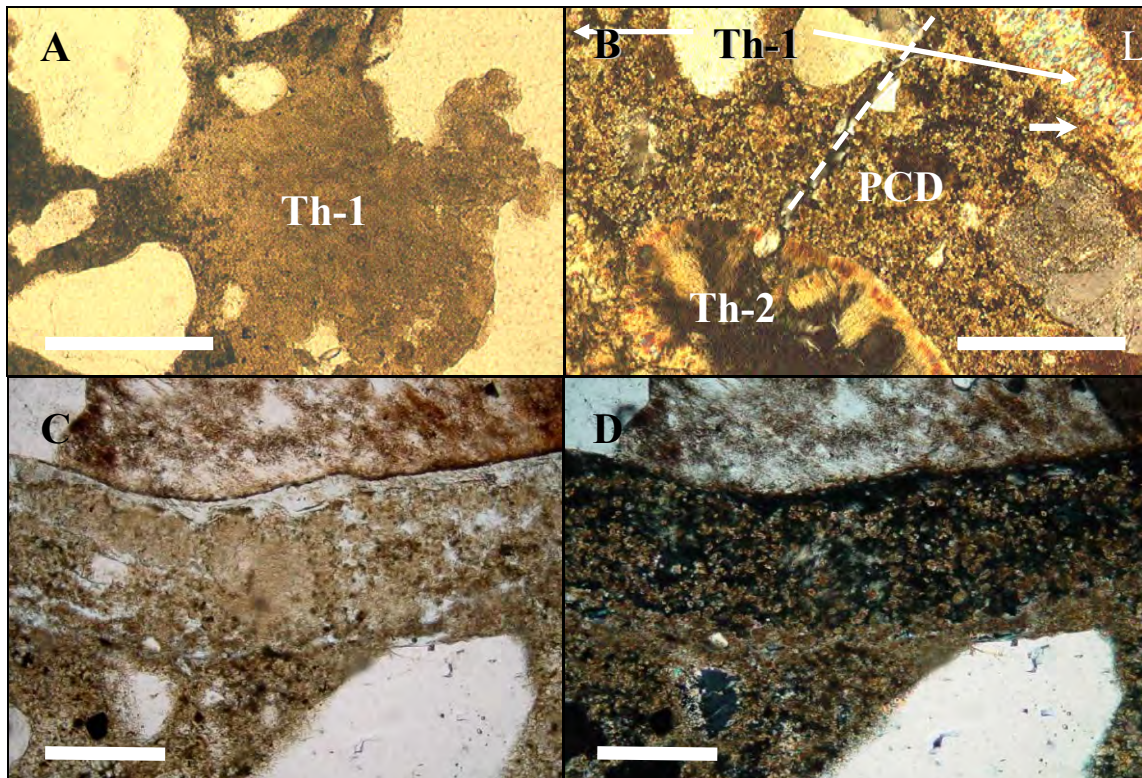


Figure 3: A) and B) Scale bars = 300 μm : A) Plane light: Sample 1647/7 (Series 12 Nor PC 85 with trass), showing evidence of Stage 1 incipient TSA (Th-1) at the expense of sound cement paste: i.e. with pristine C-S-H (left) at the edge of an air void (right). B) Crossed polars: Sample 1647/6 (Series 1 Nor PC without additives): Stage 1 TSA (Th-1) had formed locally within the cement paste matrix and along the margin with a biomicritic limestone aggregate (L). Stage 2 decalcification of C-S-H and associated Popcorn calcite deposition (PCD) at partial expense of Th-1 (small arrow). Subsequent Stage 3, full scale TSA (Th-2) formed at the expense of the assemblage PCD – decalcified C-S-H. Notice the micro crack (stippled line) restricted to the assemblage with PCD having formed at a high angle to the reaction front. C) Plane light and D) crossed polars: Scale bars = 0.2 mm: Sample 1647/6 with Stage 1 TSA associated with an adherence crack adjacent to a large granitic aggregate particle. This was followed by Stage 2 decalcification of C-S-H and PCD involving partial decomposition of thaumasite.

4.4 Microscopy of degradation products

4.4.1 Reference samples kept in tap water

The primary bonding of aggregate particles was good in all four reference samples (see Table 3). Cement paste micro cracking was rare to absent and of no significance. The general features suggest that the initial quality of test concretes was good. Samples 1647/18 (Series 8-20), 1647/19 (Series 1-20) and 1647/20 (Series 12-20) showed some local evidence of moisture transport. This was indicated by presence of minor secondary deposits of portlandite and sometimes ettringite and gypsum. Sample 1647/17 (Series 6-20: 85 % Nor PC with 15 % silica fume) with high $w/c = 0.62$ (cf. Table 2) showed almost no evidence of moisture transport after about 30 years in tap water.

4.4.2 Exposed samples displayed six reaction stages within their outer reaction zones

Microscopy of the outer friable reaction zone of each exposed sample unveiled six reaction stages developed as a rather ill defined pattern around an inner core of quite sound concrete. The overall deterioration processes were characterised by strong leaching and material loss at and near the surface, followed by ordinary carbonation, PCD and TF/TSA further inwards. The petrographic description focuses on the individual reaction stages and their interrelationship within the reaction zones. Intermingling relationships between stages 1 to 4 were common. In general there was no explicit evidence that quartz in aggregates had taken part in the thaumasite forming reactions. Terminology related to thaumasite types (I, II, III) follows the definitions in [11].*

4.4.2.1 Stage 1: TF and local TSA.

Unaffected thaumasite chiefly occurred within the deeper parts of the reaction zones. The adjacent cement paste matrix was essentially sound with evidence for some moisture transport as indicated by air voids sometimes heavily filled with secondary portlandite and – ettringite. At first non-deleterious TF formed within air voids, locally grading into incipient deleterious TSA forming at the expense sound cement paste (i.e. pristine C-S-H) (Figure 3A). Thaumasite had also formed along adhesion cracks around coarse biomicritic and sparitic limestone aggregate particles, and occasionally associated with granitoid particles. Thaumasite growth had in this case frequently developed into TSA at the partial expense of the cement paste matrix (Fig 3B, -C & -D). Simultaneous decalcification had taken place at this more advanced stage.

Thaumasite was also associated with micro cracks, which increased in abundance outwards across the reaction zones. These micro cracks were always sub-parallel to the secondary (deteriorated) outer prism surfaces. Crack bound thaumasite was notably formed within biomicritic limestone with some apparently unreacted pyrite, and was typically well developed near the outer edges of coarse aggregate particles in direct contact with apparently still intact cement paste matrix (Figure 4). The thaumasite here typically resembles plugs or wedges acting from the outside of the limestone aggregate: the remainder of the micro cracks being either completely empty or fringed with very scattered needle formed mineral (either ettringite or Type I thaumasite). The surrounding cement paste matrix here was essentially quite sound and had apparently not suffered significant decalcification. Crack bound thaumasite had also developed extensively within the cement paste matrix notably in the surface near domains of reaction zones, leading to a veined appearance. In addition, rather large calcite free aggregate sand particles had occasionally developed the same feature. Thaumasite veins swept around small relatively strong sand grains consisting of granite or quartzite and occasionally cut weaker small feldspar grains along their cleavages.

Thaumasite plugs and fillings in contact with limestone was usually characterised by highest birefringence (Type III), whilst thaumasite in air voids and in contact with cement paste and siliceous aggregate particles usually had lower birefringence (Type II). Stage 1 was well developed in both Series 1 (Nor PC) and Series 8 (Nor PC with limestone fines), whilst being of minor importance in Series 12 (Nor PC with German trass: 1647/7). In the latter case thaumasite was found in air voids with occasional transformation of C-S-H to thaumasite (incipient TSA) as well as a few incipient thaumasite “wedges” in the outermost part of limestone aggregate.

* See definitions, on page 57

4.4.2.2 Stage 2: Extensive decalcification of C-S-H and PCD

The process was characterised by variable Ca leaching of C-S-H and formation of PCD. Simultaneously early-formed thaumasite had also decomposed to PCD on a nearly isotropic substrate probably rich in silica gel (Figure 3B, -C, -D). Gypsum had occasionally formed in minor amounts upon decomposition of thaumasite suggesting that much of its sulfate were liberated for further attack. Subhedral relatively coarse calcite was deposited in air voids during this stage along with secondary portlandite and non-deleterious ettringite. Stage 2 was developed within the outer zone with thaumasite, still inside the outermost very friable concrete belonging to Stages 5 and 6. Decalcification with PCD was very important in Series 1 and 8 (Fig 3C,) whilst this assemblage was restricted to a narrow (< 1.5 mm) very scattered domain in Series 12 with natural pozzolana (sample 1647/7).

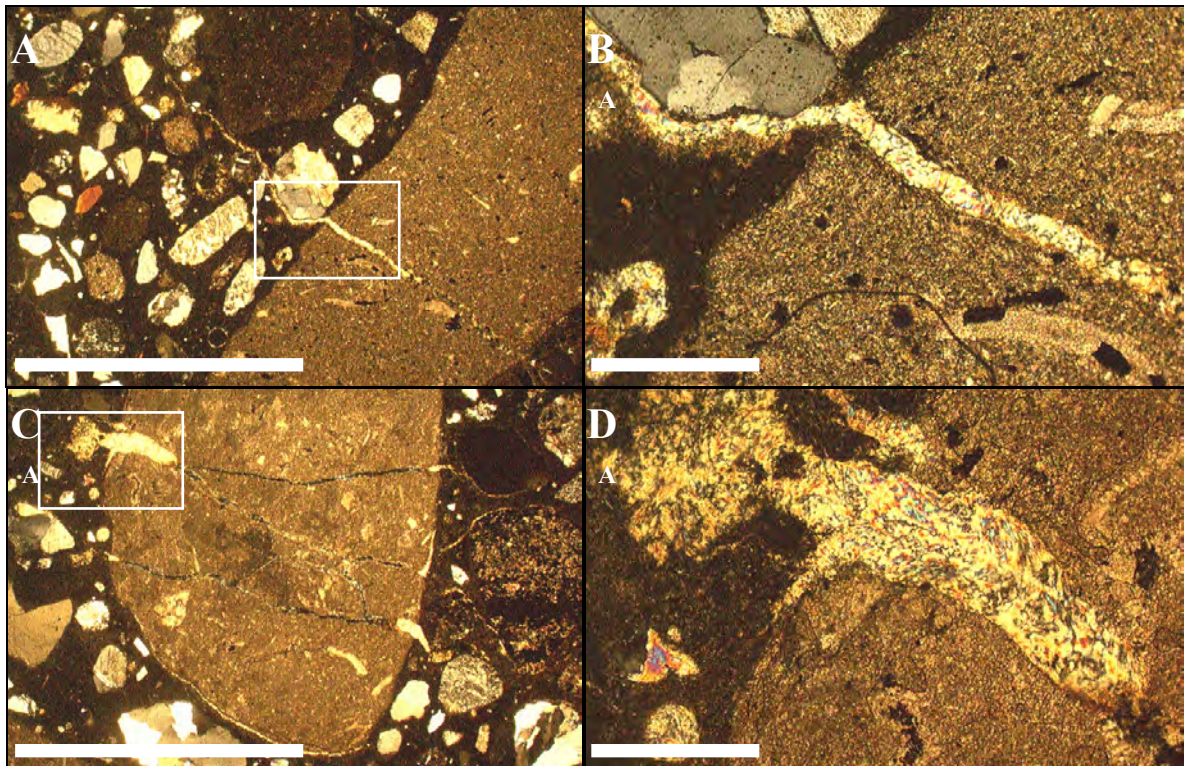


Figure 4: Crack development associated with thaumasite growth about 1-2 cm beneath the outer leached zone in Sample 1647/12 (Series 8 Nor PC with limestone fines). A) Most focused growth of thaumasite within the region where the micro crack straddles the cement paste matrix – biomicritic limestone aggregate interface. Notice that the crack dissipates in both directions. The joint in lower right was essentially open with sparse deposit of thaumasite. B) Close up detail from A showing high birefringence Type III thaumasite which grades into lower birefringence characteristic of Type II thaumasite in paste away from the interface. C) Overview of several thaumasite wedges, representing forceful growth along several micro cracks across the interface of biomicritic limestone and well-preserved cement paste matrix. Some micro cracks inside limestone were empty; others were partly filled with thaumasite or fringed with a very scattered needle shaped mineral (possibly ettringite or Type I thaumasite). D) Detail of thaumasite wedge sitting at the interface showing Type III thaumasite with 2nd order blue-green birefringence where in contact with limestone aggregate, and first order yellow birefringence (Type II) where in contact with cement paste matrix as well as at the termination at the empty crack (lower right). Notice pyrite (black) within limestone. Scale bars: A and C = 2.5 mm; B and D: = 300 μ m. Crossed polars.

4.4.2.3 Stage 3: Partial to extensive TSA at the expense of decalcified C-S-H and PCD

Interestingly the assemblage of decalcified C-S-H and PCD was found to be extensively replaced by a second generation of thaumasite (Th-2) in sample 1647/6 (Series 1 Nor PC). This reaction is illustrated in Figure 3B where a ca 1 cm² large thaumasite domain of full scale TSA had formed an embayed reaction front against the Stage 2 assemblage. The PCD rich depleted paste had developed a micro crack at a high angle to the front. Outside the image area, the thaumasite enclosed several small sand particles and the cement paste matrix was totally consumed. The growth was centred on a limestone particle. Crack bound thaumasite also formed during the second thaumasite forming phase in sample 1647/12 (Series 8 Nor PC with limestone fines), yet the relationship of Stages 1 through 4 seem to be much intermingled. Reaction Stage 3 was most explicitly demonstrated in sample 1647/6 (Series 1 Nor PC) but also occurred in other samples as thaumasite filled diffuse micro cracking which post-dated depleted cement paste matrix with PCD, typically in the middle outer parts of the reaction zone. The pozzolanic Series 12 (1647/7) with only minor effects of Stage 2 decalcification did not show any traces of Stage 3. Apparently the most extensive TSA was facilitated by pre-existing decalcification of the cement paste matrix.

4.4.2.4 Stage 4: Replacement of thaumasite by PCD.

Thaumasite belonging to Stage 1 and Stage 3 were decomposed to form PCD and a nearly isotropic substance (most likely a silica-rich gel). Also at this stage the reaction was contemporaneous with decalcification and PCD formation within the adjacent cement paste matrix. Stage 4 was extensively developed and increased in intensity towards the outermost leached domains. It involved both severely TSA affected paste as well as air void and crack bound thaumasite which ultimately was completely replaced. Also the large Stage 3 TSA area in Fig 3B showed evidence of replacement by later PCD. At the same time sparitic clear calcite formed within cracks in aggregate particles as well as air voids. Gypsum deposition was restricted to the outer domains of the overall friable reaction zone, strongly suggesting that most of the sulfate from thaumasite decomposition had been dissolved in water [3, 4]. Most features were found in all samples, except from sample 1647/7 (Series 12) within which neither thaumasite nor PCD was extensively developed.

4.4.2.5 Stage 5: Ordinary carbonation

This reaction rim, varying in thickness from about 1 to 5 mm, was characterised by an essentially fully carbonated cement paste matrix consisting of microcrystalline calcite near the surface (Figure 5). This form of carbonation shared all aspects of ordinary surface carbonation, and apparently had reached further out before the leaching reactions belonging to Stage 6 had taken over. Carbonation had caused shrinkage and development of significant micro cracking within Series 1 and 8, whilst being of less importance in Series 12 with trass.

4.4.2.6 Stage 6: Leached outermost concrete

The outermost leached domain is shown in Figure 5, as represented by sample 1647/7 (of Series 12). The same leaching pattern was found in all other samples, although much more extensively developed within Series 1 and Series 8. The surface region was directly influenced by the variable acidity of ground waters prevailing at the Blindtarmen test site (cf. Table 1).

The outermost edges of deteriorated secondary surfaces were covered by a thin (ca 200-400 µm) Fe-rust deposit, probably representing ferrihydrite or a ferric oxyhydroxide. No attempt was made to further identifying this material. Calcite fragments were found as

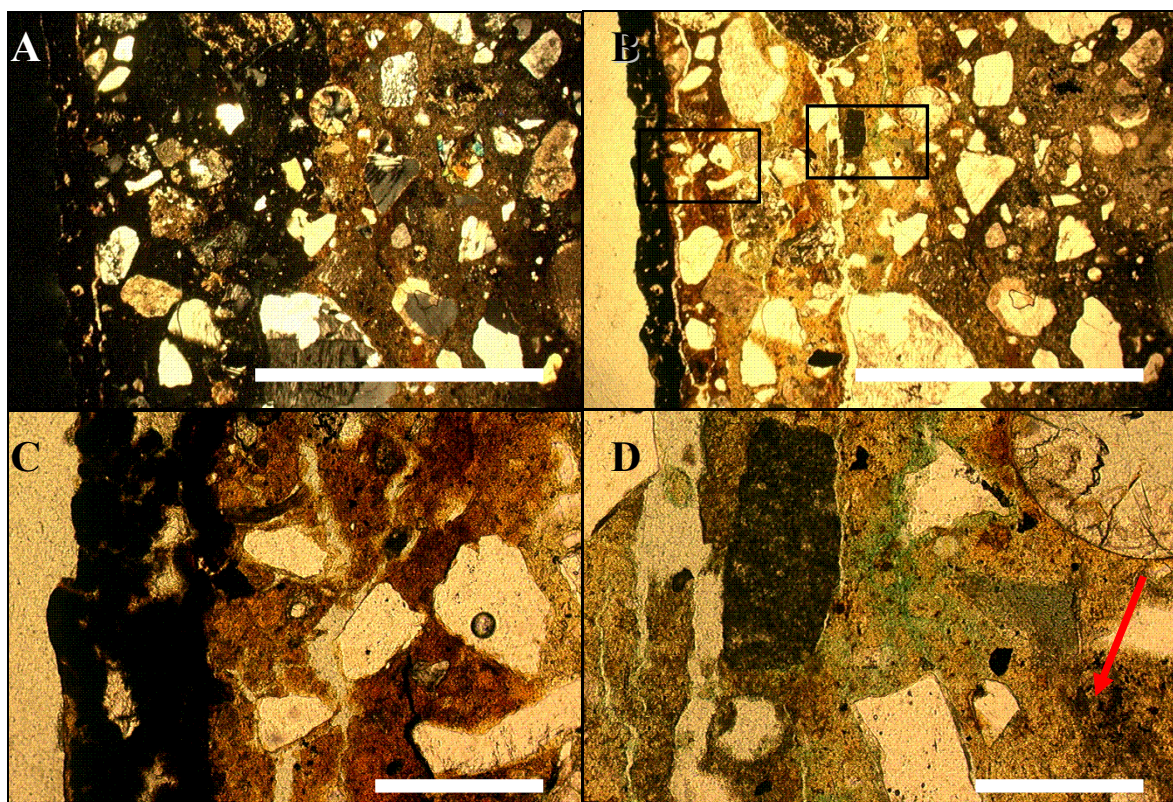


Figure 5: Effects of acid attack and carbonation in outer parts of sample 1647/7 (Series 12 Nor PC with trass). A) Crossed polars and B) plane polarised light of same domain, scale bar = 2.5 mm: Stage 6 outer ca 300 μm wide dark dense surface layer of Fe-hydroxide followed by a ca 2-2.5 mm very porous iron stained zone of extremely depleted carbonate free cement paste outside a distinct ca 2 mm thick fine grained carbonated zone (Stage 5) with somewhat Ca depleted cement paste inside (= Stage 2 far right). C) and D) in plane polarised light, scale bar = 300 μm : Outer dense Fe –deposit with calcite inclusions, sitting on extensively iron stained and microcracked very friable cement paste. D) Transition from inner leached cement paste into fine-grained carbonated zone: Lower right showing only local development of PCD (arrow) in Ca-depleted cement paste matrix. Middle right, ordinary carbonation: Upper right; air void filled with blocky calcite. Otherwise brown weak iron staining and pores (bluish green stain from preparation was not filling well; all sub-parallel microcracks appearing white are empty).

inclusions within the iron compound, presumably representing overgrown previous deposit material. Calcite had also frequently grown on the outer surface of the iron deposit. The cement paste matrix immediately beneath the Fe-deposit was characterised by an extremely Ca depleted and porous cement paste matrix usually devoid of calcium carbonate, extending from about 2.5 mm in Series 12 to about 3-5 mm in Series 1 and 8. Here the paste was strongly iron stained, the effect of which decreased inwards yet in many cases reaching into the domain of ordinary carbonation. Occasionally decalcified paste with PCD texture as well as cracks within aggregates was rust stained. Where exposed at the deteriorated surfaces, biomicritic and sparitic limestone aggregate particles were also coated by the Fe deposit. Calcite at the surface was in some cases characterised by rounded forms and in other cases the iron deposit followed the calcite cleavage pattern. It appears that calcite had sometimes been dissolved in contact with the fluids associated with deposition of Fe-compounds.

Surface (sub-) parallel micro cracking was well developed within the strongly leached and Fe-stained material. Such cracking also sometimes reached into the carbonated domains. It seems likely that the lost material at the prism margins must have been characterised by the same sort of material. The outer Fe-rust deposit was always typically *coating the outer prism secondary surfaces*. It has been reported [9] that such iron stains had frequently developed after only a short period of exposure at Blindtarmen, suggesting that the iron staining and leaching had moved inwards as deterioration proceeded.

4.5 Discussion

4.5.1 Chemical reaction mechanisms

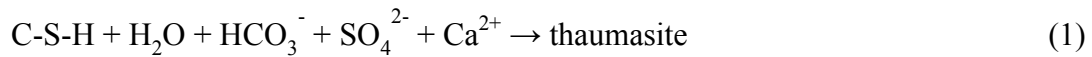
The six reaction stages within the total reaction zone represent degradation mechanisms at rather low temperatures (probably about 1-10 °C), which were triggered by the ground water chemistry at the Blindtarmen test site. This was characterised by fluctuating sulfate contents and pH, typically varying between about 2500 to 4200 mg/L and 5-6 and 2-3, respectively [9]. Available data suggest that the higher sulfate level was combined with the most acid conditions (Table 1). Moreover, since total carbonate contents in bulk concrete increased with deterioration [9] also some carbonate species must have been available in ground water. Within the pH interval 5-6 the predominating carbonate species are carbonic acid (H_2CO_3) and some bicarbonate (HCO_3^-), whilst at pH = 2.5-3 carbonic acid is prevailing (cf. Appelo and Postma [13]). Thus the ground water was characterised by presence of both carbonic- and sulfuric acid, which is very aggressive towards concrete. In contrast, pristine cement paste is characterised by a very alkaline pore fluid, and the overall deterioration must therefore be explained within the framework of a steep pH gradient across the reaction zones.

In the further discussion of the reaction stages it is necessary to understand the behaviour and stability ranges of the involved solids in presence of a neutral to acid water phase. C-S-H is stable at pH > 12.5, which formed at even higher pH during cement hydration. Below this value C-S-H dissolves incongruously by preferred leaching of Ca, which then becomes strongly enriched in the pore fluid. In the beginning, Ca leaching buffers the pH at ca 12.4 until, when present, all portlandite has been dissolved. Upon further leaching Ca is still being released at steadily dropping equilibrium pH. Having reached pH about 10.5 -11 the Ca/Si ratio in C-S-H has dropped to about 0.8 to 0.9 and dissolution is then nearly congruent [14]. The residue after extensive leaching may frequently consist of a Si-rich amorphous phase [15]. According to work summarised by Crammond [10], thaumasite ($\text{CaSiO}_3 \cdot \text{CaSO}_4 \cdot \text{CaCO}_3 \cdot 15\text{H}_2\text{O}$) may only form at pH \geq 10.5. Gaze and Crammond [16] found experimental evidence that once formed thaumasite could be stable to pH down to about 6. However, their conclusion was based on X-ray diffraction of powders, which does not discriminate between late stage and relict earlier minerals: Indeed later experimental work suggests that thaumasite under certain circumstances is unstable at pH below 12 (Jallad et al. [17]). Based on thermodynamic calculations Bellmann [18] found that increasing pore fluid pH generally requires increasing sulfate concentrations to form pure thaumasite. This “protective effect” is most efficient in C-S-H with relatively low Ca/Si ratios devoid in portlandite, where the sulfate concentrations required for thaumasite formation exceed 5000 mg/L. In marked contrast, at normal elevated Ca/Si > 1.7 in presence of portlandite or calcite, the required sulfate contents may theoretically be about 5 mg/L at pH 12.5 or 100-300 mg/L at pH 13-13.5. Calcite is stable at pH \geq 7 and the overall solubility increases by about three

orders of magnitude when pH is dropping from ca 6-7 to about 2 (cf. [13]). Gypsum is two orders of magnitude more soluble than calcite but can be stabilised in the cement paste during acid attack if saturation level is high. Collett et al. [19] studied the influence of carbonate speciation on thaumasite formation, and found that bicarbonate played an important role in TSA. The elevated water solubility of CO₂ at low temperatures was regarded as the main reason that TSA preferentially develops around 5-10 °C.

The following reactions schemes are indicated by the petrographic description of the Blindtarmen test prisms, most of which are empirical and not truly balanced. The term “C-S-H” in the below reaction schemes is to be understood that associated portlandite was also present, unless otherwise stated. The Nor PC used was rich in calcium [9].

Stage 1 incorporated several reactions, which apparently took place during an early increment in the inner parts of the reaction zones. The first formation of thaumasite (CaSiO₃.CaCO₃.CaSO₄.15H₂O) was characterised by deposition as non deleterious TF in air voids and associated incipient deleterious TSA at the expense of intact C-S-H:



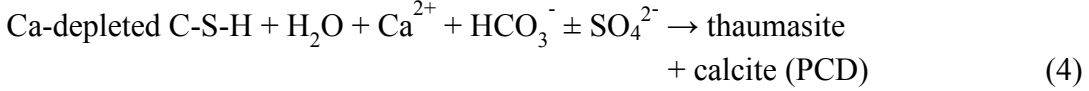
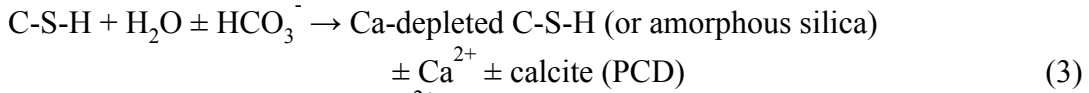
No calcite or gypsum was observed in the adjacent C-S-H (Figure 3A), indicating that bicarbonate and sulfate was provided by the water phase. Moreover no secondary ettringite predated thaumasite, and there was no portlandite formed along with thaumasite, which has been traditionally assumed when the reactants in Reaction 1 are involved (cf. [18] and references therein). In view of stability constrains given above, Reaction 1 apparently took place at pH about 12.4 (limit for portlandite dissolution) to 13.5.

Thaumasite plugs also formed as “TF” in association with micro cracks in limestone and along aggregate interfaces with more or less intact surrounding C-S-H:

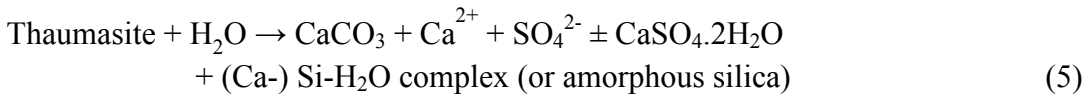


Bellmann [18] suggests that thaumasite can be formed from C-S-H along with calcite and portlandite in presence of low sulfate concentrations. In the Blindtarmen case there was no associated gypsum detected in association with thaumasite plugs, and the sulfate and possibly some calcium were provided by the concrete pore water. Reaction 2 might proceed at high pH (12.5-14) because the required sulfate is much lower than the ground water concentration. In this context it seems significant that thaumasite plugs were always well formed and that the high birefringence (Type III) was clearly associated to the direct contact with limestone (Figure 4). Accumulated analytical data at BRE suggests that Type III thaumasite contains more carbonate than Type II (Sibbick et al. [20]). Recalling that calcite dissolution and availability of bicarbonate is much enhanced at pH < 6-7, whilst thaumasite only can form at much higher pH it seems possible that the introduction of mildly acidic water could have accentuated calcite dissolution and thaumasite growth: Thus perhaps thaumasite plugs formed along a pH gradient ranging from ca 5-6 to >13. These limits represent the influence from ground water and cement paste pore fluids, respectively. This would require that the average pH was maintained at about 12. A sulfate contribution from pyrite (Figure 4) cannot be excluded.

At a more advanced stage TSA was more clearly associated with decalcification of C-S-H under influence of water. The following simultaneous reactions schemes seem relevant, reflecting pore water 10.5 < pH < 12.5:



Stage 2 involved extensive decalcification of C-S-H similar to Reaction 3 and breakdown of thaumasite according to Reaction 5. Gypsum ($\text{CaSO}_4 \cdot 2\text{H}_2\text{O}$) occasionally formed near the surface; whilst sulfate was mostly liberated for further attack. Owing to strong decalcification, formation of PCD and breakdown of thaumasite are closely related. These reactions appear to be restricted to a pore fluid pH range between about 7.0 and 10.5. This is constrained by the lower stability of calcite and a pH level typical for extensively leached C-S-H.



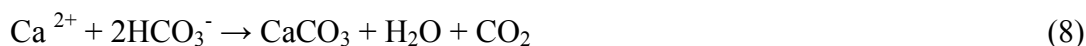
Stage 3: Full scale TSA took place at the expense of strongly decalcified C-S-H and abundant PCD. Decalcified C-S-H contains a significant amount of amorphous silica [15]. A balanced reaction, which is slightly modified after Bellmann [18], is given in Eq.6



This reaction is thermodynamically possible due to the much higher solubility of amorphous silica relative to quartz [18]. In the present case the reaction went to completion, and the PCD/substrate ratio was also very near 2:1. Evidently Reaction 6 is a very efficient pathway for the development of full scale TSA (see Figure 3B), the efficiency of which seems to be directly dependent on the extent of previous Ca leaching of C-S-H and PCD: The amount of free amorphous silica formed should represent the rate limiting step, being independent of remaining presence of partly leached C-S-H with higher Ca/Si ratios. The present authors would argue that the reaction in the Blindtarmen samples was also sustained by simultaneous release of carbon dioxide, which upon dissolution in water should assist in further reaction of Popcorn calcite (cf. [13]). Thermodynamic calculation does not consider kinetics and is, therefore, most relevant for thaumasite formation (TF). Extensive TSA and rapid conversion of the matrix, such as would occur at this stage, is therefore considered to take place at high levels of supersaturation and fast ingress of aggressive of ground water [18]. This is corroborated by the petrographic observations, showing that Stage 3 was located within the outer parts of the total reaction zones just beneath the outer porous and acid leached concrete. TSA according to Reaction 6 appears to require a local rise in pH relative to Stage 2, for example contributed by leaching of nearby intact cement paste. However, if we still accept 10.5 as a lower pH limit of thaumasite formation [16], which also allows for extensive carbonate precipitation, the reaction would proceed chiefly due to changes in outer porosity, leading to kinetically favourable conditions for full scale TSA.

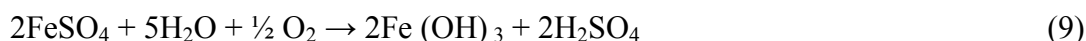
Stage 4: Thaumasite breakdown followed Reaction 5 during this stage, leading to extensive calcite formation within the outer reaction zone. Thus the pore fluid pH was about 7-10.

Stage 5: Ordinary carbonation was most probably formed in water, although we cannot exclude the possibility that the Blindtarmen samples were above water level some times. The following reactions are relevant:



The pore fluid pH is typically 8-9 in extensively carbonated cement paste [15].

Stage 6: The role of rust deposits was investigated by the Alum Shale Committee [1, 6, 9]. It was considered that the iron sulfides would give rise to soluble iron sulfate which further reacted with water and oxygen to form ferric hydroxides and sulfuric acid according to the following redox reaction:



Reaction (9) readily takes place from pH > 4-5 depending on oxidising conditions [13]. The iron deposits reflect the confrontation of acidic ground water with more neutral or alkaline fluids within the concrete. The iron staining of the matrix underneath must reflect early stage influx of dissolved ferrous iron into an already porous and permeable cement paste microstructure. Reaction 9 would produce acid until the outer rust deposit had reached a critical thickness leading to exhaustion of available dissolved iron. Accordingly sulfuric acid was allowed to penetrate further inward. Temporary acid dissolution in the outermost reaction zones led to wider access to a buffered more neutral yet sulfate laden pore fluid deeper inside. Hence all reaction stages moved inwards.

Carbonic acid was also acting from outside but was neutralised by internal fluids. At near-neutral pH bicarbonate is the essential carbon species. This would easily react with leached Ca and form calcite. This mechanism might well explain the surface near clear sparitic calcite deposits on cracks and voids. The frequent presence of such calcite, also outside and within the rust surface deposits, represents a manifestation of the fluctuating pH conditions within the Blindtarmen ground water.

4.5.2 Physical response related to thaumasite growth and decalcification with PCD

The petrographic observations suggest the existence of *two principally different forms of deleterious thaumasite growth*, namely 1) classic TSA involving partial or complete degradation of the cement paste matrix and 2) thaumasite growth giving way to deleterious crack development similar to some forms of “classic” ettringite-based sulfate attack. It was demonstrated above that classic TSA is closely associated with decalcification and PCD. Because these reactions take place at the expense of the binder, this process does not involve any significant deleterious volume change. Yet, adhesion cracks around aggregate particles seem to have developed during Stage 2 thaumasite breakdown to PCD (Figure 3C and D), which indicated shrinkage, loss of cementitious properties and strength reduction. There is also some evidence of localised action of crystallisation pressure during Stage 3: The microcracks within very fragile leached and PCD dominated matrix, at a high angle to the thaumasite growth front may well reflect this (Figure 3B).

The thaumasite plugs and wedges related to crack development did not replace the cement paste matrix, and as such represents the so-called, Thaumasite formation (TF). Crack bound thaumasite is usually regarded as a non-deleterious deposit on pre-existing flaws. However, in the present case there was no evidence for micro cracking prior to the thaumasite plugs. Indeed significant thaumasite growth was restricted to the aggregate – matrix interface, whilst the internal parts of the cracks were essentially empty, and sometimes fringed by very scattered ettringite or thaumasite needles. This contrasts markedly with passive deposition, which should have filled up along the entire crack. Thus, the thaumasite plugs seem to indicate development of microcracking by high crystallisation pressures.

A high level of supersaturation is required in order to develop a high crystallisation pressure. The above chemical considerations have shown that thaumasite can be formed according to Reaction 2 at low sulfate concentrations and high pH. Bellmann [18] calculated that only 5 mg/L of sulfate was required at pH 12.5, or 100-300 mg/L at higher pH such as pore solutions in pristine cement pastes. A realistic crystallisation pressure was calculated from the following conservative input: Considering that pH at the limestone – matrix interface was initially high we assume that the saturation of thaumasite was sustained at 300 mg/L. In contrast the ground water concentration is considered to be 2000 mg/L. Allowing for loss of sulfate to carbonated cement paste matrix farther outside we assume that the sulfate concentration at the reaction site was 1500 mg/L. This concentration is 5 times higher than the saturation level for TF. The crystallisation pressure was calculated using Equation 10 (Correns [21]):

$$P = \frac{RT}{V} \ln \left(\frac{C}{C_s} \right) \quad (10)$$

P is the crystallisation pressure in atm; R is the gas constant = 0.082 L-atm/mol; T = absolute temperature (K); V = the molar volume (dm³/mole); C = solution concentration and C_s = saturation concentration (mol/L). According to the Russian Mincrust database the molar volume of thaumasite is 0.32988 dm³/mole-degree. From these data the calculated crystallisation pressure at 5 °C = 111.188 atm, which corresponds to 10.9 MPa. This crystallisation pressure is much higher than required to induce cracking in the Blindtarmen test prisms. Accepting that the tensile strength of concrete is about 10 % of the compressive strength, the data in Table 2 (Series 1 and 8) indicates tensile strengths in the order of 3 MPa when accounting for strength loss after long term exposure. Equation 10 only gives the maximum crystallisation pressure; other factors, such as low contact angle may significantly reduce this pressure [22]. However, the contact angles between thaumasite long axes and crack walls are not generally low and the input concentrations must in fact be regarded as conservative. Yet this pressure estimate is perhaps still too high.

This calculation does support the petrographic evidence. It seems that aggressive highly supersaturated fluids were channelled along the aggregate – matrix interface. Small initial cavities on the aggregates surfaces would represent preferential sites for thaumasite growth and development of crystallisation pressures, ultimately leading to splitting. Also, thaumasite formed along aggregate grain boundaries could have developed elevated pressures. If the calculated crystallisation pressure is realistic, it should be high enough to split most concrete aggregates. Therefore the inferred process should not necessarily be restricted to moderately strong limestone aggregates, but possibly under certain circumstances lead to

cracking of large aggregate particles of any kind. For these reasons the significance of so called non-deleterious TF should always be critically assessed in each case studied.

4.5.3 Physical response related to outer carbonation, acid leaching and iron staining

Moum and Rosenqvist [1] stated that dissolved iron by entering the cement paste matrix would cause implosion of air void walls deep inside the concrete: air would be depleted in oxygen during precipitation of iron hydroxide, leading to a strong under pressure resulting in collapse. Our petrographic investigations did not lend support to this mechanism, because ferric iron deposits did not occur in air voids at depth. The outermost parts of the total reaction zone was characterised by very open porous and friable concrete, which was directly influenced by ground water interaction. Thus development of negative pressure related to iron deposition is considered impossible: Fe-compounds should rather exert a crystallisation pressure. However, instead ordinary carbonation, acid leaching and iron staining (Stages 5 and 6) led to overall shrinkage and severe micro- and macro cracking.

4.6 Comparison with modern sprayed concrete used for rock support: the durability –life time perspective

Recently, TF, TSA and PCD were reported from young steel fibre reinforced concrete used for rock support in two tunnels and a road cut in Oslo [3, 4]. These sprayed concretes were made with SRPC and silica fume (about 6-8 % by cement weight) and were employed in direct contact with the harmful Alum Shale. TF and TSA were frequently associated with contemporaneous and later stage PCD, suggesting the presence of a TF-TSA-carbonation process. Influence from acidic water was, however, only found in rare cases. The investigated sprayed concretes were of similar initial quality (w/c-ratio = 0.43-0.5) but of different age. Deterioration had started after less than 2 years of exposure and developed into local spalling and TSA-calcite mush formation after less than 13 years.

The Alum Shale Committee expected that concretes subjected to a hydraulic gradient should be more affected by Alum Shale derived attack than the Blindtarmen test samples, which were influenced by hydrostatic conditions. It is important to realise that the ground water compositions at the two different settings thus far studied were not the same. The previously investigated sprayed concretes were under influence of water characterised by sulfate (600-2000 mg/L), bicarbonate (100-275 mg/L) and pH around 7. In contrast the Blindtarmen waters were generally more acidic (pH 2-6) with a higher overall sulfate concentration (2500-4000 mg/L). The variability of Alum Shale water compositions is generally even wider, with sulfate > 5000 mg/L and pH about 1.3.

Our sprayed concrete cores were attacked from both sides of the concrete slab with a sounder internal core similar to the Blindtarmen prisms. In some sprayed concretes TF and TSA and internal carbonation had also developed along internal layers. Thus, the deteriorated thicknesses were added together (T_a = affected) and compared with the initial thicknesses (T_0). Similarly for the Blindtarmen samples, reaction zones on two opposite sides were added, and also accounting for lost material and more deteriorated corners. The three Blindtarmen samples in Figure 6 represent typical levels of deterioration for each mix (e.g. Series 1, 8 and 12). The thick stippled line is representative for the development of Nor PC with 15 % SF exposed at Blindtarmen (initial thickness = 10 cm), whilst the thick full line represents the

development of an approximately 10 cm thick sprayed concrete. Sprayed concrete sample plotting above and below this line were thinner and thicker, respectively.

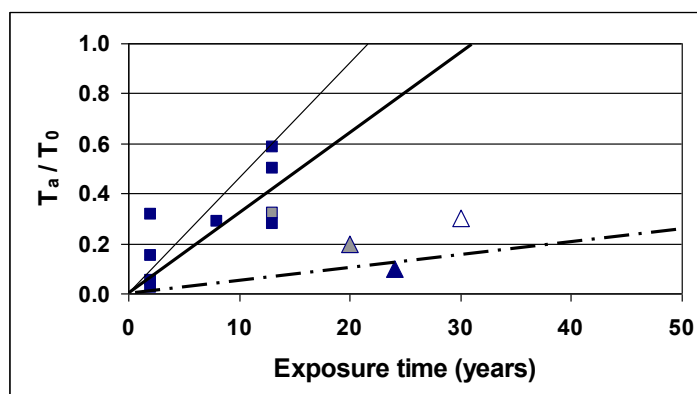


Figure 6: Comparison of deteriorated thickness (T_a) versus initial thickness (T_o) for SRPC based sprayed concrete with SF on Oslo Alum Shale (squares) [4]), with exposed Blindtarmen test prisms (triangles; filled = Series 12 Nor PC with natural pozzolana; dark grey = Series 8 Nor PC with limestone filler; open = Series 1 Nor PC reference). w/c –ratios 0.45-0.5. The thick full line approximately corresponds to initial sprayed concrete thickness = 10 cm whilst the thick stippled line represents Blindtarmen Nor PC with SF [5].

The diagram shows that the sprayed concretes with silica fume have deteriorated faster than the pozzolanic samples exposed at Blindtarmen. The designed life time for sprayed concrete in tunnels is 50 years. Using $T_a/T_o = 1.0$ (entire thickness transformed) as criterion, the hypothetical life time for sprayed concrete on Alum Shale without significant influence of acidic water corresponds to about 30 years for a 10 cm thick spray. However, sprayed concrete layers are frequently 6-7 cm thick, so the lifetime could be 20 years. It should further be noted that spalling and local mush formation had developed in concretes thicker than 10 cm. The corresponding lifetime for pozzolanic mixes under static conditions and under influence of simultaneous acid attack is much longer. We have not studied sprayed concrete deterioration in contact with waters of similar composition to the Blindtarmen test site. However, it is evident that influence of a more acidic: sulfate and bicarbonate enriched ground water should potentially lead to full deterioration of the entire sprayed concrete layer after less than 20 years.

Finally it must be admitted that the deteriorated zones in our sprayed concrete samples were less friable than the reaction zones within the Blindtarmen prisms. It is therefore possible that the sprayed concretes in contact with circum neutral water will retain their overall bearing capacity for a longer period of time than indicated by Figure 6. Indeed concrete in contact with rather dry Alum Shale should remain essentially unaffected.

4.7 Conclusions

The previous Blindtarmen test (1952-1982) designed by the Norwegian Alum Shale Committee (1947-1973) provided very important results on earlier concrete mix design. The present study is the first petrographic investigation of available test prisms from the Blindtarmen. We conclude:

- 1) The classic sulfate attack in Oslo was essentially due to Thaumalite Sulfate Attack (TSA) and Popcorn Calcite Deposition (PCD), closely associated with effects of acid attack. This stands in marked contrast to the conclusion drawn by the Alum Shale Committee.
- 2) The reaction zone around individual test prisms displayed a six stage reaction pattern involving TF-TSA and decalcification with PCD in its inner domains and significant acid leaching acting from the outside surfaces.
- 3) The details of the reaction stages clearly demonstrated that the outer deteriorations formed along a steep pH gradient, where outer acid leaching made way for deeper penetration of aggressive waters and TF – TSA – PCD where the concrete pore fluid pH was still elevated.
- 4) Full-scale TSA was most efficient after partial or complete decalcification and PCD in the cement paste matrix, the rate of which apparently depends on the amount of free amorphous silica formed by Ca leaching of C-S-H.
- 5) Isolated thaumasite growth, resembling non-deleterious TF, had developed high crystallisation pressures and deleterious microcracking of large aggregate particles, mostly limestone.
- 6) Comparison with modern sprayed concrete used for rock support in tunnels in Alum Shale suggests that concrete under influence of a significant hydraulic gradient deteriorates much faster than the Blindtarmen samples. The lifetime of sprayed concrete is apparently 20-45 years in contact with circum neutral pH. Alum Shale water, but less than 20 years in contact with acidic Alum Shale water.

4.8 Glossary of definitions and abbreviations

Thaumasite: Hexagonal mineral with composition $\text{CaSiO}_3 \cdot \text{CaCO}_3 \cdot \text{CaSO}_4 \cdot 15\text{H}_2\text{O}$.

Thaumasite Type I: A highly porous needle-like crystalline material. Colourless to very pale yellow in plane light. Birefringence; near isotropic to 1st order white (0.000-0.005).

Thaumasite Type II: Closely spaced needle-like crystals forming quite massive flow like structures. Light straw yellow to bright yellow in plane light. Birefringence; 1st order creamy white to pale yellow (0.005-0.007).

Thaumasite Type III: Dense well ordered needle-like crystals. Yellow tinted in plane light. Birefringence typically 2nd order blue-green (0.007-0.027).

Ettringite: Trigonal mineral with composition $3\text{CaO} \cdot \text{Al}_2\text{O}_3 \cdot 3\text{CaSO}_4 \cdot 31\text{H}_2\text{O}$.

C ₃ A	<i>Tricalcium aluminate</i> : Cement clinker mineral composed of $3\text{CaO} \cdot \text{Al}_2\text{O}_3$
C-S-H	<i>Calcium silicate hydrate</i> : The most abundant cement hydrate with approximate composition $\text{CaO} \cdot \text{SiO}_2 \cdot \text{H}_2\text{O}$. Responsible for concrete strength.
PCD	<i>Popcorn Calcite Deposition</i> : A form of internal carbonation with deposition of relatively coarse calcite associated with bicarbonate influx and decalcification of the cement paste matrix, ultimately leading to very friable concrete.
PC	<i>Portland Cement</i> : Cements with ordinary elevated C ₃ A contents

SF	<i>Silica Fume</i> : Amorphous bi-product from ferro-silicium manufacturing, very rich in silicium dioxide. Also referred to as microsilica.
SRPC	<i>Sulfate Resisting Portland Cement</i> : Cements with low C_3A content
TF *)	<i>Thaumasite Formation</i> : Non-deleterious early stage deposition of thaumasite within voids and pre-existing microcracks.
TSA	<i>Thaumasite Sulfate Attack</i> : Deleterious thaumasite growth forming at the expense of the cement paste matrix, ultimately degrading to a soft mush.

Thaumasite terminology based on reference [11]: *) In the present paper it was demonstrated that thaumasite deposition resembling TF may develop high crystallisation pressure on microcracks.

4.9 Acknowledgements

The authors are indebted to former head of the Geology Department at the Norwegian Road Research Laboratory Arne Grønhaug for sharing his knowledge with us. We are also grateful to Ulf Fredriksen, Jørn Grøndal and Svein Tollefsen from Oslo Municipality's Geotechnical Division for advice and help at Blindtarmen during 2000. Claus K Larsen, Norwegian Public Roads Administration Oslo, is thanked for his successful work on locating the old samples and a dirty journey together with PH to the bottom of "the Appendix". Tom Farstad, NBI Oslo, kindly provided a slice from each of the remaining test prisms. Simon Lane and Derek Metcalf, of the Building Research Establishment, Watford, UK provided invaluable technical assistance. The authors would also like to thank the UK government's Construction Directorate and Norwegian Public Roads Administration for funding the joint BRE/NPRA work on TSA. Our joint research colleague Dr. Norah Crammond formerly of the BRE is thanked for her extensive contribution to this research project.

4.10 References

1. Moum J, Rosenqvist, IT. Sulphate Attack on Concrete in the Oslo Region. Journal of the American Concrete Institute 1959; 56: Title 56-18, 8 pp.
2. Hagelia P, Grønhaug A. Thaumasite – infection causing concrete deterioration. *Våre Veger* 2000; 9: 54-55 (in Norwegian).
3. Hagelia P, Sibbick RG, Crammond NJ, Grønhaug A Larsen CK. Thaumasite and subsequent secondary calcite deposition in sprayed concretes in contact with sulfide bearing Alum Shale, Oslo, Norway. Proc 8th Euroseminar on Microscopy Applied to Building Materials, Athens, Greece, September 2001; 131-138.
4. Hagelia P, Sibbick RG, Crammond NJ, Larsen CK. Thaumasite and secondary calcite in some Norwegian concretes. *Cement and Concrete Composites* 2003; 25: 1131-1140.
5. Fiskaa O. Concrete in Alum Shale. Norwegian Geotechnical Institute 1973; Publication No. 101: 12 pp (In Norwegian with English summary).
6. Bastiansen, R., Moum, J. and I.Th. Rosenqvist. Contribution to high light certain construction problems associated with Alum Shale in Oslo. Norwegian Geotechnical Institute 1957; Publication No. 22: 69 pp (In Norwegian with English summary).
7. Sopp OI. Contribution to the understanding of the Alum Shale swelling mechanism. Thesis, University of Oslo, Oslo, Norway; 1966 (In Norwegian).

8. Antun P. Sedimentary pyrite and its metamorphism in the Oslo Region. *Norsk Geologisk Tidsskrift*; 1967; 47:3: 211-235.
9. Fiskaa, O., Hansen, H. and Moum, J. (1971): Concrete in Alum Shale, Norwegian Geotechnical Institute, Oslo, Publication No. 86. 32pp (in Norwegian with English summary).
10. Crammond NJ. The thaumasite form of sulfate attack in the UK, *Cement and Concrete Composites* 2003; 25: 809-818.
11. Department of Environment, Transport and the Regions, UK. The thaumasite form of sulfate attack: Risks, diagnosis, remedial works and guidance on new construction, Report of the Expert Group, 1999; 180 pp.
12. Hagelia P, Sibbick RG. Thaumasite sulfate attack, popcorn calcite deposition and acid attack in concrete stored at the “Blindtarmen” test site Oslo, from 1952-1982. In: Fernandes I, Guedes A, Noronha F, Teles M, Anjos Ribeiro M (Eds.), Proceedings of the 11th Euroseminar on Microscopy Applied to Building Materials (CD-rom).
13. Appelo CAJ, Postma D. *Geochemistry, ground water and pollution* (2nd Ed.): A.A. Balkema Publishers; 2005: 649 pp.
14. Harris AW, Manning MC, Tearle WM, Tweed CJ. Testing of models of the dissolution of cements-leaching of synthetic C-S-H gels. *Cement and Concrete Research* 2002; 32: 731-746.
15. Taylor HFW. *Cement Chemistry* (2nd Ed.). Thomas Telford Publishing; 1997: 459 pp.
16. Gaze ME, Crammond NJ. The formation of thaumasite in a cement: lime: sand mortar exposed to cold magnesium and potassium sulfate solution. *Cement and Concrete Composites* 2000; 22: 209-222.
17. Jallad KN, Santhanam M. Cohen MC. Stability and reactivity of thaumasite at different pH levels. *Cement and Concrete Research* 2003; 33: 433-437.
18. Bellmann F. On the formation of thaumasite $\text{CaSiO}_3 \cdot \text{CaSO}_4 \cdot \text{CaCO}_3 \cdot 15\text{H}_2\text{O}$: Part II. *Advances in Cement Research* 2004; 16: 3: 89-94.
19. Collett G, Crammond NJ, Swamy RN, Sharp JH. The role of carbon dioxide in the formation of thaumasite. *Cement and Concrete Research* 2004; 34: 1599-1612.
20. Sibbick RG, Crammond NJ, Metcalf D. The microscopical characterisation of thaumasite. *Cement and Concrete Composites* 2003; 25: 831-838.
21. Correns CW. Growth and dissolution of crystals under linear pressure. *Discussions of the Faraday Society* 1949; 5: 267-271.
22. Scherer GW. Crystallisation in pores. *Cement and Concrete Research* 1999; 29: 1347-1358.

Chapter 5

C, O and S isotopic signatures in concrete which have suffered thaumasite formation and limited thaumasite form of sulfate attack

“In order to assess the environmental state of an area, anthropogenic influences, as well as natural processes such as bedrock weathering, must be considered”

Helena Falk, Ulf Lavergren & Bo Bergbäck

Thaumasite formation (TF) and limited Thaumasite sulfate attack (TSA) has recently been discovered in sprayed concretes in contact with pyrrhotite-, pyrite- and calcite bearing Alum Shale in Oslo. In concretes, several types of calcite occur, including internal Popcorn calcite formed by replacement of both thaumasite and calcium silicate hydrate (C-S-H). In an attempt to throw further light on the origin of carbonates and sulfates involved, we have used the laser ablation probe to characterise these secondary minerals with respect to stable isotopes (C, O and S). Mitigation as well as repair may in several cases depend much on correct characterisation and location of the fluids provenance, and stable isotopic characterisation may be an appropriate tool to do so. The preliminary results of this study indicate a complex open system with influence of fluids from several sources. There is a general difference in signatures between ordinary surface carbonation and internal carbonation associated with thaumasite. Calcite deposits within the Alum Shale/concrete contact zone show highly variable isotopic signatures reflecting a composite origin, probably significantly influenced by atmospheric CO₂. The sulfur isotopes in thaumasite appear to be much lighter than the Alum Shale constituents. This might possibly be explained by a contribution from atmospheric SO₂, or alternatively by sulfide oxidation in Alum Shale assisted by bacterial activity. A certain internal contribution from gypsum in cement clinker cannot be excluded.

Keywords: Stable isotopes, thaumasite, calcite, provenance

5.1 Introduction

The use of stable isotope geochemistry has recently obtained extensive application within many environmental fields, but up to now only in a restricted way within concrete deterioration research. Basically, stable isotopes have the potential of providing information of reaction mechanisms due to fractionation during the transformations, as well as to identify the sources of the deterioration agents. Earlier work by Rafai et al. [1, 2], Letolle et al. [3]

and Macleod et al. [4, 5] have elucidated the carbonation processes in concrete structures by using carbon and oxygen isotopes. Torf & VanGrieken [6] applied sulfur isotopes to identify the sources of gypsum formation on the surfaces of limestone buildings. These workers analysed small bulk samples or separates. However, laser assisted sample extraction is a micro-analytical technique which allows for precise analysis of sub-milligram sample sizes. To our knowledge no such data have been reported for concretes. We here focus on the potential of using stable isotopes by the laser method for investigations into the mechanisms of concrete alterations by various processes, as well as a monitoring tool.

Sulfate attack in concrete represents a multitude of chemical reactions, and several paths of reaction may be observed, as dependent on concrete mix and environmental conditions. Recent work has shown that the Thaumasite form of sulfate attack (TSA) might cause significant deterioration in concretes made with Ordinary Portland Cement (OPC) and Sulfate Resisting Portland cement (SRPC) (Thaumasite Expert Group [7]; Crammond [8]). In its non-deleterious early stage, Thaumasite formation (TF), the thaumasite is restricted to pre-existing voids and micro cracks. In deleterious TSA, however, the thaumasite forms by extensive replacement of the calcium silicate hydrates (C-S-H), ultimately involving total destruction of the cement paste. This process is critically dependent on: 1) availability of sulfate- and carbonate ions (from external or internal sources); 2) a wet and cool environment (most frequently below 10-15 °C); 3) a pore fluid pH greater than 10.5 and 4) that a significant portion of the cement paste can be accessed by the carbonate- and sulfate enriched fluids and react with Ca and Si in C-S-H to form thaumasite.

Works by Hagelia et al [9] and Sibbick & Crammond [10] suggests that, in certain environments, internal carbonation represents an important late stage in the overall TF - TSA. *Both* decalcification of C-S-H resulting in cement paste depletion with Popcorn calcite formation *and* associated thaumasite decomposition to calcite with or without subordinate gypsum beneath ordinary surface carbonation [9, 10] have been observed to take place. Although this late stage may be sustained in several chemical environments, the unifying feature is a reduction in the pore fluid pH from about 13 towards neutral (cf. Gaze and Crammond [11] and [9, 10]).

The TF-TSA –carbonation process leads to strength loss, enhanced concrete permeability and reduced service life of concrete structures. It is hence of great interest to the construction engineer to be able to identify the sources of carbonate and sulfate ions. Usually chemical analysis of water, aggregates and soils are employed in conjunction with petrography. However, only isotopic characterisation may be capable of discriminating between sources with similar chemical compositions.

5.2 Background and objectives

The chemical composition of thaumasite can be written:



The mineral is hexagonal, and its crystal structure contains columns of $(\text{Ca}_6[\text{Si}(\text{OH})_6]_2 24\text{H}_2\text{O})^{8+}$ parallel to the c-axis, with $((\text{CO}_3)_2(\text{SO}_4)_2)^{8-}$ occupying the channels between them. Si in thaumasite may be substituted by some Al, and CO_3^{2-} by sulfate ions (Bensted [12]). The channel carbonate-sulfate complex is loosely bound, involving some hydrogen bonds between hydrogen in water and oxygen in carbonate (Skibsted et al. [13]). We therefore expected to achieve laser ablation and extraction of channel components sufficient to be analysed for stable isotopic composition. However, CP/MAS NMR investigations have shown that especially ^{13}C occurs in close proximity of ^1H [13], which to the present authors

may indicate that the weak hydrogen bonds favour the heavy carbon isotope. Thus, one cannot exclude the possibility that laser ablation in thaumasite may involve a fractionation towards erroneously high $\delta^{13}\text{C}$ –values.

The present study focuses on two sprayed concretes in Oslo from: a) the first reported occurrence of TSA in Norway (e.g. Hagelia and Grønhaug [14]) in a road cut at Åkebergveien (13 years old spray), and b) the Svartdal high way tunnel (2 years old). These concretes have suffered TF and limited TSA attack with contemporaneous and secondary formation of several textural types of calcite within the concrete interior. Ordinary surface carbonation was also present (cf. [9]). At both sites steel fibre reinforced concrete, made with SRPC (C_3A = about 1 %) and ca. 5-10 % silica fume, had been sprayed directly on Alum Shale. This sulfide- and calcite bearing shale contains minor monoclinic pyrrhotite, which leads to catalytic oxidation of more abundant pyrite, and historically caused extensive deterioration with formation of soft mush of cement pastes (Moum and Rosenqvist [15]). We now believe that this in fact was a severe case of TSA [9]. Although the sulfate source in this case may be considered well constrained, several possible carbonate sources, such as atmosphere, calcite fines, complex ground water and anthropogenic material can in general be expected. Thus the objectives of this study were to:

- Characterise C-S-H, calcite, thaumasite as well as local Alum Shale constituents in terms of O, C and S isotopes
- In view of these constraints, investigate the possibility that sources of carbonate and sulfate ions can be identified

5.3 Methods and samples

Samples were first investigated under the petrographic microscope, and the mineralogical compositions of characteristic micro-domains were studied in more detail by Scanning Electron Microscopy (SEM). Sample chips for laser microprobe analysis were then selected from four concrete cores (some of which contain a bit of Alum Shale behind), and one spalled outer layer (ca. 2 cm thick) immediately adjacent to a 1-2 cm wide soft thaumasite + calcite mush zone. SEM was again performed in order to confirm the phase composition in each chip. Samples from Alum Shales and a few thaumasite rich deposits within chips were also selected for bulk S isotope analysis.

Laser microprobe analyses for carbon and oxygen isotopes were performed with a high-power Nd-doped YAl garnet (Nd: YAG) Quantronix laser, producing a beam wavelength of 1064 nm. A He-Ne aiming laser producing a visible red light is incorporated into the system for focusing the beam and positioning of the beam onto a target. The laser was operated at 30-32 A DC in a pulsed mode. The diameter of the beam will vary according to the material, but was commonly about 15 micrometer, and the analyses were followed through an optical microscope. The laser-ablation technique can be used for spot analyses if a sufficient amount of CO_2 gas is released. Alternatively, as in the present case, the sample is moved slowly along an X-Y table. The concrete minerals are generally very fine grained and thus individual mineral grains were too small to be analysed. Analyses of carbon and oxygen isotopes were performed along lines parallel to the sample surface and an integrated value for a specific depth was obtained in each case. Our sample chips widths were about 10 x 20 mm and 2-3 mm thick. The gas released was carried by He to a water absorbed MgClO_4 trap, and the CO_2 is separated in a poropackQ column, followed by analysis in a Optima IRMS (Micromass, England). A minimum of 2 μmol CO_2 is required. A reproducibility of $\pm 0.2\%$ (one sigma) for both O and C is based on repeated injections of reference gas. However, the precision vary with the quality of the sample, and the precision of thaumasite and C-S-H

analyses will generally be somewhat lower (about $\pm 0.5\%$). Isotope values (C and O) are given relative to the PDB standard (cf. Faure [16]).

The procedure for laser analysis of sulfur isotopes on sulfates and sulfides is yet not fully developed at IFE, so the few $\delta^{34}\text{S}$ data presented here represent small bulk samples. Sulfur isotopic composition was analysed on liberated SO_3 in sulphides and sulfates. Isotopic values are given relative to standard Canyon Diablo triolite. The precision in $\delta^{34}\text{S}$ is $\pm 0.2\%$ for both sulfides and sulfates.

For the fundamentals of the stable isotope technique is referred to the basic books of Faure [16] and Krouse and Grinenko [19].

5.4 Results

5.4.1 Petrography of analysed micro domains

5.4.1.1 Åkebergveien road cut

Core 2 (18 cm) with near by spalled outer layer. Two sample chips were selected from this core: a) inner parts close to concrete/Alum Shale interface (Bet4) and b) outer surface exposed to air (Bet6), respectively). Bet5, representing the spalled outer layer, comprised two zones; 1) calcite dominated near the outer surface (mostly ordinary carbonation) and 2) thaumasite dominated in entrapment voids (Figure 1: close to the TSA + calcite mush zone). A small bulk sample from the void material was analysed for S isotopes. Bet6 was characterised by ordinary surface carbonation and internal carbonation, with only small amounts of ettringite/thaumasite present. Bet4 contains variable amounts of thaumasite and ettringite.

Core 4 (12 cm) from the same locality was analysed by tracks from surface to about 4 cm inwards. This core displays a distinct porous internal reaction zone with a soft mush of calcite + thaumasite 2-2.5 cm from the surface, as seen in Bet11. A bulk sample of this zone, representing the thaumasite phase, was analysed for S isotopes. Bet11 was influenced by ordinary surface carbonation (1-2 mm) and internal C-S-H with or without calcite was also analysed about 4 cm farther inside the core.

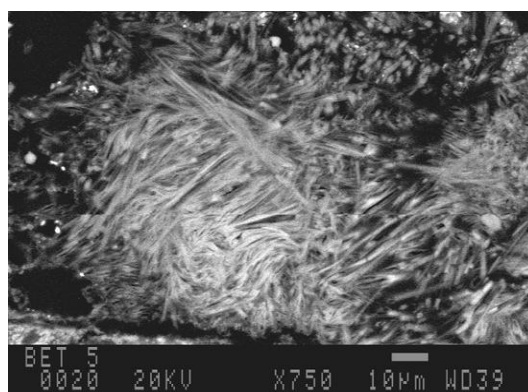


Figure 1: Thaumasite within the thaumasite+ calcite domain, Bet5 (Åkebergveien) BS image.

5.4.1.2 Svardal tunnel

Core 370A (wet, 6 cm long) is represented by Bet7 and Bet10. In this core there was a porous reaction zone with thaumasite + calcite 1-3 cm away from the interface with the Alum Shale. A bulk sample of the reaction zone was collected for S isotope analysis.

Part 1 – Black Shale environment

Bet10 represents surface carbonation; depth 1-3mm. Analyses of this sample also included internal C-S-H with or without calcite about 1.5 cm beneath the surface.

Bet7 is located close to the interface with the Alum Shale (0- 3cm). At the interface thaumasite was absent. However, coarse calcite deposits (ccd) were abundant within this fairly porous zone (Figure 2). About 1 cm away from the interface there was a complex mixed zone consisting of very fine grained C-S-H, and thaumasite/ ettringite with or without calcite. Thaumasite was also located in thin veins (Figure 3). A bulk sample of such a vein was sampled for S isotope analysis. The outer part of the Bet7 sample chip was characterised by coarser calcites (ccd) + thaumasite.

Core 320B (dry, 5 cm long). Bet9 from this core was located at the Alum Shale interface. Thaumasite was only detected close to the shale. Laser tracks up to 6 mm from this interface represent C-S-H + some calcite.

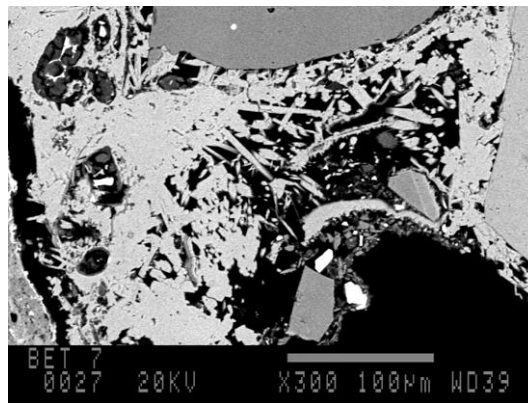


Figure 2: Coarse calcite deposits (ccd) at the Alum Shale interface in Bet7, Svartdal tunnel, BS image.

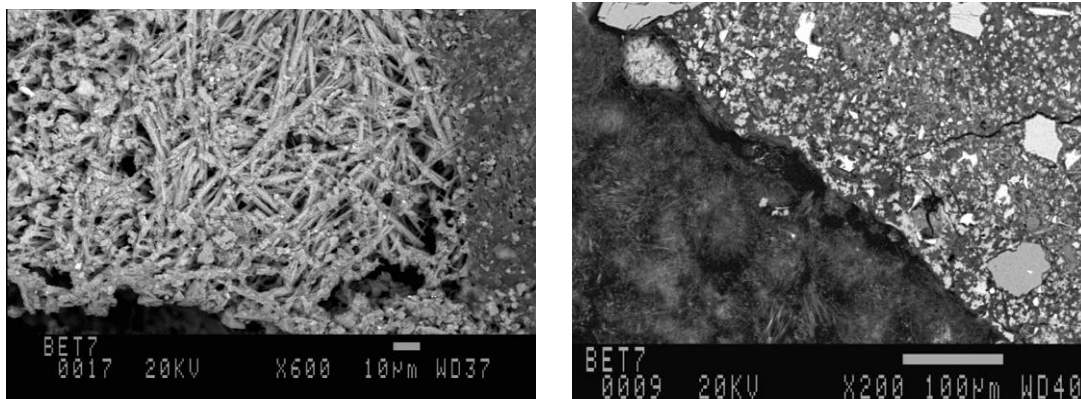


Figure 3: Thaumasite veins of different morphology in Bet7, Svartdal tunnel: Coarse-grained crystals to the left, very fine grained to the right. BS images.

5.4.1.3 Alum Shale

The petrography of the Alum Shale was not investigated in detail. At the Svartdal locality, numerous thin calcite veins at the interface with concrete have intersected the shale. The amount of carbon rich organic material was high, and small sulfide grains were scattered all over. Two bulk sulfide separates from each locality, determined by XRD to be predominated by pyrite, were analysed for S isotopic composition. One bulk analysis of shale organics from Svartdal was also included.

Part 1 – Black Shale environment

TABLE 1. Summary of investigated samples and the mineralogy of analysed domains. Predominating phases: C-S-H= somewhat depleted calcium-silicate hydrate; Th= thaumasite; cc= calcite, ccd=coarser grained calcite deposits

LOCALITY	SAMPLE	Sample no	Laser analysis	Description	Bulk analysis
Svartdaltunnelen	Core 320B (dry)	Bet9	C-S-H + Th + cc	Interface Alum Shale	S in Alum Shale sulfides
			C-S-H + cc	Interface/Internal	Organic S in Alum Shale
	Core 370A (wet)	Bet7	ccd>C-S-H + cc	Interface Alum Shale	S in thaumasite
			Cc + C-S-H	Interface Alum Shale	
			complex C-S-H mix	Internal	
Th veinlets	Internal				
Th + ccd	Internal/towards reaction zone (1-3cm from interface Alum Shale)				
	Bet10	cc>C-S-H(+Th)	Surface carbonation	S in C-S-H	
		C-S-H>cc	Internal		
Åkebergveien	Core 2	Bet6	C-S-H>cc(+Th)	Outer surface/internal	S in thaumasite S in thaumasite
		Bet4	Th + cc + C-S-H cc>C-S-H +Th	Interface Alum Shale Interface Alum Shale	
	Spall near Core 2	Bet5	cc + Th + C-S-H cc + C-S-H>Th	Inner surface near TSA mush Outer surface	
	Core 4	Bet11	cc>C-S-H cc+C-S-H cc+Th+C-S-H	Surface carbonation Surface/internal Reaction zone, 19mm from surface	

5.4.2 Stable isotopes

The stable isotope data for C and O are reported for individual laser tracks in terms of the mineral assemblages established in Table 1, and are also plotted in Figures 4 and 5. Bulk S isotopes are referred to in text.

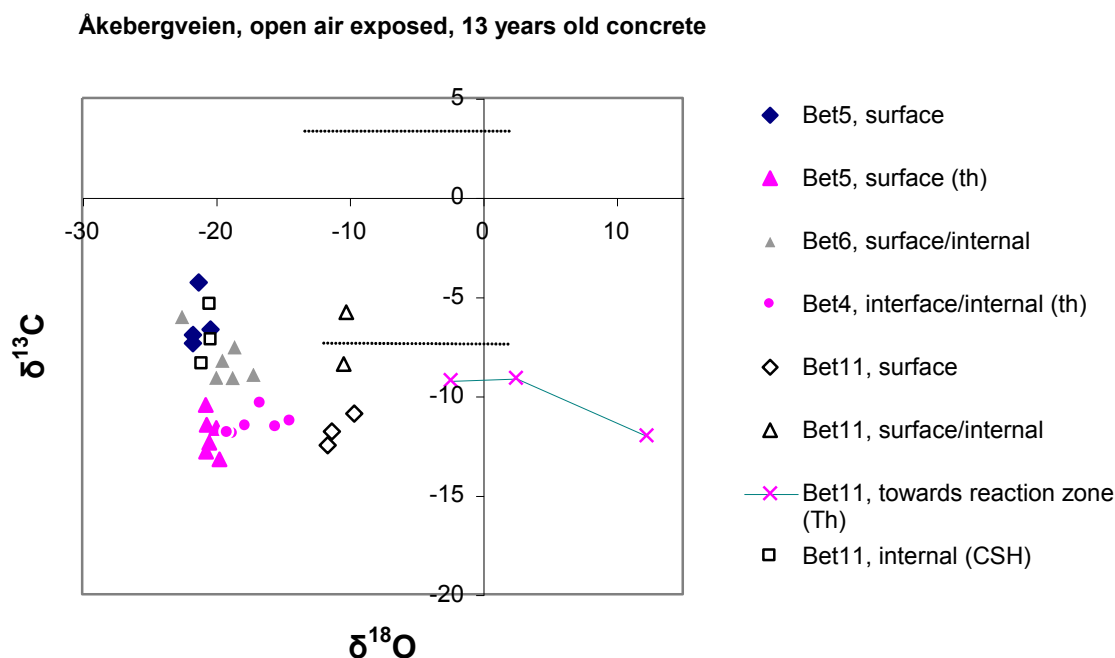


Figure 4: Carbon and oxygen isotopic variation in calcite and thaumasite from sprayed concrete at Åkebergveien in Oslo. All values are normalised to PDB. Inserted horizontal lines indicate $\delta^{13}\text{C}$ of atmospheric CO_2 (lower) and equilibrium fractionation $\delta^{13}\text{C}$ for calcite precipitated from CO_2 dissolved in water (upper). See Table 1 and text for further details.

5.4.2.1 Åkebergveien

At Åkebergveien $\delta^{13}\text{C}$ values range from -13.2‰ to -4.3‰ , yet with a significant difference between petrographic types. Thaumasite + calcite assemblages in Bet5 (pH in pore fluid probably transient from >10.5 towards 8-9) have values lower than about -10‰ . The surface carbonated zone in Bet 5 has somewhat elevated carbon, with $\delta^{13}\text{C}$ values from -7.4‰ to -4.3‰ . Pore fluid pH may be around 8-9 as judged from the assemblages. Bet6, which represents analysis from outer surface to internal carbonation is scattered between the values mentioned above.

Bet11, which represents Core 4 is different. Surface carbonates are ^{13}C depleted compared to Bet5, with $\delta^{13}\text{C}$ values from -10.9‰ to -12.5‰ . The values rise to -5.8‰ to -8.4‰ inwards, but decrease again to -9.1‰ to -12‰ towards the internal porous thaumasite + calcite mush zone. Where C-S-H dominates over calcite (Bet 11 internal) values fall within -5‰ to -8‰ .

The oxygen isotope values are also different in the two cores. The range in $\delta^{18}\text{O}$ values in Bet5, Bet6 and Bet4 is from -14.4‰ to -22.5‰ (lowest values in Bet4). The outer part of Bet11 has been enriched in ^{18}O , with $\delta^{18}\text{O}$ values from -9.6‰ to -11.3‰ . However, the internal part of this sample chip has values similar to the samples from the first core (Figure 4). The thaumasite/calcite internal reaction zone has distinctly different oxygen values, varying from -2.4‰ to $+12.3\text{‰}$.

The small bulk sample of the thaumasite + calcite reaction zone in Bet5 was analysed for sulfur stable isotopes. The $\delta^{34}\text{S}$ values range from 3.9 to 6.9‰. A void filled with thaumasite has a value of 4.0‰. C-S-H-gel was analysed in a small bulk sample, giving a $\delta^{34}\text{S}$ value of 10.6‰. This probably represents the composition of sulfur in gypsum added to the cement clinker.

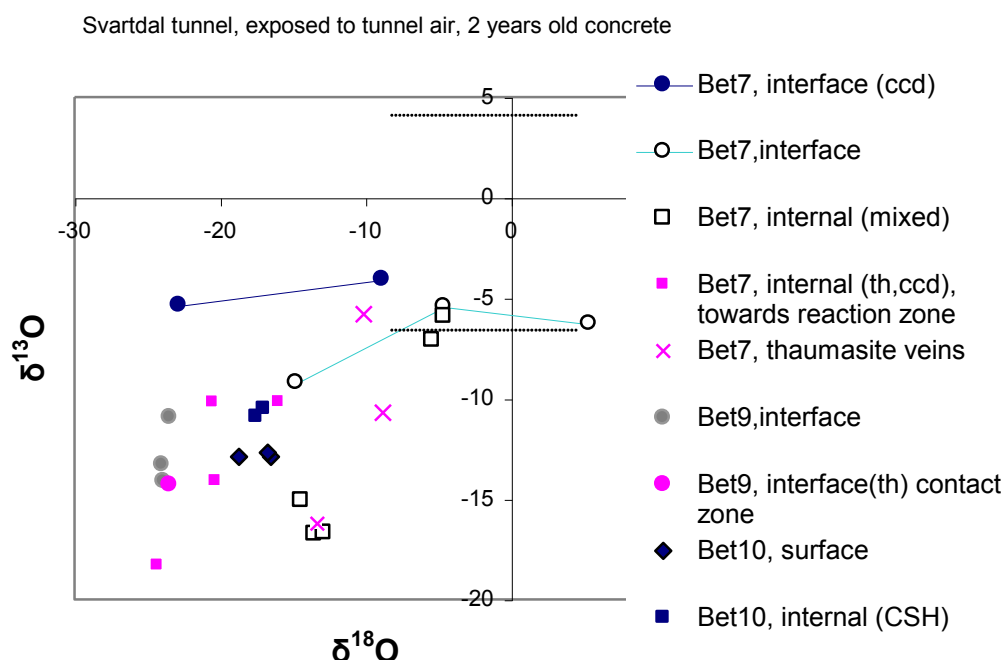


Figure 5: Carbon and oxygen isotopic variation in calcite and thaumasite from sprayed concretes in the Svartdal tunnel in Oslo. All values are normalised to PDB. Inserted horizontal lines indicate $\delta^{13}\text{C}$ of atmospheric CO_2 (lower) and equilibrium fractionation $\delta^{13}\text{C}$ for calcite precipitated from CO_2 dissolved in water (upper). See Table 1 and text for further details.

5.4.2.2 Svartdal tunnel

The isotopic scatter is more pronounced here (Figure 5). The $\delta^{13}\text{C}$ values range in total from -4.1‰ to -18.3‰ . The surface carbonation (Bet10 in Core 370) has a narrow range in $\delta^{13}\text{C}$ from -12.7‰ to -12.9‰ , which is only slightly lower than the range in internal C-S-H with or without calcite of -10.5‰ to -10.9‰ .

The mineralogical complexity of Bet7, also Core 370, extends to the isotope signatures. At the porous interface with the Alum Shale, the $\delta^{13}\text{C}$ values of the coarse calcite are fairly heavy, from -4.1‰ to -5.4‰ , decreasing to -9.2‰ towards the complex C-S-H matrix. This matrix has lower $\delta^{13}\text{C}$ values of -15.1‰ to -16.7‰ . Two analyses of small areas assumed to represent pure C-S-H matrix have values -5.9‰ to -7.1‰ (same symbol in Figure 4).

Thaumasite veinlets show highly variable values of $\delta^{13}\text{C}$ from -5.8‰ to -16.2‰ . The outer part of Bet7 with thaumasite + coarse calcite (towards the reaction zone) ranges in $\delta^{13}\text{C}$ values from -10.2‰ to -18.3‰ .

At the Alum Shale interface in Bet9 from the Core 320, the $\delta^{13}\text{C}$ value range is -10.9‰ to -14.3‰ .

$\delta^{18}\text{O}$ values of the surface carbonates (Bet10) varies from -16.5‰ to -18.7‰ . Internal $\delta^{18}\text{O}$ values are within the same range (about -17‰).

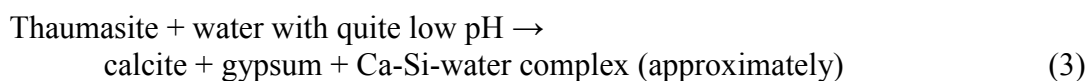
The coarse calcites (ccd) at the Alum Shale interface in Bet7 have extremely variable oxygen isotope values, $\delta^{18}\text{O}$ ranging from -8.9‰ to -22.8‰ at the contact. Coarse calcite (ccd) at the immediate vicinity range from -14.8‰ to $+5.4\text{‰}$, in total this gives a range of -22.8‰ to $+5.4\text{‰}$! The C-S-H mixed zone has $\delta^{18}\text{O}$ values from -12.2‰ to -14.4‰ , the “pure” C-S-H range from -4.6‰ to -5.4‰ . Thaumasite veins vary in $\delta^{18}\text{O}$ values from -8.8‰ to -13.3‰ , and the range in the thaumasite + coarse calcite (towards the reaction zone) is -20.3‰ to -24.3‰ .

The carbonate phase of the Bet9 core (Alum Shale interface) has a $\delta^{18}\text{O}$ value of about -24‰ .

A bulk separate of sulfides in Alum Shale, dominated by pyrite, from right behind the concrete in samples Bet9 contains very ^{34}S –enriched sulfur, with a $\delta^{34}\text{S}$ value of $+27.3\text{‰}$. Shale organics has a $\delta^{34}\text{S}$ value of $+21.2\text{‰}$. A similar sulfide separate from the shale behind Bet7 is less enriched in ^{34}S . $\delta^{34}\text{S}$ values range from $+15.8\text{‰}$ to $+22.1\text{‰}$, averaging $+18.7\text{‰}$. The isotopic signature of the reaction zone in Bet10 (thaumasite + calcite) is very different, with a $\delta^{34}\text{S}$ value of $+1.8\text{‰}$. A small bulk sample of C-S-H-gel has the value of 11.8‰ , which probably represents gypsum added to clinker. It is also possible that there is an influence from Al-sulfate admixture used as setting accelerator in this particular core [17].

5.5 Discussion

In a discussion of the isotopic signatures it is important to bear in mind the complexity of the systems investigated, which were characterised by very limited evidence of equilibrium reactions. Firstly, we assume that the isotopic signatures in concrete phases are reflecting the compositions of calcite, thaumasite and variably depleted C-S-H. Influence from portlandite and other subordinate phases should not be very great. Thus isotopic characteristics along a laser probe trail in a microscopic sub domain are expected to represent the average composition of an un-equilibrated assemblage. Schematically, the evidence suggests the following chemical reactions (cf. [9, 17]):



In addition to their age difference, the two localities have been exposed to somewhat different environments. The Åkebergveien sprayed concrete has been exposed to open air along a busy road, whereas the younger concrete at Svartdal has been influenced by tunnel air. In order to trace the sources and paths of deterioration using natural isotope systems, the sources need to be well characterised. In the case of the oxygen isotopes, the investigated systems are very complex, with many unknown participating phases (atmosphere, anthropogenic sources, meteoric water, groundwater, and oxygen bearing soluble minerals). In the following we therefore focus on the carbon and sulfur isotopes with only brief comments to oxygen.

5.5.1 Carbon isotopes

The ultimate carbon source for surface carbonation in concretes is atmospheric CO₂, which is dissolved in infiltrating water as meteoric rainwater or groundwater, or both. Precipitation of calcite in isotopic and chemical equilibrium with CO₂ gas should result in enrichment of ¹³C of about 10-11‰ at 10°C [16]. For atmospheric CO₂ the δ¹³C value is about -7‰, thus the expected δ¹³C value for precipitated calcite should be +3-4 ‰, which is certainly not the case in our samples. If the CO₂ gas transfer is diffusion dominated, a certain depletion of ¹³C will occur in the reaction product. However, interactions between water molecules and dissolved substances will reduce this effect [18]. Kinetic fractionation will also result in product ¹³C depletion, but values in the literature are highly variable. For example for the reaction CO₂ + OH⁻ → HCO₃⁻, which is dominant at high pH values (pH>10), δ¹³C values for kinetic fractionation varies from 11‰ to 39‰. Dissolution and re-precipitation of calcites should not include large fractionation effects [18].

Other carbon sources that can be present are added carbonate fillers, and also calcites within the Alum Shale. Calcite fillers are generally of marine origin, with δ¹³C values about 0‰. We estimate the contribution to the carbon isotope signatures from such fillers to be very small in our samples. Unfortunately, we do not have data from carbonate phases within the Alum Shale, but rather low δ¹³C values are presumed due to biogenic origin. Black shales usually have δ¹³C values about -25‰ [16].

Little work has been published on isotopic characterisation of concrete phases, but cement pastes with normal initial pH are reported with δ¹³C values generally below about -18‰ [1-3; 5]. Modern concretes have δ¹³C values ranging from about -10‰ to -30‰ [1]. Dietzel [20] describes two major ways of calcite sinter formation in concretes; by absorption of CO₂ in alkaline calcium hydroxide solutions within the concrete, or by deposition from ground water with dissolved CaCO₃. The first reaction will result in δ¹³C values of about -25‰, and the second in values about -13‰. Intermediate values indicate overlap of the two processes.

Although highly variable, our δ¹³C values are generally more elevated than literature data, and range from -4.3 ‰ to -13.2 ‰ in Åkebergveien, and from -4.1 ‰ to -18.3 ‰ in the younger Svartdal samples. The lowest values are seen in some thaumasite domains, although the scatter is obvious (Figure 4). Analytical enrichment in ¹³C cannot be excluded for the thaumasites, as mentioned earlier.

Surface carbonation at Åkebergveien differ in the two cores, with δ¹³C values averaging -6.3‰ and -10.8‰ respectively. At the Svartdal tunnel values at the surface are slightly lower, about -12.5‰. This is possibly due to higher concentration of exhaust fumes within the tunnel. The δ¹³C value in petroleum range from -18‰ to -34‰, and values for CO₂ from exhaust fumes should be slightly lower, probably about -25‰. A certain contribution from this source might be expected.

Carbon isotope signatures from “internal” domains are highly variable, in agreement with the presence of mixed stages of mineral reactions with various pore waters (reactions 1-5). The range in δ¹³C values is more pronounced in the younger Svartdal concrete. However, it appears that domains where C-S-H dominates over calcite have δ¹³C values as elevated as -5‰ to -8‰, in contrast to domains with C-S-H + calcite + thaumasite/ettringite. If surface carbonation results in δ¹³C values down to about -12‰, as indicated above, the lower values seen in internal domains may be ascribed to a certain supply from additional carbon sources, such as the Alum Shale. However the biogenic signatures in this shale is as yet unknown.

The porous domain of Bet7 (Svartdal) near the interface with Alum Shale has somewhat elevated δ¹³C values comparable to atmospheric CO₂. This may indicate an influx of different waters. The largest variation however is seen in the δ¹⁸O values, also indicating atmospheric influence (δ¹⁸O in CO₂ is about 10 ‰ PDB).

Highly variable $\delta^{18}\text{O}$ values are also specific for the porous reaction zone of Bet11 at Åkebergveien, extending to above atmospheric values. It is obvious that these porous zones have been available for influxes of diverse origins.

5.5.2 Sulfur isotopes

Isotopic geochemistry of sulfur compounds in water depends strongly on existing redox regimes. When oxidising conditions prevail the oxygen and sulfur isotopic composition of sulfate in waters are diagnostic of the origin of the sulfate [19]. Two possible external sulfur sources are actual in our samples: 1) anthropogenic SO_2 from ambient atmosphere oxidised to sulfates in meteoric water in contact with the surface of the concrete, or 2) circulating internal waters supplied with sulfate ions from oxidised sulfides and/or organics in the Alum Shale (or both). In addition one has to consider internal sources, such as gypsum additives.

The $\delta^{34}\text{S}$ values from the reaction zone closer to the surface in the Åkebergveien core (Bet5) vary from 3.9 ‰ to 6.9 ‰, while the values from the similar zone closer to the Alum Shale interface in the Svartdal core (Bet10) vary from 2 ‰ to 1.7 ‰. These values are rather different from $\delta^{34}\text{S}$ values of the Alum Shale phases (15.8 ‰ to 27.7 ‰). If the Alum Shale is providing the sulfate ions to the TS/TSA formation, a rather large fractionation of -12 ‰ to -25 ‰ has occurred during the sulfide/organics oxidation process. S isotope fractionation is expected to be very small during oxidation of sulfides. However, aerobic bacterial oxidation may result in significant fractionation effects [19].

SO_2 of urban air oil-gas varies in $\delta^{34}\text{S}$ from -8‰ to +30‰, but the majority lies in the range of 0 ‰ to 10 ‰ [19]. Fractionation during oxidation of anthropogenic SO_2 to sulfate is assumed to be relative low [19]. Large variations in $\delta^{34}\text{S}$ over short distances are observed at other urban localities [6], thus lack of data of local ambient atmosphere makes conclusions at this stage somewhat speculative. From the above data it is not obvious however, that the Alum Shale is the only source of the thaumasite formation in these concretes. Atmospheric SO_2 is a probable additional source. Furthermore, the $\delta^{34}\text{S}$ values of the C-S-H-gel of about 10 ‰ to 12 ‰ are considered to represent internal primary sulfur sources. Thus a certain contribution from primary source cannot be excluded either.

5.6 Conclusions

Our data are indicative of various stages of reaction, precipitation and dissolution processes with supply from different sources in an open system. We feel that this preliminary work has demonstrated the potential of applying isotopic methods in delineating the complex concrete deterioration reactions, although we are not able to pinpoint the sources of the carbonate and sulfate ions of the various calcites and thaumasites with certainty at this stage. The idea of using laser ablation for micro-scale sampling was based on the fine-grained nature of the mineral phases. In future work, however, it is recommended to supplement this micro-analytic technique by isotope analysis of small bulk samples, in order to avoid some of the very fine-scale variability. Laser analysis is suitable for local, specific problems in a petrographically well-documented sample. More systematic work is needed to trace the sources of deterioration, and all relevant sources have to be characterised in terms of their isotopic composition. In doing this, however, our understanding of the mechanisms involved in concrete deterioration will increase, and allow for the appropriate remediation actions to be taken.

5.7 Acknowledgements

The authors are indebted to Ingar Johansen and Lars Kirksæther (IFE), and Per Geir Sigursen (NPR) for technical assistance.

5.8 References

- 1 Rafai N, Letolle R, Blanc P, Person A, Gegout, P. Isotope geochemistry (^{13}C , ^{18}O) of carbonation processes in concrete. *Cement Concr. Res.* 1991; 21, pp 368-377.
- 2 Rafai N, Letolle R, Blanc P, Gegout P, Revertegat, E. Carbonation-decarbonation of concretes studied by the way of carbon and oxygen stable isotopes. *Cement Concr. Res.* 1992; 22, pp 882-890.
- 3 Letolle R, Gegout P, Rafai N, Revertegat E. Stable isotopes of carbon and oxygen for the study of carbonation/decarbonation processes in concrete. *Cement Concr. Res.* 1992; 22, 235-240.
- 4 Macleod G, Hall AJ, Fallick AE. An applied mineralogical investigation of concrete degradation in a major concrete road bridge. *Min. Mag.* 1990; 54, pp 637-644.
- 5 Macleod G., Fallick AE, Hall AJ. The mechanism of carbonate growth on concrete structures, as elucidated by carbon and oxygen isotope analyses. *Chemical geology* 1991; 86, pp 335-343.
- 6 Torfs KM, Van Grieken RE. Use of stable isotope measurements to evaluate the origin of sulfur in gypsum layers on limestone buildings. *Environ. Sci. Technol.* 1997; 31, pp 2650-2655.
- 7 Department of Environment, Transport and the Regions. The thaumasite form of sulfate attack: Risks, diagnosis, remedial works and guidance on new construction. Report of the Expert Group, DETR London, 1999, 180 pp.
- 8 Crammond N. J. 2002. The occurrence of thaumasite in modern construction – A review. *Cement & Concrete Composites* 24, pp 393-402.
- 9 Hagelia P, Sibbick RG, Crammond NJ, Grønhaug A, Larsen CK. Thaumasite and subsequent secondary calcite deposition in sprayed concretes in contact with sulfide bearing Alum Shale, Oslo, Norway. 8th Euroseminar on Microscopy Applied to Building Materials, Athens, Greece, 2001. pp 131-138.
- 10 Sibbick RG, Crammond NJ. Microscopical investigation into recent field examples of the thaumasite form of sulfate attack (TSA). 8th Euroseminar on Microscopy Applied to Building Materials, Athens, Greece, 2001. pp 261-269.
- 11 Gaze M.E., Crammond N.J. The formation of thaumasite in a cement: lime: sand mortar exposed to cold magnesium and potassium sulfate solutions. *Cement & Concrete Composites* 2000; 22: pp 209-222.
- 12 Bensted, J. Thaumasite – background and nature in the deterioration of cements, mortars and concretes. *Cement & Concrete Composites* 1999; 21: pp 117-121.
- 13 Skibstedt J, Hjorth L, Jacobsen HJ. Quantification of thaumasite in cementitious material by ^{29}Si (^1H) cross-polarization magic angle spinning NMR spectroscopy. *Advances Cem Res*, 1995; 7(26): pp 69-83.
- 14 Hagelia P., Grønhaug A. Thaumasite – infection causing concrete deterioration. *Våre veger* nr. 9 2000; pp 54-55 (in Norwegian).
- 15 Moum J., Rosenqvist ITh. Sulphate Attack on Concrete in the Oslo Region. *Journal of the American Concrete Institute* 1959; Proceedings Vol 56, Title 56-18, 8 p.
- 16 Faure, G. Principles of Isotope Geology, Second Edition. New York: John Wiley & Sons, 1989.
- 17 Hagelia P, Sibbick RG, Crammond NJ, Larsen CK. Thaumasite and secondary calcite

- formation in some Norwegian concretes. 1st International Conference on Thaumasite in Cementitious Materials, Garston, Watford, UK, 2002 (this volume).
- 18 Zeebe RE, Wolf-Gladrow D. CO₂ in seawater: Equilibrium, kinetics, isotopes. Elsevier Oceanography Series 65, 2001; 346pp.
 - 19 Krouse HR, Grinenko VA. Stable isotopes. Natural and anthropogenic sulphur in the environment. 1991. SCOPE 43, Elsevier; 440pp.
 - 20 Dietzel, M. 2000. Measurements of stable carbon isotopes in calcite sinters on concrete. ZKG International 9, pp 544-548.

Chapter 6

Sources of aqueous sulfate, bicarbonate and acid in Oslo Alum Shale with implications for concrete durability, geotechnical properties and metal leaching

*“All truths are easy to understand once they are discovered;
the point is to discover them”*

Galileo Galilei

The sulfide-bearing Norwegian Alum Shales represent a classical challenge to construction activities. This work, focusing on a local shale – concrete - water “system” based on tunnel samples, showed that the aggressiveness of Alum Shale depends on both abiotic and biotic release mechanisms. Abiotic leaching of an unweathered Alum Shale powder proved that 80 % of SO_4^{2-} aq. originated from anhydrite, as first reported herein. Monoclinic pyrrhotite was in this case not highly reactive as previously reported. In the tunnel environment iron-sulfide oxidation was somewhat more pronounced. Iron sulfides and anhydrite in the shale were isotopically much heavier ($\delta^{34}\text{S} \approx +27 \text{‰}$) than thaumasite S in deteriorated tunnel concrete ($\delta^{34}\text{S} \approx +2 \text{‰}$). The evidence can be explained by dissolution of anhydrite and partial reduction of SO_4^{2-} to H_2S within the rock mass, followed by reoxidation to sulfuric acid near the tunnel space. The process was likely sustained by sulfate reducing bacteria (SRB) and sulfide oxidation by *Acidithiobacillus sp.* Growth of such bacteria is fertilised by NH_4^+ , which can be mobilised from the shale. Hence, in general acid and sulfate release from Alum Shale is perhaps influenced by leachable ammonium. C and O isotopes confirmed that calcite at the shale/concrete interface had formed from acidic waters. Carbonate in thaumasite was derived from marine calcite and atmospheric CO_2 whilst the anthracitic-graphitic carbon was inert. In view of additional data the general Alum Shale swelling mechanism seems governed by anhydrite to gypsum conversion, gypsum precipitation from evaporating waters and possible effects from clay minerals. Metal leaching reached toxic levels even at near neutral pH.

Keywords: Alum Shale, reactive components, concrete deterioration, swelling mechanism, metal leaching

6.1 Introduction

The Norwegian Alum Shale, which is a challenge to construction activities, formed from organic-rich sediments laid down during the Lower Palaeozoic under stagnant and

reducing conditions. This sulfur -bearing black shale once covered most of Scandinavia and extended into Baltica. Due to different impacts of later geological events the present day Alum shales comprise several varieties representing different chemical and physical properties. Where unaffected by later metamorphism, the shale organics still contain bitumen and lighter hydrocarbons. Thus, certain Swedish Alum Shales were exploited for petroleum from 1925 until 1961, notably during the Second World War. A similar black shale, the so-called “kuckersitt schist”, still represents an important energy source in Estonia and was previously exploited for uranium (Ramberg et al. 2006). By contrast the Norwegian Alum shales have, with rare exceptions, lost their bitumen during later thermal events: firstly during the Caledonian Orogeny at 200-220 °C (Jensenius 1987) and secondly by variable effects of contact metamorphism related to the extensive magmatic activity within the Permo-Carboniferous Oslo Graben (Oftedahl 1955, Rosenqvist 1956, Andersson et al. 1985, Ramberg et al. 2006). Alum Shale within the Oslo Graben has historically caused severe sulfate attack in concrete, steel corrosion and shale swelling leading to heave of foundations. The Norwegian “Alum Shale Committee” (1947-1973) investigated the sources and release mechanisms of aggressives more than fifty years ago (Bastiansen et al. 1957). However, recent research has provided new perspectives and it is, therefore, necessary to take a fresh look at the Alum Shale problem.

6.1.1 Objectives and strategy

This paper summarises previous results from Oslo Alum Shale, presents a literature survey of more recent relevant research, and investigates Alum Shale – concrete - water interaction in search for the sources and release mechanisms of aggressive ions. The present work was based on a static leaching experiment on a single sample of classic Alum Shale from a road tunnel in Oslo and evidence from local sprayed concrete affected by carbonation and sulfate attack and the local tunnel water.

The strategy and idea behind was that investigations of the Alum Shale problem, as a first further step, should be based on a comprehensive understanding of a single local “system”. The implications for future work on characterisation, concrete deterioration, shale swelling, and heavy metal leaching were discussed in the light of the local evidence and some additional regional data.

6.2 Norwegian experience and recent research relevant to black shale

6.2.1 Research results from Alum Shale within the Oslo Graben

The Alum Shale Committee investigated the Alum Shale problems through site inspections, laboratory investigations and long term performance testing of concretes exposed to natural Alum Shale ground water (Bastiansen et al. 1957, Moum and Rosenqvist 1959, Fiskaa et al. 1971, Fiskaa 1973). The severe concrete degradation was interpreted to be due to ettringite sulfate attack and variable effects of acidification caused by sulfide oxidation. Groundwater sulfate concentrations in non-oxidised ground waters with pH = 5-7 were ranging from about 500 to 2500 mg/L. Sulfate in oxidised waters within the vadose zone were about 3000-5000 mg/L at pH = 2-4. The drop in pH was caused by oxidation of pyrite, release of sulfuric acid and precipitation of ferric iron.

The Alum Shale within the Oslo Graben typically consists of about 7-8 % anthracitic carbon (in “pre graphitic stage”). Recently Abreham (2008) has also found graphite. The

modal composition varies a lot and up to about wt. 50 % carbon has been reported (Bastiansen et al. 1957). Low grade metamorphic shales contain quartz, feldspars, illite, chlorite minerals, white mica, carbonates and pyrite, whilst pyrrhotite was found within contact metamorphic aureoles around Permian intrusives (further details in Table 1) (Goldschmidt 1911, Oftedahl 1955, Bastiansen et al (1957); Rosenqvist 1957; Skjeseth 1963, Antun 1967, Spjeldnes 1962, Bjørlykke 1974, Neumann 1985, Jeng 1990, 1991). Alum Shale does not contain alum but was previously used as a raw material for alum production.

The detrimental effects of Alum Shale were attributed to rapid chemical weathering under influence of water and air. The weathering reactions were triggered by the oxidation of a highly reactive and structurally disordered *monoclinic pyrrhotite* (FeS_{1.14}). This volumetrically minor phase formed through thermal metamorphism at about 150-300 °C, and was interpreted to have a catalytic effect on oxidation of the more abundant pyrite (6-7 modal %). The mechanism was interpreted to be electrochemical due to measured galvanic currents across grain boundaries of pyrite and pyrrhotite (Bastiansen et al. 1957). Moreover, the total released sulfur in the form of aqueous sulfate was much greater than the pyrrhotite contents could account for. Unweathered Alum Shale with 0.01 % pyrrhotite sulfur had reportedly caused building damage. *The Alum Shale Committee was unable to establish a threshold value* but contents of pyrrhotite sulfur < 0.001 wt. % was regarded as safe. Pyrite alone was not regarded as particularly reactive, because completely non-corroded very small pyrite cubes (≈ 10 μm or smaller) were frequently found together with surface weathering products, typically composed of gypsum and jarosite (Bastiansen et al. 1957, Antun 1967, Bjørlykke 1974, Jeng 1991). Hexahydrite, epsomite, and more rare copiapite and aluminium copiapite also occur (Neumann 1985).

Table 1: Typical constituents of Upper Cambrian - Lower Ordovician Alum Shales within the Oslo Graben. Minerals marked with *) are the author's recent findings at Gran north of Oslo. Anhydrite first reported in this work.

Phases	Low grade metamorphic	Contact metamorphic	Secondary weathering products
Main	Anthracitic carbon, illite, chlorite, white mica, feldspars, quartz, pyrite	Graphite, scapolite*, ankerite*	Iron oxides, iron oxihydroxide, jarosite, gypsum
Minors or traces	Calcite, Mg-calcite*, dolomite, barite, sphalerite, rhodochrosite, anhydrite*	Pyrrhotite, chalcopyrite, pentlandite*	Hexahydrite, epsomite, copiapite, alumino-copiapite

To protect buildings against Alum Shale, the committee found that prevention of air and water into freshly blasted shale was beneficial. Direct contact between harmful varieties of Alum Shale and concrete should be avoided, and asphalt membranes are frequently employed. An exception to this is sprayed concrete used for rock support, which is sprayed directly on the harmful Alum Shale (cf. Hagelia et al. 2001). The most resistant concrete mixes were found to be Sulfate Resisting Portland Cements or Portland cements with silica fume or other highly pozzolanic additives (Bastiansen et al. 1957, Moum and Rosenqvist 1959, Fiskaa et al. 1971, Fiskaa 1973).

The shale swelling was characterised by slow, fast and delayed heaves, which frequently amounted to several decimetres, accompanied by long lasting heat generation reflecting sulfide oxidation. Similar extensive heaves were also reported from fills containing Alum Shale. The *swelling mechanism* is however still not well understood, although it probably involves both clay minerals and formation of gypsum (Bastiansen et al 1957, Sopp

1966). Barth (1943) hypothesised that if anhydrite were present in Alum Shale it could cause swelling by hydration and volume gain and conversion to gypsum. However, anhydrite was not identified by the Alum Shale Committee.

Environmental issues were not focused in the early investigations. Yet, it is well established that Alum Shale carries environmentally unfriendly elements, leading to heavy metal leaching and radon problems caused by elevated uranium contents (30-200 ppm). A comprehensive geochemical survey of the Alum Shales stratigraphy within the Oslo Graben (Bjørlykke 1974), work by Jeng (1991,1992) and experience from construction work has provided insight into the geographical distribution and behaviour of environmentally unfriendly compounds. Uranium is easily leached during weathering and is highly mobile (Bjørlykke 1974). Pyrite and pyrrhotite usually contain traces or minor amounts of Cd, As, Cu, Ni, Zn, Mn and Pb (cf. Lapakko 2002, Lottermoser 2003). Jeng (1992) reported that pH buffering caused by calcite-bearing Alum Shales counteracted release of heavy metals: By contrast non-calcareous sulfide-bearing Alum Shales had usually developed a low pH and elevated concentrations of heavy metals in water, leading to Acid Rock Drainage (ARD).

6.2.2 Recent research into concrete degradation associated with Oslo Alum Shale

In contrast to previous interpretation of ettringite and acid attack, it has recently been established that Thaumassite Sulfate Attack (TSA), detrimental carbonation and Popcorn calcite deposition (PCD) with effects of acid attack was responsible for the cement paste deteriorations here. TSA and PCD was found both in young steel fibre reinforced sprayed concretes (Hagelia and Grønhaug 2000, Hagelia et al. 2001, 2003) and historical samples (Hagelia and Sibbick 2007, 2009). TSA is most efficient in a wet and cool environment and utilises the calcium silicate hydrates (C-S-H) in concrete and bicarbonate and sulfate from ground water or aggregate (cf. DETR 1999, Crammond 2003). In the Svartdal highway tunnel in Oslo a limited TSA had developed within less than 2 years of exposure, whilst *paradoxically* the local Alum Shale contained 0.00 % “reactive sulfur” (NPRA internal documents).

A pilot C, O and S stable isotope study of C-S-H, secondary calcite and thaumasite within sprayed concrete in contact with Alum Shale showed a complex interaction with waters from different sources (Iden and Hagelia 2003). The results suggested carbonate was derived from bicarbonate in ground water, with a possible influence of atmospheric CO₂ and shale organic carbon. Sulfate in thaumasite was possibly influenced by bacteria or anthropogenic SO₂. These and other processes are discussed further in the light of new data presented herein.

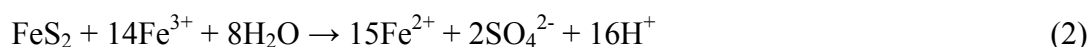
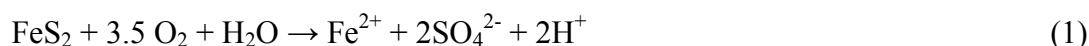
6.2.3 Outline of contemporary research progress

6.2.3.1 Sulfide oxidation- and release mechanisms of sulfur compounds and acids

Recent research has provided new perspectives on sulfide oxidation and other chemical processes relevant to the interaction of black shale with water, air and biota. In the following a brief account is given to the mechanisms which govern release of sulfate ions and generation of sulfuric acid.

Pyrite oxidation has been studied extensively over the last two decades. In general oxidation requires the presence of an electron acceptor (oxidant) which is commonly O₂ or ferric iron (Fe³⁺), but also NO₃⁻ and Cl₂ and others can accept electrons by redox reaction with iron sulfide (Nordstrom and Alpers 1999, Moncaster et al. 2000, Rimstidt and Vaughan

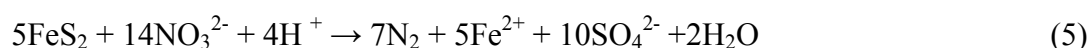
2003). Oxidation of pyrite takes place where O₂ is abundant, or by ferric iron (cf. Appelo and Postma 2005):



In low oxygenated systems Reaction 2 is rate-limiting. However, this reaction is restricted to acidic conditions at pH < 4.5 since Fe³⁺ will otherwise react with water and form iron hydroxide (goethite) (cf. Appelo and Postma 2005):



Oxidation of pyrite by nitrate at low pH leads to denitrification and sulfate formation:



Fe²⁺ in Reaction 5 also reacts further with nitrate and formation of acid, goethite and a little nitrogen. Reaction 5 probably requires bacterial catalysis (cf. Appelo and Postma 2005).

Rimstidt and Vaughan (2003) have presented an electrochemical model for pyrite oxidation. Cathodic and anodic sites exist on the pyrites surfaces due to subtle differences in chemical composition. The rate-limiting step in pyrite oxidation is taking place at the cathodic sites (e.g. Brown and Jurinak 1989) where electrons are transferred from the mineral surface to the aqueous oxidant species, usually O₂ and Fe³⁺. Charge is transported from the anodic reaction sites by replacing the electrons lost from the cathodic sites: At the anodic sites electrons are abstracted from sulfide S in *seven successive steps* through intermediate sulfoxy anion species, ultimately leading to formation of sulfate ions. The behaviour of the partly oxidised intermediate species, such as thiosulfate (S₂O₃²⁻) and polythionates (S_nO₆²⁻) are commonly oxidised to sulfite (SO₃²⁻) prior to oxidation to sulfate. This last step may be due to abiotic and biotic pathways (Williamson and Rimstidt 1994). The oxidation process is complex and depends on pH in ambient water (cf. Konhauser 2007): Sulfite rapidly oxidises to sulfate except under alkaline conditions. However, at pH > 6 the preceding intermediate species tend to be stabilised in the solution, whilst at pH < 5 these partly oxidised sulfur species remain bonded to the pyrite surfaces until fully oxidised to sulfate ions before being released into the water phase (Rimstidt and Vaughan 2003). Elemental sulfur (S⁰) may then form a *protective layer on pyrite surfaces*, thus inhibiting further oxidation. This complexity may have direct practical consequences for acidification and sulfate release from pyrite-bearing rocks, depending much on the local chemical and biochemical environment.

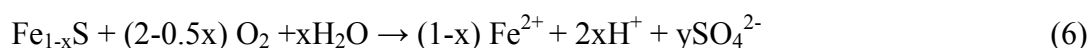
Acidophilic chemolithotrophic bacteria catalyse sulfide oxidation. *Acidithiobacillus ferrooxidans* respire aerobically and can oxidise both Fe²⁺ and sulfide but prefers sulfide for energetic reasons. *A. ferrooxidans* is frequently well attached to pyrite surfaces and oxidises and dissolves pyrite directly through enzymatic reactions. Indirect oxidation is also possible through oxidation of Fe²⁺ to Fe³⁺ which then reacts with pyrite according to Reaction 2 (cf. Konhauser 2007). *A. ferrooxidans* has also been found to colonise pyrite under initial neutral pH-conditions but developed acidity after less than two weeks in an experiment: Acidity first developed within a nano-scale layer between bacteria and pyrite (Mielke et al. 2003). On the other hand the aerobic bacterium *Acidithiobacillus thiooxidans* can only oxidise reduced sulfur, including intermediate sulfoxy anions such as tetrathionate (S₄O₆²⁻) as well as H₂S and

S^0 . Commonly, therefore, *A. thiooxidans* colonises sulfides after *A. ferrooxidans* (cf. Konhauser 2007). For long *A. ferrooxidans* was regarded as strictly aerobic but it has now been recognised that this bacterium is facultative anaerobic, i.e. also capable of surviving in absence of oxygen. In such reducing environments *A. ferrooxidans* utilises Fe^{3+} as an electron acceptor and reduced sulfur species (S^0 etc) or H_2 as electron donors. Hence acidification due to sulfide oxidation cannot always be avoided merely by excluding oxygen. Yet reducing conditions tend to favour growth of sulfate-reducing bacteria (SRB), leading to extensive formation of H_2S at the expense of Ca-sulfates. This sulfide may later form SO_4^{2-} and acid upon reoxidation (Konhauser 2007) (e.g. Reaction 11, below).

It is evident that the *growth conditions* of sulfide-oxidising bacteria exert a prominent control on the release of sulfate and acids to the environment. The optimal growth conditions for *Acidithiobacillus ferrooxidans* are at pH ca. 2-3 and elevated ammonium concentrations (100 mg/L) in presence of phosphate, leading to enhanced oxidation of ferrous iron. A similar chemical environment favours rapid cultivation of *Acidithiobacillus thiooxidans*. However, high nitrate concentrations such as 350 mg/L are regarded as *toxic* to *A. ferrooxidans*, whilst variations in phosphate concentration and temperature seem to have a lesser effect (Niemelä et al. 1994). It has further been established that certain *bacteriophages* predate on *Acidithiobacillus sp.*, thus inhibiting oxidation of iron sulfides, formation of aggressives and leaching of sulfide-bound toxic heavy metal (Meech and Suttle 2002).

An interesting recent finding is that pyrite in contact with water can be oxidised to sulfate by *radiolysis*. This mechanism is solely triggered by radioactive decay (alpha-, beta- and gamma radiation), leading to radiolytic cleavage of water molecules and formation of highly oxidising hydrogen peroxide and hydroxyl radicals. Resulting pyrite oxidation can then proceed without involvement of O_2 . The process is sensitive to pyrite grain size distribution and is especially effective for small pyrites $\leq 25 \mu m$ which can yield very elevated aqueous sulfate concentrations (Lefticariu et al. 2006, 2007).

Pyrrhotite oxidation is complex, mainly due to its variable crystal chemistry. The general formula is $Fe_{1-x}S$ where x varies from 0.125 to 0.00: representing pure monoclinic (similar to the Oslo pyrrhotite) and hexagonal pyrrhotite, respectively. Intermediate intergrowths occur and may also contain exsolved magnetite and smythite (cf. Kullerud 1986). Nicholson and Sharer (1994) found that the abiotic oxidation rate of monoclinic pyrrhotite is up to 20-100 times higher than those for pyrite:



where y depends on x . From this reaction it is also obvious that when x approaches 0, as for perfect hexagonal pyrrhotite, the potential for acid production decreases very much, whilst monoclinic pyrrhotite has a much greater potential. Thus pyrrhotite oxidation sometimes produces much less acid than pyrite. Yet pyrite and pyrrhotite oxidation rates by ferric iron are virtually the same. MEND (1998) and Janzen et al. (2000) found that characteristics of pyrrhotite, such as metal impurities and crystallographic form (e.g. monoclinic or hexagonal), do not affect oxidation rates significantly: Instead the very *high surface area* of pyrrhotite particles, which is 2-10 times greater than pyrites of similar size, is by far the most important parameter for assessment of pyrrhotite oxidation (e.g. MEND 1998).

Several authors have reported that the high reactivity of pyrrhotite leads to a surface passivation layer consisting of intermediate sulfur oxidation species and elemental sulfur (S^0), which inhibits further abiotic oxidation (cf. Janzen et al 2000). Moreover, accumulated evidence shows that Fe-poor pyrrhotite (e.g. monoclinic) is stabilised by oxygen (Kullerud 1986, Graham 1987, Kontny et al. 2000) when formed at geological temperature above about

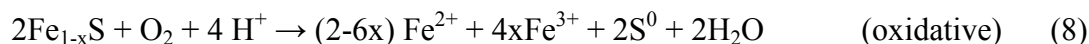
Part 1 – Black Shale environment

220 °C (Lusk et al, 1993). Many authors argue that the surface passivation layer can only be broken through bacterial activity (cf. Bernier and Warren 2005).

Bhatti et al. (1993) pointed out that *early stage pyrrhotite dissolution is characterised by acid consumption*, either by a non-oxidative redox reaction:



or by reaction with oxygen;



According to Bhatti et al. (1993) bacterial oxidation has little effect in the beginning of the oxidation process (e.g. Reactions 7 & 8). *Acidithiobacillus ferrooxidans* and *Acidithiobacillus thiooxidans* can greatly facilitate pyrrhotite oxidation by breaking the protecting layer according to Reaction 9 (Bhatti et al. 1993; Schippers and Sand 1999; Janzen et al. 2000):



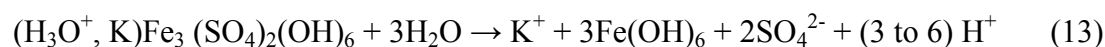
This stage is followed by bacterial and chemical oxidation of ferrous iron (Reaction 3) and formation of ferric oxihydroxide which produces acid (Reaction 4).

Efraimsson et al. (1976) investigated the role of *Acidithiobacillus ferrooxidans* on a range of sulfides involving pyrite and unspecified pyrrhotite. They found that bacterial oxidation produced much more sulfate from pyrite than pyrrhotite: while pyrite eventually was 100 % oxidised, pyrrhotite was only about 35 % oxidised. Evidently *Acidithiobacillus ferrooxidans* is not always able to completely oxidise all forms of pyrrhotite.

Once sulfuric acid has formed this may react with remaining pyrrhotite to form soluble iron sulfate and H₂S gas according to Reaction 10 (cf. Fiskaa et al. 1971). H₂S migration into oxic domains subsequently reoxidises to sulfuric acid according to Reactions 11, whilst the iron sulfate might dissolve according to Reaction 12 (Moum and Rosenqvist 1959):



Sulfurised organic carbon is another potential source of sulfate, which was not addressed by the Alum Shale Committee. It is well established that the fraction of reduced sulfur bound to organics increases with the total content of organic carbon (cf. Böttcher et al. 2005). Obviously sulfate may also be derived from dissolution of gypsum or anhydrite if present. These minerals are soluble and simply dissociate to Ca and sulfate ions without directly influencing the pH. Contrary to this, pure K-jarosite has low water solubility. However, Lapakko and Berndt (2003) found that some K-deficient jarosite (sodium, hydronium-bearing or non-ideal) dissolve according to the following acid producing reaction:

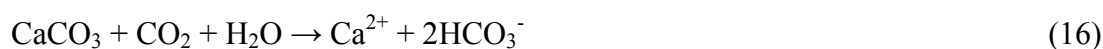


Their experimental results have shown that such jarosite may lead to pH ≈ 3.3. Also copiapite dissolution is a well known acidifier which may drive pH below 2.

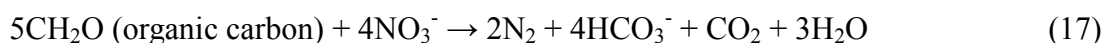
The *catalytic role* of monoclinic pyrrhotite on pyrite oxidation (cf. Bastiansen et al. 1957) is apparently not much emphasised in the literature. It is, however, established that pyrrhotite tends to behave anodically. This property is due to the non-stoichiometric relationship between iron and sulfur (Natarjan et al. 1983, Bhatti et al. 1993), being important in monoclinic pyrrhotite as characterised by vacancies and a cation deficit in the Fe (II) octahedra (Yakhontova et al. 1983). The present author feels that monoclinic pyrrhotite may catalyse or assist in further pyrite oxidation, as proposed by the Alum Shale Committee (Bastiansen et al. 1957), because the rate-limiting step in pyrite oxidation is related to the cathodic reactions (Rimstidt and Vaughan 2003). Yet intuitively the efficiency of this mechanism should depend on the connectivity of pyrite and pyrrhotite grains as well as presence/absence of sulfide-oxidising bacteria.

6.2.3.2 Carbonates, organic carbon and bicarbonate

Bicarbonate and carbonate represent very important anion species. Elevated concentrations may also cause significant concrete carbonation as well as Thaumassite Sulfate Attack when also sulfate ions are present (Crammond 2003; Collett et al. 2004; Hagelia et al. 2003). Hagelia and Sibbick (2007, 2009) reported that the most severe effects on concrete may occur when the acidity fluctuates along with sulfate and bicarbonate concentrations over time. Bicarbonate in ground waters is commonly derived from atmospheric CO₂ or dissolution of calcite:



For closed systems otherwise similar to Reaction 16, H₂CO₃ may replace CO₂. Bicarbonate may also form from organic carbon under certain circumstances (Korom 1992):



or together with H₂S upon reduction of sulfate ions (Berner 1984):



Both these redox reactions cause a rise in pH and may be relevant also for the Alum Shale environment, suggesting that bicarbonate may form either from aqueous Total organic carbon (TOC) derived from dying biota, or even from the shale carbon if available for chemical reaction.

Finally sulfuric acid can be neutralised by reaction with calcite according to the following gypsum forming reaction (cf. Appelo and Postma 2005; Jeng 1991, 1992, Lapakko 2002):



Reaction 19 may prevent acid attack in concrete and steel and sometimes also inhibiting heavy metal release. However, the reaction potentially leads to swelling and geotechnical challenges caused by the growth of gypsum.

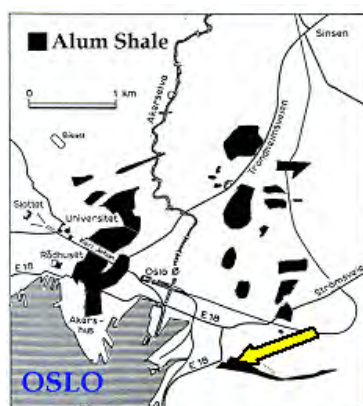


Figure 1: The main outcrops of Alum Shale within the city of Oslo. The arrow shows the location of the Svartdal tunnel.

6.3 Materials and methods

6.3.1 Field location and samples

The Alum Shale layer within the Svartdal tunnel (Figure 1) is of Upper Cambrian age. Locally abundant hydrothermal calcite veins occur. In August 2006 a previously investigated locality (Hagelia et al. 2001, 2003; Iden and Hagelia 2003) was revisited. A core (320-06U: $\Phi = 70$ mm) was extracted, consisting of an outer 5-6 cm sprayed concrete layer and inner 15-20 cm of Alum Shale. The sample station was located at chainage 320 m in the innermost part of a tunnel niche about 35 meters behind the tunnel lining. It was well protected from exhaust fumes and characterised by an overall surface wet concrete and very moist air in the form of dew. A water sample (“Tunnel water-320-06”) was collected from a big pond just beneath the core location. Field pH \approx 6.0-6.5 was measured using indicator strips. The water was typically stagnant and characterised by a rusty brown slime and a dark organic rich material. White deposits on cracks in the sprayed concrete consisted of thenardite and gypsum (Hagelia et al. 2001). Concrete core samples 320B and 370A of the previous study from the same locality were used for additional analyses.

6.3.2 Sample preparation and analytical methods

Alum Shale sample. The analytical work is summarised in Table 2. The sample for leaching was a 1.5-2 cm thick slice of Alum Shale selected from the inner part of Core 320-06U some 10-12 cm inside the concrete/shale interface. The rock sample was a carbon-rich and quite homogeneous shiny black shale without visible calcite veins, yet with diffuse very minor rust staining along two thin laminas (< 0.1 mm). This subsample was smashed up into small $ca \leq 1$ cm chips and fines using a big agate mortar, and subsequently milled to a fine powder (≤ 10 μm) in a steel swing mill. Sample crushing in air should perhaps cause rapid oxidation of monoclinic pyrrhotite and loss of reactive sulfur (Bastiansen et al. 1957). However, the sample preparation did not involve water, and reactive sulfides should hence be preserved in the initial powder. *There was no smell from H_2S or SO_2 just after milling.* A small portion (about 1-2 g) of fine powder was collected directly from the swing mill and analysed by XRD and SEM for initial composition after about 30 minutes. The powder was also controlled for grain size and homogeneity by SEM (Figure 3A). The main sub sample

Part 1 – Black Shale environment

(200-250 g) was put into a 250 ml plastic bottle immediately after milling and capped with two plastic lids in order to slow down oxidation. All of this work was completed within 15 hours after core extraction.

Table 2: Summary of analytical work on Svartdal Alum Shale powder sample 320-06U, concrete minerals, shale constituents and waters. Cores 320B and 370A were extracted in 2000.

Samples	XRD- mineral identification	SEM-imaging & chemistry	Water chemistry	Stable isotopes (bulk)
320-06U initial shale powder	X	X		
320-06U leached in Water 1	X	X		
320-06U leached in Water 2	X	X		
Bacterial slime: Tunnel water 320-06	X	X		
Calcite vein in Alum Shale 320B				C, O
Alum Shale org. in 320B & 370A				C, S
Concrete (Iden & Hagelia 2003)				C, O, S
Tunnel water 320-06			X	C, O, S
Water 1-initial			X	C, O
Water 1-final			X	C, O, S
Water 2-initial			Calculated	Calculated: C, O, S
Water 2-final			X	C, O, S

Leaching experiment. Five days later two batches of Alum Shale powder, each of 100 ± 1 gram, were placed into two 500 ml plastic bottles using a steel spatula. Two different waters were filled up to the 450 ml mark. “Water 1_{initial}” was collected from the tap at the Geology Department at NPRA whilst “Water 2_{initial}” was prepared as mixture consisting of a 200 ml of “Tunnel water-320-6” and 250 ml of “Water 1_{initial}”. The tunnel water sample was characterised by a faint brownish stain, which was not filtered. The idea with the mix was to introduce an effect from real tunnel water characteristics, yet avoiding too high initial sulfate content. Judging from the water level in the bottles, no significant effect of evaporation was indicated during the time of the experiment.

The pH and redox potential (Eh) were measured in each of the waters immediately before adding to Alum Shale powders using a Jenway Model 370 meter, accurate to $\text{pH} \pm 0.01$, and designated “zero measurements”. The two bottles were capped with an inner and outer plastic lid, which is regarded as air tight. Much of the fine powder was brought into suspension and settled after 1-2 days. pH, Eh and temperature were measured on days 4, 9, 17, 28, 39, 51 and 65. The water temperature (22.6 ± 0.3 °C) and water level (≈ 450 ml) were almost constant during the experiment. In the first part of the experiment the bottles were treated with extreme care during measurements, and recapped with two lids within about 1 minute. After measurements on day 9 the bottles were shaken for 60 seconds by hand while capped and then left open: The outer cap was left loosely on top of each bottle to counter weigh possible effects of evaporation whilst air was allowed to enter. This procedure was repeated after measurements on the 17th and 28th day. Again the bottles were capped with the two lids without any further shaking. Measurements continued until day 65 according to the same routines as before day 9. At all stages a very thin film of carbon rich material was floating on top of the bottles.

Immediately after the final measurements 77.5 ml water sub samples for stable isotope analysis were carefully collected from the top of each bottle, using 5.5 ml pipettes. Samples of the Alum Shale powders for XRD and SEM were also collected through 5.5 ml pipettes from the bottom centre of each bottle, and stored in small glasses capped with plastic lids. The remaining water was reserved for water chemical analysis. All samples were transported to

the respective laboratories on the 65th day, involving some shaking of the waters. XRD and SEM analyses were performed on the leached powders on the same day. Meanwhile the bottles were treated in accordance with standard routines and stored at 5 °C in the dark at the laboratory. Water chemical analyses started up after 12 days and the remaining Alum Shale powder was then removed by centrifugation.

XRD. Small ca 1-2 g samples of initial and leached Alum Shale powders were ground in small agate mortars under ethanol and left to dry before mounted on sample holders and run in a Siemens D 5005 Spectrometer. All spectra were run from 2° to 70° on the 2-Theta scale at 0.050° per second, and were checked versus the Powder Diffraction Files database from the International Center for Diffraction Data. Mineral proportions should be regarded as qualitative to semi-quantitative.

SEM. Bulk chemistries of the powders were analysed before and after leaching using a Hitachi 3600 N scanning electron microscope with standard Back scatter electron detector and Environmental Scanning Electron Detector (ESED) equipped with an EDS unit from Thermo Electron Corporation. The powders were mounted in thick layers on carbon tape without any pre treatment. Each run was based on the average of three small domains. For the initial homogenised powder the three different analysed frames (about 10000 µm²) gave almost the same result. The magnification was 1200x and the instrument was operated with an accelerated voltage 10 kV at high vacuum. Due to separation during the experiment final leached powders were inhomogeneous and it was necessary to scan much larger areas (about 1 x 1 mm) at 15 kV. This involved a calibration problem and the difference between initial and final shale characteristics are regarded as semi-quantitative. Back Scatter Electron (BSE) and Secondary Electron (SE) images were grabbed, and a few sulfides were analysed using 15 kV at 700x magnification. Analytical accuracy for major elements is within ± 1-2 wt. % except for carbon (± 3-4 wt. %).

Water chemistry. Before and after the leaching experiments the water samples were analysed for pH by Radiometer PHM 210 Standard pH meter. All waters were filtrated using a 0.45 µm filter prior to analysis. Total organic carbon (TOC) was analysed by a Phoenix 8000 TOC-TC analyser; Cl, F, SO₄²⁻ and NH₄⁺ by ion chromatography using a Dionex DX320 instrument. Nitrate + nitrite was analysed by a Skalar San Plus Autoanalyser, alkalinity in a Mettler DL 40 RC Memo Titrator and conductivity by a WTW inoLab Level 3 Conductivity Meter. The remaining elements were analysed as totals by ICP-AES, using a Perkin-Elmer Optima 4300 DV instrument. Detection limits depend on the available sample size (cf. Table 7). The initial chemical composition of the Water 2 was not analysed but calculated on the basis of the mix proportions of Water 1_{initial} and Tunnel water-320-06 assuming conservative mixing behaviour. Saturation indices were calculated for all waters using the computer code PHREEQC-2.

Stable isotopes. The water samples, filtrated on a 0.45 µm filter, were analysed for C and O compositions in a Finnigan Delta +XP isotope mass spectrometer. Oxygen isotopes ($\delta^{18}\text{O}_{\text{SMOW}}$) were obtained by equilibrating water with CO₂, which was cleaned for impurities by a chromatographic method prior to analysis of the oxygen in carbon dioxide. For carbon isotopes 1 ml of water was first flooded with He, then added H₃PO₄ and again flooded with He and injected into the mass spectrometer for carbon isotope ($\delta^{13}\text{C}_{\text{PDB}}$) analyses. S isotopes ($\delta^{34}\text{S}_{\text{CDT}}$) were analysed in a Micromass Optima isotope mass spectrometer: Sulfate was first precipitated as Ba-sulfate at a controlled low pH. After filtration and washing in deionised water the filtrate was burnt at 1700 °C and the liberated SO₂ was analysed for S isotopes. Solids (organic carbon and calcite vein) were first handpicked under a binocular. Organic carbon was washed in acetone and weak hydrochloric acid in order to remove possible calcite before C isotope analysis, whilst calcite was taken “as is”. Calcite and organic carbon were prepared as CO₂ gas and analysed directly in a Finnigan MAT DeltaXP Isotope Ratio Mass

Spectrometer (IRMS). Bulk sulfides (predominantly pyrite) were separated out by conventional techniques whilst Ca-sulfates were not attempted to be extracted. Sulfides and organic carbon were treated the same way as barium sulfate precipitates and analysed according to the same procedure as for waters. It should be noticed that sulfides were finely disseminated within organic carbon, implying that the true organic sulfur was not well characterised. Authorised standards from the IAEA were run as unknowns along with all samples. The individual measurements for C, O and S isotopes are accurate to within $\pm 0.1\%$, $\pm 0.2\%$ and $\pm 0.2\%$ (1 sigma), respectively.

Water 2_{initial} was not analysed isotopically but calculated from Water 1_{initial} and Tunnel water. It was assumed that the oxygen isotopes behaved like a conservative mixture, and $\delta^{18}\text{O}_{\text{SMOW}}$ was calculated according to the mix proportions. Sulfur isotopic composition ($\delta^{34}\text{S}_{\text{CDT}}$) in the mix was calculated from the sulfur weight concentrations and mix proportions of the two waters according to the following equation (based on Faure 1986):

$$\delta_{\text{mix}} = \delta_A f_A (A/M) + \delta_B (1-f_A) (B/M) \quad (20)$$

where A, B and M are the concentrations of element in end members A and B and mixture M. respectively. f_A is the fraction of A in the mix. Similarly, $\delta^{13}\text{C}_{\text{PDB}}$ for the mixture (Water 2) was calculated using total carbon, e.g. the weight concentrations of carbon in $\text{HCO}_3^- + \text{CH}_2\text{O}$ (Total Organic Carbon, TOC). The S isotopic composition of Water 1_{initial} could not be determined, since this sulfate poor sample happened to be too small. However, the composition of Water 2_{initial} is regarded as equal to the sulfate rich Tunnel water: Calculation according to Equation 20 showed that the composition of the mix (Water 2_{initial}) was insensitive to any likely compositions of Water 1_{initial} ($\delta^{34}\text{S}_{\text{CDT}} = +30$ to -30%) within the quoted analytical error.

6.4 Results

The mineralogy and chemistry of the Alum Shale sample corresponded quite well with data previously reported for Stages 2c and 2d in the local Upper Cambrian stratigraphy (cf. Bjørlykke 1974), although feldspars and illite were not detected. Most important was that also anhydrite occurred. To the present authors knowledge this is the first report of this mineral from Oslo Alum Shale, hence confirming the hypothesis of Barth (1943). Anhydrite most likely was formed after dehydration of authigenic gypsum. There was no sign of red rust deposition in the bottles during and after the leaching experiment.

6.4.1 Bacteria and bio-minerals in Tunnel water 320-06

XRD bulk analysis of a mineral rich portion from the bottom of the sample bottle showed a high and irregular background signal and low count rate typical of amorphous biogenic phases. Yet peaks of ferrihydrite, goethite, β -cristobalite (SiO_2) were identified. Sheath silicates such as clay minerals were absent.

SEM analysis was undertaken on a filtrate of suspended rusty and partly dark bacterial slime in the tunnel water sample. The investigation showed presence of heavily iron encrusted material mainly in the form of 10-100 μm sized iron rich platelets (Figure 2A). The sheath bacterium *Leptothrix ochracea* was apparently present, being intimately associated with the platelets, suggesting extra cellular biomineralisation. In addition there was an appreciable amount of smaller sized (ca 1 μm) coccoidal to rod shaped sometimes network forming

mineral encrusted bacteria, representing suspect *Acidithiobacillus thiooxidans* or *Acidithiobacillus ferrooxidans*. A few iron encrusted helix shaped *Gallionella ferruginea* also occurred (not shown). No attempt was made to further identify the microorganisms. Microchemistry (Table 3) of platelets and apparent *Leptothrix ochracea* (Figure 2A) show they were enriched in Fe, Si, with smaller amounts of S, Ca, P, N and traces of Co. Fe/O atomic ratios indicated compositions varying between goethite (FeOOH) and ferrihydrite (Fe(OH)₃). The chemistry of the suspect *Acidithiobacillus* species (Figure 2B) indicated that they consisted mainly of goethite. Nitrogen and phosphorous was present in platelets and the suspect *Acidithiobacillus sp.* (analysis B1), the latter also with traces of Co, As, Cd and Pb. The Si contents (ca. 2-4 % atomic) may represent tiny quartz grains and biogenic cristobalite embedded within the iron rich compound.

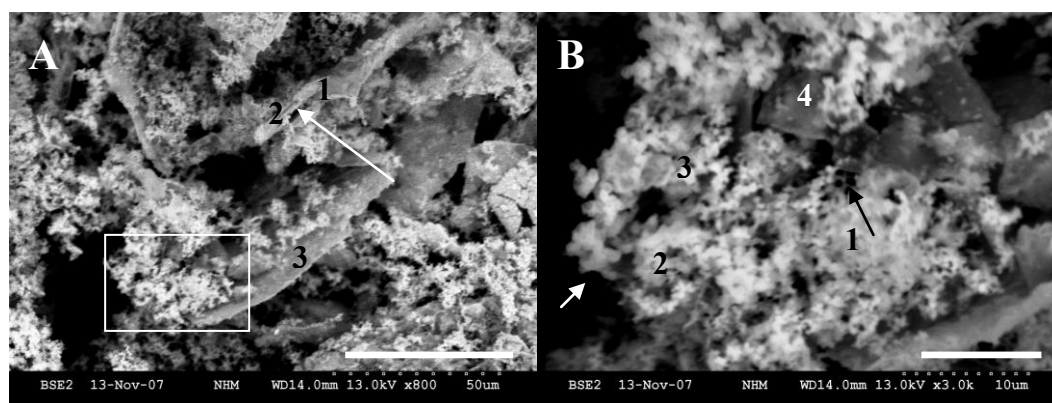


Figure 2: Bacterial deposits found in Tunnel water 320-06 (Back Scatter Images). A: Presence of apparent *Leptothrix ochracea* (arrow) and associated biominerals. B: Smaller abundant coccoidal to rod like shapes (white arrow) sometimes forming a “network” (black arrow) which likely represents *Acidithiobacillus ferrooxidans*, *Acidithiobacillus thiooxidans* or both. Numbers refer to point analyses given in Table 3. Scale bars: 50 μm and 10 μm, respectively.

Table 3: Semi-quantitative chemistry by ESED (atomic %): A & B refers to Figures 2A and 2B, respectively.

	N	O	Mg	Al	Si	P	S	Ca	Fe	Co	As	Cd	Pb
A 1	1.86	61.50		0.14	3.41		0.43	0.75	31.77	0.13			
A 2	0.77	60.95			3.84	0.02	0.24	0.70	32.76	0.72			
A 3	0.15	60.53			2.00		0.37	0.77	36.17				
B 1	0.45	60.78		0.07	3.09	0.10	0.29	0.58	34.08	0.48			0.07
B 2		60.56	0.12	0.16	2.97		0.22	0.66	35.20		0.06	0.04	
B 3		60.45	0.10	0.13	2.50	0.06	0.27	0.63	35.39	0.47			
B 4		60.83	0.08		3.04	0.20	0.51	0.75	34.56		0.04		

6.4.2 Effects of leaching on bulk mineral composition

The mineralogy of the Alum Shale sample underwent small but important changes during the leaching experiment (Table 4). The initial shale was characterised by an appreciable amount of quartz (SiO₂) and some titanomagnetite (Fe_{2.5}TiO_{0.5}O₄), almandine garnet (Al₂Fe₃(SiO₄)₃). These minerals represent detrital material. A barium and vanadium-bearing muscovite (K,Ba,Na)_{0.75}(Al,Mg,Cr,V)₂(Si,Al,V)₃O₁₀(OH,O)₂ was also important, which in view of its Ba and V contents most probably had formed from clay minerals once present in the primary sediment. Ba and V are typical constituents in shales from the marine euxinic environment (Konhauser 2007). Also a small amount of montmorillonite (Na_{0.3} Al,

$(\text{Mg})_2\text{Si}_4\text{O}_{10}\cdot\text{OH}_2\cdot 6\text{H}_2\text{O}$) was found. Pyrite (FeS_2) and pyrrhotite were ubiquitous. Diffraction lines indicated hexagonal pyrrhotite ($\text{Fe}_{0.95}\text{S}_{1.05}$) as well as monoclinic pyrrhotite ($\text{FeS}_{1.14}$) with small peaks very close to $d = 2.07196 \text{ \AA}$ and $d = 2.05838 \text{ \AA}$ (cf. Antun 1967), probably representing an intergrowth. The pyrrhotite had most likely formed during a thermal effect on the Alum Shale, likely of Permian age. A rather small amount of pure calcite (CaCO_3) and Mg-calcite ($\text{Mg}_{0.1}\text{Ca}_{0.9}\text{CO}_3$) occurred in nearly equal proportions along with a little anhydrite (CaSO_4). Traces of rhodochrosite (MnCO_3) and graphite (C) were also found, whilst anthracitic C was probably dominating.

XRD patterns of the residues were quite similar, although the following differences were noted: Montmorillonite had apparently disappeared whilst gypsum ($\text{CaSO}_4 \cdot 2\text{H}_2\text{O}$) was detected in both leached samples. Anhydrite was still present after leaching in Water 1 but had disappeared in Water 2. Mg-calcite prevailed in both samples, whilst calcite and rhodochrosite were not obvious in shale leached in Water 2. Pyrite and pyrrhotites were still present after leaching in both waters. The persistence of monoclinic pyrrhotite is somewhat surprising in view of previous results from the Alum Shale Committee, who reported that this mineral should not survive oxidation through heavy milling and later water leaching. As regards muscovite, the XRD data indicated that Ba and V had been leached.

Table 4: Qualitative mineral composition from XRD before and after 65 days leaching of Alum Shale. Qz = quartz, Mu = muscovite (Ba & V with barium & vanadium: K = ordinary), TiMt = Titanomagnetite, Alm = almandine, Anh = anhydrite, Gy = gypsum, Cc = Calcite, Mg-Cc = magnesian calcite, Mont = montmorillonite, H-Po = hexagonal pyrrhotite, M-Po monoclinic pyrrhotite. Py = pyrite, Rh = rhodochrosite, Gr = graphite. Amorphous anthracite like carbon comes in addition. Notice the presence of anhydrite in pristine shale.

Sample	Mineral composition	Remarks
320-06U initial shale	Qz, Mu (Ba & V), Py, H-Po, M-Po, TiMt, Anh, Cc, Mg-Cc, Mont, Rh, Gr	Anhydrite, Ba & V bearing muscovite
320-06U leached in Water 1	Qz, Mu (Ba), Py, H-Po, M-Po, TiMt, Anh, Gy, Cc, Mg-Cc, Rh, Gr	Anh-Gy conversion \pm dissolution. Possible Cc dissolution. Po, Py & Mg-Cc remained
320-06U leached in Water 2	Qz, Mu (K), Py, H-Po, M-Po, TiMt, Gy, Mg-Cc, Gr	All Anh converted to Gy \pm dissolution. Cc dissolved. Po, Py & Mg-Cc remained

6.4.3 Alum Shale characterisation by SEM before and after leaching

SEM imaging was first used to check for homogeneity of the powders. The initial powder was found to be very homogeneous whilst the powders after leaching were agglomerated and separated (Figure 3A and B). There was no sign of relatively coarse calcite vein material. The analysis show that the sample was very rich in carbon and most of this was represented by organic C, since bulk carbonate contents were subordinate in view of the low Ca contents. Interference with the carbon tape should be rather small in view of the thick layers of powder applied. Much of the sulfur was bound in pyrite and pyrrhotite whilst anhydrite and possibly sulfurised organic carbon account for some of this element. The initial shale contained an appreciable amount of uranium (about 300 ppm). Due to the data quality no trends may safely be established from these analyses. Yet it is noteworthy that nitrogen was detected only in the initial sample, apparently having disappeared after 65 days of leaching in both waters. This corresponded well with the overall increase in total nitrogen species released into the waters after leaching (see Table 7).

SEM imaging and a few analyses of sulfides indicated that most pyrite had survived leaching. Very small and potentially very reactive framboidal pyrites ($\leq 10 \mu\text{m}$) were

Part 1 – Black Shale environment

ubiquitous before and after leaching, as were lots of very tiny pyrite grains ($< 1 \mu\text{m}$). Also a blocky and coarser pyrite (10-50 μm) was found to be “intact”. The sulfide surfaces were generally “clean” with no obvious sign of bacterial growth during the leaching experiment. Authigenic framboidal pyrite (Figure 3) partly recrystallised to blocky pyrite is a common feature of Oslo Alum Shale (Antun 1967, Jeng 1990, Abreham 2007). Pyrrhotite was detected by XRD but not observed with certainty during screening of the Alum Shale powders. However in one case a carbon-rich domain apparently without sulfide indicated a relative excess of sulfur versus iron (Analysis nr 2-06-290606 c(3)-pt2 with C = 24.25 %, Fe = 1.31 %, S = 3,38 %, Al = 1.37 %, Si = 1.85 %, O = 67.04 % atomic): This probably reflects presence of sulfurised carbon. A few grains of FeOOH were also detected.

Table 5: Semi-quantitative chemical compositions of the Alum Shale powder from SEM scans. Notice the loss of N. Only the initial powder was truly homogeneous.

Element (wt. %)	Initial powder	Leached in Water 1	Leached in Water 2
C	19.33	19.59	19.05
O	65.26	65.35	64.67
N	0.10	0.00	0.00
K	1.62	1.47	1.63
Na	0.03	0.01	0.03
Mg	0.47	0.42	0.43
Al	3.22	3.01	3.14
Si	6.67	6.47	6.75
P	0.02	0.02	0.02
S	0.91	1.06	1.14
Ca	0.16	0.21	0.10
Ti	0.17	0.00	0.01
Fe	1.76	1.72	2.14
Mn	0.00	0.02	0.00
Ba	0.17	0.53	0.57
Th	0.05	0.00	0.03
U	0.03	0.00	0.18
Co	0.00	0.11	0.09
Sum	100.00	100.00	100.00

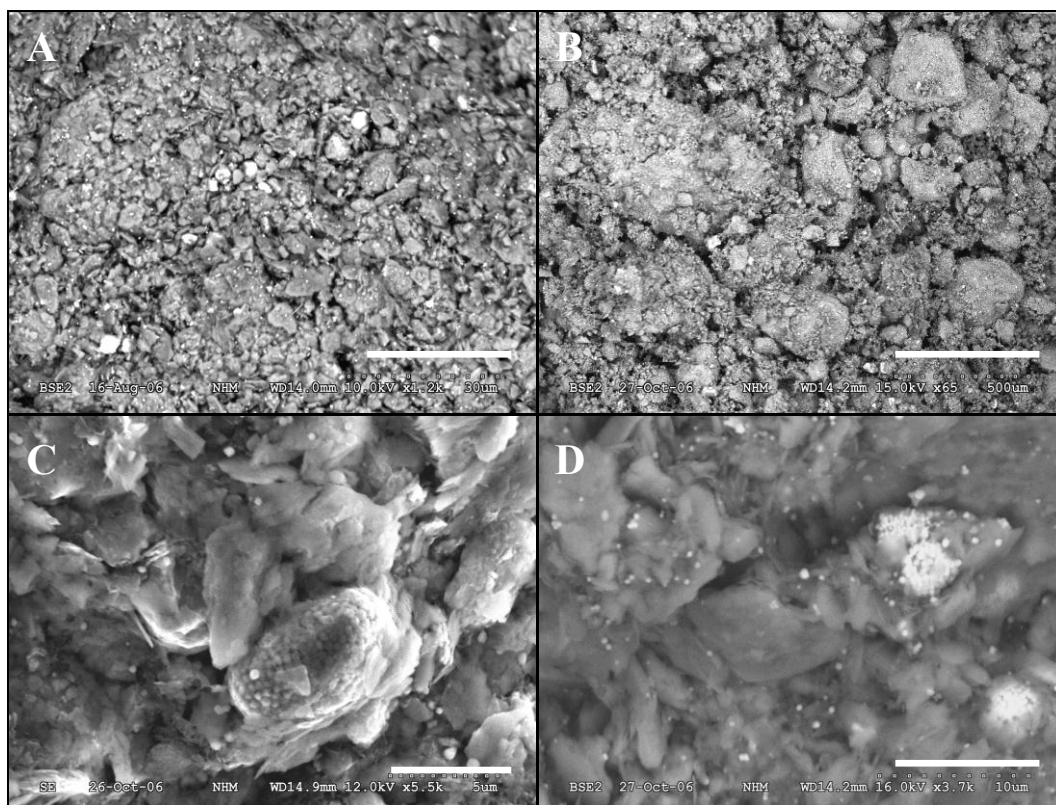


Figure 3A: Representative Back scatter electron (BSE) image of initial Alum Shale powder before the leakage experiment. Scale bar = 30 µm. B: BSE image of powder after leaching in Water 2 showing separation and agglomeration. Scale bar = 500 µm. C: Secondary electron (SE) image of apparently slightly reacted framboidal pyrite after leaching in Water 1: Scale bar = 5 µm. D: BSE image of possibly slightly reacted framboidal pyrite (bright) after leaching in Water 2: Notice also very small sulfide grains < 1 µm. Scale bar = 10 µm. There was no obvious sign of sulfide oxidising bacteria.

6.4.4 Water chemistry

6.4.4.1 pH and Eh evolution during the 65 days leaching experiment

Monitoring of Eh and pH was undertaken in order to shed light on chemical reactions during the 65 days experiment. In general Eh-pH varied within a narrow range under predominantly reducing conditions, comparable to typical variation in groundwater (cf. Appelo and Postma 2005). Both waters went through a similar 4 stage evolution up to day 65 (Table 6, Figure 4). During Stage 1 pH dropped from neutral down to 6.20 and 6.33 in Water 1 and Water 2, respectively. This was accompanied by a rise in Eh from -97 & -88 mV to -36 mV. Stage 2, from day 9 to day 17, was characterised by a rise in pH to about neutral and a drop in Eh. The onset of this development appeared to have started before day 9 when the bottles were opened and shaken but the main effect was from day 9 until at least day 17. During Stage 3, from day 17 to day 51, the pH dropped whilst Eh increased. During the final Stage 4, from day 51 to day 65, the pH was stabilised at 6.60 and a constant Eh. It was, however, noteworthy that pH measurement on day 77 in the water chemical laboratory (cf. Table 7) was higher than the pH at day 65. The tunnel water sample was slightly more acidic than the experimental waters.

Just before each measurement the bottles were smelled in order to detect possible H₂S. Water 2 had a very weak “rotten egg” like odour on day 9 with a weak “earth like” smell on days 17 and 28, whilst Water 1 had a very weak H₂S –like smell in on days 17 and 28. Thus a

very small contribution from an H₂S producing reaction seems to have started after the low pH event on day 4. However, the odours had disappeared on day 39.

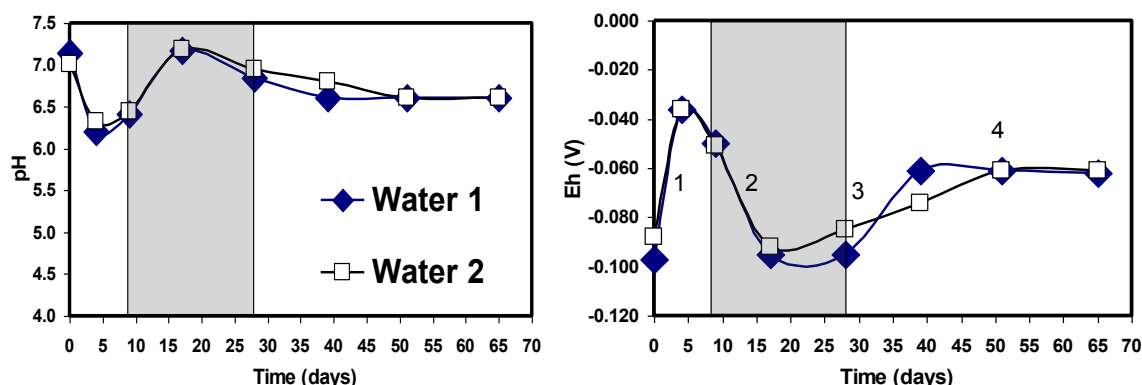


Figure 4: pH variation during the 65 days leaching experiment carried out on Alum shale powder. From day 9-28 (shaded area) bottles were kept open to air and shaken well after each measurement. Otherwise samples were undisturbed and capped with tight lids except for at each measurement. Numbers indicate stages of development.

Table 6: pH and Eh variation during 65 days leaching. Bottles were open from day 9 to day 28.

Time (days)	Water 1	Water 2	Water 1	Water 2
	pH	pH	Eh(Volt)	Eh(Volt)
0	7.12	7.02	-0.097	-0.088
4	6.20	6.33	-0.036	-0.036
9	6.42	6.44	-0.050	-0.051
17	7.17	7.19	-0.095	-0.092
28	6.85	6.95	-0.095	-0.085
39	6.60	6.80	-0.061	-0.074
51	6.60	6.60	-0.061	-0.061
65	6.60	6.60	-0.062	-0.061

6.4.4.2 Waters 1 and 2 before and after leaching compared with tunnel water

The water chemical analyses showed systematic enrichments and depletions relative to the initial water compositions. The observed variation was apparently compatible with the XRD and SEM results. The chemical data are given in Table 7 and important variations are plotted in Figure 5. Bicarbonate was calculated from alkalinity assuming no other important contributors than carbonate species.

Sulfate increased to 1080 mg/L and 1510 mg/L in the waters during the leaching experiment, greatly exceeded the level in tunnel water (541 mg/L). The Ca in all waters, reaching 430 mg/L and 565 mg/L in the final waters, displayed a good positive linear correlation against sulfate. Ca versus bicarbonate displayed a similar but less perfect correlation (Figure 5A & B). Dissolved total iron (e.g. mainly Fe²⁺) was extremely low (< 0.10 mg/L) in comparison with the sulfate contents. Tunnel water Fe was only marginally higher (Figure 5C). This was interesting in view of the fact that there was no sign of ferric iron deposition in the bottles at any stage during the leaching experiment. The total contents of nitrogen species increased during the experiment reflecting the complimentary drop in total N in Alum Shale powders: Ammonium increased from about 0.100 mg/L to 0.500-0.600 mg/L during the experiment whilst nitrate dropped from 26-148 µg/L to 3 µg/L. Total organic carbon (TOC) in the waters dropped along with the nitrate contents (Figure 5D) and was also roughly inversely correlated with bicarbonate and sulfate.

Part 1 – Black Shale environment

As regards minors and traces, Mn formed a perfect positive correlation with Ca, being enriched in the final waters. Mg was also enriched in the final waters and correlated fairly well with Ca. In addition Al, Si, Sr, Cl, F, Ba, B, K, Na and Li had increased. The metals Cd, Ni, Mo and Co increased during the experiment whilst Cu and Zn dropped. P, As, Pb, V and Cr were below the detection limits in all waters, showing no significant enrichment in the final waters. Uranium was not analysed.

Table 7: Chemical composition (mg/L), pH and conductivity of the water samples. HCO_3^- was calculated from alkalinity. Total dissolved carbon was calculated from TOC and HCO_3^- . The composition of Water 2_{initial} was calculated assuming conservative mixing.

Parameter	Water 1 _{initial}	Water 1 _{final}	Water 2 _{initial}	Water 2 _{final}	Tunnel water
pH	7.15	7.28	7.01	7.19	6.84
Conductivity (mS/m)	3.34	184.90	52.52	234.40	114.00
Alkalinity (mmol/L)	0.280	1.872	0.642	1.626	1.094
NH_4^+	0.115	0.490	0.108	0.580	0.100
$\text{NO}_3^- + \text{NO}_2^-$	0.026	0.003	0.148	0.003	0.300
TOC	0.82	0.34	1.66	0.10	2.70
HCO_3^-	17.09	114.23	39.16	99.22	66.76
Total dissolved carbon	3.69	22.60	8.37	19.56	14.21
Cl^-	2.98	5.80	9.967	29.70	18.70
F^-	0.086	0.460	0.559	0.490	0.150
SO_4^{2-}	1.14	1080	241	1510	541
S-total	0.5	377	84	524	188
Fe	0.0042	0.0381	0.079	0.0230	0.1730
K	0.3	38.3	4.2	42.6	9.09
Na	1.6	4.99	20.6	21.7	44.4
Li	<0.004	0.015	-	0.025	n.a.
Ca	3.53	430	78	565	172
Sr	0.0188	1.63	0.99	2.47	2.21
P	<0.04	<0.04	<0.04	<0.04	<0.04
Si	1.86	4.79	4.52	5.14	7.85
Al	0.007	0.029	0.006	0.007	0.004
Be	<0.0002	<0.0002	-	<0.0002	n.a.
B	0.004	0.120	0.002	0.160	n.a.
Ba	0.0110	0.0599	0.0181	0.0612	0.0270
As	<0.02	<0.02	<0.02	<0.02	<0.02
Pb	<0.01	<0.01	<0.01	<0.01	<0.01
Zn	0.2460	0.0440	0.1736	0.0771	0.0832
Cu	0.2730	0.0093	0.1539	0.0120	0.0050
Ni	0.005	0.242	-	0.419	n.a.
Cd	<0.001	0.039	<0.001	0.067	<0.001
Co	<0.002	0.064	0.035	0.109	0.0784
Cr	<0.002	<0.002	<0.002	<0.002	<0.002
V	<0.001	<0.001	<0.001	<0.001	<0.001
Mo	<0.003	0.385	0.008	0.315	0.016
Mg	0.486	17.4	9.8	26.0	21.4
Mn	0.0023	3.03	0.59	4.25	1.32

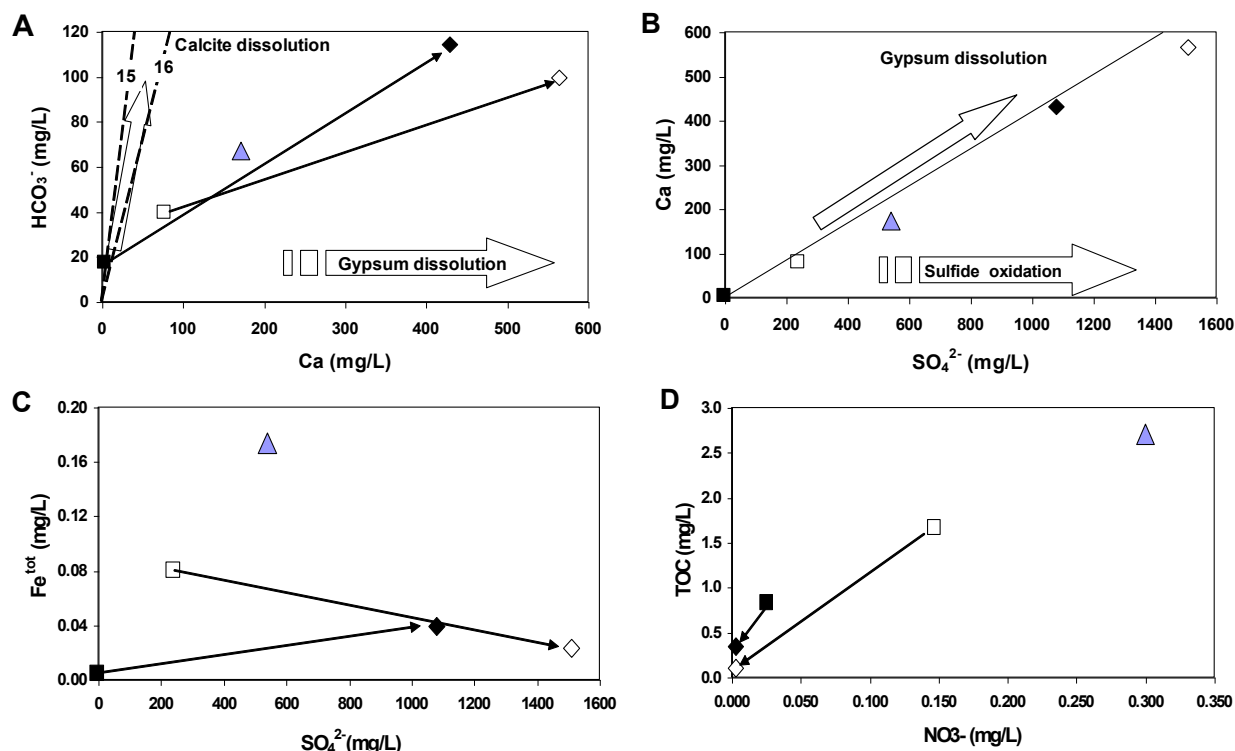


Figure 5: A: Ca vs. bicarbonate and effects from gypsum (= anhydrite) and carbonate dissolution. Stippled lines represent calcite dissolution by Reactions 15 and 16 (see text). B: Sulfate vs. Ca with arrows showing effects of gypsum dissolution and sulfide oxidation. C: Sulfate vs. total Fe. D: Nitrate vs. dissolved Total Organic Carbon. *Symbols*: triangle = tunnel water; filled symbols = Water 1; open symbols = Water 2 with evolutionary trajectories.

6.4.4.3 Saturation indices

Saturation indices (SI) were calculated from the water chemical compositions (Table 7) using the software PHREEQC-2, version 2.12.04 and the database *llnl.dat* (see references in vs. 2.12.04 of the software). This calculation assumes thermodynamic equilibrium between waters and minerals. All ions and elements were entered except those below detection limits. Alkalinity was entered instead of bicarbonate. The input redox conditions were defined by the measured Eh for initial waters and averaged Eh measurements throughout the leaching experiments for the final waters. The ion poor Water 1 initial had a poor balance (+ 44.7 %), indicating that an anion was missing in the analysis, whilst the remaining four waters showed an ion balance within + 4.47 % to + 0.54 % error.

Table 8: Saturation indices calculated from water chemistry using PHREEQC-2 and *llnl.dat*.

	Water 1 init	Water 1 final	Water 2 init	Water 2 final	Tunnel water
Rhodochrosite	-5.44	-1.84	-3.03	-1.92	-2.93
Calcite	-4.16	-1.53	-2.78	-1.63	-2.67
Magnesite	-5.28	-4.53	-3.97	-3.29	-3.88
Carbon	-12.57	-14.29	-12.11	-14.00	-12.00
Anhydrite	-4.74	-0.42	-1.44	-0.25	-0.93
Gypsum	-4.53	-0.22	-1.24	-0.05	-0.73
Barite	-2.06	1.02	0.16	1.09	0.54
Bassanite	-5.38	-1.07	-2.09	-0.90	-1.58
Ferrihydrite	-6.16	-4.73	-5.35	-5.24	-5.42

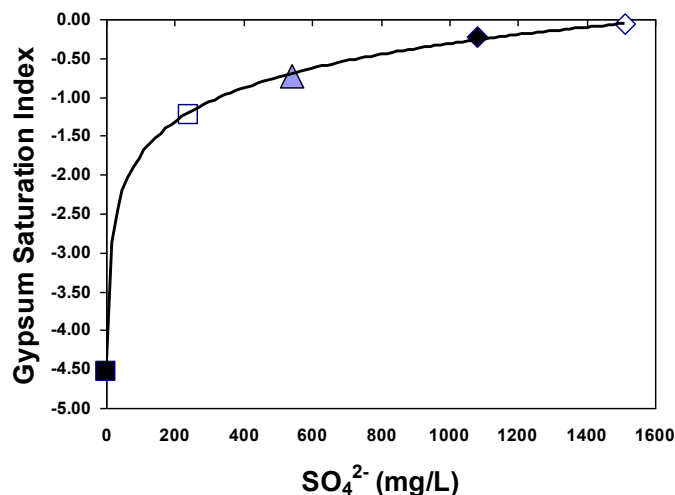


Figure 6: Sulfate concentrations plotted versus saturation indices (SI) for gypsum as calculated by PHREEQC-2. Symbols as in Figure 5.

Selected data are presented in Table 8. Figures 6 and 7 shows the saturation indices for gypsum and calcite plotted versus sulfate and bicarbonate, respectively. Gypsum was undersaturated but evolved towards near saturation in the final waters. Anhydrite followed exactly the same trend as gypsum at a very slightly more negative SI. Bassanite ($\text{CaSO}_4 \cdot 0.5\text{H}_2\text{O}$) SI's followed a parallel trend (not shown) at lower saturation level. Barite (BaSO_4) was supersaturated except from in Water 1 initial, whilst Ba had increased in the final waters: The overall effect on aqueous sulfate must have been minor due to the low concentrations of Ba. Carbonates, calcite and rhodochrosite were undersaturated and evolved towards a mild degree of undersaturation in the final waters. Magnesite (MgCO_3), representing an end-member in Mg-calcite, was well undersaturated. It should be noted that Mg-calcites (not in the *lnl.dat* database) containing a few moles of Mg is somewhat more stable than pure calcite (cf. Appelo and Postma 2005). This also seems supported by the XRD results, showing that whilst calcite dissolution was obvious Mg-calcite remained after leaching (cf. Table 4). Ferrihydrite ($\text{Fe}(\text{OH})_3$) was strongly undersaturated in all waters, as was carbon.

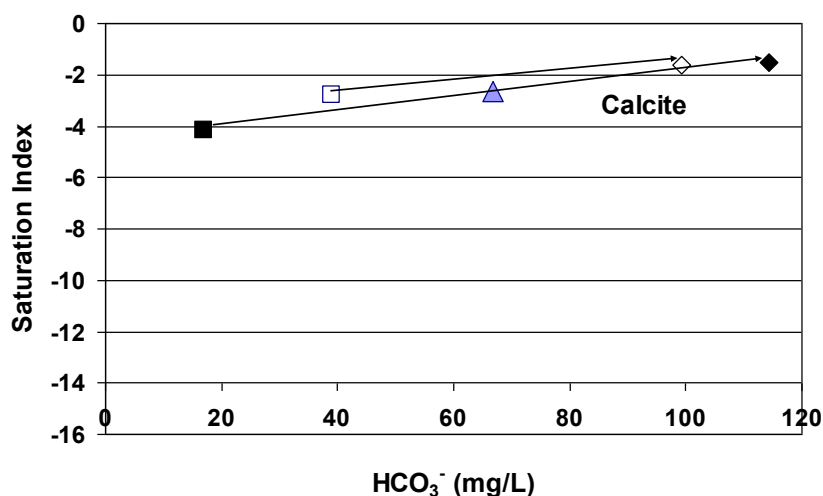


Figure 7: Bicarbonate contents plotted versus saturation indices for calcite. Symbols as in Figure 5.

Part 1 – Black Shale environment

Except for barite, the calculated saturation indices of the carbonates, sulfates and ferrihydrite represent somewhat soluble phases, which are generally regarded as reliable indicators of the saturation state. Carbon in the waters, as represented by TOC and a hypothetical contribution from Alum Shale carbon, may be present in several different forms. Therefore the calculated SI's for carbon are not necessarily meaningful. The measured redox states did not produce any reduced sulfur species in this model calculation, thus pyrite and pyrrhotite SI's were not obtained. However, due to their complex dissolution kinetics the saturation state of these sulfide minerals remains rather obscure. SI's of the remaining phases present in the Alum Shale are not reported herein, because of their complex and very sluggish dissolution kinetics, which makes interpretation of SI's difficult or meaningless.

Table 9: Stable isotopes in waters and solids from the Svartdal tunnel. A hydrothermal calcite vein in Alum Shale was taken from Cores 320B and shale organics were from Core 370A. Thauamasite data from sprayed concrete quoted from Iden and Hagelia (2003). All date in pro mill relative to isotopic standards (e.g. PDP, SMOW, CDT). * = calculated in section 6.3.2.

	Water 1 initial	Water 1 final	Water 2 Initial *	Water 2 final	Tunnel water	Calcite vein	Shale organics	Sulfide (bulk)	Thaum
$\delta^{13}\text{C}_{\text{PDP}}$	-11.3	-11.2	-12.1	-11.5	-12.3	-7.8	-30.9	na	-5.8 -16.2 -10.7
$\delta^{18}\text{O}_{\text{SMOW}}$	-10.3	-9.6	-10.7	-9.9	-11.3	5.2	na	na	+20.4 +17.1 +21.8
$\delta^{34}\text{S}_{\text{CDT}}$	nd	24.0	12.4	21.4	12.4	na	+6.7 +6.9	+26.6 +27.7	+1.8

6.4.5 Stable isotopes

Stable isotopes of C, O and S (cf. Table 9) were used in order to put further constraints on the sources of aqueous sulfate, bicarbonate and acid. The O and C isotopic compositions evolved from somewhat different values in the initial waters towards slightly heavier compositions in the final waters. The saturation indices (SI) suggested that pyrrhotite, anhydrite, gypsum, calcite and carbon were thermodynamically unstable in all waters, yet approaching chemical equilibrium (e.g. at $\text{SI} = 0$) in the final waters. Theoretically water in chemical equilibrium with soluble phases in the shale should have a uniform composition which upon mixing with waters of different isotopic compositions should fall on unique linear mixing lines being sensitive to the saturation level of each mix proportion.

It is evident that there was an almost uniform isotopic water composition in simultaneous chemical equilibrium with gypsum, anhydrite and calcite (Figure 8): For calcite, linear extrapolation of the evolutionary trends converged on an isotopic water composition of $\delta^{13}\text{C} = -11.2 \text{ ‰}$ and $\delta^{18}\text{O} = -9.5 \text{ ‰}$ at a small degree of undersaturation ($\text{SI}_{\text{Cc}} \approx -1$) (e.g. calcite in chemical equilibrium with water) Similarly, extrapolation for gypsum and anhydrite showed that the lines converged on exactly the same composition, yet in this case at a slight degree of super saturation ($\text{SI} \approx 0.5$ for both gypsum and anhydrite): At $\text{SI} = 0$ for the sulfates, $\delta^{18}\text{O}$ varied between -9.5 ‰ and -9.9 ‰ and $\delta^{13}\text{C}$ varied between -11.2 ‰ and -11.4 ‰ (Figure 8) whilst on an oxygen isotopes versus carbon isotope plot (Figure 9) the lines converged on $\delta^{13}\text{C} = -11.2 \text{ ‰}$ and $\delta^{18}\text{O} = -9.4 \text{ ‰}$. These differences are within analytical error (see section 6.3.2).

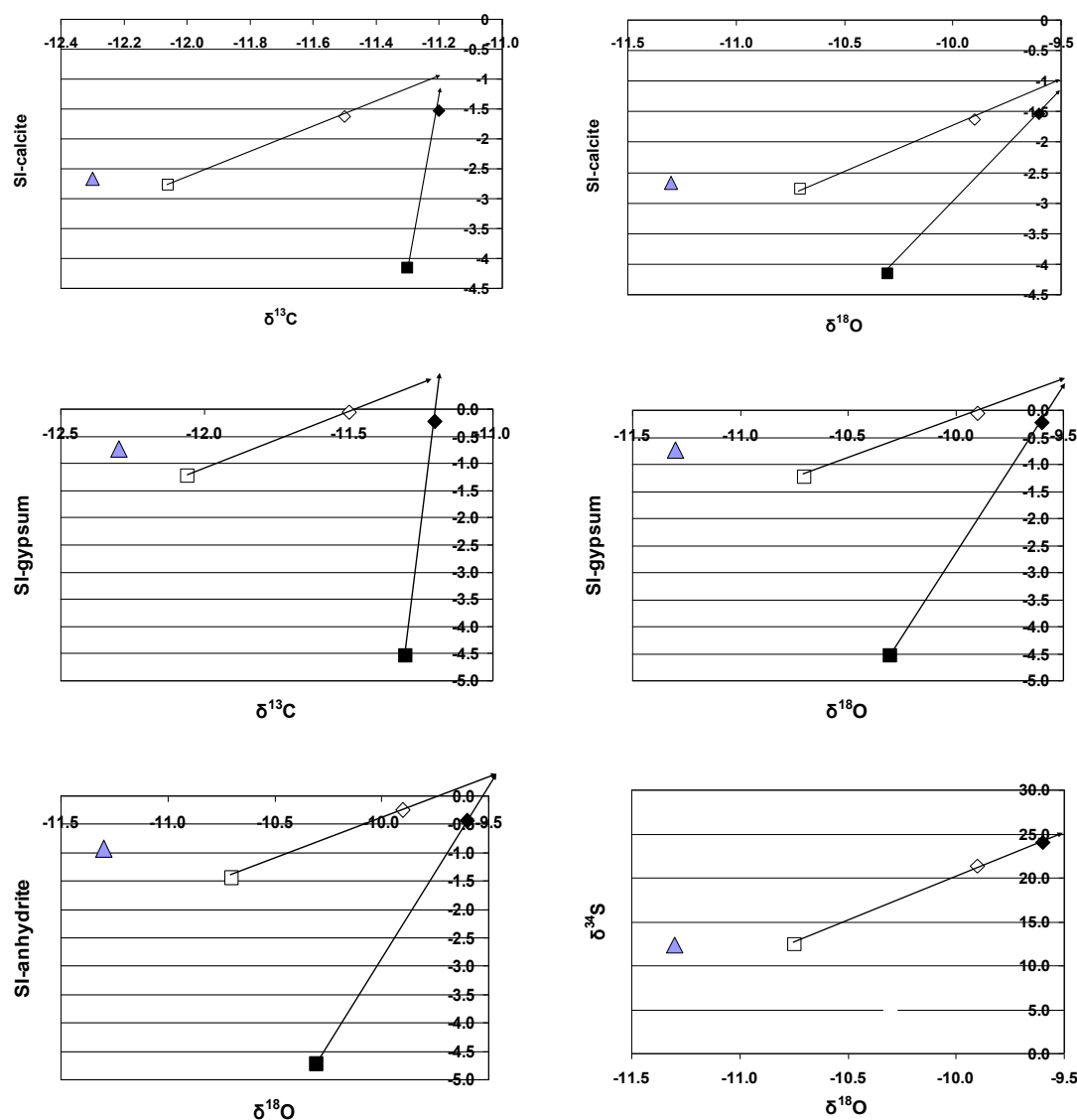


Figure 8: Stable C and O isotopes plotted versus saturation indices (SI) for calcite, gypsum and anhydrite. Symbols as in Figure 5. Note that evolutionary trends in the two waters converged on a uniform isotopic composition at equilibrium (SI = 0). This composition represents water equilibrated with Alum Shale. Also the O vs. S isotope plot indicates that the waters evolved towards a uniform heavy sulfur isotopic composition (see text for details).

The sulfur isotopes evolved towards a uniform water composition of $\delta^{34}\text{S} \approx +25 \text{‰}$ when extrapolated to $\delta^{18}\text{O} \approx -9.5 \text{‰}$ (Figure 8); holding true even though the S isotopic composition in the sulfate poor Water 1-initial is unknown. This behaviour was expected, since the same Alum Shale powder was leached in two different waters with different C, O and S isotopic starting compositions.

The C and O isotope composition of the Alum Shale secondary calcite vein was different from Cambrian Marine Carbonate (cf. Figure 10). Shale organic carbon had a very light C isotope composition ($\delta^{13}\text{C} = -30.9 \text{‰}$), which is identical to Alum Shale carbon elsewhere in Oslo ($\delta^{13}\text{C} = -29.1 \text{‰}$ to -30.9‰ ; own measurements). Sulfur associated with organic carbon yielded $\delta^{34}\text{S} = +6.7 \text{‰}$ and $+6.9 \text{‰}$. A single previous analysis of shale organics reported by Iden and Hagelia (2003) had much heavier sulfur ($\delta^{34}\text{S} = +21.2 \text{‰}$). This sample most likely contained an appreciable amount of very tiny pyrite framboids, which are

in fact very abundant (Figure 3): sulfides in Alum Shale at locality 320 were characterised by an essentially uniform $\delta^{34}\text{S} \approx +27 \text{‰}$ whilst near by Alum Shale at locality 370 ranged from $\delta^{34}\text{S} = +15.8 \text{‰}$ to $+22.1 \text{‰}$. Secondary thaumasite veins in deteriorated sprayed concrete from the Svartdal tunnel had much lighter sulfur ($\delta^{34}\text{S} = 1.8 \text{‰}$) (Iden and Hagelia 2003). The final waters developed heavy sulfate ($\delta^{34}\text{S} = +21.4 \text{‰}$ to $+24.0 \text{‰}$), which is within the range of local Alum Shale sulfide compositions (see Figure 8, Table 9). In contrast the S isotopic composition of Tunnel water from a pond rich in bacterial slime was significantly lighter ($\delta^{34}\text{S} = +12.4 \text{‰}$).

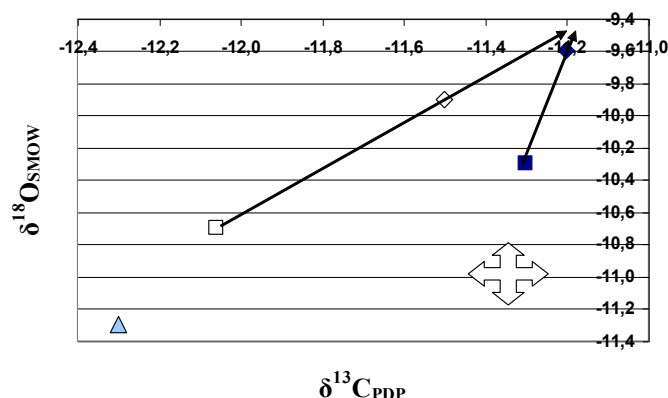


Figure 9: Stable C and O isotope trends converged on a composition identical to water equilibrated with the most soluble minerals in Alum Shale. This also suggests that effects of evaporation on $\delta^{18}\text{O}$ were minor or insignificant. Analytical errors ($\pm 1\sigma$) indicated.

6.5 Discussion

The chemical environment in the leaching experiment was somewhat different from the processes taking place in the tunnel. Surfaces of Alum Shale sulfides including the very small pyrite framboids were essentially clean after 65 days of leaching without any obvious presence of bacterial growth. In contrast the tunnel water sample was characterised by growth of a brown bacterial slime, apparently rich in *Acidithiobacillus species*. Biomineralisation here was predominated by ferric iron deposition containing some nitrogen and phosphorous. *The leaching experiment was therefore completely dominated by the abiotic part of the Alum Shale – water interaction processes, whilst the tunnel water environment also involved additional biochemical reactions.* The waters in the leaching experiment had interfered with the sulfur-, carbon- and the nitrogen cycles and was otherwise characterised by overall somewhat reducing conditions similar to ground water (cf. Appelo and Postma 2005). The results indicated that a quite small amount of soluble minerals in the shale may significantly change the water quality.

6.5.1 Chemistry of water - Alum Shale interaction

6.5.1.1 Abiotic leaching experiment

The leaching experiment must be regarded as an essentially closed system interrupted by open system behaviour from day 9 to 28, involving episodic agitation. The periods before and afterwards must have involved replenishment of air above the waters while bottles were open for measurements, representing very short incidents with lesser influence from

atmospheric CO₂ and O₂. The pH and Eh levelled off and approached some kind of equilibrium between days 40 and 65 at pH = 6.60. The subsequent rise to pH = 7.2 – 7.3 on day 77 was most likely due to more effective shale powder – water interaction caused by centrifugation of the sample, probably similar to effects after airing and agitation at day 9.

Aqueous sulfate. The saturation indices (Figures 6 and 7; Table 8) suggest that gypsum and/or anhydrite represent potential sources of aqueous sulfur species. An important contribution from iron sulfides may appear less likely in view of a) the persistence of pyrite and pyrrhotite and notably the presence of very small pyrite framboids in the residues after leaching and b) the extremely low Fe²⁺ concentrations in final waters, which might represent an argument against iron sulfide oxidation in general. There was no evidence of red rust precipitation during the leaching experiment, which agrees excellently with the strong undersaturation of Fe(OH)₃ (ferrihydrite) throughout the experiment. Moreover, (hypothetical) formation of a thin protecting layer of S⁰ on pyrite and pyrrhotite surfaces should not easily be broken in absence of sulfide oxidising bacteria, hence slowing down formation of sulfuric acid.

However, the iron sulfide grains were usually very small (frequently < 10 μm) and some amount of abiotic pyrite and pyrrhotite dissolution is therefore expected. Dissolution phenomena were apparent in SEM. This is further substantiated by the fact that at pH > 6 the intermediate sulfur species do not bond significantly to *pyrite* surfaces (Rimstidt and Vaughan 2003), and S⁰ can be oxidised abiotically to sulfate at circum neutral pH (Konhauser 2007). Presence of iron sulfides in the residues does not exclude iron sulfide dissolution but requires an explanation to the “missing aqueous Fe” in the leaching experiment. It seems possible that a contribution of SO₄²⁻ from abiotic pyrite and pyrrhotite oxidation could have developed without a notable increase in aqueous iron: Fe²⁺ might have been trapped by successive sorption to the abundant muscovite, because of its Point of Zero Charge (PZC) at 2-3 (Stumm and Morgan 1996). This strictly implies presence of a significant negative surface charge on muscovite surfaces at ambient pH = 6-7. *Sorption of Fe²⁺ would indeed explain why there was no strong acidification* and typical red rust formation taking place during the experiment. It should be recalled that the most significant acidification associated with sulfide oxidation reactions results from oxidation of the dissolved iron. When most Fe²⁺ and Fe³⁺ are removed successively from the water phase the impact of the acid producing Reactions 2, 4 and 12 will be unimportant or absent.

Bhatti et al. (1993) established that the early stages of *pyrrhotite* dissolution reactions are acid consuming. In contrast the first step of pyrite oxidation produces H⁺, SO₄²⁻ and Fe²⁺ upon reaction with oxygen and water according to Reaction 1. This might well have been the case during Stage 1 (Figure 4) when pH dropped from about 7 to 6, thus consuming initially dissolved O₂ in a closed system. Calculation based on 8.7 mg/L of dissolved oxygen at 22.6 °C (cf. standard tables) shows that total consumption of this amount of oxygen according to Reaction 1 produces 0.155 mmol/L H⁺. This corresponds to a pH drop by 0.81 which is in good agreement with the results (Table 6). The transition towards higher pH (beginning of Stage 2) took place while the bottles were closed, and at this stage (day 9) there was a suspect smell of H₂S. This suggests that non-oxidative dissolution of pyrrhotite according to Reaction 7 had started, hence consuming H⁺ which had formed through Reaction 1. Possibly an impact of Reaction 7 continued into Stage 2 while the bottles were open. However, most likely the oxidative acid-consuming Reaction 8 took over, thus stabilising S⁰ on pyrrhotite surfaces.

Bicarbonate concentrations increased during the leaching experiment. The saturation indices for initial waters strongly suggest that carbonates started to dissolve from the very beginning of the leaching experiment (cf. Table 8). Generally bicarbonate may be derived from a) carbon dioxide reacting with water (e.g. Reaction 14); b) dissolution of carbonates (Reactions 15 and/or 16 with derivatives for Mg-calcite and Mn-carbonate) and c) from

organic carbon by redox reactions involving denitrification or reduction of aqueous sulfate to hydrogen sulfide (Reactions 17 and 18, respectively). At pH = 6.3 waters contain H₂CO₃* (mainly CO₂) and bicarbonate in equal proportions, whilst at pH = 7.3 the relative bicarbonate concentration is 90 %. Thus the proportion of CO₂ varied from about 50 % of the total inorganic carbon at the transition between Stage 1 and 2 to about 10 % in the final analysed waters (pH = 7.2-7.3 at day 77). A certain contribution from shale organic carbon would seem possible due to SI < -12 for native C (Table 8). However, the C isotopic evolution showed that anthracite-like carbon (“pre- graphite stage”) did not dissolve during the leaching experiment (cf. Chapter 6.5.2), hence contrasting with carbon thermodynamic properties in the *lnl.dat* database. Therefore enhancement of bicarbonate was mainly caused by dissolution of calcite and Mg bearing calcite with a small contribution from rhodochrosite. The enhanced concentrations of Ca, Mg and Mn in the final waters partly reflect this, although some Mg and perhaps Mn were derived from breakdown of montmorillonite. A smaller amount of bicarbonate had apparently also formed from initial TOC, which was depleted in the final waters (Table 7).

The mild degree of acidification during Stage 1 suggests a certain impact of carbonate dissolution by Reaction 15 as caused by H⁺ initially derived from Reaction 1. Subsequently pH buffering according to Reaction 21 probably took place.



However, presence of atmospheric CO₂ during the first stage also suggests influence of carbonate dissolution and pH buffering according to Reaction scheme 16. CO₂ gas – water exchange is very quick (in the order of seconds; cf. Appelo and Postma 2005), and must have been replenished while the system was opened. Hence the increased pH during Stage 2 likely resulted from enhancement of bicarbonate (Reaction scheme 16) along with the H⁺ consuming Reactions 7 and 8. During Stages 3 and 4 the slow drop in pH started while the bottles were open to air, while pH levelled off at pH = 6.60 more than ten days after the bottles were closed. This may well reflect a continued small impact of pyrite dissolution (Reaction 1) and Reactions 9 and 11, which eventually halted further acid production as oxygen was consumed. Impact from carbonate dissolution by H⁺ (Reaction scheme 15) was apparently unimportant: The overall carbonate dissolution during the experiment seems due to reaction with CO₂ and water (Reaction scheme 16), as was clearly suggested by the C and O stable isotope evidence (see below).

Nitrogen species. SEM and water chemical data showed that *nitrogen was leached from the Alum Shale*. The total nitrogen contents increased in both of the final waters, being enriched in NH₄⁺ whilst NO₃⁻ was nearly exhausted (3µg/L). It is well established that ammonium occurs in Black Shales, representing a waste product after past time metabolism (Konhauser 2007). Ammonium is usually bound to clay minerals in Scandinavian Alum Shale (Lindgreen et al. 2000). In the present case it seems possible that ammonium was bound to montmorillonite, which occurred as a primary mineral in the Svartdal Alum Shale. However, the water chemical data also showed that Total Organic Carbon (TOC) became depleted along with nitrate in the waters and the degree of depletion was apparently depending on the available initial TOC contents (Figure 5D). Therefore *NH₄⁺ was most likely leached directly from the shale whilst NO₃⁻ was consumed by strong influence of a denitrification reaction*, involving breakdown of TOC to bicarbonate. Because the overall carbonate dissolution was mainly controlled by CO₂, this would seem compatible with Reaction 17 involving denitrification and CO₂-degassing.

Due to the overall reducing conditions during the experiment it is evident that ammonium derived from the Alum Shale was allowed to accumulate in the water phase, yet not excluding a small impact of Reaction 22 (cf. Appelo and Postma 2005) while the bottles were open to air and during Stage 1:



The nitrogen content in the initial Alum Shale sample, perhaps mainly ammonium, was apparently in the order of 1000 ppm (Table 5). Because high ammonium concentrations greatly enhances growth of *Acidithiobacillus sp.* the nitrogen contents of various Alum Shales should therefore have a direct bearing on their sulfide oxidising potential as well. Thus, because *Acidithiobacillus ferrooxidans* is a facultative anaerobic bacterium, NH_4^+ -enriched ground water should in certain environments sustain enzymatic *iron sulfide oxidation and acidification even in the absence of oxygen*.

6.5.1.2 Ca-sulfates contributed most of the aqueous sulfate

The plot of Ca vs. HCO_3^- (Figure 5A) shows that the final waters were much richer in Ca than calcite dissolution can account for. This “excess Ca” must have been derived from gypsum and/or anhydrite. Hence by accounting for the net bicarbonate and Ca produced from carbonate dissolution, using the $\text{Ca}^{2+}/2\text{HCO}_3^-$ weight ratio (= 0.328) of the predominating Reaction 16, it is possible to estimate the Ca which was derived from gypsum and/or anhydrite. By further allocating the “excess Ca” to Ca-sulfates it is possible to establish the relative contributions from Ca-sulfates and Fe-sulfides to the aqueous sulfate in the final waters. Two basic assumptions must be made for this model calculation: 1) the amount of bicarbonate consumed by acids during the experiment should be relatively small and 2) the contributions from Mg-, Mn-carbonates and TOC to bicarbonate should be subordinate in comparison to calcium carbonate. The pH variation (Figure 4) did not indicate very extensive acidification. Also the persistence of pyrite, the potential for sorption of Fe^{2+} and absence of bacteria suggests relatively minor total acid production: A rise in pH from 6 to 7 involves consumption of about $1 \mu\text{g H}^+$ corresponding to only $61 \mu\text{g HCO}_3^-$. Moreover, acid buffering was apparently not restricted to bicarbonate consumption but was seemingly also due to early stage abiotic pyrrhotite dissolution according to Reactions 7 and 8. The XRD results showed that calcite (CaCO_3), and Mg-calcite ($\text{Mg}_{0.1}\text{Ca}_{0.9}\text{CO}_3$) in shale powder occurs in approximately equal proportions. Thus the Ca^{2+} derived from the two calcites represents about 95 % of all calcite relative to bicarbonate on molar basis. Mg-bearing calcite is also somewhat less soluble than pure calcite (cf. Appelo and Postma 2005) and tended to remain in the residues. The contribution from Mn-carbonate (rhodochrosite) and TOC were subordinate.

A calculation was therefore made assuming that the total production of HCO_3^- is represented by the values in Table 7, and derived from dissolution of pure calcite (Reaction 16). Net production of ions was used as basis for the calculation, yet omitting the small contributions to bicarbonate from Mg-calcite, rhodochrosite and TOC. The results showed that Ca contributed from calcite was 31.9 mg/L and 19.8 mg/L in Water 1 and Water 2, respectively. The “excess Ca” derived from the Ca-sulfates was 394 mg/L and 467 mg/L, corresponding to 885 mg/L and 1049 mg/L of SO_4^{2-} in Water 1 and Water 2. This amount of aqueous sulfate makes up 80.8 % (Water 1) and 81.6 % (Water 2) of total S in the final waters, which is remarkably consistent. Evidently dissolution of anhydrite (and likely also the secondary gypsum) contributed much more aqueous sulfate than pyrite and/or pyrrhotite. This stands in marked contrast to previous conclusion by the Alum Shale Committee, stating that only the iron-sulfides were responsible.

6.5.1.3 Tunnel water and ground water involving biotic and abiotic reactions

The tunnel water shared many similarities with the waters in the leaching experiment but also reflects processes associated with Alum Shale ground water. The tunnel water sample plots at a higher $\text{HCO}_3^-/\text{Ca}^{2+}$ ratio than the final Waters 1 and 2 (Figure 5A) with a little higher sulfate content relative to Ca (Figure 5B). This implies that relatively less of its Ca originated from the Ca-sulfates and that more of its sulfate was derived from the Fe-sulfides. Simple calculation suggests that about 40 % of sulfur in tunnel water was derived from pyrite and/or pyrrhotite, which is compatible with the slightly more acidic water here. Much iron had also been released from the tunnel water, precipitated as ferric biominerals within the bacterial slime. The origin of this iron could be sulfide oxidation within the rock mass, surface steel fibre corrosion or both. Indeed, the presence of *Acidithiobacillus sp.* like bacteria in the tunnel water suggests that the potential for iron sulfide oxidation (e.g. by enzymatic reactions) was greater here than in the leaching experiment.

6.5.2 Stable isotope systematics of waters, shale constituents and deteriorated concrete

Stable isotope systematics provided independent constraints on the source materials and chemical release mechanisms. The bulk water composition in simultaneous chemical equilibrium with soluble Alum Shale constituents was $\delta^{18}\text{O} = -9.5 \text{‰}$, $\delta^{13}\text{C} = -11.2 \text{‰}$ and $\delta^{34}\text{S} = +25 \text{‰}$. This represents a uniform composition towards which Water 1 and Water 2 mixed during the abiotic leaching experiment. Temperature corrected mineral-water fractionation factors were calculated from literature using the database at Université Laval Canadian (cf. www.ggl.ulaval.ca/cgi-bin/isotope/isotope4alpha.cgi). In the Svartdal tunnel there are only two alternative calcite sources, namely hydrothermal calcite veins ($\delta^{13}\text{C}_{\text{PDP}} \approx -7.8 \text{‰}$, $\delta^{18}\text{O}_{\text{SMOW}} \approx +5.2 \text{‰}$; Table 9) and Upper Cambrian marine carbonate ($\delta^{13}\text{C}_{\text{PDP}} \approx 0 \pm 1 \text{‰}$ and $\delta^{18}\text{O}_{\text{SMOW}} \approx +25 \pm 5 \text{‰}$; cf. Faure 1986, Meidla et al. 2004) (Figure 10). However, calcite veins were not present in the leached sample. The O isotopic signature of anhydrite in Svartdal Alum Shale should be similar to Cambrian marine sulfate ($\delta^{18}\text{O} \approx +12\text{-}15 \text{‰}$; cf. Faure 1986).

The coincidence of S isotopic signatures of Svartdal bulk sulfide with sulfate agrees very well with recent data of Gill et al. (2011) for Upper Cambrian Black Shale and Alum Shale worldwide, in contrast to younger euxinic environments where pyrite S is very light ($\delta^{34}\text{S}_{\text{CDT}} \approx 0 \text{‰}$) in comparison with associated sulfate ($\delta^{34}\text{S}_{\text{CDT}} \approx +15\text{-}30 \text{‰}$) (cf. Böttcher et al. 1999, 2005).

6.5.2.1 Source materials in Alum Shale powder deduced from abiotic leaching

Carbon isotopes. The waters evolved towards a relatively heavier C isotopic signature during the leaching experiment, implying that significant influence from Alum Shale organic carbon ($\delta^{13}\text{C} \approx -31 \text{‰}$) must be disregarded. Neither should formation of bicarbonate at expense of initial light carbon (TOC) influence the bulk water C isotopic signatures. Therefore the observed shift in C isotope composition was caused by calcite dissolution. Dissolution at 22.6 °C by H^+ according to Reaction 15 involves a calcite – bicarbonate fractionation of $\delta^{13}\text{C}$ equal to 1.99 ‰ for pure calcite (Deines et al. 1974). Both pure calcite and $\text{Mg}_{0.1}\text{Ca}_{0.9}$ -calcite occurred in approximately equal proportions in the Alum Shale powder. Jiménez-López et al. (2006) found that Mg substitution into calcite increases the calcite-bicarbonate fractionation factor by 0.024 ‰ per mol% of MgCO_3 . At bulk scale we therefore consider that 1 mol of “overall calcite” contains 5 mol% Mg and 95 mol% Ca, corresponding to an increase in $\delta^{13}\text{C} = (5 \times 0.024) \text{‰} = 0.12 \text{‰}$. The equilibrium fractionation of “overall calcite” – bicarbonate: $\delta^{13}\text{C} = (1.99 + 0.12) \text{‰} = 2.11 \text{‰}$. Reaction 15 should be

for “overall calcite” – water: $\delta^{18}\text{O} = (31.80 + 0.85) \text{‰} = 32.65 \text{‰}$ (0.85 ‰ by 5 mol% Mg substitution). O isotope fractionation associated with a marine calcite – water equilibrium should produce a water isotopic signature, $\delta^{18}\text{O} = (25 \pm 5 + (-32.65)) \text{‰} = -7.65 \pm 5 \text{‰}$. The anhydrite – water fractionation factor for $\delta^{18}\text{O}$ equals 34.09 ‰ (Zheng 1999) and the gypsum-water fractionation factor is 4.08 ‰ (Fontes 1965). Rhodochrosite – water fractionation is about 34 ‰ (Zheng 1999) but this mineral was volumetrically unimportant. Considering that Cambrian sulfate is characterised by $\delta^{18}\text{O} \approx +13.5 \pm 1.5 \text{‰}$, equilibrium fractionation of anhydrite – water and gypsum – water should contribute $\delta^{18}\text{O} = -20.59 \pm 1.5 \text{‰}$ and $\delta^{18}\text{O} = +9.42 \pm 1.5 \text{‰}$, respectively: Water in equilibrium with Alum Shale ($\delta^{18}\text{O} = -9.5 \text{‰}$) therefore represents a three component mixture of the individual contributions from calcite, anhydrite and gypsum. Calculation of the absolute proportions derived from three component mixing is not possible from the current data.

The combined C and O isotopes (Figure 10, Table 9) confirm there was no impact of pure calcite vein material in the Alum Shale powder. Equilibrium fractionation by dissolution according to the main Reaction 16 should contribute $\delta^{13}\text{C} = (-7.8 + (-7) + (-1.07) + (-1.99)) \text{‰} = -17.86 \text{‰}$ and $\delta^{18}\text{O} = (5.2 + (-31.80)) \text{‰} = -26.6 \text{‰}$ to the final waters. Similarly Reaction 15 should yield $\delta^{13}\text{C} = -9.8 \text{‰}$ with $\delta^{18}\text{O} = -26.6 \text{‰}$. These isotopic signatures are very different from the water composition in equilibrium with Alum Shale powder.

Sulfur isotopes. The chemical evidence showed that bulk aqueous sulfur in equilibrium with Alum Shale powder represents a mixture with contributions from the Ca-sulfates and a smaller impact from iron sulfides. The S isotopic composition of the final waters ($\delta^{34}\text{S} = +25 \text{‰}$) is within the range of bulk sulfide in the Svartdal Alum Shale ($\delta^{34}\text{S} = +15.8$ to $+27.7 \text{‰}$) but slightly lower than the local value at the Alum Shale sample station ($\delta^{34}\text{S} = +27.15 \pm 0.55 \text{‰}$). The S isotopic composition of gypsum or anhydrite is enriched in $\delta^{34}\text{S}$ by about 1.65 ‰ relative to that of aqueous sulfate. Anhydrite-gypsum conversion does not involve S isotope fractionation. Since these Ca-sulfates contributed about 80 % of the bulk aqueous sulfur, the S isotopic signature of anhydrite should be $\delta^{34}\text{S} \approx +26.7 \text{‰}$, being identical to the bulk iron sulfides. The pyrrhotite – H₂S fractionation factor (e.g. Reaction 7, see above) for $\delta^{34}\text{S}$ is 2.86 ‰ at 22.6 °C (Li and Liu 2006). Hence, minor H₂S degassing and subsequent oxidation to aqueous sulfate during leaching should not influence the bulk aqueous S isotopes very much. No significant contribution from bulk shale organics ($\delta^{34}\text{S} = +6.8 \pm 0.1 \text{‰}$) seems likely, in agreement with the C isotopic evidence.

6.5.2.2 Additional processes deduced from sprayed concrete and tunnel environment

The processes within the *tunnel environment* are potentially different from the conditions in the leaching experiment, due to: a) a somewhat wider compositional range of Alum Shale, involving calcite veins, compared with the investigated shale powder; b) rock – water interaction by ground water flow along rock joints instead of mainly static contact with rock powder, c) presence of bacteria, d) pH about 6-6.8 and e) time of exposure.

Tunnel water. The C and O isotopic signatures of the tunnel water sample were somewhat lighter than the equilibrium composition with marine carbonate in the leaching experiment. This seems to reflect the ground water temperature which is expected to be close to 8 °C at some 10-20 m depths below surface level (Stene 1997). C isotope fractionation related to dissolution of Scandinavian Upper Cambrian marine calcite in equilibrium with CO₂ at this temperature should result in $\delta^{13}\text{C} = -12.45 \text{‰}$ in water, which is identical to the tunnel water sample (Table 9, Figure 10). Hence, there seems to have been no contribution from calcite vein material to this particular tunnel water.

The $\delta^{34}\text{S} = +12.4 \text{‰}$ in the tunnel water is much lighter than the S isotopic composition of Ca-sulfates and iron sulfides in Alum Shale. Influence of very light S in SO₂ from exhaust fumes seems unlikely because the sample station was well protected from fumes

of the main road tunnel. Mixing of rain water characterised by $\delta^{34}\text{S} \approx +4\text{‰}$ to $+6\text{‰}$ (Iden 2002) with heavy sulfur from Alum Shale can also be excluded: rain water in southern Norway contains $< 5\text{ mg/L SO}_4^{2-}$ in contrast to 541 mg/L in tunnel water, which must have been derived from the shale. Hence the compositional difference between S isotopic signatures in the tunnel water pond and the sulfur-bearing phases in Alum Shale should reflect a significant fractionation of S isotopes due to interaction of ground water and shale. This may stem from the same processes being responsible for the light sulfur in thaumasite. Influence from the sulfur poor cement paste ($\delta^{34}\text{S} = +11.8\text{‰}$) should be minor, because the outer sprayed concrete was not extensively leached.

Sprayed concrete. The isotopic signatures of secondary thaumasite and calcite in tunnel concrete reflect mainly interaction of ground water with cement pore water, and can therefore be *used as a proxy* to understanding ground water processes. The sprayed concrete degradation was characterised by a zonation pattern with contrasting isotopic signatures (e.g. Iden and Hagelia 2003): a) relatively coarse calcite deposits \pm C-S-H in porous zones at the sprayed concrete/Alum Shale interface, characterised by $\delta^{13}\text{C} \approx -4\text{‰}$ to -6‰ with a wide $\delta^{18}\text{O}$ variation from $\approx +8\text{‰}$ to $+37\text{‰}$. b) Mixed internal degradation zones in the cement paste, comprising decalcification of C-S-H and variable levels of replacement by secondary popcorn calcite and thaumasite. This bulk assemblage ranged widely from $\delta^{13}\text{C} \approx -5\text{‰}$ to -22‰ and $\delta^{18}\text{O} \approx +25\text{‰}$ to $+10\text{‰}$. c) Internal pure thaumasite veins/mush zones with C and O signatures coinciding with the mixed internal degradation zones, and with $\delta^{34}\text{S} = 1.8\text{‰}$. d) Outer ordinary surface carbonated zones facing the tunnel space was characterised by $\delta^{13}\text{C} \approx -13\text{‰}$ and $\delta^{18}\text{O} \approx +10$ to $+15\text{‰}$. Essentially pure C-S-H was characterised by a well defined composition: $\delta^{13}\text{C} \approx -6\text{‰}$ to -7‰ , $\delta^{18}\text{O} \approx +25\text{‰}$ to $+26\text{‰}$ (Figure 10) and $\delta^{34}\text{S} \approx +11.8\text{‰}$.

C and O isotopes. The rather uniform C and very variable O isotopic signatures of the *coarse calcite* rich assemblages suggests precipitation of aqueous carbonate derived from the Alum Shale under significant influence of atmospheric CO_2 . The coarse calcites displayed contrasting signatures in close proximity; implying that isotopic equilibrium was not attained. Their C isotopic composition ($\delta^{13}\text{C} \approx -5 \pm 1\text{‰}$) was heavier than the equilibrium composition with marine carbonate. It is significant that reprecipitation of dissolved carbonate may not lead to much fractionation of the C isotopes (Zeebe and Wolf-Gladrow 2001). For this reason precipitation of coarse calcite according to Reaction 16 (equilibrium with CO_2) seems impossible. Instead the isotopic signatures suggest aqueous carbonate was derived by acid dissolution of approximately equal amounts of calcite vein material and marine carbonate (Figure 10): This impact of Reaction 15 within Alum Shale near the interface with sprayed concrete shows that the tunnel environment was influenced by a carbonic and sulfuric acid regime compatible with an influence from iron sulfide oxidation or oxidation of H_2S . The process was probably sustained by bacteria. Such relatively acidic cool ground waters should readily absorb atmospheric CO_2 along open pores (observed at the concrete-shale interface; Hagelia et al. 2001), and lead to rapid kinetic precipitation of calcite with very variable O isotopic signatures when coming into contact with the high alkaline pore fluids in the cement paste.

Calcite formed by *ordinary surface carbonation* and in the *mixed internal degradation zones* plot along approximately the same trend (ellipses in Figure 10), and can be explained by the operation of *two processes being restricted to the concrete pore space*: 1) direct absorption of atmospheric CO_2 into very alkaline calcium hydroxide solution (e.g. cement pore fluid) and 2) deposition from groundwater containing dissolved calcite. These processes involve diffusion and kinetic fractionations resulting in calcite $\delta^{13}\text{C}$ values of -25‰ and -13‰ , respectively. Intermediate calcite values indicate overlap of the two processes (Dietzel 2000). The large fractionation towards very light carbon in the internal degradation zones ($\delta^{13}\text{C} < -20\text{‰}$) does not signify a further influence from the much lighter Alum Shale organic

carbon, in agreement with the conclusion from the leaching experiment. The effects on O isotopes are less systematic and depend on the signatures of inflowing water (cf. MacLeod et al. 1991). Figure 10 shows that the field of mixed internal degradation (variably developed calcite and thaumasite at expense of C-S-H) terminates at the trend of acid derived coarse calcite at $\delta^{18}\text{O} \approx +25 \text{ ‰}$, both of which coincide with pure C-S-H: Apparently the absorbed water was similar to the acidic water source of the coarse calcite deposits, being relatively enriched in carbonic acid. Yet, the characteristic $\delta^{13}\text{C} \approx -13 \text{ ‰}$ in ordinary surface carbonated zones suggests this carbonation formed by deposition from ground water (process 2) rather than by direct absorption of CO_2 . Essentially, the formation of 1) coarse calcite deposits 2) diffusion of aqueous carbonate and CO_2 into the cement paste can be regarded as aspects of the same overall process.

Recently it was established that thaumasite sulfate attack is a process closely related to internal concrete carbonation (Hagelia et al. 2001, 2003, Hagelia and Sibbick 2007, 2009). This is indeed corroborated by the coincidence of C vs. O isotopic signatures of thaumasite veins and mush zones with mixed calcite rich internal degradation zones. It is evident that the thaumasite carbonate contains an appreciable component of atmospheric CO_2 in addition to the contribution from acid dissolved carbonate derived from Alum Shale.

S isotopes. The sulfur isotopes provided additional information on processes affecting ground water chemistry. The sulfur-bearing Alum Shale minerals had much heavier S than the thaumasite in concrete ($\delta^{34}\text{S} = +1.8 \text{ ‰}$). Also bulk C-S-H in concrete, representing the bulk composition of gypsum added to cement and Al-sulfate used as setting accelerator, was different ($\delta^{34}\text{S} = +11.8 \text{ ‰}$). Thaumasite precipitation from ion rich waters does not involve any significant isotopic fractionation, and should therefore reflect the composition of the source water (Alt and Burdett 1992). There was no indication of sulfur-bearing minerals in the concrete aggregates (Hagelia et al. 2001). Hence the thaumasite sulfur source(s) must be entirely external. Airborne SO_2 from exhaust fumes could potentially represent such light sulfur (cf. Iden and Hagelia 2003) but should be ruled out in the present case, because the thaumasite had formed inside the concrete and not on its surfaces (cf. Hagelia et al 2001, 2003). The investigated location was otherwise screened from tunnel fumes.

For this reason we need to invoke a very significant sulfur isotope fractionation related to Alum Shale rock mass – ground water interaction, e.g. taking place before aqueous sulfate entered into the concrete pore space and formed thaumasite. The ground water system at this particular tunnel locality was characterised by the following ingredients: a) formation of aqueous sulfate by dissolution of anhydrite and sulfide oxidation in the approximate proportions 60:40; b) apparent presence of bacteria involving *Acidithiobacillus sp.* in oxidised zones, and hypothetically other species within anoxic domains; c) likely a somewhat variable oxidising - reducing environment related to fluctuations in the ground water level, and d) pH < 7. The local S isotopic composition of bulk sulfide just behind the analysed thaumasite - bearing concrete ($\delta^{34}\text{S} = +27.15 \pm 0.55 \text{ ‰}$) was similar to the Alum Shale anhydrite, implying fractionation of $\delta^{34}\text{S} \approx 25 \text{ ‰}$ in the ground water processes.

Only effects of bacteria (Iden and Hagelia 2003) and/or H_2S gas may explain the light S in thaumasite. Direct formation of H_2S from iron sulfides is not a sufficient step: pyrrhotite- and pyrite - H_2S fractionation factors at 8 °C are only about 3 ‰ and 5 ‰, respectively (Li and Liu 2006, Ohmoto and Rye 1979). When mixed with about 60 % anhydrite water the overall effect should be small (about 1-2 ‰). It was established above that sulfide oxidising bacteria likely had contributed to the formation of sulfuric acid from the Alum Shale rock mass by oxidation of H_2S (Reaction 11) or iron sulfides. Schnaitman et al. (1969) have shown that *Acidithiobacillus ferrooxidans* can oxidise pyrite 10^5 - 10^6 times faster than the abiotic pathways. However, most aerobic sulfide oxidising bacteria including *Acidithiobacillus ferrooxidans* cause little or no S isotope fractionation (Fry et al. 1986). An apparent exception

to this is *Acidithiobacillus thiooxidans* (previously *Thiobacillus concretivorus*), with effective fractionation varying from -10.5 ‰ to -18.0 ‰ (Kaplan and Rittenberg 1964). Yet when mixed with 60 % anhydrite water the *A. thiooxidans* may only contribute to a maximum of about 4‰ to 7 ‰ fractionation of the S isotopes. The total effect of sulfide oxidising bacteria is far too small to explain the thaumasite signature.

However, H₂S formed from reduction of SO₄²⁻ is enriched in ³²S by about 70-75 ‰ relative to aqueous sulfate (Sakai 1968; Ohmoto and Rye 1979). Upon reoxidation to aqueous sulfate near tunnel space its light isotopic signature will be retained. Sulfate reducing bacteria (SRB) are regarded as essential for breakdown of Ca-sulfates and significant formation of H₂S-gas (cf. Konhauser 2007). Hence, most likely SRB assisted in formation of H₂S from dissolved heavy sulfate under anaerobic conditions within the rock mass. It is concluded that SRB assisted formation of H₂S-gas from anhydrite reduction, followed by H₂S-degassing and re-oxidation to sulfate (sulfuric acid) represents a key process taking place within the Alum Shale rock mass. The very strong fractionation of light S into H₂S suggests that later formed sulfuric acid should have $\delta^{34}\text{S} \approx -40$ to -45 ‰. Hence the sulfate from which thaumasite formed ($\delta^{34}\text{S} \approx +2$ ‰) must have been derived from a mixture of such H₂S and dissolved non reduced anhydrite, likely with a contribution from bacterial iron sulfide oxidation. It seems possible that there was a neat interplay between the action of anaerobic and aerobic bacteria within the Alum Shale rock mass, which growth conditions should depend on fluctuations in ground water level or oxygen penetration from tunnel space.

6. 6 Regional aspects: H₂S gas and anhydrite in Alum Shale

6.6.1 H₂S gas release versus very rapid loss of pyrrhotite sulfur

H₂S-gas has frequently been reported immediately after blasting in Oslo Alum Shale, although not in the Svartdal tunnel. In the present author's opinion this clearly suggests H₂S-gas is present within some pristine Alum Shale rock masses, perhaps locked within the rock joint system. Degassing of H₂S also seems to provide a better explanation to the very rapid loss of reactive sulfur upon air exposure of Alum Shale samples than breakdown of monoclinic pyrrhotite, as was inferred by the Alum Shale Committee. This also seems corroborated by the present results, indicating the pyrrhotites were rather persistent. Yet influence from electrochemical catalysis by monoclinic pyrrhotite/pyrite interaction (Bastiansen et al. 1957) may not generally be refuted, although apparently not important in the present case. Possibly, however, the extensive non-pyrrhotite aqueous sulfate reported by the Alum Shale Committee may be due to a Ca sulfate source rather than pyrite.

6.6.2 Additional evidence of anhydrite in Alum Shale

The above new insight into a single local “system” of Alum Shale – concrete – water interaction raises the question of representativity. The result that a major portion of aqueous sulfate originated from anhydrite and to a lesser extent from iron sulfides requires further investigations. Additional available evidence suggests this is not a local phenomenon but in fact might be important at a regional scale.

Sopp (1966) analysed several samples of Oslo Alum Shale on XRD. Although anhydrite was not reported, reinvestigation of the diffractograms by the present author has revealed that several of his samples in fact show distinct small anhydrite peaks. Similarly Alum Shale from Gran north of Oslo also contains anhydrite in addition to iron sulfides.

Results of a leaching experiment demonstrated that the anhydrite bearing samples compare well with Svartdal Alum Shale (compare Figure 11 with Figure 5A, B). Also at Gran the Alum Shale leachates contained very little iron (< 1 mg/L) and no red rust had developed during the leaching experiment, suggesting similarities with the Svartdal Alum Shale (Hagelia in prep). However, each local engineering problem will always depend on relevant site specific documentation.

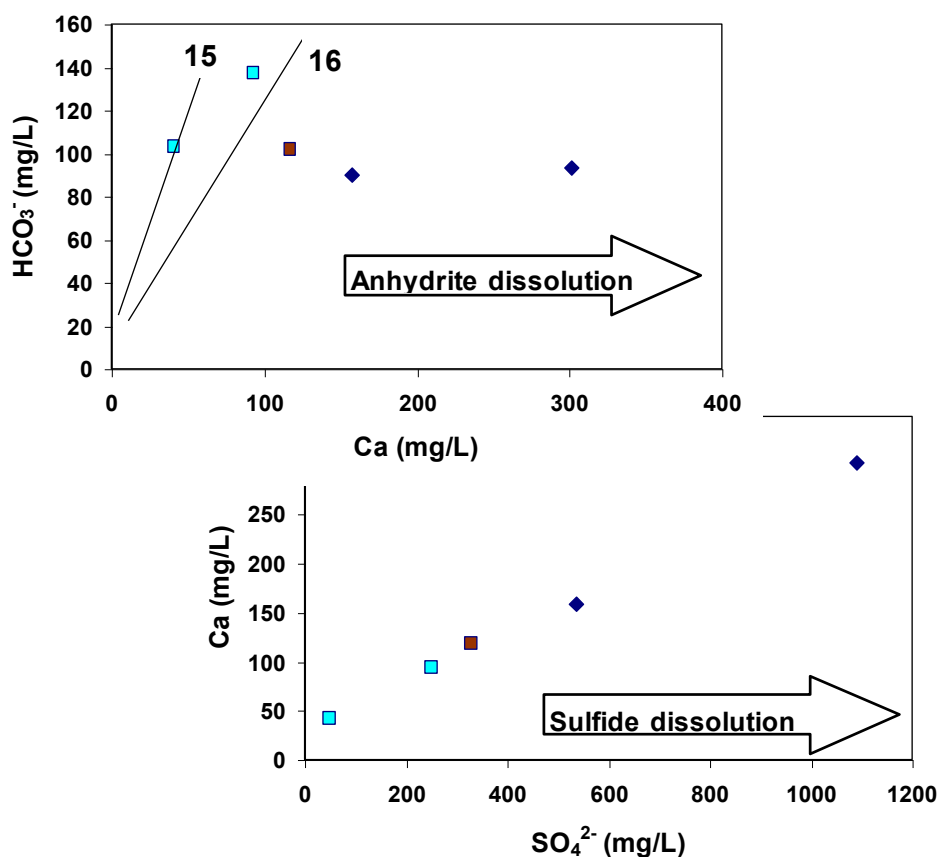


Figure 11: Results of leaching experiment on anhydrite and iron sulfide bearing Alum Shale from Gran (diamonds), black shale (dark square) and limestone (light squares). Trends for calcite dissolution according to Reactions 15 and 16 for are indicated.

6. 7 Implications

6.7.1 Concrete degradation

Ground water – Alum Shale interaction depends on the shale composition, its joint network and fluctuations in the ground water level. Thaumasite sulfate attack (TSA) and internal carbonation of the cement paste matrix is much dependent on the level of aqueous sulfate and bicarbonate, notably in acidic waters (cf. Hagelia and Sibbick 2009). The reactivity of Alum Shale towards concrete is not always dependent on its iron sulfide budget but indeed also on the contents of Ca-sulfate, calcite and involvement of bacteria. Prediction and mitigation of concrete sulfate attack should therefore potentially take great advantage of improved *on site* characterisation procedures, involving hydrogeology and microbiology. The present results also seem to suggest that atmospheric CO_2 may potentially represent the sole

source of carbonate for TSA in presence of a cool acidic and sulfate enriched ground water with very low alkalinity.

6.7.2 Shale swelling mechanism

An Alum Shale sample collected in vicinity of the investigated Core 320-06 yielded 65 % free swelling and a swelling pressure of 140 kPa (NPRA internal documents). This seems to reflect the observed anhydrite – gypsum conversion upon hydration, hence proving an old hypothesis regarding Alum Shale swelling (e.g. Barth 1943): The gypsum molar volume (74.56 cm³/mole) is larger than anhydrite (46.00 cm³/mole), which might cause a significant swelling effect in Alum Shales with more abundant anhydrite than in the present case. The compressive strength of gypsum is very high (\approx 160 MPa; Panozzo-Heilbronner 1993, Gysel 2002). Conversion of anhydrite to gypsum is also known to cause swelling in soils along with effects of swelling clays (cf. Azam et al. 1998). In a laboratory study of the Alum Shale geotechnical properties, Sopp (1966) concluded that there was *only one treatment which caused an instantaneous and permanent swelling*; namely by application of a fairly strong homogeneous stress followed by water suction. The swelling process was independent of the compositions of water and atmosphere used: e.g. distilled or sulfate rich water in presence of oxygen and nitrogen atmospheres. This seems compatible with anhydrite – gypsum conversion, notably because a stress should lead to micro fissuring, hence increasing the access of water. The swelling capacity generally increases with decreasing anhydrite grain size (Rauh et al. 2006), which may explain the significant effects sometimes encountered in very fine grained rocks such as Alum Shale.

Although the effect of anhydrite – gypsum conversion seems underestimated thus far, swelling by gypsum formation (Ca²⁺ derived from calcite or anhydrite and SO₄²⁻ rich waters derived from sulfides or anhydrite) is indeed also relevant where water is seeping into the underground and evaporation takes place: Evaporation may cause high super saturation; rapid gypsum precipitation and development of very high swelling pressures (cf. Correns 1949). This does not disregard the potential effects of swelling clay minerals when present, or perhaps other mineral transformations yet to be discovered within the Alum Shale. The geotechnical problem is always dependent on the site specific conditions.

6.7.3 Metal leaching

Cu and Zn were consumed during the experiment, whilst the elements Cd, Co, Mn, Ni and Mo were leached out. Cd reached 39-67 μ m/L, which is in the order of 8-13 times higher than most drinking water norms (5 μ m/L). Also Ni and Mn exceeded norm by about 5-10 and 60-85 times, respectively. The detection limit of As (20 μ m/L) was higher than the drinking water norms (10 μ m/L), which could hence still have reached a toxic level, whilst Pb concentrations were below drinking water norms (10 μ m/L). The experiment showed that toxic metals may be leached from Upper Cambrian Alum Shale at a near neutral pH when the contribution from sulfide oxidation was small. This appears to be somewhat conflicting with the results of Jeng (1992), which indicated that maintenance of a neutral pH (e.g. by liming) should immobilise most toxic metals. However, the release of Cd in the present experiment confirms Jeng's results for this element. It seems possible that Cd resides as Cd²⁺ in clay minerals and not in the sulfide minerals. Treatment of waste water from Alum Shale drainage should, therefore, be based on an improved knowledge of the source minerals for each

environmentally unfriendly element, involving thorough analysis of Alum Shale and waters at each site.

6.7.4 Further work

Up to now it has been established that the catalytic effect of minor monoclinic pyrrhotite on pyrite oxidation is a prerequisite for Alum Shale reactivity. In current practice Alum Shale is considered to cause swelling and concrete attack when Reactive pyrrhotite S > 0.01 % (e.g. H₂S released by boiling in HCl under N₂ atmosphere and precipitated as CdS) and *at the same time* Total S = 1.5-2 %. However, in this method any “primary” H₂S-gas residing within the shale should also be detected as Reactive S. In the leaching experiment the sulfide contributions were rather small, whilst anhydrite was responsible for about 1000 mg/L SO₄²⁻; Interestingly this corresponds to about 0.03 % Soluble S, being identical to that of local shale (Hagelia et al. 2003). Soluble S is not always used for reactivity rating but apparently reflects the Ca-sulfate content in Alum Shale. In view of the present results there is evidently a need for a revision of the test procedure. Although characterisation methods should overlap, it might be favourable to introduce separate procedures for a) swelling capacity, b) aggressiveness against concrete or steel and c) leaching of heavy metals. Development of improved engineering routines should take advantage of the mineralogical and geochemical stratigraphic record of Alum Shale, the variable impact of tectono-metamorphic events, microbiology and experience from previous construction work.

The microbiology of the Norwegian Alum Shale environments is essentially unknown. Research should focus on growth- and inhibiting conditions for sulfide oxidising- and sulfate reducing bacteria (SRB) within this environment. Each species may react differently to elemental concentration levels, redox conditions and pH. *Acidithiobacillus* species, so important for effective iron sulfide oxidation, prefer aerobic conditions despite being facultative anaerobic and otherwise favour a low pH environment in presence of, P, some K and other trace elements (cf. Konhauser 2007). NH₄⁺ can greatly enhance growth of *Acidithiobacillus ferrooxidans* (Niemelä et al. 1994). Growth of SRB and their effect on Ca-sulfate conversion to H₂S depends on the availability of essentially the same ions, albeit under anoxic conditions within the Alum Shale joint network below the vadose zone. Since high nitrate contents are toxic to *Acidithiobacillus ferrooxidans* (Niemelä et al. 1994) and SRB (cf. Bødtker et al. 2008), invasion of bacteria might be delayed after blasting. Yet, this should hypothetically be countered by the fertilising effect due to leaching of NH₄⁺ from Alum Shale.

Evidently several mechanisms being responsible for aggressive ions and swelling behaviour of Alum Shale are independent on the availability of oxygen: Future research should address a) the impact of total nitrogen content and leachable NH₄⁺, b) the regional significance of anhydrite, c) microbiology and d) the potential effect of radiolytic sulfide oxidation (e.g. Lefticariu et al. 2006): In fact reactive Alum Shale is characterised by simultaneous presence of elevated uranium contents and very small susceptible pyrite framboids. Mitigation and remedial work should always account for new findings.

6.8 Summary of findings and conclusions

This case study has demonstrated that the challenging engineering properties of Oslo Alum Shale are not only governed by iron sulfide oxidation, as interpreted by the previous Alum Shale Committee. Their hitherto established reaction mechanism, e.g. catalytic oxidation of abundant pyrite by minor amounts of very reactive monoclinic pyrrhotite, was

not confirmed. The investigation was mainly based on samples of concrete, water and Upper Cambrian Alum Shale from a classic occurrence. Together the samples represented a local quite well defined “system” useful for an integrated interpretation. The combined evidence showed that:

- The main source of aqueous sulfate was anhydrite, as first reported from Norwegian Alum Shale herein: Oxidation of pyrite and pyrrhotite accounted for only 20 % of the sulfate in an abiotic leaching experiment. In tunnel water influenced by *Acidithiobacillus*-like biota about 40 % was derived from iron sulfides.
- Other occurrences of anhydrite in Alum Shale were found, suggesting this mineral represents an important source of aqueous sulfate within several varieties of Alum Shale.
- Source anhydrite and bulk sulfides were isotopically much heavier ($\delta^{34}\text{S} \approx (+15)$ to $+27$ ‰,) than thaumasite sulfate in deteriorating concrete ($\delta^{34}\text{S} \approx +2$ ‰). This suggests partial reduction of anhydrite sulfate to H_2S within the rock mass, followed by reoxidation to sulfuric acid near the tunnels space.
- Also C and O isotope systematics suggested that calcite at the shale/concrete interface was deposited from acidic water. The overall process was most likely sustained by sulfate reducing bacteria (SRB) deep within the rock mass and sulfide oxidation assisted by *Acidithiobacillus sp.* closer to the tunnel.
- Acidification also occurs in association with weathering minerals, especially copiapite but also oxidation of ferrous iron bearing compounds and likely jarosite. These effects were not studied.
- Previous workers noticed a rapid loss of reactive sulfur from Alum Shale samples in contact with air or water, and attributed this to very reactive monoclinic pyrrhotite. However H_2S -gas release seems to be a more plausible explanation: a) monoclinic pyrrhotite was still detected by XRD after 65 days in the leaching experiment, b) H_2S has been detected after blasting operations in several Alum Shale varieties and c) H_2S represents a problem related to drinking water affected by this shale.
- Bicarbonate in investigated Alum Shale waters was derived from dissolution of Upper Cambrian marine calcite. Carbonate associated with the TF-TSA-carbonation process in concrete was derived from bicarbonate in ground water and atmospheric CO_2 , whilst anthracitic – graphitic shale carbon was inert.
- Growth of *Acidithiobacillus ferrooxidans* is fertilised by NH_4^+ , whilst a high level of NO_3^- is toxic. Hence reactivity of Alum Shale seems influenced by its leachable NH_4^+ , whilst NO_3^- available after rock blasting may delay bacterial colonisation.
- The general swelling mechanism in Alum Shale seems governed by a) anhydrite to gypsum conversion by hydration, b) gypsum precipitation by supersaturation of calcium and sulfate bearing waters and c) possible effects from clay minerals. The impact of each mechanism is site specific.
- In contrast to some previous reports, leaching of Cd, Ni and Mn reached toxic levels also when buffered by calcite to a circum neutral pH.
- Future work related to engineering and environmental issues should focus on the microbiology of Alum Shale and growth conditions for *Acidithiobacillus* species and sulfate reducing bacteria, the regional significance of anhydrite, leachable ammonium as well as the possible impact of radiolytic pyrite oxidation within uraniferous Alum Shale rock mass. Investigations of Alum Shale petrography and mineral chemistry should also be emphasised.

6.9 Acknowledgements

The author is indebted to Kjersti Iden and Ingar Johansen at IFE Kjeller for stable isotope analyses; Hans-Jørgen Berg for assistance with XRD and SEM analyses at the Museum of Natural History, University of Oslo; Ivar Dahl NIVA Oslo for water chemical analyses and Per Sydsæther, NPRA Oslo for core extraction. Professor Ignaci Casanova, Universitat Politècnica de Catalunya Barcelona, kindly commented on an early version of the manuscript. Finally the author gratefully acknowledges funding from the project Tunnel Development at NPRA.

6.10 References

- Abreham, A.Y. (2007): Reactivity of alum and black shale in the Oslo Region, Norway. MSc Thesis, University of Oslo. 95 pp.
- Alt, J.C. and Burdett, J.W. (1992): Sulfur in Pacific deep-sea sediments (Leg 129) and implications for cycling of sediments in subduction zones. In Larson, R.L. Lancelot, Y. Proceedings of the Ocean Drilling Program, Scientific Results, 129, 283-39'.
- Andersson, A., Dahlmann, B., Gee, D.G. and Snäll, S. (1985): The Scandinavian Alum Shales. Sveriges Geologiska Undersökning, Serie Ca 56, 1-50.
- Antun, P. (1967): Sedimentary pyrite and its metamorphism in the Oslo Region. Norsk Geologisk Tidsskrift. Vol. 47, No. 3, 211-235.
- Appelo, C.A.J. and Postma, D. (2005): Geochemistry, ground water and pollution. (2nd Ed.). A.A. Balkema Publishers, Leiden. 649 pp.
- Azam, S, Abduljauwad, S.N., Al-Shayea, N.A. and Al-Amoudi, O.S.B. (1998): Expansive characteristics of gypsiferous/anhydritic soil formations. Engineering Geology, 51, 89-107.
- Barth, T.F.W. (1943): Preliminary memorandum of mineralogical – chemical investigations on Alum Shale from Vikinggården. Type written report 15th April 1943 (in Norwegian).
- Bastiansen, R., Moum, J. and I.Th. Rosenqvist (1957): Contribution to high light certain construction problems associated with Alum Shale in Oslo. Norwegian Geotechnical Institute, Publication No. 22, Oslo, 69 pp (In Norwegian with English summary).
- Berner, R.A. (1984): Sedimentary pyrite formation: an update. Geochimica et Cosmochimica Acta, 48, 605-615.
- Bernier, L and Warren, L.A. (2006): Microbially driven acidity generation in a tailings lake. Geobiology, 3, 115-133.
- Bhatti, T.M., Bigham, J.M., Carlson, L. and Tuovinen, O.L. (1993): Mineral products of pyrrhotite oxidation by *Thiobacillus ferrooxidans*. Applied and Environmental Microbiology, Vol. 59, No 2, 1984-1990.
- Bjørlykke, K. (1974): Depositional history and geochemical composition of Lower Palaeozoic epicontinental sediments from the Oslo region. Norges geologiske undersøkelse, 305, 1-81.
- Brown, A.D. and Jurinak, J.J. (1989): Mechanism of pyrite oxidation in aqueous mixtures. Journal of Environmental Quality, 18, 545-550.
- Bødtker, G., Thorstenson, T., Lillebø, B-L., Thorbjørnsen, B., Ulvøen, R., Sunde, E and Torsvik, T. (2008): The effect of long-term nitrate treatment on SRB activity,

- corrosion rate and bacterial community composition in offshore water injection systems. *Journal of Industrial Microbiology and Biotechnology*, 35-12, 1625-1636.
- Böttcher, M.E., Bernasconi, S.M. and Brumsack, H.-J. (1999): Carbon, sulfur and oxygen isotope geochemistry of interstitial waters from Western Mediterranean. In Zahn, R., Comas, M.C. and Klaus, A. (Eds.) *Proceedings of the Ocean Drilling Program, Scientific Results*, 161, 413-421.
- Böttcher, M.E., Brumsack, H.-J., Hetzel, A. and Schipper, A. (2005): Sulfur isotope biochemistry and iron speciation of sediments from Demerara rise (ODP Leg 207). *Geophysical Research Abstracts*, Vol. 7, 07384, European Geosciences Union.
- Christensen, T.H., Bjerg, P.L., Banwart, S.A., Jacobsen, R., Heron, G. and Albrechtsen, H.J. (2000): Characterisation of redox conditions in groundwater contaminant plumes, *Journal of Contaminant Hydrology*, 45, 165-241.
- Collett, G., Crammond, N.J., Swamy, R.N. and Sharp, J.H. (2004): The role of carbon dioxide in the formation of thaumasite, *Cement and Concrete Research* 34, 1599-1612.
- Correns, C.W. (1949): Growth and dissolution of crystals under linear pressure. *Discussions of the Faraday Society*, Vol. 5, 267-271.
- Crammond, N.J. (2003): The thaumasite form of sulfate attack in the UK, *Cement and Concrete Composites* 25, 809-818.
- Deines, P., Langmuir, D. and Harmon, R.S. (1974): Stable carbon isotope ratios and the existence of a gas phase in the evolution of carbonate ground waters. *Geochimica et Cosmochimica Acta* 38, 1147-1164.
- DETR (1999): The thaumasite form of sulfate attack: Risks, diagnosis, remedial works and guidance on new construction, Report of the Expert Group, Department of Environment, Transport and the Regions, UK, 180 pp.
- Dietzel, M. (2000): Measurements of stable isotopes in calcite sinters on concrete. *ZKG Int*, 9, 544-548.
- Eframsen, H., Ormerød, K. and Arnesen, R.T. (1976): Microbial oxidation of sulfidic ore minerals, sulfide concentrates and crude ore with different sulfide contents. NIVA Progress Report, D2-23, B3-04 Mine drainage, 21pp (in Norwegian).
- Faure, G. (1986): *Principles of Isotope Geochemistry*. (2nd Ed.). John Wiley and Sons, 589 pp.
- Fiskaa, O., Hansen, H. and Moum, J. (1971): Concrete in Alum Shale, Norwegian Geotechnical Institute, Oslo, Publication No. 86. 32pp (in Norwegian with English summary).
- Fiskaa O. (1973): Concrete in Alum Shale, Norwegian Geotechnical Institute, Publication No 101 (Oslo, 12pp (In Norwegian with English summary).
- Fontes, J.-Cl. (1965): Fractionnement isotopique dans l'eau de cristallisation du sulfate de calcium. *Geologische Rundschau*, 55, 172-178.
- Fry, B., Cox, J., Gest, H. and Hayes, J.M. (1986): Discrimination between ³⁴S and ³²S during Bacterial Metabolism of Inorganic Sulfur Compounds. *Journal of Bacteriology*, Jan. 1986, 320-330.
- Gill, B.C., Lyons, T.W., Young, S.A., Kump, L.R., Knoll, A.H. and Saltzman, M.R. (2011): Geochemical evidence for widespread euxinia in Later Cambrian Ocean. *Nature*, 469, 80-83.
- Goldschmidt, V.M. (1911): Die Kontaktmetamorphose im Kristianiagebiet. *Vid. –Ak. Skrifter* 1, 11.
- Graham, J. (1987): Oxygen in pyrrhotite: A mechanistic model. *American Mineralogist*, 72, 610-611.
- Gysel, M. (2002): Anhydrite dissolution phenomena: three case histories of anhydrite karst caused by water tunnel operation. *Rock Mechanics & Rock Engineering*, 35, 1-21.

- Hagelia, P. and Grønhaug, A. (2000): Thaumasite – infection causing concrete deterioration, *Våre Veger* No 9, 54-55 (in Norwegian).
- Hagelia, P., Sibbick, R.G., Crammond, N.J., Grønhaug, A. and Larsen, C.K. (2001): Thaumasite and subsequent secondary calcite deposition in sprayed concretes in contact with sulfide -bearing Alum Shale, Oslo, Norway. 8th Euroseminar on Microscopy Applied to Building Materials, Athens, Greece, September 2001, 131-138.
- Hagelia, P., Sibbick, R.G., Crammond, N.J., and Larsen, C.K. (2003): Thaumasite and secondary calcite in some Norwegian concretes. *Cement and Concrete Composites* 25, 1131-1140.
- Hagelia, P. and Sibbick, R.G. (2007): Thaumasite sulfate attack, popcorn calcite deposition and acid attack in concrete stored at the “Blindtarmen” test site Oslo, from 1952 to 1982. In I. Fernandes, A. Guedes, F. Noronha, M. Teles, M dos Anjos Ribeiro (eds.), 11th Euroseminar on Microscopy Applied to Building Materials, Porto, Portugal (CD-rom).
- Hagelia, P. and Sibbick, R.G. (2009): Thaumasite sulfate attack, popcorn calcite deposition and acid attack in concrete stored at the “Blindtarmen” test site Oslo, from 1952 to 1982. In: *Materials Characterisation* 60, 686-699.
- Iden, I.K. (2002): Sulfide -bearing gneiss and pollution – application of isotopes for tracing of sources. IFE report 2002/078 (in Norwegian), 20pp.
- Iden, I.K and Hagelia, P (2003): C, O and S isotopic signatures in concrete which has suffered thaumasite formation and limited thaumasite form of sulfate attack. *Cement and Concrete Composites* 25, 839-846.
- Janzen, M.P., Nicholson, R.V. and Schärer J.M. (2000): Pyrrhotite reaction kinetics: reaction rates for oxidation by oxygen, ferric iron, and for nonoxidative dissolution. *Geochimica et Cosmochimica Acta*, 64-9, 1511-1522.
- Jeng, A.S. (1990): Morphology of pyrite in alum shale, Oslo, Norway. *Acta Agric. Scand.* 40, 11-21.
- Jeng, A.S. (1991): Weathering of some Norwegian Alum Shales I. Laboratory simulations to study the release of metal cations (Ca, Mg, K). *Acta Agric. Scand.* 41, 13-35.
- Jeng, A.S. (1992): Weathering of some Norwegian Alum Shales I. Laboratory simulations to study the influence of ageing, acidification and liming on heavy metal release. *Acta Agric. Scand.* 42, 76-87.
- Jensenius, J. (1987): Regional studies of fluid inclusions in the Palaeozoic sediments from southern Scandinavia. *Bulletin of the Geological Society of Denmark.* 36, 221-235.
- Jimenez-Lopez, C., Romanek, C.S., Huertas, F.J. Ohmoto, H. and Caballero, E. (2006): Oxygen isotope fractionation in synthetic magnesian calcite. *Geochimica et Cosmochimica Acta*, 68-16, 3367-3377.
- Jimenez-Lopez, C., Romanek, C.S. and Caballero, E. (2006): Carbon isotope fractionation in synthetic magnesian calcite. *Geochimica et Cosmochimica Acta*, 70, 1163-1171.
- Kaplan, I.R. and Rittenberg, S.C. (1964): Microbiological fractionation of sulphur isotopes. *J. Gen. Microbiology*, 34, 195-212.
- Konhauser, K. (2007): *Introduction to Geomicrobiology*. Blackwell Publishing, 425 pp.
- Kontny, A., de Wall, H., Sharp, T.G. and Pósfai, M. (2000): Mineralogy and magnetic behaviour of pyrrhotite from a 260 °C section at the KTB drilling site, Germany. *American Mineralogist*, 85, 1416-1427.
- Korom, S.F. (1992): Natural denitrification in the saturated zone: A review. *Water Resour. Res.*, 28, 1657–1668.

- Kullerud, G. (1986): Monoclinic pyrrhotite. Bulletin of the Geological Society of Finland, 58, Part 1, 293-305.
- Lapakko, K. (2002): Metal mine rock and waste characterisation Tools: An overview. Mining, Minerals and Sustainable Development, No 67, 29pp.
- Lapakko, K. and Berndt, M. (2003): Comparison of acid production from pyrite and jarosite. 6th ICARD Cairns, QLD, 7p.
- Lefticariu, L., Pratt, L.M. and LaVerne, J.A. (2006): Experimental study of radiolytic oxidation of pyrite: Implications for Mars-relevant crustal processes. Lunar and Planetary Science XXXVII. 2p.
- Lefticariu, L., Schimmelmann, A., Pratt, L.M. and Ripley, E.M. (2007): Oxygen isotope partitioning during oxidation of pyrite by H₂O₂ and its dependence on temperature. *Geochimica et Cosmochimica Acta*, 71, 5072-5088.
- Li, Y-B and Liu, J.M. (2006): Calculation of sulfur isotope fractionation in sulfides. *Geochimica et Cosmochimica Acta*, 70, 1789-1795.
- Lindgreen, H., Drits, V.A., Sacharov, B.A., Salyn, A.L., Wrang, P. and Dainyak, L.G. (2000): Illite-smectite structural changes during metamorphism in black Cambrian Alum shales from the Baltic area. *American Mineralogist* 85 No. 9 1223-1238.
- Lottermoser, B. (2003): Mine wastes – characterisation, treatment and environmental impact. Springer Verlag, 320p.
- Lusk, J., Scott, S.D. and Ford, C.E. (1993): Phase relations in the Fe-Zn-S system to 5 kbars and temperatures between 325 and 150 °C. *Economic Geology*, 88, 1880-1903.
- MacLeod, G., Hall, A.J. and Fallick, A.E. (1991): An applied mineralogical investigation of concrete degradation in a major concrete road bridge. *Mineralogical Magazine*, 54, 637-644.
- MEND (1998): Laboratory Studies of Pyrrhotite Oxidation. Mine Environment Neutral Drainage at CANMET-MMSL, MEND Report 1.21.2.
- Meech, J.A. and Suttle, C. (2002): Hunting for natural viruses to attack the bacteria that accelerate the production of ARD. <http://www.mining.ubc.ca/cerm3/phage.html>
- Meidla, T., Ainsaar, L., Backman, J., Dronov, A., Holmer, L. and Sturesson, U. (2004): Middle-Upper Ordovician carbon isotope record from Västergötland (Sweden) and East Baltica. In: O. Hints and L. Ainsaar (Eds.). WOGOGO-2004 Conference Materials, 67-68.
- Mielke, R.E., Pace, D.L., Porter, T. and Southam, G. (2003): A critical stage in the formation of acid mine drainage: colonisation of pyrite by *Acidithiobacillus ferrooxidans* under pH-neutral conditions. *Geobiology*, 1, 81-90.
- Moncaster, S.J., Bottrell, S.H., Tellam, J.H., Lloyd, J.W. and Konhauser, K.O. (2000): Migration and attenuation of agrochemical pollutants: insight from isotopic analysis of groundwater sulphate. *Contaminant Hydrology*, 43, 147-163.
- Moum, J. and Rosenqvist, I.T. (1959): Sulphate Attack on Concrete in the Oslo Region. *Journal of the American Concrete Institute, Proceedings*, Volume 56, Title 56-18, 8 pp.
- Natarjan, K.A., Iwasaki, I. and Reid, K.J. (1983): Some aspects of microbe-mineral interactions of interest to Duluth gabbro copper-nickel-sulfides. In G. Rossi and A.E. Torma (eds.), *Recent progress in biohydrometallurgy*. Associazione Mineraria Sarda, Iglesias Italy, 169-183.
- Neumann, H. (1985): The minerals of Norway. *Norges geologiske undersøkelse, Skrifter* 68, 278 pp (in Norwegian).
- Nicholson, R.V. and Scharrer, J.M. (1994): Laboratory studies of pyrrhotite oxidation kinetics. In C.N. Alpers and D.W. Blowes (eds.) *Environmental Geochemistry of Sulfide Oxidation*. American Chemistry Society, ACS Symposium Series 550, 14-30.

- Niemelä, S.I., Riekkö-Vanhanen, M., Sivelä, C., Viguera, F. and Tuovinen, T. (1994): Nutrient effects on the biological leaching of a Black-schist ore. *Applied and Environmental Microbiology* 60, No. 4, 1287-1291.
- Nordstrom, D.K. and Alpers, C.N. (1999): Geochemistry of acid mine waters. In *The Environmental Geochemistry of Mineral Deposits* (Plumlee, G.S. and Logsdon, M.J. eds.), Society of Economic Geologists, Littleton, CO, 133-160.
- Oftedal, C. (1955): On the sulphides of the alum shale in Oslo. *Norsk Geologisk Tidsskrift*, 35, 117-120.
- Ohmoto, H. and Rye, R.O. (1979): Isotopes of sulfur and carbon. In: H.L. Barnes (Ed.), *Geochemistry of hydrothermal deposits*, John Wiley & Sons, 509-567.
- Panozzo-Heilbronner, R. (1993): Controlling the spatial distribution of deformation in experimentally deformed and dehydrated gypsum. In: J.N. Boland, J.D. Fitz Gerald, (Eds.), *Defects and Processes in the Solid State: Geoscience Applications (The McLaren Volume)*. *Developments in Petrology* 14, 169-194.
- Ramberg, I.B., Bryhni, I. and Nøttvedt, A. (2006): *Landet blir til. Norges geologi*. Norwegian Geological Society, Trondheim. 608pp.
- Rauh, F., Spaun, G. and Thuro, K. (2006): Assessment of the swelling potential of anhydrite in tunnelling projects. IAEG2006 Paper no. 473, The Geological Society of London, 8pp.
- Reedy, B.J., Beattie, J.K. and Lawson, R.T. (1991): A vibrational spectroscopic ¹⁸O tracer study of pyrite oxidation. *Geochimica et Cosmochimica Acta*, 55, 1609-1614.
- Rimstidt, J.D. and Vaughan, D.J. (2003): Pyrite oxidation: A state-of-the-art assessment of the reaction mechanism. *Geochimica et Cosmochimica Acta*, 67 No 5, 873-880.
- Rosenqvist, I. Th. (1956): Investigation of Alum Shale in the Oslo region. Norwegian Geotechnical Institute, Publication No. 13, Oslo. 5 pp (in Norwegian).
- Sakai, H. (1968): Isotopic properties of sulphur compounds in hydrothermal processes. *Geochimica Journal*, 2, 29-49.
- Scherer, G.W. (1999): Crystallisation in pores, *Cement and Concrete Research* 29, 1347-1358.
- Schippers, A. and Sand, W. (1999): Bacterial leaching of metal sulfides proceeds by two indirect mechanisms via thiosulfates or via polysulfides and sulfur. *Applied and Environmental Microbiology*, 65, 319-321.
- Schnaitman, C.A., Korczynski, M.S. and Lundgren, D.C (1969): Kinetic studies of iron oxidation by whole cells of *Ferrobacillus ferrooxidans*. *Journal of bacteriology* 99, 552-557.
- Sibbick, R.G., Crammond, N.J. and Metcalf, D. (2003): The microscopical characterisation of thaumasite. *Cement and Concrete Composites* 25, 831-838.
- Skjeseth, S. (1963): Contributions to the geology of the Mjøsa districts and the classical sparagmite area in southern Norway. *Norges geologiske undersøkelse* 220, 1-126.
- Sopp, O.I. (1966): Contribution to understanding the Alum Shale swelling mechanism. Thesis, University of Oslo (In Norwegian).
- Spjeldnæs, N. (1955): Boron in some Norwegian Palaeozoic sediments. *Norwegian Journal of Geological (NGT)*, 42, 191-195.
- Spjeldnæs, N. (1962): Middle Cambrian stratigraphy in the Røyken area. *Norwegian Journal of Geology (NGT)*, 42, 196-197.
- Stene, J. (1997): *Varmepumper. Bygningsoppvarming* (3rd Ed). SINTEF Energi, klima og kuldeteknikk, Trondheim.
- Stumm, W. and Morgan, J.J. (1996): *Aquatic Chemistry*. John Wiley and Sons, New York.
- Vogel, J.C., Grootes, P.M. and Mook, W.G. (1970): Isotope fractionation between gaseous and dissolved carbon dioxide. *Z. Phys.* 230, 255-258.

Part 1 – Black Shale environment

- Williamson, M.A. and Rimstidt, J.D. (1994): The kinetics and electrochemical rate determining step of aqueous pyrite oxidation. *Geochim. Cosmochim. Acta* 58, 5443-5454.
- Yakhontova, L.K, Nesterovich, L.G. and Grudev, A.P. (1983): New data on natural oxidation of pyrrhotite. *Moscow University Geological Bulletin*, 38, 41-44.
- Zeebe, R.E and Wolf-Gladrow, D (2001): *CO₂ in seawater: Equilibrium, kinetics, isotopes*. Elsevier Oceanography Series, Vol 65, 346 pp.
- Zheng, Y.-F. (1999): Oxygen isotope fractionation in carbonate and sulfate minerals. *Geochemical Journal* 33, 109-126.

Chapter 7

Sprayed concrete deterioration due to layered Mn-Fe biofilms and saline ground waters in subsea tunnels

“It is essential that the activities of microorganisms that lead to biodeterioration of the wide range of building materials be defined, together with the microorganisms which possess these activities”

RILEM TC 183-MIB

A novel sprayed concrete deterioration process has been discovered in Norwegian subsea tunnels, resulting in disintegration of the Calcium Silicate Hydrate and destructive steel fibre corrosion. The composite reaction mechanism comprised 1) acidification and leaching caused by biomineralisation and redox reactions within layered Mn-Fe biofilms carrying *Leptothrix* and *Gallionella* species; 2) infiltration of Na^+ , Cl^- , Mg^{2+} , SO_4^{2-} and HCO_3^- enriched ground waters, leading to magnesium attack, thaumasite sulfate attack, decalcification and popcorn calcite deposition. Precipitation of brucite, Mg-calcite, aragonite and gypsum was common. Deposition of gypsum mush increased with age of exposure. Constant replenishment of Mn and Fe bearing saline waters facilitated continuous formation of layered biofilms and a sustained attack: Fe^{2+} derived from steel fibres contributed to acid producing reactions. The composite attack caused locally deep disintegration of the cement paste matrix after < 5 years involving thinning of sprayed concrete at rates varying from < 0.5-10 mm/year.

Keywords: Biodegradation; acid attack; magnesium attack; sulfate attack; carbonation

7.1 Introduction

Studies devoted to concrete degradation mechanisms most frequently focus on single processes. However in real life several degradation mechanisms frequently operate simultaneously. In fact there is a need for a wider focus, notably because the outcome of composite deterioration pathways may be quite different from the effects of single processes [1]. Yet specialist papers and comprehensive textbooks such as Taylor [2] and Biczók [3] represent significant sources of information for those who investigate concrete durability and life cycle costs.

Advances in ground water chemistry and geomicrobiology (cf. Appelo and Postma [4]; Konhauser [5]) are seldom applied for characterisation and interpretation of concrete

degradation phenomena. These research fields have focused on the interaction of solids, water and microbes for several decades. To the extent these perspectives are lacking there is always a risk we may fail in diagnosing important aspects of the chemical cycles involved in concrete deterioration.

Several researchers have reported cases of biogenic impact on concrete but it was not until recently these results were systematically gathered. Gaylarde et al. [6] summarised the work of RILEM TC 183-MIB “Microbial impacts on building materials – Weathering and conservation”, showing that concrete, steel and several other building materials may degrade under influence from microbes. Microbes involved in biodeterioration are autotrophic bacteria, such as *Acidithiobacillus sp.* (CO₂ as carbon source) and heterotrophic bacteria (organic C as carbon source), cyanobacteria, fungi and algae. The authors emphasised the importance of bioreceptivity: the ability of microbes to grow and colonise materials such as concrete. This property basically depends on a carbon source, presence of nutrient and water. Rough concrete surfaces provide favourable conditions for attachment and growth.

Steel fibre reinforced sprayed concrete used for rock support in Norwegian subsea road tunnels display suspect bacterially assisted degradation phenomena. Hansen [7] reported on loose concrete associated with rusty iron rich slimes and “black deposits” in the Flekkerøy subsea tunnel, as well as grey mush like “concrete porridge” at the interface between sprayed concrete and rock mass. Røhrsveen and Lygre [8] found grey to whitish loose sprayed concrete debris in the Freifjord subsea tunnel, which could easily be scratched off from outer surfaces or had fallen down at the base. The overall phenomenon has up to now been interpreted to represent rebound from the spraying operation. Such concrete material was otherwise characterised by destructive steel fibre corrosion [8,9].

In contrast Hagelia et al. [10] found that the friable greyish to white concrete debris in the Freifjord subsea tunnel was due to thaumasite sulfate attack (TSA) and magnesium attack associated with decalcification of the cement paste matrix, formation of internal popcorn calcite deposition (PCD) with some secondary ettringite and gypsum. Rusty and black slimes and deposits have been observed in several Norwegian subsea tunnels: These so called “algae” have hitherto been regarded as mainly harmless to concrete [9].

However, recent work by the present author has shown that deterioration of subsea sprayed concrete is closely related to bacterial black and rusty slimes [11]. The attack had started after less than 4-5 years [12,13]. This paper reports on a novel composite degradation mechanism in sprayed concrete involving a) acidification and leaching related to biomineralisation in layered Mn-Fe biofilms and b) abiotic formation of secondary non-cementitious minerals caused by infiltration of brackish to seawater like ground waters. The paper focuses on characterisation and a first look into the reaction mechanisms.

7. 2 Materials and methods

7. 2.1 Investigation and sampling of sprayed concrete in four subsea tunnels

This work was based on investigations in four Norwegian subsea tunnels (Table 1). The locations for detailed studies were selected on the basis of previous documentation ([9], [12]) and own work during 2002 to 2006. Steel fibre reinforced sprayed concrete made according to the wet method was used together with rock bolts as a final tunnel rock support. The role of the steel fibres is to sustain a ductile behaviour in case of some degree of secondary concrete cracking. The studied concrete mixes were of high initial quality and

made with innocuous aggregates, rapid setting Portland cements and silica fume, with water glass or Al-sulfate as setting accelerator. The cements had ordinary tricalcium aluminate (C_3A) contents of about 8 %. The binder contents (i.e. cement and silica fume) were between 485 and 580 kg/m^3 and the water/binder ratios varied from 0.38 to 0.47 ([9],[13]). At the time of sampling sprayed concrete ages ranged from about 5 to 16 years.

Table 1 Subsea tunnel sprayed concretes investigated. PC-rapid = Norcem RP 38 or similar. In Oslofjord also Norcem Standard Cement was partly used.

	Flekkerøy tunnel	Freifjord tunnel	Byfjord tunnel	Oslofjord tunnel
Year of opening	1989	1992	1992	2000
Years of spraying	1988 - 1989	1989-1991	1991-1992	1998-1999
Time of sampling	2002 & 2003	2000, 2003, 2006	2004	2004, 2005, 2006
Age of samples	13 & 14 years	10, 13 & 16 years	13 years	5, 6 & 7 years
First report on loose concrete	1996 /age <5 years	1996/age < 5 years	None in 2004/ age 13 years	2004/age < 5 years
Impact of loose and weak concrete	Locally important in subsea section	Common in subsea section	Minor effects in subsea section	Common in subsea section
Cement type & w/b	PC rapid/0.45-0.47	PC-rapid/0.38-0.47	PC-rapid/0.41-0.46	PC-rapid /0.41
Binder contents	550 kg/m^3	560-580 kg/m^3	485 kg/m^3	540 kg/m^3
Additives	14 % SF	1 % SF	6-8 % SF	5 % SF
Setting accelerator	Water glass	Water glass	Water glass	Al-sulfate

Chemical deterioration of sprayed concrete is usually characterised by a typical zonation pattern [e.g. 14] as aggressive agents carried by ground water attack from both sides of initially sound concrete (Fig. 1). Degradation of the cement paste matrix, involving material loss, is due to formation of secondary non-cementitious mineral assemblages at the expense of the calcium silicate hydrate (C-S-H). The first effects are usually observed adjacent to the rock/concrete interface and within the outer surface region (Layers A and C, respectively). Ca-leaching and formation of calcite stalactites may occur. Moreover, accumulation of moisture, particles and microbes is commonly observed on the outer rough and tortuous surfaces, representing ideal sites for chemical reaction. During the course of the process delamination and spalling (S) may develop, either internally within the concrete slab or along the interface with the rock mass. The attack may gradually lead to loss of bearing capacity of the overall sprayed concrete while the remaining sound Layer B is diminishing in thickness. A very similar lay-out has been reported from sprayed concrete tunnel linings in Switzerland [15].

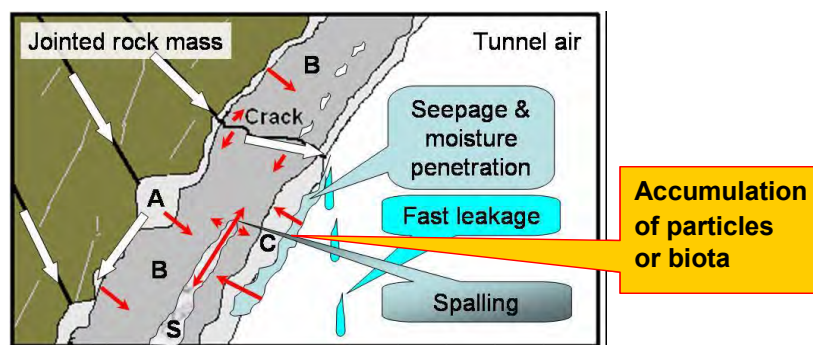


Figure 1: Cross section showing the anatomy of chemical attack within sprayed concrete. Ground water enters by advection (white arrows) or diffusion (small arrows). Layers A and C represent deteriorations, S represents spalling and Layer B remaining sound concrete.

Concrete cores ($\Phi = 50, 70$ or 100 mm) were extracted from sprayed concrete in the subsea tunnel sections, usually reaching a few centimetres into the rock mass behind. Also a few concrete spalls were collected. Separate small samples were collected from friable concrete debris, secondary deposits including black and brown crust material and bacterial slimes. Mostly all layers depicted in Fig. 1, along with interfacial and outer surface deposits, were represented within a single sample series. Water samples were taken from settings with variable water/concrete interaction and stored in plastic bottles with two tight lids prior to analysis. Seawater was collected for reference. The samples reported herein represent typical variations observed in association with the composite bacterial - saline water concrete attack.

7.2.2 Sample preparation and laboratory methods

Small sub samples (about $0.1 - 2$ g) for XRD and SEM, including Mn and Fe crust material, were systematically handpicked from concrete cores and other tunnel samples under a binocular ($50\times$) in an attempt to extract pure secondary reaction products. Such material was usually friable and also suspected to contain water soluble phases, which otherwise might have disappeared during thin sectioning. A few fresh bacterial slimes were brought to the laboratory within 5-10 hours after collection in tunnels, because biominerals can be very sensitive to aging. These small samples were collected in tight containers in order to avoid drying. Bacteria were characterised and identified by standard light microscopy and SEM.

Microscopy of thin sections and bacteria. The concrete cores were cut into two halves lengthwise by a diamond saw and washed thoroughly. Standard polished thin sections were prepared without fluorescent dye on 27×45 mm glass slides from each half core and studied under a standard polarising microscope. Most thin section series covered the entire thickness of the sprayed concrete slab and the rock behind. The preparation involved water cooling. Gypsum was preserved whilst yet more soluble phases, if present, may have been dissolved. Iron bacterial slimes were studied and identified by light microscopy at an external laboratory.

X-ray diffraction (XRD). Small samples for XRD were ground in small agate mortars under ethanol and left to dry before being mounted on sample holders and run in a Siemens D 5005 Spectrometer. All diffractograms were recorded from 2° to 70° on the 2-Theta scale at 0.050° per second, and were set to 40 kV and 40 nA using Ni-filtered $\text{CuK}\alpha$ radiation with wavelength $\lambda=1.54178$ Å. The diffractograms were checked versus the Powder Diffraction Files database from the International Centre for Diffraction Data. Mineral proportions are regarded as semi-quantitative.

Scanning Electron Microscopy (SEM). Uncoated handpicked samples and thin sections were mounted on carbon tape for analysis by SEM. Chemical point analyses ($1-2 \mu\text{m}^2$) were performed on pristine untreated sample materials and a few thin sections, using a Hitachi 3600 N scanning electron microscope with an EDS unit from Thermo Electronic Corporation. The instrument was operated with an accelerating voltage 15 kV at high vacuum. The vacuum chamber had an option for freezing, and bacterial wet samples were frozen to -30°C prior to analysis. Analytical accuracy for most elements is within 1 to 2 wt. % and may reach the accuracy of EMPA on polished surfaces. C and N analyses are less accurate. Back Scatter Electron images were captured.

Electron Microprobe Analysis (EMPA) of cement pastes and secondary phases was performed on selected carbon coated thin sections using a Cameca SX100 instrument. Selected analysed micro domains were $1-2 \mu\text{m}^2$ spot analyses. The beam current was 5.8 or 10

nA with accelerating voltage at 15 kV. The instrument was calibrated using several standards. S, Na and Cl were analysed first in the sequence. Each individual analysis was carefully checked by EDS, ensuring that all elements of significant quantity were included. The analysis totals were in most cases less than 100 %: the difference represents structurally bound- or confined water, and non bound water in capillary pores having been replaced by epoxy during preparation. Analysed major elements are accurate to within ± 0.5 wt. %. Back Scatter Electron images were captured.

Water chemical analysis. Field pH was measured using indicator strips accurate to pH ± 0.1 , and occasionally by a Jenway Model 370 meter (accurate to ± 0.01 pH units) sometimes in conjunction with measurement of redox potential. The water samples for laboratory analysis were mostly 200 or 500 ml. A few samples were collected by pipette reaching about 150 ml. Waters were first centrifuged and filtrated, using a $0.45\mu\text{m}$ filter, before analysis to avoid particles. The samples were analysed for pH by Radiometer PHM 210 Standard pH meter. Total organic carbon (TOC) was analysed by a Phoenix 8000 TOC-TC analyser; Cl, F, SO_4^{2-} and NH_4^+ by ion chromatography using a Dionex DX320 instrument. Nitrate and nitrite was analysed by a Skalar San Plus Autoanalysator, alkalinity in a Mettler DL 40 RC Memo Titrator and conductivity by a WTW inoLab Level 3 Conductivity Meter. Na, K, Ca, Mg, Mn & Fe and other elements were analysed as totals by ICP-AES, using a Perkin-Elmer Optima 4300 DV instrument.

Stable isotopes. Water samples, filtrated on a $0.45\mu\text{m}$ filter, and solids were analysed for C and S isotopic composition. For C isotopes 1 ml of water was first flooded with helium, then added H_3PO_4 and again flooded with helium before injection into a Delta +XP mass spectrometer for analysis of $\delta^{13}\text{C}_{\text{PDB}}$. The NBS19 standard was used for calibration. Bulk samples of biological material were washed in acetone and weak hydrochloric acid in order to remove influence from possible calcite. Samples were then flooded with helium and injected into a Finnigan MAT DeltaXP mass spectrometer. S isotopes ($\delta^{34}\text{S}_{\text{CDT}}$) were analysed in a Micromass Optima isotope mass spectrometer. Aqueous sulfate was precipitated as Ba-sulfate at a controlled low pH. After filtration and washing in deionised water the filtrate was burnt at 1700°C and reduced: the liberated SO_2 was analysed for S isotopes, calibrated by standards S-1 and S-2. Sulfur in solids was obtained by extraction by various procedures, then precipitated as barium sulfate and further treated according to the same procedure as for waters. Authorised standards from IAEA were run as unknowns with all samples. The individual measurements for C and S isotopes are accurate to within $\pm 0.1\text{‰}$, and $\pm 0.2 \text{‰}$ (1 sigma), respectively.

Scanning Transmission Soft X-ray Microscopy (STXM) was applied for analysis of Mn charge state distribution in Mn crust material. A concrete core sample ($\Phi = 50$ mm) with outer Mn-Fe crust was soaked in epoxy adhesive and three small cores ($\Phi = 6$ mm) were drilled through the crust into concrete. The small cores were also soaked in adhesive and cut into thin (about 1 mm) slices lengthwise. Selected sub samples were glued and mounted into copper supporting tubes. TEM thin foils were prepared by cutting, grinding and ion beam thinning in order to achieve X-ray transparency. Subsequent ion beam thinning by Ar^+ sputtering started at $\sim 10\text{kV}$ and was finished at $\sim 3\text{kV}$ in an attempt to minimise beam damage. This created a perforation around which a few transparent areas were obtained. Mn crusts were then located by EDS. A line scan across X-ray transparent Mn-oxides was performed on one selected sample at the Advanced Light Source, Lawrence Berkeley National Laboratory according the procedures of Pecher et al. [16]. The preparation procedure had, however, led to some suspect beam damage (K. Pecher personal communication 2005), which is commented on further in paragraph 3.3.6.

Part 2 – Subsea environment

Table 2: Chemistry of saline waters (in mg/L). < = below detection limit; n.a = not analysed. Rock = water from rock joint; * = Waters with some contact with concrete; ** = Waters with extensive contact with concrete: both categories characterised by presence of biofilms.

Samples	pH	Cl ⁻	SO ₄ ²⁻	Mg ²⁺	Ca ²⁺	Na ⁺	K ⁺	HCO ₃ ⁻	TOC	NH ₄ ⁺	NO ₃ ⁻	Mn ²⁺	Fe ²⁺
<i>Oslo 1, near chainage 16060 m, collected in 2005</i>													
1**	6.60	n.a	2630	1320	<u>1310</u>	8940	163	n.a	n.a	n.a	n.a	1.55	< 0.003
2**	6.64	18300	2604	1320	<u>1360</u>	8700	160	161	n.a	0.510	0.415	1.55	0.008
3**	6.89	18300	2720	1340	<u>1110</u>	8640	184	123	n.a	0.006	1.145	1.69	0.038
<i>Oslo 2, chainage 15915-15945 (V1-V6) collected in 2004, and Oslo 3 at chainage 17450 collected in 2005</i>													
V1*	7.91	19100	2640	1260	473	9170	307	132	0.66	0.091	1.535	0.773	0.003
V2*	7.89	19300	2670	1210	472	9300	308	137	0.41	0.720	0.850	1.440	0.013
V3*	7.88	19100	2640	1270	460	9180	313	146	0.37	1.630	0.006	1.460	1.140
V4*	7.93	18900	2610	1260	458	9140	316	146	0.50	1.640	0.020	1.420	1.330
V5 Rock	7.93	18600	2580	1240	442	9060	318	150	0.38	1.710	0.006	1.210	1.970
V6**	7.71	18200	2550	1321	484	9480	340	179	0.70	< 0.005	2.870	0.002	0.122
17450**	7.49	17800	2410	1270	<u>547</u>	9640	262	154	0.99	2.210	1.100	1.08	0.042
<i>Byfjord, chainage 2865 (By 1 and 2); chainage 3650 (By 3), collected in 2004</i>													
By 1*(*)	7.55	50200	3830	3280	<u>1660</u>	27800	507	137	39.1	7.400	52.000	0.524	0.004
By 2**	7.56	11400	1250	571	<u>1280</u>	5720	50.7	41	< 0.20	1.550	11.400	4.180	0.041
By 3 *	7.75	25400	3300	1790	596	14500	483	151	5.4	0.119	25.400	0.013	0.018
<i>Freifjord, chainage as sample numbers, collected in 2003</i>													
4890 **	6.00	5110	424	237	<u>1340</u>	1680	14	n.a.	n.a.	n.a	n.a	0.605	< 0.003
4930-1**	6.88	6500	510	213	<u>1600</u>	2100	10.2	23	1.6	0.096	0.081	2.32	9.34
5700*	6.00	17100	2230	1220	<u>1980</u>	8080	23	n.a	n.a	n.a	n.a	2.33	0.012
6600*	7.00	19900	2710	1310	<u>1680</u>	8550	36.9	101	1.4	< 0.005	1.335	0.121	0.054
<i>Flekkerøy, chainages 1306 (F1); 1000 (F2); 1095 (F3) and 1240 (F5), collected in 2002-2003</i>													
F1 1**	7.39	27900	2240	1420	<u>3100</u>	12800	294	43	9.2	8.100	47.000	0.101	< 0.003
F1 2	8.07	18700	2600	1310	429	10200	396	146	1.7	< 0.005	0.430	0.003	< 0.003
F1 3(*)	7.98	18300	2500	1180	<u>1020</u>	9530	297	119	1.4	0.010	1.405	0.002	< 0.003
F1 5**	7.81	17500	2300	1010	<u>1920</u>	8500	193	84	1.1	2.490	0.056	2.910	< 0.003
<i>NIVA- Solbergstranda, Osloffjord (60 m below sea level)</i>													
Seawater	7.74	18600	2630	1370	413	10800	390	144	1.2	< 0.005	0.146	0.006	0.023

7.3 Results

7.3.1 Tunnel observations and outline of forensic examination

7.3.1.1 Oslofjord subsea tunnel

The bedrock here consists mainly of granitic gneiss and pegmatite with joints and fault zones carrying clay minerals [12].

Locality Oslo 1a was characterised by severe and focused degradation of the cement paste matrix underneath a two-layer Mn and Fe biofilm (Fig. 2) with Mn-oxidising *Leptothrix discophora* (?) and Fe-oxidising *Gallionella ferruginea* (see details in Ch. 7.3.3). Adjacent barren rock mass only carried slimy manganese deposits whilst iron compounds were absent, suggesting that growth of iron bacteria on concrete was essentially sustained by the steel fibres. Small (volumetrically) saline leakages had entered through a few cracks in upper concrete; spread out over the concrete surface and caused growth of bacteria. Mn bacterial slime entered first and was followed by growth of Fe bacteria and corrosion at expense of the steel fibres. Thaumascite and calcite had formed an adjacent white rim deposit (Fig. 3) (XRD; sub sample 1-06). The Fe bacterial slime tended to remain quite soft as it accumulated, whilst hydrous Mn-oxides frequently formed about 0.1-1 mm thick black friable crust material downstream on the degrading concrete surface. Consequently a two-layer biofilm formed, consisting of inner black Mn-oxides and outer rusty Fe-rich slime.

Dark Mn-stained concrete debris with lighter coloured secondary minerals underneath the biofilms could be carved off with the finger nail, easily reaching 0.5-2 cm into the surface region (e.g. Layer C). The concrete further inside consisted of a weathered friable cement paste. The steel fibres were corroded and frequently destroyed. The extent of outer material loss was somewhat difficult to assess. However, already at age 5 years a single small narrow leakage with Mn-Fe biofilm had caused an about 4-5 cm deep groove into otherwise sound concrete (Fig. 2), which may be representative of the extent of focused attack.

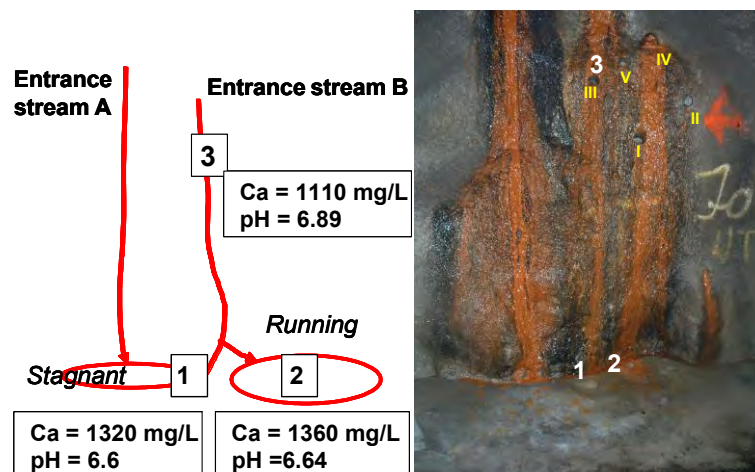


Figure 2: Locality Oslo 1a showing locations of Cores Kj I to V and water samples 1, 2 & 3: Ca was leached from concrete under influence of mildly acidic water. The small leakage on the lower right had formed an up to 4-5 cm deep groove into the concrete.

Cores K_j I, K_j II, K_j III, K_j IV and K_j V were extracted from degraded concrete together with separate small samples of concrete debris and Mn-Fe crust material (Fig. 2). The attack acted from both sides of the spray forming Layers A and C, which together with the sound Layers B had remaining total thicknesses of 25-50 mm. Adjacent dry and intact sprayed concrete was 55 to 90 mm thick (17 cores) with compressive strength about 50-60 MPa [12]).

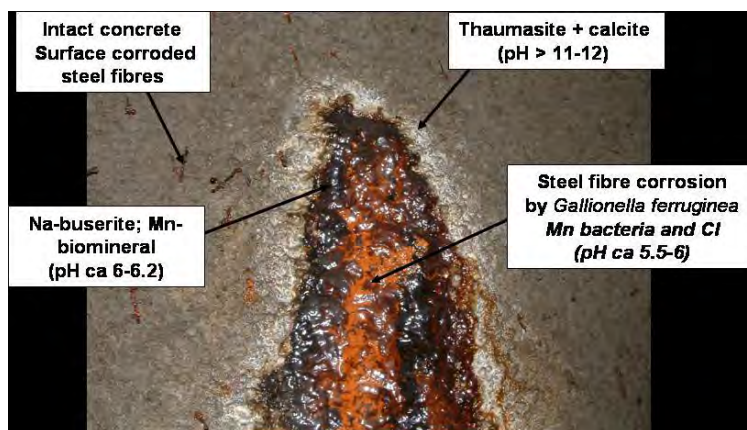


Figure 3: Locality Oslo 1a. Entrance point of saline leakage with dark Mn bacterial slime and iron bacteria leading to cement paste degradation. Image about 55 cm wide.

Mn-Fe materials were rich in hydrous Mn-oxides, Na-buserite and todorokite, and mainly amorphous Fe compounds such as ferrihydrite (cf. Ch. 7.3.3). XRD on different debris materials from underneath the biofilms (sub samples K_j II-1, 4-06 and 5-06), showed it consisted of aragonite (CaCO₃), Mg-calcite (Mg_{0.05}Ca_{0.95}CO₃), calcite (CaCO₃), magnesite (MgCO₃), gypsum (CaSO₄·2H₂O), thaumasite (CaSiO₃·CaSO₄·CaCO₃·15H₂O), and brucite (Mg(OH)₂) along with quartz and feldspars from the aggregate. Thenardite (Na₂SO₄) formed a surface deposit in a few moist areas. Dickite (a kaolinite) with a HCONH₂ group occurred on the outer surface of Core K_j V. The thin sections showed that Layers A and C in all cores were variably affected by weathering reactions, involving transformation of intact dark and dense cement paste into a typical pale yellowish-brown porous cement paste, as seen in plane polarised light. This was closely associated with formation of shrinkage cracks, deposition of brucite in paste and voids and formation of calcite (PCD). Analysis shows that such paste transformation is due to Mg substitution of C-S-H to form M-C-S-H (see Ch. 7.3.2.1). TF and TSA occurred in association with PCD, usually between sound looking cement paste and Mg infected domains. However, magnesium ingress and TSA had reached the full depth of cores K_j IV and K_j V, being characterised by a very weak and completely non-cementitious paste (Ch. 7.3.2.2). Adhesion along the rock/concrete interface varied from good to poor and permeable with open voids. Brucite deposits had sometimes formed at the interface and appeared to have weakened the adhesion to the substrate. The combined attack had led to variably destructive steel fibre corrosion with extensive rust staining of the adjacent cement paste matrix, being M-C-S-H paste with and without calcite.

All waters at this locality had interacted extensively with concrete. Water 3 was collected about 0.8 m below the upper entrance point of a small water stream B (Figure 2). Water 2 was collected directly downstream about 1.7 m below sample 3, from a pond with non-stagnant water immediately adjacent to outlet of water stream B. Water 1 was collected from a near by stagnant pond, being influenced by a separate very slow stream (A) as well as

stream B. The Ca in sample 3 was much higher than in saline ground waters with lesser contact with concrete (cf. Table 2). The Ca concentration had further increased in water 2 downstream, being similar to water 1. Bicarbonate and notably ammonium had increased downstream (3 → 2), whilst nitrate, Fe and to a certain extent sulfate decreased. Despite evidence of extensive Mn precipitation, this element was not much depleted in the downstream waters. Overall levels of Cl, Fe, sulfate and Mg were quite similar to Oslofjord seawater; Na and K were lower whilst Mn was higher. Total organic carbon (TOC) was not analysed due to small sample sizes but in view of the rich bacterial cultures it was likely high. The related pH measured in the laboratory varied from 6.89 in sample 3, dropping to 6.64 and 6.6 in samples 2 and 1, respectively. However, in the field the pH changed over time (Table 3). Lower pH values (5.5-6) were obtained when the bacterial rusty slime cover was relatively thick (early 2004). By 2005 some rusty slime had fallen down: pH dropped from (7.2) 6.6 to 6.2 downstream, which was followed by apparent stabilisation at pH = 6.5-6.6 all over during 2007-2009. Single big drops of condensed water on outer rusty steel fibres from intact dry concrete outside the area with Mn- Fe biofilm had pH ≈ 5.4-5.6.

Table 3: Locality Oslo 1a. Eh and pH measured in saline waters in contact with Mn-Fe biofilm. T = 13-14 °C. Notice increasing acidity downstream: Water 3 → 2 & 1. Field measurements except for pH* in the laboratory.

Water sample pt.	February 2004	January 2005	April 2005	September 2005
1	pH = 5.5-6.0	pH = 5.5	pH* = 6.60/Eh = 29 mV	pH = 6.3/Eh = -22 mV
2	Variations over	pH = 5.5	pH* = 6.64/Eh = 18 mV	pH = 6.2/Eh = -23 mV
3	the entire area	pH = 6.0	pH* = 6.89/Eh = 10 mV	pH = 6.6/Eh = -16 mV

Locality Oslo 2 represents a 30 m tunnel section characterised by very variable degree of attack due to contrasting impact of Mn and Fe biofilms and water leakages. *Sub localities 2a and 2b* displayed weak to moderate attack associated with surface wet concrete. The spray thickness was 60-110 mm, as judged from 10 core samples. Degradation reactions were mostly marginal (0-30 mm Layers A and C) due to brucite and aragonite deposition, formation of M-C-S-H-like paste and PCD with some TF and minor TSA. This involved local crumbling of outer 1-2 mm concrete in whitish-grey weathered concrete without biofilm. Attack underneath Mn-crust material and sparse Fe-bacterial slime was minor in surface wet concrete without running water.

By contrast *Locality 2c* was characterised by extremely friable and porous concrete surfaces underneath thick layered Mn-Fe biofilm and running saline water already at concrete age 5 years: The concrete displayed erosion phenomena and a big block and friable concrete debris had fallen down. Calcite stalactites also containing some brucite occurred scattered about. The reported sprayed concrete thickness is about 250 mm [12]. The hydraulic head here is 120 m with local rock cover less than 5 m [12], representing a very high gradient and driving force for aggressive waters [13]. One 50-100 mm thick very friable sample, *Spall V5* (Fig. 4), was broken loose by hand in 2004. Only two months later it was no longer obvious where the sample had been collected, due to extensive crumbling of the adjacent sprayed concrete. Spall V5 was characterised by extensively degraded, extremely friable and calcium-leached cement paste with loose aggregate particles set in a very porous rusty matrix. The steel fibres were more or less completely through corroded and destroyed. The iron oxidising sheath bacterium *Leptothrix ochracea* predominated over *Gallionella ferruginea*. Each of these bacteria display quite unique morphological features (cf. Appendix A5-6) as seen in

light microscopy and SEM, and are regarded as determined at species level. Thin sections showed that the remaining matrix was almost completely transformed into M-C-S-H, PCD, aragonite, fine grained carbonate and Mn-oxides along with rusty iron deposits. XRD analysis (sub samples FV-5; V5-2 and V5-3) from within the spall confirmed presence of gypsum, thenardite, aragonite and calcite.



Figure 4: Spall V5, with extremely friable cement paste matrix from underneath layered Mn and Fe biofilm. Five year's old sprayed concrete from Locality 2c, Oslofjord subsea tunnel.

Water samples from Locality Oslo 2 were taken from localities with variable interaction with concrete. Water V5 from a rock joint without interaction with concrete was rather similar to Oslofjord seawater (Table 2), yet with notably lower Na and K concentrations. Water sample V6 was collected from a stagnant pond rich in iron bacteria just beneath extensively degraded concrete similar to Spall V5: Ca and bicarbonate concentrations in water V6 were somewhat higher than rock joint water. Also total nitrogen was comparably higher. The remaining water samples from this locality (V1 to V4), collected from water bearing cracks in concrete, also had slightly higher Ca concentrations than rock joint water and seawater. As regards Mg, Cl and sulfate most samples showed seawater like concentrations. pH measured in the laboratory varied from 7.71 to 7.93. However, field pH in the stagnant pond was near neutral in 2004 but had dropped to pH = 6.4 by 2009, being associated with further extensive colonisation of iron bacteria.

7.3.1.2 Byfjord subsea tunnel

The bedrock in this tunnel consists of phyllite with quartz bearing veins and nodules [12]. The overall sprayed concrete quality was much better here than in the other investigated tunnels. The spray was generally thick (> 100 mm), mainly surface dry with only rare small leakages and associated Mn-Fe biofilm material, and with lower binder contents than in the other tunnels. Core extraction and thin section studies showed that most concrete were sound and mainly devoid of shrinkage cracks. Yet occasional detrimental effects were noted. *Core 1-2* of 200 mm thick sprayed concrete showed about 15 mm degradation in both Layer A and Layer C. Degradations involved carbonation and PCD, light brownish yellow M-C-S-H-like paste, secondary ettringite and steel fibre corrosion. Otherwise concrete and fibres were intact.

Waters collected from water panel drains (By 1 and By 3) were hypersaline, due to drought caused by tunnel fans [17]. Brackish water By 2, close by hypersaline By 1, had interacted with friable concrete without Mn-Fe biofilm. Ca/Cl ratios in samples By 1 and

especially By 2 were higher than seawater, which is compatible with localised Ca-leaching from the concrete. Bacterial activity was apparently restricted to the water panels: TOC was very high in waters By 1 and By 3 (39.1 and 5.4 mg/L) but below the detection limit in By 2 (cf. Table 2 for details).

7.3.1.3 Freiffjord subsea tunnel

This tunnel is located in a sequence of banded gneisses with beds of marble [12]. Localised crumbling had started after less than 5 years in service [8] due to formation of M-C-S-H and decalcification with PCD and TSA some secondary ettringite and gypsum [10]. The sprayed concrete in the subsea section was predominantly moist, with several widespread small water seepages. Degradation of cement paste was clearly associated with Mn-Fe biofilm material. Severely weathered concrete could sometimes be broken loose by hand, and at places only remnants of previous sprayed concrete were preserved (Fig. 5). XRD of sub sample Frei 3-06 from such rusty and black concrete contained the hydrous Mn-oxide Nambuserite, amorphous iron compounds (probably ferrihydrite), vermiculite and dickite (a kaolinite) with a HCONH₂ group.



Figure 5: Freiffjord subsea tunnel at concrete age 16 years. Left: Extensive breakdown of sprayed concrete attacked by saline ground water and Mn-Fe biofilms, overlain by grey carbon bearing gypsum mush. Notice the partly erased old core holes: Image width = 140 cm. Right: Thick carbon bearing gypsum deposit on cast concrete banquette derived from a leaky crack through decalcified and friable sprayed concrete. Image width = 200 cm.

The following sequence of events was observed on outer sprayed concrete surfaces: 1) formation of Mn-Fe biofilms, 2) Ca-leaching and formation of stalactites and calcite crusts postdating biofilms, and 3) late stage deposition of gypsum mush. *Gallionella ferruginea* occurred in several samples whilst no attempt was made to identify the Mn-bacteria. In the subsea section outer surfaces were frequently covered by a moist or wet deposit consisting of gypsum and a small amount of crystalline carbon (XRD; samples Frei 6-06, 8-06, 10-06). The colour was dark greyish and quite similar to sprayed concrete. This mush-like material occurred: a) in association with Mn-Fe biofilms and Ca leaching, b) as accumulations on water panels, drainage pipes and barren rock mass: always below concrete, c) around and below leakages through cracks and old core holes in sprayed concrete and d) as a surface deposit on cast concrete structures related to water bearing cracks through degrading sprayed concrete. The mush thicknesses ranged from about 1 mm to 20-30 mm, locally reaching 100 mm (Fig. 5).

Water samples from water panel drains and surface water on concrete varied from brackish to seawater-like, and occasional mildly hypersaline such as water 6600. Waters had interacted with the outer concrete surfaces, which partly carried Mn-Fe bacterial slimes. All waters in the subsea section had Ca concentrations greatly exceeding that of seawater (Table 2). Brackish water 4930-1, collected from a water panel, represents several small leakages with extensive contact area with concrete and Mn-Fe biofilm. The field pH associated with these degrading concrete surfaces was 5.8. Such water had caused severe cement paste degradations without gypsum precipitation, being characterised by about 5000-6500 mg/L Cl, 400-500 mg/L sulfate, 1300-1600 mg/L Ca, and about 20 mg/L bicarbonate (e.g. low buffer capacity). In general pH in Freifjord waters varied between 5.5 and 7 [17]. Waters from which gypsum precipitated had field pH = 6 - 6.2. Gypsum mush was widespread in tunnel sections with salinities similar to seawater. Further data are given in Table 2 and [17]).

7.3.1.4 Flekkerøy subsea tunnel

The bedrock consisted of amphibolite, various banded gneisses and a few weakness zones with chlorite and clayey minerals [12]. Sampling focused on outer surface material and core extraction in an area with widespread small leakages and ubiquitous Mn-Fe biofilms on sprayed concrete. Quite thick layers (5 – 50 mm) of heavily iron stained gypsum crust material had formed within *Gallionella ferruginea* slime sitting on Mn-oxide crusts. A separate sample of thick gypsum crust material showed three growth stages (Fig. 6), which were analysed for S isotopes (see Ch. 7.3.4). *Core 1373*, of 25 mm thick sprayed concrete, displayed a very smooth interface between surface deposits and concrete, suggesting some loss of cross section. A thin section showed the surface deposits consisted of 1) outermost about 5 mm thick rusty and porous gypsum-rich crust, followed by 2) layers of bacterially derived Fe-rich red rust outside Mn-oxide crust (< 0.5 mm) and 3) “coarse” calcite (0.1 mm). The concrete farther inside was friable with M-C-S-H -like paste and PCD. The adhesion zone with the rock mass was poor and permeable, containing brucite, calcite and some Na-bisulfate (NaHSO₄) (XRD on sub sample 1373). A near by *Core 1374* of 100 mm thick spray also contained additional internal brucite and thaumasite and cross cutting cracks partly filled with brucite and calcite. Shrinkage cracking and fibre corrosion was ubiquitous.

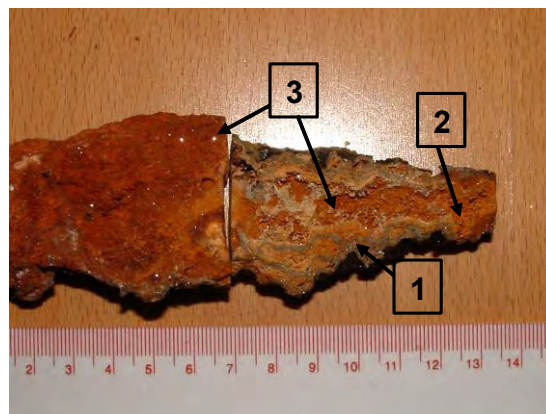


Figure 6: Rust stained hard gypsum crust (sample F8-1373) formed within *Gallionella ferruginea* slime on outer sprayed concrete surfaces in the Flekkerøy subsea tunnel, showing growth stages; Stage 1: fine grained grey to rusty gypsum; Stage 2: fine grained rusty-ochre gypsum with carbon and Stage 3: internal clear gypsum crystals.

The field pH associated with biofilm waters was about 6-6.5. Water sample F1 draining from a large water panel just above the concrete sample station was characterised by very high Ca contents and elevated TOC and nitrogen species. This water interacted extensively with sprayed concrete with some Mn and Fe slimes, and had developed hypersalinity by evaporation caused by a near by tunnel fan. Waters from elsewhere in this tunnel were enriched in calcium when having interacted with concrete, whilst one sample without interaction was similar to seawater (Table 2).

7.3.2 Micro characteristics of the abiotic saline ground water attack

7.3.2.1 Effects of Mg ingress on cement paste colour

Marginal effects. Core 5800 of quite sound 13 years old sprayed concrete (60 mm thick) from the Freifjord subsea tunnel was covered by thin outer deposits of Fe- and Mn-oxide with a little gypsum underneath (XRD sample 5800a). One thin section was analysed by EMPA. Only the outermost about 3 mm (Layer C) was influenced by significant Mg ingress, being characterised by a *pale yellowish brown cement paste matrix* with shrinkage cracks in plane polarised light. Mg concentrations in the cement paste here varied from 1.0 to 41.1 wt. %, with Ca and Si at 0.1-22.9 and 0.1-15.7 wt. %, respectively (Fig. 7). This represents leached and decalcified cement paste, M-C-S-H and brucite. Secondary calcite deposits were common and thaumasite occurred in air voids (TF) at the transition toward sounder paste at 3 mm depth. The cement paste further inside (Layer B) was dark and sound, consisting of quite ordinary C-S-H with lower Mg (0.9-1.1 wt. %). Bulk S concentrations in cement pastes were generally low (0.1-0.9 and 0.2-0.4 wt. % in Layers C and B, respectively). However, Cl concentrations were 0.19-0.23 wt. % at 24-27 mm depth, which is higher than the specified limit (0.1 %) for sprayed concrete bulk cement paste [18]: A steel fibre at 25 mm distance from the surface was marginally corroded.

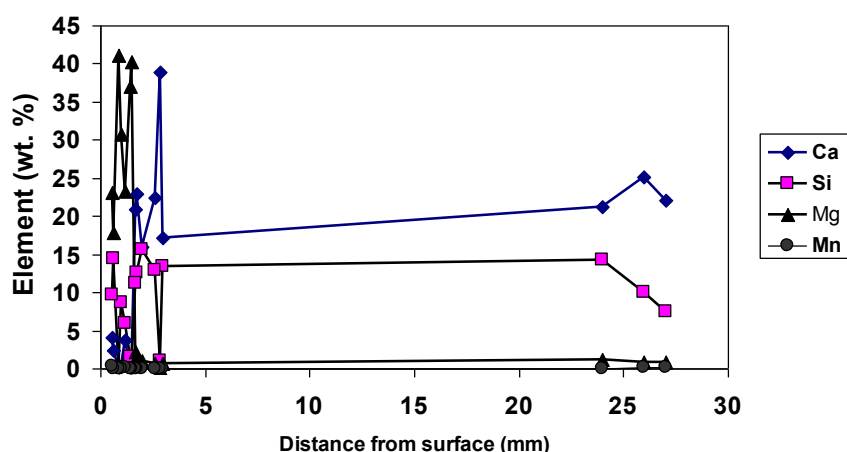


Figure 7: Element variation (EMPA) within degraded cement paste matrix in Core 5800, Freifjord subsea tunnel. The very high Ca at about 3 mm depth represents calcite. High Mg with low Si and Ca was mainly M-C-S-H with disseminated brucite. The colour of M-C-S-H in plane polarised light was pale yellowish-brown whilst intact paste at levels deeper than 3 mm was dark.

Extensive effects. A spall fragment, sample Pr-3 of 10 years old sprayed concrete from Freifjord subsea tunnel, displayed heavily degraded 25-30 mm thick outer concrete (Layer C). An outermost gypsum deposit with carbonation just underneath was observed in thin section. In plane polarised light Pr-3 was characterised by a *very pale yellowish- brown cement paste matrix* with shrinkage cracks all over. Decalcification and deposition of very fine grained PCD with associated very destructive steel fibre corrosion was ubiquitous. Also brucite veins and deposits of thaumasite occurred scattered about. EMPA (Table 4 and Fig 8) showed that ingress of saline ground water had caused formation of M-C-S-H, influencing the entire cross section of the spall and possibly also concrete farther inside. Individual analyses of the cement paste matrix (No's.15, 16, 18, 19, 20, 21) and a globular feature (No's. 13 and 14) showed presence of Al, Fe, Cl and S, suggesting mixed phases. S concentrations were quite high especially within the globules. Due to their shape and size it seems possible that the globules represent either filled air voids or perhaps even highly transformed undispersed silica fume. Thaumasite occurred in an air void (No. 8), and apparently also in the cement paste together with an Mg-rich phase (No. 9). Overall low analytical totals are compatible with a leached and porous degraded concrete.

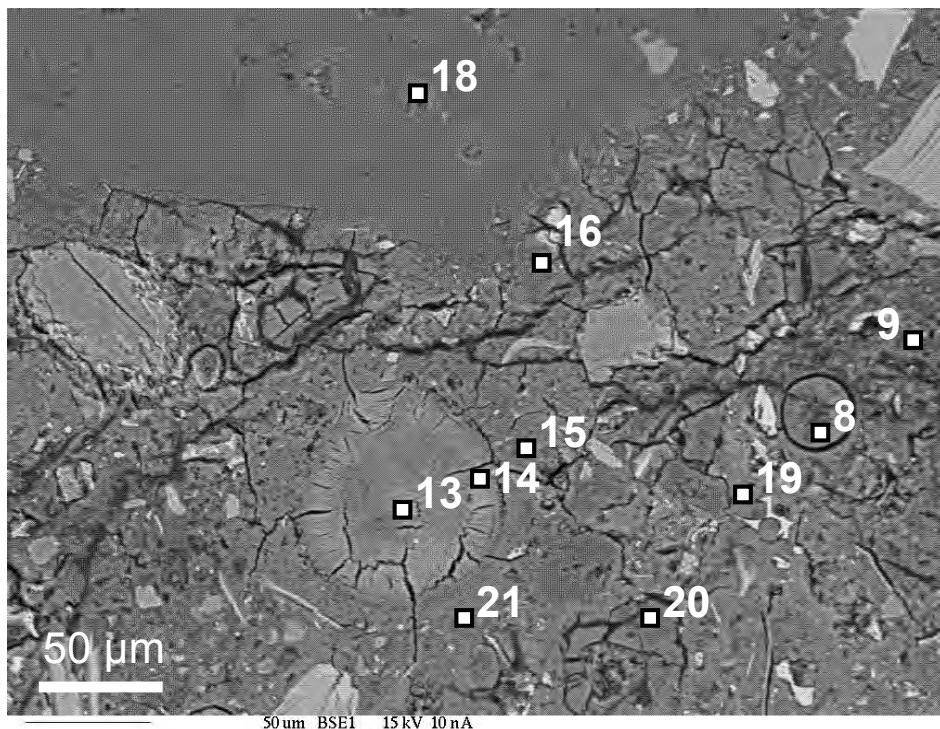


Figure 8: BSE image of sample Pr-3 about 30 mm below outer surface of sprayed concrete. M-C-S-H was well developed within cement pastes and globules and was accompanied by thaumasite. Freifjord subsea tunnel. Scale bar = 50µm.

Hence, it was evident that the pale yellowish-brown colour of cement pastes in plane polarised light was indicative of M-C-S-H, being consistent with some previous descriptions [19]. This was caused by ground waters with Cl, Mg and sulfate contents similar to seawater. However the deep ingress of Mg encountered in subsea sprayed concrete differs from cast concrete subjected to static or splashing seawater, where formation of brucite and M-C-S-H is usually restricted to the outer 1-2 mm [20].

Table 4: Typical EMPA results (weight % of oxide components) from deteriorated sample Pr-3. OM = “other minors” include TiO₂, Cr₂O₃ and P₂O₅. Analysed points correspond to Fig. 8.

Anal. Pt.	Na ₂ O	MgO	Al ₂ O ₃	SiO ₂	SO ₂	Cl	K ₂ O	CaO	MnO	FeO	OM	Total
8 void	0.03	0.69	1.63	8.80	8.96	0.95	0.02	23.08	0.00	0.11	0.13	44.39
9 paste	0.14	5.20	3.95	11.20	7.80	0.81	0.30	16.67	0.03	2.24	1.66	49.98
13 glob.	0.00	30.30	0.79	8.51	8.95	0.31	0.01	24.64	0.00	0.14	0.03	73.69
14 glob.	0.02	20.32	1.27	12.19	10.46	0.37	0.02	27.70	0.01	0.16	0.07	72.58
15 paste	0.04	30.88	2.00	25.68	1.46	0.29	0.32	3.12	0.00	1.21	0.16	65.16
16 paste	0.03	33.55	3.07	19.89	1.73	0.26	0.14	3.33	0.02	0.90	0.14	63.07
18 paste	0.00	39.76	0.13	3.53	3.76	0.37	0.00	10.14	0.00	0.09	0.08	57.88
19 paste	0.10	1.29	2.99	21.04	4.07	0.67	0.47	22.84	0.06	2.66	0.41	56.59
20 paste	0.01	17.54	4.66	27.73	0.70	0.21	0.02	6.23	0.08	4.36	0.55	62.08
21 paste	0.00	4.73	3.70	24.65	4.63	0.58	0.57	21.87	0.06	1.56	0.27	62.62

7.3.2.2 Synopsis of micro structural features in thin section

Mg attack involving formation of M-C-S-H with secondary calcite and possible secondary portlandite led to micro shrinkage cracking (Figs. 9A, B: sample H2004, Locality Oslo 1). Passive brucite deposition within entrapment voids (Fig. 9E), air voids and micro cracks were also typically related to this abiotic attack. Thaumasite Formation (TF) in air voids and entrapment voids and deleterious Thaumasite Sulfate Attack (TSA) were variably developed and usually less important than M-C-S-H formation. Yet, full scale TSA by complete transformation of the cement paste matrix was observed in association with the most focused saline water leakages (Oslo 1a, Fig. 9C, and Freifjord Core 6150-2, Fig. 9D). TSA did not appear to have caused any expansive damage. Steel fibre corrosion products frequently appeared to “soak” degraded porous cement paste matrix and did not seem to have induced expansion (Fig. 9F). Popcorn calcite-like grains were usually very small in association with Mg-substituted cement pastes (< 10 to 20 μm), such as in Figs. 9A, B and Fig. 10 (right). Also classic coarser PCD occurred in leached Ca-depleted cement paste (Fig. 10: left).

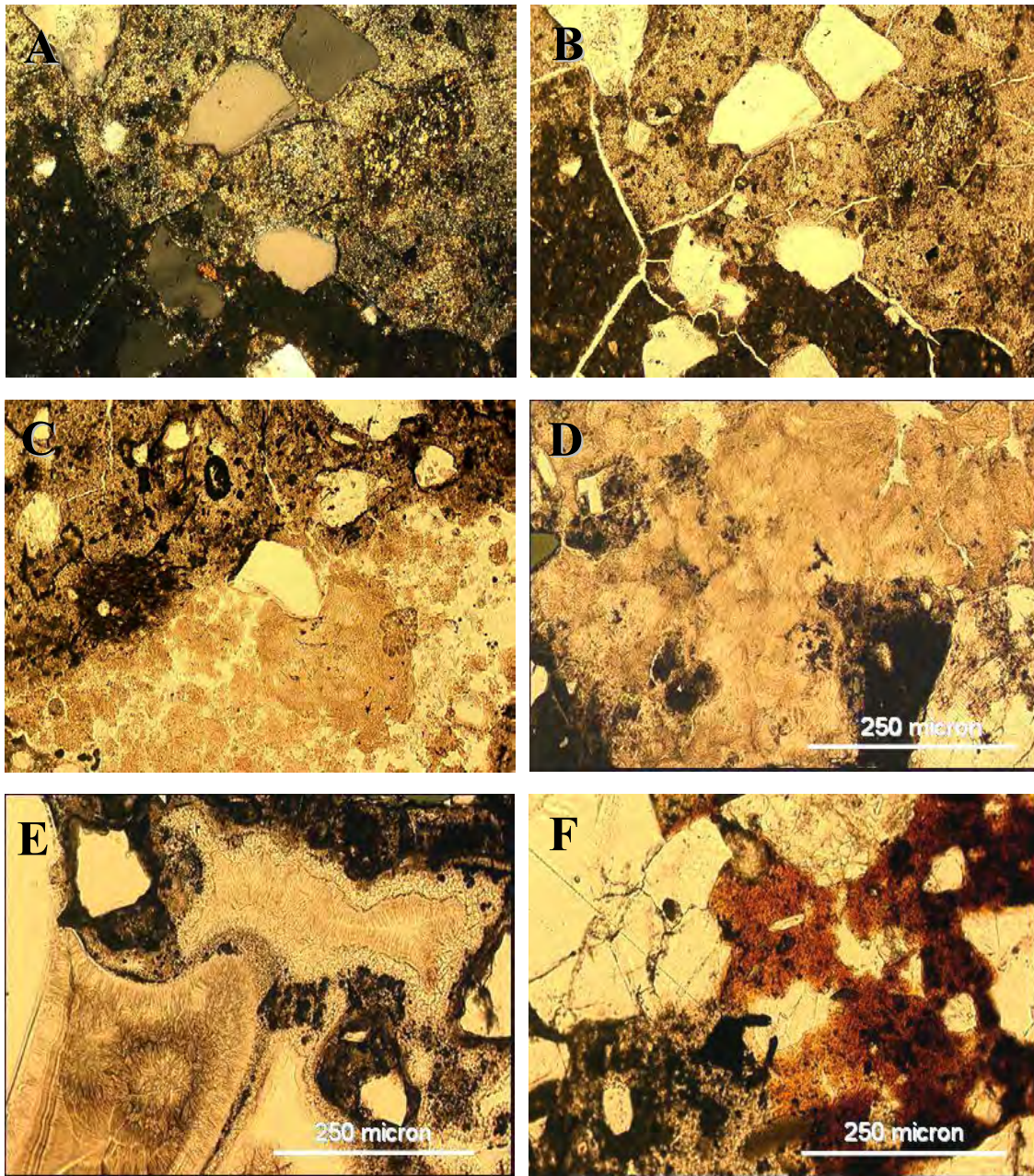


Figure 9: Typical abiotic reaction products in subsea concrete. A and B (same frame): Light coloured M-C-S-H with abundant very fine grained calcite and possible portlandite, and dark pristine paste in sample H-2004. Notice the shrinkage cracks. C: Full scale TSA mush (lower) and M-C-S-H (upper) in Core Kj V (Layer A). D: Full scale TSA mush in Core 6150 at transition between Layers A and B. E: Brucite deposits (mid Layer A) and E: rust stained porous M-C-S-H in Core 6150. Images in plane polarised light, except from A (crossed polars). Same scale. See Table 4 for further details.

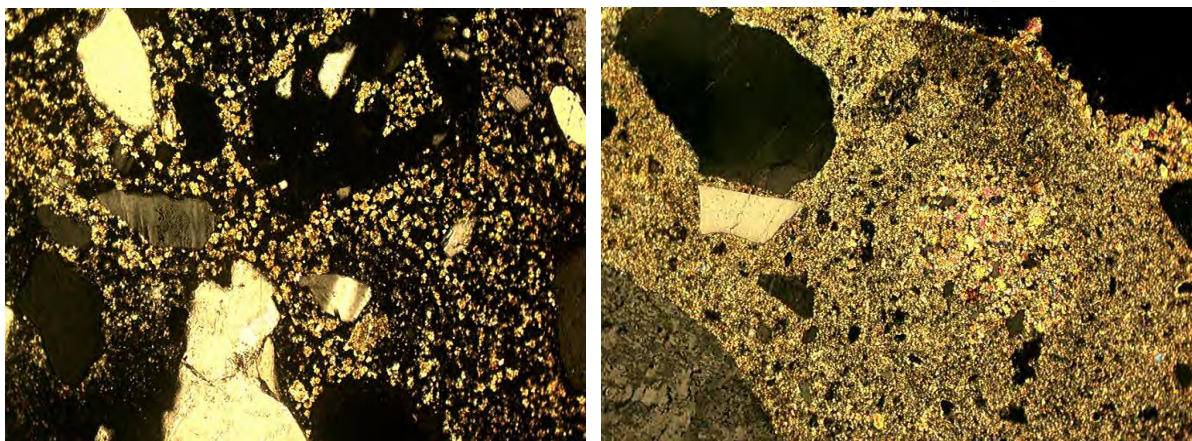


Figure 10: Left: Classic PCD within Ca depleted paste (Core 1374). Right: Popcorn like calcite precipitation within Mg infected cement paste (sample H-2004). Crossed polars: image widths = 650 μm .

7. 3. 3 Micro characteristics of Mn and Fe bacteria, biominerals and crust materials

7.3.3.1 Young Mn and Fe slimes and in situ formed Mn-platelets

Mn-Fe slime with Mn-platelets. One sample (Mn-Fe-1) of dark Mn bacterial slime with some Fe bacterial red rusty slime was collected at Locality Oslo 1a from the upper entrance of water stream B (Fig. 3). XRD analysis showed very high background, indicating significant amounts of amorphous Fe and Mn phases in the slime (Appendix A5-2). Yet, distinct peaks of Mn^{IV} in the form of hydrous phyllosulfate Na-buserite ($\text{Na}_4\text{Mn}_{14}\text{O}_{27} \cdot 21\text{H}_2\text{O}$) were found along with a small amount of todorokite (a hydrous Mn^{IV} -rich oxide). Both these minerals are frequently found in association with bacterial oxidation of Mn^{2+} , e.g. as microbially formed phases [16, 21, 22]. During mounting of the slime sample in the laboratory (e.g. before freezing in the SEM chamber) it was observed that dark Mn slime in contact with Fe-bacteria tended to reshape and form thin dark *Mn-platelets*. Back scatter imaging unveiled that the soft material consisted of “nests” of Mn coated bacteria among characteristic helix shaped stalks of Fe-bacterium *Gallionella ferruginea*. The apparent newly formed Mn-platelets were extremely thin and very brittle (Figs. 11A & B). Mn bacteria were some 5-10 μm long and consisted of several $< 1 \mu\text{m}$ disc shaped compartments, being heavily encrusted by extra cellular Mn oxide deposits. They were “fossilised” within the platelets (Figs. 11C & D). Their morphological features are similar to *Leptothrix discophora* [5, 22] (Appendix A5-6) but no further attempt was made to identify these bacteria. It may be assumed that the “nests” (Figs. 11A and B) represent the same species. Na-buserite was also detected in sample 2-06 at locality Oslo 1a (with brushite ($\text{CaPO}_4(\text{OH})_2 \cdot 2\text{H}_2\text{O}$); Locality Oslo 2 in sample V5-2 and at Freifjord (sample Frei 3-06),

SEM EDS point analyses of the various assemblages shown in Fig. 11 are presented in Table 5 and 6. The pristine Mn-bacterial slime (nests) was characterised by apparent O/Mn atomic ratios ranging from about 2 to 2.4 reflecting much Mn^{IV} , in contrast to the Mn-platelets with embedded suspect *Leptothrix discophora* apparently predominated by Mn^{III} (O/Mn = 1.4 to 1.7). Also Mn-bacterial nests located on the platelets (e.g. point D4) had similar lower O/Mn (Figs. 11D and 12). As regards *Gallionella f.* the trend was the same: O/Fe = 2.5 to 3 (amorphous ferrihydrite, $\text{Fe}(\text{OH})_3$, with some FeOOH) in the fresh soft iron bacterial slime (Figs. 11B & 12, Table 5) was higher than the scattered heavily encrusted ones

sitting on Mn-platelets (Figs. 11C & D and Fig. 13). In the latter case the *Gallionella* bacteria also contained a substantial amount of Mn, thus here the O/Fe+Mn ratio was used. It may be assumed that Na, Cl, S and Mg represent dissolved ions representing saline water in these frozen samples, which should not greatly influence the bulk O/metal ratios in the Mn and Fe material. Ca and Si were mostly within the same range in Mn and Fe bacteria and their potential impact on the O/metal ratios should be more or less the same. Ca was probably bound to the Mn and Fe biogenic compounds, as no calcite, gypsum or other Ca mineral was detected by XRD. Si probably represents amorphous silica. C was more variable and represents organic carbon with a possible impact from the carbon tape used as sample holder. The O/metal atomic ratios can be used as a semi-quantitative indication that the fresh Mn and Fe slimes underwent reduction when platelets were formed.

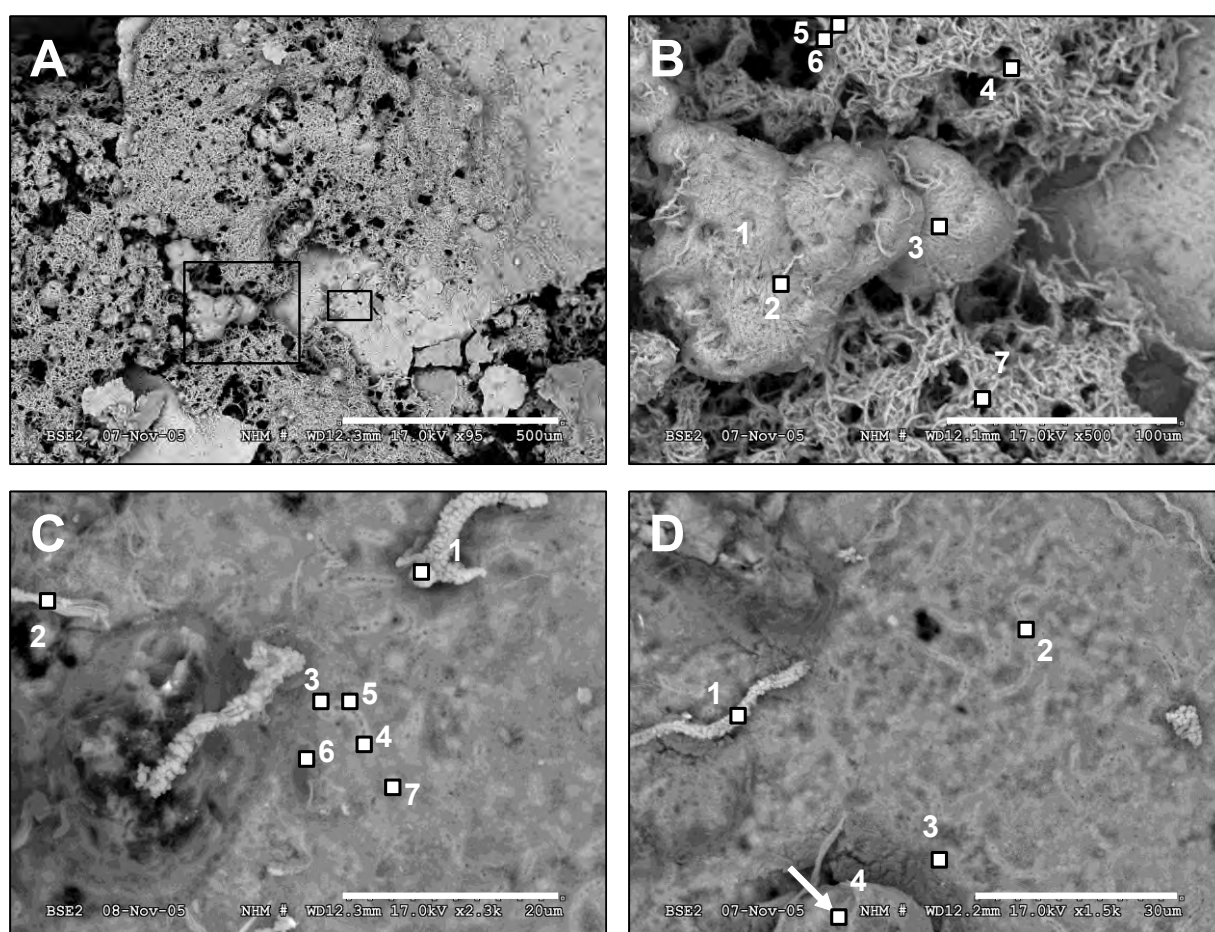


Figure 11: Sample Mn-1-05; A: Soft wet “nests” of mineralised Mn-bacteria (suspect *Leptothrix discophora*) within *Gallionella f.* slime and thin Mn-oxide rich platelets formed *in situ*. Frames show location of images B and C. B: Mn bacterial nests and helix shaped *Gallionella f.* C: Large Mn-coated *Gallionella “f-m”* and smaller suspect *Leptothrix discophora* encrusted within platelets showing extra cellular Mn-oxides. D: Similar to C, here also with reduced Mn in “nest” (arrow). BSE images: Scale bars = 500 µm, 100 µm, 20 µm & 30 µm, respectively.

Table 5: Sample Mn-1-05. SEM EDS analyses (atomic %) of Mn and Fe bacteria and crusts and one analyses of saline water (frozen). Minors (M) include, F, K, Al, As, Br Sr and P (*), N (**) in some samples. Analysed points correspond to Fig. 11.

Anal. Pt.	C	O	Na	Mg	Si	S	Cl	Ca	Mn	Fe	M
B1 Mn-bact "nest"	2.65	39.98	20.72	0.00	0.33	1.38	15.42	2.66	16.85	0.00	0.00
B2 Mn-bact"nest"	4.29	44.71	13.71	0.00	0.00	1.13	10.17	3.03	22.76	0.00	0.22
B3 Mn-slime "nest"	6.03	45.01	15.66	0.00	0.00	0.86	10.08	2.32	19.69	0.00	0.36
B4 <i>Gallionella f. slime</i>	1.42	51.07	3.67	0.00	2.59	1.34	13.18	3.21	1.85	21.32	0.36
B5 <i>Gallionella f. slime</i>	1.81	47.62	3.41	0.00	2.82	1.99	20.00	3.48	1.21	16.93	0.72
B6 <i>Gallionella f. slime</i>	2.46	54.57	2.81	2.11	3.30	2.30	8.79	3.65	1.65	17.97	0.39
B7 <i>Gallionella f. slime</i>	3.26	52.93	8.00	0.00	4.80	0.67	8.63	2.00	0.93	18.30	0.48
C1* <i>Gallionella f-m.</i>	3.77	53.20	5.17	0.98	2.79	0.42	4.25	2.10	15.54	11.26	0.49
C2 <i>Gallionella f-m.</i>	2.23	49.34	7.08	1.53	1.12	1.19	6.10	2.07	23.31	5.42	0.48
C3 <i>Leptothrix sp.</i>	2.64	49.81	3.28	1.75	0.24	0.28	2.72	2.37	35.72	0.89	0.30
C4 <i>Leptothrix sp.</i>	1.95	48.99	3.73	1.56	0.17	0.31	3.46	2.51	35.86	0.97	0.47
C5 <i>Leptothrix sp.</i>	3.88	50.05	3.17	1.64	0.22	0.00	2.87	2.25	34.61	1.11	0.19
C6/** Saline water	5.90	50.85	8.61	1.38	1.44	0.55	6.76	1.73	14.91	6.48	0.53
C7* <i>Leptothrix sp.</i>	1.79	49.97	3.54	1.51	0.94	0.28	3.22	2.35	32.39	3.49	0.20
D1* <i>Gallionella f-m.</i>	7.26	54.27	6.93	1.32	3.15	0.78	5.56	2.11	6.57	11.01	0.96
D2* <i>Leptothrix sp.</i>	5.26	51.15	3.65	2.34	0.26	0.23	2.25	1.96	31.11	0.93	0.84
D3* Mn-ox. deposit	3.42	48.77	6.90	2.49	0.38	0.36	4.35	2.27	29.42	1.22	0.41
D4* Mn-bact. "nest"	0.67	47.72	6.75	2.24	0.11	0.71	3.96	3.03	33.85	0.41	0.53

7.3.3.2 Aged Mn-crust material and aged heavily encrusted *Gallionella*

Core K_j I (Fig. 2) with aged Mn-crust material and some outermost solid Fe-deposits with *Gallionella f.* were investigated. The concrete underneath was somewhat friable, bleached and weathered with carbonation and effects of Mg ingress. Dark brittle Mn-crust material with white minerals consisted of three hydrous todorokites, i.e. mainly Mn^{IV} (NaMn₆O₁₂·3H₂O, Mn₆O₁₂·3.16H₂O and Ca_{0.8}Mn₄O₈·2H₂O); the Mn^{II} minerals manganosite (MnO) and rhodochrosite (MnCO₃) as well as calcite (handpicked sample K_j I-1B). In SEM (BSE) the Mn-crust was recrystallised and shiny showing no sign of preserved bacteria. Their O/Mn atomic ratios were 1.2-1.46, slightly lower than in the Mn-platelets (Table 5, Fig. 12). Apparently initial Na-buserite in soft Mn slime had converted into todorokite, yet involving reduction of some additional Mn compound.

Table 6: SEM EDS analyses (atomic %) of brittle and aged Mn crust material (from Core KJ-I) and aged *Gallionella sp.* slime (0-2005). Minors as in Table 5.

Anal. Pt.	C	O	Na	Mg	Si	S	Cl	Ca	Mn	Fe	M
KJI-1B pt1	1.31	49.29	2.28	0.51	0.04	0.07	0.18	2.89	41.08	0.42	1.93
KJI-1B pt2	2.68	48.84	4.13	0.99	0.14	0.00	0.25	2.94	36.32	0.36	3.35
KJI-1B pt3	2.40	49.64	3.13	1.08	0.21	0.08	0.31	3.36	36.04	1.28	2.47
KJI-1B pt5*	1.71	49.13	2.89	0.80	0.08	0.07	0.30	3.52	38.85	0.25	2.40
KJI-1B pt7	2.67	52.61	0.54	1.15	0.91	0.01	0.06	2.48	36.08	2.90	0.59
0-2005-1*	5.62	35.05	1.33	1.51	7.17	0.23	1.64	2.39	0.74	42.26	2.06
0-2005-2*	6.06	36.79	2.77	2.26	7.96	0.2	2.08	2.68	0.27	36.6	2.33
0-2005-5*	7.78	48.60	2.17	1.82	7.70	0.28	0.93	8.32	0.15	21.23	1.02

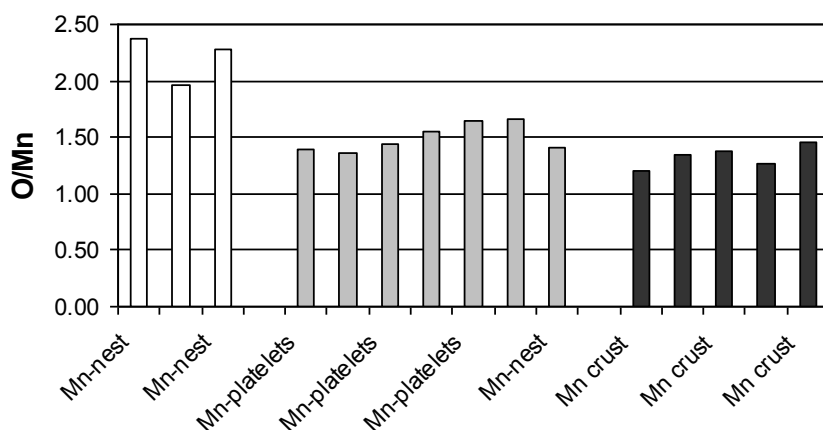


Figure 12: O/Mn atomic ratios of Mn-compounds from SEM EDS analysis (Tables 5 and 6). White = pristine Mn-bacterial slime, possibly *Leptothrix discophora*. Grey = extra cellular deposits around suspect *Leptothrix discophora* in Mn-platelets and one associated Mn-nest (reduced). Black = brittle, aged and recrystallised Mn-crust material.

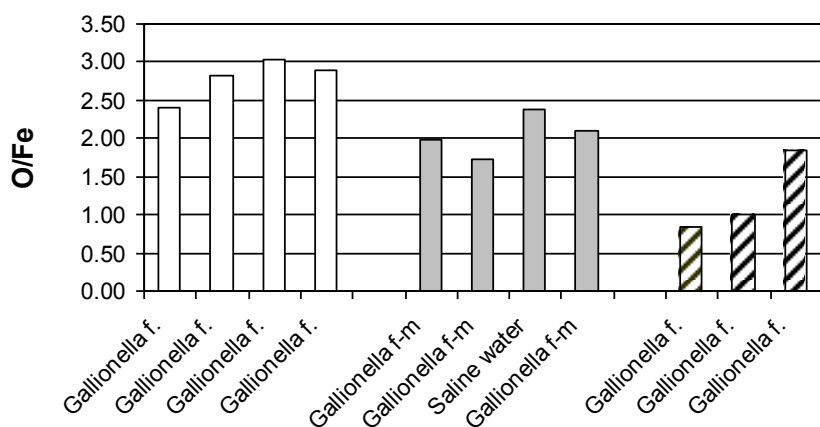


Figure 13: O/Fe (atomic ratios) of *Gallionella sp.* from SEM analyses (Tables 5 and 6). White = pristine *Gallionella ferruginea*. Grey = The Mn enriched scattered *Gallionella* on Mn-platelets (e.g. O/Fe+Mn). Hatched = Aged heavily Fe encrusted *Gallionella ferruginea*.

Sample 0-2005 from a quite deep level of thick, aged and heavily iron encrusted *Gallionella f.* slime was collected from the deteriorating concrete surface between waters 2 and 3 (Fig. 2). XRD of a sub sample (SB 2005 -125 μm) showed that this material contained Mn^{III} -oxide bixbyite (Mn_2O_3), the sulfide marcasite (FeS_2). Amorphous Fe compounds predominated in rusty brown material (sub sample SB 2005 - size fraction 0.45-125 μm). This suggests reducing conditions within aged *Gallionella* slimes. Also SEM EDS analysis confirmed this; the apparent O/Fe atomic ratios in single heavily Fe-encrusted bacteria (Table 6, Fig. 13) ranged from 0.8 to 1.8. The concentrations of cation Ca were mainly similar to the ones in the less aged Fe-material (Table 6) whilst Si was much higher.

7.3.3.3. Gypsum mush and crust deposits

Freifford subsea tunnel. In Ch. 7.3.1 it was reported that the widespread gypsum mush deposits outside sprayed concrete also comprised smaller amounts of crystalline carbon.

Sample Frei 10-06 samples was analysed by SEM EDS using BSE imaging (Table 7, Fig. 14). The crystalline carbon formed thin ribs in many respects resembling bacteria and also contained a little nitrogen. Carbon ribs and gypsum were accompanied by Na, Cl, Mg and I, representing saline ground water. Fe and Mn were absent. Gypsum also contained significant carbon. This likely represents an organic imprint, because calcite was not detected by XRD.

Flekkerøy subsea tunnel. The thick solid rust stained gypsum crust (Fig. 6, sample F8-1373) was different in that it had formed within thick *Gallionella ferruginea* slime in a “semi-confined” fashion (see also Ch. 7.3.4).

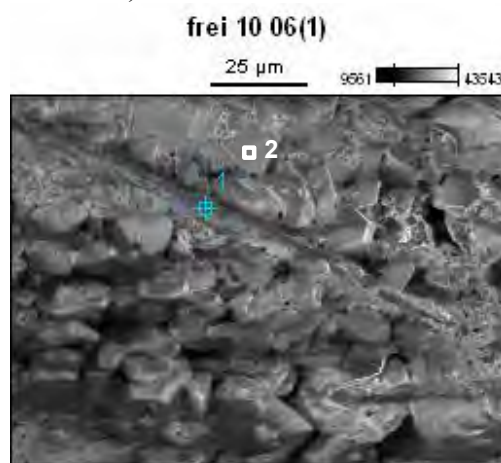


Figure 14: Gypsum mush with about 20-100 µm long ribs of crystalline carbon (no. 1) together with between gypsum crystals (no. 2).

Table 7: SEM EDS analysis of carbon ribs and impure gypsum (atomic %)

	C	N	O	Na	Mg	Al	Si	S	Cl	Ca	I
Carbon rib	30.08	0.20	63.65	1.29	1.17	0.03	0.02	0.11	2.73	0.68	0.03
Gypsum	15.66	-	64.94	1.00	0.07	-	-	7.70	0.85	9.68	0.10

7.3.3.4 Occurrence of a mellite-like carboxylate and phosphates related to saline water attack

An organic mineral deposit occurred in two different settings in Core 6150-2 from the Freifjord subsea tunnel: a) on the outer tunnel facing surface characterised by a smoothed, bleached and rust stained concrete and b) in a void about 3 mm from the concrete/rock interface (Fig 15). The compound was optically isotropic. In plane polarised light the phase was transparent light greyish with a straw yellow to pinkish tint. SEM EDS point analysis showed nearly constant C and O atomic concentrations over the entire area (about 29 % and 66 % atomic, respectively) whilst the cation contents were highly variable. Some micro domains had almost no metal- or other cation, suggesting hydrogen species may be involved in order to maintain charge balance. Elemental ratios (Table 8) suggest the compound is a benzene carboxylate hydrate similar to mellite ($\text{Al}_2\text{C}_6(\text{COO})_6 \cdot 16\text{H}_2\text{O}$). Although mellite is tetragonal, the isotropic character and highly variable composition within micro domains seems compatible with a highly disordered structure, representing a cation and H^+ or H_3O^+ substituted variety of mellite. The inner parts, about 45-50 mm (Layer A), of Core 6150-2 was otherwise extensively degraded. This involved leaching, Mg ingress with M-C-S-H formation, deposition of brucite, PCD and thaumasite. Here XRD-sample 6150-a contained calcite, aragonite, brucite and Al-hydroxide nordstrandite. XRD-sample 6150-e from severely corroded steel fibres contained several phosphates: Giniite (hydrous Fe-phosphate), Fe-hydrogen phosphates and Na-Fe-phosphate.

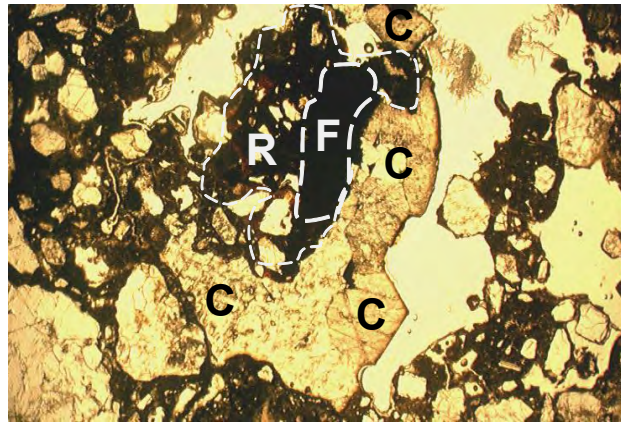


Figure 15: Core 6150-2 about 3 mm from the concrete/rock interface: A carboxylate (C) with local development of crystal faces. Also a severely corroded steel fibre (F) and rust deposit (R) in the cement paste matrix. Plane polarised light. Field of view = 500 µm.

Table 8: SEM EDS results based on atomic ratios of the carboxylate compound compared to pure Al-mellite. Cations were Mg, Al, Si, Ca, Fe and Na in highly variable proportions.

	Single point analysed	Mean (n=8):	Range	Mellite
O/C	2.27	2.31	2.02-2.80	2.33
Cations/O	0.08	0.07	0.01-0.19	0.07
Cations/C	0.18	0.18	0.01-0.52	0.17

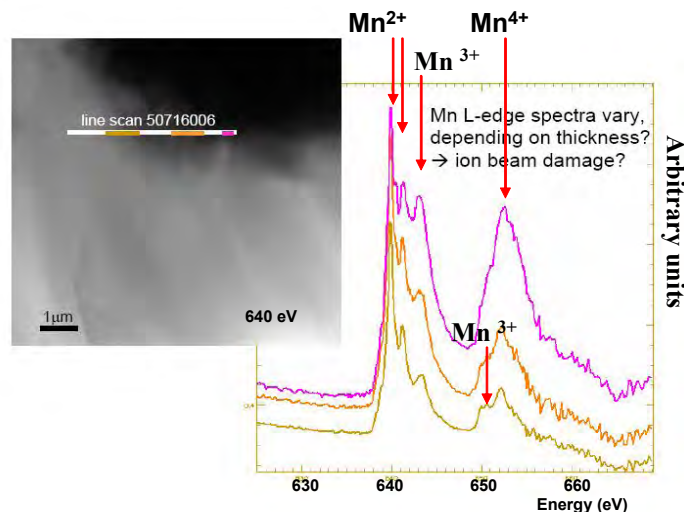


Figure 16: Left: STXM image of Mn-crust material at 640 eV with location of the line scans within the X-ray transparent region. Right: Corresponding Mn L-edge spectra.

7.3.3.5 Mn L-edge spectra of Mn-crust material

Scanning Transmission Soft X-ray Microscopy (STXM) was applied to a solid Mn-crust material from the surface of Core Kj I at Locality Oslo 1a. The analysed region was located in immediate vicinity of an outer *Gallionella ferruginea* bearing iron deposits. X-ray transparency was partly achieved using 640 eV contrast. Three Mn L-edge spectra were obtained, all of which showed distinct Mn²⁺, Mn³⁺ and Mn⁴⁺ peaks (Fig. 16). Such spectra can

be used to quantify the charge state [16]. However, the reduced species were most abundant in the thinner part of the foil, suggesting effects of beam damage during preparation. In this respect beam damage by the Ar^+ ion sputtering would perhaps seem less likely than potential reducing effects of the EDS electron beam used for locating Mn rich micro domains. Yet even the thickest part showed significant presence of the species Mn^{2+} and Mn^{3+} , being compatible with the O/Mn ratios and reduced Mn in contact with Fe compounds as established by EDS analysis on several Mn crust materials. The intermediate species Mn^{3+} is considered to reflect Mn-bacterial activity [16, 21] and is not typical for abiotic oxidation [22].

7.3.4 Stable isotopes

Some saline waters and deposits were analysed for C and S stable isotopes. Due to the differences in molecular bonding energies between heavy and light isotopic compositions, such data are used to discriminate between different processes and origins. The C and S isotopic compositions (Table 9) are presented as δ values in ‰ of their deviations from the PDP and CDT standards, respectively (cf. [23]). The data suggest isotopic fractionation took place upon interaction of saline ground waters with Mn-Fe biofilms and concrete. This effect was used to shed further light on the chemical processes involved in concrete deterioration. The S isotopic composition of Oslofjord seawater ($\delta^{34}\text{S} = 20.7$ ‰) was identical to rock water (V5), whilst $\delta^{13}\text{C}$ was -4.2 ‰ and -2.0 ‰, respectively.

Locality Oslo 1a. Surface waters showed extensive interaction with Mn-Fe biofilms and deteriorating concrete. Sample SB-2005 of predominantly rusty bacterial slime with *Gallionella ferruginea* along stream B (Fig. 2) was characterised by $\delta^{13}\text{C} = -19.1$ ‰ and $\delta^{34}\text{S} = 21.6$ ‰ in sieve fraction $0.45\text{-}125$ μm . XRD indicated mainly amorphous Fe compounds, however associated particles (>125 μm) contained the sulfide marcasite, Mn-oxide bixbyite and amorphous Fe compounds but no carbonate. The water samples showed that $\delta^{13}\text{C}$ dropped downstream: from -5.6 ‰ in water 3 to -7.2 ‰ and -8.0 ‰ in waters 2 and 1, respectively. Sulfur in water 3 ($\delta^{34}\text{S} = +23.6$ ‰), being heavier than back ground rock water, was further enriched to $\delta^{34}\text{S} = +24.3$ ‰ in Water 2 downstream. Water 1, influenced by both water streams A and B, had $\delta^{34}\text{S} = +21.1$ ‰, which is slightly heavier than seawater.

Freiffjord subsea tunnel. Brackish Water 4930-2, which had interacted extensively with outer deteriorating concrete debris and Mn -Fe biofilms, carried very heavy $\delta^{34}\text{S} = +29.8$ ‰ to $+33.6$ ‰ and light $\delta^{13}\text{C} = -14.8$ ‰. A rusty-black concrete with bacterial debris (Frei 3-06) had $\delta^{13}\text{C} = -25.0$ ‰, representing organic carbon. Gypsum deposits with some crystalline carbon (Frei 6-06 and Frei 10-06) had somewhat heavy $\delta^{34}\text{S} = +22.7$ ‰ to $+24.7$ ‰ in sulfate. The C isotopic composition representing crystalline carbon was very light ($\delta^{13}\text{C} = -25.7$ ‰ to -26.3 ‰), being nearly identical to organics in Frei 3-06.

Flekkerøy subsea tunnel. The five cm thick outer rusty gypsum crust (F8-1373, Fig. 6) displayed three growth stages. The 1st and 2nd growth stages were characterised by S isotopes somewhat heavier than seawater ($\delta^{34}\text{S} = +21.5$ ‰ and $\delta^{34}\text{S} = +23.9$ ‰, respectively), whilst the last growth stage, represented by up to 1-2 mm clear gypsum crystals within the interior, had much lighter $\delta^{34}\text{S} = +13.8$ ‰. Local hypersaline water Fl 1, draining from a large water panel associated with Mn-Fe biofilm and concrete Ca leaching, had $\delta^{34}\text{S} = +19.7$ ‰ and somewhat light carbon ($\delta^{13}\text{C} = -6.4$ ‰). In contrast the seawater-like Fl 2 without Ca enrichment (Table 2) had $\delta^{34}\text{S} = +20.0$ ‰ and $\delta^{13}\text{C} = -4.4$ ‰, which is close to Oslofjord seawater.

Table 9: S and C stable isotopes in saline waters, bacterial slimes and solids.

Samples	Material	$\delta^{34}\text{S}$ (‰)	$\delta^{13}\text{C}$ (‰)
Oslofjord	Seawater from 60 m depth	+20.7	-4.2
V5 Rock	Water from rock joint	+20.9	-2.0
<u>Oslo 1a</u>			
3	Water on Mn-Fe biofilm. Upstream of Stream B (Fig 2)	+23.6	-5.6
2	Water on Mn-Fe biofilm. Downstream of Stream B	+24.3	-7.2
1	Water on Mn-Fe biofilm. Downstream of Streams A & B	+21.1	-8.0
SB-2005 organic	<i>Gallionella ferruginea</i> slime, 45-125 μm (located along upper part of Stream B above water 3)	+21.6	-19.1
<u>Freifjord</u>			
4930-2	Water interacting extensively with Mn-Fe biofilm	+33.6/ +29.8	-14.8
Frei 3-06 organic	Rusty-black bacteria-rich concrete debris without calcite	n.d.	-25.0
Frei 6-06	Gypsum > crystalline carbon & possible Na buserite	+24.7	-25.7
Frei 10-06	Gypsum > crystalline carbon (Fig.14)	+22.7	-26.3
<u>Flekkerøy</u>			
Fl 1 (near F8)	Hypersaline water, from water panel/Mn-Fe biofilm	+19.7	-6.4
Fl 2	Seawater like, with high flow rate. No biofilm	+20.0	-4.4
F8-1373 (Fig. 6)	- 1 st growth stage, Grey-rusty gypsum, - 2 nd growth stage, Rusty gypsum w/carbon, - 3 rd growth stage, Gypsum crystals,	+21.5 +23.9 +13.8	n.a. n.a. n.a.

7. 4 Discussion

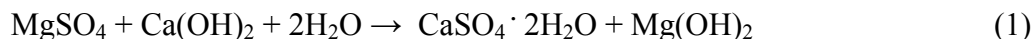
7. 4.1 Introductory remarks

This work has established a novel composite deterioration mechanism affecting sprayed concrete used for rock support in subsea tunnels. Degradation was very severe in certain zones, whilst immediately adjacent dry concrete was frequently sound looking. Also in cross section the transition from degraded into sound concrete was usually sharp. Structurally important deteriorations were characterised by cracking, spalling, leaching, degradation of the cement paste matrix and steel fibre corrosion. The rate of disintegration varied from approximately < 0.5 mm to about 10 mm/year, yet with more severe exceptions. The most extensive degradation rates seem to depend strongly on the simultaneous presence of saline ground water and favourable growth conditions for iron and manganese oxidising bacteria. A possibly related form of bacterial attack involving *Gallionella* and *Leptothrix* species has been reported by Biczók [3]. A very exhaustive discussion, for example establishing chemical reaction rates, is a bit premature and beyond the scope of this work. This discussion must be regarded as a first look into the reaction mechanisms with comments to practical issues and further work.

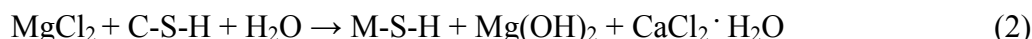
7. 4. 2 Abiotic saline water attack

The saline water attack involved a formation of M-C-S-H with precipitation of brucite. Associated PCD, Mg-calcite, aragonite and magnesite were quite ubiquitous. Secondary portlandite appeared to be less common, although small crystals might well have been

overlooked in the thin sections. Thaumasite in the form of non-deleterious TF and TSA usually occurred at the transition to sound paste, a bit deeper than M-C-S-H and brucite. Formation of brucite may take place according to the following reaction, treating saline ground water as Mg-sulfate:



or along with M-S-H formation according to the below schematic reaction scheme [24], treating saline ground water as MgCl_2 :



The typical reaction product with both brucite and M-C-S-H suggests reaction 2 was important, whilst reaction 1 might explain the apparent scarcity of portlandite. Brucite binds a substantial amount of OH^- and is very stable in saline ground waters in comparison with gypsum [2, 4], whilst hydrous calcium dichloride is highly soluble [24]. Portlandite is only stable at $\text{pH} > 12.4$ [25]. Hence, when bicarbonate is present in concentrations similar to subsea ground waters, the less soluble calcites or anhydrite will form as secondary minerals in the cement paste: Scarcity of portlandite and typical presence of carbonates suggests decalcification. The concrete pore fluid pH was somewhere within the $\text{pH} = 7-12$ range. Thaumasite formation at a deeper level near the transition to intact C-S-H is compatible with the requirement of pH above 12 for its formation [26] in presence of sulfate and bicarbonate.

M-C-S-H pastes typically showed abundant shrinkage cracking. Seemingly Mg ingress made way for subsequent thaumasite formation (TF) deeper inside. In contrast, full scale TSA was developed together with more extensive decalcification with PCD and other forms of carbonate. This lends support to previous evidence that TSA is most efficient after partial or complete Ca-depletion of the cement paste matrix [10, 14, 27].

In the present cases Mg ingress and related cement paste transformations had reached from 1-2 to >300 mm into the sprayed concrete. This stands in marked contrast to the general experience from cast concrete structures influenced by seawater splashing. Due to the relatively large size of the Mg^{2+} ion and reaction with portlandite, brucite frequently forms an insoluble protective layer on the outside of the concrete, usually restricting ingress of Mg to less than about 2 mm [20]. However, the concrete petrography of sprayed concrete used for rock support did not provide any evidence for such continuous layers of brucite, although there was evidence of some brucite deposits on outer surfaces and at the concrete/rock interface. A likely explanation to this is that the rough surfaces of sprayed concrete and uneven contact surface with rock mass do not promote formation of thin continuous protective layers. In addition tunnel concrete is influenced by hydraulic gradients, which drive the aggressive waters more efficiently into the pore space than under static loads at lesser pressure [13, 17].

7. 4. 3 The bacterial attack and the acidification processes

The acid production associated with layered Mn -Fe biofilms seems to represent a crucial mechanism in the composite deterioration mechanism, most notably in combination with the abiotic part of the attack. This is because the abiotic saline water attack tended to give way for external fluids by formation of shrinkage cracks as well as acid soluble minerals.

Abundant carbonates within micro cracked cement paste should be most vulnerable. However, also primary portlandite and C-S-H along with thaumasite are unstable phases at biofilm pH \approx 5.5 to 6.5 [25, 26]. Such mild acids are considered quite harmless to pristine concrete if the water load is static, whilst they can lead to structural defects when associated with mobile and highly mobile waters [28].

At Locality Oslo 1a the enhanced downstream Ca concentration was accompanied by dropping pH and a significant leaching of concrete due to mild acid attack. Here the most extensive Mg ingress, TSA and outer material loss had taken place underneath water streams where Mn and Fe biofilms were well developed. All waters showing extensive interaction with concrete surfaces had elevated Ca as opposed to waters with less or no interaction. Much if not all of this excess Ca must have been derived from decalcification of concrete.

7.4.3.1 Role of the metal oxidising bacteria

Microbes play a significant role in the environment and interact with inorganic matter. Bacterium *Gallionella ferruginea* is microaerophilic, which means it thrives in very low oxygenated water, typically where ground water reaches the surface or underground space. *Leptothrix ochracea* depends on a little more oxygen and therefore colonises open spaces [5]. Both these bacteria catalyse oxidation of steel [29]. According to [30] *Gallionella f.* can oxidize Fe²⁺ to Fe³⁺ about 60 times faster than in abiotic oxidation. *Leptothrix discophora* and other Mn-oxidising bacteria thrive under similar conditions, and can oxidise Mn²⁺ to Mn³⁺ and Mn⁴⁺ at much higher rates than the abiotic pathway: The oxidation mechanism is related to the activity of enzymes in metabolism, which lowers the activation energies [5, 21, 22]. For this reason these bacteria also greatly enhance corrosion of metals, including the Mn-oxidiser *Leptothrix discophora* [31]. Hence, likely the present very similar Mn bacterium (Figs. 3, 12) also enhanced the corrosion rate of steel fibres together with *Gallionella f.* Yet, the present data do not allow for a discussion regarding the quantitative impact of bacterial and electrochemical corrosion. Indeed, also chloride contributed to deep steel corrosion, along with effects of carbonation (PCD) and OH⁻ consumption by brucite.

7. 4.3.2 Mechanisms of acid production, reduction and reoxidation

The microbes also played a role in the acidification processes. Oxidation of ferrous to ferric iron involves production of two protons per mol of oxidised Fe²⁺. A commonly quoted acid producing reaction related to aerobic steel corrosion through the action of *Gallionella sp.* is given by [32], assuming Fe⁰ to Fe²⁺ conversion is not rate limiting:



Also oxidation of Mn²⁺ produces protons upon precipitation of Mn-oxides and MnOOH. It is, however, not immediately apparent why the relatively lowest pH at Locality 1a coincided with times of thick accumulation of *Gallionella* slime. In Ch. 7.3.3 it was clearly demonstrated that both the Na-buserite nests (Mn⁴⁺) as well as *Gallionella ferruginea* had become reduced when associated with the rapidly formed Mn-platelets. Also the recrystallised aged Mn-crust material on Core Kj-I was reduced, as were deeper levels of aged and heavily iron encrusted *Gallionella* slime where the iron sulfide marcasite and Mn^{III}-oxide bixbyite had formed. Bixbyite forms at more reducing conditions than the todorokites (with predominantly Mn⁴⁺) [21,33]. The semi-quantitative O/metal ratios from SEM EDS and the Mn-L-edge scans of recrystallised Mn-crust material with Mn²⁺ and Mn³⁺ show that reduction had taken place at the interface between Mn and Fe biofilm material.

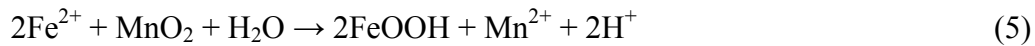
It is well established that organic carbon can reduce metals. Mn^{4+} and Fe^{3+} will be reduced while organic carbon (generally referred to as CH_2O) is transformed by redox reactions to bicarbonate [4], i.e. pH should then raise. A similar redox reaction involving sulfate reduction is commonly expressed as:



Hydrogen sulfide, which is strongly enriched in the light sulfur isotope relative to dissolved sulfate [23], may further react with ferrous iron and form pyrite or marcasite under reducing conditions [5]. Thus dissolved sulfate in water from which sulfides form will attain a complementary heavier S-isotopic signature. At Locality Oslo 1a the S-isotopic signature of sulfate increased downstream (water 3 \rightarrow 2) from $\delta^{34}S = +23.6 \text{ ‰}$ in water 3, already reduced relative to seawater and background rock water, to $\delta^{34}S = +24.3 \text{ ‰}$ in water 2. This was accompanied by a downstream drop in sulfate concentration, occurrence of marcasite within biofilm material and an increase in bicarbonate along with development of somewhat lighter C in the same direction (Tables 2 and 9). Hence, the data suggest Reaction 4 was important, notably because a contribution of bicarbonate from organic carbon here ($\delta^{13}C = -19.1 \text{ ‰}$) seems directly indicated by the downstream C isotopic variation. The brackish water having interacted extensively with biofilm material at Locality 4930 in the Freifjord subsea tunnel carried even heavier sulfate sulfur ($\delta^{34}S \approx +30 \text{ ‰}$) and light carbon ($\delta^{13}C = -14.8 \text{ ‰}$) than the Oslo case, implying locally more extensive influence of Reaction 4. Such extensive fractionation seems readily explained by reduction of organics from dying biota within the biofilms, with sulfide formation and perhaps some H_2S degassing. Although no explicit smell of H_2S was noticed at the time of sampling, this has previously been reported from the Vardø subsea tunnel of Northern Norway in presence of similar well developed biofilms [12].

Reaction 4 alone should lead to a downstream increase in pH, contrary to what was observed (Table 3). However running water and biofilms represent *a dynamic and unstable system*: biofilm material moves downstream. Thus *oxygen should enter* into some domains, hence re-oxidising some hydrogen sulfide or Fe-sulfide producing sulfuric acid. *Sulfuric acid is therefore a likely contributor*. This scenario also seems to provide a very good explanation to the S-isotopic differences between the three growth stages of gypsum in the thick rust stained gypsum crust at Flekkerøy (Fig. 6). During the first two growth stages the S-isotopic signatures increased (Table 9), hence reflecting degassing of H_2S (light S prefers the gas): No iron sulfide was detected here, which should likely be hampered by the rapid precipitation of Fe-compounds assisted by *Gallionella ferruginea* growth. However, the final growth of clear gypsum crystals with much lighter S ($\delta^{34}S = +13.8 \text{ ‰}$), forming inside the crust itself under a thick Fe- biomat, likely reflects substantial influence of sulfuric acid due to reoxidation of H_2S trapped within the biofilm. Likely also, groundwater sulfate with S isotopic composition similar to seawater was mixed in, whilst Ca for gypsum formation was readily available from degrading concrete. Sulfuric acid may also well explain the occasional formation of sodium bisulfate ($NaHSO_4$) at the concrete/rock interface in this tunnel. $NaHSO_4$ can form together with HCl in chemical reaction between sulfuric acid and Na and Cl in the saline ground water.

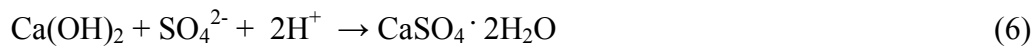
It is interesting to notice that, despite the presence of reduced Mn species in recrystallised crusts, the same material also contained todorokites (rich in Mn^{IV}). This shows that reduction was not complete all over. At the same time steel fibres were continuously oxidised, implying that both Fe^{2+} and Fe^{3+} was available all the time. For this reason it seems very likely that much of the acid production was related to the following redox reaction between Mn^{IV} -oxides and Fe^{2+} ions [34], the latter ion being derived from steel fibres:



This reaction also explains why aqueous Mn was not much depleted downstream at Locality Oslo 1a, despite extensive Mn-oxide deposition. Accordingly only aqueous Fe should become depleted downstream, as was also the case here (Table 2). Furthermore, organic weak acids formed by breakdown of organic material. The best indication of this is perhaps the occurrence of the carboxylate in Core 6150-2 (also near the interface with rock mass) in the Freifjord subsea tunnel. Carboxylate forms from carboxylic acids which are derived from breakdown of amino acids [35]. Downstream enhancement of ammonium (Oslo, Locality 1a) can be taken as additional evidence for impact of bacteria, because NH_4^+ represents a typical waste product after metabolism [5]. Also the phosphate minerals encountered (especially at Freifjord), the occurrence of nitrogen bearing dickite with a HCONH_2 group in Oslofjord and Freifjord, and occasional ammonium iron sulfate at Flekkerøy, likely represent contributions from breakdown of dying biota or even metabolism.

7.4.3.3 Evolution of the attack and the significance of gypsum deposits

Gypsum mush and crust deposits with crystalline carbon ribs, along with the occurrence of the carboxylate derived from behind the sprayed concrete at the interface with rock mass, clearly suggests that the bacterial attack eventually had reached to the back side of the sprayed concrete at an advanced stage. These carbon ribs, about 100 μm , are far too big to represent carbon derived from exhaust fumes (particle agglomerates < 1 μm [36]). Their C isotopic composition was very light ($\delta^{13}\text{C} = -25.7\text{‰}$ to -26.3‰), which strongly suggests an origin from local bacteria ($\delta^{13}\text{C} \approx -25.0\text{‰}$). Formation of gypsum according to Reaction 5 is typical of acid attack in concrete [2]: in the present case involving sulfate from saline ground water, portlandite ($\text{Ca}(\text{OH})_2$) from the cement paste matrix and acids derived from biofilm material:



This reaction consumes acid. Because the water from which gypsum formed had $\text{pH} = 6.2$, the reaction suggests that pH in saline water at the rock/concrete interface was < 6. This should indeed promote further decalcification of C-S-H, i.e. additional Ca^{2+} from C-S-H should further sustain gypsum formation. In general, however, calcium carbonate also formed in domains with $\text{pH} > 7$. Stabilisation of elementary crystalline C reflects reducing conditions [4], whilst its formation mechanism from organic carbon remains obscure.

7.4.4 Some remarks to future work

One key issue which has as yet not been studied is the effect of micro deformations on deterioration rates in tunnel sprayed concrete. Recent studies have established that permeability of concrete increases during experimental deformation. Stress induced microcracking may lead to a surge of fluid flow through concrete [37], i.e. suggesting that the water/binder ratio of the initial concrete mix may not be an entirely reliable measure of permeability in sprayed concrete used for rock support. In field exposure situations damage to concrete and the combined action of chemical and physical loads is expected to be more severe than in single mechanisms [38]. Thus, in the context of sprayed concrete, it seems

possible that strains accumulating due to an unstable rock mass should enhance degradation reaction induced by aggressive waters and biofilms. A fuller understanding of sprayed concrete durability for rock support therefore must account for the variables representing the rock mass stability, being dependent on documentation of rock mass conditions. It is interesting to note that sprayed concrete in the Byfjord subsea tunnel was very little influenced by the combined saline – bacterial attack, despite the presence of aggressive waters. However, the concrete layers here were generally thicker than in the other investigated tunnels (> 10 cm) and the binder content was lower (Table 1). Both these features should counter the effects of enhanced secondary permeability, being less prone to cement paste shrinkage and micro deformational effects.

Future work should also focus on a further understanding of the reaction mechanisms as a basis for developing improved materials and a safer concrete mix design. Investigations into the physiology of the Mn and Fe-oxidising bacteria and DNA-fingerprinting seem necessary in order to fully characterise the chemical cycles involved. In this respect recent work has shown that it is possible to discriminate between impacts of bacterial and electrochemical corrosion by the aid of Fe-isotopes [39].

7.4.5 Overall engineering judgement

The composite deterioration mechanism seems very efficient when water flow rates are low. Until a remedy can be found the focus should be on removing the most important reactants: Steel fibres took part in the acid producing reactions and should be preferably abandoned in subsea tunnel sections. Yet, a general study of the chemical stability of various fibre types is required. In new projects a more extensive grouting and thicker spray may assist in reducing the number of aggressive small leakage areas. As regards maintenance it is necessary to remove biofilms where possible, and methods for neutralising the acid should be sought. For repair, all loose material should be cleaned with a special focus on the gypsum deposits. If not removed, this will soon cause internal sulfate attack and spalling.

7.5 Conclusions

A novel sprayed concrete deterioration process has been discovered in Norwegian subsea tunnels, resulting in disintegration of the Calcium Silicate Hydrate and destructive steel fibre corrosion. The composite reaction mechanism comprised 1) acidification and leaching caused by biomineralisation and redox reactions within layered Mn-Fe biofilms carrying *Leptothrix* and *Gallionella* species and 2) infiltration of Na⁺, Cl⁻, Mg, SO₄²⁻ and HCO₃⁻ enriched ground waters, leading to magnesium attack, Thaumasite Sulfate Attack, decalcification and Popcorn calcite deposition. Precipitation of brucite, Mg-calcite, aragonite and gypsum was common. Deposition of gypsum increased with age of exposure. Constant replenishment of Mn and Fe bearing saline waters facilitated continuous formation of layered biofilms and a sustained attack: Fe²⁺ derived from steel fibres contributed to acid producing reactions. The composite attack caused locally deep disintegration of the cement paste matrix after < 5 years involving thinning of sprayed concrete slabs at rates generally varying from < 0.5-10 mm/year.

The further implication of this attack is as yet uncertain. A deeper understanding of the reaction mechanisms should be sought and experience gathered through more detailed tunnel

investigations and laboratory work. The effects on concrete permeability due to movements within unstable rock mass are not known and need to be investigated. Presently it may be concluded that steel fibres should preferably be abandoned in subsea sprayed concrete used for rock support and that gypsum deposits should be carefully removed before repair concrete is employed.

7.6 Acknowledgements

Funding from the Norwegian Public Roads Administration (NPRA) is gratefully acknowledged. The author is indebted to Claus K Larsen, Ian Willoughby, Geir Arntzen, Ove Lars Strømme, Magnus Fisketjøn (NPRA) and Dag Øystein Løyning (Mesta) for assistance with core extractions; Hans-Jørgen Berg, Museum of Natural History (NMH) Oslo for help with SEM and XRD analyses and Muriel Erambert University of Oslo for assistance with EMPA. Inger Kjersti Iden and Ingar Johansen at Institute of energy technology (IFE) Kjeller are thanked for doing the stable isotope analyses. Salah Akhavan (NMH), Lars Kirksæther (IFE) and Per Geir Sigursen (NPRA) prepared the thin sections. Ivar Dahl and Harry Efraimsen at NIVA are thanked for water analysis and identification of iron bacteria, respectively. Thanks are also due to Klaus Pecher for STXM analysis at Advanced Light Source - Berkeley University and John Walmsley SINTEF, Trondheim for preparing the thin foils. Henk Jonkers (TU-Delft) is thanked for critical comments on the manuscript.

7.7 References

- [1] P. Hagelia, There is always more than one concrete degradation mechanism involved at each site, Workshop “Forensic examination of concrete”, M.D.A. Thomas, I. Fernandes. (Org.), 5th June, 11th EMABM Porto, Portugal, 2007.
- [2] H.F.W. Taylor, Cement Chemistry, 2nd Ed. Thomas Telford Services Ltd., New York, 1997.
- [3] I. Biczók, Concrete Corrosion and Concrete Protection. Akadémiai Kiadó, Budapest, 1964.
- [4] C.A.J. Appelo, D. Postma, Geochemistry, ground water and pollution, 2nd Ed. A.A. Balkema Publishers, Leiden, 2005.
- [5] K. Konhauser, Introduction to Geomicrobiology, Blackwell Publishing, 2007.
- [6] C. Gaylarde, M. Ribas Silva, Th. Warscheid, Microbial impact on building materials: an overview, *Materials and Structures* 36 (2003) 342-353.
- [7] B.O. Hansen, Durability considerations related to sprayed concrete in subsea tunnels, *Sprayed Concrete in Subsea Tunnels*, NPRA unpublished report, 1996 (in Norwegian).
- [8] N.G. Røhrsveen, J.K. Lygre, Proper use of sprayed concrete in tunnels. Civil. Eng. Thesis. Norwegian Technical University, Trondheim (1996) (in Norwegian).
- [9] K.I. Davik, Proper use of sprayed concrete in tunnels. Part B Subsea tunnels, Norwegian Public Roads Administration, Oslo (1997), 64pp (in Norwegian).
- [10] P. Hagelia, R.G. Sibbick, N.J. Crammond, C.K. Larsen, Thaumasite and secondary calcite in some Norwegian concretes, *Cement and Concrete Composites*, 25 (8) (2003) 1131-1140.
- [11] P. Hagelia, Sprayed concrete deterioration influenced by saline ground water and Mn-Fe biomineralisation in subsea tunnels, in: B. Jamtveit (Ed.), *Mechanical Effects on*

- Reactive Systems. The 20th Kongsberg Seminar, Physics of Geological Processes (PGP) - University of Oslo, Oslo, 2007, pp. 26.
- [12] Norwegian Public Roads Administration, Internal documents (1994-2004).
- [13] P. Hagelia, Deterioration mechanisms and durability of sprayed concrete in Norwegian tunnels, in: K. Berg, C. Hauck, R. Kompen (Eds.), Fifth International Symposium on Sprayed Concrete – Modern Use of Wet Mix Sprayed Concrete for Underground Support. Lillehammer, 2008, pp. 180-197.
- [14] P. Hagelia, R.G. Sibbick, N.J. Crammond, A. Grønhaug, C.K. Larsen, Thaumasite and subsequent secondary calcite deposition in sprayed concretes in contact with sulfate bearing Alum Shale, Oslo, Norway, in: B. Georgali, E.-E. Toumbakari (Eds.), Proceedings of the 8th Euroseminar on Microscopy Applied to Building Materials, Athens, Greece, 2001, 131-138.
- [15] M. Romer, Detachment of shotcrete linings due to long term interaction with ground water, International Seminar: The Thaumasite Form of Sulfate Attack, University of Sheffield, 2003.
- [16] K. Pecher, D. McCubby, E. Kneedle, J. Rothe, J. Barger, G. Meigs, L. Cox, K. Neaslon, B. Tonner, Quantitative charge state analysis of manganese biominerals in aqueous suspension using Scanning Transmission X-ray Microscopy (STXM), *Geochimica et Cosmochimica Acta* 76 (2003) 1089-1098.
- [17] P. Hagelia, Does the EN 206-1 Exposure Classification Apply to Tunnel Concrete?, in: E.V. Sørensen, D.H. Bager (Eds.), Nordic Exposure Sites – Input to revision of EN 206-1, Workshop Proceedings from a Nordic Miniseminar, Hirtshals, Denmark, November 2008, pp. 241-263.
- [18] Norwegian Concrete Association, Sprayed Concrete for Rock Reinforcement, NB Publication 7, 2003, 78 pp. (In Norwegian).
- [19] D.A. St John, A.W. Poole, I. Sims, *Concrete Petrography – A handbook of investigative techniques*, Arnold, London, 1998.
- [20] M. Maage, S. Helland, Shore approach – 26 years experience with high quality concrete in XS3 exposure, in E.V. Sørensen, D.H. Bager (Eds.), Nordic Exposure Sites – Input to revision of EN 206-1, Workshop Proceedings from a Nordic Miniseminar, Hirtshals, Denmark, November 2008, pp. 137-152.
- [21] J.E. Post, Manganese oxide minerals: crystal structures economic and environmental significance, *Proc. Natl. Acad. Sci. USA*, (1999) 96, 3447-3454.
- [22] B.M. Tebo, J.R. Barger, B.G. Clement, G.J. Dick, K.J. Murray, D. Parker, R. Verity, S.M. Webb, Biogenic manganese oxides: Properties and mechanism of formation, *Annu. Rev. Earth Planet. Sci.* 2004, 32, 287-328.
- [23] G. Faure, *Principals of Isotope Geochemistry*, 2nd Ed. John Wiley and Sons, 1986.
- [24] D. Bonen, Composition and appearance of magnesium silicate hydrate and its relation to deterioration of cement-based material. *Journal of the American Ceramic Society*, Vol 75/10 (1992) 2904-2906.
- [25] A.W. Harris, M.C. Manning, W.M. Tearle, C.J. Tweed, Testing models of the dissolution of cements-leaching of synthetic CSH gels. *Cement and Concrete Research* 32 (2002), 731-746.
- [26] K.N. Jallad, M. Santhanam, M.C. Cohen, Stability and reactivity of thaumasite at different pH levels. *Cement and Concrete Research*, 33 (2003), 433-437.

- [27] P. Hagelia, R.G. Sibbick, Thauasite sulfate attack, popcorn calcite deposition and acid attack in concrete stored at the “Blindtarmen” test site Oslo, from 1952 to 1982. *Materials Characterisation*, 60 (2009), 686-699.
- [28] Building Research Establishment, Concrete in aggressive ground. Parts 1-4, BRE Special Digest 1, 2003.
- [29] D. Emerson, Microbial oxidation of Fe(II) and Mn(II) at circumneutral pH, in: D.R. Lovley (Ed.), *Environmental Microbe-Metal Interactions*, 2000, ASM Press, Washington DC, pp. 31-52.
- [30] E.G. Søgaard, R. Medenwaldt, J.V. Abraham-Peskir, Conditions and rates of biotic and abiotic iron precipitation in selected Danish freshwater plants and microscopic analysis of precipitate morphology, *Water Research*, 34 (2000) 2675-2682.
- [31] W.H. Dickson, F. Caccavo, B. Olesen, Z. Lewandowski, Ennoblement of stainless steel by manganese-depositing bacterium *Leptothrix discophora*. *Applied and Environmental Microbiology* 63-7 (1997) 2502-2506.
- [32] S.E. Manham, *Environmental Chemistry*, 7th Ed. Lewis Publishers, 2000
- [33] M.J. Russell, A.J. Hall, A.R. Mellersh. On the dissipation of thermal and chemical energies on the early earth, in: R. Ikan (Ed.), *Natural and Laboratory Simulated Thermal Geochemical Processes*, Kluwer Academic Publishers, 2003, 325-388.
- [34] C.A.J. Appelo, D. Postma, Variable dispersivity in column experiment containing MnO₂ and FeOOH-coated sand. *Journal of Contaminant Hydrology* 40 (1999) 95-106.
- [35] P.U.P.A. Gilbert, M. Abrecht, B.H. Frazer, The organic-mineral interface in biominerals. *Reviews in Mineralogy and Geochemistry*, Vol 59 (2005), pp. 157-185.
- [36] Braun A, Shah N, Huggins FE, Huffman GP, Wirick S, Jacobsen C, Kelly K, Sarofim AF, A study of diesel PM with X-ray microspectroscopy. *Fuel* 83 (2004) 997-1000.
- [37] M. Hoseini, V. Bindiganavile, N. Banthia, The effects of mechanical stress on permeability of concrete: A review, *Cement and Concrete Composites* 31 (2009) 213-220.
- [38] M.T. Bassuoni, M.L. Nehdi, Durability of self-consolidating concrete to sulfate attack under combined cyclic environmental and flexural loading, *Cement and Concrete Research* 39 (2009) 206-226.
- [39] E. Hutchens, B.J. Williamson, M. Anand, M.P. Ryan, R.J. Herrington, Discriminating bacterial from electrochemical corrosion using Fe isotopes, *Corrosion Science* 49 (2007) 3759-3764.

Chapter 8

Deterioration mechanisms and durability of sprayed concrete in Norwegian tunnels

“What dunnit?”
Ian Sims

Modern steel fibre reinforced concrete used for rock support in Norwegian tunnels showed chemical deterioration phenomena related to water leakages. Ground waters enriched in sulfate and bicarbonate had caused Thaumassite Sulfate Attack (TSA), detrimental internal carbonation and local acid attack. Concretes subjected to ion poor ground waters were usually sound, although sometimes affected by detrimental internal carbonation or Ca-leaching. Alkali silica reaction was unimportant. A novel deterioration process was discovered in subsea tunnels within sprayed concrete covered by layered Mn-Fe biofilms. Bio-chemical reactions within the biofilms had caused acidification of the saline waters. Acid resistance of sprayed concrete decreased with time due to simultaneous progressive development of internal carbonation, Ca-leaching, TSA, chloride and magnesium attack. This process was very aggressive and had sometimes caused deep or complete disintegrations after < 5 years. The most severe attacks involved loss of bearing capacity due to cement paste degradation, steel fibre corrosion involving thinning and strength loss of the remaining sound sprayed concrete. Depassivation of steel fibres was due to chlorides, acids, carbonation and bacterial action. Life time of significantly influenced sprayed concretes is less than the design life of 50 years. Yet where rock mass rating had been applied for design the concrete linings were much more durable. An assessment of residual life time is in each case critically dependent on rock mass conditions, spray thickness, hydraulic gradient and ground water chemistry. Consequences for further deterioration, maintenance and timing of repair are discussed.

Keywords: Ground water chemistry, concrete deterioration mechanisms, Fe-Mn biofilms, steel fibre corrosion, durability.

8.1 Introduction

Recently an accredited publication from the International Tunnelling Association (ITA) Working Group No 12 “Shotcrete Use” summarised ten years of work on the durability of sprayed concrete (Franzén et al. 2001 [1]). Their work was based on national reports involving a great number of cases, applications, materials and ground conditions. However,

the durability evolution of sprayed concrete linings in under ground space turned out to be an extremely complex subject. Generalised key data for a great number of tunnels around the world were summarised, whilst data concerning the effects of time spans of years were seldom available. In most cases the standard quality and material property parameters were available for 28-120 days old sprayed concrete only. Thus a state of the art report on durability of sprayed concrete used for rock support was considered to be a bit premature and is still missing (cf. [1]). The Working Group 12 focused much on strategies for future work and recommended the use of *four main durability aspects* pertaining to data collection:

1. Complete information about the exposure situation (i.e. chemical- and mechanical loads. based on ground water chemistry and rock mass characterisation, respectively).
2. All necessary sprayed concrete material information to be able to quantify exposure resistance parameters (documentation of the mixes used, spray thicknesses, presence of structural inhomogeneities etc.).
3. Duration of exposures, if necessary, split on the local set of processes (time elapsed since a defined diagnosed deterioration process has influenced the spray, involving mechanical loads and deformations, freeze/thaw cycles, vibrations, impacts and abrasive action, chemical attack from ground water and other liquids along with aggressive components in the atmosphere).
4. Design basis and lifetime expectancy compared to specifications and work execution (the balance between requirement and design, f. ex. permanent linings require more than preliminary).

The designed life time for Norwegian tunnels is 50 years and therefore the life time expectancy of permanent rock support including sprayed concrete and rock bolts is the same. In Norway the design is frequently based on numerical rock mass rating using the Q-system (e.g. Barton et al. [2] and later updates), although exceptions are numerous. The main purpose of rock classification is in any case to provide a long lasting safety for the tunnel traffic. Fallouts of sprayed concrete and rock should be avoided. Another concern is how to estimate the life time for sprayed concretes subjected to different environmental loads (exposure situations), since secondary weakening may represent a potential safety problem involving unforeseen maintenance costs and risks.

8.1.1 Norwegian experience, guidance and environmental classification

Norway has a very long experience with planning, construction and maintenance of tunnels within a huge variety of environments and for different purposes. The main guidance for proper use of sprayed concrete for rock support is represented by Publication 7 from the Norwegian Concrete Association [3]. This document recommends that the design of sprayed concrete linings (spray thickness etc) should be based on the Q-system, and includes the essentials of concrete mix design with reference to standards. All sprayed concrete should be made with silica fume (SF) or another pozzolanic material using the wet method. Steel fibre reinforcement is most commonly employed. Sprayed concrete for permanent rock support is specified within the Durability Classes M60-M40 with compressive strengths ranging from B25-B45 (cf. NS-EN 206-1[4]). Publication 7 also makes use of Strength Class B40 thus deviating from NS-EN standards. In most cases of aggressive grounds B45 (45 MPa) has been used in combination with M45-M40 corresponding to water/cement ratios (w/c) 0.45 to 0.40.

According to Publication 7 only *carbonation*, *calcium leaching* and *fiber corrosion* have been identified with certainty, the latter being essentially restricted to the outer few mm of carbonated sprayed concrete. Examples of chloride penetration were also reported. Deteriorations were restricted to leakages, whilst effects of freeze/thaw were unimportant. As yet, experience is too scarce to establish how deterioration will influence the service life and life cycle costs of sprayed concrete. In sub-sea tunnels the saline water leakages were of particular concern, implying special durability requirements for rock support methods. Moreover the potential for Alkali Silica Reaction (ASR) was not resolved. However, no alarming features were reported. The present day Publication 7 was to a great extent based on a national durability study undertaken about 12 years ago (Davik [5, 6]. Iron deposits and “algae” were very commonly observed within the subsea tunnels causing clogging of drains. Concrete deterioration was mostly restricted to thin sprays (< 5 cm). Occurrences of loose debris on concrete surfaces in some tunnels were interpreted to most likely represent rebound from the spraying operation.

Since 2003 NS-EN-206-1, including a National Annex (NA), has been applied in Norway. In contrast to the previous classification system this requires documentation of ground water and soil composition. The National Annex mainly reflects the Norwegian state of the art.

As regards “old” sprayed concrete, useful for a durability study, it should be noted that available concretes mostly were made just after the introduction of a previous fourfold classification scheme (1986-2003); here saline waters and sulfate ground were regarded as “Very aggressive” and “Highly aggressive”, respectively. Such conditions sometimes required special efforts including the use of Sulfate Resisting Portland Cement (SRPC) with SF.

8.1.2 Objectives

Most sprayed concrete in aggressive environments are still young and experience pertaining to durability of modern sprayed concrete is just about to emerge. The present work focused on chemical deteriorations which have not yet been studied in detail earlier. The objectives were to:

- Present a brief summary of deterioration phenomena in Norwegian sprayed concretes, as based on diagnosis by microscopy and other techniques
- Characterise the water chemical environmental loads, with a look also to mechanical effects
- Put the deterioration phenomena into a relevant hydrogeological context, and
- Discuss the implications for remediation, further deterioration, maintenance and repair.

With a few exceptions the present work was based on modern wet sprayed concrete used for rock support in tunnels.

8.2 Selection of sites, work strategy and summary of methods

8.2.1 Selection criteria

The investigated structures were selected on the basis of the following criteria: a) They should include typical ground conditions involving (hydro-) geological variation and ground water compositions, b) Deterioration characteristics should be representative and relevant for structural performance, c) Investigations should mainly focus on the most common and modern mixes, d) The age of structures should be variable, and e) Basic documentation should be available. Most of these criteria comply with the recommendations from the ITA.

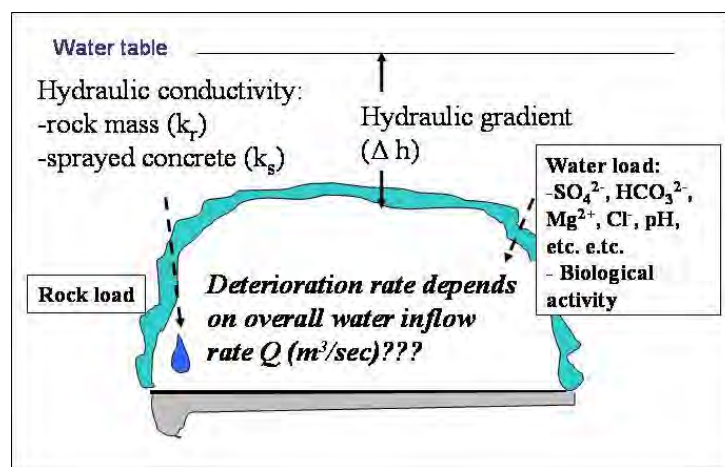


Figure 1: Principal aspects of environmental loads acting on sprayed concrete in tunnels.

8.2.2 Hypotheses and work strategy

Figure 1 gives an illustration of the principal environmental loads which act on sprayed concrete used for rock support. With this in mind it was hypothesised that chemical deterioration mechanisms are not solely dependent on the water composition but perhaps also on the “driving force” represented by the hydraulic gradient. Moreover it would seem relevant to investigate to which extent deterioration rates depend on the volumetric flow rate: It seems likely that also volumetrically small leakages, spread over large concrete outer surfaces may cause significant degradation under certain circumstances. The effects of evaporation due to tunnel draft should indeed lead to increased concentrations of aggressive ions, and this process should be most efficient in rather thin water films. Contrary to this, waters acting from behind the spray should represent more pristine ground water compositions. Adhesion (the quality of the concrete rock interface) may be influenced by water pressure, paste transformation or weak precipitates from ground water, in addition to the rock surface roughness and quality of the work. In general it must be expected that spraying directly against a quite leaky rock mass will lead to a somewhat lower quality than concrete on dryer faces, yet depending on the local volumetric flow rate: Moist surfaces or small leakages may not have influenced the initial properties of thick sprays.

8.2.3 Water categories and concrete sampling with comments to rock mass rating data

Water samples were collected from fast crack bound water (representing quite undisturbed ground waters) as well as from waters interacting with concrete surfaces *and* from metal water panels. These corrugated aluminium water panels were previously widely used for water shielding in Norwegian tunnels. It was expected that effects of evaporation should be easiest to detect in waters draining from water panels as opposed to leakages in direct contact with concrete, which are likely to absorb the aggressive ions instead. Water analytical data were arranged according to the Environmental Classes pertaining to chemical attack (NS-EN- 206-1). Core samples of sound to variably degraded concrete were extracted and concrete surface debris samples were also included. Most concrete samples corresponded directly to a particular water quality.

Systematic documentation of rock mass parameters (Q-values) was only available from two of the investigated tunnels whilst general geological data were available.

8.2.4 Materials and methods

The cases and materials studied represent “real world” sprayed concrete used for rock support, most of which were modern concretes with a high initial quality. This work represents the first systematic petrographical study of sprayed concretes in Norwegian tunnels within a water chemical context. About 100 cores ($\Phi = 50, 70$ or 100 mm) were extracted from ten different structures (cf. Table 1) along with several big spalls and small debris samples. More than 200 thin sections were prepared from concrete cores and spalls and investigated under a standard polarising microscope in the Technology Department at NPRA. Surface debris including microbes and other loose and potentially water soluble materials from within degraded zones in the cores were analysed by X-Ray Diffraction (XRD) and Scanning Electron Microscopy (SEM) at the Museum of Natural History, Oslo. Compressive strength was determined for a few cores at Sentrallaboratoriet (NPR) and NIVA Oslo analysed the waters and some microbes.

8.3 Results and discussion

8.3.1 Anatomy of chemical attack and consequences for sprayed concrete thickness

Deterioration may lead to 1) Fallout of strong thick concrete slabs (sometimes involving the rock material behind or 2) Focused or widespread weakening, thinning and spalling. The *first case* was facilitated by early cracking across the sprayed concrete slab in at least two directions, combined with absence or later weakening of adhesion. Cracking was mostly due to readjustments in the rock mass. Aggressive waters easily attacked the steel fibre reinforcement on cracks and contributed to transformations along the adhesion zone. Experience from the Oslofjord subsea tunnel and other places have demonstrated that fallout might take place at an early age. The *second case* involved bulk diffusion of aggressive waters from the back side of the concrete slab with water penetration along minor cracks, leading to concrete-water interactions also from the outer concrete surfaces on the tunnel facing side.

Figure 2 illustrates the general anatomy of chemical attack (Hagelia et al. [7]). Concrete within Layer A at the interface and Layer C of the outer surface region may be

transformed, depending on the nature and extent of the attack, whilst Layer B represents more sound concrete. Aggressive ions attack from both sides and eventually lead to a complete breakdown of the bearing capacity of the concrete as Layer B is diminishing. Spalling (S) and calcite stalactites may develop during the course of this process. A very similar lay-out has been reported by Romer [8] from sprayed concrete tunnel linings in Switzerland. Sprayed concrete in tunnel space as well as in open air tend to accumulate particles and sometimes biological material on the rough outer surfaces. This again attracts moisture which might facilitate chemical reaction or growth of for example bacteria. Exhaust fumes may also take part in the reactions but these effects were not studied.

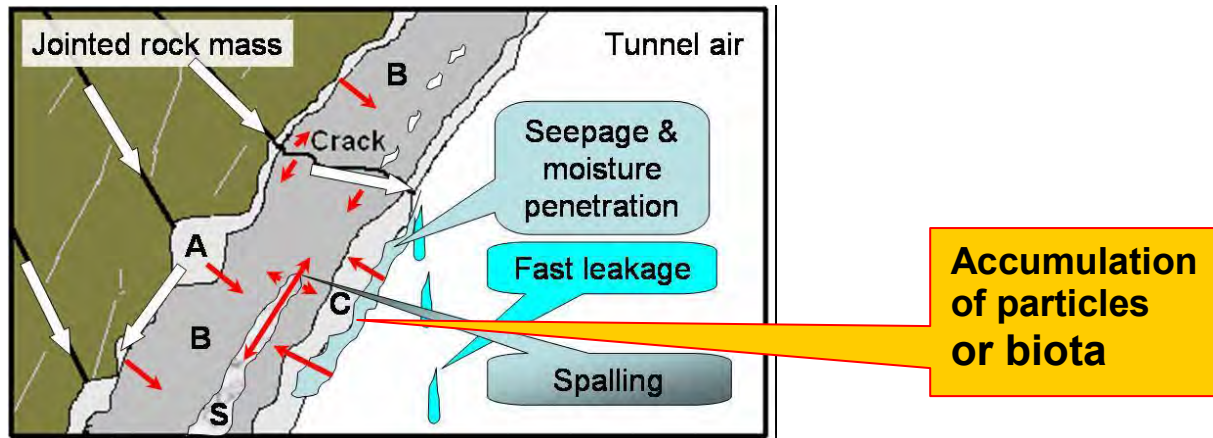


Figure 2: Anatomy of chemical attack within sprayed concrete. Ground water enters by advection (white arrows) or diffusion (small arrows). Layers A, B, C & S are explained in text.

8.3.2 Concrete degradation phenomena studied within three water categories

A summary of the investigated structures and material properties of sprayed concretes is given in Table 1. Material properties are mostly given by a reported range as based on previous work, representing most of the real variation. The structures are represented by subsea tunnels as well as land tunnels within different geological environments. Several of the sprayed concretes were investigated around 1996 within the previous durability project. Table 2 gives a summary of the overall water chemical compositions at each site. An outline of the main durability problems, maintenance work and sprayed concrete thicknesses for each case are presented in Table 3. The accumulated data are based on the investigation of the present author as well as Davik [5], Hagelia et al. [7, 9], and other available documents [10].

The exposure conditions comprised 1) freshwaters in land tunnels and land sections of subsea tunnels; 2) sulfate enriched ground sulfide derived from Oslo Alum Shales, and 3) saline ground waters within subsea tunnel sections. Concretes were studied within these three water categories as shown in Table 2. Mostly several deterioration mechanisms were acting together and their impact varied from being rather insignificant to having important structural effects.

Part 3 – Summary of deteriorations & engineering aspects

Table 1 Summary of investigated structures and material properties. Tunnels marked with *) were also included in a previous study (cf. Davik [5]). PC = Portland cement, PC-standard = Norcem Standard Cement, PC-rapid = Norcem RP 38, SRPC = Norcem Sulfate Resisting Portland Cement; SF = Silica fume (SF). Wet method except for “Dry” = dry method). Åkeberg road cut **) includes an older SRPC based sprayed concrete from 1970 without SF with w/c ratio about 0.5 and steel grid instead of steel fibres. The Harpefoss aggregate was marginally susceptible to Alkali silica reaction otherwise aggregates were innocuous.

Locality (year of concrete placement)	Type of structure	Concrete age at time of sampling (years)	Rock conditions	Cement type & w/b ratio	Additives (% by cement weight) & accelerator	Binder contents (equiv. in kg/m ³) / Designed strength (real range, cube)	Reinforcement. Fibres in kg/m ³ : Designed/real range
Lier *) Dry SE Norway (1965-1971)	Railroad tunnel	Ca 25*), Ca 35	Granite, dolerite Extensive rock burst Fractures with clay	PC (not specified) 0.4-0.6)	HS-3 (2.5-5 %) (= portlandite + C3A + PC-rapid)	Ca 500/B50-B60	Steel grid & none
Harpefoss E Norway (1984)	Access tunnel to hydropower plant	13, 16	Metasediments with black gneiss	PC (MP30?) Ca. 0.4-0.5	Possibly Fly ash & water glass	No documentation	None
Åkeberg Oslo (1970 & 1987) **)	Road cut in city centre	13 (30**)	Alum Shale, syenite	SRPC 0.45-0.50	SF & water glass (** no SF)	Ca 500 / Ca B45	Steel fibre (**steel grid)
Ekeberg Oslo (1992)	Urban highway tunnel	8	Alum Shale, clay stone	SRPC 0.45	SF (8 %) & water glass	Ca 530/Ca B45	Steel fibre
Svardal Oslo (1998)	Urban highway tunnel	2, 8	Alum Shale	SRPC 0.39	SF (5 %) Al-sulfate	530/B40	Steel fibre
Oslo city Dry (about 1970)	Abandon civil defence shelter	Ca. 30	Alum Shale (swelling)	SRPC Ca. 0.5-0.6 **)	No documentation	No documentation	None
Freifjord *) NW Norway (1990-1991)	Subsea road tunnel (highway)	5*), 9, 13, 16	Gneisses, local marble Joints including chlorite etc	PC-rapid 0.38-0.47	SF (6-8 %) & water glass	560-580 /B45 (30-58 MPa)	Steel fibre 50-70/26-44
Flekkerøy *) S Norway (1988)	Subsea road tunnel	8*), 13, 15	Gneiss, amphibolite, Joints with illite and other clay	PC-rapid 0.45-0.47	SF (14 %) & water glass	550 /B45 (27-41)	Steel fibre 45/36-56
Byfjord *) SW Norway (1990- 1991)	Subsea road tunnel (highway)	14	Phyllite, schist, gneiss Joints with chlorite etc	PC rapid 0.41-0.46	SF (1 %) & water glass	485 /B45 (30-36 MPa)	Steel fibre 55/30-52
Oslofjord SE Norway (1998)	Subsea road tunnel (highway)	5, 6, 7	Granitic gneiss, pegmatite, amphibolite Joints and fractures with montmorillonite, kaolinite & illite	PC-standard PC-rapid 0.41	SF (5 %) & Al- sulfate	540 /B40 (54-66 MPa)	Steel fibre 45/36-49

Part 3 – Summary of deteriorations & engineering aspects

Table 2: Tunnel water chemistry given as range within each category, excluding ditchwater. n = number of water samples at each locality; n.a. = not analysed. Subsea tunnel sections in freshwater and saline water are denoted “f” and “s”, respectively. The seawater sample was collected from 60 m depth at NIVA Solbergstrand, Oslofjord. Bicarbonate contents calculated from alkalinity. Data from this study except: Harpefoss, Åkeberg and Ekeberg (Hagelia et al. [9]) and a few samples from Freifjord, Flekkerøy and Byfjord (Davik [5]). Exposure classes for concrete influenced by water; See text for details and discussion. Explanation of XSA I given I Appendix 7.

Locality (n)	pH	Cl ⁻ mg/L	NH ₄ ⁺ µg/L	NO ₃ ⁻ µg/L	SO ₄ ²⁻ mg/L	HCO ₃ ⁻ mg/L	Na ⁺ mg/L	K ⁺ mg/L	Mg ²⁺ mg/L	Ca ²⁺ mg/L	Exposure classes: NS-EN-206-1
Lier (1)	8.18	2.8	< 5	< 1	22.3	173	15.0	0.79	12.1	44.5	X0 (XA1?)
Harpefoss (4)	5.7-6.1	12.2-16.9	n.a.	< 1.	102-111	n.a.	3.2-11	0-7.8	1.5-3.9	38.5-59.9	X0 (XA1?)
Freifjord, f (2)	7.0-9.16	24-26	n.a.	n.a.	124-146	n.a.	168	5.8	0.89-1.0	2.54-13.3	X0
Byfjord, f (1)	8.33	260	< 5	465	51.2	141	193	14.3	15.4	14.6	X0
Oslo, f (3)	7.43-8.16	9.4-123	<5-41	55-570	13.3-21.1	64 -165	12.8-76.3	1.6-3	2.98-5.57	20.7-39.6	X0
Åkeberg (1)	7.6	29	n.a	25000	1841	274	26	22	110	615	XSA
Ekeberg (2)	7.0 (4-5)	10	n.a	14000-18000	592-2031	56 -100	25-43	16-22	20-74	106-574	XSA
Svardal (1)	6.84	18.7	100	300	541	67	44.4	9.09	21.4	172	XSA
Freifjord, s (12)	5.5-7.33	5110-19900	<5-96	81-1335	410-2710	23 -101	1680-8550	11-36.9	158-1310	1340-4040	XA1-XA3 (XSA?)
Flekkerøy, s (7)	7.12-8.07	11100-27900	<5-8100	56-47000	1380-2600	43 -146	5080-12800	136-369	745-1420	429-3100	XA2-XA3 (XSA?)
Byfjord, s (6)	7.50-8.15	1000-50200	119-7400	290-52000	50-3830	41-151	5720-27800	50.7-507	998-3280	562-1660	XA2-XA3 (XSA?)
Oslo, s (10)	6.64-7.83	16900-19300	6-1710	5-1535	2550-2740	132 -161	8640-9300	160-348	1180-1340	394-1360	XA3 (XSA?)
Seawater Oslofjord (1)	7.74	18600	< 5	146	2630	144	10800	390	1370	413	(XA3)

Part 3 – Summary of deteriorations & engineering aspects

Table 3. An outline of the main durability status. It should be noticed that cement paste degradation was most typically developed within subsea tunnels, involving thinning and loss of bearing capacity. *) = Minor signs of ASR. See text for further explanation.

Locality & age of concrete	Practical problem related to concrete	Type and extent of deterioration	Maintenance work up to now	Spray thickness
Lier, E Norway (1965-1973) <i>Dry method: old technology</i>	Extensive spalling and falloff. Expensive long term maintenance	Early age sulfate attack & extensive carbonation (also internal)	Removal of weak concrete twice in a year	2 – 25 cm
Harpefoss, E Norway (1984)	No big problem	Minor TSA & PCD apparently slow. *)	Nothing done	2 – 12 cm
Åkeberg road cut, Oslo (1970 & 1987)	Local spalling and deformations started at age <13 yrs	TSA & PCD at age < 13 yrs	Previous 1970 spray replaced in 1987	6 – 18 cm
Ekeberg, Oslo (1992)	Some weakened concrete observed	TSA and PCD at age < 8 yrs	Nothing done	3 – 10 cm
Svardal, Oslo (1998)	Not yet problematic	Some TSA and PCD at age < 2 yrs	Nothing done	5 – 11 cm
Oslo, civil defence shelter (ca. 1970) <i>Dry method: old technology</i>	Abandoned mainly due to ground conditions, locally severe spalling and -cement paste crumbling	TSA, PCD, Ettr. Shale swelling probably due to gypsum	Several times in past years	5 – 12 cm
Freifjord, NW Norway (1990-1991)	Cement paste crumbling started at age < 5 yrs	Complex seawater attack: very widespread in undersea section *)	Occasional new spray recently	6.5 – 14 cm
Flekkerøy, S Norway (1988)	Some cement paste crumbling started at age < 5 yrs	Complex seawater attack: locally extensive in subsea section	Occasional new spray recently	4 – 15 cm
Byfjord, SW Norway (1990-1991)	Very limited cement paste crumbling	Complex seawater attack: minor effect	Nothing done	2 – 17 cm
Oslofjord, SE Norway (1998)	1) Local rock fall on the road; < 5 years of service: 15 weeks closed 2) Cement paste crumbling started at age < 5 yrs	1) Early age cracking combined with rock load 2) Complex seawater attack: common in subsea section	Repair & extensive replacement locally at age ca 5 years Also due locally to saline ground water	5 – 18 cm

The chemical Exposure Classes of NS-EN 206-1 were applied. It was, however, also possible to address the impact from chlorine and carbonation, as has been done in a several cases below. Although there may be some uncertainties as regards the initial quality of sprayed concrete at a detailed level, there seems to be no reason to infer that the observed deterioration phenomena reported herein were caused by low quality and poor workmanship. Instead in many cases deteriorations had indeed influenced well documented high quality concrete.

Surface dry sprayed concrete was usually found to be in a good shape showing up to a few mm of surface carbonation without any other obvious secondary transformations of the cement paste matrix. However, it is important to realise that where draw-down of the water table has occurred at some stage, a dry concrete surface might still hide weaknesses caused by previous water attack. This problem is briefly discussed below. Moreover internal

deteriorations related to components in the concrete aggregate were also considered (cf. Alkali silicate reactions below). In general, however, almost all of the sprayed concretes were made with a high quality aggregate without aggressive or reactive components.

8.3.3 Sprayed concrete in freshwater environments

8.3.3.1 Exposure conditions

The water compositions (Table 2) in the investigated cases classify mainly as non-aggressive.

8.3.3.2 Deterioration mechanisms and examples

The concretes subjected to freshwater loads were essentially intact although some Ca leaching and calcite stalactite formation occurred, which in the general case has no impact on structural performance. This is indeed the most typical observation.

It should be noticed that the presence of bicarbonate dissolved in ground water may enter into concrete and cause some degree of leaching and internal carbonation. There is also some concern about the effects of slightly elevated sulfate contents (< 200 mg/L, i.e. lower than in Exposure Class XA1) because sulfates such as ettringite and thaumasite do not require a very high concentration to form (cf. [11] and references therein).

Locally, however, sulfate attack also was found both at the Harpefoss and the Lier tunnel despite sulfate concentrations < 150 mg/L in these ground waters. At Harpefoss thaumasite had formed locally at the concrete/rock interface in quite modern wet sprayed concrete less than 16 years old [9]. The Lier tunnel [10] was characterised by severe rock burst problems during construction about 40 years ago, and an early stage sulfate attack. This attack was obviously due to significant early water leakages into the tunnel since intergrowth of thaumasite and ettringite as well as large portlandite- and hydrated calcium silicate crystals were found in the large air voids. Presently the concrete is essentially dry, extensively laminated and carbonated. This sulfate attack was obviously due to high concrete permeability and porosity, which also made way for very extensive deep carbonation and severe spalling which is still continuing.

Although the concrete in question represents an expensive maintenance problem for the owner (Table 3) this old dry-spray is not at all representative for the performance of modern wet sprayed concrete mixes. The main lesson to be learned is that ground water loads are not constant and that even the aggressive ion concentrations may change with time.

8.3.4 Sprayed concrete in the Alum Shale environment

8.3.4.1 Exposure conditions

The exposure conditions were similar to the ones reported by the previous Alum Shale Committee (cf. Bastiansen et al. [12] and Fiskaa et al. [13]) being characterised by very high sulfate concentrations (2000- 5000 mg/L) and pH varying from < 2 to 6-7. As such the Alum Shale environment sometimes involves characteristics of Acid Rock Drainage (ARD). In NS-EN 206-1 these conditions are represented by the Exposure Class XSA, which has been introduced nationally, among others, due to the well known sulfate attack related to Oslo Alum Shale.

8.3.4.2 Deterioration mechanisms and examples

The Alum Shale Committee reported on a severe form of sulfate attack causing rapid degradation of the cement paste matrix and severe corrosion of steel. This was attributed to a sulfuric acid attack and ettringite formation induced by the high ground water sulfate concentrations which are derived from sulfide oxidation. However, Hagelia and Grønhaug [14] found that this was instead due to the Thaumasite Sulfate Attack, the effect of which has been detailed in a series of recent papers from NPRA and BRE UK [7, 9, and 11]: The main feature of the attack is formation of thaumasite in air voids and cracks (called Thaumasite formation; TF) and detrimental Thaumasite Sulfate Attack (TSA) at the expense of the cement paste matrix. Thaumasite also contains carbonate, and entrance of bicarbonate from ground water and simultaneous formation of large calcite grains leading to internal detrimental carbonations (referred to as Popcorn Calcite Deposition, PCD). The overall process has been termed TF-TSA-Carbonation (e.g. [7, 9]) and has caused variable effects of structural weakening. It is significant that thaumasite also forms in Sulfate Resisting Portland Cement (SRPC) with silica fume (SF) (see Tables 1 and 3). TSA is well known from the UK and takes place in a moist and cool environment such as in tunnels (cf. DETR [15] and Crammond [16]).

In present day concretes based on SRPC with silica fume (Table 2) the effects of TSA are quite small in comparison with the classic problem in Oslo some 50-70 years ago. As a matter of fact the Alum Shale Committee was first to discover the beneficial effects of SF! Spalling and deformations have still been recorded in modern steel fibre reinforced wet sprayed concrete about 13 years old (e.g. the Åkebergveien road cut, see Table 3). Hagelia et al [9] reported that the effect of the attack depended on the spray thickness, and that if acids were present there is a potential for sprayed concretes breakdown (6-10 cm thick) within less than 20 years. Although very young (< 2 years) TF-TSA-Carbonation was found in the Svartdal tunnel ([7, 9], later sampling at concrete age 8 years indicated that the process has halted here (P. Hagelia in prep).

Recently the leaching mechanisms related to Alum Shale were studied in detail. The results, including stable isotope analysis, suggested that the source of sulfate involved sulfide oxidation assisted by *Acidothiobacillus sp.* as well as anhydrite/gypsum dissolution (Hagelia [17]).

8.3.5 Sprayed concrete in saline ground water

8.3.5.1 Exposure conditions involving occurrences of hypersaline waters

Sprayed concretes subjected to the saline ground waters within the subsea tunnel sections have up to now been regarded as similar to seawater conditions and compared to seawater attack in bridge foundations. Thus the Exposure Class XA3 or similar has been applied. Yet in NB Publication 7 it is also obvious that the subsea tunnel environment is of special concern and that SF and low w/c ratios are specified. However, the present results imply that this should be reconsidered, since significant effects of evaporation has been found in waters draining from Al water panels both in the Flekkerøy- and Byfjord subsea tunnels. Here some waters had become hypersaline: chloride- magnesium- and sometimes sulfate concentrations greatly exceeded those of ordinary seawater (Table 2). The *hypersaline waters were typically encountered in relatively slow leakages from water panels in immediate vicinity of fast and busy tunnel fans*. It was obvious that draft from the fans had caused this

evaporation and that such extremely aggressive waters therefore also must have influenced the near by sprayed concretes.

Hypersaline waters were not encountered within small leakages running over sprayed concrete surfaces. Instead SEM investigations showed that these concretes were consistently influenced by a seawater-like attack, involving elevated Cl, Na, Mg and sulfate in the paste. Evidently the sprayed concretes had absorbed these aggressive ions. Small leakages in direct and permanent interaction with saline ground waters had unusually high Ca contents (ca 1000 to 3000 mg/L) in contrast to background and seawater at some 400 mg/L. Ca concentrations also increased downstream on a severely deteriorated concrete surface in the Oslofjord tunnel (Figure 3), implying breakdown of the cement paste matrix (Hagelia [18]).

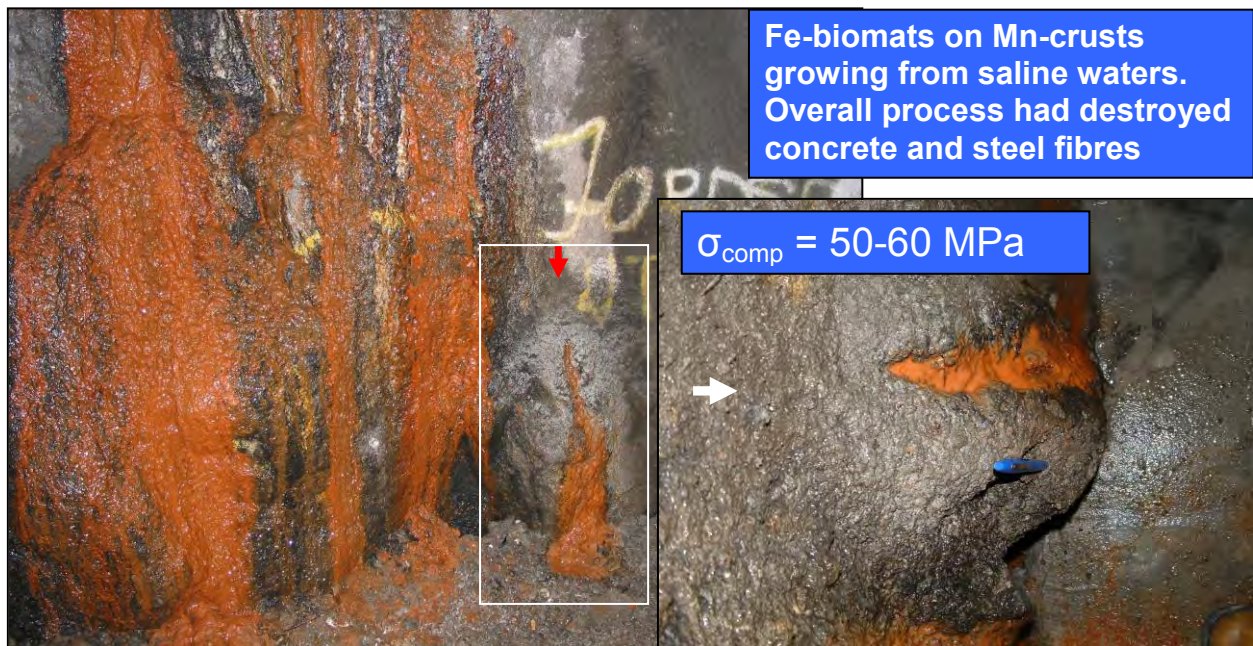


Figure 3: Complex seawater attack in the Oslofjord subsea tunnel facilitated by mild acid attack due to chemical reactions within two layer biofilm consisting of *Gallionella ferruginea* and *Leptothrix sp.* The process also attacks initially strong concrete from the outer surface (inset).

8.3.5.2 Deterioration mechanisms and examples

A novel concrete deterioration process was discovered in the subsea tunnels (e.g. [18]). Steel fibre reinforced concrete used for rock support was attacked by saline ground waters along the concrete/rock interfaces as well as at the outer very rough and reactive concrete surfaces. The process had frequently led to total disintegration of the cement paste matrix and steel fibres after < 5 years (< 0.5 to 10 mm/year) and was closely related to growth of Mn and Fe biofilms. The typical feature was a bacterially derived black Mn-oxide concrete surface deposit covered by a rusty slime consisting of iron bacteria and Fe-hydroxide (Figure 3).

The reaction mechanisms comprised two principal aspects: 1) redox reactions with production of mild acids with pH about 5.5 to 6.5 and 2) a through solution process leading to secondary mineral transformations. Both processes had caused breakdown of portlandite and

Calcium Silicate Hydrate (C-S-H) in the cement paste matrix, and depassivation of steel. The redox regime was strongly influenced by bacterial activity. Initial oxidation of ground water Mn^{2+} by *Leptothrix discophora* (?) led to formation of Na-buserite in pristine dark slime around leakage entrance points through concrete. Buserite quickly transformed into todorokite and birnessite, forming solid black Mn (IV)-rich crusts downstream. *Gallionella ferruginea* and sometimes *Leptothrix ochracea* accumulated outside. These bacteria catalysed oxidation of steel fibres and Fe^{2+} from the ground water, forming ferric compounds such as amorphous ferrihydrite. Also Mn-bacteria, chloride and concrete carbonation assisted in corrosion. Acid production was apparently mostly related to redox reactions between partly oxidised iron compounds and Mn (IV) crust material as was suggested by micro structural relationships, occurrence of Mn crust material with very low O/Mn ratios and preliminary Mn-L-edge spectra. Internally, portlandite and C-S-H had partially broken down through leaching and Ca depletion, bi-carbonation, Mg substitution, brucite ($Mg(OH)_2$) formation and thaumasite sulfate attack. Precipitates of Mg-calcite and aragonite were predominating over calcite on outer and inner surfaces. Most of these minerals are soluble in weak acids.

At an advanced stage gypsum had formed extensively at the expense of cement paste, building up deposits on the outer concrete surfaces. Growth and accumulation of biomass led to reducing conditions and sulfide formation. Stable S-isotopes suggested gypsum sulfate ($\delta^{34}S \approx 13-25\text{‰}$) was derived both from slightly reduced seawater and oxidised H_2S formed through temporary reduction of seawater sulfate underneath dying biota. Crystalline large fibrous carbon with $\delta^{13}C \approx -25$ to -26‰ being incorporated within gypsum also pinpoints the link to the bacterial processes. The combined effects of biotic activity and abiotic secondary mineral transformations resulted in microcracking due to both positive and negative volume changes. Constant replenishment of saline Mn and Fe enriched waters facilitated continuous formation of layered Mn and Fe biofilms and a sustained acid attack, being increasingly effective as microcracking continued to develop. The process also attacked high quality concrete (50-60 MPa; Figure 3).

It is obvious that the so called “algae” reported from several subsea tunnels in previous investigations in fact represent iron and manganese bacteria. Their negative effects were in fact noticed by Hansen [19] already many year ago, who stated that especially the “black deposits” (e.g. manganese deposits) were most harsh to the sprayed concretes.

The effects of this attack is summarised in Table 3 for each subsea tunnel (cf. “complex seawater attack”). The impact of this composite deterioration mechanism had apparently increased with age at several locations. It is important that gypsum layers appeared to accumulate with age; in fact within the Freifjord tunnel a wet mush like greyish gypsum rich slime has been build up within large areas in the deepest part of the tunnel. This implies that the acid attack has moved into the adhesion zone as was also seen in thin sections. Also cast concrete in this tunnel was affected. This type of deposit was by some investigators thought to represent rebound, whilst XRD analyses have shown then to consist of mainly gypsum and occasionally also thaumasite.

The Oslofjord and the Flekkerøy tunnels were also typically influenced by the “complex seawater attack”, whilst these effects were quite minor in the Byfjord tunnel. It seems likely that this reflects a more relevant spray thickness as well as less water leakage. As regards dry or fairly dry concretes the durability was apparently quite normal in the subsea tunnels, without any obvious alarming features. Yet localised calcite stalactites (sometimes with internal brucite deposits) or other leaching phenomena occurred.

8.3.6 Steel fibre corrosion due to chlorides, carbonation and bacterial attack

It was established above that steel fibres were severely attacked in connection with Fe and Mn deposits and bacteria. The steel fibres were attacked by several mechanisms which at places led to their ultimate destruction. Obviously chlorides had a severe effect. But also contact with secondary internal calcite in the form of PCD was important both within the Alum Shale environment and the subsea tunnels. This is due to the infiltration of bicarbonates in ground water which reduced the pore fluid pH to about 8-9.

An interesting “pre-rusting effect” was found within most concretes from subsea tunnels: The steel fibres here had a strong tendency to corrode initially shiny fibres on the core surfaces soon after extraction, even after having been washed in ion poor water. In contrast steel fibres in concrete cores from the freshwater environment always remained uncorroded. Obviously the influence from the saline ground water attack had already contributed to some depassivation of the steel. Investigations by Electron Microprobe Analysis has shown that Cl concentrations in mildly affected C-S-H may exceed 0.5 wt % of the cement paste yet excluding microcracks and micro pores which frequently contained more concentrated Cl. The phenomenon of prerusting has previously been treated by Novak et al. [20]. Finally steel fibre corrosion was facilitated by fast bacterial iron oxidation (see above) and by manganese oxidising bacteria which are known to cause ennoblement of steel (cf. Dickson et al. [21]).

8.3.7 Insignificant traces of Alkali Silica Reaction (ASR)

ASR in Norwegian bridges and dams develop very slowly and usually only becomes apparent after several decades. Wigum [22] evaluated the possibility for ASR in sprayed concrete and argued that their typically high cement contents combined with a susceptible aggregate and possible presence of undispersed silica fume could perhaps lead to reaction.

Within the present study two cases of ASR were identified, both of which in fact just represent curiosities. The first was in the Harpefoss tunnel where the aggregate contains about 20-25 % reactive aggregate (rich in microcrystalline quartz [23]). Here ASR gel was developed as a very thin marginal deposit within extremely few air voids in 13 and 16 years old concrete. Although ASR might develop further it is rather unlikely in view of its rarity. The second case was related to ASR gels formed locally at the expense of undispersed silica fume in the Freifjord tunnel. The observation was made in a sample from just five years old concrete. However later inspection 11 years later did not indicate any negative structural effects. Moreover none of the other thin sections from this tunnel indicated ASR, since most of the silica fume was well dispersed. Microscopy of more than 200 thin sections indicated that the silica fume is generally extremely well dispersed, which means that the pozzolanic effect was very effective.

It may be concluded that ASR in modern Norwegian sprayed concretes is unimportant. This contrasts with experience from Iceland where ASR seems to be present in certain environments (Harðarson et al. [24]).

8.3.8 Compressive strength of samples from subsea tunnels

Concrete cores from the Freifjord-, Byfjord- and Oslofjord subsea tunnels were selected for testing of compressive strength (relating to cube) as based on petrographic

criteria. Some long cores were cut into two, thus testing the inner and outer layer. All cores were visibly quite sound without any obvious cracks and flaws, whilst petrography had indicated various impacts of magnesium attack with traces of thaumasite and internal carbonation (P. Hagelia in prep). The main conclusion was that scattered internal influence of the saline ground water attack did not seem to have a very strong influence on the compressive strength (yielding about 40-55 MPa), whilst when about 40-70 % of the cement paste matrix had been transformed into MSH with brucite and a little thaumasite the strength had dropped by about 50 % or more (about 25 MPa). There was a tendency that outer layers influenced by saline waters from the tunnel side were weaker than concrete further inside. This was partly due to the magnesium attack which was characterised by extensive shrinkage and microcracking in MSH dominated pastes.

Samples with full scale TSA and magnesium attack were much weaker and could not be tested. It is expected that their compressive strengths were in the order of a few MPa (maximum) with almost no tensile strength. Obviously the still weakest concrete was represented by debris which readily was washed away or had fallen down.

8.4 The geological context

8.4.1 Significance of rock mass rating as regards sprayed concrete durability

Although the Q-system is well embedded in NB Publication 7 the reality is quite often different, ranging from no documentation to a qualitative engineering judgement based on registration of weakness zones, occurrences of clay etc. The consequence is that we frequently do not know precisely the rock mass condition behind a particular spray, implying that the effect on stability due to deteriorations is difficult to judge. It is important to realise that the Q-system also accounts for presence of water through the important term J_w (*Joint Water Reduction Factor*). Thus accordingly the Q-values may be reduced significantly depending on the characteristics of water inflow. The Q-system readily states that a water load should be compensated by a thicker sprayed concrete layer.

Since water flow slows down as a function of the thickness of the traversed medium, it is expected that appropriate application of the Q-system should contribute to an extended durability of the sprayed concrete linings also with respect to water loads. In this respect it is very interesting to note that the degradation rate in the Byfjord tunnel was very insignificant despite the presence of highly aggressive waters here. Also in the Svartdal tunnel, where early stage (< 2 years) thaumasite and internal carbonation was detected, later observations at a concrete age of 8 years suggested the attack has halted or slowed down. It is possibly significant that only in these tunnels a systematic rock mass rating had been undertaken: In fact the final sprayed concrete thicknesses applied here were in both cases complying well with the prediction by the Q-system (Bøyeie [25], Hval [26]). However, changes over time in rock mass hydraulic parameters or ground water chemistry may also lead to an overall less aggressive environment towards concrete in some instances (drawdown of the water table, depletions of aggressive ions along rock joints etc.).

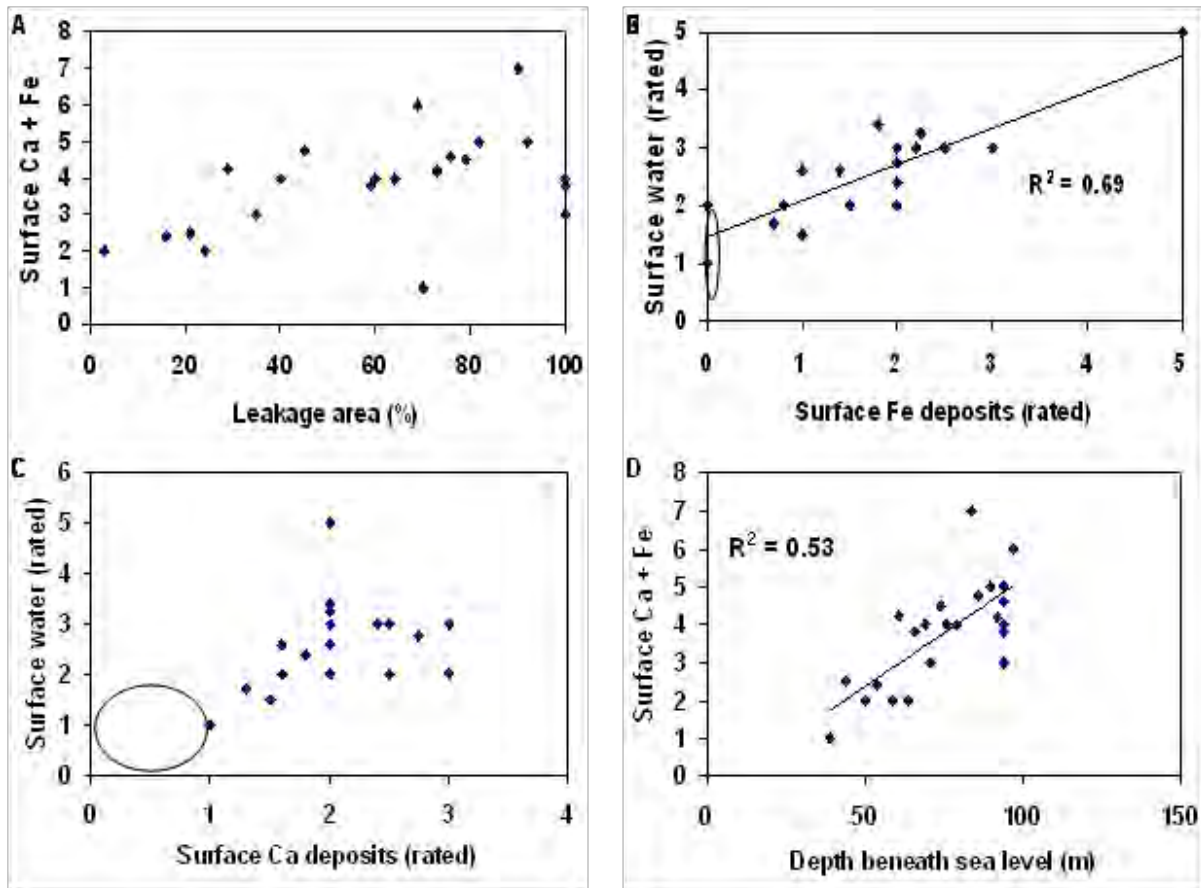


Figure 4: Surface deposits of iron ± manganese (Fe) and Calcite (Ca) show positive correlation with leaching area (A); local surface waters (B, C) and hydraulic gradient (D). Data from the Flekkerøy subsea tunnel. Ellipses represent variation in the fresh water sections under land.

8.4.2 The hydrogeological environment and effect of hydraulic gradient

Deteriorations of all kinds were for all practical purposes restricted to water leakages and the typical situation was a large contact area between concrete and aggressive water. Røhrsveen and Lygre [27] have previously rated surface phenomena including calcite precipitation/stalactite formation and iron deposits in several subsea tunnels using a scale from 0 (no influence) to 5 (most influenced). In view of the detrimental effects related to the iron deposits these data were investigated further: Compilation of data from the Flekkerøy subsea tunnel (averaged pr 50 m in order to minimise scale effects) shows that there is a positive correlation between Ca and Fe deposits and the size of tunnel areas influenced by saline leakages (Figure 4B and C, see also Appendix A6-7). Previously Hagelia [28, 29] reported that the total leakage area, X (the % of a unit tunnel area influenced by spread and volumetrically small water leakages) obeyed the following preliminary empirical equation:

$$X = \frac{h - 30.2(h_r / J)^{0.27}}{0.07(h_r / J)} \quad (1)$$

where h = hydraulic gradient, h_r = rock cover and J is the number of steeply dipping joints/m² (60° – 90°). J simulates the hydraulic conductivity of the rock mass in a rough sense, and variations could under favourable circumstances also be detected on resistivity profiles (Hagelia [30]). Combined with the data in [28] it could further be substantiated that there is a rough positive correlation between registered Fe + Ca surface deposits and the total leakage area X in eq. (1) (Figure 4A). Even more important, there is a steep positive correlation between the same surface deposits and the hydraulic gradient (depth beneath sea level; Figure 4D).

These results prove that concrete deterioration in the subsea environment depends on the hydro geological lay out; the effects of chemical deterioration are not solely depending on the NS EN-206-1 exposure classes but indeed also on the hydraulic gradient (driving force). Preferably future systems should be incorporating these effects as a better basis for planning, exposure classification, cost analysis and forecasting of maintenance costs.

8.5 Practical implications

8.5.1 Characterisation and classification of exposure conditions

An important finding was that deterioration pattern in sprayed concrete deviated from those found in cast concrete, such as bridges and others. Influence from high hydraulic gradient and/or biofilms frequently has had a profound negative effect within otherwise aggressive environments, implying that environmental loads on sprayed concrete represent to a certain extent a new field of experience.

In general saline ground waters in subsea tunnels have up to now been regarded as the same as seawater. NS-EN 206-1 only considers static water loads and the consequences of mobile water are not well explained. Yet in some countries including the UK the mobile and highly mobile ground waters are accounted for by Exposure classes (cf. Building Research Establishment [31] including references to British Standard). This is due to the experience that the highly mobile waters (defined as slowly moving ground waters such as in tunnels) have a different impact on concrete than static waters. In fact, whilst mildly acidic water usually has no effect when static, a highly mobile water with the same pH (about 5.5 to 6) usually has detrimental effects. The same holds true for aggressive ions which is due to the constant replenishment provided by the running water. Highly mobile waters are not easily allowed to buffer or equilibrate with concrete surfaces and hence build up a protective layer. Protective layers such as outer carbonation and $Mg(OH)_2$ which are well known from coastal bridges do not easily build up in the same way when concrete is influenced by running aggressive waters driven by a gradient. This is precisely why magnesium deposits and carbonation in the form of PCD can form deeper within sprayed concretes along with thaumasite.

The additional effect from the “driving force” as represented by the hydraulic gradients acting on the sprayed concrete linings makes the situation perhaps even worse. As such the present author would advice that all subsea tunnel concrete used as rock support should be classified as XSA (“Especially aggressive environment”) in the same way as for the TF-TSA-PCD sources in Alum Shale. In this respect it is important to note that the complex attack, sometimes being influenced by highly evaporated hypersaline waters, indeed involves TSA and PCD with addition significant impact from magnesium, chloride and acids produced within biofilms.

Finally it should not be forgotten that the rock mass stability conditions represent a very important issue as regards exposure conditions. Inappropriate rock mass classification has up to now led to erroneous design of the rock reinforcement involving sprayed concrete thickness. This practice has caused instabilities and even severe collapse within several modern Norwegian tunnels during recent years. Although chemical degradations are at work and should be monitored for their long term effects, the experience so far is that the collapse situations were not due to low material qualities.

8.5.2 Mitigation and remediation for new constructions, maintenance and repair

The question is mainly relevant for the attacks from Oslo Alum Shale and saline ground waters. Although the use of high quality concrete with SRPC and SF has combated the severe effects of TSA the process is still slowly working. Studies in the UK have revealed that certain slag cements are even more successful than silica fume [16, 31] and should perhaps also be tried out in Norway. It should still be recalled that revision of a well proven regime sometimes might involve difficulties also to the disfavour of the concrete durability.

The attack in subsea tunnels was in most respects more serious than the present cases of Alum Shale attack. Since steel fibres represent an important reactant in the acid production within the biofilms in an otherwise corrosive subsea environment, it would seem logical to dispense from the use of steel fibres within the mostly leaky subsea tunnels. At least this represents a realistic remediation since there are now several other alternative fibres available on the market. As a matter of fact the Norwegian Public Roads Administration has already specified polymer fibres of non-corrosive material for highly corrosive environments such as in the subsea part of subsea tunnels (cf. Kompen [32]). It is also possible to introduce somewhat thicker sprayed concrete layers than usually specified, because this would slow down water penetration and at the same time serve as a sacrificial layer. A better control and low w/c –ratios might of course also improve the durability.

As regards maintenance work it seems important to remove biofilms systematically where possible. This is not always the case since the sprayed concrete lining sometimes is not accessible through ordinary maintenance procedures.

Repair should, when required, always involve a thorough characterisation with location of important occurrences of biofilms and identification of degraded sprayed concrete. This should take advantage of geological tunnel maps and rock mass rating charts prepared already during construction. The occurrence and distribution of surface gypsum deposits should be identified and completely removed along with deteriorated concrete, otherwise dissolution of this sulfate will soon take place and lead to sulfate attack on new concrete and also lead to spalling along the old outer surface. Finally the new spray should preferably be made with an inert fibre.

8.5.3 Optimal timing of repair? A general socio-economic approach

It is expected that the most severe deteriorations observed within Norwegian tunnels will lead to a problematic situation earlier than the designed life time of fifty years. An evaluation of the residual life time requires pertinent *site specific* documentation which may only be obtained through a systematic maintenance scheme, including information on rock mass conditions (Q-value, block movements etc), initial spray thickness, hydraulic gradient

and ground water chemistry. Presently no clear cut criteria exist as to where, when and how such a scheme should be applied but it would seem logical to set up a monitoring programme in some tunnels in order to establish deterioration rates. Once having established the rate of deterioration it should be possible to make a socio-economically feasible decision on when to undertake repair. Indeed the optimal timing of repair is also a site specific problem which depends on the local traffic conditions and a safety analysis. If for example the residual life time of a given sprayed concrete can be estimated to be 20 ± 5 year it would seem most feasible to undertake an operation after less than 15 years both due to public safety as well as for accessibility. Traffic prognoses usually indicate a steadily increasing trend. The consequences of a late repair after about 25 years would certainly involve greater risks as regards traffic safety and transportation costs.

8.6 Conclusions

The present study involved a multidisciplinary investigation of sprayed concrete durability exposed to variably aggressive ground waters. Modern steel fibre reinforced concrete used for rock support in Norwegian tunnels showed chemical deterioration phenomena related to water leakages. Ground waters enriched in sulfate and bicarbonate had caused Thaumassite Sulfate Attack (TSA), detrimental internal carbonation and local acid attack. Concretes subjected to ion poor ground waters were usually sound, although sometimes affected by detrimental internal carbonation or Ca-leaching. Alkali silica reaction was unimportant.

A novel deterioration process was discovered in subsea tunnels within sprayed concrete covered by layered Mn-Fe biofilms. Bio-chemical reactions within the biofilms had caused acidification of the saline waters. Acid resistance of sprayed concrete decreased with time due to simultaneous progressive development of internal carbonation, Ca-leaching, TSA, chloride and magnesium attack. This process was very aggressive and had sometimes caused deep or complete disintegrations of the sprayed concrete after < 5 years.

The most severe attacks involved loss of bearing capacity due to cement paste degradation, steel fibre corrosion involving thinning and strength loss of the remaining sound sprayed concrete. These deteriorations were not only depending on the exposure classes but also on the effect of ambient hydraulic gradients. Depassivation of steel fibres was due to chlorides, acids, carbonation and bacterial action. The life time of significantly affected sprayed concretes is regarded as less than the design life of 50 years. Yet where rock mass rating had been applied the concrete linings were much more durable. An assessment of residual life time is in each case critically dependent on rock mass conditions, spray thickness, hydraulic gradient and ground water chemistry.

8.7 Acknowledgements

Funding from the Norwegian Public Roads Administration (NPRA) is gratefully acknowledged. The author is indebted to Ted Sibbick and Norah Crammond, formerly with the BRE, Watford UK for collaboration on thaumasite attack. Reidar Kompen and Claus K Larsen (NPRA) are thanked for fruitful discussions during several years. Ove Lars Strømme, Ian Willoughby, Bente McGonnel, Per Geir Sigursen (NPRA); Hans-Jørgen Berg, Salah

Akhavan (Museum of Natural History) and Ivar Dahl (NIVA) provided invaluable technical assistance.

8.8 References

- [1] Franzén T, Garshol, K.T. and Tomisawa, N. (2001): Sprayed concrete for final linings. ITA/AITES Accredited Material: ITA Working Group Report. Tunnelling and Underground Space Technology, 16, 295-309.
- [2] Barton N., Lien R. and Lunde J. (1974): Engineering classification of rock masses for the design of tunnel support. Rock Mechanics, 6, 189-236.
- [3] Norwegian Concrete Association (2003): Sprayed Concrete for rock reinforcement. NB Publication No. 7, 78 pp. (in Norwegian).
- [4] Norwegian Standard NS-EN 206-1, 2003, Concrete Part 1: Specification, performance, production and conformity.
- [5] Davik K.I. (1997): Proper use of sprayed concrete in tunnels. Parts A, B, C, D, E and Final report, Norwegian Public Roads Administration (in Norwegian).
- [6] Davik K.I. (1998): Proper use of sprayed concrete in tunnels. Nordic Road and Transport Research 1998-1, 16-17.
- [7] Hagelia P., Sibbick R.G., Crammond N.J. Grønhaug A. and Larsen C.K. (2001): Thaumassite and subsequent secondary calcite deposition in sprayed concretes in contact with sulfate bearing Alum Shale, Oslo, Norway. 8th Euroseminar on Microscopy Applied to Building Materials, Athens, Greece, 131-138.
- [8] Romer M. (2003): Detachment of shotcrete linings due to long term interaction with ground water. International Seminar June 2003: The Thaumassite Form of Sulfate Attack, University of Sheffield. 6 pp.
- [9] Hagelia P., Sibbick R.G., Crammond N.J. and Larsen C.K. (2003): Thaumassite and secondary calcite in some Norwegian concretes. Cement and Concrete Composites, 25, 1131-1140.
- [10] Norwegian Public Roads Administration (internal documents).
- [11] Hagelia P. and Sibbick R.G. (2007): Thaumassite sulfate attack, popcorn calcite deposition and acid attack in concrete stored at the “Blindtarmen” test site Oslo, from 1952 to 1982. 11th Euroseminar on Microscopy Applied to Building Materials, Porto, Portugal. 20 pp.
- [12] Bastiansen R., Moum J. and Rosenqvist I. Th. (1957): Contribution to high light certain construction problems associated with Alum Shale in Oslo. Norwegian Geotechnical Institute, Publication No 22, 69 pp (in Norwegian with English summary).
- [13] Fiskaa O., Hansen H. and Moum J. (1971): Concrete in Alum Shale. Norwegian Geotechnical Institute, Publication No 86, 32 pp (in Norwegian with English summary).
- [14] Hagelia P. and Grønhaug A. (2000): Thaumassite – infection causing concrete deterioration. Våre Veger, 9, 54-55 (in Norwegian).
- [15] DETR (1999): The thaumassite form of sulfate attack: Risks, diagnosis, remedial work and guidance on new construction. Report from the Expert Group, Department of Environment, Transports and Regions, UK, 180 pp.
- [16] Crammond N. (2003): The thaumassite form of sulfate attack in the UK. Cement and Concrete Composites, 25, 809-818.

- [17] Hagelia P. (2009): Sources of aqueous sulfate and bicarbonate in Norwegian Alum Shale with implications for concrete durability and geotechnical properties. Submitted to GFF.
- [18] Hagelia, P. (2007): Sprayed concrete deterioration influenced by saline ground water and Mn-Fe biomineralisation in subsea tunnels. In: Jamtveit, B. (ed.): Mechanical effects on reactive systems. The 20th Kongsberg Seminar, Norway (Extended abstract/invited talk).
- [19] Hansen B.O. (1996): Durability considerations related to sprayed concrete in subsea tunnels. Sprayed Concrete in Subsea Tunnels, NPRA Unpublished report October 1996 (in Norwegian).
- [20] Novak P., Mala R. and Joska L. (2001): Influence of pre-rusting on steel corrosion in concrete. Cement and Concrete Research, 31, 589-593.
- [21] Dickson W.H., Caccavo F., Olesen B. and Lewandowski Z. (1997): Ennoblement of stainless steel by manganese-depositing bacterium *Leptothrix discophora*. Applied and Environmental Microbiology, 63-7, 2502-2506.
- [22] Wigum B.J. (1998): Evaluation of the potential for alkali aggregate reactions in sprayed concrete based on literature studies and international experience. P-533 Durable Concrete Structures. Internal report 2009 Norwegian Road Research Laboratory, 47 pp (in Norwegian).
- [23] Norwegian Concrete Association (2004): Durable concrete containing alkali reactive aggregates. NB Publication No. 21, 22 pp with appendices (in Norwegian).
- [24] Harðarson B.A., Wigum B.J., Guðmundsson G., Loftsson M. and Sveinbjörnsson S. (2004): Condition survey of sprayed concrete. Hönnun report. 102 pp (in Icelandic).
- [25] Bøyeie A.E. (1994): Classification of the rock mass in the RENNFAST tunnels using the Q-method, The RMR-method and the RSR-method. Internal report 1708 Norwegian Road Research Laboratory, 66 pp with appendices (in Norwegian).
- [26] Hval O. (2000): Comparison of the rock mass rating systems RMR, Q and RMi – experience from practical application in Tåsentunnelen and Svartdaltunnelen. Cand. Scient Thesis, University of Oslo. 230 pp (in Norwegian).
- [27] Røhrsveen N.G. and Lygre J.K. (1996): Proper use of sprayed concrete in tunnels. Thesis, Norwegian Technical University, Trondheim (in Norwegian).
- [28] Hagelia P. (1992): Semi-quantitative estimation of water shielding requirements for subsea road tunnels using geological and hydrological data. Internal report 1569, Norwegian Road Research Laboratory, 35 pp.
- [29] Hagelia P. (1994a): Semi quantitative estimation of water shielding requirements and optimisation of rock cover for subsea road tunnels. In: M.E. Abdel-Salam (ed.), Tunnelling and Ground Conditions, Balkema 485-492.
- [30] Hagelia P. (1994b): Detection of leakage sensitive joint systems using resistivity measurements in connection with subsea tunnels. In: J. Krokeborg (ed.), Strait Crossings, Balkema, 371-378.
- [31] Building Research Establishment (2003): BRE Special Digest 1 Concrete in aggressive ground. Parts 1-4. London CRC.
- [32] Kompen R. (2008): Specifications for sprayed concrete, EN 14487 for sprayed concrete generally, Norwegian Concrete Association Publication No. 7 for rock support and NPRA Specifications for Road Tunnels. In: K. Berg, C. Hauck, R. Kompen (eds.), 5th International Symposium on Sprayed Concrete – Modern Use of Wet Mix Sprayed Concrete for Underground Support, Lillehammer, Norway 21-24 April 2008, 256-261.

Chapter 9

Does the EN 206-1 Exposure Classification Apply to Tunnel Concrete?

“We have an interest in the design of structures so that effects from degradation is minimized”

Vagn Askegaard

This paper gives an outline of chemical deterioration mechanisms affecting sprayed concrete used for rock support, and provides a discussion of the consequences. The most severe degradations, found in subsea tunnels, were due to a composite saline ground water attack in close association with acidification caused by reactions within Mn-Fe layered biofilms. Thaumassite Sulfate Attack associated with Alum Shale still represents a concern, whilst degradations within the freshwater environment are uncommon. The NS-EN 206-1 Exposure Classes did not predict the extent and rate of severe degradations in high quality mixes. Tunnel concrete is also influenced by effects of hydraulic gradients, bacterial activity and evaporation. As yet the standard does not mention sprayed concrete. Revised Exposure Classes should preferably include bio-degradation, bicarbonate and hydro-geological context, emphasising the importance of “Life Time Exposure Classification” for dynamic water environments.

Keywords: Sprayed concrete, freshwater, Alum Shale environment, saline ground water, biodegradation.

9.1 Introduction

Sprayed concrete used for rock support in tunnels differs from cast concrete in many respects. This material is special in that the main quality parameters are sensitive to the execution process and also because sprayed concrete is directly exposed to variable ground water and rock mass conditions. However, quality routines and good workmanship involving certification of nozzle-men has developed the technology. Modern sprayed concretes therefore, usually display a quite uniform quality. Yet sprayed concrete layers are potentially influenced by instabilities within the surrounding rock masses as well as ground waters of variable chemical composition.

Steel fibre reinforced sprayed concrete is used as a final tunnel rock support method together with rock bolts within a wide range of rock mass conditions. Spray thicknesses vary from about 5 to 30 cm, and are usually designed on the basis of rock mass classification systems such as the Q-system (e.g. [1], and later updates). When the rock support has been established according to rock mechanical principals there is still a possibility that chemical deteriorations may cause thinning and weakening of the sprayed concrete in the long run. Loss of bearing capacity might hence lead to destabilisation of the rock mass. Therefore relevant exposure classification is necessary to ensure long term safety of tunnels.

9.1.1 Background, motivation and objectives

The life time expectancy of sprayed concrete linings in Norwegian tunnels is fifty years, which corresponds to the designed life time. Durability investigations up to 1997 indicated that the situation was not alarming. Ca-leaching, carbonation and steel fibre corrosion was apparently restricted to very thin sprays (< 5 cm) and freeze-thaw damage was regarded as unimportant. The concrete strengths and mixes were in most cases found to comply with the design criteria [2]. However, the aggressive subsea environment was regarded as an important topic for future investigations. The experience up to 1997 is embedded in NB Publication 7 [3], which is the Norwegian specification for sprayed concrete for rock reinforcement. The specification was introduced already in 1979 and has been revised several times. This reflects the leading role Norwegian engineers have had in the development of modern sprayed concrete technology. Presently NB Publication 7 is under revision*, mainly due to the need for harmonisation with the recent EN- 14487, EN 14488 and EN 14489 standards for sprayed concrete. Further details may be found in [4].

However, investigations by the present author from 2000 throughout 2007 have demonstrated that several deterioration mechanisms are affecting tunnel concrete. The mechanisms and structural impact summarised by [5,6], showed that lifetime of sprayed concretes located within certain chemically aggressive environments is much shorter than fifty years. Hence, it was necessary to compare these findings with the NS-EN 206-1 and establish whether the extent and rate of deteriorations was predictable in view of the Exposure Classes. If not predictable, it would seem logical to address the status of the standard and provide a basis for future revisions. The objectives of this paper were to:

- Summarise the characteristics of Norwegian sprayed concrete used for rock support, and establish the main environmental variables affecting concrete within tunnel space.
- Present the main deteriorations in sprayed concrete and the characteristics of associated aggressive groundwaters.
- Undertake exposure classification according to the NS-EN 206-1 Exposure Classes [7] and compare the actual Durability Classes with observed degradations.
- Discuss the findings vs. status of (NS-)EN 206-1 and propose improvements.

** The new revised NB Publication was published in August 2011. The main changes were description of test methods for energy absorption, requirements for fibre distribution on concrete loads prior to spraying and changes to regulations regarding inspection and quality assurance documents.*

9.2 Norwegian sprayed concrete in tunnels

9.2.1 Norwegian specifications for sprayed concrete versus investigated concrete

According to NB Publication No. 7 [3], Norwegian sprayed concrete for rock support should be made according to the following range of specifications:

- Wet method
- CEM I with added 4-15 % silica fume (SF) by cement weight or other pozzolana with a proven effect similar to SF
- Setting accelerators, usually Al-sulfate; previously water glass
- Strength Classes B25, 30, B35, B40 and B45. B40 is not a NS-EN 206-1 Strength Class.
- Durability Classes M40, M45 and M60.
- Binder contents 400-530 kg/m³
- w/c = 0.60-0.40: mostly w/c = 0.40 - 0.45
- Steel fibre reinforcement for ductility (40-50 kg/m³)

NB Publication No. 7 and NS-EN 14487 utilises the NS-EN 206-1 Exposure Classes as a normative reference. The studied sprayed concretes were all made according to the wet method, using a rapid setting Portland cement (PC rapid) or Sulfate Resisting Portland Cement (SRPC) with mostly 5-16 % SF. Strength Classes and Durability Classes were B40 or B45 and M40 or M45, respectively. The binder contents varied from 485 to 580 kg/m³ and the w/b-ratios were ranging from 0.38 to 0.47 (0.50). Steel fibre contents were within the 30 to 60 kg/m³ range. In general it was concluded that the investigated sprayed concretes were complying with NB Publication 7 and NS-EN 206-1. They represent “real life” sprayed concretes made according to a quality scheme, and there was no indication that deteriorations were due to poor workmanship. A more specific relationship between Exposure Class, Durability Class and state of deterioration for individual cases is given in Table 2.

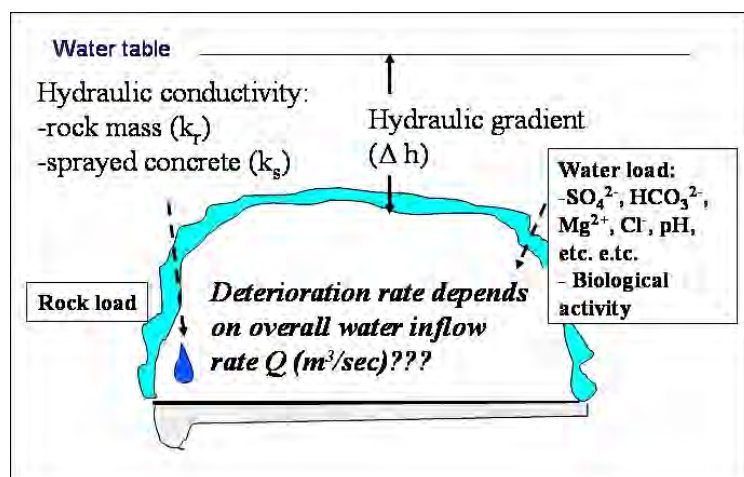


Figure 1: Environmental loads acting on sprayed concrete in tunnels. In addition the effects of evaporation within tunnel space should be considered.

9.2.2 Context of sprayed concrete in tunnels

Steel fibre reinforced sprayed concrete usually takes the shape of the blasted rock mass behind and is characterised by a tortuous and rough outer surface. The surface of sprayed concrete frequently accumulates particles and biota and attracts moisture. This is a favourable environment for chemical reaction and growth of microbes [5,6]. The principal aspects of environmental loads acting upon sprayed concrete linings in tunnels are illustrated in Figure 1. The tunnel environment is characterised by differential mechanical loads from the rock mass, variably aggressive waters and variable hydraulic gradients. Drought in tunnels might also cause evaporation and lead to increased ionic strength of leakage waters within the tunnel space. Moreover, the effects from exhaust fumes cannot be excluded, although this was not studied.

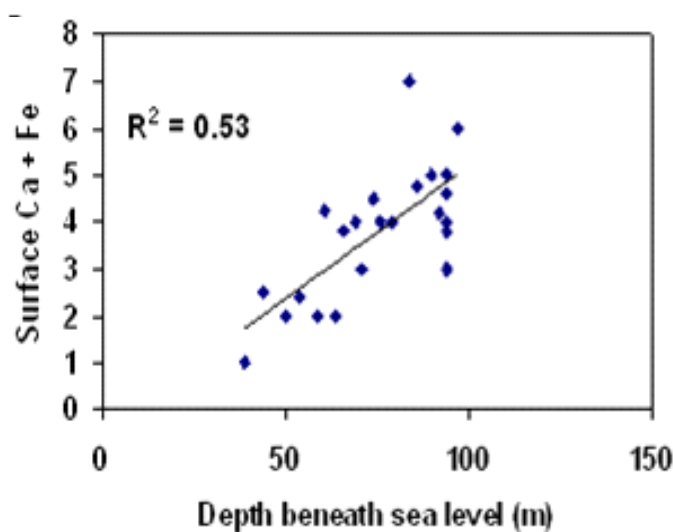


Figure 2: Surface deposits (rated) of calcite (leached Ca from cement paste) and iron ± manganese oxides (Fe) in the Flekkerøy subsea tunnel, showing a positive correlation with hydraulic gradient (depth beneath sea level) (cf.[5,6]).

Investigations in a subsea tunnel have shown that Ca-leaching of sprayed concrete and Mn-Fe surface deposition increased significantly with the depth beneath sea level (Figure 2). Hence there can be no doubt that the magnitude of the hydraulic gradient represents a very important environmental variable affecting the sprayed concrete lining. In view of the rather thin concrete layers involved (frequently 5-10 cm), aggressives should enter more easily into the pore space of sprayed concrete than into thick layers of cast concrete [5,6]. This is mainly due to the differences in concrete water conductance, which increases with thickness of the concrete layer. In contrast to subsea tunnel sections, tunnels under land are influenced by a variable water table with a less constant water pressure. Shifting of ground water level also leads to variable redox conditions within the rock mass which may effect temporal changes in the water chemistry: It is well established that lowering of the water table leads to sulfide oxidation and formation of aqueous sulfate within Alum Shale [8].

Large water leakages are rare in tunnels due to pre-grouting. Instead volumetrically small leakages with low flow rates are representative of the typical water loads on tunnel concrete. Such leakages may be spread over large concrete surface areas or be more focused. Evaporation has been found near tunnel fans [5,6] and the effect is most efficient in thin water films, corresponding to volumetrically small and spread water leakages. The evaporation rate

is suppressed at high relative humidity (RH). However, RH in tunnels commonly range from 60 to 70 % [9], suggesting there is a significant potential for increased aggressiveness by evaporation.

9.2.3 An outline of the structural deterioration phenomena in sprayed concrete

The investigations indicated that, although most sprayed concretes still appear to be intact there are many examples of deeply weathered concretes which are in the process of losing their integrity. Structural deterioration of sprayed concrete is characterised by cracking, spalling, leaching and degradation of the cement paste matrix. These features are almost exclusively related to the presence of water leakages acting from behind the sprayed layers and from the outer surface. Destructive steel fibre corrosion may take locally along cracks or more generally associated with secondary minerals (see chapter 3).

Chemical degradations may lead to 1) fallout of strong thick concrete slabs or 2) focused or widespread weakening and thinning due to leaching, spalling and formation of concrete debris (Figure 3). These mechanisms have caused structural damage at early age (< 5 years), although they mainly should be regarded as somewhat “long term processes”. The first process is facilitated by cracking across the sprayed concrete layers leading to local transformations of the cement paste along cracks and the interface with the rock mass. Destructive steel fibre corrosion occurs, notably in the subsea environment, causing loss of sprayed concrete ductility. It is significant that the adhesion zone quite commonly is weak and sometimes permeable [11]. The second process involves bulk diffusion of aggressive waters from both sides of the sprayed concrete layers. This process has caused significant thinning of the sprayed concrete layers, typically occurring within the saline ground waters environment.

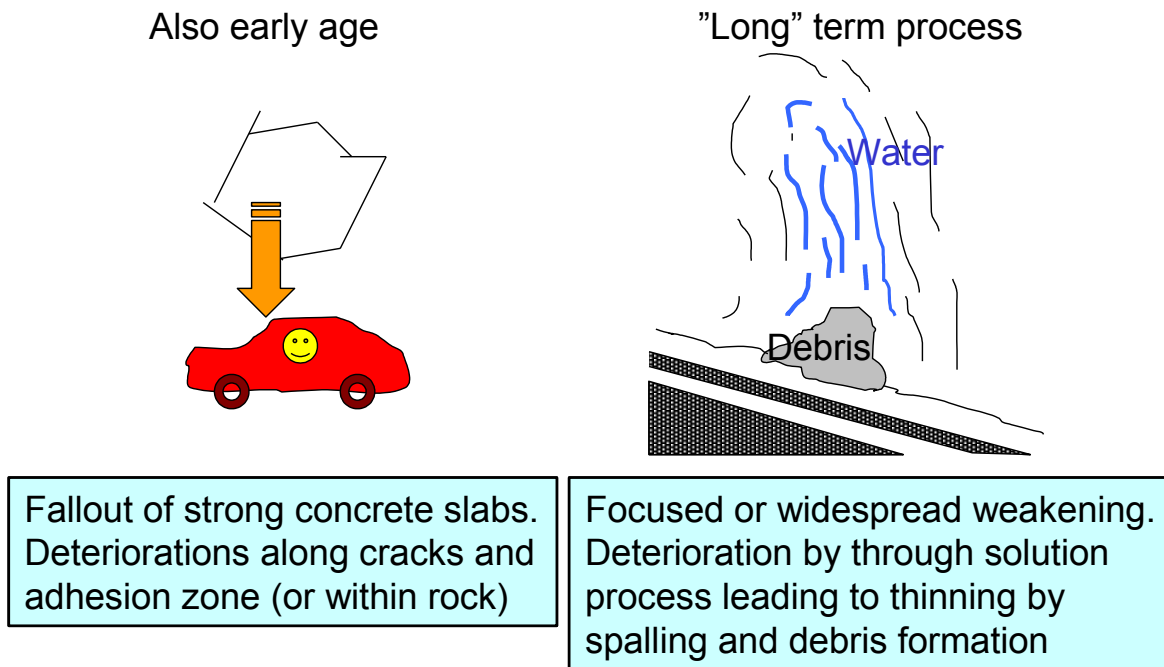


Figure 3: Two principal types of structural deterioration in sprayed concrete linings.

Part 3 – Summary of deteriorations & engineering aspects

Table 1: Chemical & stable isotope data for waters. Subsea tunnel samples in italics were collected from fresh waters under land. Water chemical analyses from the previous Blindtarmen test site from [16] (I to IV) and [17]. * = waters with some interaction with concrete; ** = waters with extensive interaction with concrete (upstream from sample stations). Ammonium concentrations were generally low .

Samples	Characteristics	$\delta^{18}\text{O}$	$\delta^2\text{H}$	pH	Cl ⁻	Na ⁺	K ⁺	Ca ²⁺	Mg ⁺	SO ₄ ²⁻	HCO ₃ ²⁻
		‰	‰		mg/L	mg/L	mg/L	mg/L	mg/L	mg/L	mg/L
<u>Subsea tunnels</u>		SMOW									
Flekkerøy 1**	Water shield w/Mn (?) bacteria	-4.4	-37	7.39	27900	12800	294	3100	1420	2240	43
Flekkerøy 2	Water shield, large leakage	-0.8	-4.5	8.07	18700	10200	396	429	1310	2600	146
Flekkerøy 3*	Water shield w/Fe bacteria	-1.2	-10.8	7.98	18300	9530	297	1020	1180	2500	119
Flekkerøy 4*	Water shield w/Mn bacteria	-3.7	-28.3	8.02	11100	5080	136	1060	754	1380	117
Flekkerøy 5*	Interface rock/concr w/ Fe bact	-2.6	-23.4	7.81	17500	8300	193	1920	1010	2300	84
Byfjord 1*	Water shield; w/possible Fe bact	-0.4	-15.9	7.55	50200	27800	507	1660	3280	3830	137
Byfjord 2**	Via degraded concrete surface	-6.2	-47.4	7.56	11400	5720	50.7	1280	571	1250	41
Byfjord 3*	Water shield	0.1	-6.1	7.75	25400	14500	483	596	1790	3300	151
Byfjord 4*	Water shield	-6.7	-48.8	8.33	260	193	14	15	15.4	51.2	141
Oslofjord V1*	Via degraded surf.;Mn-Fe bact	-0.1	-1.8	7.91	19100	9170	307	473	1260	2640	132
Oslofjord V2*	Via degraded surf.;Mn-Fe bact	n.a	n.a	7.89	19300	9300	308	472	1210	2670	137
Oslofjord V3	Crack in concrete, large leakage	-0.3	-0.4	7.88	19100	9180	313	460	1270	2640	146
Oslofjord V4*	Crack in concrete w/Mn-Fe-bact	0.6	1.9	7.93	18900	9140	316	458	1260	2610	146
Oslofjord V5	From rock joint	-0.4	-5	7.93	18600	9060	318	442	1240	2580	150
Oslofjord V6**	Ditch under degraded; Mn-Fe-b.	0.8	2.6	7.71	18200	9480	340	484	1321	2550	179
Oslofjord 1**	Degraded surface w/Mn-Fe bact	0.4	-4.2	6.60	n.a	8940	163	1310	1320	2630	n.a
Oslofjord 2**	Degraded surface w/Mn-Fe bact	-1.7	-10.1	6.64	18300	8700	160	1360	1320	2604	161
Oslofjord 3**	Degraded surface w/Mn-Fe bact	-1.1	-5.6	6.69	18300	8640	184	1110	1340	2720	123
Oslofjord F1*	From rock mass w/ Fe-bacteria	n.a	n.a	7.80	18500	8990	318	435	1240	2550	139
Oslofjord F1-2005*	Ditch below F1 w/ Fe-bacteria	-0.8	-13.7	7.30	17800	9740	316	419	1230	2440	179
Oslofjord V10	Average water at pump station	-5.1	-32.9	7.67	9990	5110	161	370	725	1410	135
Oslofjord V10II	Average water at pump station	-4.8	-40.5	7.60	10600	5690	155	391	763	1450	144
Oslofjord 17450**	Below degr. surf. w/Mn-Fe-bact	-1.0	-14.3	7.49	17800	9640	262	547	1270	2410	154
Oslofjord T4-1	Crack in concrete	-0.4	-4.3	7.83	16900	9280	348	394	1180	2740	135
Oslofjord T4-2	Ditch below T4-1 w/ Fe-bact	-0.6	-4.3	7.82	17500	9320	349	398	1190	2840	135
<i>Oslofjord SOS31</i>	<i>Ditch water</i>	<i>-10.2</i>	<i>-74.7</i>	<i>8.03</i>	<i>9.4</i>	<i>12.8</i>	<i>2</i>	<i>40</i>	<i>4</i>	<i>13.6</i>	<i>139</i>
<i>Oslofjord SOS 8</i>	<i>Rock water, slow</i>	<i>-10.5</i>	<i>-74.2</i>	<i>8.16</i>	<i>59.6</i>	<i>63</i>	<i>2</i>	<i>31</i>	<i>6</i>	<i>21.1</i>	<i>165</i>
<i>Oslofjord B1</i>	<i>Rock water large basin</i>	<i>-11.1</i>	<i>-81.5</i>	<i>7.43</i>	<i>123</i>	<i>76.3</i>	<i>3</i>	<i>21</i>	<i>3</i>	<i>13.3</i>	<i>64</i>
Oslofjord A2*	Stalactite water in saline zone	n.a	n.a	7.00	1910	1040	16	131	57	334	n.a

Part 3 – Summary of deteriorations & engineering aspects

Freifjord 6600**	Drain w/Mn-Fe bacteria	n.a	n.a	7.00	19900	8550	37	1680	1310	2710	101
Freifjord 6650**	Dropping on c surface/Mn-Fe b.	n.a	n.a	6.50	19200	6700	33	2950	1250	3130	n.a
<i>Freifjord 3135*</i>	<i>Ditch</i>	<i>n.a</i>	<i>n.a</i>	<i>7.00</i>	<i>24</i>	<i>168</i>	<i>6</i>	<i>13</i>	<i>1</i>	<i>146</i>	<i>n.a</i>
Freifjord 5910**	Water shield w/Fe-Mn bacteria	n.a	n.a	6.00	17100	7300	34	2480	1270	1930	n.a
Freifjord 4930**	Water shield under Mn-Fe bact	n.a	n.a	5.50	5680	2050	11	1610	205	410	n.a
Freifjord 5700**	On surf. w/Mn-Fe-bact	n.a	n.a	6.00	17100	8080	23	1980	1220	2230	n.a
Freifjord 4890*	Via degraded surf. w/Mn-bact	n.a	n.a	6.00	5110	1680	14	1340	237	424	n.a
Freifjord 6915*	Drain under Mn-Fe bact	n.a	n.a	5.50	15700	6580	34	2420	1170	1780	n.a
Freifjord 4930-1**	Water shield under Mn-Fe bact	-15.5	-115.1	6.88	6500	2100	10.2	1600	213	510	23
Oslofjord seawater	60 m depth NIVA Solbergstrand	0.2	-0.77	7.74	18600	10800	390	413	1370	2630	144
<u>Freshwater</u>											
Lier 44265	Drain in railroad tunnel	-11.8	-82.1	8.18	2.8	15.0	0.8	44.5	12.1	22.3	173
Harpefoss 1	Crack in concrete	n.a	n.a	5.70	16.9	3.2	7.8	59.9	2.3	111.0	n.a
Harpefoss 2	Crack in concrete	n.a	n.a	5.67	13.2	3.5	4.4	38.5	2.8	106.0	n.a
Harpefoss 3	Crack in concrete	n.a	n.a	5.66	15.8	11.0	5.0	58.5	1.5	102.0	n.a
Harpefoss 4	Crack in concrete	n.a	n.a	6.06	12.8	3.4	n.d.	38.9	3.9	105.0	n.a
<u>Alum Shale water, Oslo</u>											
Åkeberg 1*	Drainage hole, TSA aff. concr.	n.a	n.a	7.60	29	26.0	22.0	615.0	110.0	1841	274.0
Ekeberg 1**	Stalactite water, TSA aff. concr.	n.a	n.a	7.00	10	25.0	16.0	106.0	20.0	592	100.0
Ekeberg 2**	Crack in TSA affected concrete	n.a	n.a	7.00	10	43.0	22.0	574.0	74.0	2031	56.0
Svartdal 320-06	Pond below TSA aff. concrete	-11.3	n.a	6.84	18.7	44.4	9.1	172	21.4	541	66.8
<u>Alum Shale water, Blindtarmen Test Site - Oslo 1952 - 1973</u>											
I	Ground water (isolated from air)	n.a	n.a	5.38	421	n.a	n.a	n.a	n.a	2772	n.a
II	Ground water (isolated from air)	n.a	n.a	6.14	491	n.a	n.a	n.a	n.a	653	n.a
III	Ground water (isolated from air)	n.a	n.a	5.00	343	n.a	n.a	n.a	n.a	2530	n.a
IV	Ground water (isolated from air)	n.a	n.a	4.89	347	n.a	n.a	n.a	n.a	2523	n.a
Sept 55 B	Bottom of tunnel	n.a	n.a	6.22	420	n.a	n.a	n.a	n.a	2772	n.a
22/5/63 B	Bottom of tunnel, oxidised	n.a	n.a	3.91	210	37	7	760	110	4116	n.a
22/5/63 H1	Hole I oxidised ground water	n.a	n.a	2.95	190	37	10	740	150	4284	n.a

9.3 Water environments

9.3.1 Freshwater environment

The concretes in contact with freshwater loads were visually mainly intact. Local Ca-leaching and calcite stalactite formation was observed. The water analyses reported in Table 1 indicate somewhat elevated sulfate concentrations < 150 mg/L, which is less than Exposure Class XA1. However there is some concern related to impact of sulfate attack. This is due to the fact that secondary ettringite and thaumasite can be stabilised at rather low sulfate concentrations: In fact a local thaumasite attack at Harpefoss, detected when this sprayed concrete was 16 years old, [12] had formed at sulfate concentrations about 110 mg/L. In the Lier railway tunnel there was evidence of an old sulfate attack (ettringite-thaumasite) which took place at a time when leakages were abundant. Presently the tunnel concrete is typically dry due to a permanent lowering of the water table. The single water chemical analysis from this tunnel shows a very low sulfate content, which if representative, might also indicate that the sulfate source within the rock mass has been exhausted [9]. The present problem is due to extensive spalling and falloff, related to very extensive outer carbonation. The Lier sprayed concrete was made in 1965-1971, representing old technology of no direct relevance to a study of the durability of modern concrete. The investigations within the freshwater environment were not very comprehensive because other environments were obviously more important.

9.3.2 Alum Shale environment

The Norwegian Alum Shale Committee (1947-1973) concluded that the well known quick cement paste degradation in the Oslo region was due to secondary ettringite and variable impact from acid attack [8]. However, this has recently been refuted. Petrography of young sprayed concrete used for rock support and old test samples from the previous “Blindtarmen” test site (1952-1982) has demonstrated that this classic “ettringite case” in fact was caused by Thaumasite Sulfate Attack (TSA) in close association with decalcification and internal detrimental carbonation in the form of Popcorn calcite and other relatively coarse calcite. There was also a variable impact of acid attack. Non-deleterious Thaumasite Formation (TF) was quite common, suggesting TSA is under way several places. Modern cases are represented by the Åkebergveien road cut and the Ekeberg and Svartdal road tunnels (Table 1) [11,12,14].

Thaumasite growth requires a source of sulfate and carbonate, usually a cool and moist environment, and otherwise utilises Ca and Si in the cement paste matrix. TSA leads to partial or complete degradation of the cement paste matrix, in contrast to expansion and map cracking caused by ettringite. Recent investigations have proven that extensive Ca-leaching and calcite formation greatly facilitates the development of full scale TSA [14]. Oxidation of Alum Shale sulfides (pyrrhotite and pyrite) was previously regarded as the main source of sulfate ions, whilst research by the present author has demonstrated that also primary anhydrite in the shale may contribute significantly to the aqueous sulfate concentration. The sulfide oxidation mechanisms are complex, and bacterial oxidation assisted by *Acidithiobacillus species* appears to play a significant role [18]: These investigations have also shown that the source of thaumasite carbonate is both bicarbonate derived from calcite dissolution and atmospheric CO₂.

Part 3 – Summary of deteriorations & engineering aspects

Water chemistry implies that sulfate concentrations within the 500-4000 mg/L range, coupled with ordinary bicarbonate contents of around 100-275 mg/L, are responsible for the overall TF-TSA-carbonation process. Associated ground water pH ranges from circum neutral to strongly acidic ($\text{pH} < 3$). Lower pH causes efficient leaching of the outer cement past matrix and an increased porosity, making the overall concrete more open for sulfate and bicarbonate ions. The overall rate of the TF-TSA-carbonation increases in presence of acidic water where thaumasite and Popcorn calcite form in an intermediate position between pristine paste and the acid leached domains [14].

In reality the chemical composition and acidity of Alum Shale ground water varies at each site, as shown by the analyses from the Blindtarmen test site (Table 1). The important lesson is that ground water compositions under land are not constant. They vary over time reflecting the complex chemical interaction between jointed rock mass and a shifting water table, likely responding to variations in precipitation and drying. Alum Shale represents Exposure Class XSA (NS-EN 206-1; NA.11) and sprayed concretes are now usually made with SRPC and silica fume in line with the findings of the previous Alum Shale Committee. These concrete mixes have countered the severe attacks. However, Hagelia et al.[11,12] reported on the occurrence of TF and TSA in a modern steel fibre reinforced concrete less than 2 years old (Svardal highway tunnel) and the overall TF-TSA-carbonation process had caused spalling, thaumasite-calcite mush formation and destructive steel fibre corrosion after less than 13 years at the Åkeberg road cut (Figure 4). There was no indication of internal sources related to the concrete aggregate. For this reason TSA still represents a concern within the Alum Shale provinces.



Figure 4: Spalling after less than 13 years in a 1987 steel fibre reinforced concrete (SRPC and SF), due to TSA and carbonation due to PCD. A previous spray had been severely affected and was replaced after 17 years in service. Alum Shale environment, Åkebergveien Oslo.

Popcorn Calcite Deposition (PCD) is another concern where bicarbonate bearing ground waters enter deep into concrete in a through solution process. This sort of carbonation is different from ordinary surface carbonation in that it forms relatively coarse calcite grains as a direct consequence of decalcification of CSH, hence influencing the strength. In contrast, ordinary surface carbonation only reaches a few mm and is essentially harmless unless it

reaches steel reinforcement. Steel fibres in sprayed concretes are always corroded within the surface carbonated zone [2], whilst effects of PCD can have detrimental effects even in absence of TSA [12,14].

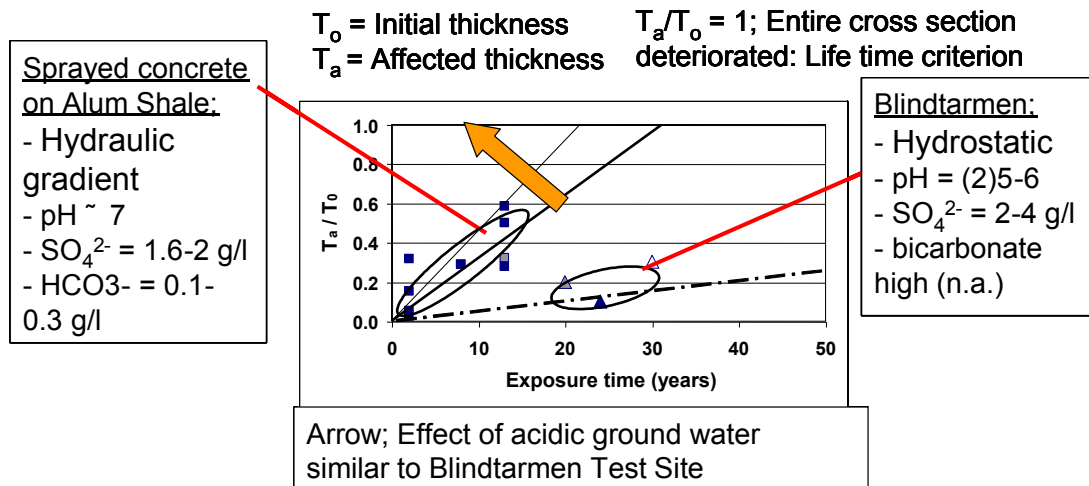


Figure 5: Lifetime of sprayed concrete under a hydraulic gradient is potentially shorter than concrete immersed under hydrostatic conditions, such as the Blindtarmen test samples. Thick continuous line represents 10 cm thick sprayed concrete (SRPC and 5 % SF) the thick stippled line 10 cm thick Blindtarmen test prisms (PC and 15 % SF)[14].

Comparison of deteriorated zones (“affected thickness”) with initial thicknesses can be used as a proxy to life time studies (Figure 5). Sprayed concrete on Alum Shale at near neutral pH was somewhat more affected by the TF-TSA-carbonation process than the Blindtarmen test specimens that had suffered events of acid attack. Modern sprayed concrete in contact with Alum Shale and additional sulfuric acid attack can be expected to remain in service for less than 20 years, in contrast to some 20 to 30 years at pH neutral conditions [14]. The combined effects of acid attack and TSA on sprayed concrete influenced by a hydraulic gradient remains to be studied directly. Yet the effect is less pronounced when spray thicknesses exceed 10-15 cm [12].

9.3.3 Saline ground water environment with localised development of hypersalinity

9.3.3.1 A novel mechanism involving bacterial degradation

A novel sprayed concrete deterioration process has been discovered in Norwegian subsea tunnels (e.g. [13]). The process ultimately resulted in complete disintegration of the cement paste matrix and destructive steel fibre corrosion (Figure 6), even in the strongest concrete (Strength Class B45) [5,6]. The composite reaction mechanism comprised 1) acid production due to redox reactions within layered Mn-Fe biofilms inhabited by *Leptothrix* and *Gallionella* species forming biominerals, and 2) infiltration of saline Cl^- , Mg^{2+} , SO_4^{2-} and HCO_3^- enriched ground water, leading to formation of magnesium silicate hydrate, Thaumassite Sulfate Attack, Popcorn Calcite Deposition (PCD) and associated precipitation of brucite, Mg-calcite, aragonite and gypsum. The development of these secondary minerals generally decreased the acid resistance of the concrete. The bacterial acid attack initially acted

from the outside surface, whilst the saline infiltration acted from both sides of the spray. Eventually the acid attack also entered the interface against the rock mass.

In contrast to static conditions, the hydraulic gradient facilitated magnesium attack several cm inside sprayed concrete, causing shrinkage, increased inflow of aggressives and consumption of hydroxyl ions. Constant replenishment of saline Mn and Fe bearing waters resulted in continuous formation of layered biofilms and a sustained attack. The deterioration had caused outer debris formation and thinning of sprayed concrete layers at rates varying between < 0.5 up to 5-10 mm/year, leading to deep and complete disintegration of the cement paste matrix after less than five years at several places. These rates were estimated on the basis of visual observation where an approximate control level could be established. However, in absence of the Mn-Fe biofilms the attack by saline infiltration was mostly slower. At an advanced stage gypsum had formed extensively at the expense of cement paste, building up crusts on the outer sprayed concrete surfaces. Gypsum crust thicknesses have been found to exceed 5 cm, forming either within/underneath rusty bacterial slimes or as precipitates. Such crust material should be removed prior to repair sprays in order to avoid sulfate attack soon afterwards.

Steel fibres delivered Fe^{2+} to the acid producing reactions, and should therefore be abandoned in subsea tunnel concrete. The steel fibre corrosion leads to a loss of sprayed concrete ductility which is a very important property when used for rock support. In general steel fibre corrosion is also triggered by more familiar mechanisms, such as chloride penetration, carbonation, and Mg-attack [5,6,13,15]. An interesting “pre-rusting” effect was found in most subsea sprayed concretes: Steel fibres in freshly cut and washed core material from sound concrete were mostly intact and shiny but exhibited pronounced surface corrosion after a few hours. In contrast steel fibres in concrete from the freshwater environment remained unaffected.



Figure 6: Old core locations in the Freifjord subsea tunnel showing extensive breakdown of the sprayed concrete 16 years later. Rusty and black areas (right) consist of iron oxihydroxide from *Gallionella ferruginea* and manganese oxides derived from *Leptothrix* sp. Grey deposits consist of gypsum formed from Ca in concrete and sulfate from seawater.

9.3.3.2 Significance of salinity, hypersalinity and evaporation

The ground waters in the subsea tunnel sections appear to represent mixtures of fresh water and seawater like saline ground waters in different proportions, with some effects from interaction with rock mass. However some drain waters collected from aluminium water panels in the Flekkerøy and Byfjord tunnels were much more saline than seawater (hypersaline). These waters were exposed to drought near busy tunnel fans and represent evaporation, as is also indicated by their Na/Cl ratios which are similar to seawater or any mixture of seawater and freshwater (Figure 7). Apparently some sodium at some localities has been bound within the rock mass, possibly due to exchange with clay minerals. Also sample 6650 (Freifjord) leaking over concrete indicated some degree of hypersalinity in direct contact with concrete (Table 1). Most waters on water panels had drained over concrete surfaces before they entered the panels. In contrast to aluminium sheaths, cement pastes certainly also had absorbed Cl, Na, Mg and sulfate, as shown by SEM analysis [15]. Leakages showing extensive interaction with concretes influenced by the composite bacterial and saline water attack (indicated with ** in Table 1) had been strongly enriched in Ca relative to background water (e.g. seawater, rock water and fast leakages through concrete cracks with Ca = 394-460 mg/L). Ca concentrations also increased downstream: Water sample “Oslofjord 3”, from about 1 m downstream from a leakage entrance point, had Ca = 1110 mg/L whilst “Oslofjord 2”; 2 m further below had reached 1360 mg/L. This excess Ca must be derived from the cement paste, since this particular location showed extensive cement paste degradation due to Mn-Fe biofilms and saline water attack.

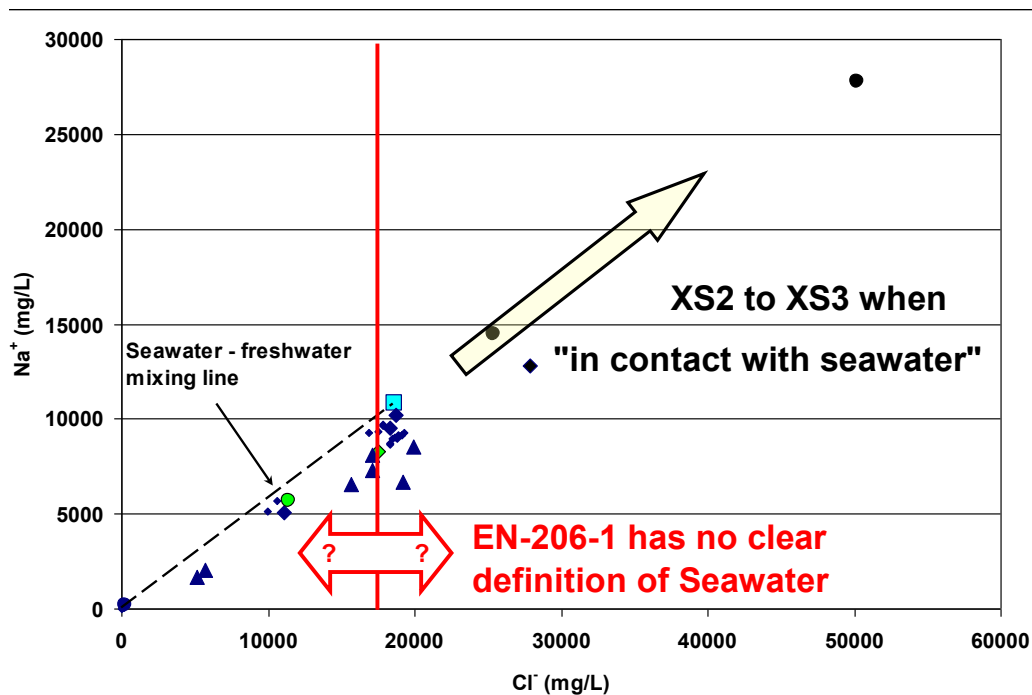


Figure 7: Chloride and sodium variation in waters collected in subsea tunnels and land tunnels. Circles = Byfjord; triangles = Freifjord; diamonds = Flekkerøy; small diamonds = Oslofjord, and square = seawater. Big arrow, trend of evaporation.

9.3.4 Characterisation of waters by hydrogen and oxygen stable isotopes

Stable isotopes are extensively applied within environmental fields. Hydrogen and oxygen isotopes were in this case used in order to distinguish between origins of waters, with focus on hypersaline waters. The main issue related to the EN 206-1 exposure classification is to find out the potential for development of “excess” aggressiveness due to evaporation within tunnel space. In water the heavy ^2H (deuterium) and ^{18}O isotopes make up small fractions, whilst ^1H and ^{16}O are far more abundant. Due to the differences in weight (e.g. molecular bonding energies) isotopic fractionation takes place, reflecting different processes and origins. The isotopic composition of H and O is expressed as the ratio of the heavy to light isotopes relative to a standard composition, referred to as “Standard Mean Ocean Water” or SMOW. A further introduction to the basics of stable isotope systematics may be found in [19]. Figure 8 shows a plot of oxygen isotopes versus hydrogen isotopes, presented as δ values in ‰ of the deviation from SMOW. According to convention SMOW plots at (0,0) and the real seawaters are not very different (see Table 1). All analysed samples plot on a trend which indicates an overall mixture of seawater like ground water (near 0,0) and freshwaters (at very negative values). This trend nearly coincides with seawater, falling below the Meteoric Water Line (MWL), which represents river water, rain and snow from all over the world. The seawater like ground waters (cf. chemical compositions in Table 1) with $\delta^{18}\text{O}$ and $\delta^2\text{H}$ within 0 to – 1 ‰ and 0 to – 5 ‰ ranges, respectively, are strongly predominated by the seawater component, whilst the most negative signatures mainly represent freshwaters. Freshwaters always have quite negative H and O isotopic compositions and melt waters derived from snow and ice are most depleted in the heavy isotopes.

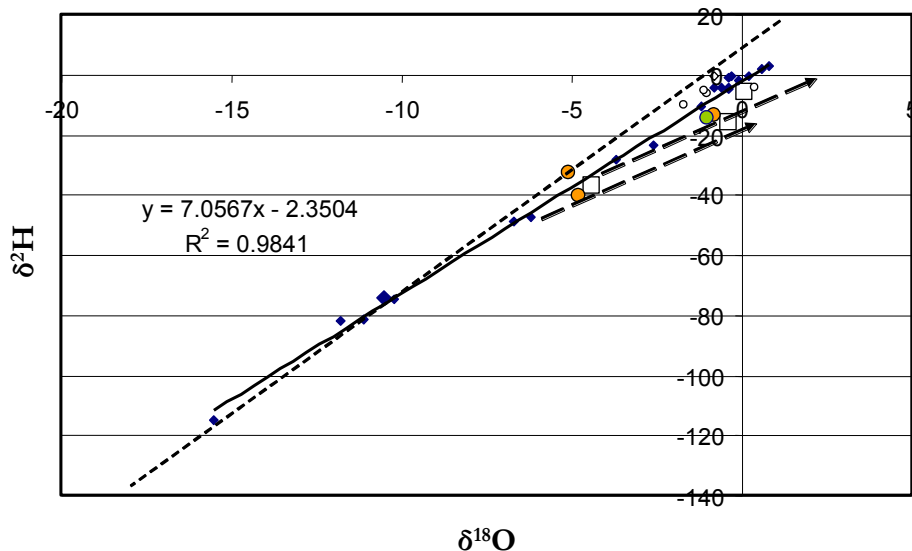


Figure 8: Stable H and O isotopes of waters collected in subsea tunnels and freshwater tunnels. The open squares represent strongly evaporated waters on the lower side of the main trend. Arrows corresponds to the slopes of evaporating waters from two arbitrary initial compositions along the freshwater – seawater mixing line (thick line and regression). Open squares; evaporated hypersaline waters. Thin stippled line is the Meteoric Water Line.

Evaporation of any water composition will lead to enrichment in their heavy isotopic compositions, because the light isotopes prefer the vapour. Accordingly the H and O compositions in remaining waters become progressively more positive as evaporation proceeds. Evaporated waters derived from different starting compositions fall below the actual freshwater – seawater mixing line on separate trends with similar nearly constant slopes, as illustrated in Figure 8. Initial compositions prior to evaporation are somewhere along or near this mixing line. In general all of the hypersaline waters fell below the main seawater – freshwater mixing line in keeping with evaporative effects. The hypersaline water from the Flekkerøy subsea tunnel (“Flekkerøy 1”) had a very negative composition in comparison with seawater, and originated from a water mixture with a significant portion of freshwater. This means that the initial water composition before evaporation most likely was brackish water. Similarly the most evaporated water from the Byfjord subsea tunnel (“Byfjord 1”) extrapolated backwards to the main mixing line show it was derived from an isotopic composition which is characteristic of brackish water. “Byfjord 3” had the largest seawater component among the hypersaline waters. Thus, undoubtedly the effects of evaporation within tunnel space can increase the waters aggressivity against concrete very extensively. This will be elaborated further in the next chapter dealing specifically with EN 206-1 Exposure classification.

9.4 Exposure classification according to NS EN 206-1

9.4.1 Introduction

Table F.1 in EN 206-1 is not used in Norway. Instead Table NA.11 has been introduced in National Annex NA.F, showing the relationships between Exposure Class and Durability Class. Table NA.11 also introduces Exposure Class XSA nationally for “Especially aggressive environment”, such as Alum Shale ground water, and XA4 for manure cellars. According to [3] sprayed concrete for rock support does not require classification of frost environment. NS-EN 206-1 states that if a relevant environmental classification has been made and the mix design complies with recommendations in this standard, then the concrete life time should be 50-100 years. Obviously this was not always the case.

9.4.2 Classification and comparison with real life tunnel concrete

The classification was based on water chemistry reported in Table 1 and documentation of initial concrete quality [2,9]. The durability status of several sprayed concretes up to 2008 was compared to Strength Classes and Durability Classed as derived from the concrete quality documentation. Table 2 gives a summary of the results. Most samples were cores from 2 to 16 years old concrete. Judgement about the durability status was based on detailed petrography as well as visual inspections. It should be noted that although the degradations are typical, they are overrepresented in the summary. In general the choice of Exposure Classes for corrosion caused by carbonation and seawater was a bit tricky, because no verbal statement in the standard refers explicitly to sprayed concrete and tunnel environments.

Part 3 – Summary of deteriorations & engineering aspects

Table 2: Comparison of NS-EN 206-1 classes and real life durability of sprayed concrete used for rock support. Concrete sample numbers from [15]. Deterioration mechanisms: Mn-Fe & saline = bacterial acid attack and saline gr. water load; Saline = saline gr. water load without acid; TF-TSA-PCD = Thaumassite Formation-Thaumassite Sulfate Attack-internal carbonation. Destructive steel fibre corrosion in extensive attacks. Ordinary surface carbonation was always present.

Location (age) & concrete samples	Water samples (Table 1)	Exposure Class	Strength Class	Durability Class	Real life durability & influence of mechanism	Deterioration mechanism
<u>Subsea sections</u>						
<i>Flekkerøy (1988)</i>						
1373, 1374	1 (hypersaline), 5	XC2, XS2, XA3	B45	M45	<u>Extensive thinning; ≥ 5 cm gypsum crust</u>	<i>Mn-Fe & saline/gypsum</i>
1070, 1074	3	XC2, XS2, XA3	B45	M45	Thinning?, weak paste, 4-6 cm deep Mg	<i>Mn-Fe & saline</i>
<i>Byfjord (1990-1991)</i>						
1-2 at 2868 m	1&3 (hypersaline)	XC2, XS2, XA3	B45	M45	Good performance, local Mg, 14 yrs	<i>Saline (minor Mn-Fe)</i>
Visual at 2862 m	2	XC2, XS2, XA2	B45	M45	Good performance, leached surface, 14 yr	<i>Saline (minor Mn-Fe)</i>
<i>Oslofjord (1998)</i>						
Slab H2004	1,2,3	XC2, XS2, XA3	B45	M40	<u>Replaced after 5 years service: >5 cm Mg.</u>	<i>Saline</i>
Kj I, II, II, IV, V	1,2,3	XC2, XS2, XA3	B45	M40	<u>0.5-5 cm loss of thickness; age < 5 yrs</u>	<i>Mn-Fe & saline</i>
Kj 1, 2, 3, 4, 5	V1 trough V6	XC2, XS2, XA3	B45	M40	Possible loss, some paste transformation	<i>Mn-Fe & saline</i>
Kj 6, 7, 8, 9, 10	V1 trough V6	XC2, XS2, XA3	B45	M40	No loss, weak transf. paste: Mg deep	<i>Saline</i>
Spall V5	V1 trough V6	XC2, XS2, XA3	B45	M40	<u>Extr. friable, > 6cm compl. transformed.</u>	<i>Mn-Fe & saline</i>
<i>Freifjord (1990-1991)</i>						
Visual at 4930	4890, 4930-1	XC2, XS2, XA1	B45	M45	<u>Extensive paste degradation, ages 5-16 yrs</u>	<i>Mn-Fe bact + saline</i>
5700, 5800	5700, 5910	XC2, XS2, XA3	B45	M45	Some thinning and internal degradation	-- " – w/ gypsum crust
6080	5910	XC2, XS2, XA3	B45	M45	Some thinning and internal degradation	-- " – w/ gypsum crust
6150	5910, 6650 (hyp)	XC2, XS2, XA3	B45	M45	<u>4 cm deep Mg attack (thinning?), 13 years</u>	<i>Mn-Fe & saline</i>
<u>Alum Shale</u>						
Structures in Oslo						
Åkebergveien (1987); Cores 1,2,3,4	1	XC2, XSA	≈ B45	≈ M45	Spalling and localised mush formation after < 13 years. Still in service: 21 years	<i>TF-TSA-PCD</i>
Ekeberg (1992); C 1,2	1,2	XC2, XSA	≈ B45	M45	Leaching, stalactites, some friable paste	<i>TF-TSA-PCD</i>
Svartdal (1998); Cores 320A,B; 370A,B; 320O,N; 370H,V	320-06	XC2, XSA	B45	M40	Leaching, small structural effects after 8 years, process started at < 2 yrs, some friable paste	<i>TF-TSA-carbonation</i>

Table continued overleaf...

Part 3 – Summary of deteriorations & engineering aspects

Location & concrete samples	Water samples (Table 1)	Exposure Class	Strength Class	Durability Class	Real life durability & influence of mechanism	<i>Deterioration mechanism</i>
<u>Freshwater</u>						
Harpefoss (1984); 1,2,3	1,2,3 &4	XC2, (X0)	No docum.	M45-M60	Small local effects after 16 years	<i>TF-TSA-carbonation</i>
Freifjord (1990); 3132	3135	XC2, (X0)	B45	M45	High quality, no effect	<i>None</i>
Byfjord (1990); 3 at 4410 m	4	XC2, (X0)	B45	M45	High quality, no effect	<i>None</i>
Oslo (visual inspections)	SOS8, SOS31,B1	XC2, (X0)	B45	M40	High quality, no effect	<i>None</i>

9.4.2.1 Freshwater environment

In the few included examples corrosion class XC2 by carbonation was considered as the most close to the verbal statement in the standard. Much of the concrete was dry and X0 is then the relevant classification. Concretes from Harpefoss, Freifjord, Byfjord and Oslofjord were considered, mainly representing M45. Only the concrete at Harpefoss was marginally affected by TSA with only small structural effects after 16 years in service. According to [12] early leaching with surface efflorescence of calcite and thenardite occurred. However there are some uncertainties regarding the initial quality and the Durability Class of the concrete was M45-M60. Yet it might be concluded that the durability of sprayed concrete in the freshwater environment is in agreement with the predictions implied by NS-EN 206-1. These concretes had a higher designed quality than strictly demanded by the chemical exposure conditions.

9.4.2.2 Alum Shale environment

This environment is by definition XSA and due to frequent moist conditions XC2 seemed relevant. The Durability Class of sprayed concrete at the Åkebergveien road cut and Ekeberg tunnels was around M45, whilst the concrete in the Svartdal tunnel classifies as M40. NS-EN 206-1 gives a relevant environmental classification, but since the effects of the TF-TSA-carbonation process still results in some structural disintegration after quite a few years this represents a concern. Yet the XSA Exposure Class requires Durability Class M40, which was not fulfilled for the most affected concrete at Åkebergveien. However, the effect of early sulfate attack (< 2 years) in the Svartdal M40 concrete suggests some problems related to formulation of an optimal mix still remains. As stated in Figure 5, the effects of acidic Alum Shale ground water should be more aggressive, and have not yet been studied.

9.4.2.3 Saline environment

The saline environment was mainly characterised by Exposure Classes XC2, XS2, XA3. The Durability Classes of sprayed concrete were M45 except for M40 in the Oslofjord subsea tunnel. Table 2 shows that extensive deteriorations occur at places. Sample H2004 represents sprayed concrete within the service tunnel down to the pump station. This concrete was strongly weathered and influenced by saline ground water attack with extensive Mg penetration (brucite and MSH) and development of TSA and PCD. No acid attack related to Mn-Fe biofilm was involved here. The life time of this approximately 10-12 cm thick spray was only 5 years, as it was demolished and replaced in 2004. Presently the new concrete is characterised by extensive water penetration, being very well developed already by the end of 2005.

Although Mg attack with or without TF-TSA and PCD has influenced subsea concrete deep inside, additional acid attack related to bacterial activity definitely had the most severe effects. This composite attack has led to severe cement paste deterioration with extensive debris formation in concretes belonging to Durability Classes M45 and M40, even in waters belonging to Exposure Class XA1 (Freifjord tunnel location 4930). The late stage outer gypsum deposits related to the acid production had formed in thicknesses reaching at least 6 cm in the Flekkerøy subsea tunnel at one location, but were uncommon in the young Oslofjord subsea tunnel. Previous reports [2] suggest that the capillary suction of the Freifjord sprayed concrete is somewhat elevated, which might be one of the factors assisting degradation here. The composite bacterial – saline attack appears to be present in most subsea tunnels. However, sprayed concrete in the Byfjorden subsea tunnel performs well. This is

most likely due to the overall thicker spray here (10-15 cm) and much lesser abundance of Mn-Fe biofilms.

At one location in the Oslofjord subsea tunnel (Spall V5) sprayed concrete influenced by Mn-Fe biofilms and saline ground waters was extremely friable: This big spall (5-6 cm thick) was collected in winter 2004 and could easily be broken off, leaving a visible “scar”. When returning to the location after two months degradation in adjacent concrete had been so fast there was no sign of the spalling any longer. Petrographic investigations showed that quite coarse calcite, Mn- oxides and ferric iron compounds had been deposited throughout the spall, which in fact disintegrated extensively while drying in the laboratory. This concrete has as yet not been replaced.

The most severe attacks outlined in Table 2 had occurred in concrete at least 100 m below sea level. Thus there is a complex relationship between the chemical loads and the “driving force” represented by the hydraulic gradient.

Preliminary data on compressive strength (P. Hagelia in prep) have shown that as long as the saline water attack by Mg substitution and thaumasite and internal carbonation is rather scattered the strength is not very significantly influenced (yielding about 40 -55 MPa). However when these secondary minerals exceed some 40-70 % of the cement paste matrix the strength drops by about 50 % or more.

Based on the compiled data in Table 2 it can be stated that, despite that initial concrete properties largely complied with the specifications given in NS-EN 206-1, the extent of the attacks were by no means predicted by this standard. It should be emphasised that the investigated tunnels are still (in 2009) only 11 to 21 years old.

9.5 Discussion of NS-EN 206-1

9.5.1 Evaporation and classification

Evaporation in tunnel space leads to increased salinities and aggressiveness of waters with implications for exposure classification according to NS-EN 206-1. Jørgensen [20] established experimentally the relationship between chloride and stable isotope enrichment during evaporation. Using these results it was possible to estimate the initial salinities of evaporated hypersaline waters assuming that the initial water composition fall close to the seawater – freshwater mixing line (Figure 9). Although this is a strait forward and conventional application of H isotopes, it seems possible that additional processes might have contributed to the scatter near the mixing line. The uncertainty may perhaps reach about 2500 mg/L on the Cl scale. Yet this does not alter the main conclusion: In fact the samples that had experienced most evaporation appear to have increased the chloride contents from about 5000 mg/L to 50000 mg/L.

Thus, having established the approximate chloride contents in the hypersaline waters prior to evaporation, trajectories of evaporative effects were then plotted on Cl vs. Mg and Cl vs. SO_4^{2-} diagrams and compared to the Exposure Classes (Figures 10 & 11). Evidently evaporation can cause a 100 % to 1000 % increase in concentrations. Judging from the length of the trajectories it can be envisaged that low saline waters less aggressive than XA1 can develop into highly aggressive waters belonging to Exposure Class XA3 at very high ionic strengths. For obvious reasons evaporation influences waters on concrete surfaces as well as metal water panels to a similar extent. Therefore, wherever possible, tunnel fans should be installed at a sufficient distance from widespread aggressive leakages. Undoubtedly

unfavourable location of tunnel fans may directly contribute to unnecessary aggressive loads and a shorter service life of sprayed concrete.

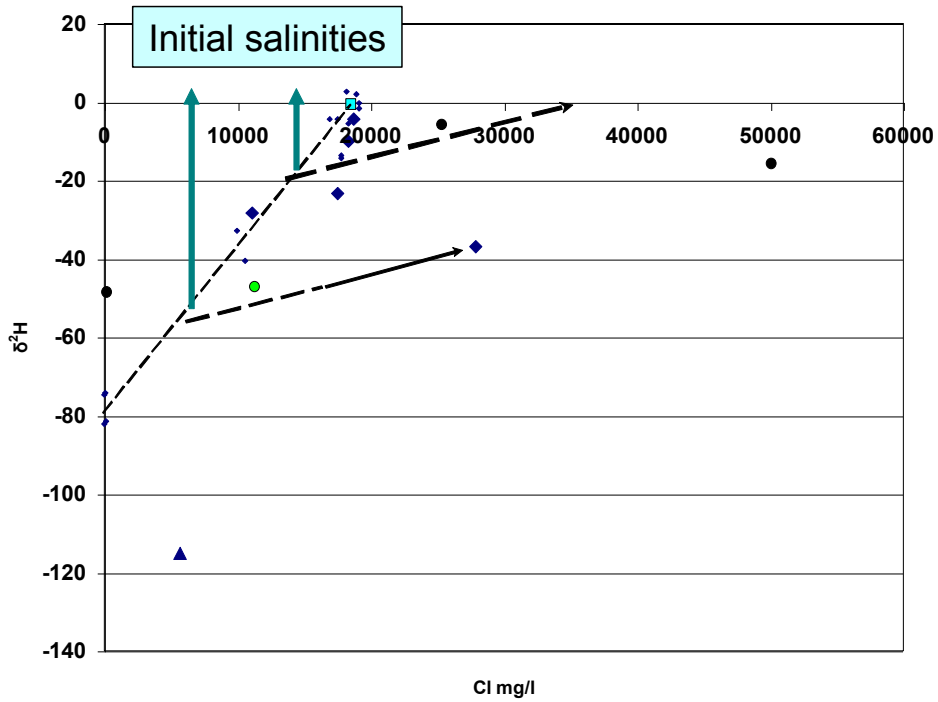


Figure 9: Chlorine concentrations versus H isotopes of waters collected in subsea tunnels. Stippled arrows represent effects of evaporation. Thin stippled line is the mixing line of seawater and freshwater and thick arrows indicate initial salinities prior to evaporation.

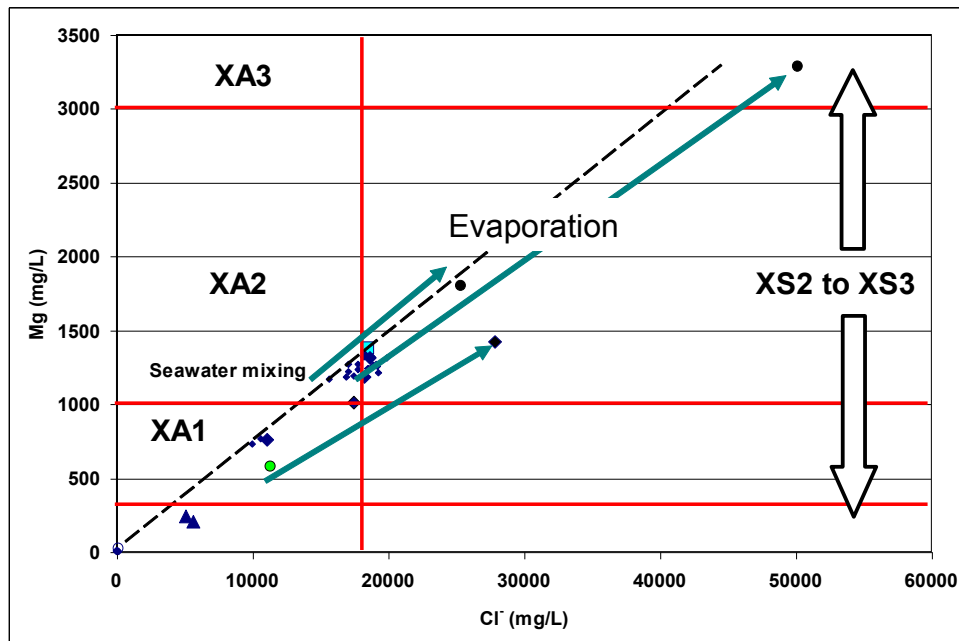


Figure 10: Chlorine vs. magnesium showing trends of evaporations projected onto the EN-206-1 Exposure Classes.

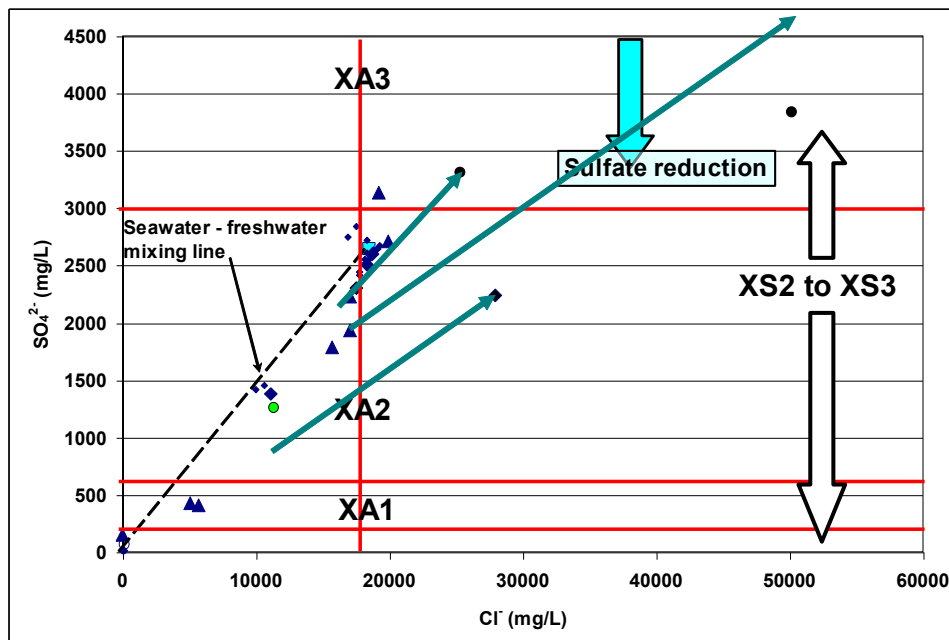


Figure 11: Chlorine vs. sulfate showing trends of evaporations projected onto the EN-206-1 Exposure Classes.

9.5.2 Significance of dynamic water environments

The present investigation has clearly demonstrated that the tunnel environment is characterised by a dynamic water system, implying that the water loads change character from location to location and from time to time. The main features can be summarised as follows:

9.5.2.1 Natural background

- 1) Hydrogeological changes in subsea section; frequent lowering of volumetric flow rate due to clogging or mineral deposition on rock joints [9].
- 2) Hydrogeological changes in land sections; lowering or fluctuations of ground water level with effect on hydraulic gradients (i.e. changing driving force for aggressives).
- 3) Hydro-chemical changes: Aggressive reservoirs may become depleted or activated (Alum Shale and others).

9.5.2.2 Dynamics in tunnels

Tunnel drought, due to tunnel fans and others: small spread leakages are most prone to evaporative effects and development of “excess” aggressiveness. Salinities may increase by 100 % – 1000 % from initial.

Tunnel air: exhaust fumes, dust and particles, bringing external components into contact with concrete surfaces (not investigated).

In general the deterioration rate of sprayed concrete is a function of w/c, spray thickness, rock mass stability, hydraulic gradient, water chemistry and bacteria. The concrete standards and other specifications should preferably focus on this broad perspective.

9.5.3 What the standard does not tell: some recommendations

NS-EN 206-1 considers mainly static water and does not really account for mobile waters, typical of the tunnel environment and many other contexts. In the United Kingdom the classification for concrete in aggressive ground covers a wider range of applications than (NS)EN-206-1 [21]. Mobile and highly mobile waters are accounted for due to the experience that such waters generally are more aggressive than static waters. For example mildly acidic waters (pH = 5.5-6) may have very small structural effects when static but cause deteriorations when mobile. It would be a great advantage to incorporate this reality in EN-206-1.

The present investigation has unveiled practical problems: NS-EN 206-1 does not provide any example related to sprayed concrete and tunnel environments, despite that the EN- 14487, EN 14488 and EN 14489 standards for sprayed concrete refer to EN-206-1. In particular the problem is that the standard does not cover the entire durability problem.

In the first place there is no clear-cut definition of what seawater is (is the brackish Black Sea, a seawater or not?). It was not very clear what the differences between XS2 and XS3 represents when applied to tunnel concrete. The standard considers various contact relations between “seawater” and concrete without taking notice to the different salinities encountered. Preferably variable salinity (chloride) should be included in EN-206-1, because degradation rates are always sensitive to concentration levels of all aggressive ions. Moreover there was some uncertainty as regards carbonation. The examples given by the standard seem “coloured” by one of the carbonation mechanism, namely the effect of atmospheric carbon dioxide. There is no mention of the role of bicarbonate, which is very important for the development of internal detrimental carbonation in the form of Popcorn calcite. Amendments should, therefore, make a clear distinction between the two different types and contexts of carbonation, by including bicarbonate (alkalinity) on the list of parameters to be analysed. This would also provide information about the buffering capacity for acids, as well as capacity for TSA when sulfate also is present.

Also the effects of biological material should be included in EN-206-1. Recently RILEM summarised the results of microbial impact on concrete and other building materials, and stated that a multidisciplinary approach to concrete durability is necessary [22]. As a first approach the present author would suggest that EN-206-1 includes XSA (Especially aggressive) and splits into subclasses with bacterial attack and acid rock drainage (similar to some Alum Shale environments). Subsea tunnel sections should be integrated in the existing XSA Exposure Class and the potential effect of evaporation should be accounted for.

Finally the hydrogeological context is important to understand. Temporal changes in water pressure and water chemistry are governed by the interaction of water and rock mass. The durability development of buried concrete depends on the time integrated exposure conditions. Thus classification of hydrogeological environments should help unveiling the changing exposure conditions during the service life of concretes. There is hence a direct relationship between geological characterisation/classification and water exposure classification for tunnel concrete. For these reasons the concept of “*Life time exposure classification*” is introduced herein. The concept should be developed for various applications of concrete in different environments and geological settings based on hydro-geochemical and hydrological interpretation.

9.6 Conclusions

The NS-EN 206-1 Environmental Classes did not predict the extent and rate of the more severe attacks found in sprayed concrete used for rock support in tunnels. Tunnel concrete is also influenced by effects of hydraulic gradients, bacterial activity and evaporation. Ground water chemical loads can be very aggressive and may vary over time. Revision of the standard should involve biodegradation, bicarbonate contents and hydro-geological classification. There is also a need to differentiate better between the most aggressive exposure conditions and “Life Time Exposure Classification” based on hydro-geochemical and hydrological interpretation.

9.7 Acknowledgements

The author is indebted to the Norwegian Public Roads Administration (NPRA) for funding this project. Hans-Jørgen Berg, Salah Akhavan, Berit Løchen Berg and Muriel Erambert, University of Oslo; Inger Kjersti Iden and Lars Kirksæther, Institute for Energy Technology Kjeller; Ivar Dahl, NIVA Oslo; Per Geir Sigursen, Ove Lars Strømme, Bente McGonnel, Øystein Lahaug, Ian Willoughby and Per Sydsæther, NPRA, provided invaluable technical assistance. Collaboration on thaumasite attack with Ted Sibbick and Norah Crammond, formerly with BRE Watford UK, and fruitful discussions with Reidar Kompen and Claus K Larsen, NPRA, are gratefully acknowledged.

9.8 References

1. Barton, N., Lien, R. & Lunde, J., “Engineering classification for rock masses and for the design of tunnel support”. *Rock Mechanics* 6, (1974) pp. 189-236.
2. Davik, K.I., “Proper use of sprayed concrete in tunnels” Parts A, B, C, D, E and Final report. Norwegian Public Roads Administration, 1997 (in Norwegian).
3. Norwegian Concrete Association, “Sprayed Concrete for rock reinforcement”, NB Publication 7, 2003, 78 pp. (In Norwegian).
4. Kompen, R., “Specifications for sprayed concrete, EN 14487 for sprayed concrete generally, Norwegian Concrete Association Publication No. 7 for rock support and NPRA Specification for Road Tunnels”, In: K., Berg, C., Hauck, R., Kompen (Eds.), 5th International Symposium on Sprayed Concrete – Modern Use of Wet Mix Sprayed Concrete for Underground Support. Lillehammer, 2008, pp. 256-261.
5. Hagelia, P., “Deterioration mechanisms and durability of sprayed concrete in Norwegian tunnels”, In: K., Berg, C., Hauck, R., Kompen (Eds.), 5th International Symposium on Sprayed Concrete – Modern Use of Wet Mix Sprayed Concrete for Underground Support. Lillehammer, 2008, pp. 180-197.
6. Hagelia, P., “Deterioration mechanisms and durability of sprayed concrete in Norwegian tunnels”. In: K., Fossum, G., Gjæringen, E., Moe (Eds.). *Underground Openings – Operations, Maintenance and Repair*. Norwegian Tunnelling Society, Publication 17, 2008, pp. 45-58.
7. NS-EN 206-1, “Concrete Part 1: Specification, performance, production and conformity”

8. Bastiansen, R., Moum, J., & Rosenqvist, I.Th., “Contribution to high-light certain construction problems associated with Alum Shale in Oslo”. Norwegian Geotechnical Institute, Publication No. 22, 1957, 69 pp., (In Norwegian with English summary).
9. Norwegian Public Roads Administration, Internal documents.
10. Franzén, T., Garshol, K.T., & Tomisawa, N., “Sprayed concrete for final linings”. ITA/AITES Accredited Material: ITA Working Group Report. *Tunnelling and Underground Space Technology* 16, 2001, pp. 295-309.
11. Hagelia, P., Sibbick, R.G., Crammond, N.J., Grønhaug, A., & Larsen, C.K., “Thaumasite and subsequent secondary calcite deposition in sprayed concrete in contact with sulfate bearing Alum Shale”, 8th Euroseminar on Microscopy Applied to Building Materials, Athens, Greece, 2001, pp. 131-138.
12. Hagelia, P., Sibbick, R.G., Crammond, N.J., & Larsen, C.K., “Thaumasite and secondary calcite in some Norwegian concretes”, *Cement and Concrete Composites*, 25, 2003, pp. 1131-1140.
13. Hagelia, P., “Sprayed concrete deterioration influenced by saline ground water and Mn-Fe biomineralisation in subsea tunnels”, In: B., Jamtveit (Ed.), *Mechanical Effects on Reactive Systems*, the 20th Kongsberg Seminar, 2007, abstract/invited talk.
14. Hagelia, P., & Sibbick, R.G., “Thaumasite Sulfate Attack, Popcorn Calcite Deposition and Acid Attack in Concrete Stored at the “Blindtarmen” Test Site Oslo, from 1952 to 1982”, 11th Euroseminar on Microscopy Applied to Building Materials, Porto, Portugal, 2007.
15. Hagelia, P., “Sprayed concrete deterioration due to layered Mn-Fe biofilms and saline ground waters in subsea tunnels: Structural effects, characterisation and preliminary reactions”, Manuscript, 2009.
16. Moum, J., & Rosenqvist, I.Th., “Sulphate attack on concrete in the Oslo region”, *Journal of the American Concrete Institute*, Proceedings, Vol. 56, Title 56-18, 1959, 8 pp.
17. Fiskaa, O., Hansen, H., & Moum, J., “Concrete in Alum Shale”, Norwegian Geotechnical Institute, Publication No. 86, 1971, 32 pp., (In Norwegian with English summary).
18. Hagelia, P., “Sources of aqueous sulfate and bicarbonate in Norwegian Alum Shale with implications for concrete durability and geotechnical properties”, 2008, Submitted to *Chemical Geology*.
19. Faure, G., “Principles of Isotope Geochemistry”, 2nd Ed., John Wiley and Sons, 1986, 589 pp.
20. Jørgensen, N.O., “Origin of shallow saline groundwater on the island of Læsø, Denmark”, *Chemical Geology*, 184, 2002, pp. 59-370.
21. Building Research Establishment, “Concrete in aggressive ground”, Parts 1-4, BRE Special Digest 1, 2003.
22. Gaylarde, C., Ribas Silva, M., & Warscheid, Th., “Microbial impact on building materials: an overview”, *Materials and Structures*, 36, 2003, pp. 342-353.

Chapter 10

Conclusions, implications and further work

*“The durability of the present conclusions
remains to be studied”*

P.H.

10.1 General

This chapter gives a summary of the main conclusions made in Chapters 3 through 9, along with main supporting evidence. Furthermore, the implications are discussed along with consequences for contemporary engineering. Finally recommendations for further investigations and research are presented.

10.2 Main conclusion of the thesis

10.2.1 Part 1 - The Black Shale environment

10.2.1.1 Reaction mechanisms in concrete

Investigation of modern *steel fibre reinforced sprayed concrete* and *historical concrete samples* from the Blindtarmen test site in Oslo confirmed that concrete deterioration was caused by Thaumasite Formation (TF), detrimental Thaumasite Sulfate Attack (TSA) and Popcorn Calcite Deposition (PCD) with variable effects of acid attack. This stands in marked contrast to the significant role of secondary ettringite, as was previously suggested (Bastiansen et al. 1957). This external attack was caused by sulfate and carbonate bearing groundwater with acidic to neutral pH derived from Alum Shale.

Conclusions related to *modern sprayed concrete* used for rock support, made with Sulfate Resisting Portland Cement (SRPC) and silica fume (SF) and w/b ratios 0.4-0.5 were:

- The sulfate attack was closely tied to decalcification and Ca-depletion of C-S-H with Popcorn Calcite Deposition (PCD) and other forms of internal carbonation, rather than by direct decomposition of undepleted C-S-H. Internally in concrete, thaumasite also decomposed to calcite under liberation of sulfate ions; available for further attack.
- The process required fluid flow through the bulk cement paste matrix, and the reaction progress was sensitive to the spray thickness. Alum Shale ground water had mildly acidic to neutral pH; about 600-2000 mg/L aqueous sulfate and 100-275 mg/L bicarbonate. Influence of TF-TSA-carbonation in older Black shale (Eocambrian) was

Conclusions, implications and further work

very minor: The ambient pH was 5.5-6 with about 100-110 mg/L sulfate (bicarbonate not analysed).

- The TF-TSA-carbonation process was not markedly sensitive to C₃A contents within the 1-8 % range: Infected concretes were made with Sulfate Resisting Portland Cements (SRPC) or Portland cement (PC), always with well dispersed silica fume. There was no indication that formation of secondary ettringite occurred prior to thaumasite, which has been suggested by some researchers to be a prerequisite for TSA (cf. Bensted 2003).
- Destructive steel fibre corrosion began in the presence of PCD and other internal carbonation, and also occurred in soft thaumasite + calcite mush formation leading to spalling.
- The lifetime of TF-TSA-PCD affected sprayed concrete is shorter than the design life time (50 years): Spalling had occurred after less than 13 years in modern steel fibre reinforced sprayed concrete.
- Some data presented in this thesis suggested that SRPC based sprayed concrete made with Al-sulfate accelerator were possibly slightly more vulnerable to Ca-leaching and TF-TSA-carbonation than SRPC based sprayed concrete made with water glass. This is in apparent agreement with the research results of Paglia et al. (2003).

Investigations of *historical test prisms from the Blindtarmen test site* showed they were characterised by an outer reaction zone formed along a steep pH gradient. Six reaction stages were established, representing a complete record of acid attack and associated TF-TSA-carbonation (details given in Chapter 4):

- Outer leaching due to sulfuric acid (and carbonic acid) led to an increased porosity, which made way for penetration of aggressive waters. This facilitated TF-TSA and PCD at somewhat deeper levels where concrete pore solution pH was still relatively high (pH ≈ 12).
- The most resistant concrete mix investigated in this thesis, based on Norwegian Portland cement with natural pozzolana (German Trass), was only marginally affected by the TF-TSA-carbonation process. In contrast, test prisms based on Norwegian Portland cement were severely affected by all six reaction stages (as defined in Chapter 4) and significant loss of outer material. A similar concrete with added limestone fines had performed even worse.
- Two novel reaction mechanisms were found; a) Development of apparent high crystallisation pressure associated with Thaumasite Formation, leading to surface parallel microcracking and b) Full scale TSA was most efficient after partial or complete decalcification of C-S-H: Thaumasite had formed directly at the expense of Popcorn calcite and severely Ca-depleted cement paste rich in amorphous silica. This finding stands in apparent contrast to Bellmann (2004) who stated that thaumasite generally does not form in fully carbonated concrete. Moreover, because the severely Ca-depleted pastes did not contain ettringite, the latter mechanism represents additional evidence that early formed secondary ettringite is *not* a prerequisite for TSA.
- Direct transformation of C-S-H into thaumasite was apparently inefficient: The reaction mechanisms in the old test samples were similar to the processes taking place in modern sprayed concrete.
- A notable feature was decomposition of thaumasite to calcite *without* gypsum formation in internal concrete, reflecting different solubility of these minerals. In

contrast, both calcite and gypsum formed by decomposition of thaumasite near outer surfaces, where drying caused precipitation of the more soluble gypsum.

- The time integrated exposure conditions at the Blindtarmen test site showed a much wider variation in pH (ca 2-6) and sulfate concentrations than the studied cases of sprayed concrete on Alum Shale (pH \approx 7). Yet the total affected volume of the TF-TSA-carbonation reaction was higher in sprayed concrete than in the Blindtarmen test samples, reflecting significant influence of the hydraulic gradient. It may be inferred that sprayed concrete under influence from sulfuric acid is less than 20 years, as yet to be confirmed.

10.2.1.2 Sources and release mechanisms of aggressive substances

The sources and release mechanisms of aggressive substances were constrained by a pilot stable isotope study and a subsequent multidisciplinary (multiproxy) investigation into Alum shale – concrete – water interaction. The investigation was mainly based on samples of concrete, water and Upper Cambrian Alum Shale from a classic occurrence. Together the samples represented a local quite well defined “system” useful for an integrated interpretation. The combined evidence showed that:

- The main source of aqueous sulfate was anhydrite, as first reported from Norwegian Alum Shale in this thesis: Oxidation of pyrite and pyrrhotite, hitherto regarded as the main reason for all construction problems in Norwegian Alum Shale, accounted for only 20 % of the sulfate in an abiotic leaching experiment. In tunnel water influenced by *Acidithiobacillus*-like biota about 40 % was derived from iron sulfides.
- Other occurrences of anhydrite in Alum Shale were found, suggesting this mineral represents an important source of aqueous sulfate within several varieties of Alum Shale.
- Source anhydrite and bulk sulfides were isotopically much heavier ($\delta^{34}\text{S} \approx +27 \text{‰}$), than thaumasite sulfate in deteriorating concrete ($\delta^{34}\text{S} \approx +2 \text{‰}$). This suggests partial reduction of anhydrite sulfate to H_2S within the rock mass, followed by reoxidation to sulfuric acid near the tunnels space. Also C and O isotope systematics suggested that calcite at the shale/concrete interface was deposited from acidic water. The overall process was apparently sustained by sulfate reducing bacteria (SRB) deep within the rock mass and subsequent sulfide oxidation assisted by *Acidithiobacillus sp.* closer to the tunnel.
- Previous workers noticed a rapid loss of reactive sulfur from Alum Shale samples in contact with air or water, and attributed this to very reactive monoclinic pyrrhotite. However H_2S -gas release seems to be a more plausible explanation, because: a) In the present investigation, monoclinic pyrrhotite was still detected by XRD after 65 days in the leaching experiment, b) H_2S has been detected after blasting operations in several Alum Shale varieties and c) H_2S represents a problem related to drinking water affected by this shale.
- Bicarbonate in investigated Alum Shale waters was derived from dissolution of Upper Cambrian marine calcite. Carbonate associated with the TF-TSA-carbonation process in concrete was derived from bicarbonate in ground water and atmospheric CO_2 , whilst anthracitic – graphitic shale carbon was inert.
- Growth of *Acidithiobacillus ferrooxidans* is fertilised by NH_4^+ , whilst a high level of NO_3^- is toxic. Hence reactivity of Alum Shale seems influenced by its leachable NH_4^+ , whilst NO_3^- , available after rock blasting, may delay bacterial colonisation.
- The general swelling mechanism in Alum Shale seems governed by 1) anhydrite to gypsum conversion by hydration, 2) gypsum precipitation by supersaturation of

calcium and sulfate bearing waters and 3) possible effects from clay minerals. The impact of each mechanism is site specific.

- In contrast to some previous work, leaching of Cd, Ni and Mn reached toxic levels also when buffered by calcite to a circum neutral pH. Apparently the impact of Alum Shale compositional variation is more diverse than previously reported.

10.2.2 Part 2 – The subsea environment

10.2.2.1 Reaction mechanisms in concrete

A novel composite deterioration mechanism was discovered in subsea tunnels, resulting in disintegration of C-S-H and destructive steel fibre corrosion. Other structurally important deteriorations were cracking, spalling and Ca-leaching. Degradation was severe in some domains affected by water leakages, whilst dry concrete remained sound. The phenomena were investigated through a multidisciplinary approach. The deteriorations were caused by bacterial and abiotic reaction mechanisms:

- Acidification and acid leaching occurred in association with layered biofilms, consisting of inner black Mn deposits with *Leptothrix sp.* and outer rusty Fe deposits and slime with *Gallionella sp.* Associated minerals were hydrous Mn^{IV} rich-oxides (biominerals); Na-buserite, todorokites and birnessite, Mn^{II} minerals (manganosite and rhodochrosite) and Fe-hydroxide and Fe-oxihydroxide, respectively. Mn^{III}-oxide bixbyite and Fe-sulfide (marcasite) occurred within thick biofilms.
- The bacterial attack mainly acted on the outer concrete surface from the tunnel and was related to volumetrically small saline water leakages through minor cracks in concrete. The pH of bulk waters in the biofilms was about 5.5 -6.5 and varied over time, whilst the ground water pH was 7.5-8.0.
- A simultaneous abiotic attack caused by infiltration of Na⁺, Cl⁻, Mg²⁺, SO₄²⁻ and HCO₃⁻ enriched mostly seawater-like ground waters, leading to decalcification, magnesium attack, TF-TSA and Popcorn calcite deposition. The Mg-attack reached from about 2 mm to 35 mm depth (occasionally even deeper) and resulted in shrinkage cracking. Thaumasite was usually in the form of TF but full scale TSA occurred where leakages were focused. Precipitation of brucite, Mg-calcite, aragonite and gypsum was common on outer surfaces and at the rock/concrete interface.
- At advanced stages gypsum mush and crusts had formed at the outer concrete surface. Gypsum mush contained an amount of crystalline carbon, which originated from waters seeping over the outer surface and along the concrete/rock interface. A carboxylate phase and phosphate minerals also occurred in both these settings.
- The overall attack acted from both sides of the sprayed concrete layer and caused locally deep disintegration of the cement paste matrix after < 5 years. This involved thinning of sprayed concrete at rates varying from < 0.5 mm/year to at least 10 mm/year. The most extensive examples of degradation were found in deep subsea tunnel sections where the hydraulic gradient was high or where both biotic and abiotic attacks were simultaneously present.

10.2.2.2 Sources and release mechanisms of aggressives

The *acidification* process within the biofilm was governed by complex interaction between bacteria, water and concrete. Initial soft Mn and Fe bacterial slimes were associated with extensive biomineralisation and formation of hydrous Mn-oxide and Fe-compounds, respectively. Brittle black Mn-crusts formed adjacent to concrete surfaces, and outer mobile

Conclusions, implications and further work

and Fe encrusted bacterial slime occurred while bacteria accumulated. The gravitationally unstable nature of biofilm material resulted in very variable and transient redox conditions within layered biofilms. Several acidification processes were involved:

- Acid production related to oxidation of Fe^{2+} with deposition of Fe-hydroxide (ferrihydrite), as greatly facilitated by *Gallionella sp.* The source of iron was essentially the steel fibres in sprayed concrete. Also Mn^{2+} oxidation likely contributed.
- Sulfuric acid originating from oxidation of H_2S and iron sulfide. Sulfides were derived through temporary reduction of ground water sulfate by organic matter within the biofilms. Tunnel leakages associated with the biofilms carried SO_4^{2-} with consistently heavier S isotopic signatures than ground water and seawater. This clearly suggests that sulfate reduction and sulfide formation was taking place continuously whilst reoxidation to sulfuric acid occurred where oxygen was allowed to enter.
- Acid producing redox reaction between Fe^{2+} and Mn^{IV} -oxides. This was due to a) continuous supply of Fe^{2+} by steel fibre corrosion and b) inhomogeneous nature of Mn-reduction; Mn^{IV} -rich minerals and reduced Mn-compounds occurred “side by side”.
- Organic acids, involving carboxylic acid derived through breakdown of amino acids from dying biota.
- The rather mild acidity in bulk water may be explained by a) inflow of saline ground water, b) dissolution of carbonates and c) gypsum formation, which consumes acid.
- Crystalline carbon within gypsum mush originated from dying bacteria as suggested by their nearly identical C isotopic compositions ($\delta^{13}\text{C} \approx -25 \text{‰}$ to -26‰). Gypsum – carbon mush was partly derived from waters at the concrete/rock interface, indicating that the bacterial attack also may enter the interfacial region at an advanced stage.

The *abiotic* part of the attack was sustained by the ground water chemistry. Several of these mineral transformations are quite well established, except for their rather significant impact after only few years. Important findings were:

- Decalcification of CH and C-S-H seems to represent an important first step: The TF-TSA – carbonation process also occurred in subsea tunnel concrete, and PCD and other forms of internal carbonate were closely associated with formation of M-C-S-H.
- The ground water sulfate and magnesium concentrations in subsea sections were usually, but not exclusively, similar to seawater.
- The combination of micro shrinkage cracking and formation of acid soluble secondary carbonates apparently made way for a significant degradation of the cement paste matrix due to acid attack from Mn-Fe biofilm.
- Depassivation of steel fibres and corrosion was caused by PCD and other forms of bicarbonation, chloride, acids and consumption of OH^- by brucite deposition.

10.2.3 Part 3 – Summary of deteriorations and engineering aspects

Chapters 8 and 9 were based on results in Part 1 and 2 and additional investigations including the fresh water environment. Most of the investigated concretes were complying with design requirements and were therefore regarded as “real world sprayed concrete”, made according to a modern quality scheme. It was concluded that:

Conclusions, implications and further work

- Degradation of sprayed concrete used for rock support within the freshwater environment was uncommon.
- TF – TSA – carbonation associated with Alum Shale still represents a concern.
- The most severe degradations were due to the composite attack caused by Mn-Fe biofilms and saline ground waters in subsea tunnels.
- Alkali Silica Reaction was found to be unimportant.
- The service life of the most affected sprayed concretes was less than the present design life of 50 years for rock reinforcement in Norwegian tunnels.
- The thickness of sprayed concrete had an effect on the durability (*see also section 10.4*). There were some indications that when thickness was designed according to rock mass rating (e.g. the Q-system, accounting also for water leakages) the concrete performance was better than in cases where no rigorous rock mass classification had been undertaken.
- Investigations in a subsea tunnel demonstrated that Ca-leaching and Mn-Fe surface deposition increased significantly with tunnel depth below sea level. The magnitude of the hydraulic gradient represents a very important environmental variable affecting the durability of the sprayed concrete lining.
- Effects of deterioration and residual life time at each site is critically dependent on local characteristics being mainly: a) rock mass hydraulic conductivity, b) hydraulic gradient, c) hydraulic conductivity and thickness of sprayed concrete, d) age of concrete and e) aggressiveness of water and f) the role of microbes.
- The NS-EN 206-1 Exposure Classes did not predict the extent and rate of the most severe degradations in high quality mixes: This standard does not either provide examples related to sprayed concrete or tunnel environments.
- Using H and O stable isotopes, it was found that some high saline and hypersaline tunnel waters were derived from brackish waters. Evaporation within tunnel space can cause a 100 % to 1000 % increase in ionic concentrations. Hence a brackish water belonging to Exposure Class XA1 as it leaks into the tunnel may be transformed into Exposure Class XA3 due to tunnel drought.
- It was recommended that future revision of the concrete standard should include classification according to biodegradation, bicarbonate contents, hydro-geological context and the importance of “Life time exposure classification” when exposed to a dynamic water environment. The subsea environment should be classified in the national XSA (“Especially aggressive”) together with Alum Shale environment.

10.3 Implications and consequences based on present knowledge

This subsection deals with the implications and consequences which can be drawn on the basis of current knowledge including the conclusions of the present thesis.

10.3.1 Concrete in the Black shale environment

The service life of modern sprayed concrete exposed to sulfuric acids was not available for an investigation (case not approached), but it was inferred that a full transformation of the sprayed concrete layer into non-cementitious material may take less than 20 years. It is therefore necessary to search for tunnel sections in Alum Shale which have been exposed to such an environment for a period of time. Continuing monitoring of the

Conclusions, implications and further work

investigated sprayed concrete, exposed to a near neutral pH in Alum Shale, is also required in order to obtain insight into the impact of such common exposure conditions over a much longer time span.

For new projects it will be important to undertake thorough site investigations, among others on the basis of findings in this thesis. Activities should primarily involve:

- Characterisation of different Alum Shale varieties with emphasis on mineralogy and other constituents, with a focus on the contents of anhydrite, iron sulfides, carbonate and the weathering minerals.
- Establishing different *on-site* properties of surface weathered and unweathered shale through relevant leaching experiments.
- Eventually test concrete mixes which have been used with some success to combat TSA elsewhere. For example binders consisting of 30 % Portland cement and 70 % ground granulated blast furnace slag (ggbfs) have proven very resistant to TSA (cf. Crammond 2003).

10.3.2 Concrete in subsea tunnels

The presently reported tunnels should be monitored for further development of the composite subsea attack, and several other subsea tunnels should be included. The reason for this is twofold:

- The subsea attack has not been described earlier and it remains uncertain as to whether the loss of outer concrete and other loss of cementitious properties will continue at the same pace, as indicated in the present thesis.
- The impact of degradation due to Mn-Fe biofilms and saline ground water is virtually absent in several subsea tunnels, which calls for more data and improved insight.

As regards maintenance and repair of old and new-build tunnels, the following should be done:

- Mn- Fe biofilms should be removed, where possible to reach, and at regular intervals within the existing maintenance regime.
- Repair concrete should not be employed before gypsum mush and gypsum crust material has been thoroughly removed, in order to prevent future sulfate attack: So far this has been done in one subsea tunnel.
- Steel fibres should preferably be abandoned in subsea tunnel sections: Recently synthetic fibres have been specified by NPRA for new projects as well as repair concrete. The initial motivation was the high level of chlorides in the subsea environment, whilst the presently reported new degradation mechanism represents an additional argument for the new specification.
- As regards the “additional aggressiveness” due to evaporation, it is advised that tunnel fans to the extent possible should be placed at a distance from widespread tunnel leakages.

10.3.3 Durability and engineering aspects

Current knowledge and experience (Davik 1997 and later accumulated evidence) should be summarised systematically with respect to durability data from a large number of tunnels:

- Empirical data from existing sprayed concrete in all environments should be compared to timing of repair, in order to establish possible development trends on the basis of statistics.
- This should always be accompanied by proper diagnosis of deterioration mechanisms, degree of degradation and characterisation of the ambient water loads, including hydro-geological variables and if possible also rock loads.
- Monitoring sites should be established and followed up for at least 10-15 years.
- The investigations should otherwise be based on the recommendation of the International Tunnelling Association (Franzén et al. 2001).

10.4 Recommendations for further work

Future investigations should be based on a scientific approach in order to solve remaining practical issues. In the following some topics are recommended for in depth studies.

10.4.1 A comment to the claimed beneficial effect of increased sprayed concrete thickness

In Chapter 3 and several later chapters of this thesis it has been argued that an increased sprayed concrete thickness should be beneficial for long lasting performance in aggressive ground. In the previous Norwegian durability project this was in fact a main conclusion, and it was advised that the minimum sprayed concrete thickness should be increased from 5 cm to 6 cm (Davik 1997). In current NPRA practice a minimum thickness of 8 cm is employed.

Using the ratio “Affected thickness/Initial thickness” (t_a/t_0) it was apparent in Chapter 3 that the proportion of affected concrete decreased with an increasing sprayed concrete thickness. However, looking at the data in more detail, this might appear to have been a too hasty conclusion (Figure 1). This is particularly demonstrated by the 13 years old concrete, implying that the volume of deteriorated concrete increases with an increasing spray thickness. This feature seems incompatible with Darcy’s law, which states that the resistance to bulk flow should increase as a function of the thickness of the material when permeability and hydraulic gradient are constant.

However, the parameter t_a/t_0 represents a simplified approach, which does not account for the complex interaction of concrete permeability; structural flaws and layer parallel permeable zones. The impact of deteriorations due to an aggressive environmental load depends on: a) the permeability of bulk concrete, which is determined by the initial w/c-ratio and secondary microcracking, b) cross cutting meso-scale cracks and spall zones, facilitating localised water flow with potential for diffusion into concrete, and c) layer parallel domains with individual flow properties (see concept illustrated in Figure 1: Chapter 7).

In the cases of TF-TSA-carbonation (Chapter 3) the w/c-ratios were about 0.4 to 0.5. The secondary microcracking, due to deformational loads and continuing chemical

Conclusions, implications and further work

deteriorations, was not quantified. Moreover the impact of cross cutting cracks was not considered, although the field investigations indicated presence of scattered mostly minor cracks. The affected thicknesses were not only restricted to domains of outer concrete and domains adjacent to Alum Shale, but in fact also involved deteriorations within layer parallel domains internally within the concrete. It is perfectly possible to envisage that some of the affected layers formed in response to aggressive waters from cross cutting minor cracks. Possibly the affected internal layers of sprayed concrete were initially more permeable than the rest, thus being more prone to degradation. Therefore, due to this complexity, *it is not generally expected that the simple parameter “Affected thickness” should correlate negatively with “Initial thickness”*. Only if sprayed concrete of same age and mix and under same hydraulic gradient is mainly homogeneous and free of cross cutting cracks such a relationship may be ubiquitous.

However, this does not disregard the beneficial effects of relatively thick sprays. Presently, in view of the previous Norwegian durability project and results of this study, it may be concluded that an increased sprayed concrete thickness should contribute to a longer service life time.

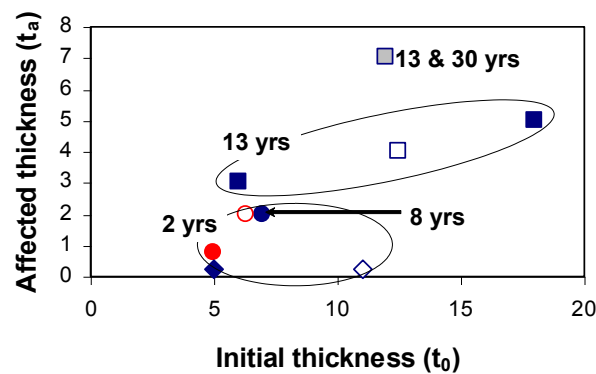


Figure 1: Data from Chapter 3 apparently suggest that the deterioration (t_a) increases with increasing sprayed thickness (t_0) (cm). Symbols as in Chapter 3: Squares represent 13 years old concrete. The open square contains an internal 2 cm mush zone. The grey square represents a composite core consisting of completely transformed 30 years old concrete (4 cm) and 13 years old concrete.

Yet, future research should investigate the combined effects of bulk paste permeability crack permeability and diffusion on overall resistance to attack by aggressive waters.

10.4.2 Black shale environment

Further understanding of reaction mechanisms related to the TF-TSA-carbonation process should focus on the conditions required for the transition from non-deleterious TF into full scale TSA. It is as yet not straight forward to evaluate the fate of structures characterised by TF. Within this context it would seem important to investigate the relationship of thaumasite supersaturation and development of crystallisation pressure as a possible path for development of secondary porosity and faster reaction kinetics.

Another important research objective is the role of atmospheric carbon dioxide in cool acidic and sulfate enriched waters with very low alkalinity. In view of the very significant impact of atmospheric CO₂ reported in Chapter 6 it seems possible that TSA may be sustained

without any other carbonate source. This is of particular importance, because waters with very low alkalinity also are the most acidic waters, which should make way for extensive decalcification and full scale TSA within the interior of sprayed concrete.

Generally prevention of TF-TSA-carbonation process requires a dense low permeable concrete mix design. The present work has demonstrated that the level of decalcification is very important for the progress of this degradation mechanism. Future research should, therefore, look into the role of Al-sulfate setting accelerator and the possibility that certain dosages promote decalcification (cf. Paglia et al. 2003).

The Alum Shale reactivity should be further investigated with emphasis on microbial characterisation and growth conditions under reducing and oxidising conditions. As yet sulfate reducing bacteria have not been observed, although stable isotope systematics strongly suggests they are present in the rock mass. The impact of *Acidithiobacillus sp.* on the Alum Shale acidification potential seems especially important to understand: the role of leachable and fertilising ammonium should be focused on. All research results should be seen in view of the relative impact of anhydrite and iron sulfides. Finally, the potential role of radiolytic pyrite oxidation should be investigated in uranium bearing Alum Shale (Lefticariu et al. 2006).

10.4.3 Subsea environment

Future work should focus on the complex reaction mechanisms involved in the composite concrete attack. Appropriate microbiological characterisation and further identification of bacteria in the layered Mn-Fe biofilms is necessary in order to understand better the relative impact of biotic and abiotic reactions. Also a remedy which may combat acidification in biofilms should be searched for.

Because decalcification is a very important consequence of the composite attack in subsea tunnels, the role of the commonly used Al-sulfate setting accelerator is especially important to understand.

Another important research topic concerns the effects of imposed stresses and strains on sprayed concrete permeability in response to variable rock mass loads. It would be desirable to investigate performance in relation to variations in rock mass parameters and sprayed concrete thickness.

10.4.4 Engineering aspects and durability prediction

Experience gathered through characterisation and testing in tunnels is a prerequisite for development of performance tests in the laboratory. Consequently, a new test site has already been established in a subsea tunnel (Hagelia 2011). The main variables to be investigated are effects of variable sprayed concrete thickness, different concrete mixes and fibre types. The test site is located in a tunnel section with a proven record of fast degradation due to Mn-Fe biofilm and saline ground water attack. Such “real world laboratories”, inspired by the previous Blindtarmen test site, are expected to provide reliable results of practical value after several years.

Computer modelling of future durability development of sprayed concrete should be attempted, but there are many pit-falls. The main problem is the typical inhomogeneous development of sprayed concrete deteriorations, changing rock conditions and the very variable and complex impact of water leakages. It must be expected that computer modelling

for this purpose will be a very difficult task. The responsible owner of tunnels will likely have to rely on monitoring as a basis for durability prediction for many years to come.

10.5 References

- Bastiansen R, Moum J and Rosenqvist ITh (1957): Contribution to high light certain construction problems associated with Alum Shale in Oslo. Norwegian Geotechnical Institute, Publication No. 22, Oslo, 69 pp. (In Norwegian with English summary).
- Bellmann F (2004): On the formation of thaumasite $\text{CaSiO}_3 \cdot \text{CaSO}_4 \cdot \text{CaCO}_3 \cdot 15\text{H}_2\text{O}$: Part II. *Advances in Cement Research*; 16: 3: 89-94.
- Bensted J (2003): Thaumasite – direct, Woodfordite and other possible formation routes. *Cement and Concrete Composites*, 25, 873-877.
- Crammond NJ (2003): The thaumasite form of sulfate attack in the UK. *Cement and Concrete Composites*, 25, 809-818.
- Davik KI (1997): Proper use of sprayed concrete in tunnels, Parts A, B, C, D, E and Final report (in Norwegian). Norwegian Public Roads Administration 1997.
- Franzén T, Garshol KF and Tomisawa N (2001): ITA/AITES Accredited Material. Sprayed concrete for final linings: ITA working group report. *Tunnelling and Underground Space Technology* 16, p 295-309.
- Hagelia P (2011): Sprayed concrete in aggressive subsea environment – The Oslofjord Test Site. In: T. Beck, O. Woldmo, S. Engen (Eds.), 6th International Symposium on Sprayed Concrete – Modern Use of Wet Mix Sprayed Concrete for Underground Support. Tromsø, Norway, pp. 161-175.
- Lefticariu L, Pratt LM and Ripley EM (2006): Experimental study of radiolytic oxidation of pyrite: Implications for Mars-relevant crustal processes. *Lunar and Planetary Science XXXVII*. 2p.
- Norwegian Standard NS-EN 206-1, Concrete Part 1: Specification, performance, production and conformity (in Norwegian).
- Paglia C, Wombacher F and Böhm H (2003): The influence of alkali-free and alkaline shotcrete accelerators within cement systems. Influence of the temperature on the sulfate attack mechanisms and damage. *Cement and Concrete Research*, 33, 387-395.

Appendix 1: Additional documentation to Chapter 3

- A1-1 Summary of samples with systematic petrography**
- A1-2 X-ray diffraction data**
- A1-3 Micro analyses of thaumasite**
- A1-4 Images of thaumasite, decalcified cement paste matrix & secondary calcite**

A-1 Summary of samples with systematic petrography

The samples studied were concrete cores with a chip of rock inside. Also spalls and smaller samples were investigated. Thin sections were made usually covering the entire thickness of the spray and some rock behind. The results are presented as a core log according to the zoned nature of the deterioration phenomena (e.g. zones A, B, C and S, as illustrated in Fig. 1 of Chapter 7 and Figure 2 of Chapter 8). Notice that silica fume (SF) was well dispersed, except from in a very few cases where some SF globules were observed.

Table A-1-1: Summary of samples studied in Chapter 3. Notice that core samples from the Svartdal tunnel collected later (2006) are included for comparison. Abbreviations: OC = ordinary carbonation. PCD = Popcorn calcite deposition; Cc = calcite; TF = Thaumaside formation; TSA = Thaumaside Sulfate Attack; MSH = severely Mg substituted CSH; CH = portlandite; ASR-gel = Alkali-silica gel; SF = silica fume.

Locality, & age of spray Sample/thickness (thin section no.)	Rock types, joint material & stability problem	Zone A Rock-concrete interface & deposits	Zone A Inner concrete degradation	Zone B Sound internal	Zone C Outer concrete degradation	Zone C Outer surface characteristics and deposits	Zone S Characteristics & location of spalling zone	Water conditions
<i>Oslo civil defence shelter</i>								
<i>Ca. 1970</i>								
<i>Collected</i>								
<i>Nov. 2000:</i>								
Spall Bag 2 (1570/21) - ca 6 cm	Alum Shale with internal swelling	Adhesion lost Jarosite Gypsum Fe-oxy-hydroxide	3 mm TF/TSA Surf. parallel cracks w/ Gyp in strongly Ca-depleted w/PCD + Cc and sec. CH	Sound micro domains scattered within Ca-depleted paste w/ PCD, Cc & sec. CH	Ca 20 mm OC	Outer surface w/ white paint	1) spalling adjacent to shale 2) internal spalling in concrete	Very moist environment
Spall Bag 7a (1570/25) - Ca 5-6 cm	Alum Shale with internal swelling	Adhesion lost Jarosite Gypsum Fe-oxy-hydroxide	5 mm TSA adjacent to shale: Extensive macro cracking with calcite	Not much remaining. Aggregate particles degraded Depleted CSH with PCD & Cc	5-15 mm OC Surface parallel micro cracks with thaumasite, ettringite, gypsum and calcite	Outer surface white paint, stained by rusty Fe deposits	Spalling along rock/concrete Fragments as sludge at the base	Very moist environment

Appendices – Black shale environment

Locality, & age of spray Sample/thickness (thin section no.)	Rock types, joint material & stability problem	Zone A Rock-concrete interface & deposits	Zone A Inner concrete degradation	Zone B Sound internal	Zone C Outer concrete degradation	Zone C Outer surface characteristics and deposits	Zone S Characteristics & location of spalling zone	Water conditions
<i><u>Harpefoss tunnel 1984</u></i>								
<i>Collected April 1997:</i>								
Core 1.1 (1.1-1; 1.1-2) - 6.5 cm	Banded quartz rich gneiss with dark carbon bearing layers	Good adhesion	< 0-2 mm ettringite + thaumasite	55 mm normal paste, some aggregate ASR susceptible, Some entrapment voids with local carbonation	1 mm very weak and diffuse OC	Initial surface preserved, no deposit	No spalling	Dry surface
Core 2 (2-1) - 7 cm	Not preserved in core	Split along interface	Seemingly unimportant (judged from core only)	60-65 mm Residual clinker. Few shrinkage cracks. Entrapment voids with minor ASR-gel	5-10 mm diffuse OC	Initial surface intact: 0.5 mm calcite & thernardite deposit	No spalling	Previously wet: now dry surface
Core 3.2 (3.2-1; 3.2-2) - 5.5 cm	Dark gneiss (not preserved in core)	Split along interface	Seemingly unimportant (judged from core only)	40-45 mm sound. Possible Fly ash particle.	1-1.5 cm very diffuse OC	Initial surface preserved	No spalling	Dry surface
Core 4 (4-1, 4-2,4-3) - 6.5 cm	Banded quartz rich gneiss with dark carbon bearing layers	Good adhesion	Very minor ettringite	60-65 mm sound with internal micro cracks and local carbonation, minor ASR-gel	0.5 mm OC	Initial surface preserved	No spalling	Surface wet

Appendices – Black shale environment

Core 5 (5-1) - 8 cm	Not present in core	Split along interface	Unimportant	70 mm well preserved paste	10-15 mm OC	Initial surface preserved	No spalling	Dry surface
Core 6 (6-1) - 6 cm	--"--	Some adhesion Minor carbonation	Unimportant	45-50 mm normal paste	10-15 mm OC	Initial surface preserved	No spalling	Surface wet
<i>Collected Nov. 2000:</i>								
Core 1 (1570/1) - 2 cm	Dark carbon bearing gneiss	Split along interface	5-10 mm TSA & subsequent PCD. Ettringite on crack	5 mm rather sound paste Surface parallel cracks with TF and Gyp	10 mm OC	Initial surface preserved but friable. Dark thin deposit; undefined	Spalling within Zone A	Moist
Core 2 (1570/2) - 11 cm	Grey mylonite	Partial adhesion 0.5 mm deposit Fe-stained Cc	Not well developed	95-10 mm fairly sound	10-15 mm OC	Initial surface preserved (no thin section). Thenardite	No spalling	Moist
Core 3 (1570/3) - 11 cm	Black carbon rich gneiss	Good adhesion No deposit	2-5 mm w/entrapment voids filled with water glass	Ca 90 mm fairly sound	5-10 mm OC	Initial surface preserved Thenardite	No spalling	Moist

Appendices – Black shale environment

Locality, & age of spray Sample/thickness (thin section no.)	Rock types, joint material & stability problem	Zone A Rock-concrete interface & deposits	Zone A Inner concrete degradation	Zone B Sound internal	Zone C Outer concrete degradation	Zone C Outer surface characteristics and deposits	Zone S Characteristics & location of spalling zone	Water conditions
<i><u>Åkeberg road cut; 1987</u></i>								
<i>Collected July 2000:</i>								
- Spall 2 (Pr 1, Pr 2) outer steel fibre free layer - ca 2 cm	(Alum Shale, “mænaite = syenite”) Not represented in sample	Not present in sample	Not present in sample	Local presence of sound concrete; Outer layer fibre free	Inner part full scale TSA + PCD, outer part less affected with 1-3 mm OC. SF globules	Initial surface preserved yet friable	Spalling along mushy debris with fully corroded & destroyed steel fibres	Moist
Mushy debris behind above Spall 2	--“--	Not present in sample	Not present in sample	Not present in sample	Calcite, gypsum thaumasite <i>Steel fibres completely destroyed by corrosion</i>	Not present in sample	Spalling material	Moist
<i>Collected Nov. 2000:</i>								
Core 1 (1& 2 + 1570/27) - 8 cm	Syenite sill (Alum Shale near by)	Good adhesion: 0.1 mm Cc, thaumasite deposit	30 mm less sound p. mildly depleted	30 mm sound Grading into Zones A & C SF globules	2-3 mm OC & 20 mm mildly depleted to sound paste SF globules	Initial surface preserved	Spalling	Moist

Appendices – Black shale environment

Core 2 (1, 2 & 3 + 1570/28) - 18 cm	Alum Shale, with 1 cm crosscutting jarosite vein against cement	Weak contact: permeable Breakdown of jarosite w/ Fe precipitation and acid generation	a) 0.5-7 mm strong acid attack against jarosite. CSH dissolved w/ minor Cc rims on remaining CSH- aggreg. particles: b) 25 mm Ca – depleted p; PCD, TF/TSA	12-13 mm rel. sound: Ca-depleted CSH w/PCD and some TF frequently associated to entrapment voids. Cc in fines	2-3 mm OC 20-30 mm leached depleted	Initial surface preserved, yet quite friable	No spalling; yet potential weakness planes	Moist
Core 3 (1570/29) - 6 cm	Alum Shale w/some jarosite	Weak contact Permeable thin Cc deposit	- 5 mm acid leached: permeable - 5-15 mm depleted w/ TF/TSA, Cc, CH (Br)	20-35 mm, yet <i>not sound</i> ; Cross cutting crack, internal leached zone Limestone in fines	1-3 mm OC 15-20 mm very depleted paste	Initial surface not well preserved	No spalling; yet potential weakness planes along acid leached zones	Moist
Core 4 <u>1987 spray</u> (1570/30) - 6 cm	Alum Shale	Adhesion to 1970 spray fair, with Cc and TSA, Fibre corrosion	- 25-35 mm TSA and sec PCD w/ fibre corrosion: depleted w. PCD (TF, CH)	- Diffuse rather sound grading into Zones A & C. Fibres intact.	1-3 mm OC 25-30 mm OC on void + depleted w PCD (TF)	Initial surface rather well preserved	Ca 1-5 mm Delaminated Carbonated	Moist
Core 4 <u>inner remnant of 1970 spray</u> (1570/30) - 4 cm	Alum Shale	Calcite and thaumasite deposit, permeable TF. Steel corrosion	- 40 mm; 1) Cc and TSA near shale; 2) TF, depletion with PCD	Locally preserved in outer part	Not present: reported to have been extensively degraded	Removed & replaced by new spray in 1987	Extensive spalling of 1970 spray reported	Moist
Sample 1 Spall. Outer layer without fibres (1570/32) - 2 cm	Not present in sample	Not present in sample	Not present in sample	Local presence of sound concrete	2-3 mm OC with local gypsum near surface, inner domains full scale TSA, PCD	Initial surface intact. Spall broken	Spalling along mushy debris with fully corroded & destroyed steel fibres	Moist

Appendices – Black shale environment

Mushy debris behind; Sample 1 (XRD 1570/33)	Not present in sample	Thaumasite, calcite <i>Steel fibres completely destroyed by corrosion</i>	Not present in sample	Spalling material	Moist			
---	-----------------------	-----------------------	-----------------------	-----------------------	--	-----------------------	-------------------	-------

Appendices – Black shale environment

Locality, & age of spray Sample/thick- ness (thin section no.)	Rock types, joint material & stability problem	Zone A Rock-concrete interface & deposits	Zone A Inner concrete degradation	Zone B Sound internal	Zone C Outer concrete degradation	Zone C Outer surface characteristics and deposits	Zone S Characteristics & location of spalling zone	Water conditions
<i><u>Ekeberg tunnel</u></i>								
<i><u>1992</u></i>								
<i><u>Chainage 1730</u></i>								
<i><u>Northbound</u></i>								
<i>Collected</i>								
<i>Nov. 2000:</i>								
Core 1 (1570/37) - 3 cm	Syenite sill	Good adhesion No deposit	Not well developed	Sound normal Shrinkage cracks with local Cc and TF Moisture transport	1-2 mm OC large voids rimmed with Cc (TF)	Initial surface quite intact. Rust and calcite efflorescence	No spalling yet some outer delamination	Surface wet
Core 2 (1,2 & 3 + 1570/40) - 8 cm	Alum Shale	Good-fair adhesion Ca 0.5 mm Cc & TF/TSA	ca 10 mm w/ Ca-depleted paste TSA PCD	70 mm fairly sound; sparse TF and PCD; local ASR gel	3 mm OC 5-10 mm depleted	Initial surface intact; Cc deposit	No spalling	Surface wet

Appendices – Black shale environment

Locality, & age of spray Sample/thickness (thin section no.)	Rock types, joint material & stability problem	Zone A Rock-concrete interface & deposits	Zone A Inner concrete degradation	Zone B Sound internal	Zone C Outer concrete degradation	Zone C Outer surface characteristics and deposits	Zone S Characteristics & location of spalling zone	Water conditions
<u><i>Svardal tunnel</i></u> <u><i>Eastbound</i></u>								
<u><i>1998; Chainage 320 & 370</i></u>								
<i>Collected Aug. 2000:</i>								
Core 320a (1 & 2) - 5 cm	Alum Shale	Somewhat permeable contact, TF	0.5-2 mm TF, TSA	42 mm sound	2 mm OC	Thenardite, gypsum deposit	No spalling	Surface wet
Core 320b (1, 2 & 1570/49) - 5 cm	Alum Shale	TF also within Alum Shale	0.5-5 mm TF, TSA	45 mm sound yet vein with TF, PCD	2 mm OC	Initial surface intact	No spalling	Surface dry
Core 370a (1, 2 & 1570/46) - 6.3 cm	Alum Shale	TF, permeable	1-20 mm TSA, PCD, OC porous	50-55 mm sound	5-10 mm OC TF, TSA, PCD	Initial surface intact/friable	No spalling	Surface wet
Core 370b (1 & 2) - 11 cm	Alum Shale	TF	0.5 mm TSA 1 mm depleted	10 mm sound	2-3 mm OC	Initial surface intact	No spalling	Surface dry
<i>Collected Aug. 2006:</i>							No spalling	
Core 320 O (1) - 2.5 cm	Alum Shale	TF	1 mm PCD	20 mm sound	1-2 mm OC	Initial surface leached	No spalling	Moist
Core 320 N (1) - 3.5 cm	Alum Shale	TF	0.25 mm PCD	30 mm sound	1-2 mm OC	Initial surface leached	No spalling	Moist
Core 370 V (1,2,3 &4) - 13 cm	Alum Shale	Permeable contact: TF	5 mm jarosite PCD	125 mm sound w carbonation on single crack	1 mm OC	Initial surface leached	No spalling	Moist
Core 370 H (1,2 & 3) - 10 cm	Alum Shale	0.2 mm TF	5 mm TF, TSA, PCD & Fe deposit	90 mm sound	1-2 mm OC	Initial surface leached	No spalling	Moist

Appendices – Black shale environment

Locality, & age of spray Sample/ (thin section no.)	Rock types, joint material & stability problem	Zone A Rock-concrete interface & deposits	Zone A Inner concrete degradation	Zone B Sound internal	Zone C Outer concrete degradation	Zone C Outer surface characteristics and deposits	Zone S Characteristics & location of spalling zone	Water conditions
<i><u>Freifjord</u></i> <i><u>subsea tunnel</u></i> <i><u>1991</u></i>	NB! ONLY OUTER SPALLS & FRAGMENTS				ALL SAMPLES BELONG TO ZONE C			
<i>Collected</i> <i>Nov 2000:</i> Spall 1 /6800 m (Pr. 1)	Gneiss	Not observed	Not in sample	Not in sample; sound looking	0.5-1 mm OC 2 cm sound paste with signs of ASR in part related to SF globules. 20 % mylonite in aggregate	No deposit	Outer spall in Zone C	Moist, saline
Fragment 3 /6180 m (Pr 3)	Gneiss	Not observed	Not in sample	Not in sample; not much sound	3 cm fully degraded paste, MSH, brucite, PCD, TF, TSA, Shrink. cracks, Extensive fibre corrosion	Not preserved	Some spalling in Zone C	Wet, saline
Spall 5b /5940 m (Pr.5b)	Gneiss	Not observed	Not in sample	Not clearly represented	0.5 mm OC 2 cm fully degraded paste, TF, TSA, PCD, MSH, shrink. cracks, Extensive fibre corrosion	Stalactites	Several spalls in Zone C	Wet, saline

A1-2 X-ray diffraction data

Figure 1. XRD plot for Akerbergveien Cutting Sample 2

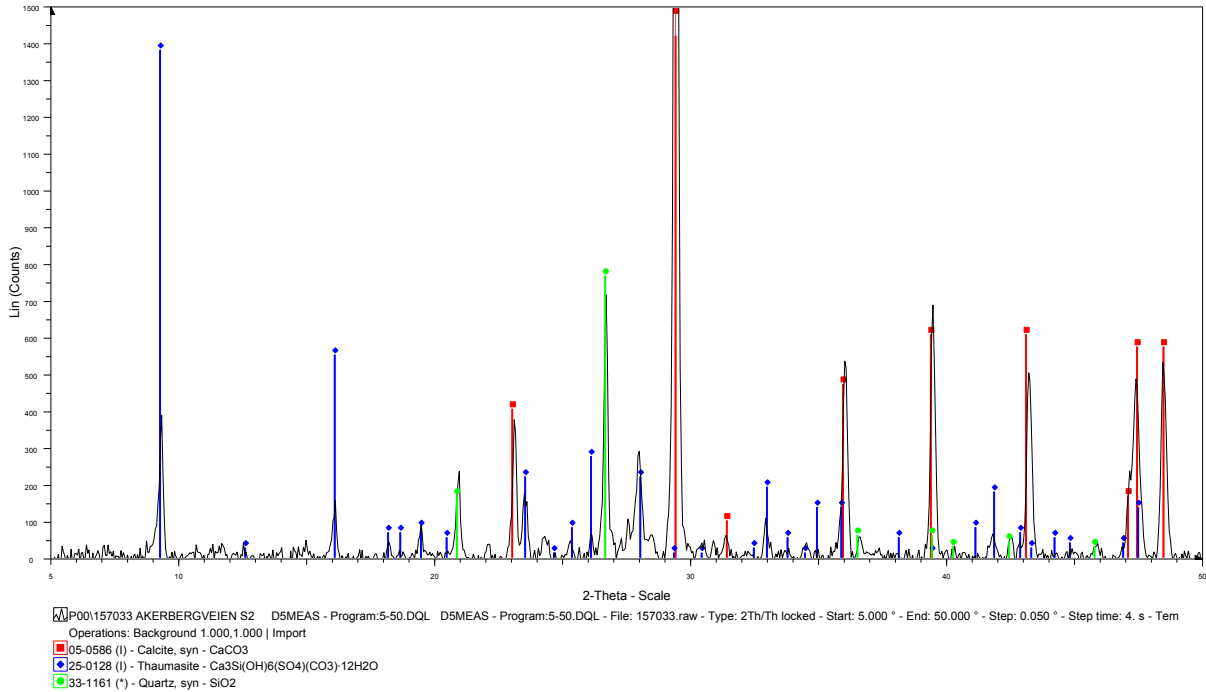


Figure A1-2-1: X-ray diffractogram of a 1-2 cm wide concrete mush behind Spall 2 Sample 2: BRE – P00/1570/33 (see field photos: Figure A1-4-2).

Table A2-1-1: Summary of main XRD results. ID is file number at Museum of Natural History, Oslo or BRE numbers (1570/nn). All samples collected in 2000.

Sample	Location/chainage	Material	Minerals	ID
Sample 1 Åk	Åkebergveien/-	Mushy concrete from spalled area	Gypsum, calcite, quartz, plagioclase	170800-hagelia-B.RAW
Sample 2 Åk (fig A1-2)	Åkebergveien/-	Mushy concrete from spalled area	Thaumasite, calcite, quartz	1570/33
Core 4-shale interface (Åk)	Åkebergveien/-	Concrete debris with Alum Shale	Thaumasite & possible buetschliite	1570/34
Sample 4 Åk	Åkebergveien/-	Mushy concrete from spalled area	Calcite, quartz, gypsum and thaumasite	1570/42
Sample 1 Ek	Ekeberg tunnel/ca 1600 m Southbound	White from pop-out on sprayed concrete surface	Thaumasite, calcite	1579/36
Sample 320 Svartdal	Svartdal tunnel/ 320m Near cores 320a & b Eastbound	White deposit on crack in sprayed concrete	Thenardite, gypsum, calcite, quartz	160800-hagelia-per320.RAW
Sample 1 Freifjord	Freifjord tunnel/5260 m	Subsea degraded concrete with white deposits	Gypsum, calcite, thaumasite, quartz	1570/44

A1-3 Micro analyses of thaumasite

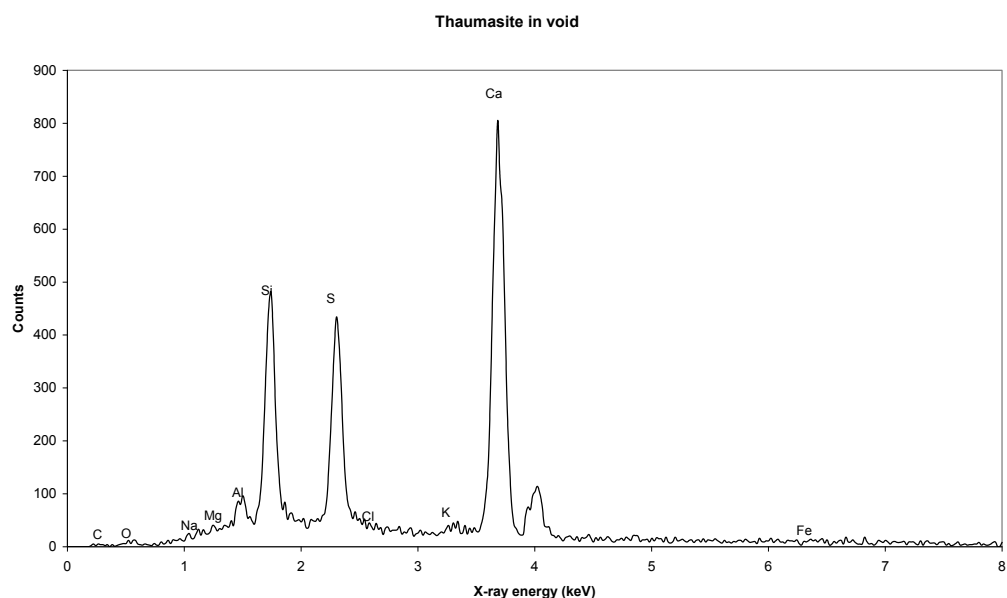


Figure A1-3-1: EDS spectrum of thaumasite filling an entrapment void in < 2 years old sprayed concrete from the Svartdal tunnel, Oslo. Core 370a.

Table A1-3-1: Electron microprobe analyses of thaumasite in 13 years old sprayed concrete from Åkebergveien road cut, Oslo. First conclusive evidence of TSA in Norway. Sample: Spall 2: thin section Pr-2. Concentrations are given in wt. %.

	SO3	P2O5	Cl	K2O	SiO2	Al2O3	MgO	CaO	FeOt	Total
Pr 2a-1	19.05	0.55	0.04	0.00	13.73	2.00	0.00	45.36	0.00	80.74
Pr 2a-2	19.43	0.48	0.10	0.00	12.17	2.40	0.00	40.65	0.09	75.32
Pr 2a-3	19.83	0.62	0.06	0.02	12.94	1.76	0.00	42.00	0.09	77.32
Pr 2a-4	18.68	0.53	0.07	0.02	13.01	1.49	0.00	40.90	0.32	75.02

A1-4 Images of thaumasite, decalcified cement paste matrix & secondary calcite



Figure A1-4-1: Effects of swelling Alum Shale and sulfate attack in abandoned civil defence shelter in 2000. This now ca. 40 years old (in 2010) sprayed concrete was made with SRPC (dry method, no steel fibre reinforcement). The thickness was about 5-6 cm and severely infected by TF-TSA-carbonation associated with ettringite and gypsum. The cement paste matrix was severely leached and porous. The exposed Alum Shale surface was heavily coated with secondary jarosite and also carried gypsum and iron-oxyhydroxides. Notice the heavy accumulation of completely disintegrated concrete fragments at the base. Image width = 3 m.



Figure A1-4-2 *Left*: Overview of sprayed concrete Åkebergveien road cut, city of Oslo in 2000, sitting on Lower Ordovician Alum Shale interbedded with Upper Carboniferous syenite sills (“mænaite”). Cores 1-4 were extracted here. This is the first published case of TSA in Norway (Hagelia and Grønhaug 2000; Hagelia et al. 2001). This steel fibre reinforced wet sprayed concrete was 13 years old and made with SRPC and silica fume. A previous SRPC based 1970 spray was demolished and replaced in 1987. Notice spalling and ferric iron stains, reflecting effects of iron sulfide oxidation. Deformations were also observed. *Right*: Detail of the spalling (sample “Spall 2) along a 2 cm white mush zone consisting of thaumasite and calcite due to TSA and PCD. Steel fibres were totally destroyed by corrosion in the process. The 1987 spray has not yet been replaced (2010) and is now about 23 years old.

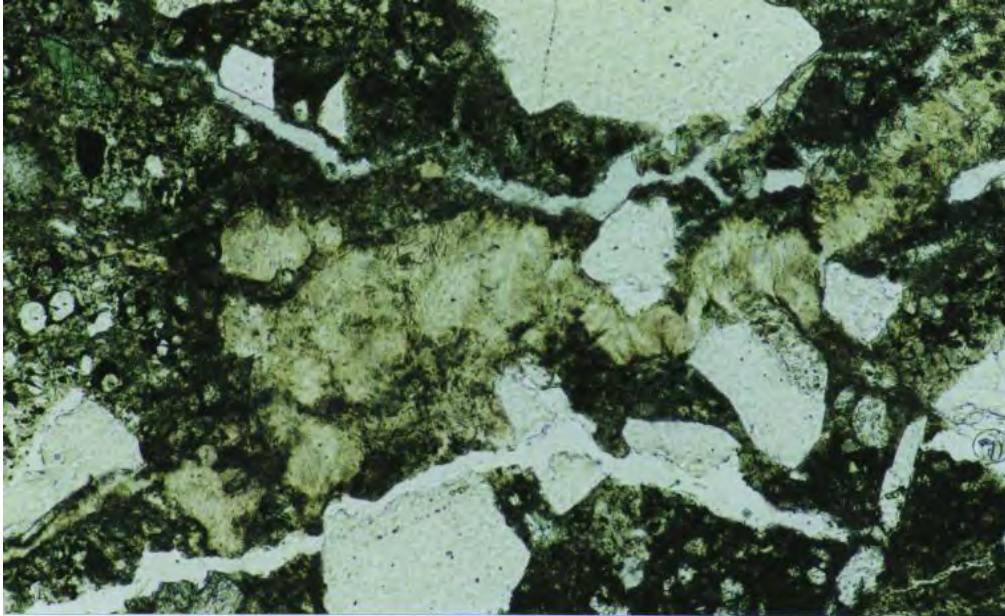


Figure A1-4-3a. Thaumascite Sulfate Attack (TSA). Thaumascite replacing the cement paste matrix in the 13 years old Åkebergveien sprayed concrete. Plane polarised light; lower: crossed polars. Core 2, thin section 1570/28. Width of field = 1.8 mm.

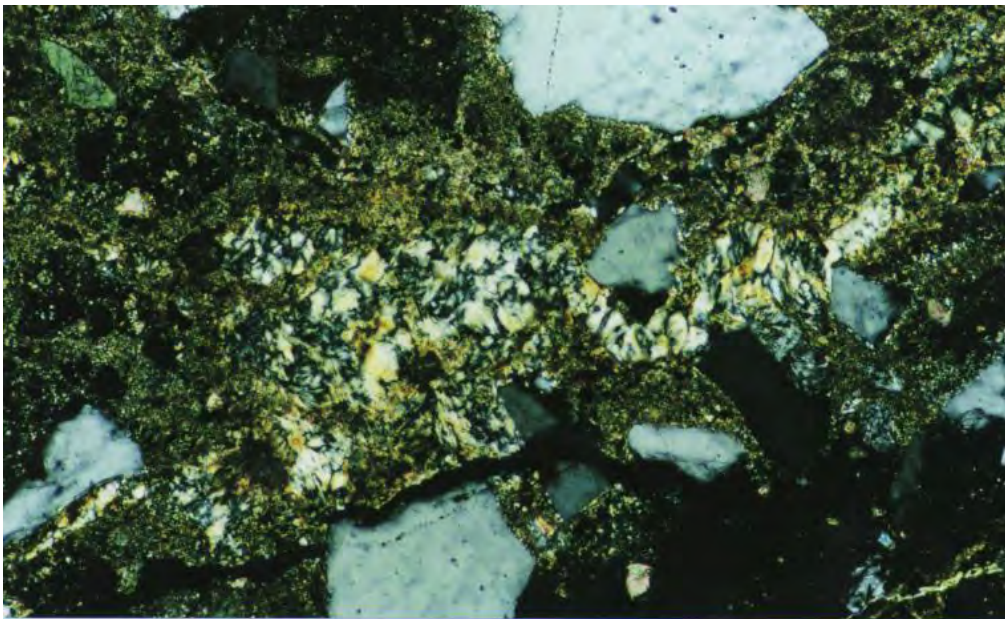


Figure A1-4-3b: Same view as above. Crossed polars. Width of field = 1.8 mm.

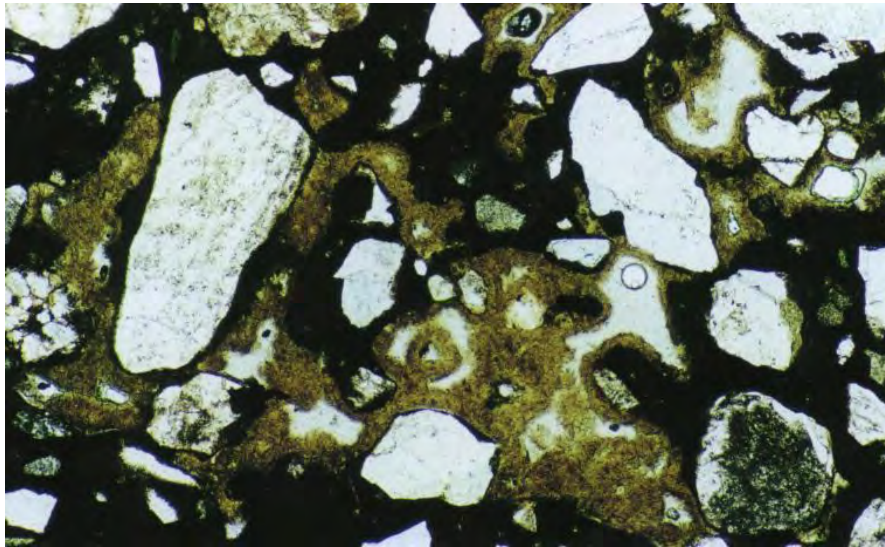


Figure A1-4-4: Thaumasite deposited in entrapment voids (TF) and occasionally replacing the cement paste matrix (TSA) in the 13 years old Åkebergveien sprayed concrete. Plane polarised light. Core 4, thin section 1570/30. Width of field = 1.8 mm.

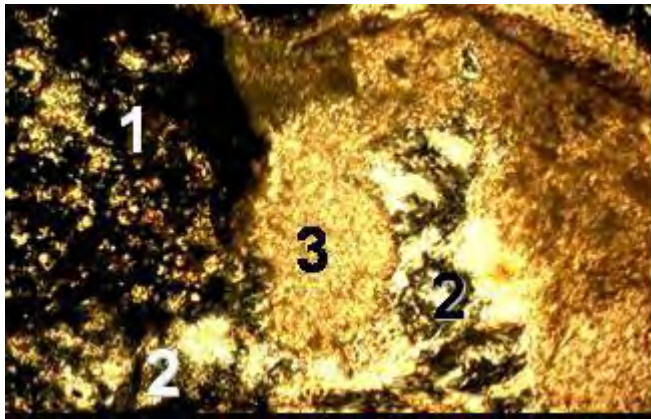


Figure A1-4-5: Sprayed concrete in the Svartdal tunnel, city of Oslo (< 2 years old). Extensively Ca-depleted paste (dark) with Popcorn calcite deposition (1) was replaced by thaumasite (2) which was replaced by large Popcorn calcite (3). Core 370a: thin section no. 1. Width of field = 0.3 mm.

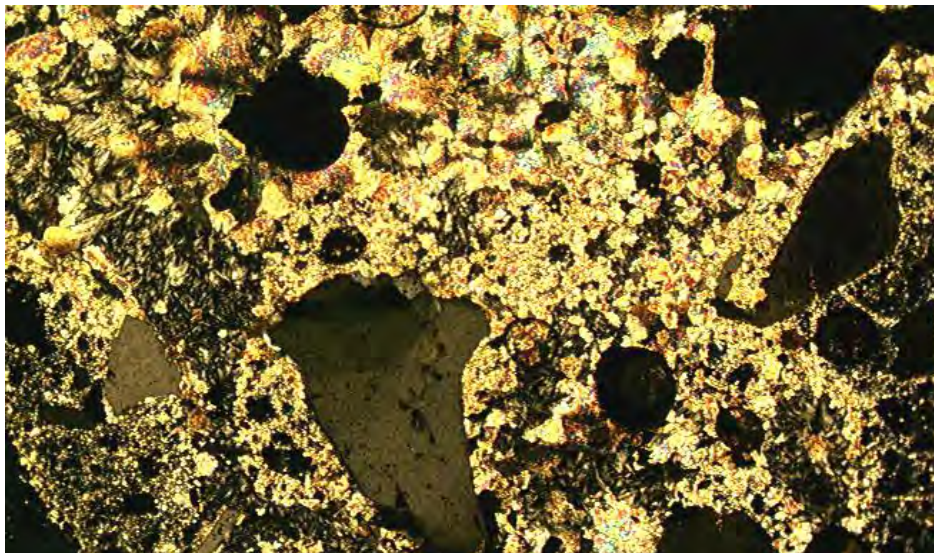


Figure A1-4-6: Sprayed concrete in the Åkeberg road cut. Spall 2, thin section Pr.1. 13 years old. Thaumasite (left central) and Ca-depleted cement paste (lower left and right) extensively replaced by secondary calcite representing the *end product of the TF-TSA-carbonation* process, which leads to internal release of sulfate ions. The resulting cement paste is friable, permeable and sensitive to acid attack: Crossed polars, Width of field: 1.5 mm.

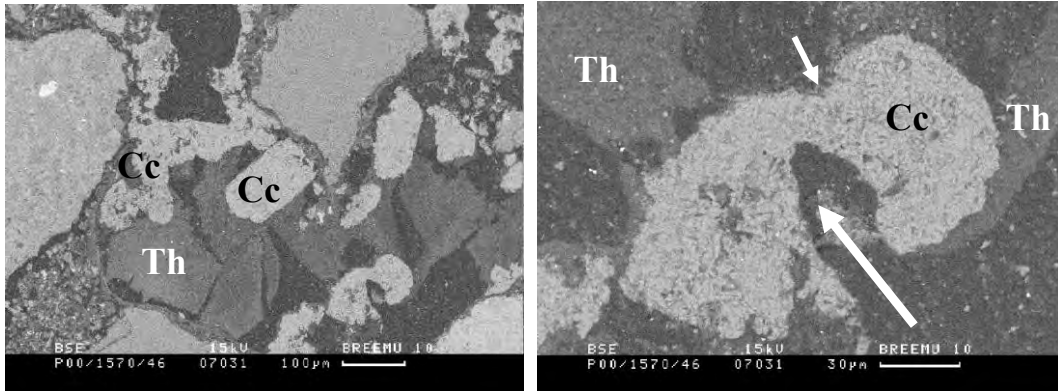


Figure A1-4-7: Sprayed concrete from the Svartdal tunnel (Core 370a, thin section 1570/46) showing co-precipitation of thaumasite (TF) and calcite in an entrapment void. Notice the original crystal faces only in direct contact with thaumasite. Right: detail showing dissolution (arrows) of calcite and thaumasite due to later acid attack. Back Scatter images. Scale bars: 100 µm and 30 µm, respectively.

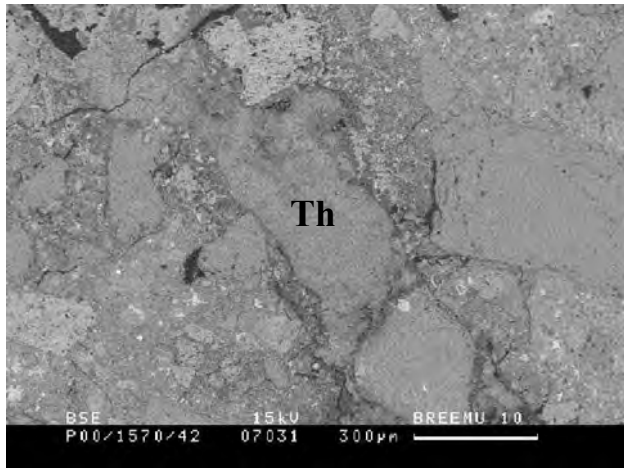


Figure A1-4-8: Thaumasite (Th) mass replacing cement paste (TSA) at Åkeberg road cut. Spall 2, thin section 1570/42: Back Scatter. Scale bar: 300 µm.

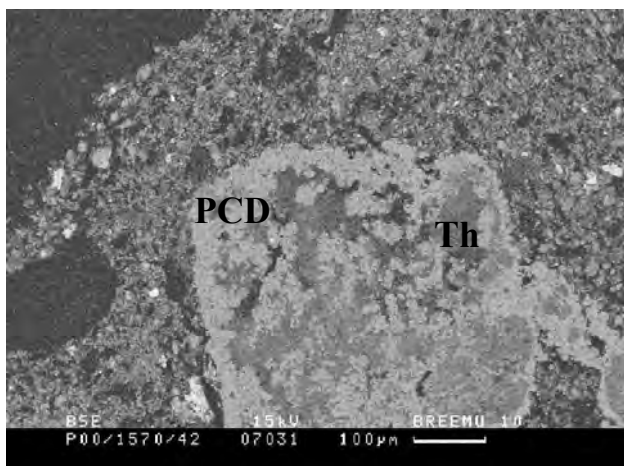


Figure A1-4-9: Extensive formation of Popcorn calcite (PCD) at the expense of thaumasite (Th). Thaumasite had initially formed at the expense of cement paste (TSA). Outermost part of 13 years old sprayed concrete in the Åkeberg road cut. Spall 2, thin section 1570/42. Back Scatter. Scale bar: 100 µm

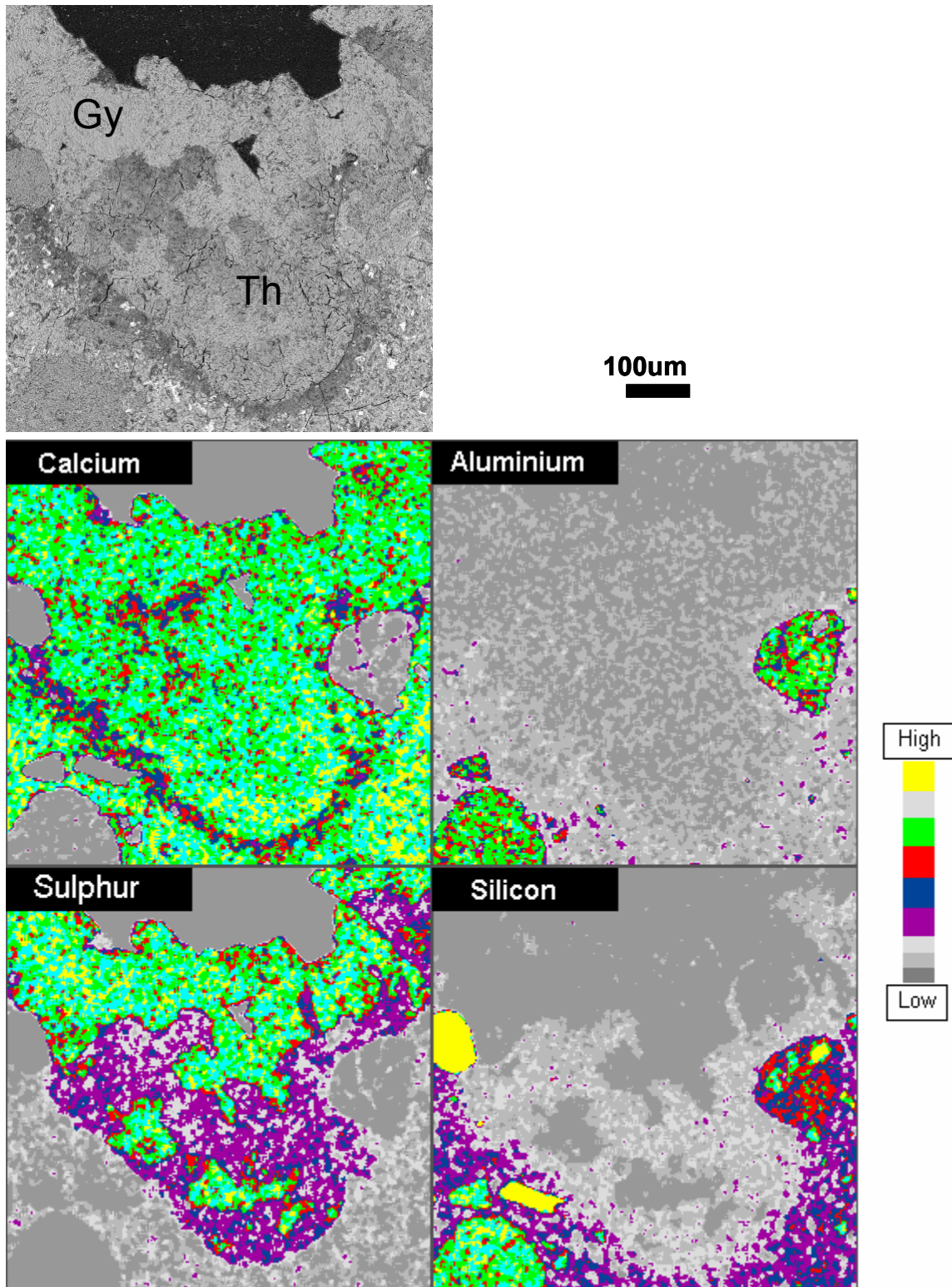


Figure A1-4-10: Back Scatter image and corresponding X-ray maps of thaumasite (Th) and coexisting gypsum (Gy) deposited within an entrapment void in Åkebergveien sprayed concrete. Notice the ca 25 µm wide rim of Ca-depletion (lower) within surrounding cement paste matrix at the contact adjacent to thaumasite. Core 4, thin section 1570/30.

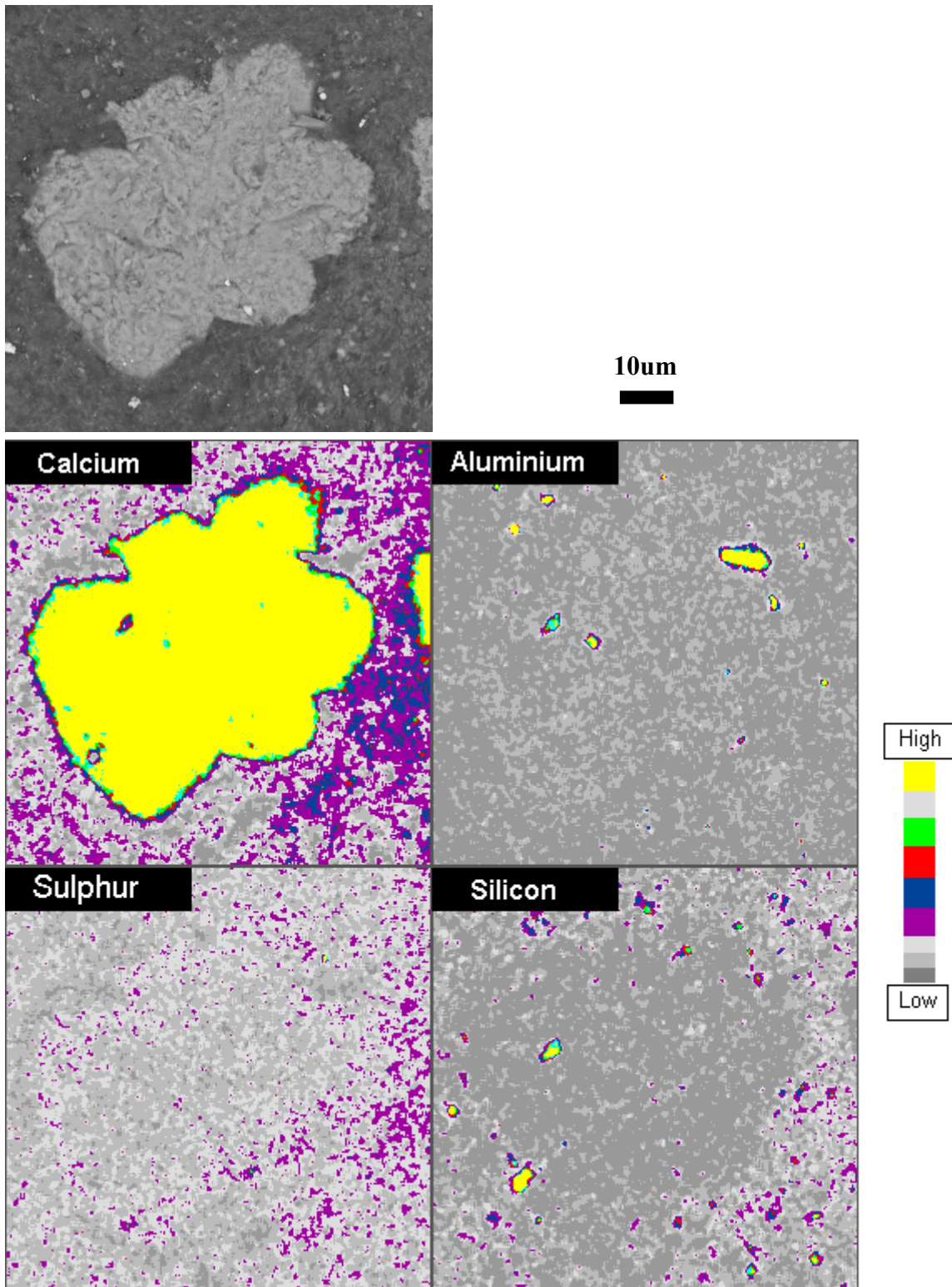


Figure A1-4-11: Back Scatter image and corresponding X-ray maps of a Popcorn calcite grain within thaumasite in Svartdal sprayed concrete. The calcite rim is somewhat sulfurised and thaumasite is depleted in calcium at the margin with Popcorn calcite. Core 370a, thin section 1570/46.

Appendix 2: Additional documentation to Chapter 4

- A2-1 Forensic examination and identification of unknown samples from the Blindtarmen test site**
- A2-2 Outer reaction zones in exposed samples**
- A2-3 Microscopical images**

A2-1 Forensic examination and identification of unknown samples from the Blindtarmen test site

The Alum Shale Committee tested sixteen different concrete mixes at the Blindtarmen test site. Altogether 212 individual concrete prisms were exposed and the committee provided a detailed record of their durability from 1952 to 1972. Some remaining test- and reference specimens had been stored at NBI (Norsk Byggforskningsinstitutt) since around 1982 when all samples had been picked up for further investigations of effects of silica fume etc. No report was prepared for the period 1972-1982, because the main researcher had passed away and the results were lost. Tom Farstad (NBI) kindly provided slices of both exposed specimens and reference samples in 2001. Most of the previously exposed old samples had lost their sample and series numbers. By using a forensic approach it was possible to relate most of the unknown samples to original Series numbers given by the Alum Shale Committee, whilst further identification of individual sample numbers in each Series was impossible. The approach was based on microscopy of unknown samples (standard petrographic microscope and SEM) and comparison with the detailed documentation by the Alum Shale Committee as well as available reference samples of known composition. The references cited in this appendix are the ones given in Chapter 4.

Microscopy of concrete aggregate and characteristics of inner sound paste

Coarse aggregate. In all samples coarse aggregate consisted of angular to rounded particles of size range 20 mm down to about 5 mm. It was composed of micro-crystalline limestone usually micritic and biomicritic but sometimes also sparitic. Lesser amounts of metamorphosed limestone (assemblages with epidote and calcite) also occurred. These observations are in perfect agreement with the documentation of the Alum Shale Committee, which tells us that the coarse fraction consisted solely of crushed Franzefoss limestone [5, 9].

Fine aggregate. The fine aggregate (mostly < 5 mm) consisted of angular to rounded sand grains composed primarily of granitic material with some basalt, meta-quartzite, amphibolite, chert like fragments, single fragments of quartz, feldspar and opaque minerals (apparently no pyrite) and others. This conforms to reports of the Alum Shale Committee. The unknown samples 1647/8 and 1647/12 also contained some small grains (< 100 microns) of angular biomicritic limestone similar to the coarse aggregate. These samples were very similar to reference sample 1647/18 (Series 8, Nor PC with added limestone filler). There was however no so-called “Aktivitt” (=coarser grained crushed calcite) as in Series 9 in any of the available samples (Table 2 of Chapter 4). Slag particles were not found either.

Cement paste in the less affected domains. In all samples the cement paste matrix was composed of Portland cement with no obvious signs of air entrainment. In all samples residual cement clinker grains were rather abundant. Unknown samples were mostly characterised by moderate levels of capillary porosity and occurrence of fine grained and evenly distributed portlandite throughout. Secondary larger grains of portlandite and/or non-deleterious ettringite were also present on aggregate-paste interfaces and air voids, indicating moisture transport.

Sample 1647/7, which was a lot less deteriorated than the other exposed samples, was characterised by a little more brownish cement paste in plane polarised light than most other samples. The good performance of this sample suggested it belongs to one of the mixes containing pozzolana or SRPC's. Observed in plane polarised light sample 1647/7 compared well with reference sample 1647/20 (Series 12 with 15 % Trass): Both these samples had a somewhat lighter brown cement paste in comparison with obviously darker brown paste in reference sample 1647/17 (Series 6; Nor PC with 15 % with silica fume (SF)). In the reference

sample 1647/17 the SF was very well dispersed without any traces of SF-globules, making discrimination based on presence/absence of SF impossible. Based solely on visual characteristics of the cement paste matrix under the polarising microscope it appeared that the mix with Norwegian silica fume (e.g. Series 6) was possibly not represented among the exposed samples, whilst one of the series with German trass *or* with SRPC remained good candidates. Yet sample 1647/7 was lacking signs of fine crushed calcite replacement such as in Series 13 with trass and crushed calcite fines (cf. Table 2 in Chapter 4 for mix details). Unfortunately we did not have access to reference samples of Series 14, which was made with 45 % trass and 10 % portlandite. None of the exposed samples had visual characteristics similar to the reference sample made with English sulfacrete (sample 1647/19), which had a distinct grey appearance on cut surfaces.

SEM-EDX results from quite sound paste

Cement colour and other visual features were not regarded as entirely safe discrimination criteria, and the samples were therefore analysed chemically by semi-quantitative SEM-EDX, using defocused beam within domains with relatively sound cement pastes. The analytical results are presented in Figure A2-1-1. In general the degree of scatter within each analysed block is thought to represent variations in distribution of very fine grained aggregate and possible effects of secondary mobility of elements, most likely Ca. Comparison of unknowns with reference samples showed that the very durable sample 1647/7 (unknown block 7) compares neither with English Sulfacrete nor Norwegian Portland Cement with 15 % silica fume, both of which have low Al/Si ratios. On the contrary, this sample is very similar to sample 1647/20 (Nor PC with trass). Moreover, the chemistry of the unknown sample 1647/8 (= block 8) plots at somewhat elevated Ca contents together with reference sample 1647/18 (= block 18; Series 8 Nor PC with crushed limestone fines), with the exception of one outlier at low Ca (possibly representing decalcified paste). Most of the remaining unknown samples plot within the field of block 3 (= Nor PC, Series 1).

Conclusions on sample identity

The overall results seem to rule out the presence of Nor PC with silica fume and SRPC based concretes, as none of the investigated unknown samples had comparably low to very low C₃A contents (cf. Figure A2-1-1) & Table 2 in Chapter 4). Thus, series 2, 3, 4, 6, 15 and 16 should be eliminated. The apparent lack of air entrainment in the investigated samples suggests that neither Series 5 nor Series 10 were represented. It also seems unlikely that Series 7 (Nor PC with 15 % slag) was present: This particular slag contained 37 wt. % CaO [9]; more total Ca than in the 8 % lime stone added mix, and should plot above the cluster of blocks 3 (Series 1 Nor PC) and block 18 (Series 8 Nor PC with limestone fines). Sample 1647/7 appears to be identical to Series 20 with respect to its matrix chemistry, performance and paste microscopical characteristics, and was interpreted as Norwegian PC with 15 % German Trass (block 20). Sample 1647/12 shared all petrographic characteristics of Nor PC with crushed biomicritic limestone fines, and could safely be interpreted as belonging to Series 8 even if no chemical analysis was undertaken. Series 9 could also readily be ruled out since this mix was made with coarse calcite crushed to size fractions around 30 µm, being much different from biomicritic limestone. The remaining more severely attacked unknown samples were interpreted to represent Nor PC Series 1, because matrix analyses cluster around block 3 and paste properties and aggregates used were otherwise comparable.

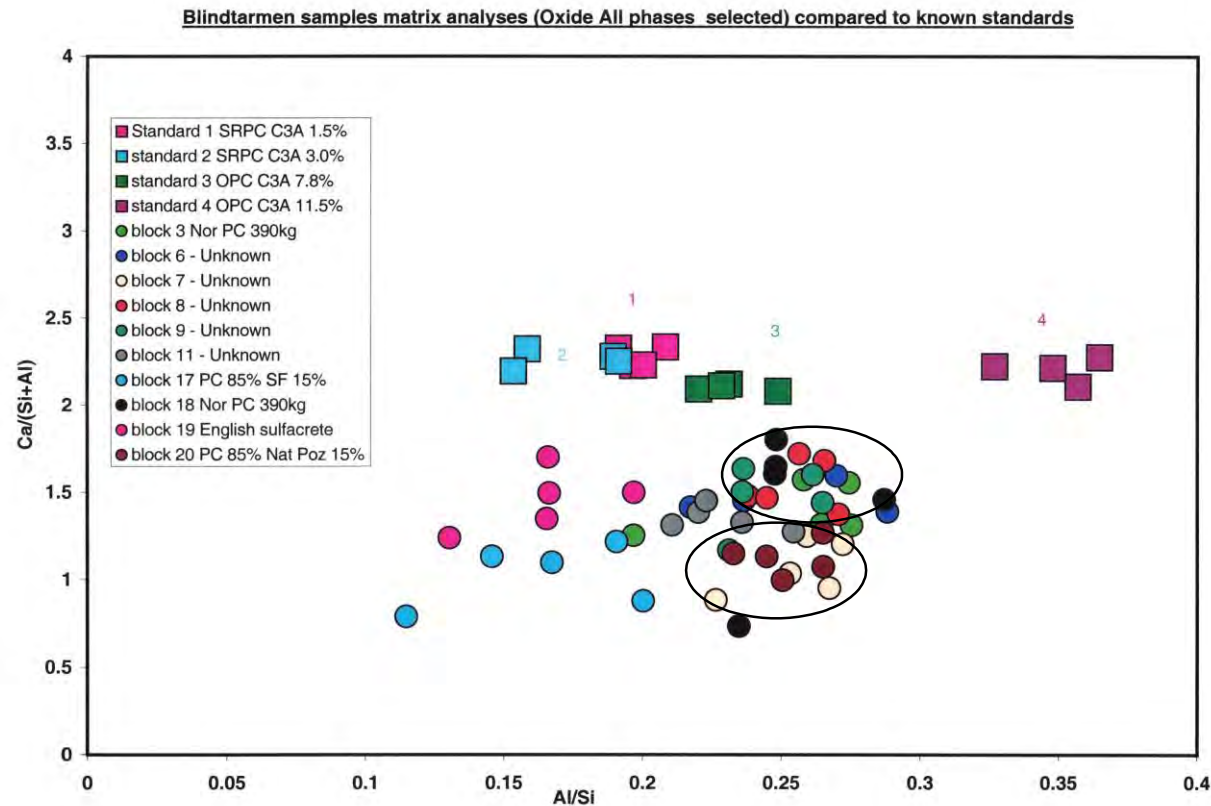


Figure A2-1-1: Chemical composition of internal sound cement paste matrix (cf. Figure A2-2-2) in unknown Blindtarmen samples (blocks 6-11) compared with different British cements standards (1-4) and Blindtarmen reference samples (blocks 17-20). The *lower ellipse* indicates the compositional variation in unknown block 7 (sample 1647/7), which compares well with Series 12: Nor PC with 15 % trass (block 20 = sample 1647/20). The *upper ellipse* represents the variation of the unknown sample 1647/8 sample (block 8, red), which is similar to 1647/18 (block 18, black) Series 8 Nor PC with limestone additives. The remaining unknown samples cluster around block 3 (Series 1 Nor PC without additives. Analyst: Derek Metcalf, BRE, Garston-Watford, UK).

A2-2 Outer reaction zones in exposed samples

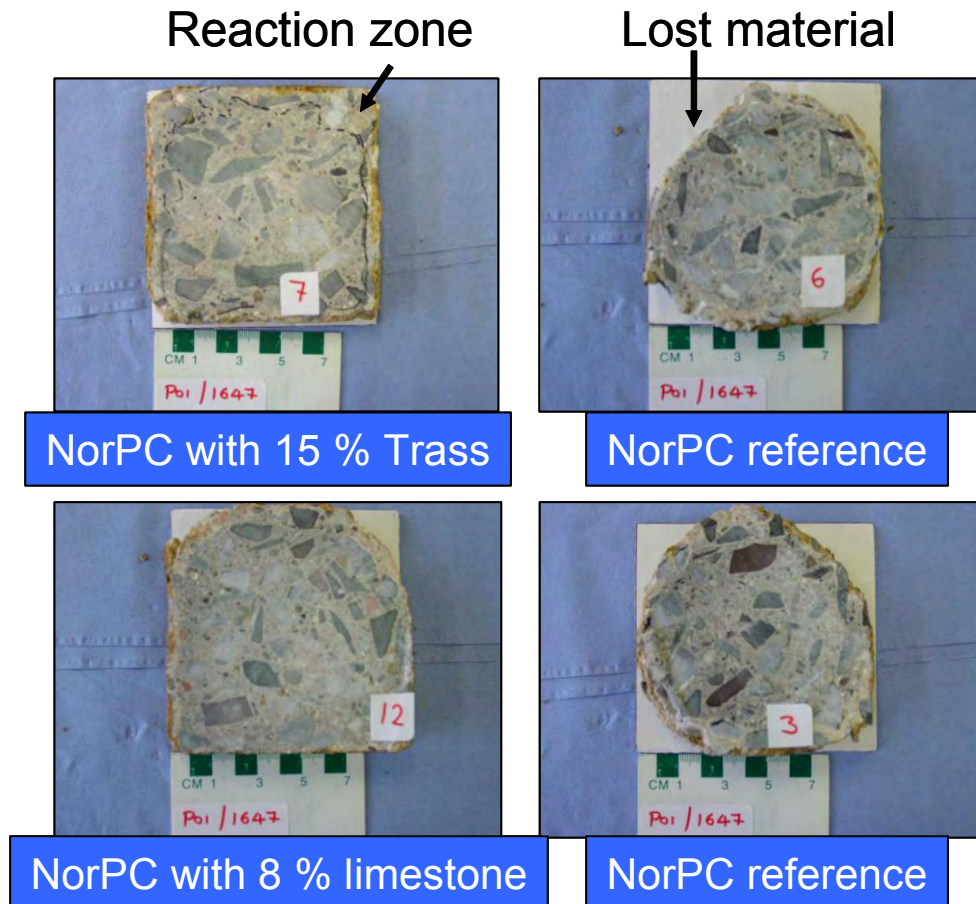


Figure A2-2-1: Typical examples of sliced Blindtarmen test prism. The cross sections were initially 10 cm x 10 cm as indicated by the white cardboard plates behind. Sample 1647/7, representing Norwegian Portland Cement (Nor PC) with 15 % trass (Series 12 of the Alum Shale Committee) was exposed for 24 years, being the most durable concrete among the remaining samples. Sample 1647/12 (Series 8) Nor PC with 8 % limestone fines in the sand fraction was exposed for 20 years, whilst the reference samples (Series 1) were exposed for 30 years. Notice the bleached reaction zones and severe loss of material in the samples without pozzolana. Irrespective of state of degradation *all* samples had an outer ferric iron deposit with rust stained concrete just underneath.

A2-2 continued:

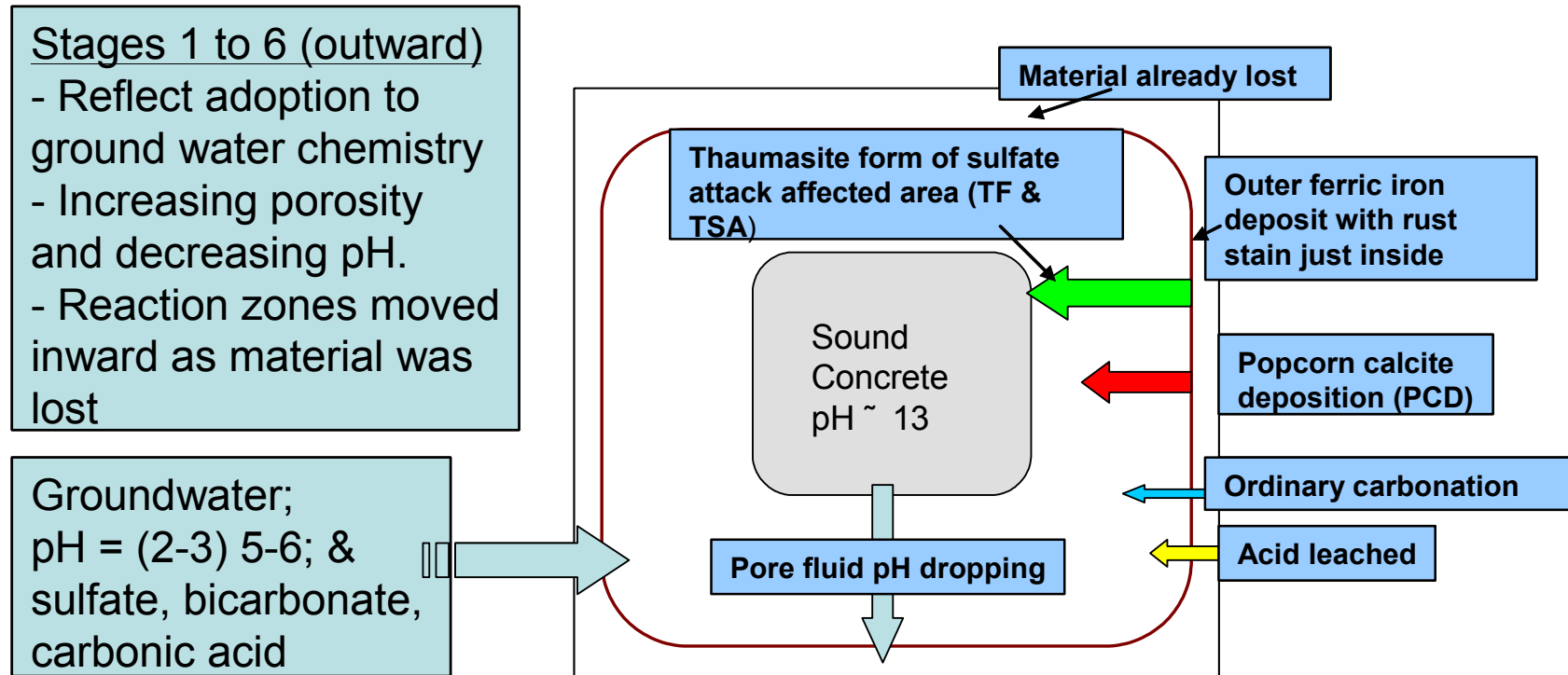


Figure A2-2-2: Idealised sketch of the reaction stages within outer parts of the Blindtarmen test concretes.

A2-3 Microscopical images

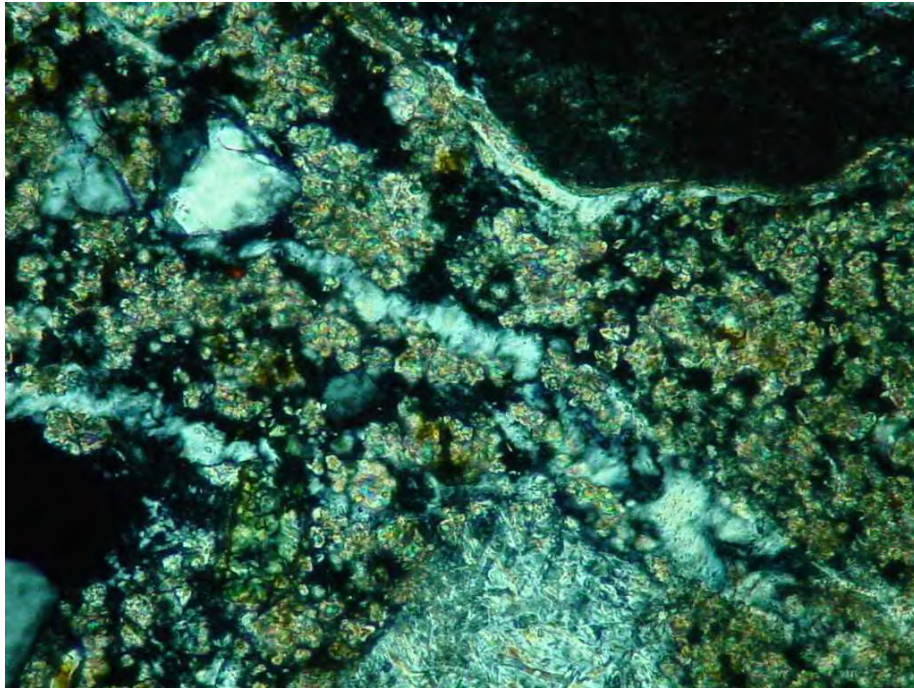


Figure A2-3-1: Blindtarmen, sample 1647/8 (Series 1 Nor PC), showing decomposition of thaumasite (dark and barely visible in substrate) to Popcorn calcite and gypsum veins (light grey) along microcracks. Gypsum only precipitated in the outer dried concrete, whilst breakdown of thaumasite within the interior just liberated sulfate ions to the pore solution (Figure A2-3-2). Large grains are aggregates. Width of field = 150 μ m. Crossed polars.

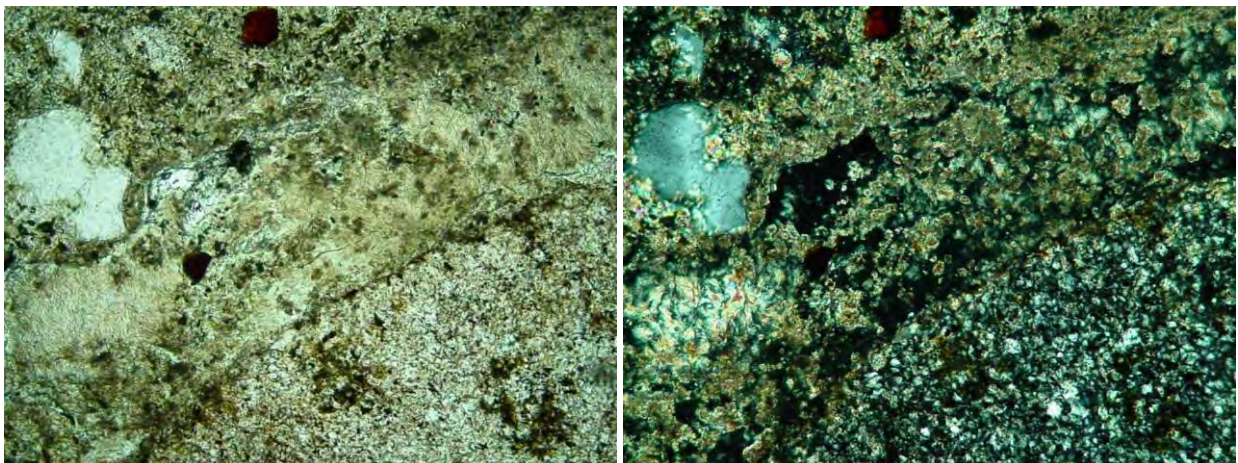


Figure A2-3-2: Blindtarmen, from the interior of Sample 1647/3 (Series 1-18 Nor PC). Plane polarised light (left image) and crossed polars (right image). Thaumasite (lower left with 2nd order birefringence), was extensively replaced by Popcorn calcite whilst thaumasite sulfate was liberated to the pore solution for further attack. Width of field = 0.9 mm.

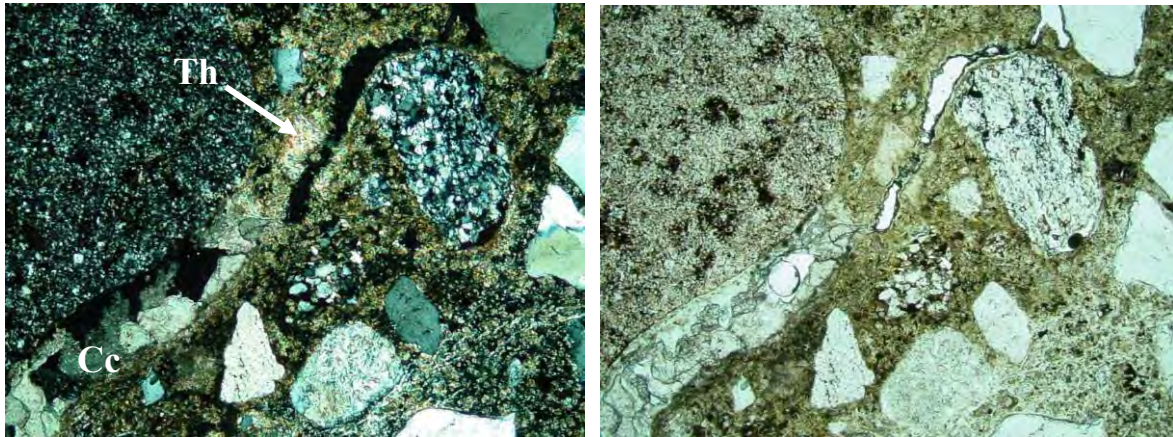


Figure A2-3-3: Sample 1647/3 Norwegian PC showing a vein of thaumasite (Th) and calcite (Cc). Notice also finer calcite formed at expense of thaumasite. Image width 1.8 mm.

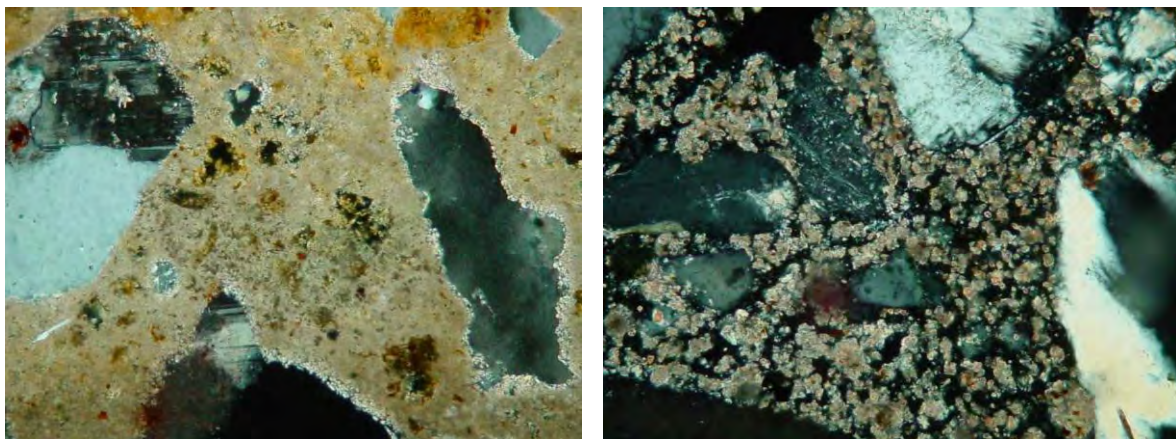


Figure A2-3-4: Blindtarmen sample 1647/8 (Series 1 Nor PC), showing the typical difference between full scale ordinary carbonation in outer concrete prisms (left image) and Popcorn Calcite Deposition (PCD) deeper inside (right image); the latter having formed through extensive Ca-depletion of the CSH under influx of bicarbonate ions. Image widths = 0.9 mm. Crossed polars.

Appendix 3: Additional documentation to Chapter 5

- A3-1 C, O and S stable isotope data of thaumasite and secondary calcite in sprayed concrete in contact with Alum Shale**
- A3-2 Outline of stable isotope systematics**

A3-1 C, O and S stable isotope data thaumasite and secondary calcite in sprayed concrete in contact with Alum Shale

Laser microprobe data

Small samples (Bet.) were prepared from cores described in Appendix 1. Th = thaumasite; cc = calcite; CSH = calcium silicate hydrate, somewhat depleted; ccd = coarser grained calcite deposits. C and O isotopic data normalised to the PDP standard. Alum Shale at Åkebergveien and Svartdal are of Lower Ordovician and Upper Cambrian ages, respectively.

Table A3-1-1 Åkebergveien road cut (13 years).

Bet5(th/carb)			Bet5(carb)		
$\delta^{18}\text{O}$	$\delta^{13}\text{C}$	Assemblage	$\delta^{18}\text{O}$	$\delta^{13}\text{C}$	Assemblage
-19.7	-13.2	Th+cc+CSH	-21.71	-7.36	cc+CSH>th
-20.7	-10.5	Th+cc+CSH	-21.69	-6.93	cc+CSH>th
-20.7	-12.8	Th+cc+CSH	-21.26	-4.29	cc+CSH>th
-20.7	-11.5	Th+cc+CSH	-20.39	-6.67	cc+CSH>th
-20.5	-12.4	Border zone			
-19.9	-11.6	Border zone			

Table A3-1-2 Åkebergveien road cut (13 years).

Bet 6(surface + intern carb.)			BET4 (th+cc+CSH)		
$\delta^{18}\text{O}$	$\delta^{13}\text{C}$	Assemblage	$\delta^{18}\text{O}$	$\delta^{13}\text{C}$	Assemblage
-20.0	-9.0	CSH>cc	-15.5	-11.6	Th+cc+CSH
-19.5	-8.2	CSH>cc	-18.7	-11.9	Th+cc+CSH
-18.7	-9.1	CSH>cc	-19.1	-11.9	Th+cc+CSH
-17.2	-8.9	CSH>cc	-17.8	-11.5	cc+Th+CSH
-18.6	-7.5	CSH>cc	-14.4	-11.3	cc>CSH+Th
-22.5	-6.0	CSH+cc?	-16.6	-10.4	cc>CSH>Th

Table A3-1-3 Åkebergveien road cut (13 years)

BET11 Surface carbonation					
$\delta^{18}\text{O}$	$\delta^{13}\text{C}$	Assemblage			
-11.3	-11.8	cc>CSH Surface			
-11.6	-12.5	cc>CSH Surface			
-9.6	-10.9	cc>CSH			
-10.2	-5.8	CSH+cc			
-10.4	-8.4	CSH>cc?			
-2.4	-9.2	cc+Th>CSH		Towards reaction zone	
2.5	-9.1	cc+Th>CSH			
12.3	-12.0	cc+Th>CSH		19mm from surface	
-21.0	-8.4	CSH>cc		Internal carbon.	
-20.3	-7.2	CSH>cc		4cm from surface	
-20.4	-5.4	CSH>cc			

Table A3-1-4 Svartdal tunnel (2 years)

Bet7(del1)	(outer part)		Bet7(del2)	interface part	
$\delta^{18}\text{O}$	$\delta^{13}\text{C}$		$\delta^{18}\text{O}$	$\delta^{13}\text{C}$	
-24.3	-18.3	Th>cc			
-20.5	-10.2	Th>cc	-14.8	-9.2	CSH>cc
-20.3	-14.1	Th>cc	-4.6	-5.4	CSH+cc
-16.0	-10.2	Border	5.4	-6.3	ccd>CSH+cc
-5.4	-7.1	CSH>?	-8.9	-4.1	ccd>CSH+cc
-14.4	-15.1	CSH mix	-22.8	-5.4	ccd+CSH+cc
-13.5	-16.7	CSH mix			
-12.9	-16.7	CSH mix			
-4.6	-5.9	CSH>?			
-12.9	6.0	Th			
-10.1	-5.8	Th			
-8.8	-10.7	Th			
-13.3	-16.2	Th>			

Table A3-1-5 Svartdal tunnel (2 years)

Bet9	interface with alum shale		BET10	Surface carbonation	
$\delta^{18}\text{O}$	$\delta^{13}\text{C}$		$\delta^{18}\text{O}$	$\delta^{13}\text{C}$	
-23.9	-14.1	csh>cc	-16.5	-12.9	Surface carb. Cc>csh (+th?)
-24.0	-13.3	csh>cc (intern.)	-18.7	-12.9	Surface carb. Cc>csh
-23.5	-10.9	csh>cc	-16.7	-12.7	Surface carb. Cc>csh
-23.5	-14.3	csh+th>cc	-17.5	-10.9	CSH>cc Internal
			-17.0	-10.5	CSH>cc Internal

Conversion to the SMOW standard:

$$\delta^{18}\text{O}_{\text{SMOW}} = 1.03086 \delta^{18}\text{O}_{\text{PDP}} + 30.86$$

Small handpicked samples

Table A3-1-6. Sulfur isotopes. All data normalised to the CDT standard.

Sample no (IFE)	Sample	$\delta^{34}\text{S}$	Description
Svartdal tunnel			
Upper Cambrian			
2001.1660	Bet8, Core370A	15.8	Sulfide separate, alum shale
		22.1	-"
		18.5	-"
2001.1159	Bet8, Core370A	6.7	Organics, alum shale
		6.9	-"
2001.2394	Bet10, Core370A	11.9	CSH-gel
	Bet10, Core370A	1.8	Thaumasite, mush zone
2001.1661	Bet9, Core320B	27.7	Sulfide separate, alum shale
		26.8	-"
	Bet9, Core320B	21.2	Organics, alum shale (possibly w/ small pyrites)
Åkebergveien road cut			
Lower Ordovician			
2001.1156	Bet5, Core2	3.9	Thaumasite, mush zone
2002.3230		4.7	Organics, alum shale, opposite Core2
2002.3229	Core2	2.1	Sulfide in alum shale (OK)
2002.3230		7.8	Sulfide in alum shale, opposite Core2 (small signal)
2002.3229	Core2	4.0	Thaumasite within pores
2002.3230		2.1	Jarosite, surfaces within alum shale, opposite Core2
2002.3229	Core2	10.7	CSH-gel
2001.2395		Bet11, Core4	10.5

A3-2 Outline of stable isotope systematics

Stable isotopic ratios of light elements vary much in nature. These variations generally record the results of chemical, physical or biological processes. In Chapters 5, 6, 7 and 9 the non-radioactive stable isotopes of carbon, sulphur, oxygen and hydrogen were applied in order to throw light on the sources and release mechanisms of aggressive waters. Isotopic data were also used together with results from other techniques, representing an integrated “multiproxy” approach. Both waters and solids were analysed, as appropriate for each topic in question.

Isotopes are atoms that contain the same number of protons but differ in the number of neutrons, e.g. mass. The relevant isotopes of C, S, O and H are tabulated along with abundance in Table A3-2-1 with the numbers of neutrons for each element using standard notation for nuclides. A brief outline of stable isotope systematics is given below, and further details may be found in textbooks such as Faure (1989), cited in Chapter 3.

Table A3-2-1. Stable isotopes of H, C, O and S and abundance from standard tables.

Element	Isotopes	Relative abundance
Hydrogen (H)	¹ H	99.985
	² H (D)	0.015
Carbon (C)	¹² C	98.90
	¹³ C	1.11
Oxygen (O)	¹⁶ O	99.762
	¹⁷ O	0.032
	¹⁸ O	0.200
Sulfur (S)	³² S	95.02
	³³ S	0.75
	³⁴ S	4.21
	³⁶ S	0.02

The table shows that the light isotopes are by far the most abundant. In natural samples of minerals, water, biological material and others, the isotopic ratios deviate from the table due to the source materials and processes involved. The behaviour of H, C, O and S stable isotopes is mostly mass dependent. In general the lighter isotopes favour the less dense compound: for example water vapour instead of water and H₂S gas instead of sulfate or iron sulfide. Light isotopes also accumulate in bacteria and other organic matter. This is referred to as *isotopic fractionation*, which reflects the fact that molecules containing heavy isotopes are more stable (i.e., have a higher dissociation energy) than molecules with lighter isotopes.

Stable isotope analysis usually involves various techniques for converting/purifying the elements of interest into a stable gas. The isotopic ratios (for example ¹⁸O/¹⁶O) are then measured in an isotopic mass ratio mass spectrometer, and are commonly expressed by delta notation, for example:

$$\delta^{18}\text{O} = \left(\frac{\left(\frac{^{18}\text{O}}{^{16}\text{O}}\right)_{\text{sample}}}{\left(\frac{^{18}\text{O}}{^{16}\text{O}}\right)_{\text{standard}}} - 1 \right) * 1000 \text{ ‰}$$

or in general:

$$\delta = (\text{Ratio in sample}/\text{Ratio in standard} - 1) * 1000 \text{ ‰}$$

The isotopic compositions are reported relative to international standards (δ in pro mill (‰)) recommended by the International Atomic Energy Agency (IAEA). For δD (δ^2H) and $\delta^{18}O$ the international standard are VSMOW (Vienna - Standard Mean Ocean Water); for $\delta^{13}C$ the VPDB (Vienna - Pee Dee Belemnite). SMOW and PDB are equivalent standards. $\delta^{34}S$ is reported relative to CDT (Canyon Diablo Triolite).

Isotopic fractionation occurs in relation to two main phenomena: *isotope exchange reactions* and *kinetic processes*. Chemical, physical, and biological processes can be viewed as either reversible *equilibrium* reactions or irreversible unidirectional *kinetic* reactions. The fractionation associated with the equilibrium reaction between two substances *A* and *B* (i.e., the fractionation of *A* relative to *B*) can be expressed by use of the isotope fractionation factor α (alpha):

$$\alpha_{A-B} = R_A / R_B$$

where R = the ratio of the heavy isotope to the lighter isotope (i.e., $^2H/^1H$, $^{13}C/^{12}C$, $^{18}O/^{16}O$, $^{34}S/^{32}S$) in compounds *A* and *B*. Considering that *A* is a mineral and *B* is an ionic species dissolved in equilibrium with *A*, or alternatively exchange between two different minerals, the difference between the isotopic composition of *A* and *B* is commonly expressed as:

$$\varepsilon_{A-B} \sim \delta_A - \delta_B \sim 1000 \ln \alpha_{A-B}$$

where ε denotes the difference in isotopic composition between *A* and *B*. Fractionation factors are usually expressed as “1000 ln α ”. Fractionation factors for the different compounds may be found in databases and scientific literature, and are the same whether equilibrium fractionation or kinetic fractionation is involved.

Appendix 4: Additional documentation to Chapter 6

- A4-1 Scanning Electron Microscopy (SEM)**
- A4-2 X-ray diffraction (XRD)**
- A4-3 Water chemical calculation using the computer code
PHREEQC-2**
- A4-4 Contribution of Ca-sulfates and Fe-sulfides to aqueous sulfate**
- A4-5 Images of tunnel water with bacterial slime and Alum Shale
sample**
- A4-6 Microbes found in the Alum Shale environment**

A4-1 Scanning Electron Microscopy (SEM)

SEM data files at the Museum of Natural History (NHM), University of Oslo.

The data file names are summarised in the following tables and related to sample numbers and topics described in Chapter 6.

Table A4-1-1. Semi-quantitative bulk chemical analysis of Alum Shale powder (Table 5 in Chapter 6)

Sample no.	Characteristics	NHM-files
320-06U initial shale	Homogeneous (three different domains)	Hagelia 2006-08-16 01.29.35.doc Hagelia 2006-08-16 01.36.45.doc Hagelia 2006-08-16 01.40.53.doc
320-06U leached in Water 1	Some separation (five different domains)	Hagelia 2006-10-27 01.03.37.doc Hagelia 2006-10-27 01.06.56.doc Hagelia 2006-10-27 01.17.24.doc Hagelia 2006-10-26 22.46.10.doc Hagelia 2006-10-26 22.55.06.doc
320-06U leached in Water 2	Some separation (three different domains)	Hagelia 2006-10-27 01.38.15.doc Hagelia 2006-10-27 01.46.10.doc Hagelia 2006-10-27 01.50.21.doc

Table A4-1-2. Quantitative micro chemical analysis of Alum Shale constituents by SEM

Sample no.	Reference to Chapter 6	NHM-files
320-06U initial shale	Goethite, sulfide + sulfurised C Pyrite Pyrite (chapter 6.4.3)	Hagelia 2006-08-16 01.53.39.doc Hagelia 2006-08-16 02.15.29.doc Hagelia 2006-08-16 02.03.54.doc
320-06U leached in Water 1	Blocky pyrite (chapter 6.4.3)	Hagelia 2006-10-27 01.24.59.doc
320-06 tunnel water bacterial slime	Table 3 (A1, A2, A3); Fig 2A Table 3 (B1, B2, B3, B4); Fig 2B	Hagelia 2007-11-13 22.52.41.doc Hagelia 2007-11-13 23.09.51.doc

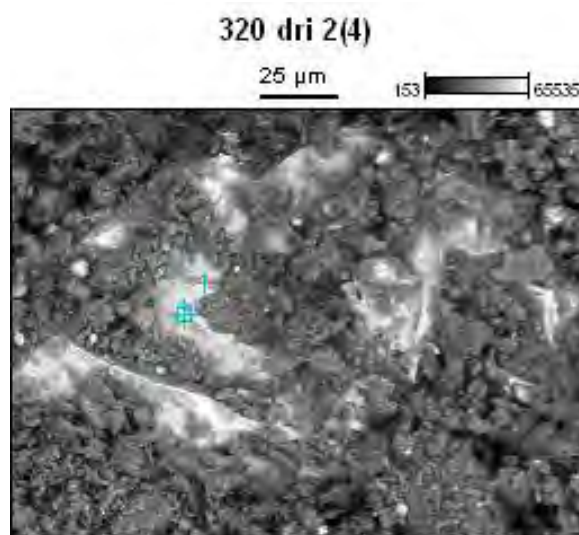


Figure A4-1-1: Blocky pyrite in the leached Alum Shale powder. Fe/S atomic ratio = 0.5.

A4-2 X-ray diffraction (XRD)

XRD- data files at Museum of Natural History (NHM), University of Oslo.

The file names, sample numbers and mineral contents are given in the table below for reference.

Table A4-2-1: Summary of main XRD results from Svartdal tunnel Alum Shale sample powder prepared for the leaching experiment. The sample was extracted from chainage 320 m eastbound. ID is file number at NHM.

Sample	Minerals	ID
320-06U initial shale	Quartz, Ba-V- muscovite, pyrite, hexagonal-pyrrhotite, monoclinic-pyrrhotite, Ti-magnetite, anhydrite, Mg-calcite, calcite, montmorillonite, almandine, rhodochrosite, graphite	160806 320 oppe.RAW
320-06U leached in Water 1	Quartz, Ba-muscovite, pyrite, hexagonal-pyrrhotite, monoclinic-pyrrhotite, Ti-magnetite, anhydrite, gypsum, Mg-calcite, calcite, almandine, rhodochrosite, graphite	271006 320 dri.RAW
320-06U leached in Water 2	Quartz, K-muscovite, pyrite, hexagonal-pyrrhotite, monoclinic-pyrrhotite, Ti-magnetite, almandine, Mg-calcite, graphite	271006 320 tun.RAW
320-06 tunnel water slime	Essentially amorphous, yet distinct lines of cristobalite, goethite and ferrihydrite	141107 320 06.RAW

A4-3 Water chemical calculation using the computer code PHREEQC-2

Short introduction

PHREEQC is a computer program for speciation, batch reaction, inverse modelling and one-dimensional transport, designed for low-temperature aqueous geochemical calculation. The aqueous model uses ion association and Debye-Hückel theory to account for the non-ideality of aqueous solutions. The program is distributed free of charge by the U.S. Geological Survey and can be downloaded together with User's Guide from <http://www.xs4all.nl/~appt/index.html>. Further documentation of PHREEQC may be also found in Appelo and Postma (2005; referred in Chapter 6).

In the present work PHREEQC (version 2.12.04) was used to compute saturation indices (SI's) for relevant minerals in tunnel water and experimental waters before and after leaching of an Alum Shale powder. Solubility of minerals in water is generally described by the law of mass action and based on calculated activities. The activities represent dimensionless "effective concentrations" derived from ionic concentrations obtained from chemical water analysis. The activities are related to the molal ion concentrations by activity coefficients which corrects for non-ideal behaviour. In reality anions and cations are not infinitely diluted (ideal); they interact with other ions and complexes in the solution.

The software calculates activities and ionic speciation through iterative procedures based on the input ionic concentrations, redox conditions, pH, T etc. using thermodynamic databases. The SI's are calculated by comparing the solubility product K (e.g. at thermodynamic equilibrium) with the *ion activity product (IAP)* in the actual water samples.

For example:

$$K_{\text{gypsum}} = [\text{Ca}^{2+}][\text{SO}_4^{2-}] = 10^{-4.6} \text{ (activities of the ions at equilibrium)}$$

$$IAP_{\text{gypsum}} = [\text{Ca}^{2+}][\text{SO}_4^{2-}] \text{ (activities of the ions in the sample)}$$

The IAP/K –ratio represents the saturation state (Ω):

$$\Omega = IAP/K$$

When $IAP = K$, there is equilibrium ($\Omega = 1$): the mineral is saturated in the water and will start to precipitate. The definition of SI is:

$$SI = \log (IAP/K)$$

Hence when $SI = 0$ equilibrium is attained, whilst $SI < 0$ and $SI > 0$ represents subsaturation and supersaturation, respectively. SI's calculated by PHREEQC are more close to real world saturation states than those based on simple calculation from molal concentrations.

PHREEQC-2 input files

The water chemical data in Table 7 (Chapter 6) was the basis for the input file. The redox conditions were defined by measured Eh and pH in the waters. Temperature used was 22.6 °C (laboratory conditions), whilst a separate calculation for the tunnel water at ambient tunnel temperature (8 °C) did not change the saturation states very significantly. The relevant saturation indices in Table 8 were plotted versus different other parameters in figures 6 & 7 & 8 in Chapter 6.

The input file is given below. Lines marked with # are not used in calculation. For example Alkalinity was used instead of #Total carbon (C).

```
#ALUM SHALE SAMPLE: FROM CORE 320U-06, ABOUT 10-12 CM DEPTH #UNDERNEATH  
SPRAYED CONCRETE  
#LOCATION: SVARTDAL TUNNEL, CITY OF OSLO (CHAINAGE 320 IN NICHE)  
#ALUM SHALE AGE: UPPER CAMBRIAN (Stage 2 c-d),  
#SAMPLES: TWO PARALLEL'S (EACH 100g) OF FINE POWDER LEACHED FOR 65 #DAYS IN TWO  
DIFFERENT WATERS: WATER 1 AND WATER 2  
#DATABASE USED: llnl.dat  
#PHREEQC -2
```

```
SOLUTION 1 WATER 1 INITIAL  
temp 22.6  
pH 7.15  
pe -1.64 #BASED ON Eh MEASURED: pe = Eh/0.059  
Alkalinity 0.280  
units mg/L  
density 1.00  
Na 1.6  
Cl 2.98  
F 0.086  
S(6) 1.14 # Sulfate by chromatography  
#N(5) 0.026  
#N(-3) 0.115  
#C 3.69 # Total carbon calculated from TOC and HCO3-  
#S 0.5 # S-tot by ICP
```

Appendices – Black shale environment

K 0.3
Ca 3.53
Sr 0.0188
Si 1.86
Al 0.007
B 0.004
Ba 0.0110
Zn 0.2460
Cu 0.2730
Mg 0.486
Mn 0.0023
Fe 0.0042
END

SOLUTION 2 WATER 1 FINAL # Composition after 65 days reaction with 100 grams of Alum shale powder
temp 22.6
pH 7.28
pe -1.18 #based on average Eh measurements during the 65 days experiment
Alkalinity 1.872
units mg/L
density 1.000
Na 4.99
Cl 5.8
F 0.460
S(6) 1080 # Sulfate by chromatography
#N(5) 0.003
#N(-3) 0.490
#S 377 # S-tot by ICP
#C 22.6 # Total carbon calculated from TOC and HCO₃-
K 38.3
Ca 430
Sr 1.63
Si 4.79
Al 0.029
B 0.120
Ba 0.0599
Zn 0.044
Cu 0.0093
Mo 0.385
Mg 17.4
Mn 3.03
Fe 0.0381
END

SOLUTION 3 WATER 2 INITIAL (WATER 1 Initial 250 ml/450 ml + TUNNEL WATER 320U-06 200 ml/450 ml)
assuming conservative mixture
temp 22.6
pH 7.01
pe -1.49 #BASED ON Eh MEASURED: pe = Eh/0.059
Alkalinity 0.642
units mg/L
density 1.000
Na 20.6
Cl 9.967
F 0.559
S(6) 241 # Sulfate by chromatography
#N(5) 0.148
#N(-3) 0.108
#C 8.37 # Total carbon calculated from TOC and HCO₃-

Appendices – Black shale environment

K 4.21
Ca 78.4
Sr 0.99
Si 4.52
Al 0.006
B 0.002
Ba 0.018
Zn 0.174
Cu 0.154
Co 0.035
Mo 0.008
Mg 9.8
Mn 0.59
Fe 0.079
END

SOLUTION 4 WATER 2 FINAL #Composition after 65 days reaction with 100 grams of Alum shale powder
temp 22.6
pH 7.19
pe -1.16 #based on average Eh measurements during the 65 days experiment
Alkalinity 1.626
units mg/L
density 1.000
Cl 29.7
F 0.490
S(6) 1510 # Sulfate by chromatography
#N(5) 0.003
#N(-3) 0.580
#S 524 # S-tot by ICP
#C 19.6 #calculated from TOC and HCO₃-
K 42.6
Na 21.7
Ca 565
Sr 2.47
Si 5.14
Al 0.007
B 0.160
Ba 0.0612
Zn 0.0771
Cu 0.0120
Ni 0.419
Cd 0.067
Co 0.109
Mo 0.315
Mg 26.0
Mn 4.25
Fe 0.0230
END

SOLUTION 5 TUNNEL WATER 320-06
temp 22.6 #in lab
pH 6.84
pe -1.3 #BASED ON Eh MEASURED: $pe = Eh/0.059$
Alkalinity 0.642
units mg/L
density 1.00
Cl 18.7
F 1.150
S(6) 541 # Sulfate by chromatography
#N(5) 0.300

#N(-3) 0.100
 #C 14.2 #calculated from TOC and HCO3-
 K 9.09
 Na 44.4
 Ca 172
 Sr 2.21
 Si 7.85
 Al 0.004
 Ba 0.027
 Zn 0.0832
 Cu 0.0050
 Mo 0.016
 Mg 21.4
 Mn 1.32
 Fe 0.1730
 END

Ion balance for the different water samples

Cation versus anion balance according to;

$$\text{Percent error} = 100 * (\text{Cations} - \text{Anions}) / (\text{Cations} + |\text{Anions}|) \quad (\text{A4-3-1})$$

Table A4-3-1: Results at 22.6 °C. Ion balance within 5 % error is regarded as a good analysis

	Water 1 initial	Water 1 final	Water 2 initial	Water 2 final	Tunnel water 320-06
Balance (%)	44.72	4.28	4.47	0.54	3.72

The ion poor Water 1-initial had a poor balance, suggesting that an anion was missing in the analytical procedure.

Thermodynamic data from the hydro-geochemical data base llnl.dat

This database is one of several included in PHREEQC, and was chosen for two reasons 1) it contains very many phases relevant for studies at the ground water - concrete interface, and 2) it has been extensively used in modelling of concrete, reactive barrier, ground water systems. The following selected data were copied from the llnl.dat database. These phases were relevant to the investigation, some of which were present in the initial Alum Shale sample (cf. Table 8 in Chapter 6).

Anhydrite

```
CaSO4 = + 1.0000 Ca++ + 1.0000 SO4--
log_k      -4.3064
  -delta_H-18.577 kJ/mol # Calculated enthalpy of reaction  Anhydrite
#   Enthalpy of formation:  -342.76 kcal/mol
-analytic -2.0986e+002 -7.8823e-002 5.0969e+003 8.5642e+001 7.9594e+001
#   -Range: 0-300
```

Barite

```
BaSO4 = + 1.0000 Ba++ + 1.0000 SO4--
log_k      -9.9711
  -delta_H25.9408 kJ/mol # Calculated enthalpy of reaction  Barite
#   Enthalpy of formation:  -352.1 kcal/mol
-analytic -1.8747e+002 -7.5521e-002 2.0790e+003 7.7998e+001 3.2497e+001
#   -Range: 0-300
```

Bassanite

$\text{CaSO}_4 \cdot 0.5\text{H}_2\text{O} = + 0.5000 \text{H}_2\text{O} + 1.0000 \text{Ca}^{++} + 1.0000 \text{SO}_4^{--}$
 log_k -3.6615
 -delta_H-18.711 kJ/mol # Calculated enthalpy of reaction Bassanite
 # Enthalpy of formation: -1576.89 kJ/mol
 -analytic -2.2010e+002 -8.0230e-002 5.5092e+003 8.9651e+001 8.6031e+001
 # -Range: 0-300

C

$\text{C} + 1.0000 \text{H}_2\text{O} + 1.0000 \text{O}_2 = + 1.0000 \text{H}^+ + 1.0000 \text{HCO}_3^-$
 log_k 64.1735
 -delta_H-391.961 kJ/mol # Calculated enthalpy of reaction C
 # Enthalpy of formation: 0 kcal/mol
 -analytic -3.5556e+001 -3.3691e-002 1.9774e+004 1.7548e+001 3.0856e+002
 # -Range: 0-300

Calcite

$\text{CaCO}_3 + 1.0000 \text{H}^+ = + 1.0000 \text{Ca}^{++} + 1.0000 \text{HCO}_3^-$
 log_k 1.8487
 -delta_H-25.7149 kJ/mol # Calculated enthalpy of reaction Calcite
 # Enthalpy of formation: -288.552 kcal/mol
 -analytic -1.4978e+002 -4.8370e-002 4.8974e+003 6.0458e+001 7.6464e+001
 # -Range: 0-300

Fe(OH)₃

$\text{Fe(OH)}_3 + 3.0000 \text{H}^+ = + 1.0000 \text{Fe}^{+++} + 3.0000 \text{H}_2\text{O}$
 log_k 5.6556
 -delta_H-84.0824 kJ/mol # Calculated enthalpy of reaction Fe(OH)₃
 # Enthalpy of formation: -823.013 kJ/mol
 -analytic -1.3316e+002 -3.1284e-002 7.9753e+003 4.9052e+001 1.2449e+002
 # -Range: 0-300

Gypsum

$\text{CaSO}_4 \cdot 2\text{H}_2\text{O} = + 1.0000 \text{Ca}^{++} + 1.0000 \text{SO}_4^{--} + 2.0000 \text{H}_2\text{O}$
 log_k -4.4823
 -delta_H-1.66746 kJ/mol # Calculated enthalpy of reaction Gypsum
 # Enthalpy of formation: -2022.69 kJ/mol
 -analytic -2.4417e+002 -8.3329e-002 5.5958e+003 9.9301e+001 8.7389e+001
 # -Range: 0-300

Magnesite

$\text{MgCO}_3 + 1.0000 \text{H}^+ = + 1.0000 \text{HCO}_3^- + 1.0000 \text{Mg}^{++}$
 log_k 2.2936
 -delta_H-44.4968 kJ/mol # Calculated enthalpy of reaction Magnesite
 # Enthalpy of formation: -265.63 kcal/mol
 -analytic -1.6665e+002 -4.9469e-002 6.4344e+003 6.5506e+001 1.0045e+002
 # -Range: 0-300

Rhodochrosite

$\text{MnCO}_3 + 1.0000 \text{H}^+ = + 1.0000 \text{HCO}_3^- + 1.0000 \text{Mn}^{++}$
 log_k -0.1928
 -delta_H-21.3426 kJ/mol # Calculated enthalpy of reaction Rhodochrosite
 # Enthalpy of formation: -212.521 kcal/mol
 -analytic -1.6195e+002 -4.9344e-002 5.0937e+003 6.4402e+001 7.9531e+001
 # -Range: 0-300

A4-4 Contribution of Ca-sulfates and Fe-sulfides to aqueous sulfate

Tables A4-4-1 and A4-4-2 show the details of the model calculation in chapter 6.5.1.2. The results for both experimental waters compare very well (about 80 % sulfate derived from Ca-sulfate, i.e. primary anhydrite) whilst the tunnel water suggests a relatively higher contribution from the Fe-sulfides.

Table A4-4-1: Leaching experiment: Calculation of the sulfate contributions from gypsum/anhydrite and Fe-sulfides.

Water	Net production (final - initial). Units: mg/L. Derived from Table 7					
	Ca ²⁺	Mg ²⁺	Mn ²⁺	HCO ₃ ⁻		SO ₄ ²⁻
Water 1	426	16.9	3.03	97.1		1079
Water 2	487	16.2	3.66	60.1		1269

Ca from bicarbonate:		$Ca = \text{net HCO}_3^- \times (40.1/61.02 \times 2)$
Water 1	31.91	
Water 2	19.75	$CaCO_3 + CO_2 + H_2O \rightarrow Ca^{2+} + 2HCO_3^-$ (Reaction 16)

Ca from gypsum/anhydrite:		$Ca_{Gy/anh}^{2+} = \text{net Ca}^{2+} - Ca_{Cc}^{2+}$
Water 1	394.09	
Water 2	467.25	

SO ₄ ²⁻ from gypsum/anhydrite		$SO_{4\ Gy/anh}^{2-} = Ca_{Gy/anh} \times (90.06/40.1)$
Water 1	885.09	
Water 2	1049.40	

SO ₄ ²⁻ from Fe- sulfides:		$SO_{4\ Fe-sulfides}^{2-} = \text{net SO}_4^{2-} - SO_{4\ Gy/anh}^{2-}$
Water 1	193.91	
Water 2	219.60	

SO ₄ ²⁻ from gypsum/anhydrite and Fe- sulfides:		
	% Gy/anh	% pyrite/pyrrh
Water 1	82.03	17.97
Water 2	82.69	17.31

Table A4-4-2: Tunnel water. Calculation of the sulfate contributions from gypsum/anhydrite and Fe-sulfides.

*) Net calculated using ion poor Water 1 as model for ground water starting material

Water	Net production (final - initial). Units: mg/L. Derived from Table 7					
	Ca ²⁺	Mg ²⁺	Mn ²⁺	HCO ₃ ⁻		SO ₄ ²⁻
Tunnel water	168	21	1.32	50		540

Ca from bicarbonate:	$Ca = \text{net } HCO_3^- \times (40.1/61.02 \times 2)$
Tunnel water	16.43

Ca from gypsum/anhydrite:	$Ca^{2+}_{Gy/anh} = \text{net } Ca^{2+} - Ca^{2+}_{Cc}$
Tunnel water	151.57

SO ₄ ²⁻ from gypsum/anhydrite:	$SO_4^{2-} \text{Gy/anh} = Ca_{Gy/anh} \times (90.06/40.1)$
Tunnel water	340.41

SO ₄ ²⁻ from Fe- sulfides:	$SO_4^{2-}_{Fe-sulfides} = \text{net } SO_4^{2-} - SO_4^{2-}_{Gy/anh}$
Tunnel water	199.59

SO ₄ ²⁻ from gypsum/anhydrite and Fe- sulfides:	
	$\% \text{ pyrite/pyrrh}$
Tunnel water	36.96

A4-5 Images of tunnel water with bacterial slime and Alum Shale sample



Figure A4-5-1: Svartdal tunnel water sample 320-06 and rusty and dark bacterial slime was collected from this pond just beneath the Alum Shale core sample station (before drilling).



Figure A4-5-2: Svartdal tunnel Alum Shale core sample 320-06U after first manual crushing, representing a pure Black Shale without secondary calcite vein material.

A4-6 Microbes found in the Alum Shale environment

In Chapter 6 it was inferred that bacterial matter depicted in Figure 2, represent *Acidithiobacillus sp.* The evidence was mainly the shape and size as well as the Alum Shale environment and influence of sulfide oxidation within the Svartdal tunnel, which is regarded as a typical environment for *Acidithiobacillus sp.* The colour of the biofilm material was rusty brown. The shapes of bacteria were rod-like to coccoidal (1-2 μm), sometimes forming apparent “networks” where individual rods seemed to have grown into each other (Chapter 6, Figure 2B). This resembles some features in Konhauser (2007; Figure 5.13 page 216). The chemistry of the biofilm material (Chapter 6) involved high levels of Fe (34-36 atomic %), but little S (0.22-0.51 atomic %). Si (about 3 atomic %, reflecting β -cristobalite, see Table A4-2-1), a little Al, Mg, Ca, N and P were detected along with small amounts of Co, Cd, As and Pb.

According to “Bergey’s Manual of systematic bacteriology” (2005) and other literature this is compatible with *Acidithiobacillus sp.* However, it must be admitted that also other bacteria may share similar features, and the present evidence must therefore be regarded as permissive only. Future investigations should take advantage of DNA-fingerprinting and rigorous identification of all microorganisms associated with the Alum Shale, notably also the possibility that Sulfate Reducing Bacteria (SRB) occur with the rock mass (as was concluded from the stable isotope study).

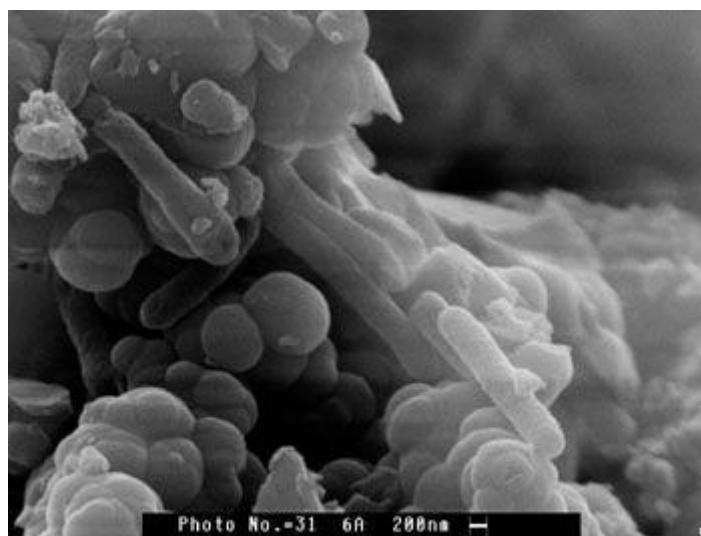


Figure A4-6-1: *Acidithiobacillus ferrooxidans* as seen in SEM (Secondary electron mode).

Source:

<http://www.educa.madrid.org/web/cc.nsdelasabiduria.madrid/Ejercicios/2b/Biologia/Microbiologia/biolixiviacion.htm>

Appendix 5: Additional documentation to Chapter 7

- A5-1 Results from Scanning Electron Microscopy (SEM)**
- A5-2 Results from X-ray diffraction (XRD)**
- A5-3 Results from Electron Microprobe Analysis (EMPA)**
- A5-4 Images of tunnel concrete and biota**
- A5-5 Summary of concrete samples with systematic petrography**
- A5-6 Microbes found in the subsea environment**
- A5-7 Mn L-edge spectra and STXM**

A5-1 Results from Scanning Electron Microscopy (SEM)

SEM – data files at the Museum of Natural History (NHM), University of Oslo.

The following SEM results on sub samples arranged according to the same system as in Chapter 7. Most SEM samples were picked from the outer surface (O) of the concrete cores; a few were from the rock/concrete interface (I). The sample numbers refer to results summarised in A5-5, and analyses of additional samples (marked with *) reported in Tables 5, 6 and 7. Mn-bacteria resembled taxonomical features of *Leptothrix discophora*.

Table A5-1-1: Oslofjord subsea tunnel. Summary of SEM work and related NHM-files.

Sample no.	Reference to Chapter 7	NHM-files
<i>Oslofjord 1b: Focused cement paste destruction associated with Mn-Fe biofilm</i>		
Mn-Fe 1-05*	<i>Leptothrix discophora</i> ? “nest”, <i>Gallionella f.</i> (Table 5)	Hve 2005-11-08 03.17.09.doc
--“--*	Mn-platelets with Mn & Fe bacteria (Table 5)	Hve 2005-11-08 03.15.26.doc
--“--*	Mn-platelets with Mn & Fe bacteria (Table 6)	Hve 2005-11-07 23.45.43.doc
Mn-Fe 3*	Mn platelet with “nest” (Table 5)	Hve 2005-11.07 02.48.17.doc
Kj-I-1B*	Aged Mn-oxide crust material (Table 6)	Hagelia 2005-05-09 12.55.26.doc
0-2005*	<i>Gallionella ferruginea</i> (Table 6)	Hagelia 2005-04-27.11.53.20.doc
Kj-II-1 (O)	<i>Gallionella ferruginea</i> (A5-5)	Hagelia 2005-09-15 15.49.57.doc
Kj-II-4 (O)	Gypsum (A5-5)	Hagelia 2005-05-10 13.50.13.doc
Armeringsjern*	Uncorroded steel fibre; Fe \approx 97.5 wt %, Mn \approx 1.5 wt %	Hagelia 2005-04-27 10.54.53.doc
<i>Oslofjord 2a: Cement paste deterioration with Mn –(Fe) biofilm</i>		
Kj 1-1	<i>Leptothrix discophora</i> (?) in Mn crust (A5-5)	Hagelia 2005-04-25 10.28.25.doc
<i>Oslofjord 2c: Severe cement paste destruction with Mn-Fe biofilm</i>		
V6*	<i>Leptothrix ochracea</i> (rusty bacterial slime in pond beneath concrete surface with Mn & Fe bacteria)	Hagelia 2005-11-30 03.35.13.doc

Table A5-1-2: Freifjord subsea tunnel. Summary of SEM work and related NHM-files,

Sample no.	Reference to Chapter 7	NHM-files
Frei 10-06*	Gypsum (Table 7)	Hagelia 2006-09-24 23.02.13.doc
--“--	Carbon rib (--“--)	Hagelia 2006-09-24 22.58.24.doc
6150 (I)	Mellite like carboxylate (Table 8)	Hagelia 2009-02-25 10.38.15.doc
--“--	--“-- (--“--)	Hagelia 2009-02-25 10.46.23.doc

A5-2 Results from X-ray diffraction (XRD)

XRD- data files at Museum of Natural History (NHM), University of Oslo.

The sample numbers, full mineral contents and file names are given in the table below. Sample names correspond to the cores, slabs or related material they were taken from. Locations are the ones described in Chapter 7 and a few additional samples from these tunnels. The relationship to transformed layers (Fig. 1 in this chapter) is indicated by I = interface with rock mass; A = inner deteriorated domain, C = outer deteriorated domain and O = outer surface. Presence of amorphous phases was indicated by high irregular background combined with generally low counts. The clay mineral dickite (#), being a variety with a HCONH₂ group, was found on several outer surfaces in association with organic Mn-Fe biofilms/crusts.

Appendices – Subsea environment

Table A5-2-1: Oslofjord subsea tunnel. Summary of XRD results from samples referred to in Chapter 7, except from *) = additional samples. ID is file number at NHM.

Sample	Minerals: amorphous phases indicated by high back ground	ID
Oslo 1b		
H 2004b (C)	Aragonite, thenardite, calcite, quartz	090505h2004b.RAW
Oslo 1a		
* Mn-Fe 1-05 bulk bacterial slime (O)	Amorphous Mn- and Fe-compounds with Na-buserite and some todorokite (rusty = <i>Gallionella sp.</i> ; black = <i>Leptothrix sp.</i>)	071105 MnFe1.RAW
* 1-06 (C-O)	Thaumasite, calcite, quartz (<u>white deposit</u> on concrete near Mn-Fe 1)	130606 1_06.RAW
* 2-06 (C)	Na-buserite, brushite (<u>brown deposit</u> within Mn-Fe slime)	120606 2_06.RAW
* 4-06 (C)	Aragonite, Mg-calcite (<u>debris</u> behind Mn-Fe crusts/slime)	130606 4_06.RAW
* 5-05 (C)	Gypsum, calcite, thaumasite, brucite, quartz, albite (<u>debris</u> behind Mn-Fe crusts/slime)	130606 5_06.RAW
Kj I-1A (O)	Calcite, todorokite, manganosite & amorphous Mn- & Fe compounds (<u>outer rusty, dark and whitish</u> crust material)	100505KJI .RAW
Kj I-1B (O)	Calcite, todorokite, hydrous Ca-todorokite, hydrous Na-todorokite, manganosite, rhodochrosite & Mn- & Fe amorphous (--“--)	100505KJI 1B.RAW
Kj II-1 (O)	Calcite, magnesite, quartz	26042005kjII-1.RAW
Kj III (O)	Brucite, aragonite, calcite, albite, quartz	081105 kj III ytre.RAW
Kj V (O)	Buserite (?) calcite, quartz, microcline, anorthoclase	161105 Kj V ytre.RAW
Kj V-1 (O)	Aragonite, Mg-calcite, quartz, anorthite	100505KJV-1.RAW
Kj V-2 (O)	Mg-calcite, <u>dickite #</u> , quartz, plagioclase, rutile	220705 kj V 2.RAW
* SB2005 Gallionella slime: 125-45 µm (O)	Amorphous Fe- and Mn-oxide compounds with traces of buserite; albite (outer thick <u>rusty slime</u> along water stream B collected just beneath Core Kj I, Fig. 3 in Chapter 7)	081105 sb2005.RAW
* SB2005 particles: >125 µm (O)	Bixbyite, marcasite, quartz, anorthite, anorthoclase (<u>the sample was dried at room T</u>).	301105 SB2005 rest.RAW
Oslo 2a		
Kj 1-1 (O)	Buserite (?), todorokite, thaumasite (?), quartz, amorphous Mn (dark crust)	240405kj1-1.RAW
Kj 5-1 (I)	Aragonite, calcite, quartz, plagioclase (white deposit)	290405 kj5-1.RAW
Kj 5-2 (O)	Birnessite, amorphous Fe-compound, calcite, quartz, (<u>rusty domain</u> with dark and white material)	26042005kj5-2.RAW
Oslo 2b		
Kj 9-1 (O)	Todorokite (?), quartz, albite, microcline	27042005kj9-1.RAW
Kj 9-2 (I)	Brucite, aragonite, calcite, magnesite, quartz, Fe-chlinochlore	26042005kj9-2.RAW
Kj 10 (I)	Brucite, calcite, quartz (white)	26042005kj10-1.RAW
* Kj 8 (I)	Brucite, aragonite, quartz (white)	kjerne 8.RAW
* FF (O-C)	Gypsum, calcite, aragonite, quartz, plagioclase (grey degraded paste)	sement f-f.RAW
* FH (O)	<u>Dickite #</u> , calcite, todorokite (?), quartz, plagioclase (grey)	sement f-h.RAW
Oslo 2c		
Spall V5/ FV-5 (O-C)	Calcite, aragonite, sodium calcium sulfate hydrate, thenardite, quartz	100505FV-5.RAW
SpallV5-2 (C)	Buserite, birnessite, albite, quartz	301105oslo2.RAW
SpallV5-3 (C)	Birnessite, amorphous Fe compound, quartz, anorthite, albite (<u>50-60 mm below outer surface</u> in very friable concrete)	240605 Oslo 3.RAW
SementFV5 (O-C)	Calcite, gypsum, thenardite, quartz, microcline (degraded <u>rust stained cement paste</u> , from near Spall V5)	Sement fv5.RAW
V6 IIa organic	Halite, Mg-calcite, amorphous Fe compound with <i>Leptothrix ochracea</i> from below Spall V5 (<u>dried at room T</u>).	301105V6II organisk.RAW
Chainage 11777		
* A33 stalactite (O)	Calcite, brucite, aragonite (collected from stalactite material leached under strong influence of saline ground water and Mn-Fe biofilm)	sement A33.RAW

Table A5-2-2: Freifjord subsea tunnel. Summary of XRD results from samples in Chapter 7, except from *) = additional samples. ID is file number at NHM

Sample	Minerals: amorphous in organic rich with high back ground	ID
* Frei 3-06	Buserite, dickite #, vermiculite, quartz, plagioclase	290606 frei 3 06.RAW
* Frei 6-06	Gypsum, crystalline carbon (no fluorescence in Black light blue)	290606 frei 6 06.RAW
* Frei 8-06	Gypsum, crystalline carbon (no fluorescence in Black light blue)	290606 frei 8 06.RAW
* Frei 10-06	Gypsum, crystalline carbon (no fluorescence in Black light blue)	290606 frei 10 06.RAW
5800-a (O)	Ammonium iron sulfate, biotite (=var. annite) (brown outer skin)	110804hagelia 5800-a.RAW
5800-b (O)	Gypsum, quartz (white material on corroded steel fibre)	170804hagelia5800-b.RAW
6150-a (A)	Aragonite, calcite, nordstrandite, brucite (white deposit with pinkish- white in Black light blue)	170804hagelia6150-a.RAW
6150-b (A)	Aragonite, quartz, plagioclase (amber-coloured deposit with creamy -yellow fluorescence in Black light blue)	170804hagelia6150-b.RAW
6150-c (I)	Calcite, laumontite, Ca-Al-Fe oxide, quartz, and possible phenyl phosphate hydrate with Al, Ni or Co (grey deposit on crack entering rock mass)	170804hagelia6150-c.RAW
6150-d (O)	Brushite, gypsum (deposit on severely corroded steel fibre)	100804-Hagelia-6150-d.RAW
6150-e (A)	Brushite, Fe-hydrogen phosphate, Fe-hydrogen phosphate hydrate, Na-Fe-phosphate, giniite, plagioclase (--“--)	100804-Hagelia-6150-e.RAW
CORROSION PRODUCTS FROM CORES NOT DESCRIBED IN CHAPTER 7:		
6935-1a (O)	Goethite, lepidochrosite and amorphous Fe comp. (steel fibre corrosion product)	100804-Hagelia-6935-1a.RAW
6935-1b (I)	Goethite, lepidochrosite and amorphous Fe comp. (steel fibre corrosion product)	100804-Hagelia-6935-1b.RAW

Table A5-2-3: Flekkerøy subsea tunnel. Summary of XRD results. ID is file number at NHM

Sample	Minerals: amorphous in organic rich with high back ground	ID
1373 (I)	Na- bisulfate, calcium oxide, calcium silicate hydroxide, ferrite, calcite, margarite, quartz (interfacial pale deposit)	010405sement1373C.RAW
1374 (I)	Brucite, calcite, quartz, margarite (interfacial white deposit)	010405sement1374.RAW
F8-1373 1 st stage	Gypsum (brown crystals)	160806 1786.RAW
F8-1373 2 nd stage	Gypsum, minor carbon (brown ochre, high back ground: some amorphous)	160806 1786b.RAW
F8-1373 3 rd stage	Gypsum clear crystals (Identified in thin section at Norwegian Public Roads Administration)	(No XRD)

Selected XRD diffractograms (overleaf)

Oslofjord subsea tunnel

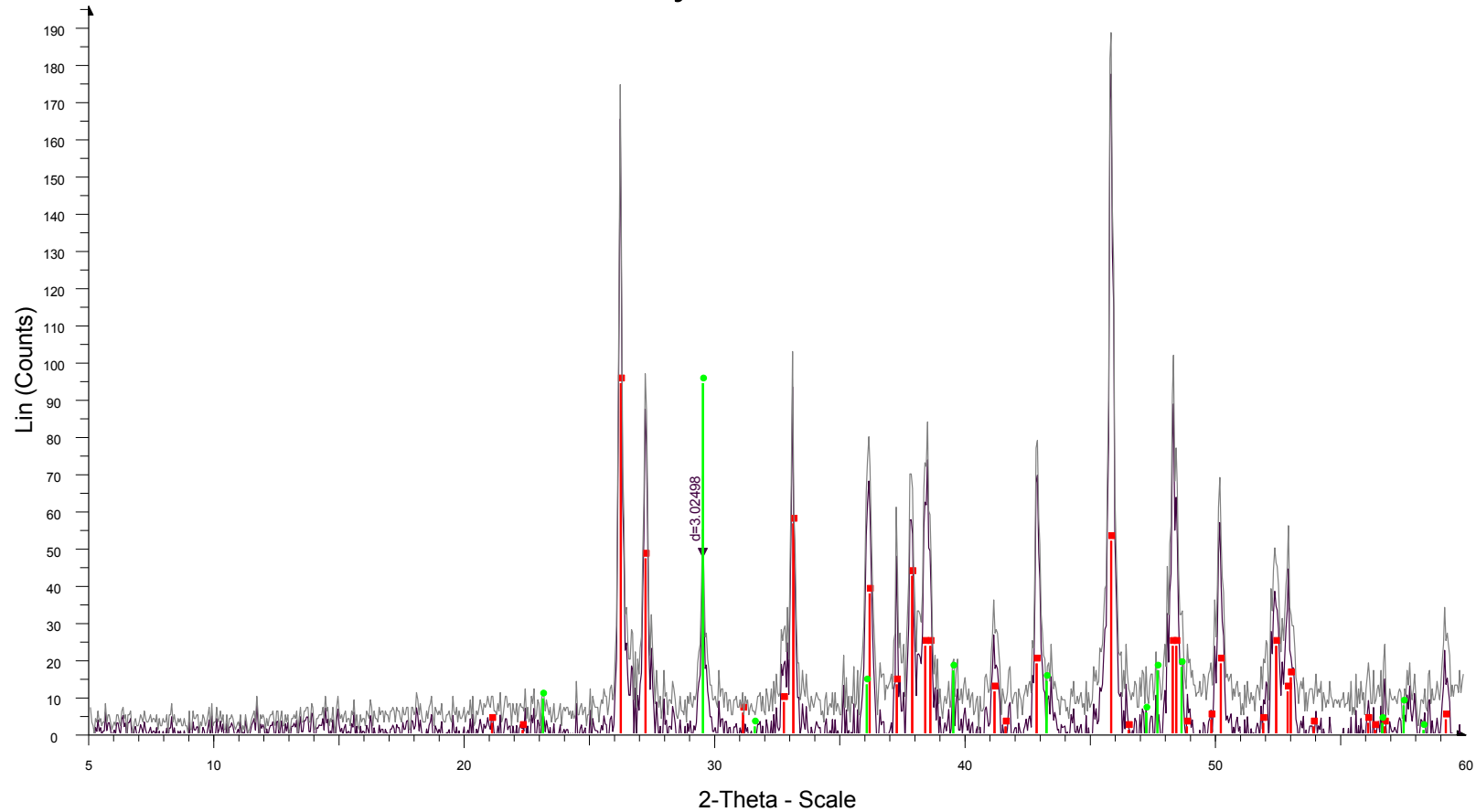
Freifjord subsea tunnel

Flekkerøy subsea tunnel

Appendices – Subsea environment

Locality 1a Oslofjord subsea tunnel. Concrete debris underneath Mn-Fe biofilm:

4-06 lyst i litt brunt



4-06 lyst i litt brunt - File: 130606 4_06 .RAW - Type: 2Th/Th locked - Start: 5.000 ° - End: 60.000 ° - Step: 0.050 ° - Step time: 1. s - Temp.: 25 °C (Room) - Time Started: 7 s - 2-Theta: 5.000 ° - Theta: 2.500 ° - Phi: Operations: Import

4-06 lyst i litt brunt - File: 130606 4_06 .RAW - Type: 2Th/Th locked - Start: 5.000 ° - End: 60.000 ° - Step: 0.050 ° - Step time: 1. s - Temp.: 25 °C (Room) - Time Started: 7 s - 2-Theta: 5.000 ° - Theta: 2.500 ° - Phi: Operations: Background 1.202,1.000 | Import

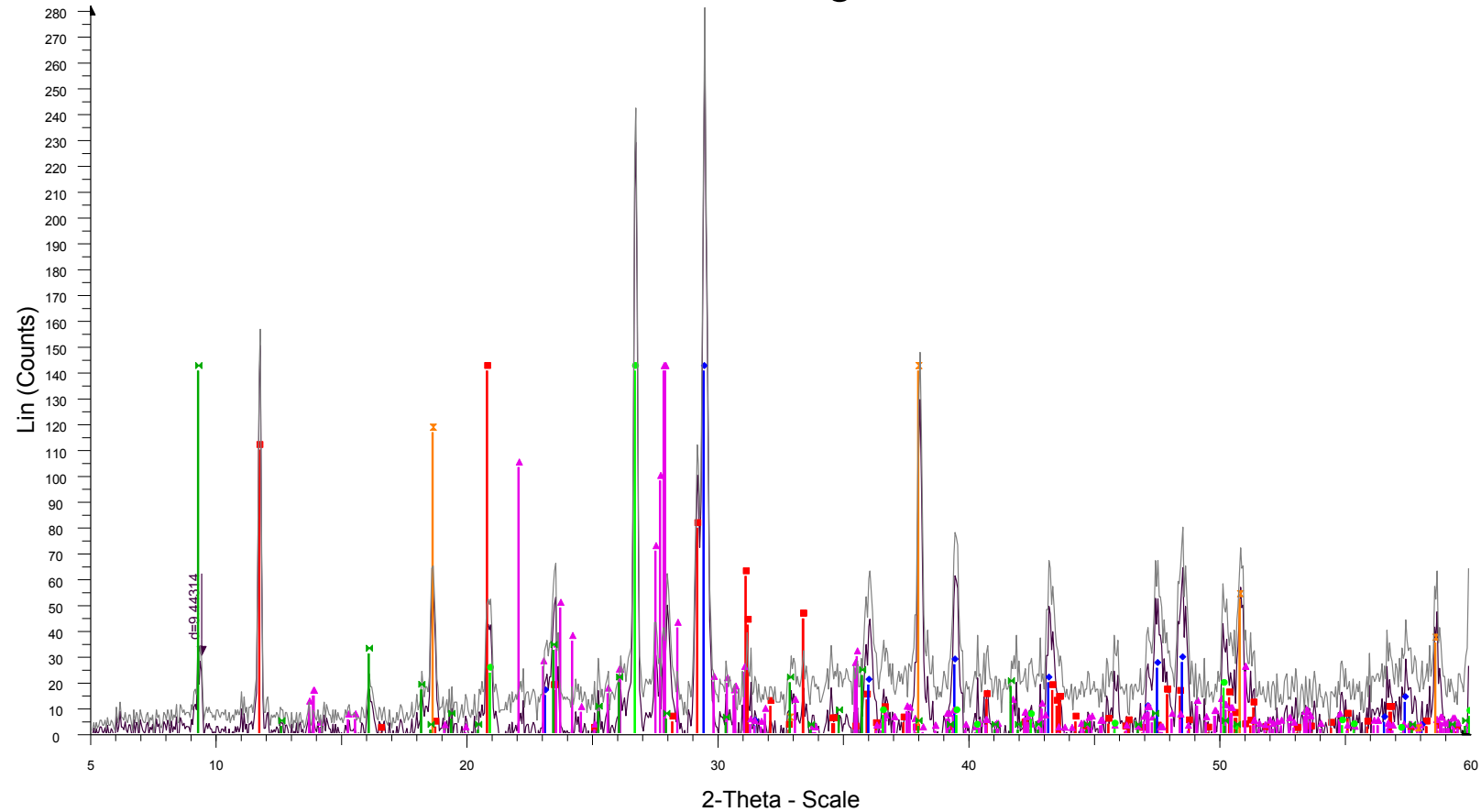
00-041-1475 (*) - Aragonite - CaCO₃ - Y: 50.00 % - d x by: 1. - WL: 1.5406 - Orthorhombic - I/lc PDF 1. - S-Q 75.7 % -

01-089-1304 (C) - Magnesium calcite, syn - (Mg_{0.03}Ca_{0.97})(CO₃) - Y: 50.00 % - d x by: 1. - WL: 1.5406 - Rhombo.R.axes - I/lc PDF 3.1 - S-Q 24.3 % -

Appendices – Subsea environment

Locality 1a Oslofjord subsea tunnel. Concrete debris underneath Mn-Fe biofilm:

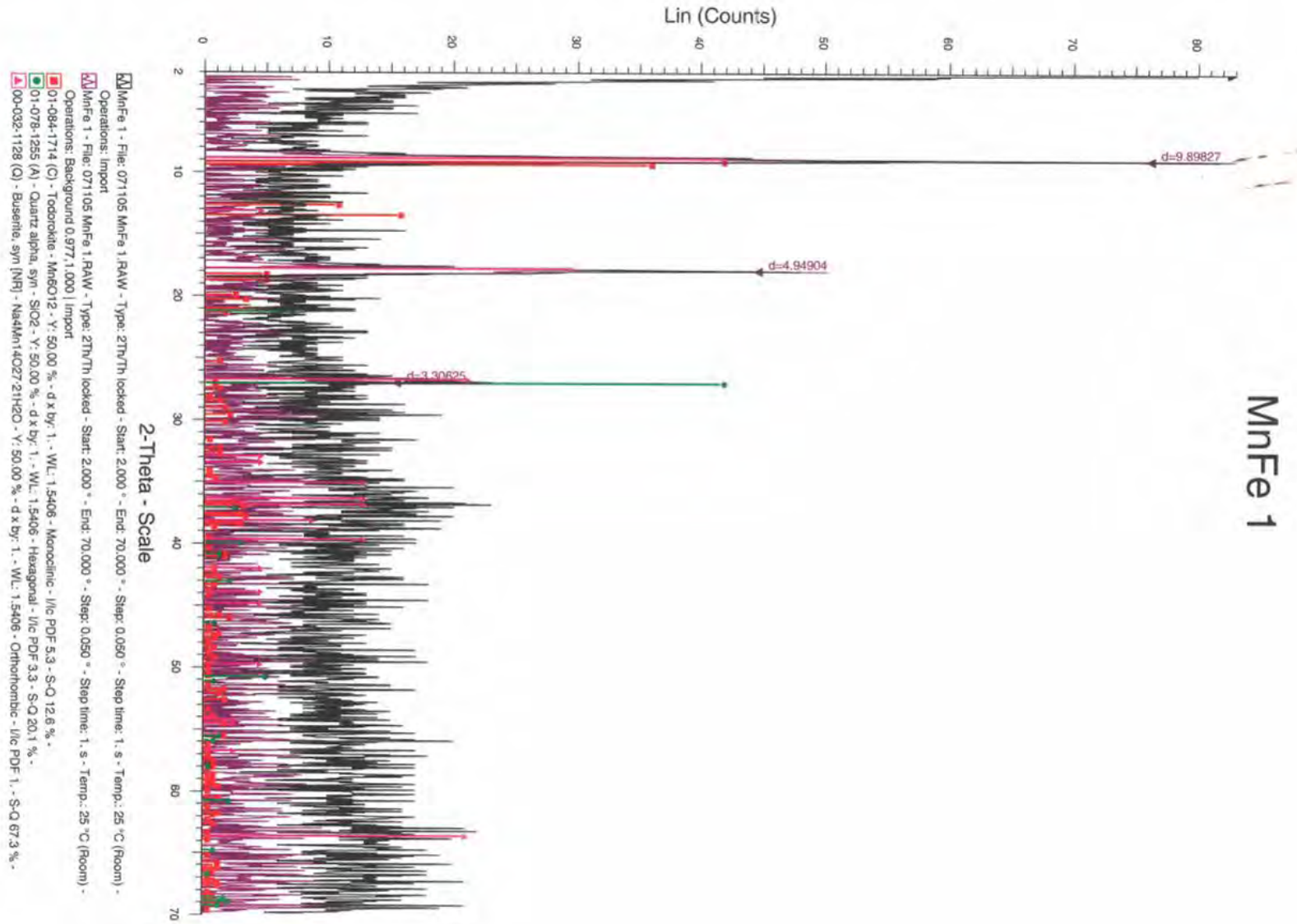
5-06 mørk/grå



- 5-06 mørk/grå - File: 130606 5_06 .RAW - Type: 2Th/Th locked - Start: 5.000 ° - End: 60.000 ° - Step: 0
Operations: Import
- 5-06 mørk/grå - File: 130606 5_06 .RAW - Type: 2Th/Th locked - Start: 5.000 ° - End: 60.000 ° - Step: 0
Operations: Background 0.309,1,000 | Import
- 01-074-1904 (C) - Gypsum - $\text{Ca}(\text{SO}_4)(\text{H}_2\text{O})_2$ - Y: 50.00 % - d x by: 1. - WL: 1.5406 - Monoclinic - a 5.68
 - 01-072-1214 (C) - Calcite, syn - CaCO_3 - Y: 50.00 % - d x by: 1. - WL: 1.5406 - Rhombo.H.axes - a 4.98
 - 01-083-1658 (C) - Albite high - $(\text{K}_0.22\text{Na}_0.78)(\text{AlSi}_3\text{O}_8)$ - Y: 50.00 % - d x by: 1. - WL: 1.5406 - Triclinic -
 - 01-078-1253 (A) - Quartz alpha, syn - SiO_2 - Y: 50.00 % - d x by: 1. - WL: 1.5406 - Hexagonal - a 4.9120
 - 01-083-0114 (C) - Brucite - $\text{Mg}(\text{OH})_2$ - Y: 50.00 % - d x by: 1. - WL: 1.5406 - Hexagonal - I/c PDF 2.2 -
 - 00-046-1360 (*) - Thaumasite - $\text{Ca}_3\text{Si}(\text{OH})_6[\text{CO}_3][\text{SO}_4]\cdot 12\text{H}_2\text{O}$ - Y: 50.00 % - d x by: 1. - WL: 1.5406 -

Appendices – Subsea environment

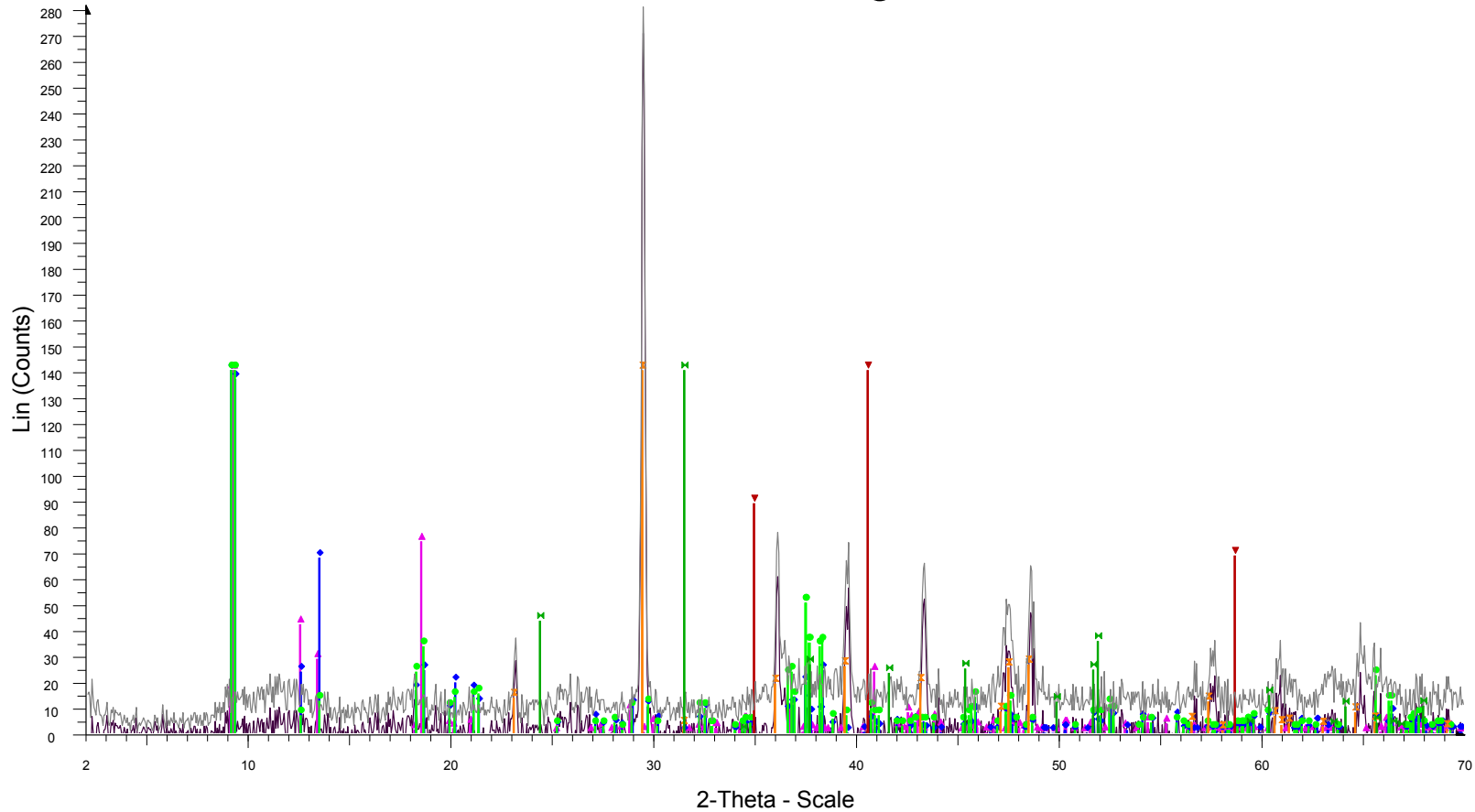
Locality 1a Oslofjord subsea tunnel. Soft Mn –rich slime (*Leptothrix discophora?*) with Mn-platelets:



Appendices – Subsea environment

Locality 1a Oslofjord subsea tunnel. Aged and recrystallised Mn crust material:

KJI-1B utfelling



☒ KJI-1B utfelling - File: 100505KJI 1B.RAW - Type: 2Th/Th locked - Start: 2.000 ° - End: 70.000 ° - Step: Operations: Import
☒ KJI-1B utfelling - File: 100505KJI 1B.RAW - Type: 2Th/Th locked - Start: 2.000 ° - End: 70.000 ° - Step: Operations: Background 1.445,1.000 | Import

☒ 01-071-3699 (*) - Calcite, syn - $\text{Ca}(\text{CO}_3)$ - Y: 50.00 % - d x by: 1. - WL: 1.5406 - Rhombo.H.axes - a 4.9
☒ 01-086-0173 (A) - Rhodochrosite, syn - $\text{Mn}(\text{CO}_3)$ - Y: 50.00 % - d x by: 1. - WL: 1.5406 - Rhombo.H.axes

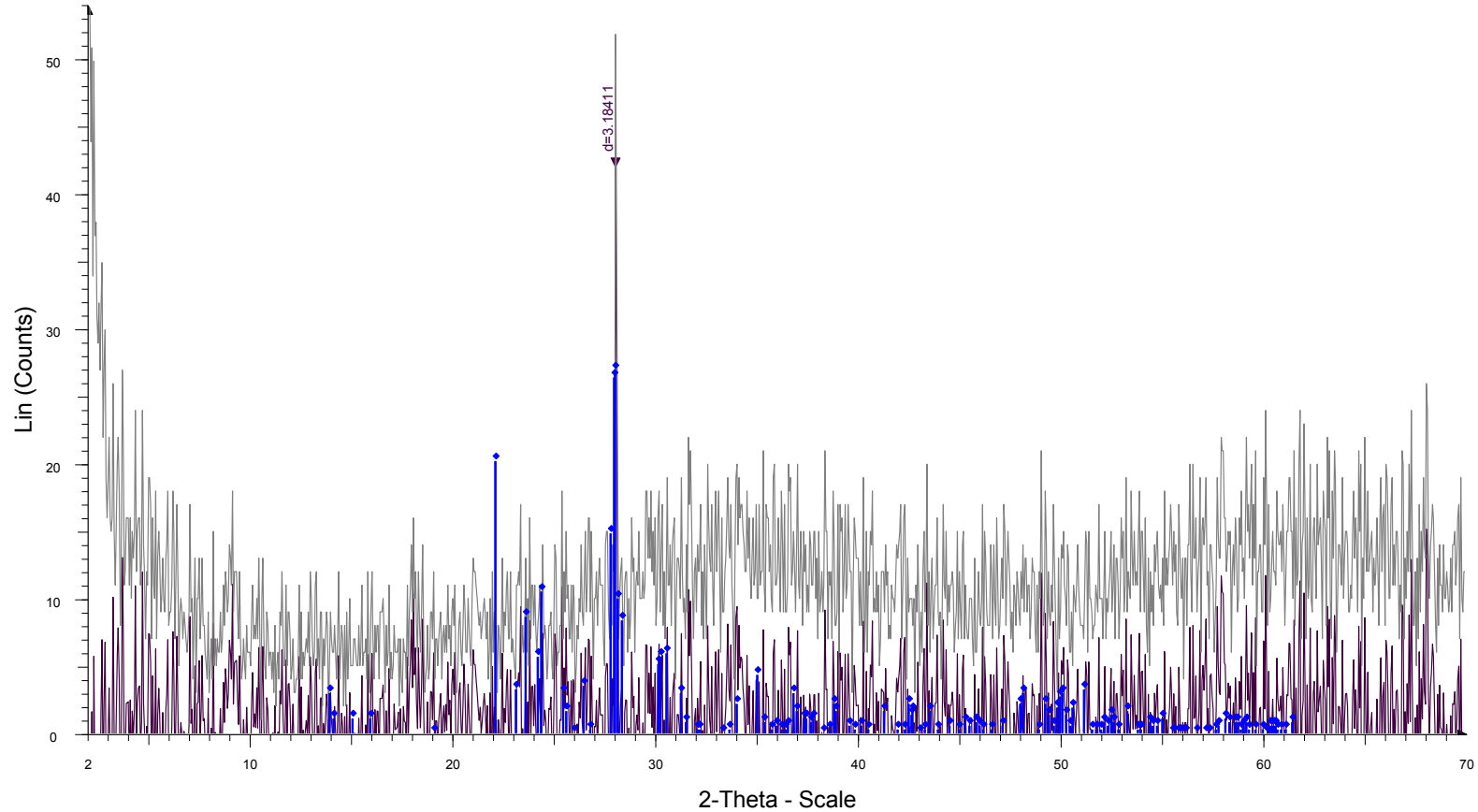
☒ 01-087-0389 (N) - Todorokite - $\text{Ca}_0.8(\text{Mn}_4\text{O}_8)(\text{H}_2\text{O})_2$ - Y: 50.00 % - d x by: 1. - WL: 1.5406 - Monoclinic
☒ 01-084-1712 (I) - Todorokite - $\text{Mn}_6\text{O}_{12}(\text{H}_2\text{O})_3 \cdot 16$ - Y: 50.00 % - d x by: 1. - WL: 1.5406 - Monoclinic - a
☒ 00-038-0475 (I) - Todorokite - $\text{NaMn}_6\text{O}_{12} \cdot 3\text{H}_2\text{O}$ - Y: 50.00 % - d x by: 1. - WL: 1.5406 - Monoclinic - a 9
☒ 01-075-1090 (*) - Manganosite, syn - MnO - Y: 50.00 % - d x by: 1. - WL: 1.5406 - Cubic - a 4.44600 - b

Appendices – Subsea environment

Locality 1a Oslofjord subsea tunnel.

Soft slime of heavily Fe encrusted *Gallionella ferruginea* (within biofilm). Sieve fraction 0.45 – 125 μm :

SB2005



SB2005 - File: 081105 sb2005.RAW - Type: 2Th/Th locked - Start: 2.000 ° - End: 70.000 ° - Step: 0.050 ° - Step time: 1. s - Temp.: 25 °C (Room) - Time Started: 7 s - 2-Theta: 2.000 ° - Theta: 1.000 ° - Phi: 0.00 ° - A
Operations: Import

SB2005 - File: 081105 sb2005.RAW - Type: 2Th/Th locked - Start: 2.000 ° - End: 70.000 ° - Step: 0.050 ° - Step time: 1. s - Temp.: 25 °C (Room) - Time Started: 7 s - 2-Theta: 2.000 ° - Theta: 1.000 ° - Phi: 0.00 ° - A
Operations: Background 2.138,1.000 | Import

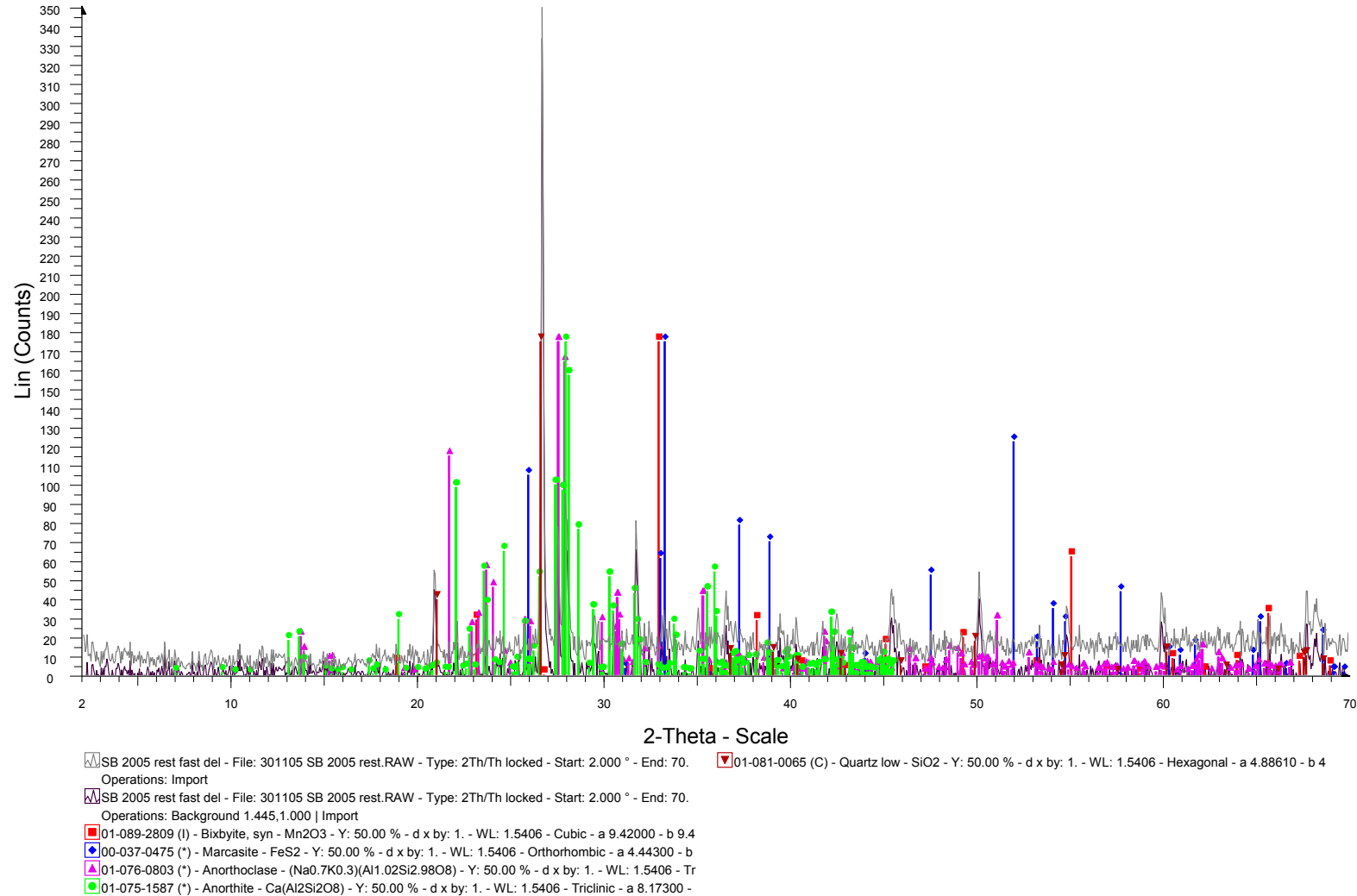
01-076-0758 (C) - Albite low - Na1.09(Al1.09Si2.91O8) - Y: 50.00 % - d x by: 1. - WL: 1.5406 - Triclinic - I/Ic PDF 0.7 - S-Q 100.0 % -

Appendices – Subsea environment

Locality 1a Oslofjord subsea tunnel.

Soft slime of heavily Fe encrusted *Gallionella ferruginea* (within biofilm): Sieve fraction >125 µm:

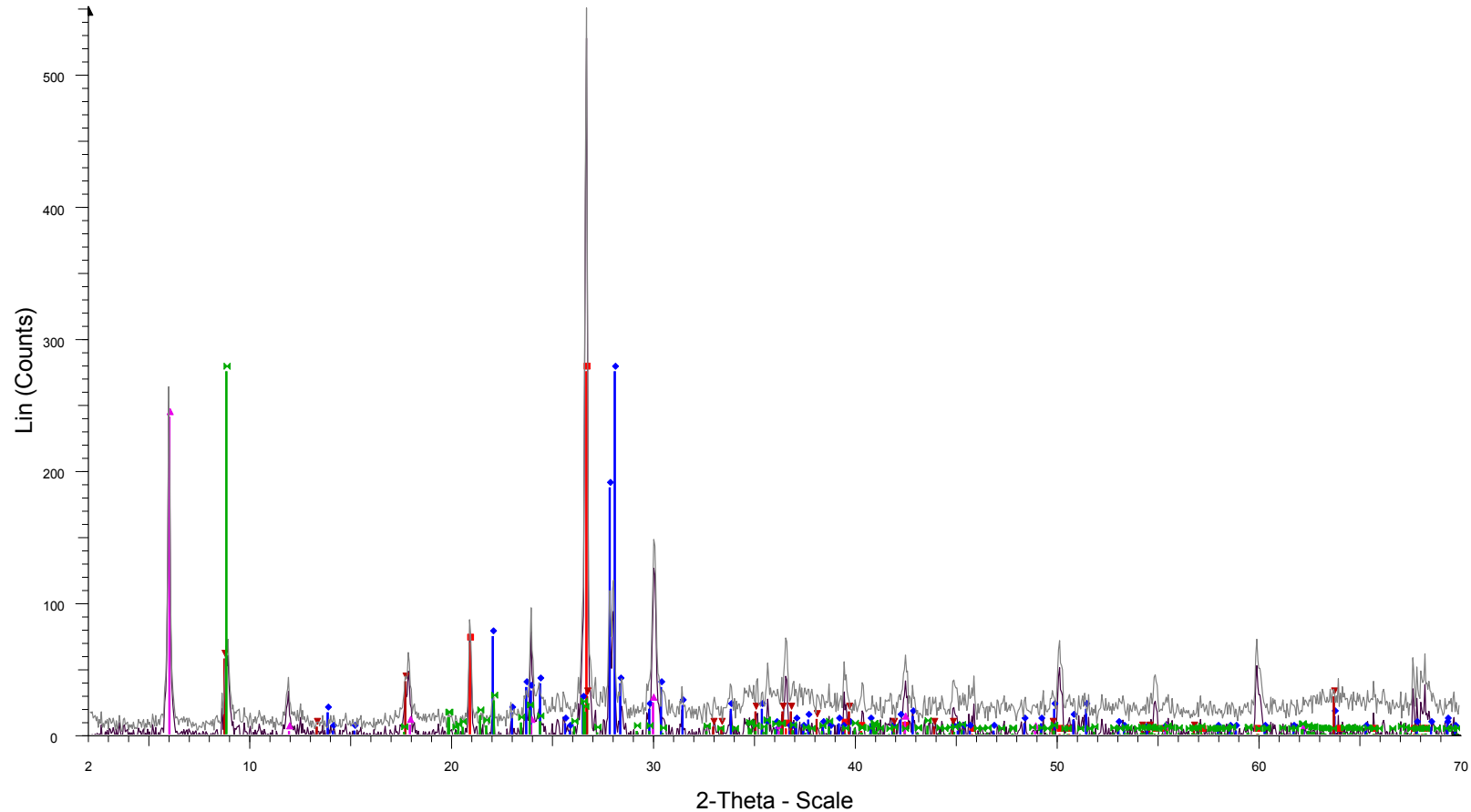
SB 2005 rest fast del



Appendices – Subsea environment

Freifjord subsea tunnel. Concrete debris with Gallionella ferruginea and Mn-bacteria:

Frei 3-06



Frei 3-06 - File: 290606 frei 3 06.RAW - Type: 2Th/Th locked - Start: 2.000 ° - End: 70.000 ° - Step: 0.05 01-074-1758 (C) - Dickite - Al₂Si₂O₅(OH)₄(HCONH₂) - Y: 50.00 % - d x by: 1. - WL: 1.5406 - Monoclinic
Operations: Import

Frei 3-06 - File: 290606 frei 3 06.RAW - Type: 2Th/Th locked - Start: 2.000 ° - End: 70.000 ° - Step: 0.05
Operations: Background 1.778,1.000 | Import

01-085-0335 (C) - Quartz low - SiO₂ - Y: 50.00 % - d x by: 1. - WL: 1.5406 - Hexagonal - a 4.91340 - b 4

00-041-1480 (I) - Albite, Ca-rich, ordered - (Na,Ca)Al(Si,Al)₃O₈ - Y: 50.00 % - d x by: 1. - WL: 1.5406 - T

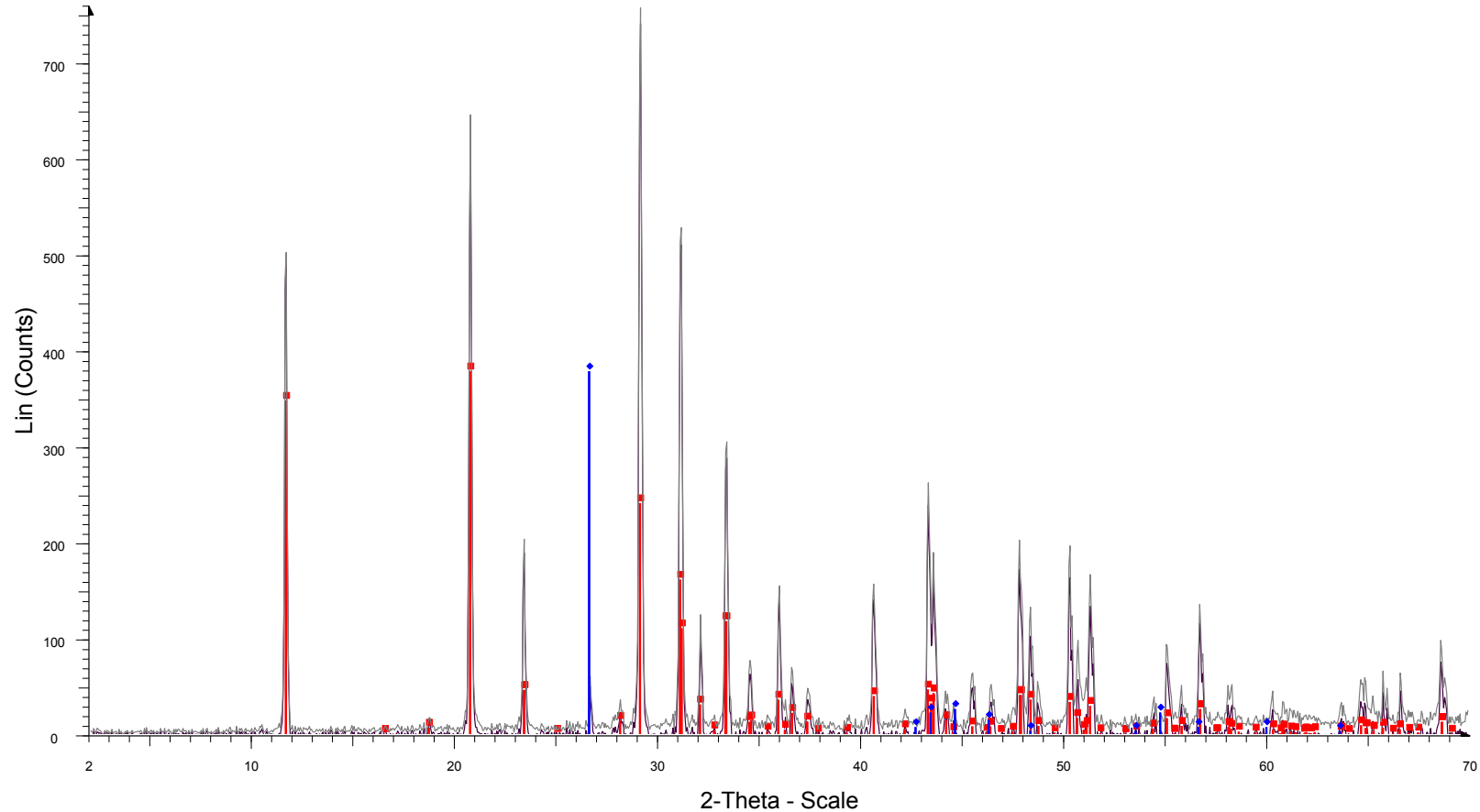
00-029-1235 (N) - Sodium Magnesium Iron Aluminum Silicate Hydroxide - Na_{0.5}(Mg,Fe,Al)₃(Si,Al)₄O₁₀(

00-032-1128 (Q) - Buserite, syn [NR] - Na₄Mn₁₄O₂₇·21H₂O - Y: 10.42 % - d x by: 1. - WL: 1.5406 - Ort

Appendices – Subsea environment

Freifjord subsea tunnel. Gypsum mush with crystalline carbon from outer concrete surface:

Frei 10-06



Frei 10-06 - File: 290606 frei 10 06.RAW - Type: 2Th/Th locked - Start: 2.000 ° - End: 70.000 ° - Step: 0.050 ° - Step time: 1. s - Temp.: 25 °C (Room) - Time Started: 5 s - 2-Theta: 2.000 ° - Theta: 1.000 ° - Phi: 0.00 °
Operations: Import

Frei 10-06 - File: 290606 frei 10 06.RAW - Type: 2Th/Th locked - Start: 2.000 ° - End: 70.000 ° - Step: 0.050 ° - Step time: 1. s - Temp.: 25 °C (Room) - Time Started: 5 s - 2-Theta: 2.000 ° - Theta: 1.000 ° - Phi: 0.00 °
Operations: Background 11.220,1.000 | Import

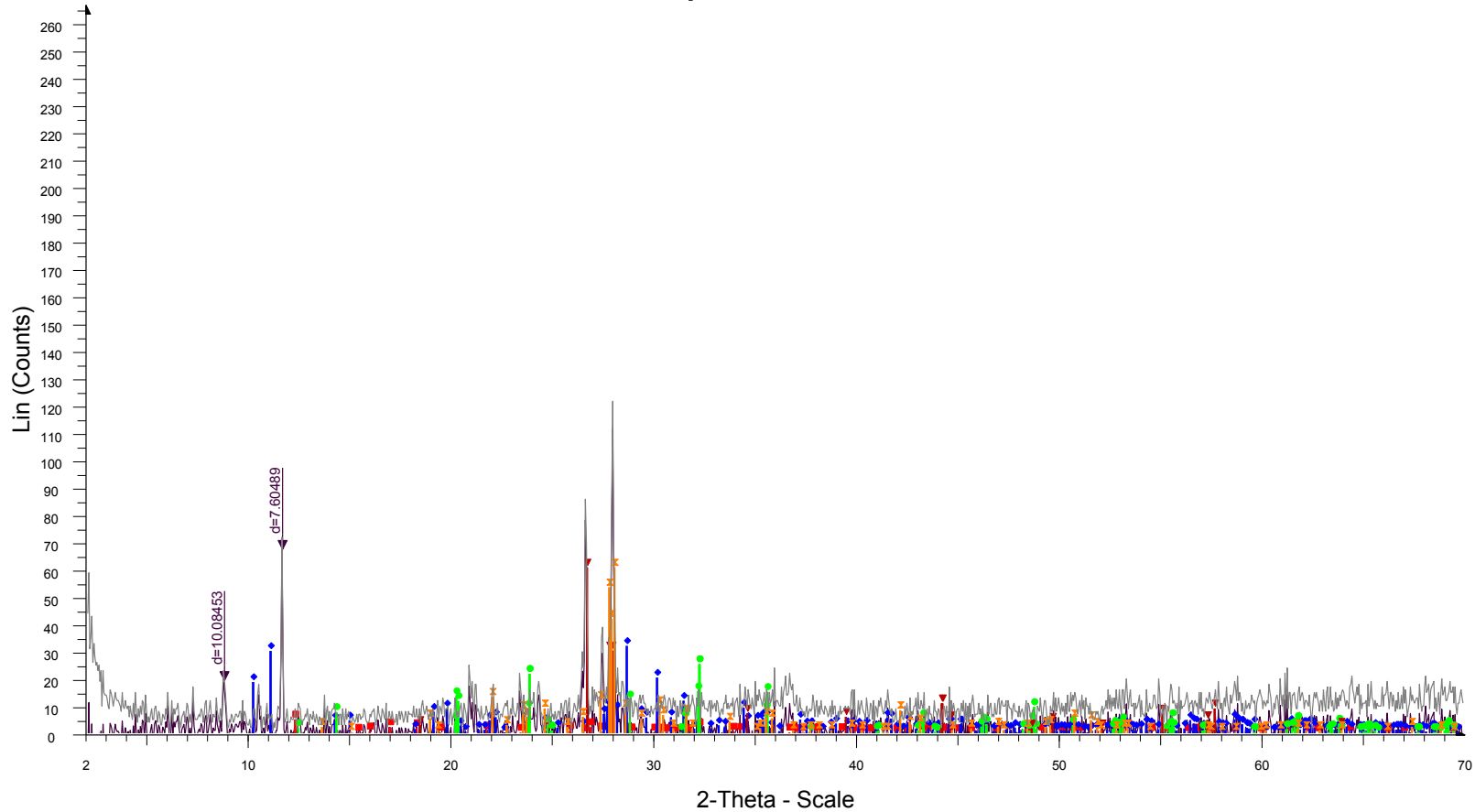
01-074-1433 (C) - Gypsum - $\text{Ca}(\text{SO}_4)(\text{H}_2\text{O})_2$ - Y: 50.00 % - d x by: 1. - WL: 1.5406 - Monoclinic - a 5.67900 - b 15.20200 - c 6.52200 - alpha 90.000 - beta 118.430 - gamma 90.000 - Body-centered - I2/c (0) - 4 - 495

00-026-1076 (C) - Carbon - C - Y: 50.00 % - d x by: 1. - WL: 1.5406 - Hexagonal - a 2.45600 - b 2.45600 - c 20.08800 - alpha 90.000 - beta 90.000 - gamma 120.000 - Primitive - P-6m2 (187) - 12 - 104.936 - I/c PDF

Appendices – Subsea environment

Freifjord subsea tunnel. Phosphates within deteriorated concrete near rock/concrete interface:

Sementprøve 6150e

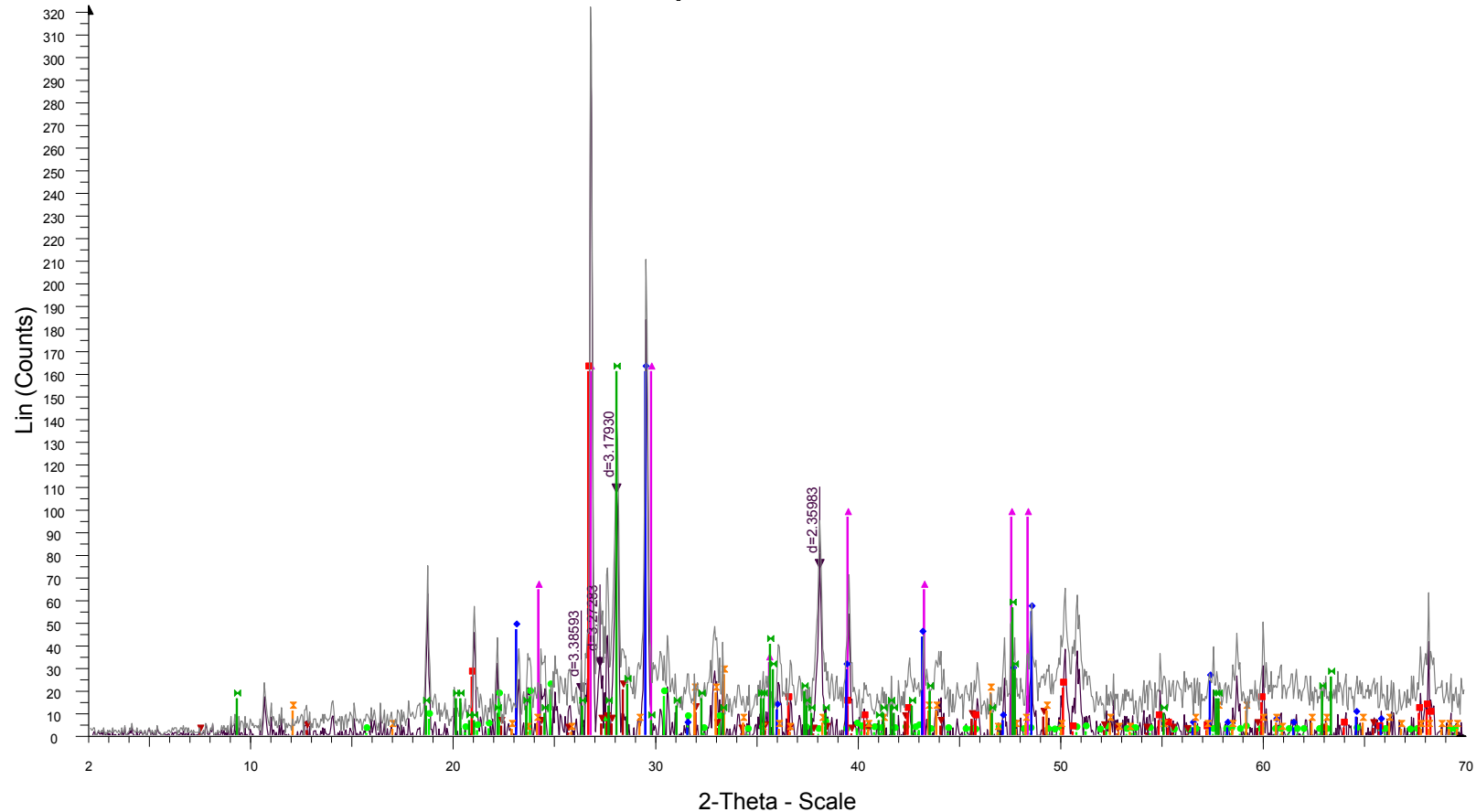


- ☒ Sementprøve 6150e - File: 100804-Hagelia-6150e.RAW - Type: 2Th/Th locked - Start: 2.000 ° - End: 70. Operations: Import ☒ 00-041-1486 (*) - Anorthite, ordered - CaAl₂Si₂O₈ - Y: 50.00 % - d x by: 1. - WL: 1.5406 - Triclinic - a 8.
- ☒ Sementprøve 6150e - File: 100804-Hagelia-6150e.RAW - Type: 2Th/Th locked - Start: 2.000 ° - End: 70. Operations: Background 1.000,1.000 | Import
- ☒ 00-045-0500 (Q) - Iron Hydrogen Phosphate Hydrate - FeH₃P₂O₈·4H₂O/FeH₃(PO₄)₂·4H₂O - Y: 4.17 %
- ☒ 00-045-0121 (C) - Iron Hydrogen Phosphate - Fe₅P₄O₂₀H₁₀ - Y: 26.39 % - d x by: 1. - WL: 1.5406 - Mo
- ☒ 00-045-0319 (*) - Sodium Iron Phosphate - Na₃Fe₂(PO₄)₃ - Y: 20.83 % - d x by: 1. - WL: 1.5406 - Mono
- ☒ 00-045-1436 (I) - Giniite, Fe-rich, syn - Fe₅(PO₄)₄(OH)₃·2H₂O - Y: 50.00 % - d x by: 1. - WL: 1.5406 - O

Appendices – Subsea environment

Flekkerøy subsea tunnel. Sodium bisulfate and other compounds at rock/concrete interface:

sementprøve 1373 C



- sementprøve 1373 C - File: 010405sement 1373C.RAW - Type: 2Th/Th locked - Start: 2.000 ° - End: 70. Operations: Import
- sementprøve 1373 C - File: 010405sement 1373C.RAW - Type: 2Th/Th locked - Start: 2.000 ° - End: 70. Operations: Background 3.802,1.000 | Import
- 00-026-0960 (*) - Sodium Hydrogen Sulfate - NaHSO₄ - Y: 6.25 % - d x by: 1. - WL: 1.5406 - Monoclinic
 - 00-028-0775 (N) - Calcium Oxide - CaO - Y: 50.00 % - d x by: 1. - WL: 1.5406 - I/Ic PDF 1. - S-Q 27.0 %
 - 00-029-0381 (I) - Calcium Silicate Hydroxide - Ca₄Si₅O_{13.5}(OH)₂ - Y: 6.25 % - d x by: 1. - WL: 1.5406 -
 - 00-046-1045 (*) - Quartz, syn - SiO₂ - Y: 50.00 % - d x by: 1. - WL: 1.5406 - Hexagonal - I/Ic PDF 3.4 - S
 - 00-024-0027 (D) - Calcite - CaCO₃ - Y: 50.00 % - d x by: 1. - WL: 1.5406 - Rhombo.R.axes - I/Ic PDF 1.
 - 00-019-0222 (D) - Calcium Iron Oxide - Ca₂Fe₂O₅ - Y: 8.33 % - d x by: 1. - WL: 1.5406 - Orthorhombic -
 - 00-018-0276 (I) - Margarite-2M1 - CaAl₂(Si₂Al₂)O₁₀(OH)₂ - Y: 50.00 % - d x by: 1. - WL: 1.5406 - Mono

Appendices – Subsea environment

A5-3 Results from Electron Microprobe Analysis (EMPA)

Table A5-3-1: Results from Electron Microprobe Analysis (EMPA). Freifjord subsea tunnel. Variably degraded cement pastes in Core 5800.

Freifjord tunnel; Core 5800		Chainage 5,800 /h.s						Concrete age: 13 years											
Thin section 2 Outer concrete (0-30 mm)																			
Profile		Context: Saline water seepage with growth of Gallionella f. and Mn-bacteria (Leptothrix discophora?)																	
Beam 5.8 nm, 15 keV, defocused (10 µm)																			
Analysis of Cement Paste Matrix		Main elements (wt. %)											Total all elements						
Points analysed	Distance from outer surface/mm	Ca	Si	Mg	Al	Fe	Mn	S	Cl	Na	K	including O							
e-95#	27.00	22.12	7.48	0.86	3.99	2.75	0.09	0.21	0.19	0.23	0.17	61.30							
d-93#	26.00	25.18	10.05	0.93	3.56	2.40	0.17	0.38	0.23	0.10	0.44	70.45							
d-94#	24.00	21.31	14.27	1.13	4.20	1.78	0.01	0.24	0.21	0.53	0.24	74.86							
c-91#	3.00	17.21	13.38	0.69	2.94	1.64	0.06	0.47	0.34	0.00	0.12	63.42							
c-80#	2.88	38.81	1.09	0.00	0.10	0.06	0.00	0.87	0.09	0.00	0.00	59.69							
c-75#	2.63	22.47	12.87	0.69	2.44	1.06	0.02	0.55	0.25	0.20	0.28	68.34							
c-72#	2.00	16.02	15.69	0.98	1.30	1.24	0.00	0.52	0.73	0.18	0.25	64.52							
c-69#	1.75	22.89	12.64	1.56	2.41	2.18	0.05	0.61	0.33	0.12	0.17	71.52							
c-67#	1.65	20.88	11.26	2.13	2.99	2.63	0.08	0.77	0.50	0.23	0.26	70.35							
b-62#	1.50	0.19	0.43	40.32	0.06	0.03	0.02	0.13	0.05	0.00	0.01	68.61							
b-61#	1.45	0.09	1.45	37.02	0.06	0.03	0.00	0.22	0.23	0.00	0.01	65.57							
b-56#	1.20	3.73	6.00	23.21	2.46	4.17	0.13	0.11	0.15	0.01	2.07	70.99							
b-53#	1.00	0.38	8.63	30.77	0.65	0.14	0.00	0.17	0.18	0.00	0.00	72.14							
b-49#	0.85	0.15	0.09	41.06	0.03	0.07	0.00	0.22	0.15	0.00	0.00	69.91							
b-46#	0.65	2.38	14.38	17.80	2.12	1.52	0.06	0.26	0.06	0.00	0.03	70.65							
b-42#	0.55	4.13	9.73	23.11	0.37	0.07	0.34	0.21	0.17	0.06	0.00	66.92							

A5-4 Images of tunnel concrete and biota

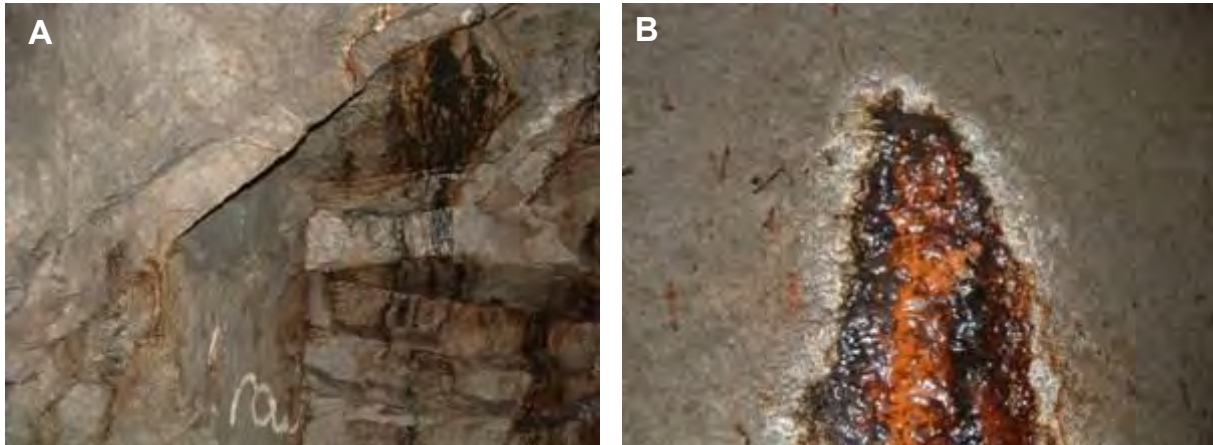


Figure A5-4-1: Locality Oslo 1a: A. Local barren rock with black Mn-oxides and Mn biofilm suggesting Mn^{2+} was mainly derived from ground water: B) Entrance point of a leakage showing black slime consisting of Mn-oxidising bacteria (resembling *Leptothrix discophora*) and the biomineral Na-buserite. Red rust (central) was derived from oxidation of steel fibres which was catalysed by Fe-oxidising bacterium *Gallionella ferruginea*. The white outer halo consisted of thaumasite and calcite.

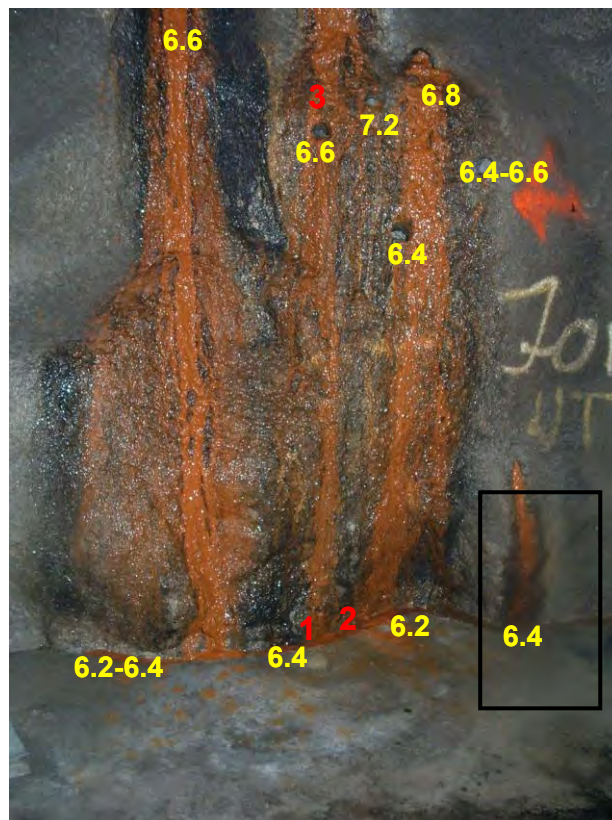


Figure A5-4-2: Locality Oslo 1a in September 2005 (concrete age \approx 6 years) showing pH variation in water and locations of the three sample stations for water chemistry (1, 2 & 3; cf. Table 2 in Chapter 7). Notice that the overall pH dropped by up to one pH unit downstream within the Mn-Fe biofilm, but pH as low as 5.5 was measured at other times (Table 3 in Chapter 7).

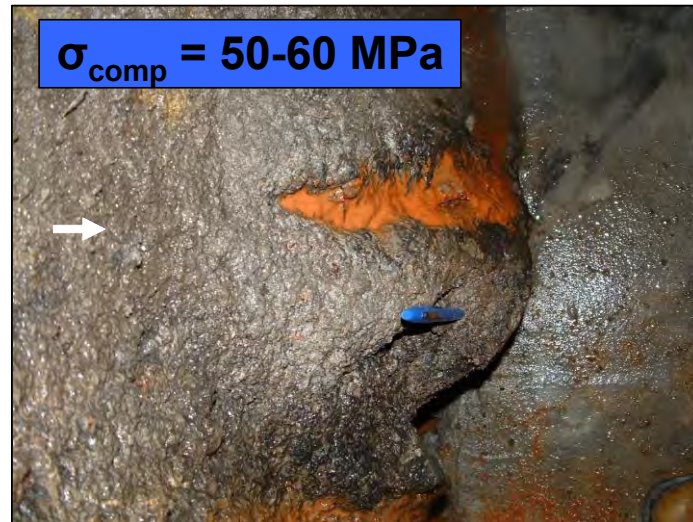


Figure A5-4-3: Small leakage (frame of previous figure) showing a groove with up to 4-5 cm of material loss related to acid producing reactions within Mn-Fe biofilms. Notice the smoothed surface (arrow) with minor loss also in the moist surrounding area. Nearby dry concrete some 1-2 m away had ordinary strength, which likely represents the initial quality of the domains now degraded by the composite bacterial - saline water attack.

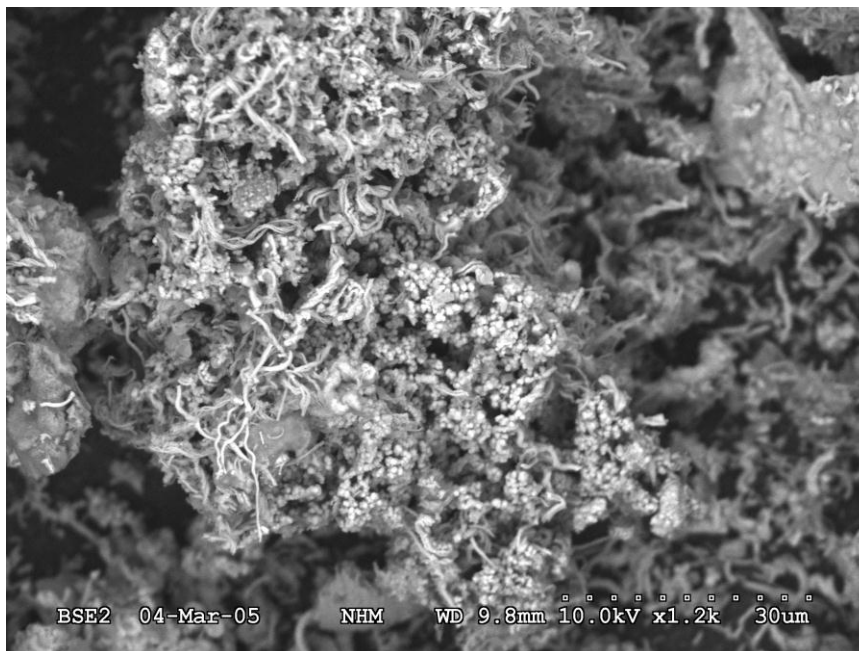


Figure A5-4-4: Locality Oslo 1a. Sample 0-2005 of *Gallionella ferruginea* slime (here aged) was the most commonly observed iron bacterium in the subsea tunnel sections. Width of field = 105 μm . SEM micro chemical data are given in Table 6 in Chapter 7.

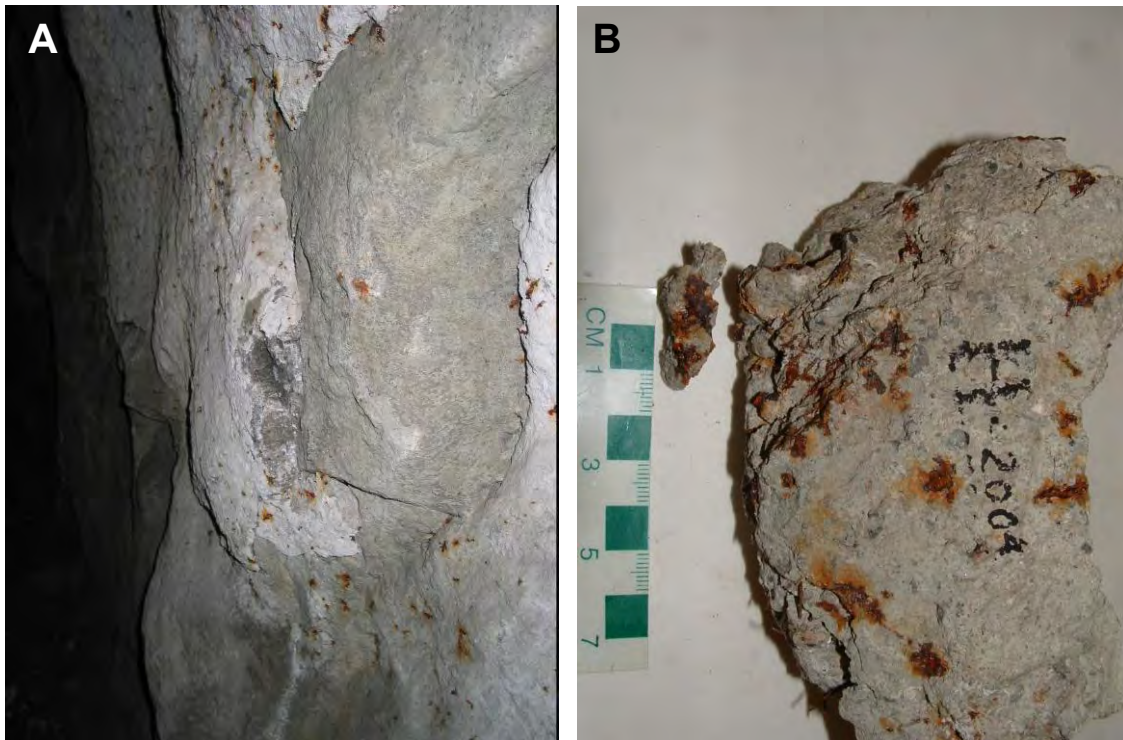


Figure A5-4-5: Locality Oslo 1b. February 2004. A: White weathered friable sprayed concrete influenced by saline water attack. Destructive steel fibre corrosion. Concrete replaced after about 4-5 years in service. B: Sample H-2004 from outer parts (Layer C). The cement paste matrix of white paste was transformed into MCSH and PCD and scattered TF with local TSA.

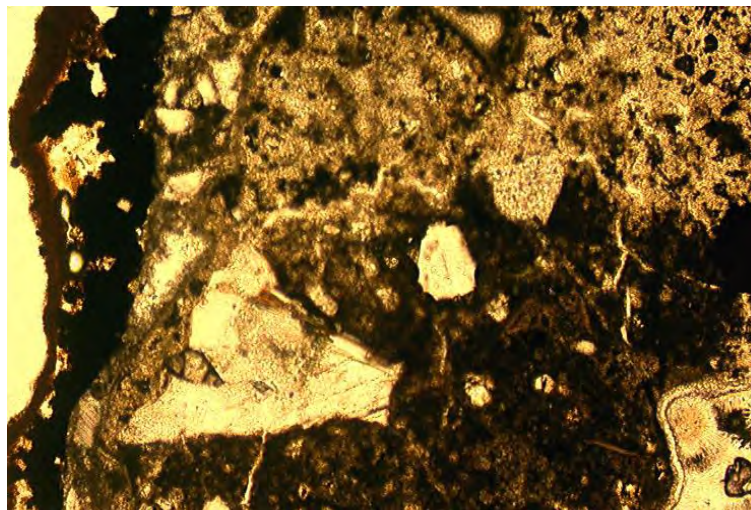


Figure A5-4-6: Locality Oslo 2a. Thin section from Core Kj 2 in plane polarised light. Width of field = 0.6 mm. Outermost Fe crust with *Gallionella sp.* (left) just outside black Mn-oxide crust (opaque) derived from Mn-oxidising *Leptothrix sp.* In this case deterioration was minor (0-5 mm) with pale yellowish brown paste (upper part) consisting of Mg substituted paste with some carbonation and entrapment voids rimmed with brucite and internal fibrous aragonite (lower right corner). Otherwise dark normal paste. Concrete age \approx 5 years.



Figure A5-4-7: Iron bacterium *Leptothrix ochracea* with suspect heavily Fe-encrusted *Gallionella ferruginea* (image centre) from ditch water at Location Oslo 2c. (BSE image: width of field 50 μm).



Figure A5-4-8: Freifjord subsea tunnel. Extensively deteriorated sprayed concrete due to interaction with Mn-Fe biofilms and saline ground water. pH = 5.8 in small leakages. Black and rusty crust material consisted of Na-buserite (hydrous Mn-oxide biomineral), amorphous Fe (likely ferrihydrite), the clay minerals vermiculite and dickite (with a HCONH_2 group), quartz and plagioclase. Situation from June 2006: concrete age 16 years.



Figure A5-4-9: Freifjord subsea tunnel. Sampling of water 4930-1 from leakages draining across a water panel within 15-20 meters of the location in Figure A5-4-8. The water leakages behind this panel were associated with Mn-Fe biofilms, showing extensive interaction with degraded concrete in the tunnel crown. The water was brackish (Table 2, Chapter 7) and sulfur isotopes showed very significant influence of sulfate reduction (Table 9).

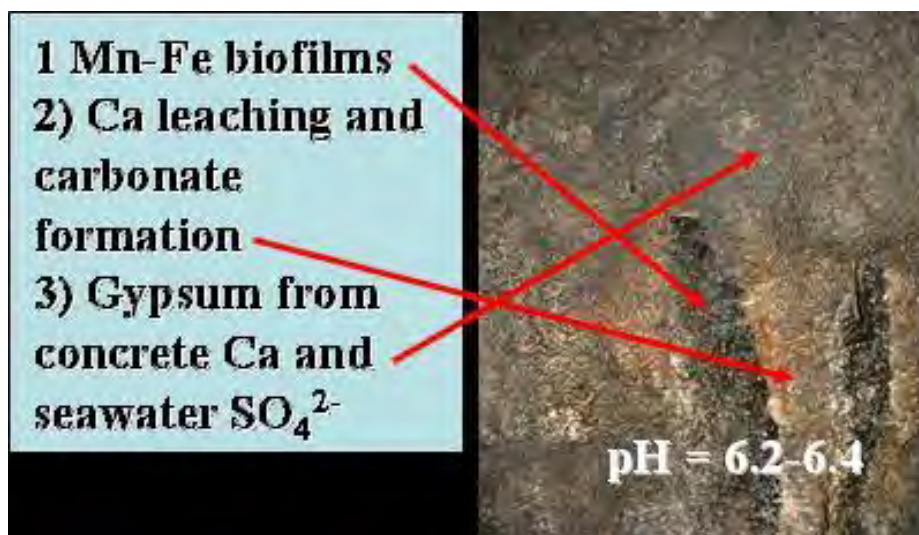


Figure A5-4-10: Freifjord subsea tunnel. Concrete age: \approx 16 years. Chronology of attack: 1 Establishment of biofilm, e.g. source of acids, 2) Ca – leaching and calcium carbonate formation, and 3) gypsum mush formation.



Figure A5-4-11: Freifjord subsea tunnel in 2006. Concrete age: \approx 16 years. Surface deposits of gypsum with some crystalline carbon precipitating from saline water draining at the concrete/rock interface. Core 6150-2 from 2003 = left hole with pH = 6.2 in 2006. The other cores were older and had accumulated much more gypsum. Note the smoothed rust stained and bleached concrete surface. Gypsum formation consumes acid suggesting pH in water behind the sprayed concrete layer was $<$ 6. The carbon was derived from dead bacteria occurring at the concrete/rock interface. Core holes (Φ = 50 mm).



Figure A5-4-12: Freifjord subsea tunnel. Concrete age: \approx 16 years. Gypsum deposit with crystalline carbon (5-10 mm thick).



Figure A5-4-13: Freifjord subsea tunnel. Concrete age: \approx 16 years. Very extensive deposition of gypsum mush associated with a leaky crack through weathered decalcified, friable and rust stained sprayed concrete, running over a cast concrete banquette (“Rivers of gypsum”). On either side the sprayed concrete was covered by a similar thin gypsum deposit.



Figure A5-4-14: Freifjord subsea tunnel. Concrete age: \approx 13 years. Core 6150-2 with 45-50 mm degraded friable sprayed concrete and destructive steel fibre corrosion within Layer A against the rock mass (right). The degradation was characterised by Mg ingress (forming MCSH and brucite) and local Thaumassite Sulfate attack (TSA) at the transition to more sound concrete. Calcite, laumontite, aragonite and nordstrandite also occurred. Impact from microbial activity acting from behind the spray was indicated by the presence of several phosphate minerals, a possible phenyl phosphate hydrate (Table A-5-2) and a carboxylate (an organic mineral) formed: a) within concrete 3 mm from the concrete/rock (Figure A5-4-15) and b) as a microscopic thin deposit on the outer surface (left).

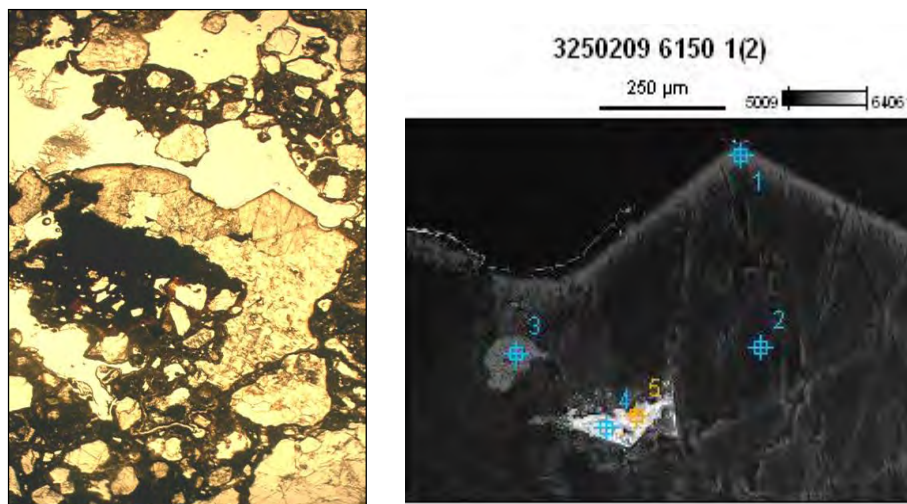


Figure A5-4-15: Freifjord subsea tunnel, Core 6150-2, Layer A about 3 mm from the concrete/rock interface. Occurrence of a metal bearing carboxylate derived from organic acids in a pore in concrete. Left image in plane polarised light, showing the light greyish with a straw yellow to light pinkish tint organic mineral with partial development of crystal faces. The compound was optically isotropic. Vertical width of field = 500 µm. Right image seen in Back Scatter under SEM.

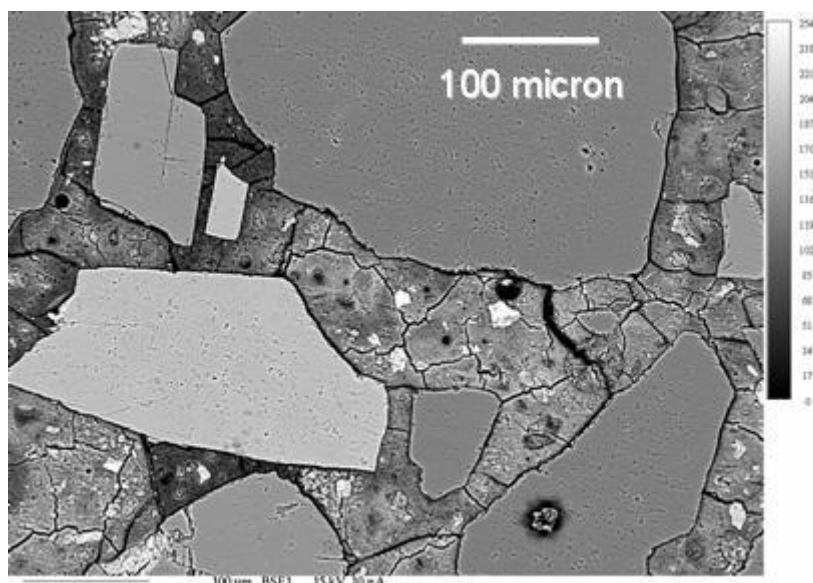


Figure A5-4-16: Flekkerøy subsea tunnel. BSE image of thin section from Core 1373. Note the extensive development of shrinkage cracks in the cement paste matrix, which was partly substituted by Mg from saline ground water forming MCSH.

A5-5 Summary of concrete samples with systematic petrography

The samples studied were concrete cores with a chip of rock inside. Thin section series usually cover the entire thickness of the spray and some rock behind. Spalls and smaller samples were also investigated. Table A5-5-1 (overleaf) summarises the petrographic features according to Layers A, B and C as defined in Figure 1, Chapter 7. Note that silica fume (SF) was well dispersed in all investigated concretes (i.e. rarely any sign of SF globules).

Appendices – Subsea environment

Table A5-5-1: Characteristics of subsea sprayed concrete layers and affected thicknesses. n = number of thin sections in each sample. Destructive steel fibre corrosion (*): PCD = Popcorn calcite deposition: Cc = carbonate: MCSH = Magnesium Calcium Silicate Hydrate ± brucite. TF = Thaumassite Formation, TSA = Thaumassite Sulfate Attack. 1-5 mm outer normal carbonation was always present. Additional XRD and SEM data referred to in Chapter 7.

Sample (n) Tot. thickness	Interface region (I)	Layer A inner	Layer B sound	Layer C, outer	Outer surface region (O)	XRD on sub samples (layer)	SEM on sub samples (layer)	pH-range on site
<i>Oslofjord 1a; Focused cement paste degradation associated with Mn-Fe biofilm, collected in 2004</i>								
Core Kj II (1) 40 mm Friable	Poor adhesion Brucite; 0.5-1mm	Diffuse layer: MCSH, PCD ± TF; 20 mm Fibre corr.	Partly preserved Diffuse areas of MCSH ± PCD ≥ 10 mm Some fibre corr.	Diffuse layer: MCSH, PCD Shrinkage 2-10 mm Fibre corr.*	Some pure Fe biofilm Minor loss Fibre corr.*	Calcite, magnesite (O)	Gypsum (O) <i>Gallionella</i> <i>ferruginea</i> (O)	5.5-6.6
Core Kj III (2) 30 mm remaining Friable	Good adhesion No deposit	Diffuse layer: some MCSH, PCD,± TF/TSA 5 mm. Fibre corrosion.	Partly preserved Diffuse areas of MCSH 10 mm Some fibre corr.	Diffuse layer: MCSH, PCD: Shrinkage 15 mm Fibre corr. *	Smooth with Mn-Fe crust 1-2 mm loss Fibre corr.*	Calcite, brucite, aragonite (O)	–	5.5-6.6
Core Kj IV(2) Two fragments: Extremely friable concrete (35 of 50 mm)	Not obtained Weak debris lost while drilling	Debris lost; Full scale MCSH, TSA, PCD: Shrinkage Fibre corr.*	Not preserved Fibre corr.	Debris lost; Full scale MCSH, PCD ± TF: Shrinkage Fibre corr.*	Weak debris Mn-Fe biofilm ≥ 20 mm lost Fibre corr. *	–	–	5.5-6.8
Core Kj V (2) 25 mm remaining Very friable	Fair adhesion Permeable No deposit	Full scale TSA MCSH, PCD: Shrinkage Fibre corr.*	Not preserved Fibre corr. *	Full scale TSA MCSH, PCD: Shrinkage Fibre corr. *	Mn-Fe biofilm 10-20 mm loss of very friable Fibre corr. *	Mg-calcite, Calcite, aragonite, dickite, busserite? (O)	–	5.5-7.2
<i>Oslofjord 1b; Spalled and weathered concrete without biofilms replaced after 4-5 years in service, collected in 2004</i>								
Spall 1 (4) (big flake) 100 mm	No adhesion Brucite Fibre corr.*	MCSH, calcite 1-2 mm Fibre corr.*	Very high quality: No shrinkage ≥ 90 mm Intact fibres	MCSH and carbonation Minor TF 1-10 mm Fibre corr.	No loss No biofilm Fibre corr.*	–	–	7 – 7.4
H-2004 (3) outer 45 mm of 80-100mm Very friable	Not collected	Not collected, features as for Layer C Fibre corr.*	Not collected, not sound: bleached Fibre corr.*	MCSH, brucite PCD ± TF/TSA (≥ 45 mm): Shrinkage Fibre corr.*	Smooth Minor loss No biofilm Fibre corr.*	Calcite, aragonite, thenardite (C)	–	n.a.

Appendices – Subsea environment

Sample (n) Tot. thickness	Interface region (I)	Layer A inner	Layer B sound	Layer C, outer	Outer surface region (O)	XRD on sub samples (layer)	SEM on sub samples (layer)	pH-range on site
<i>Oslofjord 2a: Cement paste degradation with Mn-Fe biofilm, collected in 2004</i>								
Core Kj 1 (2) Fairly sound 100 mm	Poor adhesion Brucite	Not developed Intact fibres	Sound (thin bleeding zone) ≥ 95 mm No shrinkage Intact fibres	MCSH, PCD ± TF: ≤ 5mm Shrinkage Fibre corr.	Smooth w/Mn-crust Some loss (<0.5 mm) Fibre corr.	Todorokite, (buserite?) amorphous Mn (O)	<i>Leptothrix discophora</i> (?) embedded in Mn-oxide platelets	≈ 7-7.5
Core Kj 2 (2) Fairly sound 58 mm	Good adhesion No deposit	Not developed	Well preserved 52 mm Local shrinkage in sound paste Intact fibres	Carbonation, MCSH, brucite, aragonite, TF- TSA: 0-5 mm Fibre corr.	Smooth w/Mn-Fe crust (loss?) Fibre corrosion	–	–	≈ 7-7.5
Core Kj 5 (3) 80 mm	Poor adhesion Aragonite, calcite	MCSH, carb. Shrinkage 5 mm Fibre corrosion	Sound (local bleeding). No shrinkage 70 mm Intact fibres	Carbonation aragonite (MCSH minor) 5 mm Fibre corrosion	Smooth w/Mn-Fe crust (loss?) Fibre corrosion	Birnessite, amorphous Fe, calcite (O)	-	≈ 7-7.5
<i>Oslofjord 2b: Cement paste degradation without biofilm, collected in 2004</i>								
Core Kj 9 (2) Friable 70-75 mm	Brucite, aragonite calcite, magnesite (1 mm)	Diffuse MCSH with PCD (no TSA) 10-30 mm Fibre corr.	Not quite sound: diffuse areas like A & C 50 mm Intact fibres	Diffuse MCSH with PCD Shrinkage 4-5 mm Fibre corr.*	Smooth friable minor loss. Grey deposit Fibre corr.*	Todorokite? (O). Brucite, calcite, aragonite, magnesite (I)	-	(moist) n.a
Core KJ 10 (3) A bit friable 110 mm	Brucite, calcite (0.5-1 mm)	Diffuse MCSH with PCD, TSA 3-4 mm Fibre corr.	Not quite sound, diffuse areas: carbonation & MCSH: Shrink ~ 100 mm Intact fibres	MCSH with small PCD (no TSA) Shrinkage 10-12 mm Fibre corr.	Smooth. Minor loss, Fibre corr. *	Brucite, calcite (I)	–	(moist.) n.a

Appendices – Subsea environment

Sample (n) Tot. thickness	Interface region (I)	Layer A inner	Layer B sound	Layer C, outer	Outer surface region (O)	XRD on sub samples (layer)	SEM on sub samples (layer)	pH-range on site
<i>Oslofjord 2c: Severe cement paste destruction with Mn-Fe biofilm, collected in 2004</i>								
Spall V5 outer 60 mm of ca 300mm Extremely friable w/debris	Not collected	Not collected	Probably no sound concrete left	Disintegrated paste: MCSH, Cc & internal Mn-oxides. 50-100 mm Fibre corr. *	Mn-oxide and Fe slime of <i>Leptothrix</i> <i>ochracea</i> & <i>Gallionella</i> <i>ferruginea</i>	Birnessite, buserite, gypsum aragonite, calcite thenardite, Na- Ca-sulfate hydrate (C)	Aragonite (C) <i>Leptothrix</i> <i>ochracea</i> (O)	≈ 7-7.5
<i>Byfjord: Minor cement paste degradation without biofilm, collected in 2004</i>								
Core 1-2 (6) 200 mm	No sub sample	PCD, MCSH ± ettringite Shrinkage ≤ 15mm Fibre corr. *	Well preserved, entrapment voids No shrinkage 170-175 mm Intact fibres	Cc w/ettringite ± MCSH 12-15 mm Fibre corr.*	Calcite deposits (related to stalactites)	-	-	<i>dry</i>
<i>Freifjord: Cement paste degradation with Mn-Fe biofilm, collected in 2003</i>								
5800 (2) 60 mm	Fair adhesion, permeable	Carbonation 1 mm Marginal fibre corrosion	Sound w/a bit shrinkage 56 mm Marginal fibre corrosion	MCSH, PCD, brucite, TF 5 mm Fibre corr. *	Fe-Mn-biofilm Smooth surface w/ some loss	NH ₄ -Fe-sulfate, gypsum (O)	EMPA anal.: Chapter 7.3.2	6-7
6150-2 (5) w/friable zones 140 mm	Adhesion quite good Calcite, laumontite	Very friable w/ MCSH, brucite, TSA, carbonate Al-hydroxide phosphates, Carboxylate 45-50 mm Fibre corr. *	Well preserved Some shrinkage 80-85 mm Intact fibres	Carbonation 5 mm Fibre corr. *	Carboxylate, gypsum,	<u>Degraded paste:</u> Aragonite, Mg- calcite, brucite, nordstrandite(A); Calcite, laumontite (I) <u>Corroded fibres:</u> Brushite & other phosphates (O & A); Gypsum (O)	Carboxylate (I) Chapter 7.3.3	<i>n.a</i>

Appendices – Subsea environment

Sample (n) Tot. thickness	Interface region (I)	Layer A inner	Layer B sound	Layer C, outer	Outer surface region (O)	XRD on sub samples (layer)	SEM on sub samples (layer)	pH-range on site
<i>Flekkerøy: Cement paste degradation with Mn-Fe biofilm, collected in 2003</i>								
Core 1373 (2) - 25 mm remaining	Adhesion lost, permeable; Na- bisulfate + clinker min.	MCSH PCD/Cc 10-15 mm Fibre corr. *	Not well preserved. Diffuse areas with MCSH Intact fibres	MCSH, PCD/Cc 10-15 mm Fibre corr. *	5 mm rusty gypsum crust outside Fe and Mn crusts Some loss	Na-bisulfate, calcium silicate hydroxide, CaO, ferrite calcite (I)	–	<i>n.a.</i>
Core 1374 (6) - 100 mm	Poor adhesion Permeable zone w/ brucite, calcite	Diffuse MCSH w/carbonation 10-20 mm: Layer parallel permeable crack (1-2 mm) w/brucite ± Cc Some shrinkage Local fibre corr.	Not well preserved Cross cutting permeable crack (1-2 mm) w/brucite ± Cc Mainly intact fibres	MCSH, PCD, brucite, local TF 5-20 mm Some shrinkage Fibre corr.	Mn-(Fe)biofilm 0-3 mm calcite, brucite deposit Insignificant loss	Brucite, calcite (I)	–	<i>n.a.</i>

Appendices – Subsea environment

A5-6 Microbes found in the subsea environment

The iron bacteria were identified by a microbiologist at NIVA – Oslo, using light microscope and acid to remove Fe –encrustation. The samples were taken from typical red rusty slime. Table A5-6-1 gives a summary to the main samples and reports.

Table A5-6-1: Summary of iron bacteria encountered in samples from subsea tunnels, with reference to NIVA reports. * = completely dominating.

Sample	Bacteria and observations	NIVA-report
<i>Oslofjord loc. 1a</i> SB 2005	<i>Gallionella ferruginea</i> *	O 25011 04
<i>Oslofjord loc. 2a</i> V1L1	Little organic material, precipitation of Fe-sulfide	O 25011 06
<i>Oslofjord loc. 2c</i> V5L2	<i>Leptothrix ochracea</i> >> <i>Gallionella ferruginea</i> In open ditch, same as Fig. A5-4-7.	O 25011 06
<i>Freifjord</i> 5215 6085 6660	<i>Gallionella ferruginea</i> * <i>Gallionella ferruginea</i> * <i>Gallionella ferruginea</i> *	O 25011 06
<i>Flekkerøy</i> 3/okt 2002 II/01-09.2002 III/01-09.2002	<i>Gallionella ferruginea</i> * <i>Gallionella ferruginea</i> * <i>Gallionella ferruginea</i> and some unidentified	O 22022 11

Gallionella sp. are characterised by small bean shaped cells (0.5-2.5 µm), with attached twisted to helix shaped stalks (20-400 µm), which are formed mostly during the late growth stages. These stalks may be heavily encrusted by Fe. *Leptothrix ochracea* is typically characterised by tube-like nearly empty sheets about 1-2 µm thick and about 10-100 µm long (Bergey's Manual of Systematic Bacteriology, Part 3, 2005).

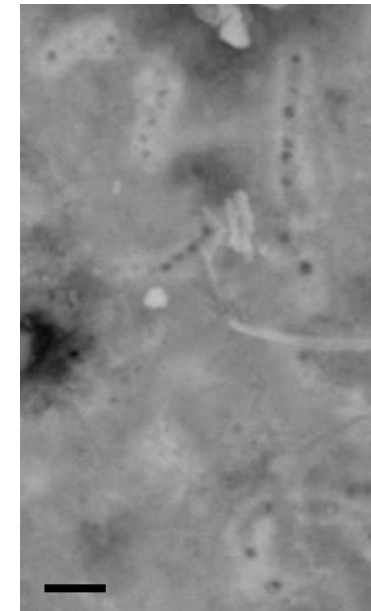
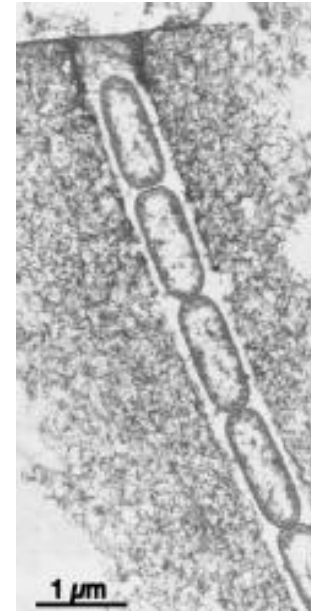
Appendices – Subsea environment

The Mn-oxidising bacterium seems very similar to *Leptothrix discophora* as interpreted from SEM-imaging by the author (Chapter 7 states this with a question mark). The colour of such biofilm material was black-brown with a metallic tint. The pertinent features of a well-chosen sample from the present study are compared with data from Bergey's Manual in Table A5-6-2. Yet, there is indeed a need to investigate this further by using modern approaches, involving DNA-fingerprinting.

The attached figure (*left*) is an example of *Leptothrix discophora* (cf. B.M. Tebo, J.R. Barger, B.G. Clement, G.J. Dick, K.J. Murray, D. Parker, R. Verity, S.M. Webb, Biogenic manganese oxides: Properties and mechanism of formation, *Annu. Rev. Earth Planet. Sci.* 2004, 32, 287-328). The figure to the *right* represents Mn-oxidising bacteria from Oslofjord subsea tunnel (locality 1a, sample Mn-1-05, scale bar = 2µm)

Table A5-6-2: Comparison of Mn-oxidising bacterium with data for *Leptothrix discophora* taken from (Bergey's Manual 2005) and other literature.

	Sample Mn-1-05	<i>Leptothrix discophora</i>
Cells	Disc-shaped	Disc-shaped
- Width	0.5-1 µm	0.6-0.8 µm
- Length	0.5-2 µm	2.5-12 µm
Sheets		
- Width	≈ 1 µm	≈ 1 µm
- Length	≈ 5-15 µm	≈ 5-100 µm (not well constrained)
Cells confined within sheets	Yes	Yes
Occurrence of single cells	Yes	Yes
Extracellular Mn-oxide	Yes	Yes



A5-7 Mn L-edge spectra and STXM

Scanning Transmission Soft X-ray Microscopy (STXM) has recently been used for quantitative determination of charge state distribution of Mn in bio-minerals (Pecher et al. 2003, quoted in Chapter 7). A first attempt was made in this thesis and a friable Mn-crust material was prepared as TEM thin foils, using abrasives and a finish with Ar⁺ sputtering as described in Chapter 7. This was followed by EDS for location of Mn-oxide. The STXM measurements were performed at the Advanced Light Source at Lawrence Berkeley National Laboratory, by Dr Klaus Pecher. The main idea was to investigate possible differences in Mn-charge state in profiles from outer Fe-crust material and further inward within Mn-crusts.

Due to suspect beam damage, the full potential for quantitative charge state spatial mapping was not utilised. The damage was likely most significant in the thinnest parts of the TEM thin foil, as can be substantiated by the different distributions of Mn-species at different thicknesses (Figure 16, Chapter 7). The thinnest zones were characterised by the highest abundance of Mn^{II}, (most reduced), implying that the damage was due to electrons (the EDS screening), rather than the Ar⁺ sputtering. It is considered that a better solution would have been to analyse very small pieces of pure Mn-crust material, without too much complicating preparation.

Analysis of Mn-charge states (Mn is a 3d transition metal) requires a probe which can reach deep into the atomic structure. Due to large Coulomb interaction between the 2p and 3d levels, the dipole transition energies depend on the local electronic structure of the absorbing ion. Discrimination between charge states of Mn is possible because the absorption energies, to a great extent, reflect the Mn charge state. However, it has proven more feasible to use model compounds (Mn compounds with different oxidation states) for fitting purposes. Analysis of Mn L-edge spectra using STXM in this way has proven to be a powerful tool (see Pecher et al. 2003 for details).

The STXM technique utilises so-called zone plate optics to focus a monochromatic x-ray beam onto a very small spot (40 nm, or so). It is significant to utilise samples which are thin enough to achieve X-ray transparency. The sample is raster-scanned through the focused x-ray beam, and the intensity of transmitted photons is detected to form a 2D image of the variation in photoelectric absorption signal through a column of material. A sequence of images (referred to as a stack), can be acquired at finely spaced incident monochromatic energy intervals (for Mn around 640-660 eV) in the Mn 2p region. Additional techniques are used in order to calibrate the instrument. Further details of the technique may be found in Pecher et al. (2003) and references therein.

Appendix 6: Additional documentation to Chapter 8

- A6-1 Introduction**
- A6-2 Freshwater environment**
- A6-3 Lier railway tunnel**
- A6-4 Alum Shale environment**
- A6-5 Saline environment**
- A6-6 Alkali-Silica Reaction (ASR)**
- A6-7 Rating of water loads, Ca- and Fe-Mn deposits on subsea tunnel concrete**

A6-1 Introduction

The background documentation for each location reported in the summary Chapter 8 was gathered from several of the other papers and appendices. The intention of Appendix 6 is to systemise the sources of the most important data for easy reference. Moreover, data from the Lier railway tunnel were just briefly referred to in Chapter 8, and further documentation is provided herein.

A6-2 Freshwater environments

Harpefoss tunnel and land sections in subsea tunnels

The Harpefoss tunnel is the access tunnel leading down to an underground power station, as referred to in Chapter 3, which included site descriptions from 1997 and 2000, summary of concrete petrography and chemical analyses of local leakage waters. The details of concrete petrography from 1997 and 2000 are tabulated in Appendix 1 in this thesis.

The freshwater section under land in subsea tunnels were just investigated briefly within this study and were based on tunnel observations and few concrete cores and water chemical analyses. Generally the sprayed concrete was visually in a good condition, and cores were extracted from apparently typical quality. The water chemical compositional ranges given in Table 2 of Chapter 8 were based on the individual analysis reported in Chapter 9 (Table 1) and the Lier water analysis (Table A6-3-1). The documentation of sprayed concrete is given in Table A6-2-1 below. Steel fibre corrosion was restricted to the surface carbonated domain and was then not severe.

Table A6-2-1 Outline of main features of sprayed concrete in freshwater sections in subsea tunnels. n = number of thin sections.

Core sample (n)	Adhesion	Internal concrete	Internal steel fibre corrosion	Surface carbonation	Total spray thickness
<u>Flekkerøy, chainage 2143</u>					
2143 (2)	Fair permeable	Sound w/extensive PCD near interface	None	3-4 mm	8 cm
<u>Freifjord, chainage 3132 m</u>					
3132 (3)	Very good	Sound	None	10-20 mm	7 cm
<u>Byfjord, chainage 4410 m</u>					
Core 3-2 (4)	Very good	Sound	None	2-3 mm	9.5 cm
Core 3-3 (3)	Very good	Sound	None	2-3 mm	7-12 cm

A6-3 Lier railway tunnel

The sprayed concrete in the Lier railway tunnel is old, made some time between 1965 and 1971. The tunnel was opened for traffic in 1973. The main problem with the sprayed concrete is the presence of extensive and continuing spalling within an outer about 1-5 cm layer of heavily carbonated concrete (Figure A6-3-1). Maintenance work is required usually two times per year, mostly involving manual removal of very friable 0.5-2 cm thick concrete spalls (Kjell Bjarne Saglia, personal communication 2006).

The sprayed concrete was probably the first used for rock support in a Norwegian tunnel and was used to prevent effects of widespread rock bursts. It was experienced that the rock burst problem vanished soon after spraying (Anders Heltzen, personal communication 2004). The main rock type is Permian granite with abundant dolerite dykes. Several clay infected weakness zones occur.

The sprayed concrete was made according to the dry method and was partly reinforced by a steel grid, which was at places severely corroded within thick carbonated outer layers. The concrete mix was based on a standard Portland Cement (likely rapid setting), an innocuous aggregate rich in fines and 2.5-3 % HS-3 accelerator, which consisted mainly of water glass, portlandite and calcium aluminate (Odd Tjugum, personal communication 2004).

The concrete lining is presently usually very dry, whilst water leakages were very common during excavation. Evidently draw down of the water table has reduced the volumetric water flow into the tunnel. Several cores and spalls were collected during spring 2004.

The outer surface of the concrete was covered by a black or dark material, which is typical of all railroad tunnels (mainly electrified) and represents dust from brake systems, electrical sparks and diesel locomotives (Stian Wesøy, personal communication 2004). SEM analysis (ID: Hagelia 2004-09-07) showed the cover material was rich in carbon and iron.

Petrography of thin sections of concrete samples has shown that the outer carbonated zone was typically laminated and very brittle/friable, consisting of fine grained carbonate similar to ordinary surface carbonation as well as Popcorn calcite (PCD) or similar coarser calcite. The sprayed concrete had suffered a sulfate attack in early years, being most typically developed in the inner parts of the concrete layer and adjacent to the rock mass. The sprayed concrete had an initial rather variable quality and contained abundant large entrapment voids reaching several mm in widths. These voids were usually filled with large secondary portlandite, crystalline calcium silicate hydrate needles and an intergrowth of ettringite and thaumasite (SEM EDS analysis). The ettringite-thaumasite and the Ca-bearing phases had in part grown at the expense of the cement paste matrix, and a tendency for swelling could be seen (Figure A6-3-2). The sizes of the secondary minerals in some cases exceeded 0.5 mm, which explicitly attests to an event of early bulk water diffusion. There was also some apparent evidence for later stage dissolution of the ettringite-thaumasite minerals (Figure A6-3-3). The interface region between concrete and rock was usually permeable and sometimes carried an ettringite deposit (XRD analysis).

The water chemical analysis given in Table A6-3-2 shows elevated concentration of bicarbonate which is typically associated with PCD. Present sulfate concentration is probably not representative for earlier years with sulfate attack.

This description was based on investigations of three concrete cores and several spalls (Internal documents, NPRA).

Table A6-3-1 Water sample collected from a water drain at chainage 44265 m (mg/L)

pH	Cl	F	SO₄²⁻	Na	K	Ca	Mg	Fe	HCO₃⁻
8.18	2.89	1.35	22.3	15.0	0.79	44.5	12.1	1.5	173



Figure A6-3-1 Spalling in dry extensively carbonated sprayed concrete at chainage 43720 m in the Lier tunnel. Two 50 mm cores were extracted for thin sectioning. The concrete was frequently sounder deeper inside, yet showing evidence of a sulfate attack in previous years. The dark outer surface represents dusts mainly consisting of carbon and iron.

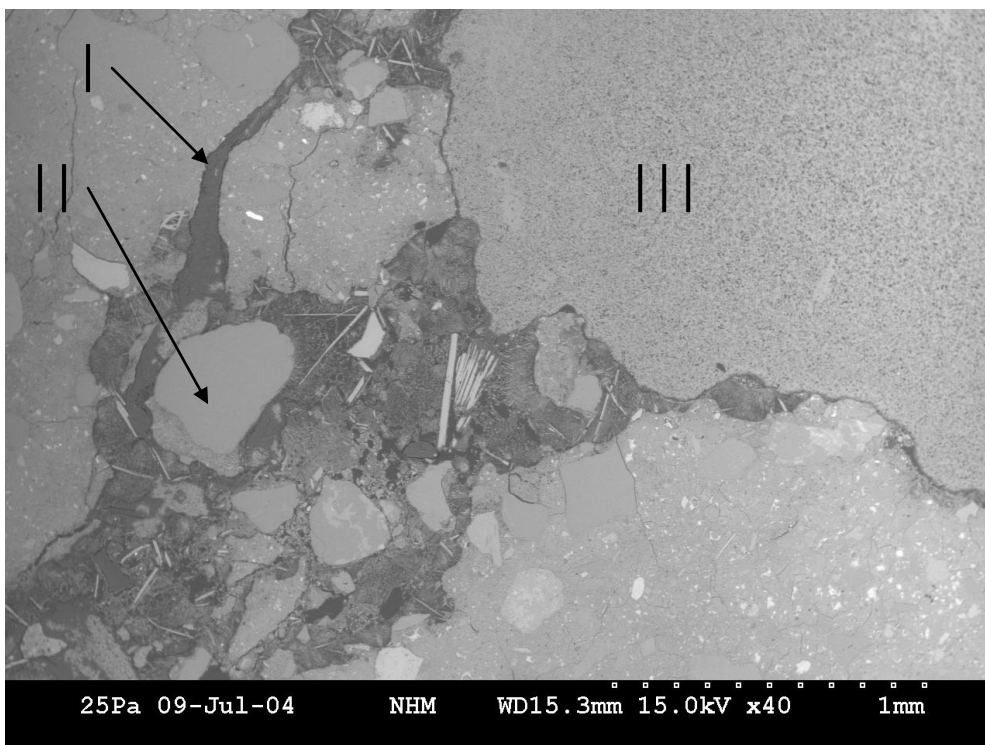


Figure A6-3-2 Extensive deterioration of the cement paste matrix in the Lier tunnel due to replacement by (dark) ettringite –thaumasite (E-T) and needle shaped crystals (light) of portlandite and a calcium silicate hydrate. I = apparent expansion due to E-T; II = Aggregate particle with a small remnant of sound paste (lower part); III = entrapment void. Lower right domain = sound concrete (SEM, Back scatter, width of field = 3 mm).

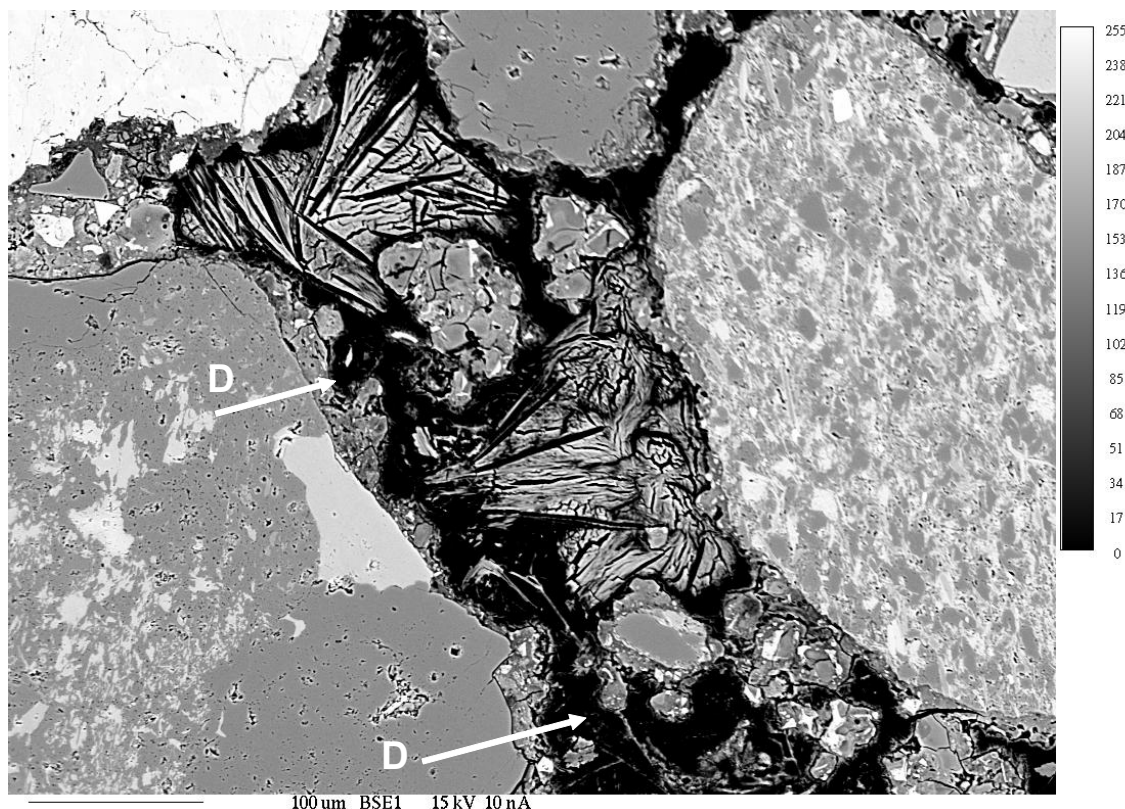


Figure A6-3-3. Sulfate attack in Lier sprayed concrete, showing extensive replacement of cement paste by intergrowth of ettringite and thaumasite. Remaining paste preserved in contact with some aggregate grains was mainly cracked and friable. The secondary assemblage had apparently been subjected to dissolution (D) later on. Back Scatter Image. Scale bar 100 μm .

A6-4 Alum Shale environment

Åkeberg road cut, Ekeberg & Svartdal highway tunnels

The basic results from these sprayed concretes were reported in Chapter 3 and the detailed petrography was tabulated in Appendix 1 (Table A1-1-1). In Chapter 8 the status of Svartdal tunnel concrete in 2006 was also referred to, and the petrographic description was included in Appendix 1; Table A1-1-1 along with the samples from 2000. The water chemical range given in Chapter 8 was based on data in Chapter 3 and Chapter 7.

A6-5 Saline environment

The main results from the subsea sections were based on selected concrete samples, concrete debris samples, bacterial slimes and water samples in Chapter 7 and Appendix 5. The full water chemical data for saline tunnel waters are reported in Chapter 9 (Table 1).

A6-6 Alkali-Silica Reaction (ASR)

ASR was in general absent in the investigated sprayed concretes, when found the effects had no structural influence: A few thin sections indicated incipient ASR at Harpefoss which contained reactive aggregate particles (thin sections from Core 1.1; Core 2 and Core 3;). The material was collected in 1997 when the concrete was 13 years old (see Appendix 1, Table A-1-1). Occasional traces of ASR were also observed in the 2000 material.

In the Freifjord subsea tunnel some silica fume (SF) was not well dispersed and ASR-gel had occasionally formed at the expense of SF (Figures A6-6-1 & -2). This form of ASR was found by the present author through reinvestigation of the few thin sections made as part of the previous durability project (Davik 1997). The location, within the niche at the pump station, was characterised by rather thick sprayed concrete. The age of the concrete was about 6 years at the time of sampling. The location was inspected visually in June 2006 (at age 16 years), showing no indication of map cracking or any other superficial sign of distress, suggesting this form of ASR had no significant structural effects. This seems corroborated by the lack of microcrack development into the cement paste matrix adjacent to ASR gel (Figure A6-6-1 and -2).

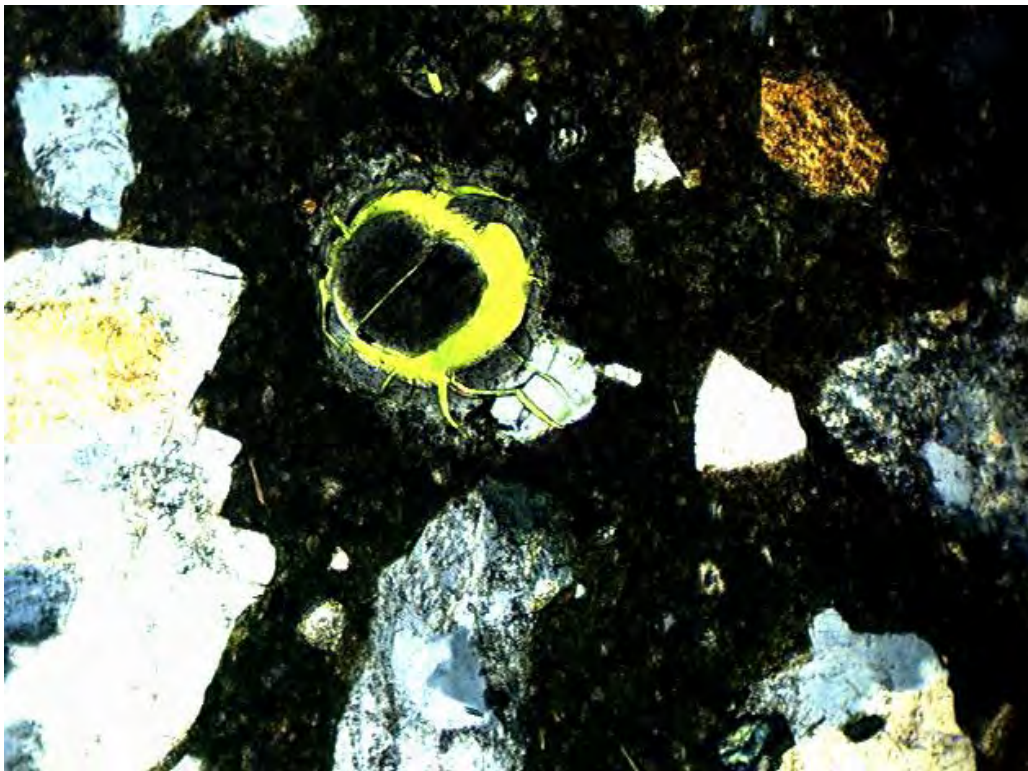


Figure A6-6-1 ASR-gel had formed locally at the expense of a silica fume SF globule within the Freifjord subsea tunnel after 6 years. Fluorescence impregnated thin section. Crossed polars with mica plate inserted. Width of field = 500 μ m.

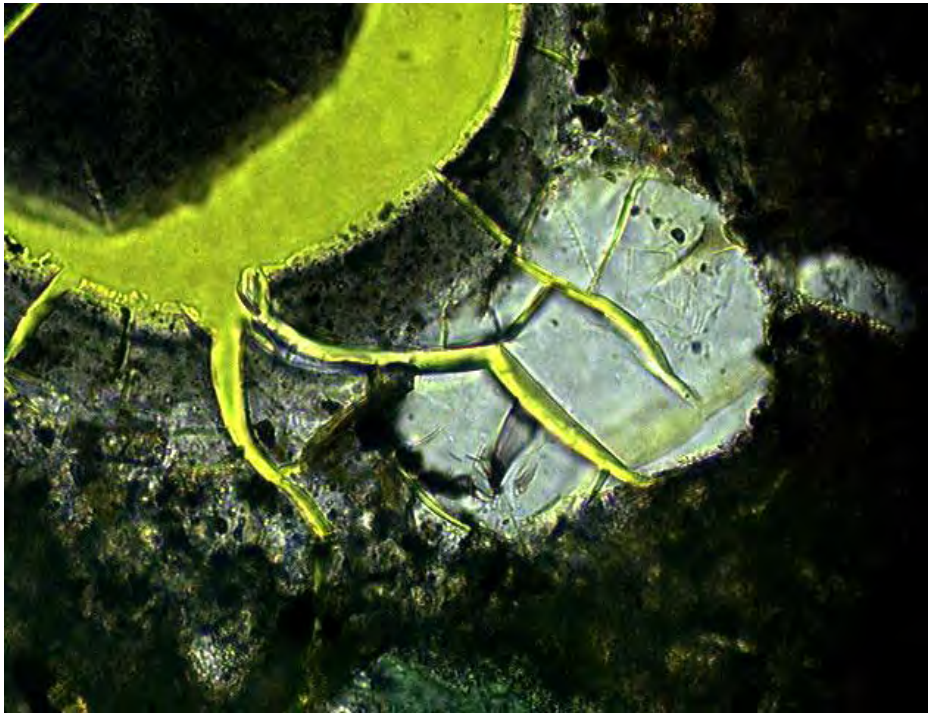


Figure A6-6-2 Detail of previous image showing SF with ASR-gel (light grey) which had formed at the margin against sound cement paste. Later desiccation cracks within SF and ASR gels. Note the absence of microcracks in the surrounding sound cement paste. Crossed polars (Width of field 150 μm).

A6-7 Rating of water loads, Ca- and Fe-Mn deposits on subsea tunnel concrete

During the previous durability project “Proper use of sprayed concrete in tunnels” (Davik 1997, quoted in Chapter 8), several subsea tunnels were mapped systematically. A rating system was used to characterise the outer secondary effects/features on sprayed concrete used for rock support: The secondary effects were defined as “Water load”, “Ca bearing deposits” (mainly calcium carbonate derived from leaching) and “Fe-algae deposits” were registered for each ten metre of tunnel in both land sections and subsea sections (Røhrsveen and Lygre 1996, quoted in Chapter 8). My own tunnel investigations and photo documentation of each type of feature by these authors clearly shows that the Fe-“algae” deposits incorporated both rusty brown ferric iron bacterial slime (not algae) as well as black Mn deposits. Also rating of concrete roughness and adhesion was tried but not followed up systematically due to difficulties.

The rating system was based on a scale ranging from 0 to 5 for each of the features. Thus 0 represents no significant effect whilst 5 represents full impact. Ratings 1, 2, 3 and 4 represent intermediate classes. The system did not account for variable sprayed concrete thickness, thus each of the mapped 10-meter intervals were treated as if they had the same cover of concrete. The overall conclusion was that subsea tunnel sections were more influenced (e.g. by water, Ca-leaching and Fe-“algae” deposits) than the freshwater sections under land, even though most investigated subsea tunnels were young.

Appendices – Summary of deteriorations & engineering aspects

In the present work (Chapters 7, 8 and 9) it was reported that the saline ground water ingress into sprayed concrete was characterised by Ca- leaching (due to decalcification of the cement paste by abiotic and biotic processes) with and without calcite deposition *and* acid attack derived from Mn and Fe bacterial deposits. It was concluded (e.g. Hagelia 2007, quoted in Chapters 7, 8, 9) that these processes were intimately related and frequently operating simultaneously. Yet the relative impact of the different mechanisms varies from place to place. The Ca- rating and Fe- “algae” rating of Røhrsveen and Lygre (1996) represent surface features of the overall saline ground water deterioration process: The sum of rated “Ca leaching” and “Fe-algae deposits” is therefore a relevant parameter, which was investigated in Chapter 8.

Table A6-7-1 Flekkerøy subsea tunnel. Surface water and surface deposits on sprayed concrete by 50 m tunnel sections. X (%) = leakage area in % of a unit tunnel area, and h = hydraulic gradient (cf. Hagelia 1994). The remaining parameters represent averaged 10 m results from Røhrsveen and Lygre (1996).

Tunnel section	X (%)	h (m)	Sum Cc + Fe	Calcite deposit	Mn-Fe deposit	Water load
1500-	4					
1550-	9	55				
1600-	17	56				
1650-	29	61	4.25	2	2.25	3.25
1700-	59	66	3.8	2	1.8	3.4
1750-	35	71	3	2	1	2.6
1800-	40	76	4	2	2	3
1850-	45	86	4.75	2.75	2	2.75
1900-	82	90	5	2.5	2.5	3
1950-	73	92	4.2	2	2.2	3
2000-	100	94	3	1.6	1.4	2.6
2050-	76	94	4.6	2.4	2.2	3
2100-	100	94	4	2	2	3
2150-	92	94	5	3	2	2
2200-	69	97	6	3	3	3
2250-	100	94	3.8	1.8	2	2.4
2300-	90	84				
2300-	90	84	7	2	5	5
2350-	64	79	4	2	2	2
2400-	79	74	4.5	2.5	2	2
2450-	60	69	4	2.5	1.5	2
2500-	3	64	2	2	0	2
2550-	24	59	2	2	0	2
2600-	16	54	2.4	1.6	0.8	2
2650-	24	50	2	1.3	0.7	1.7
2700-	21	44	2.5	1.5	1	1.5
2750-	70	39	1	1	0	1

Figure 4 in Chapter 8 shows some pertinent data for the Flekkerøy subsea tunnel. All data of Røhrsveen and Lygre (1996) were recalculated for 50 m tunnel intervals (see Table A6-7-1). These 50 m tunnel intervals were calculated to match previous data from this tunnel (cf. Hagelia 1994, quoted in Chapter 8): In this previous work “leakage areas” in % of 50 tunnel meters (corresponding to about 1000 m² tunnel areas as unit areas) were measured directly in the tunnel. Data from leakage areas averaged by 50 tunnel meters were used since this procedure tends to cancel out scale effects (cf. Hagelia 1994). Figures 4B and 4C

(Chapter 8) clearly demonstrated that there is a positive correlation between rated surface water and Ca-deposits/leaching as well as Mn-Fe deposits, respectively. Figure 4A shows that there is a rough but well defined positive correlation between “Leakage area (%)” from Hagelia (1994) and the sum of scores of surface Ca- and Fe-“algae” deposits from the data of Røhrsveen and Lygre (1996). Moreover, Figure 4D shows that the surface Ca and Fe-“algae” deposits are positively correlated with the hydraulic gradient (e.g. depth beneath sea level) as based on the same 50 m tunnel sections. Since the surface effects represent a variable impact of the saline ground water attack it may be concluded that the hydro-geological parameters have a direct impact on the deterioration rate.

Also for the other subsea tunnels (cf. data in Røhrsveen and Lygre 1996) it was obvious that the effects of deterioration features on sprayed concrete surfaces were most pronounced in the deep subsea sections, coinciding with the steepest hydraulic gradients. Thus the example from the Flekkerøy tunnel can be regarded as typical. Yet the local quantitative effects of deterioration will depend on local characteristics being mainly: 1) the rock mass hydraulic conductivity, 2) the magnitude of the hydraulic gradient, 3) the hydraulic conductivity and thickness of the sprayed concrete, 4) the age of the concrete and 5) the aggressiveness of water and biofilm material.

Appendix 7: Additional documentation to Chapter 9

- A7-1 Relationships of Durability Class and Exposure Class according to NS-EN 206-1**
- A7-2 Characteristics of sprayed concrete versus cast concrete**

A7-1 Relationships of Durability Class and Exposure Class according to NS-EN 206-1

According to this standard a given Exposure Class determines which Durability Class should be applied. In the Norwegian Annexes the **Exposure Class XSA** has been introduced for especially aggressive environments such as Alum Shale ground water: When the aqueous sulfate concentration exceeds 600 mg/L (e.g. XA2 or XA3) sulfate resisting concrete should be specified, which in practice is either Sulfate Resisting Portland Cement or Portland Cement with added silica fume (SF). In sprayed concrete used for rock support SF or other pozzolanic material is always specified. Table A7-1-1 indicates the Durability Classes (“Bestandighetsklasse”) mostly used for sprayed concrete (M40 and M45).

The Norwegian Concrete Association Publication no. 7 (NB 7) does not specify air content to ensure frost resistance in sprayed concrete. Instead experience has shown that sprayed concrete seldom exhibit frost deterioration, whilst the weakness lies in the bond zone. According to NB 7 water should be drained where freeze-thaw cycles occur: The Durability Classes MF40 and MF45 are, therefore, not used in Norway. Further details may be found in NS-EN 206-1 and Chapter 9.

Table A7-1-1. The National Annex of NS-EN 206-1, showing the relationship between Durability Class and Exposure Class, with classes (highlighted) for Alum Shale environment (M40 and XSA) and classes involving seawater exposure (M45 and XS1, XA1, XA2 or M40 and XS2, XS3, XA3).

Tabell NA.11 – Valg av bestandighetsklasse avhengig av eksponeringsklasse

Eksponeringsklasse	Bestandighetsklasse					
	M90	M60	M45	MF45	M40	MF40
X0	X	X	X	X	X	X
XC1, XC2, XC3, XC4, XF1		X	X	X	X	X
XD1, XS1, XA1, XA2 ^{a)} , XA4 ^{b)}				X		X
XF2, XF3, XF4				X		X
XD2, XD3, XS2, XS3, XA3 ^{a)}						X
XSA ^{a)}	Betongsammensetning og beskyttelsestiltak fastsettes særskilt. Betongsammensetningen skal minst tilfredsstille kravene til M40.					

^{a)} Om det i eksponeringsklasse XA2, XA3 eller XSA er mulighet for kontakt med sulfater i konsentrasjoner høyere enn grenseverdien for XA2, skal det i produksjonsunderlaget være presisert at det skal anvendes sulfatbestandig sement

^{b)} For konstruksjoner utsatt for husdyrgjødsel skal det i produksjonsunderlaget være angitt at det skal anvendes minst 4 % silikastøv

A7-2 Characteristics of sprayed concrete versus cast concrete

Sprayed concrete is a mortar which is conveyed through a hose and pneumatically projected at high velocity on to a surface. The surface mostly needs to be cleaned by water before the spraying operation, for example a rock surface. Modern sprayed concrete for tunnelling is applied by robotic equipment, but the skills of the operator (the nozzle man) are especially important: certification for the nozzle man is an important issue for the International Tunnel Association (ITA). Sprayed concrete technology is very flexible and is used in connection with ground support of all kinds, for fire protection of panels for water/frost protection and several other purposes. There are two different application methods for sprayed concrete, among which wet mix completely dominates in tunnelling:

- *Dry mix*: The ingredients (cement, aggregate, fibres, admixtures) are pre-blended and then placed into the delivery equipment. Compressed air conveys the concrete material through a hose, at high velocity to the nozzle, where water is added.
- *Wet Mix*: All ingredients, including water, are mixed and placed into the delivery equipment. The wet concrete mix is pumped to the nozzle where compressed air is added to provide high velocity and consolidation of the material.

This application method and use of sprayed concrete differs much from cast concrete: Cast concrete commonly needs to be vibrated, whilst self-compacting concretes are also in frequent use. Sprayed concrete mixes are designed in order to achieve good pumpability, good bonding to the substrate, optimal stiffness of fresh concrete, early age setting and rapid build-up thick layers in a single spraying round. In contrast to cast concrete, early setting is a prerequisite for sprayed concrete: Setting accelerators are used. Also mineral admixtures, aggregate grading with low D_{max} , elevated binder contents and super-plasticisers assist in avoiding internal lamination and structural flaws within the final sprayed concrete layer. Several other differences between sprayed concrete and cast concrete are tabulated below.

Table A7-2-1. Some common characteristics of current wet sprayed concrete and cast concrete. * the example is given for compressive strength of cylinders ≥ 35 MPa (B35)

Property	Wet sprayed	Cast concrete	Remark
Water/binder ratios	(0.35) 0.40-0.55	0.35-0.55	Common ranges
Aggregate grading (mm)	0-16	0-25	Common ranges
Binder contents	380-500 kg/m ³	350-450 kg/m ³	Common ranges
Silica fume or pozzolana	“Always”	Common	
Setting accelerator	Always used	Not common	Al-sulfate e.t.c.
Fibres	Very common	Less common	
Surface characteristics	Rough & tortuous	Plan and even	
Drying shrinkage	0.8-1.2 vol-%	0.4-0.6 Vol-%	Approximate
E-modulus, example*	≈ 22 GPa	≈ 28 GPa	Approximate
Layering/inhomogeneity	Not uncommon	Less common	Air void structure
Rebound (of total vol.)	≤ 5 vol-%	Irrelevant	Includes fibres

Sprayed concrete is more susceptible to creep and drying shrinkage than cast concrete, which usually results a certain degree of micro cracking. This is reflecting their differences in binder contents. Moreover, in-homogeneities as regards porosity tend to be more common in sprayed concrete than in cast concrete, although not generally. Hence some sprayed concrete should potentially be more vulnerable to aggressive external waters than cast concrete.